TU ILMENAU

DOCTORAL THESIS

Perception of Color Break-Up

A thesis submitted in fulfillment of the requirements
for the degree of Doctor of Engineering

in the

Faculty of Computer Science and Automation

by

Markus LEICHT, M. Sc.

1. Reviewer: Prof. Dr.-Ing. habil. Jens HAUEISEN
2. Reviewer: Prof. Dr.-Ing. Sascha KLEE
3. Reviewer: Prof. Dr. Stephan DEGLE

Day of Submission: August 13, 2022
Day of Defense: Mai 5, 2023

URN: urn:nbn:de:gbv:ilm1-2023000099
DOI: 10.22032/dbt.57446

Declaration of Authorship

I, Markus LEICHT, M. Sc., hereby declare that this thesis titled "Perception of Color Break-Up" and the work presented therein has been generated by me as the result of my own original research. I confirm that:

— This work was done entirely within the framework of a doctorate at the TU Ilmenau.

— The work has not been submitted to an examination authority in the same or a similar form, neither at the TU Ilmenau nor at any other institution.

— Where I have consulted the published work of others, this is always clearly attributed.

— Where I have quoted from the work of others, the source is always given.

I certify that I have completed this work without unauthorized help of third parties and without the use of aids other than those indicated:

— Software development (CBU Scenario Player) for content presentation during the empirical studies by Stefan Sandig, Dipl.-Inf. (FH), from the SeeReal Technologies GmbH.

— Expert advice on the statistical analysis of empirical and model data by Prof. Dr. Mario Walther from the EAH Jena.

— LaTeX template from Vel (2017) used as the framework for writing the doctoral thesis (licensed under CC BY-NC-SA 3.0).

— Proofreading of the doctoral thesis by Henrice C. Stöbesand, M. Phil.

No other people were involved in the content-related creation of the present work. In particular, I did not use any paid help from intermediary or consulting services (PhD supervisors or other persons) for this purpose. No one has received direct or indirect monetary benefits from me for work related to the content of the submitted dissertation.

I have been informed that the incorrectness of this declaration will be considered as an attempt of deception, which will result in the discontinuation of the doctoral procedure according to Section 7 (10) of the doctorate regulations of the TU Ilmenau in the version of the tenth amendment of October 13th 2017.

Signed:

Place/Date:

"You make different colors by combining those colors that already exist."

Herbie Hancock

TU ILMENAU

Abstract

Faculty of Computer Science and Automation
Institute of Biomedical Engineering and Informatics

Doctor of Engineering

Perception of Color Break-Up

by Markus LEICHT, M. Sc.

Background. A color-distorting artifact called *Color Break-Up* (CBU) has been investigated. Disturbing CBU effects occur when eye movements (e.g., pursuits or saccades) are performed during the presentation of content on *Field-Sequential Color* (FSC) display or projection systems where the primary colors are displayed sequentially rather than simultaneously. ***Methods.*** A mixed design of empirical research and theoretical modeling was used to address the main research questions. Conducted studies evaluated the impact of hardware-based, content-based, and viewer-based factors on the sample's CBU perception. In a first step, visual performance parameters (e.g., color vision), short-term state (e.g., attention level), and long-term personality traits (e.g., affinity to technology) of the sample were recorded. Participants were then asked to rate the perceived CBU intensity for different video sequences presented by a FSC-based projector. The applied setup allowed the size of the CBU-provoking content (1.0 to 6.0°), its luminance level (10.0 to 157.0 $\mathrm{cd/m^2}$), the participant's eye movement pattern (pursuits: 18.0 to 54.0 deg/s; saccadic amplitudes: 3.6 to 28.2°), the position of retinal stimulation (0.0 to 50.0°), and the projector's frame rate (30.0 to 420.0 Hz) to be varied. Correlations between independent variables and subjective CBU perception were tested. In contrast, the developed model predicts a viewer's CBU perception on an objective basis. The model graphically reconstructs the intensity and color characteristics of CBU effects. The visual CBU reconstruction is then compressed into representative model indices to quantify the modeled scenario with a manageable set of metrics. Finally, the model output was compared to the empirical data. ***Results.*** High interindividual CBU variability within the sample cannot be explained by a participant's visual performance, short-term state or long-term personality traits. Conditions that distinctly elevate the participant's CBU perception are (1) a foveal stimulus position on the retina, (2) a small-sized stimulus during saccades, (3) a high eye movement velocity, and (4) a low frame rate of the projector (correlation expressed by exponential function, $r^2 > .93$). The stimulus luminance, however, only slightly affects CBU perception. In general, the model helps to understand the fundamental processes of CBU genesis, to investigate the impact of CBU determinants, and to establish a classification scheme for different CBU variants. The model adequately predicts the empirical data within the specified tolerance ranges. ***Conclusions.*** The study results allow the determination of frame rates and content characteristics (size and position) that avoid exceeding predefined annoyance thresholds for CBU perception. The derived hardware requirements and content recommendations enable practical and evidence-based CBU management. For CBU prediction, model accuracy can be further improved by considering features of human perception, e.g., eccentricity-dependent retinal sensitivity or changes in visual perception with different types of eye movements. Participant-based data from the empirical research can be used to model these features.

Acknowledgements

This doctoral thesis was written within the framework of a cooperative doctorate jointly supervised by Prof. Dr.-Ing. habil. Jens Haueisen (TU Ilmenau, Faculty of Computer Science and Automation) and Prof. Dr. Stephan Degle (EAH Jena, Faculty of SciTec). I am deeply grateful for their trust and support along the way.

I worked on this doctoral project while employed by the SeeReal Technologies GmbH (extra-occupational doctorate), a company that develops seminal FSC-based display technologies and therefore benefits from the findings of this work. I am grateful for their provision of the bulk of the technical setup and their technical support.

I particularly wish to thank SeeReal's CTO, Hagen Stolle, for providing me with the opportunity to delve into this fascinating topic, and to continuously learn and grow.

Among the many other colleagues at SeeReal, I would like to especially thank Stefan Sandig, Dipl.-Inf. (FH), for the constructive and committed teamwork on a day-to-day basis.

Furthermore, I would like to thank the EAH Jena for providing me with the space and the technical equipment for preliminary light measurements to conduct my empirical studies.

A special thanks to Prof. Dr. Mario Walther (EAH Jena) for his invaluable professional advice on carrying out the statistical analysis.

I want to make particular mention of Henrice C. Stöbesand, M. Phil., for patiently proof-reading the dissertation — thanks a million.

A loving hug goes to my awesome parents, Margit and Ansgar. You have supported me my entire life with everything you have. Okay, I know that just one hug won't do it — it should be way more hugs. I think that there is no other way than giving you all the hugs I have, hug by hug.

I am sorry that there is no good news for you, Meena. A few seconds ago, I gave away all my hugs. Now I only have kisses left. Sorry. But don't worry, you will get all of them. That's only fair. You always stood by my side and encouraged me when I needed it most.

The sad thing is that from now on, I only have handshakes left for the rest of you. However, you can be sure that they will be warm.

Contents

List of Figures

List of Tables

List of Abbreviations

ACR	**A**bsolute **C**ategory **R**ating
AM	**Am**etropia
ANOVA	**An**alysis **o**f **Va**riance
AP	**A**djustment **P**oint
AR	**A**spect **R**atio
AU	**A**rbitrary **U**nit
B	**B**lue
BFR	**B**ase **F**rame **R**ate
BINO	**Bino**cular
BP	**B**lue **P**hase
BS	**B**lurring **S**trength
BT	**B**loch **T**ime
C	**C**yan
CAT	**Ca**tegory
CBU	**C**olor **B**reak-**U**p
CBUA	**C**olor **B**reak-**U**p **A**ngle
CE	**C**yclops **E**ye
CF	**C**olor **F**actor
CFA	**C**olor **F**ield **A**rrangement
CH	**C**ontent **H**eight
CIE	**C**ommission **I**nternationale de l'**É**clairage
CM	**C**ontent **M**ovement
CMD	**C**ontent **M**ovement **D**istance
CMF	**C**olor **M**atching **F**unction
CMV	**C**ontent **M**ovement **V**elocity
CN	**C**urrent **N**umber
CO	**Co**nes
COBUS	**Co**lor **B**reak-**U**p **S**tudy
CP	**C**ontent **P**osition
CPB	**C**enter-to-**P**eriphery **B**ias
CRF	**C**ase **R**eport **F**orm
CS	**C**ontrast **S**ensitivity
CT	**Coun**t
CTB	**Con**tri**b**ute
CTO	**C**hief **T**echnical **O**fficer
CTR	**Cen**te**r**
CV	**C**olor **V**ision / **C**orneal **V**ertex
CW	**C**ontent **W**idth
D	**D**ark / **D**istance
DA	**D**irectional **A**rrow

DC **D**uty **C**ycle
DD **D**isplay **D**iagonal
DIN **D**eutsches **I**nstitut für **N**ormung
DIV **Div**ision
DLP **D**igital **L**ight **P**rocessing
DMD **D**igital **M**icromirror **D**evice
DU **D**isplay **U**nit
DVA **D**ynamic **V**isual **A**cuity
DVS **D**ominant **V**isual **S**aliency
D2U **D**own-**t**o-**U**p

EC **E**thics **C**ommittee
ECC **Ecc**entricity
EM **E**ye **M**ovement
EMD **E**ye **M**ovement **D**istance
EMV **E**ye **M**ovement **V**elocity
EOC **E**xample **o**f **C**hoice
EP **E**ye **P**osition

FC **F**rame **C**ycle
FCC **F**rame **C**ycle of **C**hoice
FFF **F**licker **F**usion **F**requency
FIX **Fix**ation
FLC **F**erroelectric **L**iquid **C**rystal
FOV **F**ield **o**f **V**iew
FR **F**rame **R**ate
FRR **F**rame **R**ate **R**ange
FRT **F**oveated **R**endering **T**echnique
FSC **F**ield-**S**equential **C**olor
FT **F**ixation **T**arget

G **G**reen
GDPR **G**eneral **D**ata **P**rotection **R**egulation
GP **Gap**
GPD **G**lobal **P**rimary **D**esaturation

H **H**ypothesis
HC **H**abitual **C**orrection
HDMI **H**igh-**D**efinition **M**ultimedia **I**nterface
HMD **H**ead-**M**ounted **D**isplay
HOR **Hor**izontal
HUD **H**ead-**U**p **D**isplay
H3D **H**olographic **3D**

I **I**ntersection
IA **Inter**a**ction**
ID **Id**entifier
IDX **Ind**e**x**
ISO **I**nternational **O**rganization for **S**tandardization
ITU **I**nternational **T**elecommunication **U**nion

JCC	**J**ackson **C**rossed **C**ylinder
L	**L**ong
LC	**L**iquid **C**rystal
LCD	**L**iquid **C**rystal **D**isplay
LE	**L**eading **E**dge
LED	**L**ight-**E**mitting **D**iode
LL	**L**uminance **L**evel
LPD	**L**ocal **P**rimary **D**esaturation
L2R	**L**eft-**t**o-**R**ight
M	**M**edium
MCS	**M**ixed **C**olor **S**equential
MD	**M**ovement **D**irection
ME	**M**ain **E**ffects
MI	**M**otion **I**nterpolation
MN	**Mea**n
MONO	**Mono**cular
MOS	**M**ean **O**pinion **S**core
MP	**M**ovement **P**attern
MV	**M**ovement **V**elocity
MVA	**M**ulti-domain **V**ertical **A**lignment
NI	**N**o **I**rregularity
NV	**N**o **V**iolation
OCB	**O**ptically **C**ompensated **B**end
OD	**O**culus **D**exter
OS	**O**culus **S**inister
P	**P**osition
PAR	**Par**ticipant
PD	**P**rojection **D**istance
PEM	**P**ursuit **E**ye **M**ovement
PH	**Ph**ase
PI	**P**erceived **I**rregularity
PP	**P**ixel **P**itch
PPT	**P**ower **Point**
PRT	**Part**
PV	**P**ower **V**ector
PX	**P**i**x**el
R	**R**atio / **R**ed
RA	**R**icco **A**rea
RBP	**R**homboid **B**asic **P**oint
RE	**R**efractive **E**rror
REF	**Ref**erence
REG	**Reg**ular
REQ	**Req**uirement
RES	**Res**olution
RL	**R**adiance **L**evel
RO	**Ro**ds

RR **R**etinal **R**adius
R2L **R**ight-**t**o-**L**eft

S **S**hort
SAC **Sac**cade
SCN **Scan**
SCR **Scor**e
SD **S**tandard **D**eviation
SDIV **S**ub**div**ision
SEC **Sec**tor
SEQ **Seq**uence
SF **S**ub**f**rame / **S**ub**f**ield
SFC **S**ub**f**rame **C**ycle / **S**ub**f**ield **C**ycle
SFR **S**ub**f**rame **R**ate / **S**ub**f**ield **R**ate
SGL **S**ing**l**e
SL **S**accadic **L**ength
SME **S**imple **M**ain **E**ffects
SMPTE **S**ociety of **M**otion **P**ictures and **T**elevision **E**ngineers
SN **S**ubstitution **N**umber
SP **S**timulus **P**osition
SPL **S**am**pl**e
SPX **S**ub**pix**el
SS **S**timulus **S**ize
ST **St**imulus
STICA **S**patio-**T**emporal **I**ntensity & **C**olor **A**nalysis
SUC **Suc**cess Rate

T **T**ime
TE **T**railing **E**dge
TFT **T**hin-**F**ilm **T**ransistor
TI **T**exas **I**nstruments
TOA **T**hreshold **o**f **A**nnoyance
TOP **T**hreshold **o**f **P**erceptibility
TP **T**ime **P**eriod
TS **T**emporal **S**ummation
TTL **T**ot**al**
TV **T**ele**v**ision

U **U**nion
ULH **U**niform **L**ying **H**elix
U2D **U**p-**t**o-**D**own

V **V**isit
VA **V**isual **A**cuity
VD **V**iewing **D**istance
VER **Ver**tical
VOL **Vol**ume

W **W**hite / **W**idth

Y **Y**ellow

List of Symbols

α	angular content position at display level (CBU model)	deg
β	angular eye position at display level (CBU model)	deg
β^*	exponent of power function (Power law)	—
γ	angle btw. content and eye position at display level (CBU model)	deg
γ'	angular content position at retinal level (CBU model)	deg
δ	angular pixel distance at display level (CPB)	deg
ϵ	angle btw. optical axis and visual axis (human eye)	deg
η	angle btw. optical axis and fixation line (human eye)	deg
ϕ	physical magnitude of stimulation (Power law)	—
ψ	subjective magnitude of perception (Power law)	—
F	first principal focus (human eye)	—
F'	second principal focus (human eye)	—
I	electric current	A
J_0	second power vector component (Jackson vector)	D
J_{45}	third power vector component (Jackson vector)	D
k	measurement unit-dependent constant (Power law)	—
L_e	radiance	$\mathrm{W}/(\mathrm{sr}\times\mathrm{m}^2)$
L_v	luminance	cd/m^2
M	first power vector component (spherical equivalent)	D
N	first nodal point (human eye)	—
N'	second nodal point (human eye)	—
x	first chromaticity coordinate	—
X	first tristimulus value	—
y	second chromaticity coordinate	—
Y	second tristimulus value	—
Z	third tristimulus value	—
Z'	center of rotation (human eye)	—

For Ida.

Chapter 1

Introduction

In general, there are two methods to trigger human color perception via digital display systems. Both methods have in common that they generate a multitude of different color impressions by additive mixing of a limited number of basic colors of light (Maxwell, 1857, 1860). However, the methods must be distinguished in terms of their general approach.

The first, more common method is based on the *spatial summation* of colored stimuli by the viewer's visual system. This form of color mixture has its starting point at the display level. Each individual pixel consists of subpixels as the smallest presentation units which in most cases are arranged side-by-side and displayed simultaneously. The subpixels — which classically cover the emission of red, green, and blue light as the three primary colors of additive color mixing — are so small that the human visual system cannot perceive them independently of their neighboring subpixels. The additive combination of the primary colors emitted by the subpixels results in the viewer perceiving a mixed color that depends on the proportions of the primary colors (R. H. Chen, 2011). This is the conventional method of generating an appropriate color gamut for a large share of all types of displays, such as the traditional Thin-Film Transistor Liquid Crystal Display (TFT-LCD) used in smartphones, tables, desktop monitors, and televisions.

The second, alternative method for digital color creation is the so-called Field-Sequential Color (FSC) technology, which is based on the *temporal summation* of colored stimuli. Unlike the conventional method, the primary colors are not presented simultaneously side-by-side, but sequentially via subframes/subfields – embedded within a frame cycle – at the same spot at the display level. A fast temporal succession of single subframes enables the human eye to combine the RGB primaries to create the desired color impression (R. H. Chen, 2011). The general FSC principle was developed for color television application in the 1940s (Goldmark, 1949), but did not become widely accepted at that time. A first application within Liquid Crystal Displays (FSC-LCD) was later realized by Hasebe and Kobayashi (1985). Nowadays, FSC projectors based on Digital Light Processing (DLP) are widely used. Future applications of seminal Head-Mounted Displays (HMD) such as Microsoft's HoloLens (Poulos et al., 2018) or CREAL's light-field hardware (Sluka et al., 2021) are also based on sequential color reproduction. This technical aspect also applies to the Holographic 3D Displays (Häussler et al., 2017, H3D) and Head-Up Displays (Teich et al., 2022, HUD) from SeeReal Technologies.

FSC technology offers great advantages in terms of optimizing the available native resolution and light emission (including a wider color gamut) of a digital display unit, since no color filters are required during the sequential presentation of primary colors.[1] Furthermore, FSC systems are generally more energy-efficient due to the higher light efficiency, and are characterized by a flatter design and lower material costs (Guenther & Steel, 2018). However, FSC technology has a much smaller market share than the conventional method,

[1] In the present work, the term *digital display unit* (or digital display system) is used as a collective term for all electronic output devices that allow displaying digital content. The term includes all types of visual output devices such as direct-view systems or projection-based systems.

mainly due to one major drawback: Under certain conditions, the time-shifted subframe presentation leads to a disturbing effect of color distortion known as *Color Break-Up*, or CBU for short. The digital color reproduction is affected by CBU as soon as the viewer's eyes move, while potentially CBU-triggering content is presented via the FSC system. Subframes presented sequentially at the same spot at the display level are spatially separated on the viewer's retina due to eye movements such as pursuits or saccades. As a result, the time-delayed RGB contents within the three subframe periods fall on different retinal areas and cannot be temporally summed. In this case, the viewer will not perceive a completely white object, as assumed with harmonized RGB mixing. Instead, s/he will see slight color artifacts at the leading and trailing edges of the object perpendicular to the eye movement direction, or even stronger color distortions affecting the entire object.

To achieve high consumer acceptance, the CBU effect needs to be overcome. Therefore, this work seeks to elucidate fundamental, causal processes at an early stage of CBU emergence and, furthermore, improve the understanding of how certain determinants affect the highly variable features of CBU perception (magnitude and color structure). Overall, this work aims to provide new insights that will form the basis for future improvements towards a CBU-free FSC technology.

The present thesis is organized as follows: First, the basic operating principles of FSC technology and the scientific literature on CBU perception — including genesis, factors, compensation techniques, evaluation, and prediction — as well as other relevant topics, such as a viewer's eye movement behavior and various aspects of his/her visual perception are reviewed (see Chapter 2). Second, the emergence of the CBU effect is investigated using a theoretical MATLAB model (see Chapter 3) that simulates the visual impression of CBU on the viewer's retina under certain conditions. The self-developed model allows prediction of human CBU perception based on a Spatio-Temporal Intensity & Color Analysis (STICA), which considers the CBU effect's retinal positioning/timing, light intensity, and color characteristics. This establishes a fundamental understanding of early stage CBU formation processes. Third, the implementation of empirical studies (see Chapter 4) allows the investigation of the influence of hardware-based (frame rate), content-based (size, position, and luminance), and viewer-based factors (eye movement behavior, visual performance, and personal characteristics) on human CBU perception. For this purpose, study participants were invited to evaluate various CBU-provoking scenarios presented via a DLP projector. Finally, the model's output and the empirical evidence are critically compared (see Chapter 5), and avenues for future research are provided (see Chapter 6).

Chapter 2

Literature Review

2.1 Digital Color Creation

Digital display systems generate colors based on the additive color mixing of light (Maxwell, 1857, 1860). Classically, the primary colors red, green, and blue (RGB) are used for color mixing. Different RGB compositions produce different colors. Yellow content, for example, can be created by mixing red and green components. White content originates from a harmonized RGB primary presentation. The total range of achievable colors defines the color gamut of a digital display system. The size of the gamut depends on the light sources used.

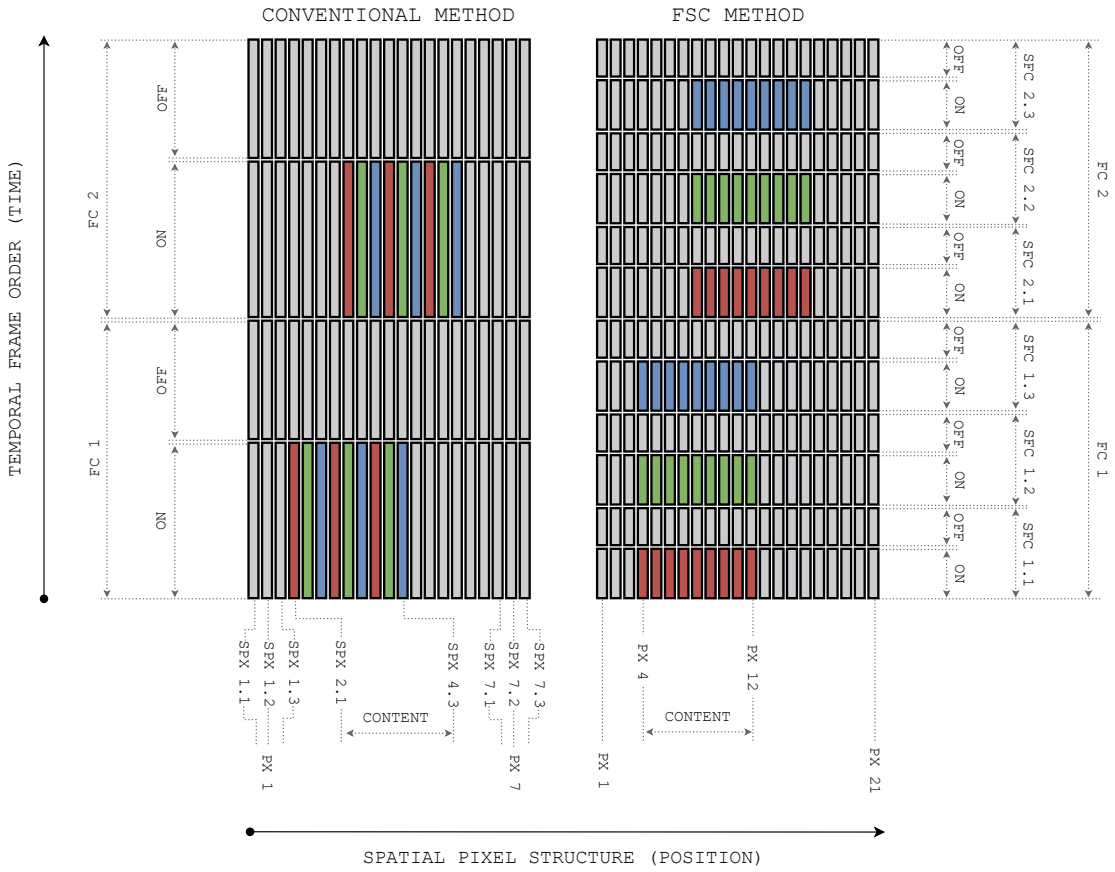

FIGURE 2.1: Principle of color creation via digital display unit applying conventional (left) and FSC method (right). Illustration of spatio-temporal RGB primary structure on a pixel-based display unit over two frame cycles (FC = frame cycle, SFC = subframe/subfield cycle, PX = pixel, SPX = subpixel).

Additive color mixing is the foundation of color creation via a display or a projection system. As outlined, there are two different methods of mixing primary colors — the conventional vs. the FSC method (see Chapter 1). The functional principle of a digital FSC system

for temporal mixture of primary colors is fundamentally different from the conventional method of spatial color mixing. Figure 2.1 illustrates the spatial pixel structure over two full frame cycles for a schematic display unit with a defined pixel range for both methods. In the example shown, the RGB pixel structure of the display unit is activated to (1) create color-mixed content that is (2) moving from left to right.

To understand the first aspect of digital color creation, it is necessary to analyze the temporal and spatial processes *within* one separate frame cycle. The conventional method of digital color creation is based on a simultaneous presentation of the primary RGB colors emitted by subpixels arranged side-by-side (see Figure 2.1, left graphic). To achieve the desired perception of color-mixed content, the viewer must process the displayed RGB content by spatially fusing the adjacent RGB subpixels. To ensure spatial summation, the subpixel structure must not exceed a certain size so that the individual subpixels cannot be resolved separately by the viewer's visual system. In contrast, the classic RGB pattern during FSC presentation is displayed in rapid succession at the same pixel spots at the display level (see Figure 2.1, right side). The color creation of the FSC method works by the temporal summing of the RGB contents within the sequential subframes over time.[1] Again, the temporal summation of the individual RGB stimuli to create color-mixed content depends on the viewer and his/her visual processing of the scene (R. H. Chen, 2011). However, the viewer's eye (including subsequent cognitive processes) can only ensure temporal summation of the subframes within a frame cycle as long as the frame rate does not fall below a minimum value.

Regardless of these differences in terms of color creation within a single frame cycle, both methods have in common that the second aspect of content movement is realized by displaying a rapid succession *across* several frame cycles. In Figure 2.1, the displayed content of the two consecutive frame cycles is shifted by a few pixels, resulting in a short movement of the content with a velocity of four pixels per frame cycle. If further frame cycles with the same content shift were added, the viewer would perceive a continuous movement of the content from left to right. With this basic principle of pixel-based image sequences, a digital presentation of colored and moving content is possible.

2.2 Color Break-Up

Sections 2.2.1 to 2.2.4 highlight relevant scientific findings on the genesis, factors, compensation techniques, and approaches to assess, evaluate, and predict the CBU effect.

2.2.1 Genesis

Four conditions are pivotal for the appearance of CBU. The first two conditions are technical, and have to do with the digital display system. First, the subframes of a display or projector system — classically three subframes with RGB pattern — must be displayed in temporal succession, as in FSC systems (see Section 2.1). Second, at least two subframes

[1] The term *subframe* (subfield or field) refers to the time interval in which light is emitted by one primary light source of an FSC display unit — red, green, or blue (see Figure 2.1). This time interval is also called on-time. Correspondingly, the time interval in which the light source is switched off is called off-time. Both intervals form one subframe cycle of one primary light source. The duty cycle is calculated by dividing a subframe cycle's on-time by the time span of a complete subframe cycle (on- and off-time). The time period of one full subframe cycle corresponds to the technical specification of the subframe rate as its reciprocal value. The subframe cycles of all included light sources (red, green, and blue) define one full frame cycle. Consequently, the frame rate as the reciprocal value of the frame cycle's duration is one third of the subframe rate, assuming an RGB color pattern with three subframe cycles (e.g., three subframe cycles with a subframe rate of 180 Hz lead to a frame rate of 60 Hz). This section focuses on findings that are applicable to all FSC systems rather than addressing specific FSC approaches (e.g., FSC-LCD or DLP projector).

within a frame cycle must be active and emit light to create color-mixed content, for example, a yellow object by mixing light from the first (R) and second (G) subframe cycles. In most cases, however, all subframes are activated and contribute to the final color creation. A balanced display of the primary colors (RGB) would be necessary to generate color-mixed white content (see Figure 2.2).

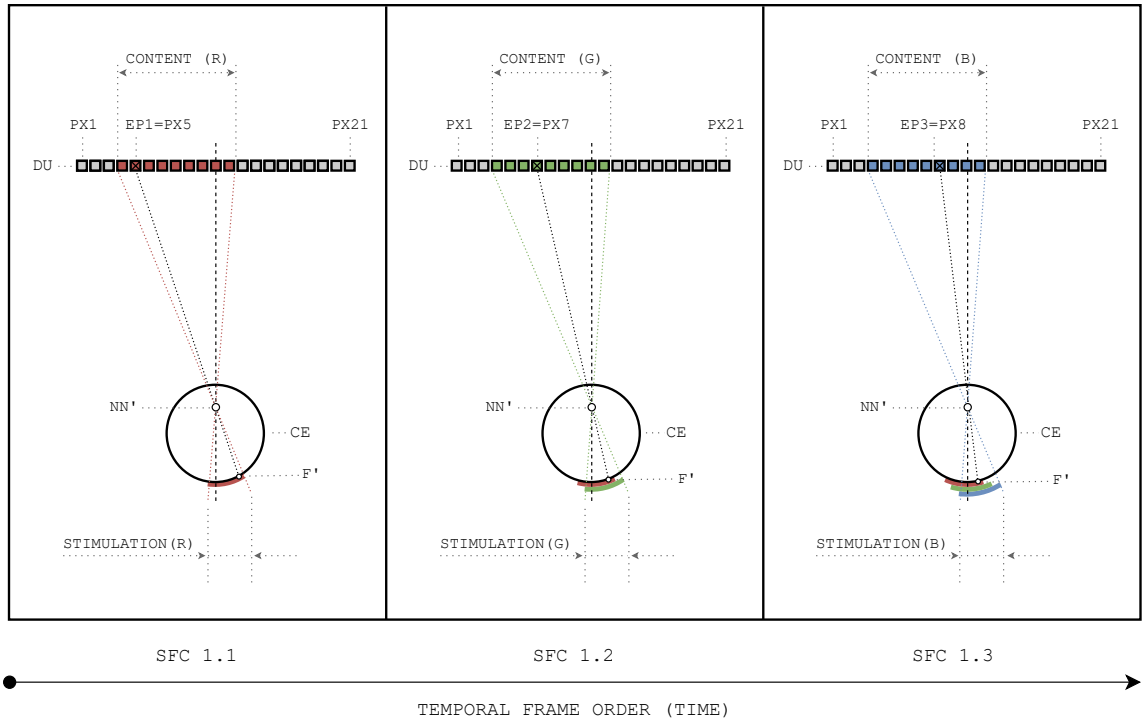

FIGURE 2.2: Principle of CBU origin during FSC presentation on a schematic display unit (DU) covering 21 pixels, viewed by a simplified cyclops eye (CE). Illustration of three time-shifted RGB subframe cycles (SFC) within one full frame cycle (FC), RGB content is presented consecutively at the same pixel spots at display level to create a color-mixed white object with a width of nine pixels (conditions refer to first frame cycle illustrated in right graphic of Figure 2.1), cyclops eye's position (EP) at display level changes with a movement velocity of two pixels per subframe cycle, eye movement during FSC presentation leads to a spatial separation of the stimulation with red, green, and blue content at retinal level (N = first nodal point, N' = second nodal point, F' = second principal focus).

The other two conditions pertain to the viewer of a digital scene shown on the FSC display or projector. First, the viewer must execute eye movements during the presentation of color-mixed content via the FSC system.[2] Eye movements can be triggered, for example,

[2]The author classifies a scenario in which a viewer maintains stable fixation onto a static point in a digital FSC-based scene including moving (white) stimuli as *not* CBU-provoking. In other words, the author asserts that content movement is not relevant for the genesis of CBU (other than eye movement). This assertion is based on the defined conditions that have to be fulfilled to trigger CBU, and is confirmed by own empirical pre-tests. Deviant assertions by other researchers such as P. V. Johnson et al. (2014) are based on insufficient experimental methods/setups or incorrect result interpretations. First, during psychophysical CBU experiments, participants might misinterpret other distorting effects (e.g., motion blur) as CBU. The evaluation of scenes with fast moving content is particularly challenging. A systematic instruction helps increase the quality of the participant's evaluation. However, this measure alone does not guarantee errorless CBU evaluations. Second, involuntary eye movements (tremor, drifts, and microsaccades) are likely to occur during fixation tasks — potentially triggering CBU. Furthermore, reflexive eye movements are easily provoked by content movement within the participant's field of view. Undesired eye movements cannot be ruled out even if the participant is tasked to fixate. Monitoring undesired eye movements by implementing eye-tracking systems would allow to cleanse data sets from erroneous trials. In previous research on CBU, this is not the standard procedure. Most experimental setups do not include eye-tracking, see P. V. Johnson et al. (2014). The stated disruptive factors lead to CBU overestimation during scenarios with content movement and stable fixation. The author postulates that the exclusion of these factors leads to zero CBU perception during these scenarios.

by a moving object that is slowly and smoothly pursued by the viewer's gaze, or by an object that suddenly appears in the peripheral field of view, leading to a fast saccade. When the first three conditions are met, the time-delayed subframes (RGB) at the display level are spatially separated on the viewer's retina due to the simultaneous execution of eye movements (see Figure 2.2). As a result, certain retinal areas are not stimulated by all activated subframe cycles. Therefore, the spatial components of the RGB content cannot be temporally summed by the viewer's visual system. This fact potentially leads to the occurrence of CBU. However, whether CBU is actually perceived depends on the fulfillment or violation of the fourth and last condition: The color-distorted content must fall on retinal areas that have sufficiently high sensitivity during motion (see Section 2.3.2) to perceive the existent CBU effect on the retina. Assuming that all four conditions are met, the viewer will not perceive a completely white object as intended. Instead, the viewer will perceive color artifacts at the leading and trailing edges of the white object perpendicular to the direction of eye movement as one possible CBU color pattern (see Figure 2.3).

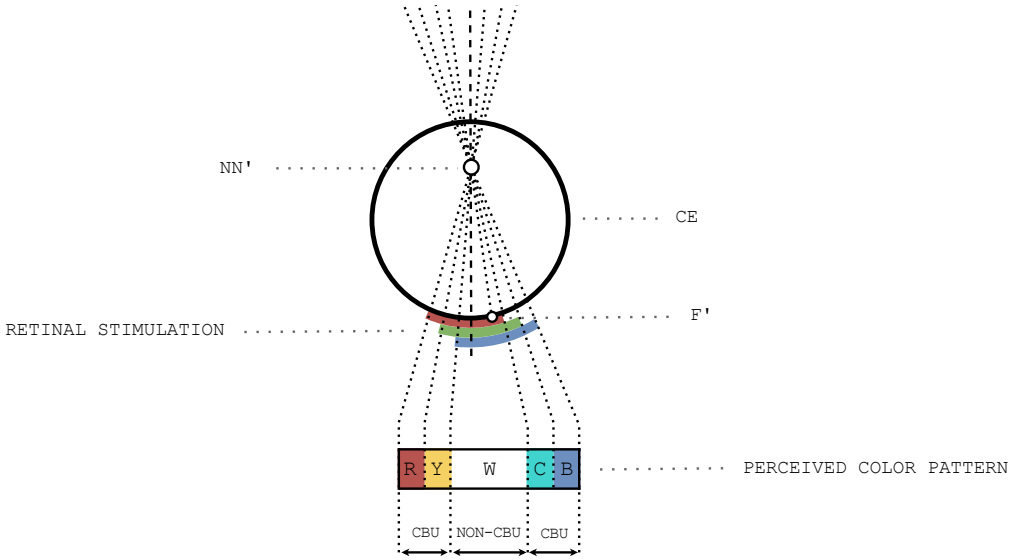

FIGURE 2.3: Retinal color pattern resulting from sequential RGB stimulation via FSC display unit while viewer executes eye movement (cyclops eye in the right graphic in Figure 2.2, magnified view). Temporal summation of full RGB pattern leads to central CBU-free stimulation (white), color-distorted CBU areas at leading/trailing content edges due to incomplete stimulation with one or two primaries only: red and yellow (red + green) on the left, blue and cyan (blue + green) on the right.

Chapter 3 provides an in-depth analysis of the CBU genesis and introduces a theoretical model for the prediction of CBU.

2.2.2 Factors

The factors that determine the magnitude of CBU perception can be broadly categorized into three groups:

— viewer-based factors

— presentation-based factors

— surrounding-based factors

The following Table 2.1 lists relevant studies that improve our understanding how those factors affect CBU perception. The listed work focuses on empirical studies based on (subjective) human CBU perception. Investigations with an objective approach such as a rotatable

high-speed camera setup developed by Järvenpää (2005) are not included. With few exceptions, most findings relate to the FSC presentation of the classic RGB pattern. The samples of the various studies all have in common that they included only healthy participants, with sample sizes varying considerably from a few participants to larger groups.

Viewer-based Factors

Viewer-based factors that influence CBU perception relate to several performance parameters of the observer's visual system. First and foremost, of course, is color perception, but visual acuity and contrast sensitivity can also be strong predictors of CBU perception. Additionally, saccadic or pursuit eye movement (PEM) behavior has to be considered (see Section 2.3). However, to the author's best knowledge, research on the impact of visual performance parameters is limited to aspects of eye movement behavior (e.g., velocity and precision) and the resulting retinal target velocity of the CBU-provoking stimulus, which certainly has a major impact on CBU perception. In summary, research shows that increasing retinal target velocities elevate the magnitude of CBU perception, regardless of whether the target movement on the retina is triggered by actual eye movements like pursuits (P. V. Johnson et al., 2014; Koma & Uchida, 2003) and saccades (Miettinen et al., 2008; X. Zhang & Farrell, 2003) or by the experimental setup itself, without the need to perform eye movements at all (Mori et al., 1999; Post et al., 1998; Post et al., 1997).[3] Researchers have also found out that, in particular, saccades performed with the same amplitude but in different directions (horizontal, vertical, or diagonal) produce different magnitudes of CBU. Vertical and diagonal saccades provoke less CBU perception than horizontal saccades (Kobayashi et al., 2010). The reason for this is that the velocity of a saccade depends on the direction in which it is executed. For example, a horizontal saccade can be executed with a higher velocity than a vertical saccade (see Section 2.3.1). This means that the actual cause of the differences in CBU perception is — once again — retinal target velocity.

Cognitive processes are another subcategory of viewer-based factors. Yohso and Ukai (2006) studied CBU perception during saccades and compared the perceived magnitude of CBU (width of colored area in eye movement direction) with the theoretically assumed magnitude of CBU based on eye movement velocity and exposure time. The researchers found out that participants perceived CBU narrower than theoretically calculated. The reason for the differences between perceived and calculated CBU effects lies in perceptual changes during saccadic eye movement (see Section 2.3.2). More precisely, saccadic compression is probably the main reason, since saccadic suppression does not work well for highly saturated color stimuli like CBU.

Finally, more general aspects such as the viewer's attention, concentration, and motivation are likely to play a role in the perception of CBU. Unfortunately, we know little about how a viewer's current state might influence CBU perception. Demographic parameters such as age (Baron & Chase, 2004) or gender (Seelmacher, 2017) do not influence CBU perception.

Presentation-based Factors

The second group of presentation-based factors includes hardware-related (e.g., frame rate) and content-related parameters (e.g., stimulus dimension and brightness). With respect to hardware-related parameters, CBU perception decreases with rising frame rates. The duty cycle, on the other hand, does not seem to have an effect on CBU. While there is general agreement on the negative correlation between frame rate and CBU perception, available

[3] The effect of a saccade's velocity on CBU perception is empirically investigated by requesting participants to execute saccades with different amplitudes leading to different saccadic speeds.

TABLE 2.1: Literature review on factors that influence the intensity of CBU perception (chronological order).

Author	Target	Factor	Constant
Post et al. (1997)	frame rate threshold (CBU detection task)	frame rate (up to 2 kHz), retinal target velocity (0, 6, 34, 85, and 200 deg/s), background luminance (0, 5, 43, 497, and 2,131 cd/m^2), and stimulus luminance modulation (0.4, 0.5, 0.7, 0.85, and 1.0)	stimulus width (not specified) and duty cycle (1.0)
Post et al. (1998)	frame rate threshold (CBU detection task)	frame rate (up to 2 kHz), retinal target velocity (6, 34, 85, and 200 deg/s), background luminance (0, 5, 49, 468, and 2,223 cd/m^2), and stimulus luminance modulation (0.47, 0.56, 0.66, 0.8, and 0.96)	stimulus width (not specified) and duty cycle (1.0)
Mori et al. (1999)	frame rate threshold (CBU detection task)	frame rate (not specified), retinal target velocity (not specified), stimulus luminance (12.6 and 250 cd/m^2), and room illumination (dark vs. 100 lx)	stimulus width (not specified), stimulus-to-background-contrast (not specified), and duty cycle (not specified)
Koma and Uchida (2003)	CBU score (5-point impairment scale) during PEM	stimulus movement velocity (8 to 25 deg/s) and path (not specified)	stimulus width (7 mm in viewing distance of 360 mm), stimulus and background luminance (not specified), frame rate (55 Hz), duty cycle (not specified)
X. Zhang and Farrell (2003)	CBU detection task during SAC	stimulus width (1, 2, and 4°), saccadic length (10 and 18°), background luminance (1, 4, and 15 cd/m^2), and stimulus-to-background contrast	stimulus luminance (85 cd/m^2), frame rate (120 Hz), and duty cycle (not specified)
Baron and Chase (2004)	luminance threshold (CBU detection task) during SAC	stimulus luminance (not specified) while contrast ratio was stable and background luminance (not specified) while stimulus luminance was stable, additional investigation of age-related effects	stimulus width (0.4°), frame rate (60 Hz), saccadic amplitude (48°), and room illumination (30 cd/m^2)
Yohso and Ukai (2006)	CBU width (in eye movement direction) during SAC	stimulus presentation time (Experiment 1 vs. Experiment 2), stimulus height (Experiment 2)	saccadic amplitude (20°), stimulus width (1°), stimulus (30 cd/m^2) and background luminance (0.22 cd/m^2), frame rate (60 Hz), and duty cycle (not specified) [a]
Y.-P. Huang et al. (2007)	indistinguishable CBU angle	stimulus luminance (18, 28, 42, and 56 cd/m^2), surrounding illuminance (0, 27, and 195 lx), and target movement velocity (100 to 800 mm/s)	stimulus width (not specified), frame rate, and duty cycle (both not specified)
S.-C. Chen et al. (2007)	indistinguishable CBU angle	stimulus luminance (18, 100, 180, and 425 cd/m^2), target movement velocity (200 to 800 mm/s, 200 mm/s steps), and viewing distance (not specified)	stimulus width (not specified), surrounding illuminance (0 lx), frame rate (60 Hz), and duty cycle (not specified)
Yan et al. (2007)	indistinguishable CBU angle	stimulus luminance (18, 28, 42, and 56 cd/m^2), surrounding illuminance (0, 27, and 195 lx), and target movement velocity (100 to 800 mm/s)	stimulus width (not specified), frame rate (60 Hz), and duty cycle (not specified)
Miettinen et al. (2008)	frame rate threshold (CBU detection task) during SAC	frame rate (6 to 1666 Hz, 1 Hz steps), saccadic length (2, 4, 8, and 14°), and stimulus luminance (2, 31.5, and 500 cd/m^2)	Michelson stimulus-to-background contrast (approx. 1.0), stimulus width (8 mm in viewing distance of 155 cm), and duty cycle (0.13)
Kobayashi et al. (2010)	CBU score (5-point visibility scale) during SAC	saccadic movement direction (horizontal, vertical, and diagonal), stimulus luminance (1.5, 4.3, 12.2, 34.9, 100, and 286.7), and stimulus-to-background contrast ratio	saccadic length (24.5°), frame rate (approx. 75 Hz), duty cycle (1.0), and background luminance (0.15 cd/m^2)
Kobayashi et al. (2011)	CBU detection/allowance threshold during SAC	frame rate (80 to 480 Hz, 40 Hz steps) and stimulus width (not specified)	saccadic length (58.4°), stimulus luminance (15.25 cd/m^2), background luminance, and duty cycle (both not specified)
Yoshida et al. (2011)	CBU detection/allowance threshold during SAC	frame rate (80 to 480 Hz, 40 Hz steps) and stimulus width (not specified)	saccadic length (not specified), stimulus luminance (15.25 cd/m^2), background luminance, and duty cycle (both not specified)
Y. Zhang et al. (2012)	CBU score (5-point visibility scale) during SAC	chromaticity (various primary hue/saturation settings) and luminance of stimulus (38 to 380 cd/m^2), stimulus-to-background contrast ratio (multiple values tested, see paper)	stimulus width (2°), saccadic amplitude (20°), frame rate (60 Hz), and duty cycle (0.15)
P. V. Johnson et al. (2014)	MI offset testing (CBU detection task) during PEM/FIX	target movement velocity without tracking (2, 6, 10, 20, and 30 deg/s) and with tracking (2, 6, and 10 deg/s), stimulus width (0.5, 1, 2, and 4°) , various MI offsets (9)	frame rate (40 Hz) and duty cycle (not specified), stimulus and background luminance (both not specified)
Seelmacher (2017)	CBU score (10-point perception scale)	frame rate (40 to 580 Hz, 60 Hz steps) and duty cycle (0.3 and 0.6), additional parameters tested (e.g., age, gender, optical correction)	stimulus width (0.17°) and luminance (457 cd/m^2), background luminance (0.17 cd/m^2), retinal target velocity (55 deg/s)
Wang, Zhang, Li, et al. (2017)	color saturation threshold (CBU detection task) during SAC	variation of saturation for different color hue combinations of two subfields	stimulus width (2°), stimulus luminance (18.2 cd/m^2), background luminance (dark, not specified), saccadic length (20°), frame rate (60 Hz), duty cycle (not specified), room illumination (below 0.5 lx)

Note. Stimulus width refers to the stimulus dimension in eye/content movement direction. Stimulus height refers to the stimulus dimension perpendicular to the eye/content movement direction. SAC = saccade; PEM = pursuit eye movement; FIX = fixation.
[a] Specifications refer to Experiment 1. In Experiment 2, a different projector (different frame rate and color pattern) was used and luminance levels of stimulus and background were altered (see paper for detailed description).

data on the effect of the duty cycle on CBU perception are limited (see explanations on subframe timing in Section 2.2.3).

Content-related parameters such as the stimulus width in eye movement direction also have an impact on CBU perception. There is agreement that a larger stimulus width results in a reduction of CBU perception during saccades (Kobayashi et al., 2011; Yoshida et al., 2011; X. Zhang & Farrell, 2003). However, theoretical model simulations by P. V. Johnson et al. (2014) predict little effect of stimulus width on CBU visibility during pursuits (no empirical data available).

Comparing CBU perception for two different luminance levels (12.6 vs. 250 cd/m^2) of a stimulus, Mori et al. (1999) found differences in CBU detection thresholds at an early date (background luminance unchanged). A decade later, Y.-P. Huang et al. (2007) and Yan et al. (2007) discovered that luminance level variation within the range of 18 to 56 cd/m^2 of CBU-provoking stimuli has only little impact on CBU perception. Findings from S.-C. Chen et al. (2007) even suggest that the stimulus luminance range can be extended from 18 to 425 cd/m^2 without significant effect on CBU perception, which was confirmed by Y. Zhang et al. (2012) for a slightly smaller luminance level range (38 to 380 cd/m^2). The results from Mori et al. complement rather than contradict the findings of the other researchers. The effect of the stimulus luminance level alone (without changing background luminance) seems to be marginal, up to the point where a certain luminance level threshold is undershot. In this context, two other experiments are of particular interest, where the included stimulus luminance levels were around and below 10 cd/m^2 while the background luminance was kept constant (to the greatest possible extent). Kobayashi et al. (2010) found that perceived CBU only slowly decreases for stimulus luminance levels ranging from 286.7 to 34.9 cd/m^2 (analogous to previous findings) whereas a much steeper decline is observed for the three lowest luminance levels tested (12.2, 4.3, and 1.5 cd/m^2). Tests by Miettinen et al. (2008) showed that the two highest stimulus luminance levels tested (31.5 and 500 cd/m^2) result in similar CBU effects whereas the lowest luminance level (2 cd/m^2) leads to a more distinct reduction of CBU perception. These additional findings confirm the assumption of a luminance threshold above which changes in luminance do not significantly affect the magnitude of CBU effects and below which changes in luminance lead to a significant alteration in CBU perception. According to the previous findings, such a luminance threshold might be determined at a luminance level around 15 cd/m^2. It follows that the relation between stimulus luminance and CBU perception could be adequately described by a power function. Accordingly, Post et al. suggest a formula for CBU detection thresholds that implements a power function term with stimulus luminance as a variable base and exponent values of 0.10 (1997) and 0.08 (1998).

The proposed formula by Post et al. also considers the contrast ratio between the CBU-provoking stimulus and its background as an important factor in determining CBU detection thresholds. In this context, Miettinen et al. (2008) and Y. Zhang et al. (2012) independently conclude that the contrast ratio between the CBU-provoking stimulus and its background has a much stronger effect on CBU perception than stimulus luminance alone. For example, increasing the background luminance while keeping the stimulus luminance constant (resulting in a decline of the contrast ratio between stimulus and background) leads to a substantial decrease of CBU perception (X. Zhang & Farrell, 2003).

Baron and Chase (2004) investigated the relationship between stimulus and background luminance variation, and examined luminance thresholds for CBU detectability at variable stimulus luminance levels with stable contrast ratio (to the greatest possible extent) and at variable background luminance levels with stable maximum stimulus luminance (variable contrast ratio). Results show a statistically significant yet moderate correlation between both

luminance thresholds ($r = .40$, $p = .023$). However, there was large variation in participants' CBU sensitivity under variable luminance conditions.

In addition to the effects of luminance levels, the relationship between subfield colors in terms of hue and saturation is also very important. In general, CBU is effectively reduced by creating a compressed color gamut through the application of desaturated subfield colors (Y. Zhang et al., 2012). Moreover, relative low sensitivity to CBU can be achieved by applying colors along the blue-yellow path, which is not the case for the magenta-cyan path (Wang, Zhang, Li, et al., 2017). The positive effect of hue, brightness, and saturation on CBU is used for various compensation techniques (see Section 2.2.3).

Surrounding-based Factors

Finally, it is important to consider surrounding-based factors such as room illumination and viewing distance when discussing CBU effects. Room illumination has only a small effect on CBU perception (Y.-P. Huang et al., 2007),[4] whereas decreasing viewing distance increases the ability to perceive smaller shares of CBU because of a magnification due to approach (S.-C. Chen et al., 2007; Yan et al., 2007).

2.2.3 Compensation

Generally, compensation techniques for mitigating CBU are characterized by a deviation from the standard subframe presentation (RGB) in terms of its basic features. Accordingly, available techniques for CBU compensation can be classified by considering the following subframe characteristics:

— subframe order and count

— subframe hue, brightness, and saturation

— subframe position

— subframe timing

Researchers have proposed several compensation techniques to reduce CBU. However, almost all of these techniques have been applied to FSC-LCDs. Therefore, the existing compensation techniques need to be validated with regard to their applicability to other display or projection techniques.

Subframe Order and Count

A simple compensation technique proposed by Makino et al. (2003) does not change the conventional presentation of three color fields, but changes the order of the subframes from frame to frame. The typical RGB order is varied in three consecutive frames: RGB – GBR – BRG. This approach is called Color Field Arrangement (CFA). However, in CFA at frame rates of 60 Hz, the second and third green subframes are displayed with a time delay that

[4] The slight effect of room illumination on CBU perception is surprising as it has a strong effect on color perception across the retina, which is explained by the retinal adaptation processes and their influence on the degree of rod and cone activity (see Section 2.3.2). It was expected that these retinal processes would also significantly affect CBU perception. The surprising results from Y.-P. Huang et al. (2007) might be explained by the fact that retinal adaptation processes during their experiments not only depend on room illumination but also on the CBU-provoking stimulus within the observer's field of view (displayed via FSC-LCD). In other words, the status of retinal adaptation not only depends on room illumination but also on the luminance level of the displayed content. This weakens the share of the effect of room illumination on the final state of light adaptation as the trigger for color perception alterations.

represents a repetition under 36 Hz. Under consideration of the color-dependent threshold for the perception of flickering (the human eye is most sensitive to the color green), it is likely that this approach provokes flickering effects. It is proposed that the application of the 4-Color Field Arrangement (4-CFA) can suppress this annoying flicker effect, implementing an additional color field to shorten the time interval between green subframes. The four subframes within one 60 Hz frame period occur in alternating order (RGBR – GBRG – BRGB) from frame to frame (C.-H. Chen et al., 2009; Hsu et al., 2007; Y.-P. Huang et al., 2007). Judging the effectiveness of this approach, "the degree of static CBU reduction is relatively marginal" (Yang et al., 2016, p. 673).

Sekiya et al. (2006) investigated the effect of Blanking on CBU perception on a theoretical basis. By doubling the field rate, the typical subframes (RGB) can be displayed in the first half of a frame cycle. The second half is blacked or blanked (KKK). This solution only works in combination with a higher field rate in order to keep the frame rate at least constant (field rate of 360 Hz when assuming a frame rate of 60 Hz). In this context, technical limitations such as the response time of LCs have to be accepted. Sekiya et al. conclude that Blanking can effectively reduce CBU when the field rate is doubled at the same time. F.-C. Lin, Huang, and Shieh (2010) confirm this finding: Compared to the conventional three-field image presentation (RGB) at a field rate of 180 Hz, doubling the field rate with included Blanking (RGBKKK) shows better results with a relative CBU reduction of 43.4% on average than merely doubling the field rate (RGBRGB), which reduces CBU only by 18.9%. They used an objective color difference index to quantify CBU while Srivastava et al. (2019) applied a camera system to objectively visualize CBU, confirming the positive effect of Blanking (see Section 2.2.4 for methods of CBU evaluation and prediction).

Different to previous approaches for CBU compensation, the Mixed Color Sequential (MCS) technique changes the subframe order temporally (RGBK – RGKB – RKGB – KRGB – BRGK) at a field rate of 240 Hz, and spatially, as the RGB-LED backlight consists of 48 separately controllable blocks (Y.-F. Chen et al., 2007a, 2007b).

Subframe Hue, Brightness, and Saturation

This section deals with compensation techniques characterized by additional changes in the hue, brightness, and/or saturation of a subframe (in addition to the possibility of varying subframe order and count). They can be divided into three categories: Color-Mixed Fields, Multi-Color Fields, and Field Desaturation.

The compensation technique of Color-Mixed Fields includes one or more additional color fields that complement or replace the typical primary color fields (RGB). The extra color-mixed fields — for example cyan (C), yellow (Y), or white (W) — are presented over the whole display area. Chu et al. describe the basic idea as follows: "Generating the color overlay by adding another sub-color field to minimize the color difference of the edge stagger causes the human eye to be less perceptive of the CBU" (2010, p. 324). In other words, the color hues of the subframes lie closer together, resulting in a weakened CBU effect.[5]

Sekiya et al. (2006) propose one additional color-mixed field (Y) for CBU compensation with different successions of the four subframes/fields (RYGB or YBGR). In this approach, the characteristics (color and intensity) of the extra field are fixed. A more complex approach uses a Gray Level Redistribution towards a fourth field that is added to the classic RGB presentation. The brightness of the first (R), second (G), and third (B) field is decreased while the missing shares of RGB are redistributed into the fourth dominant color field (D-field). In contrast to the approach proposed by Sekiya et al., the D-field is adaptive, i.e.,

[5] To reduce CBU, the addition of more subframes is only effective in combination with higher field rates, keeping the frame rate at least stable.

its characteristics can be chosen depending on the entire content of the displayed image to ensure the greatest possible effect on CBU reduction (C.-H. Chen et al., 2008; Chu et al., 2010; Y.-P. Huang, Chen, et al., 2008). A disadvantage of this solution is that the iterative processing of the D-field calculation requires a high computational effort. A smarter algorithm concentrates on the image areas where CBU is most likely to occur (high-contrast image boundaries). The Edge-Directed FSC method can be used in addition to almost all of the CBU reduction methods presented in this section (F.-C. Lin et al., 2019; F.-C. Lin, Teng, Chang, et al., 2016; F.-C. Lin, Teng, Huang, et al., 2016).

The development of so-called Spatial-Temporal Color Displays (Silverstein, 2005) or Spectrum-Sequential Displays (Jak et al., 2005) as a hybrid technology also aims at reducing CBU. Langendijk (2007), for example, combined two 120 Hz color fields (yellow and cyan) with two specific color filters (magenta and green), resulting in the availability of four primary colors (as in previous approaches). This approach reduces the required field rate to 120 Hz to achieve a frame rate of 60 Hz (with three fields, the required field rate would raise to 180 Hz). Furthermore, such displays have a higher transmission and spatial resolution compared to a conventional LCD and cause less CBU than a typical FSC-LCD based on three color fields (RGB). However, the CBU effect is still noticeable (Langendijk et al., 2009).

Some research groups even tested five color fields with a specific RGBYC sequence (Eliav et al., 2005; Langendijk et al., 2006) or with multiple color orders and color ratios of five color fields (CBRYG, YCRGB, RCYBG, etc.) including Gray Level Redistribution (H.-C. Cheng et al., 2010).

The method of Multi-Color Fields mostly uses RGB-LED backlight arrays (direct-lit) to enable fields consisting of multiple colors simultaneously presented on different parts of the displayed area. In contrast to the color-mixed fields, which are displayed globally with one specific coloration over the whole display area, mixed-color fields are presented with local variations in coloration within a field.

Y.-K. Cheng et al. (2009) introduced a two-field driving scheme that does not require additional color filters (see description of Spatial-Temporal Color Displays). Instead of filters, Y.-K. Cheng et al. used a spatially modulated color backlight that allowed the generation of multi-color fields. CBU is suppressed by reducing the contrast sensitivity between the two color fields. Similarly, F.-C. Huang et al. (2017) used two multi-color fields by applying a local RGB-LED backlight without additional filters. They conclude that their approach is preferable because the "primaries are fully content-adaptive, while theirs [Y.-K. Cheng et al.] adapt only to local brightness with color hue limited to R+B (magenta) and G+B (cyan)" (p. 2), which does not allow a full-color reproduction (severe image distortion). Furthermore, the CBU effect is not sufficiently suppressed as the maximum display gamut is used for the primary color characteristics (F.-C. Lin et al., 2015).

The Stencil-FSC method addresses this issue by collecting most of the luminance in an initial multi-color field using a backlight that consists of a homogeneous matrix arrangement of multiple RGB-LEDs. The backlight enables the creation of a rough spatial full RGB color pattern, which is sharpened by the transmission through the LC panel. Merging most of the image information in the first field offers the possibility to reduce the luminance of the subsequent field images. During eye movements, the subframes still fall on different retinal spots, but the shift of the main luminance to the first subframe and the consequent reduction of the luminance in the following subframes reduces CBU perception, because the second, third, and maybe fourth subframes are perceived less intensely — CBU is suppressed. The Stencil-FSC method was developed using four color fields with a field rate of 240 Hz (Y.-P. Huang, Lin, Wei, et al., 2008; F.-C. Lin et al., 2009, 2010; F.-C. Lin et al., 2008), three 180 Hz fields (Y.-P. Huang et al., 2009; F.-C. Lin, Huang, & Shieh, 2010; F.-C. Lin et al., 2012), and even only two 120 Hz fields (Shieh et al., 2009) to ensure a frame rate of 60 Hz.

While Stencil-FSC suppresses CBU significantly, "the luminance difference between the multi-color field and the mono-color fields might be too large, leading to a flicker issue, especially for images with much more white information" (Teng et al., 2016, p. 809). By concentrating the image information in two instead of one multi-color field, the luminance differences between all applied color fields can be drastically reduced. This Deflicker-FSC method can reduce potential flicker issues, but results in lower effectiveness of CBU compensation compared to Stencil-FSC (Teng et al., 2016).

In the Field Desaturation technique, each color field is composed of different portions of all three primaries (RGB) to desaturate the resulting color fields. This minimizes the color gamut required to represent all colors in a given scene and consequently reduces CBU. Y. Zhang et al. (2016) distinguish two subgroups: Global Primary Desaturation (GPD) and Local Primary Desaturation (LPD). GPD calculates the primaries for the entire screen based on the entire image to be displayed (Bergquist & Wennstam, 2006; Hu et al., 2011). In contrast, LPD calculates primaries for smaller parts of the image until the complete image is covered (F.-C. Lin et al., 2011a, 2011b; Y. Zhang, Lin, et al., 2011). The smaller the defined image areas, the more the desaturated color gamuts are compressed, resulting in a higher effectiveness of CBU reduction. To realize local primary features, LPD requires a spatially addressable backlight. However, F.-C. Lin (2018) highlights the high costs of LPD, as "three convolutions are required to evaluate backlight intensities for three field images when using LPD. This computational complexity causes a high hardware cost to execute LPD" (p. 24).

All previously mentioned methods of CBU reduction are categorized as Decompensation Techniques. A few approaches combine two or more of these techniques. For example, Y. Zhang, Langendijk, Hammer, and Lin (2011) introduced a hybrid Spatial-Temporal Color Display with an LPD backlight scheme. Other researchers used a combined Stencil-LPD method for a 120 Hz two-field display (Chang et al., 2012; F.-C. Lin et al., 2015), because the backlight requirements are similar for both compensation techniques. Yang et al. (2016) suggest a content-dependent multi-primary presentation (four-field, 240 Hz) including Field Desaturation and Gray Level Redistribution.

In general, all of the above Decompensation Techniques can be applied to all kinds of eye movements (pursuits and saccades) provoked by specific content movement patterns (including CAT2 and CAT3, see Section 3.3.1).

Subframe Position

Over the years, various journal articles, conference proceedings, and patents (Baron et al., 1996; Crisler et al., 2018; Koma & Uchida, 2003; Sekiya et al., 2003; Van Dijk & Shimizu, 2004, 2009; Welch & Fernie, 1997) have been published on Motion Interpolation (MI). Different from the previously described compensation techniques, MI is based on changing the subframe position rather than changing subframe characteristics. The main principle of MI is the implementation of a spatial offset between the individual subframes/fields within a frame cycle. The purpose of this offset is to compensate for the retinal displacement of the displayed subframe content that occurs when subframes are presented sequentially during the execution of eye movement. The magnitude of the spatial offset depends on the eye movement velocity and the field/frame rate of the display or projector. Faster eye movements and lower frame rates lead to a larger spatial offset required for CBU compensation. Precise MI can only be implemented if information on the direction and velocity of eye movements is available (assuming the frame rate is known). Such information can be provided by suitable gaze-tracking systems. However, gathering and implementing eye movement data during MI processing in real time is a technical challenge — especially for fast eye movements like saccades.

As long as no information on eye movement behavior is available, a simpler solution would be to assume that eye movement velocity is equal to content movement velocity. This might be the case in a situation where a single object is presented with limited movement velocity, eliciting a smooth and precise PEM. In such a case, the spatial offset could be calculated based solely on the content's velocity and the frame rate: "As long as the eyes track the moving object correctly, this method gives the best motion image quality in FSC LCD applications; No color breakup is caused" (Sekiya et al., 2006, p. 1662). A violation of the central assumption of equal eye and content movement velocity reduces the effectiveness of this simple MI approach without gaze-tracking. However, deviations from the ideal match of spatial offset (as calculated based on content velocity) and actual eye movement velocity during a pursuit task are tolerable within a certain range to still benefit from reduced CBU (P. V. Johnson et al., 2014). This finding is confirmed by a psychophysical experiment (pursuit task) conducted by Wang, Zhang, Weng, et al. (2017). A gradual change in spatial offset in either direction toward over- or undercompensation results in a symmetric, linear, and moderate decrease in MI effectiveness rather than a sudden decline. While less precise pursuits might slowly reduce the effect of CBU compensation, a fast saccade in the opposite direction of the compensated object in a more complex scene with multiple stimuli actually leads to higher CBU perception. The lack of a gaze-tracking system therefore limits the application of MI to simple scenes where precise pursuits (CAT3) can be assumed.

Subframe Timing

The CBU effect can be reduced by displaying color fields in faster succession by increasing the field/frame rate. DLP projectors, for example, are usually capable of displaying digital content at a very high frame rate. In contrast, direct-view FSC-LCDs which use various liquid crystal modes such as Multi-domain Vertical Alignment (MVA), Optically Compensated Bend (OCB), or Ferroelectrics (FLC), have lower potential due to their relatively slow-switching LC modes. However, two relatively new LC modes — Blue Phase (BP) and Uniform Lying Helix (ULH) — are capable of providing faster and thus superior switching speeds in the sub-millisecond range, which is necessary for high frame rates that can more effectively reduce CBU effects (Siemianowski et al., 2016).

The empirical studies described below investigated the effect of variable frame rate ranges on CBU perception under the condition of a time-sequential presentation of the classic RGB pattern without further compensation techniques (different experimental setups). Most studies were based on small samples ($N \leq 10$).

A few studies have tested frame rate thresholds for horizontal saccades. For example, Miettinen et al. (2008) determined that the frame rate for the CBU detection threshold is 1200 Hz in the worst case (max. stimulus luminance at 500 cd/m^2, max. saccadic length of 14°). At the most distinct reduction of luminance level (2 cd/m^2) and saccadic length (2°), the threshold for frame rate is slightly above 200 Hz. The stimulus width (8 mm) in the direction of the saccade was kept stable during the experiment (viewing distance of 155 cm). In this context, it should be noted that the frame rate threshold (detection task during saccades) strongly depends on the stimulus width (Kobayashi et al., 2011; Yoshida et al., 2011).

Other studies stimulated CBU perception at variable retinal velocities by using devices with a rotating filter wheel (Post et al., 1998; Post et al., 1997) or a rotating chopper blade (Mori et al., 1999) to generate FSC targets (both methods feature a duty cycle of 1.0). During these experiments, participants did not execute any eye movement (fixation task). The CBU genesis differed from that of the empirical studies discussed previously, which were based on eye movement. The experimental setups themselves provoked CBU. These experiments ignored the process of change in human perception during eye movement (see Section 2.3.2). The detection thresholds of Post et al. have been evaluated under variation of

retinal velocity and stimulus/background luminance. The worst-case scenarios (high retinal stimulus velocity of 200 deg/s, high stimulus-to-background contrast ratio) required frame rates of 1000 Hz or more to reach the CBU detection threshold. Similarly, Mori et al. found that the threshold frequency increases with retinal velocity and target luminance. However, with increasing retinal velocity, the threshold frequency eventually saturates. They report a significantly lower frame rate threshold around 450 Hz for the conditions most conducive to CBU emergence (stimulus luminance level of 250 cd/m^2 and retinal stimulus velocity of 400 deg/s), leading to an inconsistent picture regarding frame rate requirements for CBU detection thresholds.[6] A more recent study by Seelmacher (2017) also investigated CBU perception in dependency of the applied frame rate range (40 to 580 Hz) without eye movements. Seelmacher used a light-emitting diode (constant stimulus width, stimulus luminance of 457 cd/m^2, background luminance of 0.17 cd/m^2) sliding laterally at a velocity of 55 deg/s on a horizontal rail. Results based on a larger sample ($N = 49$) show that the relation between CBU perception and frame rate is best described by applying a quadratic function. A transition from strong to medium CBU is detected at 122 Hz and from medium to mild CBU at 331 Hz (no detection threshold established).

Seelmacher (2017) also studied the effect of another subframe timing parameter — the duty cycle — on CBU perception. However, he found no significant difference in CBU perception when changing the duty cycle from 0.3 to 0.6, as assumed by Baron and Chase (2004) on a theoretical basis. Based on their theoretical CBU model simulation (see Section 2.2.4), Wang, Zhang, Weng, et al. (2017) conclude that lowering the duty cycle over a wider range from 1.0 to 0.5, 0.2, and 0.1, leads to the effect that "the CBU edges become more separated from each other" (p. 659). As a result, the observer perceives CBU more clearly. Thus, unlike motion blur effects, which can be reduced by lowering the duty cycle (den Boer, 2005), CBU perception is not affected or sometimes even enhanced by reducing the duty cycle.

All of the above studies share a high interobserver variability for CBU perception, as CBU perception is highly individual. Furthermore, all available studies on the relationship between CBU perception and frame rate variation refer to saccadic eye movement or artificially stimulate CBU-provoking retinal target velocity while the observer's eyes do not move at all. So far, there is no scientific data on the effect of frame rate variation during PEM. Another aspect to consider: In order to test wide frame rate ranges, some researchers have built experimental setups as substitutes for available FSC-based technology with limited potential to display frame rates up to the highest range. In other words, when transferring the experimental results in practice, more or less restrictive technical limits have to be kept in mind, depending on the technology used (e.g., switching speed of older LC approaches).

Effectiveness of Approaches

Y. Zhang et al. (2016) reviewed compensation techniques for CBU suppression and classified them in terms of their effectiveness and application areas. They found that MI can completely eliminate CBU under ideal conditions. However, technical limitations significantly restrict the application areas. A realistic MI scenario could enable CBU elimination during pursuits in clearly arranged scenes. Increasing frame rates can also have a strong effect on reducing CBU to the point of making it imperceptible. However, very high frame rates are necessary to eliminate CBU for the observer — this requires technological progress. Among the techniques that do not rely on changes in subframe positioning or timing, LPD and Stencil-FSC/Deflicker-FSC are promising approaches because they significantly reduce CBU. An even higher CBU reduction can be achieved with the Edge-Directed FSC method.

[6] Different detection thresholds might be due to small sample sizes and high interobserver variability of CBU perception, as well as different study-dependent FSC apparatuses and content characteristics.

Emphasizing these statements, Qin et al. (2018) provide a comparison of objective CBU indices for LPD, Stencil-FSC, and Edge-Directed FSC (classic RGB pattern without compensation as reference) based on the distinguished Dominant Visual Salience method (see following Section 2.2.4). Given the effectiveness of the highlighted techniques, it is expected that merging these techniques (e.g., Stencil-LPD) may further increase their effect on CBU reduction.

2.2.4 Evaluation and Prediction

Several approaches for objective CBU evaluation and models for CBU prediction have been developed in the course of research on CBU-associated factors (see Section 2.2.2) and compensation techniques (see Section 2.2.3). The evaluation and prediction of CBU effects requires either visualization or quantification processes.[7]

Visualization

One approach to objectively assess CBU is to use a movable high-speed camera that simulates eye movement across a displayed scenario with potentially CBU-provoking stimuli. For this purpose, the camera can be placed on a linear motion track (C.-H. Chen et al., 2008; C.-H. Chen et al., 2009; Y.-K. Cheng et al., 2009; Y.-P. Huang et al., 2009; F.-C. Lin, Huang, Wei, & Shieh, 2010) or integrated in a rotatable camera setup (Järvenpää, 2005; F.-C. Lin et al., 2019; Y.-J. Lin et al., 2018; Qin et al., 2018). Camera-based CBU evaluation to visualize the CBU effect is widely used but often not specified further (Y.-F. Chen et al., 2007b; Hsu et al., 2007; Koma & Uchida, 2003; F.-C. Lin et al., 2015; F.-C. Lin et al., 2012; F.-C. Lin, Teng, Chang, et al., 2016; F.-C. Lin et al., 2011a).

As an alternative, some researchers have used computational simulations for CBU visualization (H.-C. Cheng et al., 2010; Langendijk, 2007; Langendijk et al., 2009; Yoshida et al., 2011; Y. Zhang, Langendijk, Hammer, & Lin, 2011). Shifting and overlapping the field images to integrate them creates a simulation of the perceived CBU image. The spatial shift between the single field images depends on the defined conditions that the simulation is to represent. For example, the frame rate of the display system and the eye movement velocity are important factors. In addition, the color and brightness of the individual fields must be considered when overlapping and integrating the fields.

Quantification

Some researchers used formulas that include the most relevant factors for CBU perception to describe CBU. Such formulas vary in complexity and range from simple to more elaborate approaches. Some available formulas consider only spatio-temporal aspects related to the display system and its observer, such as the frame rate or the duty cycle, the eye/content movement velocity or the stimulus width in the direction of motion. For example, such a simple approach that calculates the Color Break-Up Angle (CBUA) at the leading and trailing edges of the potentially CBU-provoking stimulus has been proposed by researchers of the National Chiao Tung University (S.-C. Chen et al., 2007; Y.-P. Huang et al., 2007; Yan et al., 2007). Another formula for calculating the angular CBU expansion, which contains only a few spatio-temporal parameters, was defined by Koma and Uchida (2003). A more comprehensive formula-based approach by Sekiya et al. (2006) additionally considers the luminance characteristics of the presented content at a basic level. However, these approaches are based on simplistic assumptions on CBU and its genesis. The most accurate simulation

[7] A review of assessment methods for the evaluation and prediction of CBU is available in a short (Qin, Lin, et al., 2019) and an extended version (Qin, Zhang, et al., 2019).

of spatio-temporal relations during light stimulation within a frame cycle was performed by Wang, Zhang, Weng, et al. (2017). The formula-based calculations at pixel level lead to an accurate description of the color and luminance characteristics of the entire CBU stimulus. However, the model was designed for ideal PEM only, i.e., it assumes identical velocities of eye and stimulus motion. The model predictions of Wang, Zhang, Weng, et al. show high correlation to subjective CBU perception.

Unlike the previous formulas, which share a theoretical origin, Post et al. (1998) and Post et al. (1997) established their CBU formula based on observers' subjective CBU assessment. The formula generally allows to determine the threshold field rate at which CBU is no longer perceptible and includes stimulus luminance, contrast between stimulus and background, and retinal velocity of the stimulus as main factors. In the course of statistical analysis of the data set, Post et al. applied a nonlinear regression to determine the best-fitting coefficients in the equation and were able to provide an accurate representation of human CBU perception.

The formula-based approaches can be useful to calculate the spatial dimension of the CBU effect for certain conditions or to determine the cut-off frequency for the field rate. As Y.-K. Cheng and Shieh (2009) conclude, however, "the utility is limited due to the lack of generality and efficiency" (p. 379). That is due to the fact that the formulas derived from the above approaches are based on a specific technical setup. The application of a different display system under changed viewing conditions can influence the validity of the formula.

In the following paragraphs, device-independent methods that focus on the displayed content are discussed. These methods provide an objective index that can condense CBU perception to a single number, with the goal of quantifying CBU on an objective basis and accurately predicting the viewer's subjective CBU perception. To this end, some color difference indices have been developed. Those indices calculate the color differences between the ideal (original) image and the distorted CBU image. The resulting color difference index, which represents the theoretical CBU intensity, has been defined by various researchers based on the CIELAB (F.-C. Lin, Huang, Wei, & Shieh, 2010; Yang et al., 2016), CIELUV (Y.-P. Huang, Chen, et al., 2008), or CIEDE2000 color difference equation (Chang et al., 2012; Y.-P. Huang et al., 2009; F.-C. Lin et al., 2015; F.-C. Lin, Huang, & Shieh, 2010; F.-C. Lin et al., 2012; F.-C. Lin, Teng, Chang, et al., 2016; F.-C. Lin et al., 2011a; Teng et al., 2016) by summing up the color differences between ideal and distorted image pixel by pixel.

Similarly, Kim et al. (2014) based their adapted CBU formula on the comparison between the original undistorted and distorted CBU image in the CIELUV color space. In addition, the output of their formula was optimized by physiological experiments, resulting in improved performance. Yang et al. (2016) recommend another measure that is also based on the CIELUV color space but uses a different approach. The researchers define the number of pixels belonging to so-called static CBU-free areas. The more pixels are concentrated in these CBU-free areas, the less pronounced the perceived CBU effect.

In particular, the first mentioned simple color difference indices are often unable to adequately represent subjective CBU perception. With the motivation of developing an improved objective metric for CBU visibility, Y. Zhang et al. (2012) proposed a revised CBU index that is mainly determined by considering two aspects: the chromaticity difference between individual fields and the contrast between the CBU-provoking stimulus and its surrounding content. In perceptual experiments with humans, the researchers found that these two aspects are more influential than the absolute luminance value of the stimulus (see Section 2.2.2).

The so-called Dominant Visual Saliency (DVS) method represents a further improvement of the introduced CBU indices. It allows to determine an advanced CBU metric referring to the picture level. The DVS method assumes that CBU perception is mainly determined in DVS regions that contain content with high potential to provoke CBU. Consequently,

color differences within these regions are weighted higher than the color differences in the rest of the image. Compared to basic CBU metrics based on unweighted color difference calculations, the DVS method shows higher correlation with subjective CBU scoring (F.-C. Lin et al., 2019; Y.-J. Lin et al., 2018; Qin et al., 2018).

Some vision-based methods even go a step further by considering the subjective response of the human visual system to objective stimulation (P. V. Johnson et al., 2014; Langendijk et al., 2006). These models use spatio-temporal filtering of the luminance and color-opponent channels of human perception to create a robust single-valued index that is closer to the observer's actual CBU perception. In this context, both Yi (2008) as well as Y.-K. Cheng and Shieh (2009) calculated the RCS value, which strongly correlates with CBU scores obtained by psychophysical experiments.

The evaluation and prediction of CBU described in Section 2.2.4 is closely related to Chapter 3, in which a self-developed CBU model is introduced. The model aims to objectively predict CBU by calculating a theoretical CBU index that is as close as possible to a viewer's subjective CBU perception.

2.3 Human Visual System

The performance of the human visual system (e.g., visual acuity and color perception) and its ability to adapt to external conditions (e.g., ambient brightness) are of paramount importance for accomplishing everyday tasks. However, the great features of the human eye are useless if eye movements cannot be performed adequately. This section summarizes scientific findings on the oculomotor system (see Section 2.3.1) and the perceptual aspects of vision (see Section 2.3.2) that are relevant in the context of CBU perception.

2.3.1 Eye Movement

A basic requirement for the occurrence of CBU is the presence of eye movements (see Section 2.2.1). Following a functional classification, there are a five types of eye movements: vestibular, optokinetic, smooth pursuit, saccadic, and vergence eye movement (Enderle, 2010; Leigh & Zee, 2015). Gaze-stabilizing reflexes (e.g., vestibular, optokinetic, or smooth pursuit eye movements) aim to ensure a stable image on the retina in general and the fovea in particular, whereas gaze-shifting eye movements (e.g., saccades) redirect the line of sight to a new object of interest. All eye movement types are of equal importance since they all serve different purposes. Of particular interest, however, are fast saccades and smooth pursuits, since the present research refers explicitly to these types of eye movements (see Chapters 3 to 5). A distinction between saccades and pursuits was already made early in the last century by Dodge (1903). More than 100 years later, however, it is known that the architecture of the saccadic and pursuit systems have more in common than previously assumed. Krauzlis (2004) recapitulates recent scientific work pointing in this direction:

> As an alternative to the traditional view of pursuit and saccades as distinct oculomotor subsystems, the control of pursuit and saccades might be viewed as different outcomes resulting from a single cascade of sensory–motor functions. From this view-point, the several obvious differences between pursuit and saccades illustrate the variety of outcomes that are possible with these layers of control, rather than indicate the presence of independent systems of control. (p. 599)

In the following, saccades and pursuits are briefly introduced as separate parts of the oculomotor system by accentuating their different functional features. For a more detailed review, see Kowler (2011) or Klein and Ettinger (2019).

Pursuits

Smooth PEM allows to track small moving targets with or near the fovea to minimize retinal image motion and collect as much detailed visual information as possible. Visual stimulation (e.g., a passing car) is required as the trigger to initiate and execute smooth pursuits (Robinson, 1965). PEM is a selective rather than a reflexive process, i.e., a viewer can make a selective choice about which target to track in a complex scene (Collewijn & Tamminga, 1986; Kowler et al., 1984). However, the basis of pursuit lies in "processes that sense retinal motion and can induce eye movements without active participation" (Barnes, 2008, p. 309). The first 100 ms after the onset of PEM (open-loop phase) is driven by visual motion information (retinal image velocity). The subsequent phase of pursuit maintenance (closed-loop or steady-state phase) is controlled by visual feedback and prediction of target velocity to compensate for retinal misalignments — called the retinal slip (Spering & Montagnini, 2011).

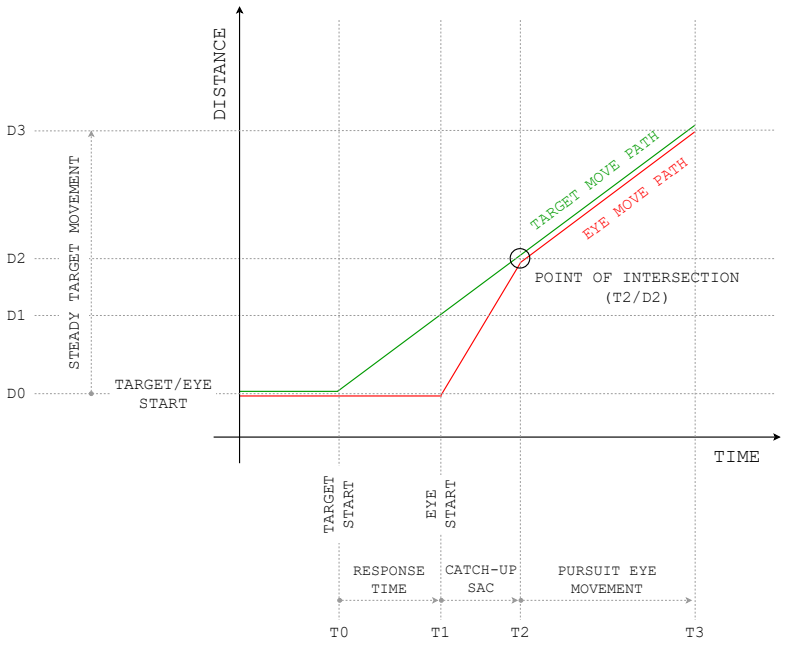

FIGURE 2.4: Target movement path with characteristic of a ramp stimulation, and resulting eye movement path.

Precise and smooth pursuit can only be performed at a limited target movement velocity. Regarding thresholds for smooth PEM, there are different basic definitions ranging from 30 deg/s (Mallot, 2000) to 50 deg/s (Fischer, 1999) up to 70 deg/s (Enderle, 2010). Meyer et al. (1985) have shown in an experimental setup that even for target velocities up to approximately 90 deg/s, a gain up to 0.9 can be achieved in most cases.[8] At higher speeds, the precision of pursuit steadily decreases. The resulting deviation between target and gaze position is corrected by compensatory saccades. To meet the demands of everyday life, a combination of pursuits and saccades is always used. This aspect can be further clarified by considering the PEM latency. The latency between the onset of target motion and the initiation of PEM typically ranges from 80 to 130 ms (Lisberger et al., 1987) and depends on the target's luminance, size, velocity, and position (Lisberger & Westbrook, 1985; Tychsen & Lisberger, 1986). This delay — caused by the viewer's response time — and the resulting gap between target and gaze position is initially compensated by so-called catch-up saccades (de

[8]The so-called gain describes the precision of eye movements that are triggered by a moving target. A perfectly precise tracking of a moving target by the viewer's eyes corresponds to an ideal gain of 1.0, whereas inaccurate eye-tracking leads to a gain below/above 1.0 for eye movements that are either too slow or too fast.

Brouwer et al., 2002) before the actual PEM can be executed. As an example, the characteristics of a target movement path with a ramp stimulation (assuming steady movement from start to stop position) and the resulting eye movement response are illustrated in Figure 2.4 (compare with Robinson, 1965, p. 571).

For experimental setups investigating PEM without any saccadic shares, a step-ramp stimulation can be used (Rashbass, 1961). Step-ramp stimulations avoid catch-up saccades because of the initial step of the fixation target in the opposite direction to the subsequent steady movement of the target (see Figure 2.5, compare with Robinson, 1965, p. 572). Subsequent steady movement of the fixation target causes the point of intersection between eye and target movement path to be reached after the viewer's response time. This means that the eye can follow the fixation target smoothly as it passes.

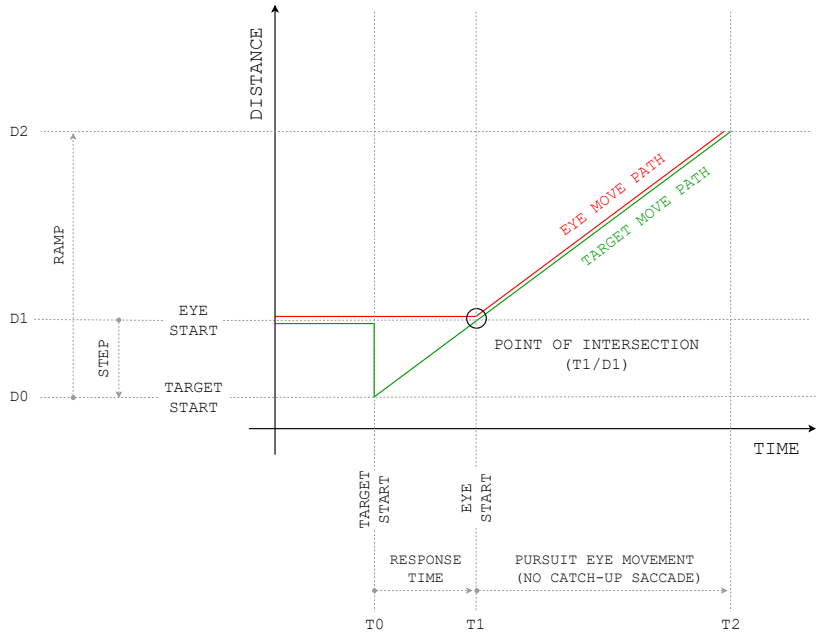

FIGURE 2.5: Target movement path with characteristic of a step-ramp stimulation, and resulting eye movement path.

In the phase of pursuit maintenance, the gain is greater for horizontal pursuits than for vertical pursuits. In the initiation phase, however, vertical pursuits tend to show faster accelerations than horizontal pursuits (Rottach et al., 1996). Furthermore, older people show a reduced gain during pursuits provoked by moderate to high target velocities (Sharpe & Sylvester, 1978; Spooner et al., 1980; Zackon & Sharpe, 1987), and the onset of pursuits is delayed (Knox et al., 2005).

Saccades

Saccades are rapid ballistic and conjugate eye movements that shift the gaze direction from one visual target to another in a short period of time. This allows to position the object of interest in the fovea, where visual acuity is highest.[9] Saccades can be divided into two subgroups — quick phase saccades and voluntary saccades (Leigh & Zee, 2015). Quick phase saccades are executed involuntarily by a "visual grasp reflex" (Klinke & Silbernagl, 2005, p.

[9]The viewer's choice of a certain sequence of visual targets in a scene has been of great scientific interest. A review on the control of saccadic target selection and its main determinants (i.a. salience and object recognition) is provided by Schütz et al. (2011).

695), which can be triggered by visual, auditory, or even tactile stimuli. In contrast, voluntary saccades are caused by a conscious decision, which is based on voluntary cognitive control processes.[10]

Saccades are typically characterized by their amplitude, duration, velocity or peak velocity, gain, and latency. In general, saccades exhibit typical spatial and temporal behavior that varies little among different individuals. Between the start and stop of a saccade, the saccade accelerates rapidly toward the peak velocity, followed by fast deceleration until the initial state of stability is reached (i.e., zero movement velocity or constant movement velocity without acceleration). The temporal ratio between the phases of acceleration and deceleration depends on the amplitude of the saccade. For example, a 12° saccade can reach a peak velocity of nearly 400 deg/s and terminates after a duration of only 50 ms (Gilchrist, 2011). The relationship between the amplitude of the saccadic eye movement and its peak velocity and duration is consistent — it is known as the main sequence (Bahill, Clark, et al., 1975).

The maximum peak velocity during saccadic eye movements is reached at about 600 to 700 deg/s for a saccadic amplitude of around 20° (Bahill, Clark, et al., 1975). However, most saccades in normal viewing situations do not exceed a saccadic length of 15° because head movements are involved at a certain point (Bahill, Adler, et al., 1975). Comparing durations and peak velocities of saccadic eye movements in different directions, horizontal saccades are executed faster and in a shorter time than vertical saccades. This equally applies for quick phase and voluntary saccades (Garbutt et al., 2003).

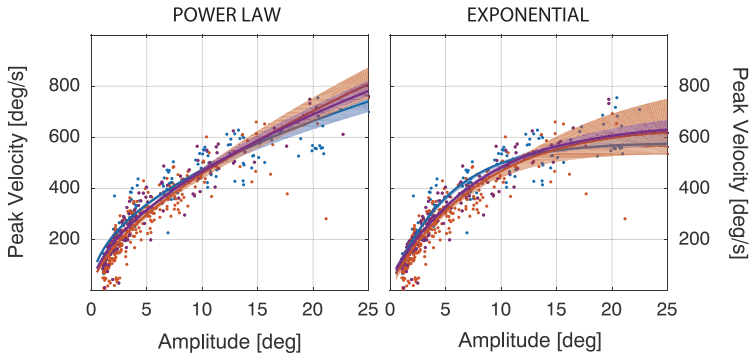

FIGURE 2.6: Model fitting of single participant's main sequence (solid line = median curve, 1st/3rd quartile = colored area, bootstrap analysis). Guided saccadic monitor task with horizontal amplitudes (blue) and free gaze exploration task in rendered images of natural environments for horizontal saccades (purple) and all directions (orange). Adapted from "The saccade main sequence revised: A fast and repeatable tool for oculomotor analysis," by A. Gibaldi and S. P. Sabatini, 2021, *Behavior Research Methods*, *53*(1), p. 183 (https://doi.org/10.3758/s13428-020-01388-2). CC BY 4.0.

Due to the stereotypical behavior of the main sequence, this feature can be used as a fast and repeatable tool for oculomotor analysis that extends to numerous fields of research (Gibaldi & Sabatini, 2021). To date, there is no agreement on how to describe the main sequence with a mathematical model (peak velocity as a function of amplitude, see Figure 2.6). Some researchers propose a model based on an exponential function (Baloh et al., 1975; Smit et al., 1987), while others recommend a power function as the best fit (Lebedev et al., 1996).

When saccades are initiated, a latency between stimulation and execution must be considered for neural processing and motor execution. A typical value for saccadic latency is reported to be around 200 ms (Carpenter, 1988). However, saccadic latency shows high

[10] Aside from the superordinate classification into quick phase and voluntary saccades, there are other possibilities to classify saccades. A more application-oriented classification refers to the saccadic direction towards or away from a peripheral target (Awater & Lappe, 2004, pro-saccade vs. anti-saccade) or the availability of a saccade-provoking target (M. R. G. Brown et al., 2004, visually-guided vs. memory-guided saccade).

inter- and intraindividual variability, ranging approximately from 100 to 1,000 ms (Gilchrist, 2011). In addition to the type of the saccade (quick phase vs. voluntary saccade), latency also depends on the characteristics of the saccade-eliciting target. For example, latencies rise with decreasing stimulus intensity/contrast or with increasing spatial frequency of the target (Kalesnykas & Hallett, 1994; Ludwig et al., 2004). The eccentricity of the saccadic target also affects saccadic latency (Kalesnykas & Hallett, 1994). Furthermore, timing aspects play a role. A saccade can be initiated faster if the fixated target disappears before the new saccade-provoking target appears — this is called the gap effect (Saslow, 1967). Walker et al. (1997) showed how a distracting object synchronized with the appearance of the saccadic target increases the observer's processing time for saccadic motion, called the remote distractor effect. Even by leaving the mentioned influences out of consideration and keeping the experimental conditions stable, there is still considerable intraindividual latency spread.

A certain period of time before the start of the saccade, the saccadic behavior is determined based on the information gathered up to this point. A change in conditions such as the target position of the saccade within this period of no return — the so-called dead time — does not change the behavior of the executed saccade. The dead time is often defined with a time value of 80 ms (Findlay & Harris, 1984; Ludwig et al., 2007). However, it is well known that certain dependencies lead to a variation of dead time under different conditions (Becker & Jürgens, 1979).

There are also age-related changes in saccadic behavior. Saccadic reaction times vary systematically with age. The fastest reaction times are found in teenagers and young adults (approximately aged from 13 to 31 years). Younger and older participants show slower latencies with higher intrasubject variance (Bono et al., 1996; Fischer et al., 1997). In contrast, the dynamics of a saccade (amplitude, peak velocity, and duration) and its accuracy vary only moderately with increasing age — at least for saccades that do not exceed a path length of 20°, for larger saccades the age differences are more pronounced (Moschner & Baloh, 1994; Munoz et al., 1998; Sharpe & Zackon, 1987).

2.3.2 Visual Perception

The following section summarizes scientific findings on the perceptual aspects of vision that are thought to play a major role in CBU perception.

Retinal Sensitivity

Subjective perception of light intensity and color depends on the eccentricity of the stimulated retinal area. In general, "chromatic sensitivity ... is about 7 times higher than luminance sensitivity in the fovea but falls faster with eccentricity, so that luminance and chromatic sensitivities are similar at eccentricities of 20° or less" (Stromeyer et al., 1992, p. 1865). Further detailed studies of perceptual aspects in dependency of retinal eccentricity have been conducted by various research groups. Figure 2.7 compares the findings of Martin et al. (2001), Mullen and Kingdom (2002), Mullen et al. (2005), and Hansen et al. (2009) in terms of sensitivity changes with rising retinal eccentricity for three different perceptual channels — the two chromatic red-green and blue-yellow channels and an additional achromatic channel.[11] As expected, all three channels show a decrease of sensitivity with increasing eccentricity. However, the red-green channel (left graphic) shows a faster decrease than the two other channels for blue-yellow color perception (middle graphic) and perception

[11] The signals from the three retinal cone types (S, M, and L) are processed by an achromatic and a chromatic system. The achromatic system consists of the achromatic channel [M + L] and the chromatic system consists of the blue-yellow [S - (M + L)] and the red-green channel [L - M]. All channels are supplied by additive/subtractive combinations of the three cone signals as described in square brackets (Blake & Sekuler, 2006).

of light intensity (right graphic), which are comparable to some extent. This behavior of an accentuated sensitivity reduction in the red-green channel is particularly noticeable for a stimulation within a retinal areal of eccentricities up to 20°. At larger retinal eccentricities, the results of Martin et al. (2001) and Hansen et al. (2009) show a slowed decrease in red-green color sensitivity (downward triangle graph and circle graph). In contrast, the results of Mullen et al. (2005) suggest a continuous steep decline of L/M contrast sensitivity over their entire test range up to the maximum tested eccentricity of 30° (square graph) leading to "the complete loss of L/M cone opponency at the behavioural level by 25–30 deg of eccentricity" (p. 956). The reasons for these discrepancies could be due to different experimental methods and setups. For example, the experiments used different stimulus sizes and shapes (see explanations below) and different background characteristics, which have a proven effect (Abramov et al., 1992). Furthermore, the experiments included only small samples that might not be representative since in most cases three or fewer participants were investigated.

When comparing the outcomes of all research groups illustrated in Figure 2.7, global differences in retinal sensitivity levels become apparent, especially in the red-green channel (cf. graphs in left-side graphic). This can be explained in large part by the fact that the target size is a critical parameter for the experimental testing of color perception across the retina. Every measure of color perception in the periphery of the human eye can be improved by applying a larger stimulus (Abramov et al., 1991; M. A. Johnson, 1986; Kuyk, 1982). For comparison, Hansen et al. (2009) presented colored disks of 8° (circle graph) whereas Mullen et al. (2005) used a circular ring segment covering a considerably smaller retinal area (downward triangle graph) which consequently results in a significant attenuation of the global sensitivity level over the entire eccentricity test range.

If one distinguishes between color perception for red and green stimulation in the retinal periphery, the sensitivity for green stimuli is lower than for red stimuli. Such a clearly asymmetric behavior in the detectability of red and green stimuli can be observed at eccentricities greater than approximately 14° (Stromeyer et al., 1992). Newton and Eskew (2003) determined asymmetry factors for perceptual differences between red and green sensitivity with 1.4 to 2.0.

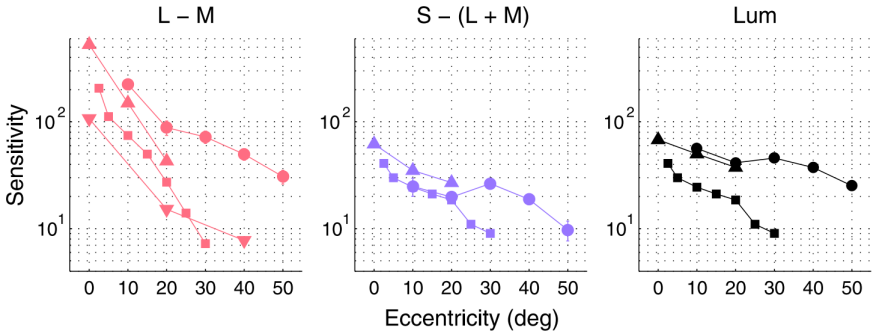

FIGURE 2.7: Cone contrast sensitivity in dependency of retinal eccentricity for chromatic red-green (left graphic) and blue-yellow channel (middle) as well as achromatic channel (right). Comparison of data from Martin et al. (2001, downward triangles, only red-green channel), Mullen and Kingdom (2002, upward triangles), Mullen et al. (2005, squares), and Hansen et al. (2009, circles). From "Color perception in the intermediate periphery of the visual field," by T. Hansen, L. Pracejus, and K. R. Gegenfurtner, 2009, *Journal of Vision*, *9*(4), p. 5 (https://doi.org/drq36h). Copyright 2009 by the Association for Research in Vision and Ophthalmology. Reprinted with permission.

All illustrated data sets in Figure 2.7 have in common that a detection task was performed to determine the channel-dependent cone contrast sensitivity. Therefore, the illustrated results

of Hansen et al. (2009) also refer to a detection task, which raises the question if the participant detects a more or less peripheral stimulus at all (without the need to assign a color). In addition, Hansen et al. integrated another experimental setup based on an identification task. In the identification task, it was necessary to identify the specific color of the stimulus presented. By comparing both tasks, it was found that there was no difference between the detection and identification thresholds for the red-green channel and negligible differences for the blue-yellow channel. The detection of a stimulus within the field of view and the identification of its color happen synchronously with no or only slight discrepancy. Another color identification task by Dalhaus and Gunther (2012) showed that red/green performance is stable until it declines rapidly at an eccentricity of about 40° (the stimulus size of 2.5° must be considered again). The identification of blue/yellow stimuli is stable over an even larger retinal area up to eccentricities of 45° until the performance drops. More specifically, the highest sensitivity to identify colored stimuli in the retinal periphery is observed for blue stimuli followed by yellow, red, and green stimuli in that order.

The simple identification of a stimulus color has no informative value for quantitative aspects of color perception. How do color characteristics (hue and saturation) change in perception across the retina? With increasing retinal eccentricity, a stimulus becomes increasingly desaturated and the perceived hue of the stimulus changes (Boynton et al., 1964; Gordon & Abramov, 1977; Ikeda et al., 1985; McKeefry et al., 2007; B. Stabell & Stabell, 1979). A detailed investigation of perceptual alterations of color hue and saturation at different retinal orientations reveals perceptual differences in horizontal and vertical direction. For the perception of saturation, there is a naso-temporal asymmetry that causes a faster reduction of saturation on the temporal side of the retina than on the corresponding nasal locus (Abramov et al., 1992; Ayama & Sakurai, 2003; Sakurai et al., 2003; U. Stabell & Stabell, 1982). The same stimulus appears more saturated on the nasal retina than on the temporal. In addition to the horizontal asymmetry, the reduction of saturation in the inferior part of the retina is stronger than on the superior retina. Stimuli are perceived as more saturated in superior retinal direction (Sakurai et al., 2003).[12] Regarding hue perception, it can be concluded that the blue-yellow channel is largely unaffected with increasing eccentricity (only saturation decreases). This stability in color perception applies to all retinal orientations (nasal, temporal, superior, and inferior). However, color perception in the red-green channel deteriorates with increasing eccentricity in all directions. Red and green stimuli shift towards a yellowish perception (Sakurai et al., 2003). While this perceptual shift for the primary colors red and green (as well as blue and yellow) was not observed by Yujiri and Hamada (2003) and Hamada and Yujiri (2004), intermediate colors with a yellow component (yellow-red and green-yellow) showed a yellow shift with increasing eccentricity. Furthermore, intermediate colors with a blue component such as blue-green and red-blue shifted towards blue color perception. The authors interpret these findings as a strengthened dominance of the blue-yellow channel response compared to the red-green channel response in peripheral vision. In line with these findings, another experiment by Ayama and Sakurai (2003) confirmed the general stability of the blue-yellow channel, and showed a shift towards yellow color perception for the primary colors of red and green, a blue shift for intermediate colors with a blue component (e.g., red-blue), and a yellow shift for intermediate colors with a yellow component (e.g., green-yellow). These color shifts in the retinal periphery were more pronounced in temporal direction than in nasal direction (an investigation of the vertical retinal meridian was not part of the experiment).

[12] Orientations on the retinal surface have to be inverted when transferring the results to the field of view. The nasal retina (inner part) corresponds to the outer field of view, whereas the temporal retina (outer part) corresponds to the inner field of view. The superior retina (upper part) is connected with the lower field of view and the inferior retina (lower part) corresponds to the upper field of view (see Figure 4.22).

The surrounding illuminance has a strong influence on color perception across the retina, since the surrounding illuminance triggers retinal adaptation processes and influences the degree of rod and cone activity. Chromatic sensitivity deteriorates and hue perception alters with decreasing illuminance levels (wide test ranges from 0.01 to 1,000 lx) from fovea to periphery in all retinal directions (Hamada & Yujiri, 2004; Yujiri & Hamada, 2003). B. Stabell and Stabell (1980) and U. Stabell and Stabell (1981) conclude that rod intrusion in a dark-adapted state strongly affects peripheral color vision.

Perception during Motion

While visual perception does not change during fixation periods, it changes during saccades and pursuits. Why is this perceptual change necessary? Eye movements inevitably lead to retinal image shifts of the entire scene during saccades and at least the non-tracked background during pursuits. These retinal shifts do not correspond to the actual movement or non-movement behavior of targets in the perceived scene. To avoid misinterpretation of the retinal movement, it is necessary to distinguish between its two possible causes — a real-world object's movement or just eye movement — to ensure perceptual stability of static targets during eye movements (even if these targets move across the retina). Therefore, signal processing is required during eye movements for visual stabilization. In this context, visual reafference, proprioception, and corollary discharge are relevant.[13] The following paragraphs address the changes in basic visual features at the time of eye movements.

Visual perception and potential changes during PEM are discussed for the performance categories of visual acuity, contrast sensitivity, and color perception. The question how detailed a moving target can be observed while being tracked by the viewer can be answered by investigating the minimum angular resolution during pursuit, and subsequently deriving the dynamic visual acuity (DVA). Ludvigh and Miller (1958) investigated the DVA for a range of angular velocities from 10 to 170 deg/s. As assumed, the DVA decreases with rising target velocities. Initially, the decrease of visual acuity is moderate with rising target velocity up to 50 deg/s (average decimal visual acuity approx. 0.35) but rapidly accelerates to a drastic reduction in DVA at the highest target velocity (average decimal visual acuity approx. 0.09). The collected data also show that there are significant interindividual differences in the participants' DVA that increase with rising target velocity. B. Brown (1972) tested the hypothesis that the decline of DVA is due to the increase of retinal error (target is no longer positioned foveally) while faster pursuits are required. He found that the reduction in DVA actually corresponds to the retinal error which he considered to be the main determinant of DVA.

Contrast sensitivity during PEM behaves similarly. The contrast sensitivity when tracking a moving test target is comparable to the results of stationary testing (stable fixation) as long as pursuits are executed accurately and the retinal image velocity (oscillating grating as test target) is the same in both cases. This finding holds at least for high spatial frequencies — there are inconsistent findings for low spatial frequencies (Flipse et al., 1988; Murphy, 1978). In other words, contrast sensitivity is limited primarily by retinal positioning and velocity errors caused by inaccurate pursuit, rather than by pursuit itself.[14] Schütz, Braun, and Gegenfurtner (2007) conclude that the suppression of contrast sensitivity during precise pursuits is insignificant compared to the strong effects of saccadic suppression.

[13] Signal processing reviews are provided by Bridgeman et al. (1994) and Wurtz (2008).

[14] Studies on detectability of non-tracked background targets during PEM show that contrast sensitivity is attenuated (Schütz, Delipetkos, et al., 2007). This is not surprising as background targets always show a retinal shift. However, non-tracked background targets during PEM are only slightly affected by motion blur when compared to target motion during stable fixation provoking identical retinal target velocity (Bedell & Lott, 1996).

Furthermore, detection thresholds for briefly flashed luminance-defined stimuli with high spatial frequency are even lower during pursuit than during fixation. This implies that under specific conditions, visual sensitivity can improve during pursuits. In contrast, visual sensitivity for stimuli with low spatial frequency is moderately reduced (Schütz et al., 2008).

This effect of sensitivity improvement was also found for colored stimuli, including red-green and blue-yellow stimuli. Detection thresholds during pursuit were lowered by 16% on average compared to tests during fixation (Schütz et al., 2008). The results of Schütz et al. were later confirmed by Braun et al. (2017). In addition, PEM improves the temporal resolution of color perception by elevating the critical chromatic fusion frequency. The fusion frequency shifts from 21.3 ± 0.7 Hz during fixation to 23.2 ± 0.8 Hz during pursuit (Terao et al., 2010).

PEM also has an effect on the perceived velocity (Turano & Heidenreich, 1999) and movement direction (Souman et al., 2005) of non-tracked targets. There is also evidence that flashed stimuli are misinterpreted with respect to their location during PEM – a forward shift in the direction of motion can be observed (Brenner et al., 2001; Kerzel et al., 2006; Rotman et al., 2002).

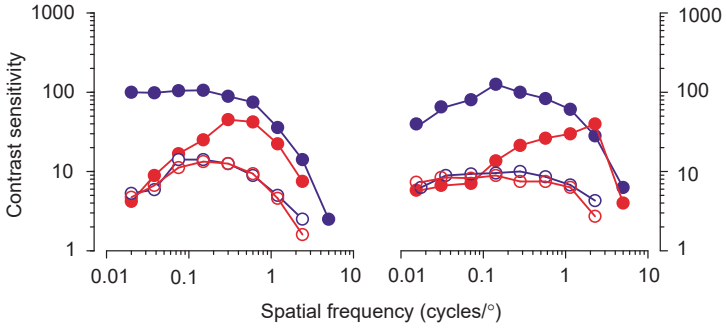

FIGURE 2.8: Contrast sensitivity in dependency of spatial frequency for Participants DB (left graphic) and MCM (right). Detection task of briefly flashed horizontal gratings with variable spatial frequencies during fixation (blue symbols) and shortly after the onset of a large horizontal saccade (red symbols), gratings were modulated with regards to luminance (filled circles) or equiluminant color (open circles). Originally from Burr et al. (1994, p. 511), adapted from "Changes in visual perception at the time of saccades," by J. Ross, M. C. Morrone, M. E. Goldberg, and D. C. Burr, 2001, *Trends in Neurosciences*, *24*(2), p. 114 (https://doi.org/10.1016/S0166-2236(00)01685-4). Copyright 2001 by Elsevier. Adapted with permission.

Human visual perception also changes during the execution of saccadic eye movement. Perceptual processes during saccades include saccadic suppression, mislocalization, and compression; see Ross et al. (2001) for an in-depth review. Saccadic suppression results in a reduction of retinal contrast sensitivity. This effect of sensitivity reduction is increasing with decreasing spatial frequencies. For high spatial frequencies, there is only little or no effect (Volkmann et al., 1978; Wolf et al., 1978). Reducing the luminance level leads to a downward shift of the spatial frequency threshold, which is accompanied by sensitivity loss when undershot (Burr et al., 1982). It is remarkable that the effect of retinal sensitivity reduction is mainly limited to the magnocellular pathway. In contrast, the parvocellular pathway is only affected briefly. This means that retinal sensitivity to luminance is drastically reduced (for low spatial frequencies), whereas retinal sensitivity to equiluminant color perception is only slightly affected (Burr et al., 1994), see Figure 2.8 for illustration. There is evidence that saccadic suppression of luminance-modulated low frequency stimuli is not only based on masking effects caused by retinal image motion but also includes non-visual extraretinal sources of control (Diamond et al., 2000). In general, the magnitude of saccadic suppression increases with saccadic amplitude (Mitrani et al., 1970; Ridder & Tomlinson, 1997; Stevenson et al., 1986).

Furthermore, the perceived localization of brief stimuli before, during, and after saccades is not stable over a time period of 200 ms (Bischof & Kramer, 1968; Honda, 1989, 1991; Matin & Pearce, 1965). The effect starts less than 100 ms before the execution of a saccade (locational shift in direction of saccade) and reaches the maximum of mislocalization approximately at the time of saccadic onset. After the start of the saccade, the shift steadily reverses in the opposite direction (see Figure 2.9). It is assumed that this behavior is part of the retinal stabilization process by compensating the shift of the retinal image during the saccadic eye movement.

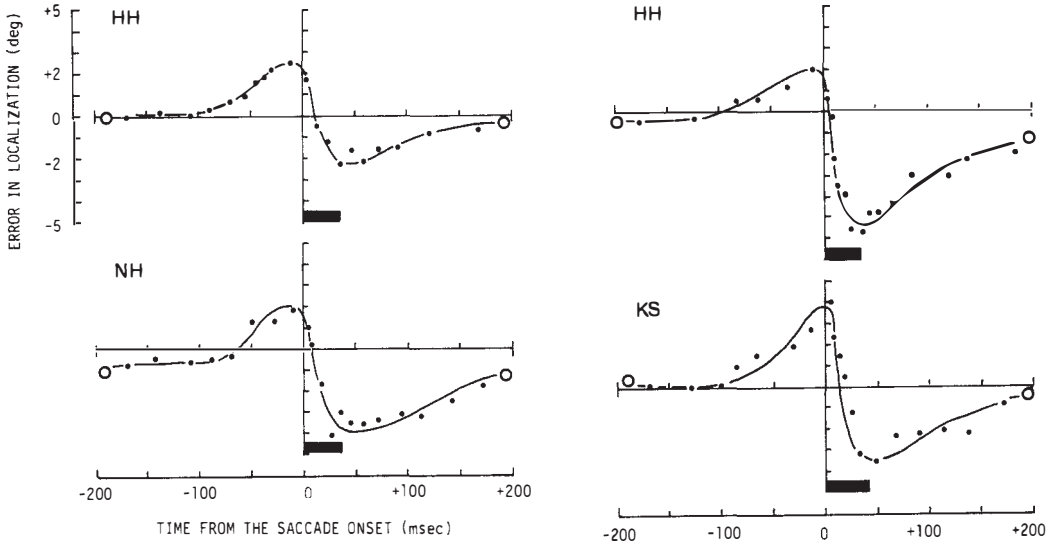

FIGURE 2.9: Time course of perceptual mislocalization of a small, briefly flashed light (target) around the time of saccadic eye movement with amplitude of 8° in vertical (two left graphics) and horizontal direction (two right graphics), illustrated for three participants (HH, NH, and KS). Abscissa represents time interval between onset of saccade and target presentation, ordinate indicates the mislocalization of the target while positive/negative values refer to a mislocalization in the same/opposite direction of the saccade, dots represent averaged values from 10 to 60 trials, black horizontal bars show mean duration of the executed saccade. From "The time courses of visual mislocalization and of extraretinal eye position signals at the time of vertical saccades," by H. Honda, 1991, *Vision Research*, *31*(11), p. 1917 (https://doi.org/10.1016/0042-6989(91)90186-9). Copyright 1991 by Elsevier. Reprinted with permission.

However, the described characteristic of mislocalization is not always present, since its magnitude and direction strongly depend on the position of the mislocalized object in the visual field. A mislocalization of different parts of visual space in opposed direction leads to saccadic compression parallel to the saccadic movement path which can have a strong impact on perception (Ross et al., 1997). Lappe et al. (2000) found out that this effect only occurs as long as visual references are available. For experimental testing in complete darkness, saccadic compression cannot be observed. Apart from the spatial effects of compression as described, saccades also provoke a compression of time perceived (Morrone et al., 2005).

Chapter 3

Color Break-Up Model

3.1 Aim & Scope

The theoretical CBU model aspires to forecast a viewer's CBU perception on an objective basis for predefined scenarios. The model scenario always includes (1) an FSC display system presenting digital content and (2) a viewer observing this content. Under certain conditions, such a scenario potentially leads to the occurrence of CBU effects (see Section 2.2.1). The model aims primarily to graphically reconstruct the intensity and color characteristics of an occurring CBU effect. The visualized CBU reconstruction is then compressed into representative model indices to quantify the extent of the CBU effect with a manageable set of metrics. Modeling of potentially CBU-provoking scenarios is advantageous in many ways. First, the knowledge gained in the course of model development and application allows to better understand the fundamental processes of CBU genesis. Second, the impact of certain determinants on CBU characteristics can be easily determined at the push of a button. And third, the model can be used to establish a classification scheme for CBU variants with different color patterns.

3.2 Platform & Structure

The model code »cbu model« was written down in MATLAB (Version R2018b, The MathWorks, Inc.). The entire code has been made freely available as open source, accessible on GitHub (https://github.com/markusleicht/ColorBreakUp) and additionally archived via Zenodo (https://doi.org/10.5281/zenodo.6749170).

The CBU effects are computed by the model in a multi-stage process. The fundamental structure of the model and its segmental build-up are illustrated in Figure 3.1. The functional principle of CBU modeling provides that various *model input* parameters must be entered to first specify the frame conditions of the model scenario. The display unit's technical specifications, the characteristics of the presented content, the viewer and his/her behavior, and other surrounding conditions are defined in detail (see Table 3.2). Based on the model input, light intensity and color characteristics (hue and saturation) of the displayed content (*physical stimulus*) that potentially provokes CBU are quantified. Furthermore, the content's size, its position at display level, and the exposure time of light emission are defined. Taking into account the underlying FSC principle of content creation (see Section 2.1), the content characterization is executed at subframe level, i.e., every single subframe is separately specified at first. This allows the CBU genesis to be deconstructed to its starting point. Subsequently, the interactions of the individual subframes within a full frame cycle are computed to create a realistic copy of the displayed content. The corresponding *stimulation of the viewer* is calculated under consideration of the determined content characteristics, leading to the exact description of retinal stimulation within the viewer's eye. The model predicts the retinal zone of stimulation and the intensity and color characteristic profile within this area. This

finally allows the discrimination between CBU-free and CBU-loaded retinal zones by creating a model-based replication of the perceived scene. In other words: The *model output* predicts a real viewer's visual impression that is provoked by the defined scenario.

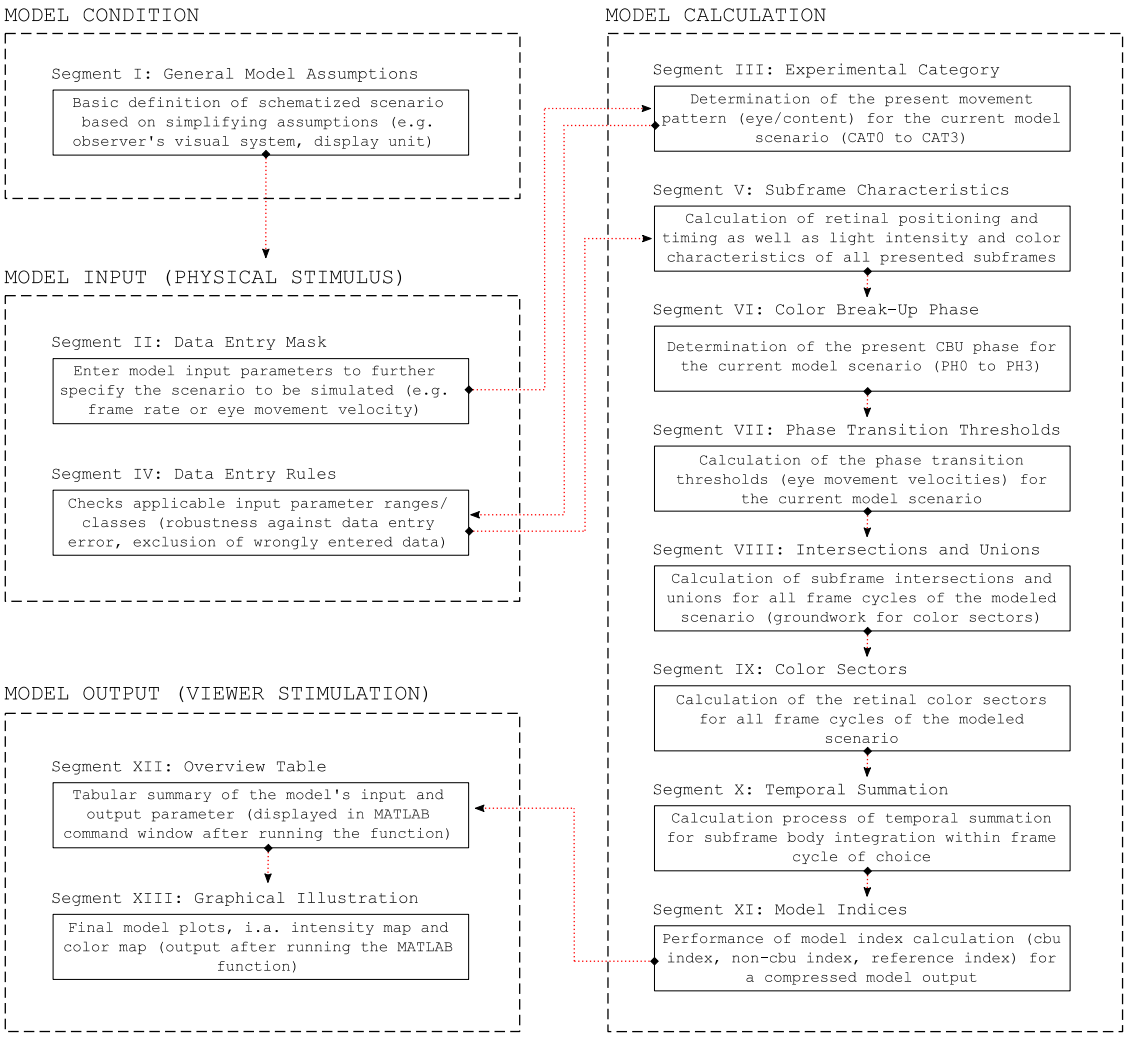

FIGURE 3.1: Segmental structure of the CBU model's source code (MATLAB). A basic code description is embedded in the code itself. References to the Segments I to XIII can be found in Chapter 3.

A more detailed model description is provided in the following sections. At first, the model's area of application is specified (see Section 3.3), followed by a step-by-step description of the model operations (see Sections 3.4 to 3.6) and the demonstration of the model results (see Section 3.7). In a final discussion, the set objectives for the newly developed model are checked, the model is compared with external approaches for the evaluation and prediction of CBU, and possible model add-ons for model improvement are addressed (see Section 3.8).

3.3 Application Range

3.3.1 Movement Pattern

Digital content presentation via an FSC system and the response of the viewer's eye movement to the displayed content are decisive for the appearance or absence of CBU (see Section 2.2.1). Therefore, it is essential to determine the eye and content movement patterns

that must be covered by the model. Table 3.1 lists all possible eye and content movement combinations.

TABLE 3.1: Categorization of possible movement patterns of a viewer-to-display setup.

Category		Eye Movement	Stimulus Movement	Head Movement
CAT0	—	stable fixation	static	stable
CAT1	—	stable fixation	mobile	stable
CAT2	A	pursuit	static	stable
	B	saccade	static	stable
CAT3	A	pursuit	mobile	stable
	B	saccade	mobile	stable

Note. CAT = category. Head movement is assumed to be non-existent (stable head position) since an additional variable would increase the number of possible combinations drastically.

It is necessary to distinguish between combinations of eye/content movement that do or do not provoke CBU. Obviously, CAT0 does not provoke CBU perception because there is neither eye nor content movement triggering CBU perception. It is controversial if CAT1 provokes CBU perception. In this dissertation, CAT1 is classified as a non-provoking category with respect to CBU perception (see Footnote 2 in Section 2.2.1). Consequently, CAT0 and CAT1 are not considered in the CBU model or in the empirical studies (see Chapter 4). CAT2 and CAT3 potentially provoke CBU perception as both categories meet the prerequisite of the presence of eye movement. Therefore, this thesis focuses on CBU perception during CAT2 and CAT3. Both categories can be further subdivided into pursuit and saccadic eye movement (see Section 2.3.1). As in most investigations on CBU, this thesis refers only to research conditions in which a saccade is executed while the CBU-provoking stimulus is static (CAT2B), or in which a moving stimulus is precisely followed by smooth pursuit eye movement (CAT3A). Therefore, these two subcategories of movement patterns will be referred to below by the abbreviations CAT2 and CAT3.[1]

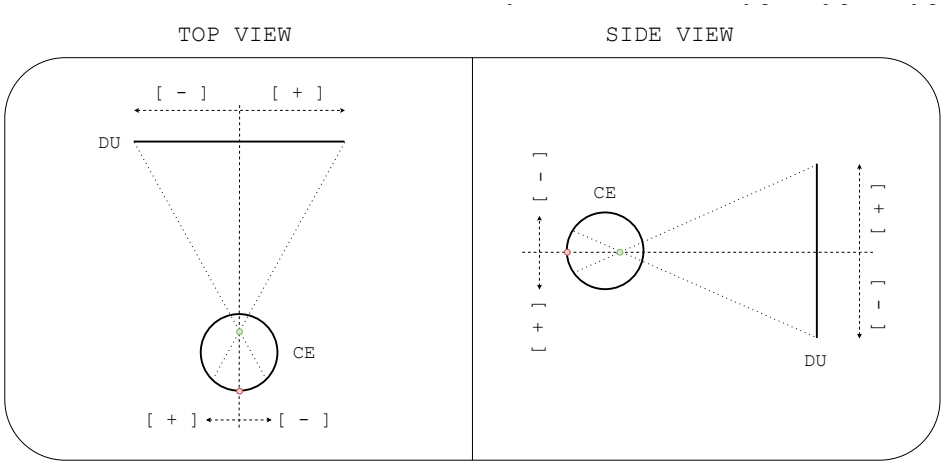

FIGURE 3.2: Model's sign conventions for retinal positions of a viewer's cyclops eye (CE) and field of view positions on the display unit (DU).

To describe eye and content positions and their movement patterns, it is required to define local reference systems with their specific sign conventions and points of origin. Figure 3.2 illustrates two reference systems referring to the viewer's retina and the observed display unit. The display unit's point of origin is positioned at its horizontal and vertical center.

[1]The category of the eye and content movement pattern for the current model conditions is defined in Segment III of the model's MATLAB code.

Positive position values are assigned in right/up direction, negative values are assigned in left/down direction. The point of origin of the retina coincides with the *fovea centralis*. Due to the image inversion on the retina, an adequate connection of both reference systems requires an adjustment of the assignment of positive and negative values in the retina's reference system. In consequence, positive retinal values are assigned in left/down direction and negative values are assigned in right/up direction.

3.3.2 Basic Assumptions

The model cannot ideally represent all possible real-world scenarios. Consequently, the model's focus is on simulating schematized scenarios based on simplifying assumptions about the anatomical aspects of the observer's visual system and its adjustment to the display unit, which is generally assumed to have a plane surface. Furthermore, eye/content positions, movement paths (dimension and direction), and movement velocities are restricted by the following assumptions:

— The observer's visual system is represented by a cyclops eye whose fovea centralis coincides with the horizontal/vertical center of the display system in primary eye position.

— The optical axis, visual axis, and fixation line of the cyclops eye are assumed to be equally aligned, which means that angle ϵ (btw. optical axis and visual axis) and angle η (btw. optical axis and fixation line) are assumed to be zero.

— The fixation line of the cyclops eye is perpendicular to the plane of the display system (no tilt of display system).

— The eye/content positions can be determined in horizontal and vertical direction within the limits of the display system's dimension.

— The eye/content movement paths can only be linear in positive horizontal direction (left-to-right movement) by defining a horizontal start and stop position within the limits of the display system's dimension (no vertical or transversal movements).

— The eye/content movement velocities are constant from start to stop position (no positive or negative acceleration).

— The transition of the presented content's angular position on the display system to the angular position on the cyclops eye's retina is carried out via nodal points N and N' (see Section 3.4.1).

In addition, further assumptions on temporal aspects must be made to create a model environment that allows a definite calculation of CBU:

— Eye and content movement always start at the same point in time *T0* with no delay.

— The displayed content disappears immediately when the stop point of the content movement path is reached.

The listed assumptions (1) guarantee a controlled model calculation of positions and timings at display and retinal level and (2) assure the model's predictive power within a defined tolerance range.[2]

[2]The basic model assumptions can be found in Segment I of the MATLAB code.

3.3.3 Input and Output

The aim is to provide a flexible model that allows to represent various CBU-provoking conditions (input) and subsequently predict the corresponding CBU effect (output). At first, the model's input parameters need to be determined. These parameters can be divided into the following main groups:

— display system (e.g., frame rate or duty cycle)

— viewer (e.g., eye movement behavior)

— surrounding (e.g., viewing distance)

The model needs to strike a balance between structural simplicity and predictive accuracy. Therefore, only input information that are either indispensable for a realistic reproduction of relevant scenarios or that are assumed to have a high impact on the quality of the model output are provided to the model. Table 3.2 lists the model's input parameters that can be entered to determine the condition for which the CBU effect has to be calculated.[3] The upper and lower value limits for all listed input parameters are given (see Column 4). Within these borders, input parameters can be chosen as required. The final choice of specific input parameters for an exemplary model calculation (see Column 5) was made with the intention to reproduce a specific experimental setup of the empirical studies conducted (COBUS1, see Chapter 4). The hardware specifications (e.g., frame rate) and the surrounding conditions (e.g., viewing distance) of the study were transferred to the model. In addition, aspects of the presented content (e.g., content width) and the participant's response (e.g., eye movement velocity) were taken from one specific experimental arm during the study — the provocation of precise pursuit eye movements (CAT3) during a stimulus presentation with a movement velocity of 36.0 deg/s over a horizontal path length of 21.3° (frame-to-frame shifts of 8 px/fr over path of 432 px). The determined input parameters define the example of choice (EOC) which will be continuously referred to during the following step-by-step explanation of the model build-up. The intermediate model results and the final numerical model output, which compresses the complexity of CBU perception to a few objective indices, refer to the described EOC pursuit task (see following Sections 3.4 to 3.7).

3.4 Subframe Characterization

Subframes, as the smallest units involved in CBU genesis, are characterized by applying a Spatio-Temporal Intensity & Color Analysis — STICA for short. The analysis concentrates on a detailed description of the position and timing of a subframe (see Section 3.4.1) and quantifies its light intensity and color characteristics (see Section 3.4.2). STICA aims to provide a comprehensible approach by complementing basic calculations with graphical illustrations towards a better understanding of the CBU genesis. A step-by-step introduction is provided in the following subsections.[4]

3.4.1 Positioning and Timing

The model concentrates on the simulation of eye/content movement in horizontal direction. In vertical direction, stable eye/content positions are assumed. Hence, all explanations in

[3] The model's input parameters can be viewed/altered in Segment II of the MATLAB code, and applicable parameter ranges as well as further data entry rules are specified in Segment IV.

[4] Positioning and timing as well as light intensity and color characteristics of all subframes within all calculated frame cycles are listed in matrix tables in MATLAB Segment V (see code description on table structure).

TABLE 3.2: Possible ranges and determined values of CBU model calculation for various input parameters concerning display system, viewer characteristics, and surrounding condition.

Classification		Input Parameter	Abbrev.	Range	Value	Unit
display	hardware	frame rate	FR	20.0 – unlimited	90.0	Hz
		subframe number	SF_{CT}	2 – 6	3	—
		duty cycle	DC	0.0 – 1.0	0.3	—
		native resolution (hor.×vert.)	RES	positive integers $\neq 0$	912×1140	px
		aspect ratio	AR	positive values $\neq 0$	1.60	—
		display diagonal	DD	positive values $\neq 0$	0.54322	m
	lighting [a]	radiance level	RL	0.0 – unlimited	0.1224 / 0.2456 / 0.1576	$W/(sr \times m^2)$
		luminance level	LL	0.0 – unlimited	27.39 / 126.03 / 5.14	cd/m^2
		chromaticity coordinate (x value)	x	ltd. by color space	0.6912 / 0.3018 / 0.1527	—
		chromaticity coordinate (y value)	y	ltd. by color space	0.3078 / 0.6276 / 0.0240	—
	content	width (regular)/height [b]	CW_{REG} / CH	integer w/i display lmt.	40 / 80	px
		vertical position [c]	CP_{VER}	integer w/i display lmt.	+40	px
		mov. positions (hor. start/stop) [d]	CP_{T0} / CP_{T1}	integer w/i display lmt.	-236 / +196	px
		movement velocity (hor.) [e]	CMV	0 – unlimited (integer)	+8	px/fr
viewer	anatomy [f]	$\overline{\text{CV-N}}$ (relaxed)	—	—	0.00706	m
		$\overline{\text{CV-N'}}$ (relaxed)	—	—	0.00736	m
		$\overline{\text{CV-F'}}$ (relaxed)	—	—	0.02389	m
		$\overline{\text{CV-N}}$ (accommodated)	—	—	0.00656	m
		$\overline{\text{CV-N'}}$ (accommodated)	—	—	0.00691	m
		$\overline{\text{CV-F'}}$ (accommodated)	—	—	0.02125	m
		$\overline{\text{CV-Z'}}$	—	—	0.01350	m
		radius of retina	RR	—	0.01200	m
	cognition	Bloch time (cones) [g]	BT_{CO}	0.0 – unlimited	0.0 (inactive)	s
		Bloch time (rods)	BT_{RO}	0.0 – unlimited	0.0 (inactive)	s
		Ricco area (rods/cones) [h]	$RA_{RO/CO}$	0.0 – unlimited	0.0 (inactive)	m
	eye	vertical position [i]	EP_{VER}	integer w/i display lmt.	0	px
		mov. positions (hor. start/stop) [j]	EP_{T0} / EP_{T1}	integer w/i display lmt.	-216 / +216 (PEM)	px
		movement velocity (hor.) [k]	EMV	0 – unlimited (integer)	+8 (PEM)	px/fr
surrounding		viewing distance [l]	VD	positive values $\neq 0$	0.57169	m

Note. *CV* = corneal vertex; *N* = first nodal point; *N'* = second nodal point; *F'* = second principal focus; *Z'* = eye's center of rotation.

[a] For every single subframe, all lighting parameters are specified separately under consideration of the determined number of three subframes within one frame cycle (*SF1* = red / *SF2* = green / *SF3* = blue).

[b] Content is assumed to have a simple geometrical shape. In this case, it is a quadratic stimulus with a width of 40 px and a height of 80 px corresponding to an angular side length of 2.0° in horizontal and vertical direction (angular side length in [deg] is valid for content in a central display position in horizontal/vertical direction, undistorted content at display level).

[c] Vertical content position is defined by the upper content edge at display level (constant), point of origin is vertical center of the display unit (down = negative, up = positive), determined vertical content position for model calculation (+40) leads to a vertically centered display position which deviates from COBUS1 presentation setting with one upper (+160) and one lower stimulus (-80) since model only allows the determination of one stimulus in a defined position.

[d] Horizontal movement path is defined by position of left content edge (display level) at the time movement starts (*T0*) and after movement is finished (*T1*), point of origin is the horizontal center of the display unit (left = negative, right = positive).

[e] Horizontal content movement velocity of +8 px/fr corresponds to an angular velocity of +36.0 deg/s for the defined conditions (angular movement velocity in [deg/s] refers to a rotation around the eye's center of rotation *Z'*, angular movement velocity is only valid for a central display position, positive values = left to right movement, negative values = right to left movement).

[f] Anatomical parameters of standard observer eye refer to Gullstrand-Emsley's schematic human eye model (except retinal radius), *relaxed* values refer to anatomical status of no accommodative effort, *accommodated* values refer to status of an accommodative effort of 10.9 D (Emsley, 1936); simplistically, it is assumed that the schematic retina has a spherical shape with a radius of 12.0 mm (Smith & Atchison, 1997).

[g] Bloch time is defined as time period for which temporal summation of light stimulation is assumed.

[h] Ricco area is defined as area for which spatial summation of light stimulation is assumed (no differentiation for rods and cones).

[i] Constant vertical eye gaze position (cyclops eye's fixation line at display level), point of origin is vertical center of the display unit (down = negative, up = positive).

[j] Movement path is defined by eye gaze position (cyclops eye's fixation line at display level) at the time movement starts (*T0*) and after movement is finished (*T1*), point of origin is the horizontal center of the display unit (left = negative, right = positive), eye movement path for model calculation is determined to follow CBU-provoking content with idealized PEM, eye gaze position during PEM determined to be in the horizontal/vertical center of the CBU-provoking content at the start of every frame cycle.

[k] Horizontal eye movement velocity of +8 px/fr corresponds to an angular velocity of +36.0 deg/s for the defined conditions (angular movement velocity in [deg/s] refers to a rotation around the eye's center of rotation *Z'*, angular movement velocity is only valid for a central display position, positive values = left to right movement, negative values = right to left movement).

[l] Distance from display level to corneal vertex of cyclops eye.

the following subsections refer to the dynamics of positioning and timing in the context of horizontal stimulation.[5]

Display-to-Retina Transition

Section 3.3.1 provides a definition of the reference systems for the display and the retinal level (sign convention, point of origin). During data entry of the model's input parameters, the positions of the cyclops eye and the content are determined pixel-perfect at display level for the complete sequence (see Table 3.2). In case of a static behavior of eye/content during the defined sequence, the fixed display position of eye/content is defined by its pixel-based horizontal and vertical display position. In case of eye/content movement during the defined sequence, the complete movement path is defined by the movement's start and stop point in [px], and the movement velocity in [px/fr]. As a result, the pixel-based display positions of both eye and content are known for every frame cycle of the sequence. This allows an accurate description of the sequence for which CBU perception must be calculated.

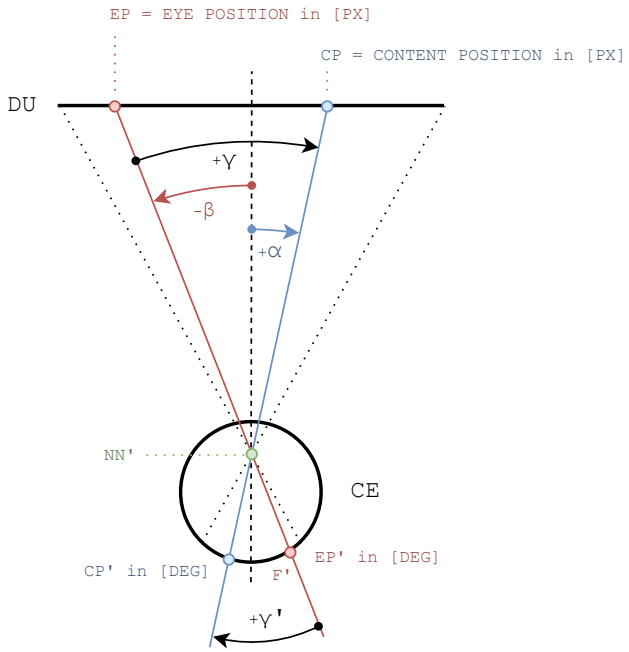

FIGURE 3.3: Angular position transfer from display level (object space) to retinal level (image space); angles α and β refer to the reference system of the display with its horizontal/vertical center as point of origin, angles γ and γ' refer to the retinal reference system with fovea centralis as point of origin.

Figure 3.3 illustrates an exemplary static scene in which the cyclops eye fixates a point at display level that is left from the display's point of origin (red dot, negative pixel value), and the presented content is positioned on the right side (blue dot, positive pixel value). Generally, the pixel-based eye/content positions at display level in object space can be transferred to angular positions using the Formulas 3.1 and 3.2.[6] Applying the formulas leads to a

[5] Calculating the stable vertical positions of stimulation from the stable eye/content positions is uncomplicated (compared to calculations of the dynamics of horizontal eye/content movement) as they can be inferred from the display-to-retina transition of eye/content positions (following subsections are not relevant).

[6] Abbreviations in the transition formulas: CP = content position at display level in [px], EP = eye position at display level in [px], PP_{HOR} = pixel pitch as the absolute size per pixel in horizontal direction in [m/px], VD = viewing distance from display level to corneal vertex of observer's eye in [m], $\overline{CV\text{-}N}$ = distance from corneal vertex to first nodal point of observer's eye in [m], AR = aspect ratio of display unit, DD = display diagonal in [m], RES_{HOR} = horizontal native resolution of display unit in [px].

negative angle β for the eye position and a positive angle α for the content position:

$$\alpha = \arctan\left[\, CP \times PP_{HOR} \,/\, \left(\, VD + \overline{CV\text{-}N} \,\right) \,\right] \tag{3.1}$$

$$\beta = \arctan\left[\, EP \times PP_{HOR} \,/\, \left(\, VD + \overline{CV\text{-}N} \,\right) \,\right] \tag{3.2}$$

The angular positions of eye/content can be calculated using the input parameters provided in Table 3.2. However, the display unit's horizontal pixel pitch PP needs to be calculated based on Formula 3.3 (see Table 3.2 for formula input):

$$PP_{HOR} = \left(\, 1 \,/\, \sqrt{1 + AR^{-2}} \,\right) \times DD \,/\, RES_{HOR} \tag{3.3}$$

Contrary to the description of a pixel-based position in object space via model input, the model output of the corresponding stimulation at retinal level in image space is defined via angular values in [deg]. Since the retina's point of origin corresponds to the fovea centralis and in most cases does not coincide with the point of origin of the display unit (unless the eye fixates the horizontal/vertical center of the display), the content position on the retina (positive γ') must be recalculated under consideration of the retinal reference system using Formula 3.4:

$$\gamma = \alpha - \beta = \gamma' \tag{3.4}$$

Therefore, the angular content position can be calculated in reference to the eye position in object space ($\gamma = \alpha$ - β), which is identical to the content position on the retinal reference system in image space ($\gamma' = \gamma$). This circumstance is due to the fact that the transition of the optical path from the display unit through the viewer's eye to the retina is carried out under the assumption that the optical path goes through the first (N) and second nodal point (N') of the viewer's eye (see Figure 3.3). This has the benefit that the angle of the incident light ray is similar to the angle of the outgoing light ray — no additional calculations are necessary.[7]

Basic Subframe Geometry

The previous subsection dealt with the general procedure necessary to calculate the retinal position of displayed content. As STICA needs to consider not only the spatial but also the temporal properties of retinal stimulation, the approach of spatial positioning has to be complemented by timing aspects of stimulation. The basic idea is to deconstruct the CBU effect, starting from its origin. For this purpose, the smallest parts in the process of CBU genesis — subframes as subcategories of a frame cycle — need to be characterized by their elementary geometrical shape. This paves the way to a better understanding of CBU and its perception.

[7] This approach works perfectly well as long as the relevant retinal positions can be expressed as angle value in [deg]. If the retinal position has to be stated as distance value in [m], a conversion from angle values in [deg] to distance values in [m] for the retinal position is necessary. Unfortunately, the retinal position in [deg] cannot be transferred to the retinal position in [m] by simply calculating the circular arc under consideration of the retinal radius and the already calculated emergent angle from the second nodal point (N') towards the retinal position of interest. This is because the second nodal point (N') does not coincide with the midpoint of the circle that represents the retinal shape. Instead, the circular arc calculation must be performed on basis of the eye's center of rotation (Z') as the midpoint of the circular retinal shape (simplified approximation). Therefore, further calculation steps to determine the emergent angle from the center of rotation (Z') towards the retinal position of interest are required. Afterwards the calculation of the circular arc can be operated by using assumed retinal radius and emergent angle starting from the center of rotation (Z') to determine the retinal position as a distance value in [m]. The calculation process from an angular retinal position in [deg] to a retinal position based on distance values in [m] can be viewed in the MATLAB code's Segment V.

The stimulation of a moving eye's retina by light emitted during one single subframe cycle can be described geometrically by considering the two dimensions of time and space (see Figure 3.4). At the beginning of light exposure, subframe-based light stimulation covers the retina across the regular content width (distance from point A to C). When eye movement leads to retinal rotation, the stimulated retinal area shifts until it reaches a new retinal position at the end of the subframe's on-time (distance from point E to G). Like an accordion, the stimulated area $\overline{AC}$ is stretched temporally and spatially towards area $\overline{GE}$.

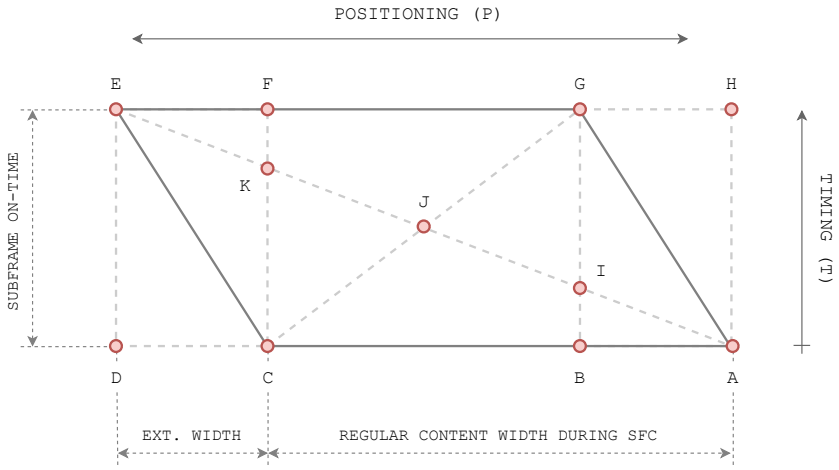

FIGURE 3.4: Two-dimensional rhomboid representing a single subframe's spatial and temporal stimulation at retinal level (rhomboid's basic points A to K included).

The resulting two-dimensional geometrical shape is a rhomboid, representing the spatial and temporal properties of retinal stimulation during eye movement (without eye movement, a rectangular shape would represent the retinal stimulation). The rhomboid can be unambiguously described by determining the time and space components of the four basic points A, C, E, and G (see following subsections).

Subframe Positioning

The following Formulas 3.5 to 3.8 can be universally applied to calculate the retinal positions of the rhomboid's basic points, since they are valid for both CAT2 and CAT3.[8] The formulas are based on the general approach to calculate the position of retinal stimulation (γ') considering the content position (α) and the eye position (β) as in Formula 3.4. The basic relation

[8] Abbreviations in the positioning formulas: CP_{T0} = content position referring to the left edge of the content in horizontal direction at display level at point of time $T0$ in [deg], CW_{REG} = regular content width in [deg], CM_{FC} = content movement during a full frame cycle in [deg], CMV = content movement velocity in [deg/s], EP_{T0} = eye position at point of time $T0$ in [deg], EM_{SFON} = eye movement during subframe is switched on in [deg], EM_{SFOFF} = eye movement during subframe is switched off in [deg], EM_{FC} = eye movement during the presentation of all subframes (on- and off-times) included within one full frame cycle in [deg], EMV = eye movement velocity in [deg/s], SF_{CT} = subframe count, FR = frame rate in [Hz], and DC = duty cycle. Due to the display unit's plane surface (assumption), the initially defined input parameters CW_{REG} in [px] and CMV/EMV in [px/fr] as listed in Table 3.2 — describing a fixed content width and a stable content/eye movement velocity — are converted to display position-dependent variable parameters CW_{REG} in [deg] and CMV/EMV in [deg/s]. The position-dependency of these angular parameters is caused by the display unit's plane surface (stated angular content widths and content/eye movement velocities refer to a central display position unless otherwise stated, angle values decrease in the periphery). The angular movement parameters CM_{FC}, EM_{SFON}, EM_{SFOFF}, and EM_{FC} in [deg] which are based on CMV/EMV in [deg/s] also vary with display position (see Formulas 3.11 to 3.14). The position-dependent variability of these angular parameters is considered when calculating the positions of the basic points A, C, E, and G of all relevant subframes/frame cycles (see Formulas 3.5 to 3.10). The model's position-dependent basic points are calculated in MATLAB Segment V.

between eye and content position and the resulting retinal position ($\gamma' = \alpha$ - β) is indicated by the lower indices outside the square brackets of the formulas below. The listed Formulas 3.5 to 3.8 describe the positioning within a single subframe by calculating the angular positions P of the rhomboid's basic points A,C, E, and G of the first subframe *SF1* within the first frame cycle *FC1*:

$$[\,P_{A\,(FC1/SF1)}\,]_{\gamma'} = [\,CP_{T0} + CW_{REG}\,]_{\alpha} - [\,EP_{T0}\,]_{\beta} \tag{3.5}$$

$$[\,P_{C\,(FC1/SF1)}\,]_{\gamma'} = [\,CP_{T0}\,]_{\alpha} - [\,EP_{T0}\,]_{\beta} \tag{3.6}$$

$$[\,P_{E\,(FC1/SF1)}\,]_{\gamma'} = [\,CP_{T0}\,]_{\alpha} - [\,EP_{T0} + EM_{SF\,ON}\,]_{\beta} \tag{3.7}$$

$$[\,P_{G\,(FC1/SF1)}\,]_{\gamma'} = [\,CP_{T0} + CW_{REG}\,]_{\alpha} - [\,EP_{T0} + EM_{SF\,ON}\,]_{\beta} \tag{3.8}$$

To enable the description of all other subframes within *FC1*, the transition from subframe to subframe must be defined. Therefore, the position of the basic point A of the second subframe (*SF2*) can be calculated using Formula 3.9:

$$[\,P_{A\,(FC1/SF2)}\,]_{\gamma'} = [\,CP_{T0} + CW_{REG}\,]_{\alpha} - [\,EP_{T0} + EM_{SF\,ON} + EM_{SF\,OFF}\,]_{\beta} \tag{3.9}$$

The other basic points C, E, and G of *SF2* can be calculated by applying Formulas 3.6 to 3.8. This pattern of basic point calculation and the following calculative jump from subframe to subframe can be used to calculate all relevant basic points of all subframes within a frame cycle. To calculate positions across frame cycle borders, the calculative transition from frame to frame must be considered. Formula 3.10 refers to the angular position of the basic point A of the second frame cycle's first subframe (*FC2*/*SF1*):

$$[\,P_{A\,(FC2/SF1)}\,]_{\gamma'} = [\,CP_{T0} + CW_{REG} + CM_{FC}\,]_{\alpha} - [\,EP_{T0} + EM_{FC}\,]_{\beta} \tag{3.10}$$

Having determined the first basic point of *FC2* as reference point, the process starts from the beginning, allowing to calculate the positions of all following basic points of all subframes within *FC2*. By systematically applying Formulas 3.5 to 3.10, all required basic points of all subframes within all frame cycles not explicitly named can be determined with the same pattern as described above since the structure repeats.

$$[\,CM_{FC}\,] = CMV \times FR^{-1} \tag{3.11}$$

$$[\,EM_{SF\,ON}\,] = EMV \times DC \times (\,FR \times SF_{CT}\,)^{-1} \tag{3.12}$$

$$[\,EM_{SF\,OFF}\,] = EMV \times (\,1 - DC\,) \times (\,FR \times SF_{CT}\,)^{-1} \tag{3.13}$$

$$[\,EM_{FC}\,] = EMV \times FR^{-1} \tag{3.14}$$

The content movement (*CM*) and eye movement (*EM*) in the positioning formulas are calculated using the Equations 3.11 to 3.14. The input for the equations is given by the EOC input parameters of the model as listed in Table 3.2. Hence, all positions P can be calculated with the originally defined input parameters of the model.

Subframe Timing

In a next step, the formulas describing the exposure time of subframe stimulation on the retina are presented. All timing formulas below can be used universally for the movement

categories of CAT2 and CAT3.[9] At first, the points of time T within one subframe ($FC1/SF1$) are determined by defining the basic points of the representative rhomboid using the Formulas 3.15 to 3.18:

$$[\, T_{A\,(FC1/SF1)} \,] = 0 \tag{3.15}$$

$$[\, T_{C\,(FC1/SF1)} \,] = [\, T_{A\,(FR1/SF1)} \,] \tag{3.16}$$

$$[\, T_{E\,(FC1/SF1)} \,] = [\, T_{A\,(FR1/SF1)} \,] + [\, TP_{SF\,ON} \,] \tag{3.17}$$

$$[\, T_{G\,(FC1/SF1)} \,] = [\, T_{E\,(FR1/SF1)} \,] \tag{3.18}$$

Hereafter, the transition from subframe to subframe within $FC1$ must be calculated. On basis of the first subframe's ($SF1$) basic point A, Formula 3.19 allows to calculate the timing T of the basic point A of the second subframe $SF2$:

$$[\, T_{A\,(FC1/SF2)} \,] = [\, T_{A\,(FR1/SF1)} \,] + [\, TP_{SFC} \,] \tag{3.19}$$

Finally, the frame-to-frame transition is made by calculating the time component of the first subframe's ($SF1$) basic point A of the second frame cycle ($FC2$) based on the same basic point within the first frame cycle (see Formula 3.20):

$$[\, T_{A\,(FC2/SF1)} \,] = [\, T_{A\,(FR1/SF1)} \,] + [\, TP_{FC} \,] \tag{3.20}$$

The application of Formulas 3.15 to 3.18 for basic point calculations within a subframe, Formula 3.19 for jumps across subframe borders, and Formula 3.20 for frame cycle jumps, allows the timing calculation of all subframes' basic points within all relevant frame cycles that are not explicitly named.

$$[\, TP_{SF\,ON} \,] = DC \times (\, FR \times SF_{CT} \,)^{-1} \tag{3.21}$$

$$[\, TP_{SFC} \,] = (\, FR \times SF_{CT} \,)^{-1} \tag{3.22}$$

$$[\, TP_{FC} \,] = FR^{-1} \tag{3.23}$$

The time periods TP in the formulas for timing calculation can be calculated using the Equations 3.21 to 3.23. The input of these equations refers to the EOC (see Table 3.2). Therefore, all points in time T can be calculated with the originally defined EOC input parameters of the model.

The representative EOC rhomboids for a whole frame cycle are illustrated schematically in Figure 3.5. Three subframes with classic RGB pattern are included. By applying the positioning and timing formulas as described, the rhomboid's spatio-temporal coordinates P and T can be quantified. Exemplarily, the positioning and timing coordinates of the basic point E of the initial frame cycle's second subframe are P_E = -1.1302° and T_E = 0.0048 s, while the coordinates of the basic point G of the same frame cycle's third subframe are P_G = 0.6722° and T_G = 0.0085 s. The finally defined rhomboid serves as the two-dimensional representation of subframe stimulation over time and space.

[9] Abbreviations in the timing formulas: $TP_{SF\,ON}$ = time period a single subframe is switched on in [s], TP_{SFC} = time period of a full subframe cycle including a subframe's on/off-time in [s], TP_{FC} = time period of all subframes (on- and off-times) included within a full frame cycle in [s], SF_{CT} = subframe count, FR = frame rate in [Hz], and DC = duty cycle.

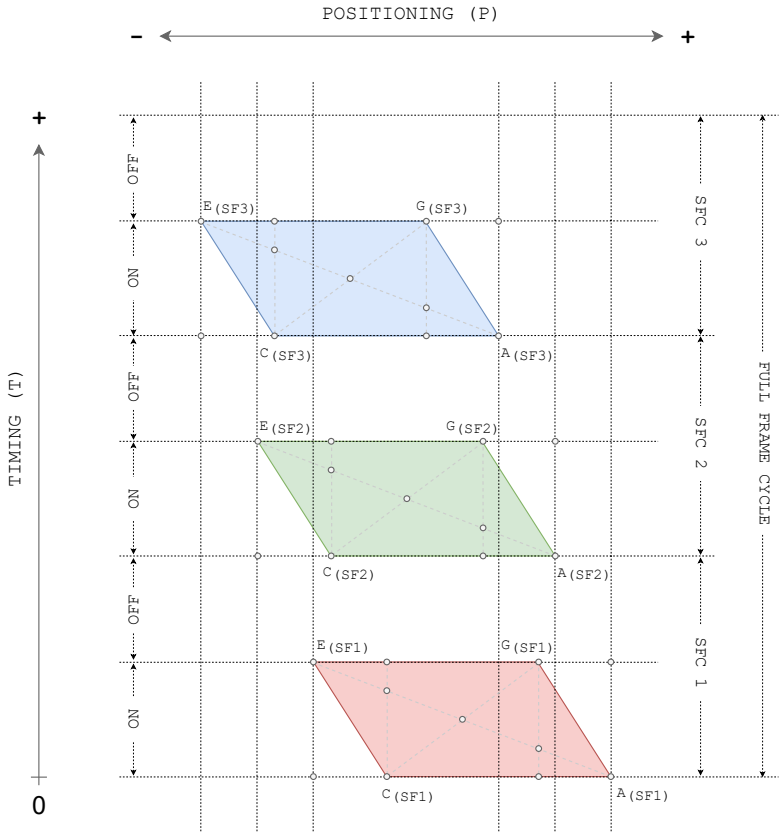

FIGURE 3.5: Interaction between three subframes of one full frame cycle under consideration of positioning and timing (illustration refers to EOC).

3.4.2 Intensity and Color

The next step is to specify the emitted light intensity and color characteristics during a subframe period. Since STICA is explained by mirroring specific EOC conditions, the light sources of interest are the LEDs of the applied DLP projector during COBUS1 (see Appendix A.3.1 for a device specification and Appendix B.1 for pre-testing results of the LEDs' light emission behavior).

Subframe Intensity

Regarding the EOC, the three succeeding subframes that are relevant for the model calculation feature the following light intensities: first, red-colored subframe with a radiance of $L_e = 0.1224\,\mathrm{W/(sr \times m^2)}$ and a luminance of $L_v = 27.39\,\mathrm{cd/m^2}$, second, green-colored subframe with $L_e = 0.2456\,\mathrm{W/(sr \times m^2)}$ and $L_v = 126.03\,\mathrm{cd/m^2}$, and closing third, blue-colored subframe with $L_e = 0.1576\,\mathrm{W/(sr \times m^2)}$ and $L_v = 5.15\,\mathrm{cd/m^2}$.[10]

[10] Light intensity can be specified by physical and photometric measurands. Radiance L_e in $[\mathrm{W/(sr \times m^2)}]$ is the physical quantity related to the power of light, yet ignores any aspect of human perception (i.e., the human eye's wavelength-dependent sensitivity). The wavelength-dependent sensitivity of the retinal photoreceptors (S, M, and L cones) can be included by measuring the luminance L_v in $[\mathrm{cd/m^2}]$ as the photometric measurand. Both measurands were chosen from a range of light measurement parameters considering a projection-based approach (DLP projector applied during COBUS series). The measured light intensities during the single subframe periods are frame rate-averaged values (30.0 to 420.0 Hz) referring to the highest luminance level that is achievable with the applied projector ($157.0\,\mathrm{cd/m^2}$, full frame cycle, see Table B.7). The light intensities and color characteristics of the single subframe periods were determined to create a white stimulus.

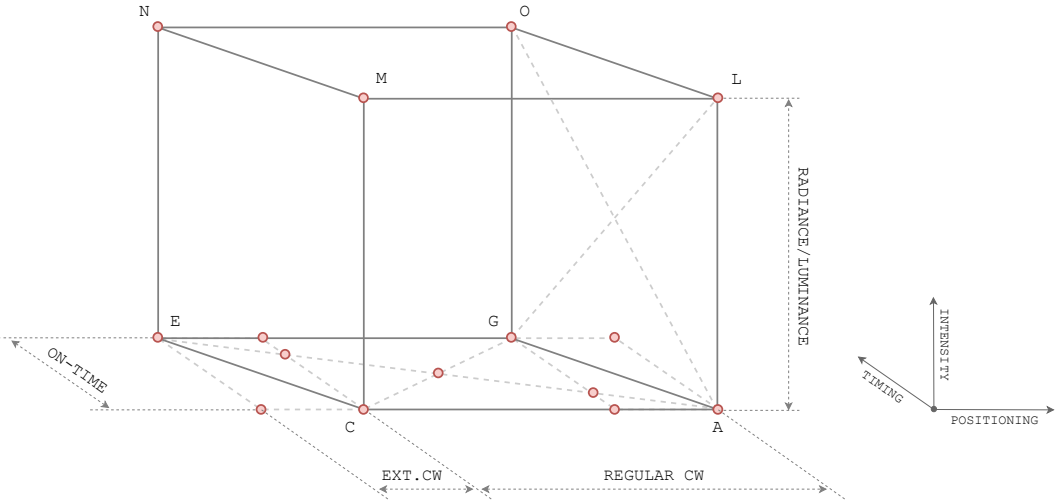

FIGURE 3.6: Three-dimensional subframe body representing spatial and temporal retinal stimulation (xy-plane, rhomboid) with defined light intensity (z-axis).

A three-dimensional subframe body illustrates all previous specifications at subframe level (see Figure 3.6). The body consists of a rhomboidal basis representing spatio-temporal aspects of retinal stimulation. The emitted light intensity is visualized in vertical direction, perpendicular to the subframe body's space-time basis.[11] Figure 3.7 displays the subframe bodies of three subframes within a full frame cycle (classic RGB pattern). The subframe bodies are positioned in a three-dimensional coordinate system with the dimensions of position (x-axis), time (y-axis), and intensity (z-axis). The subframes' intensities in this space-time-intensity plot are illustrated schematically based on the mentioned luminance levels L_v.

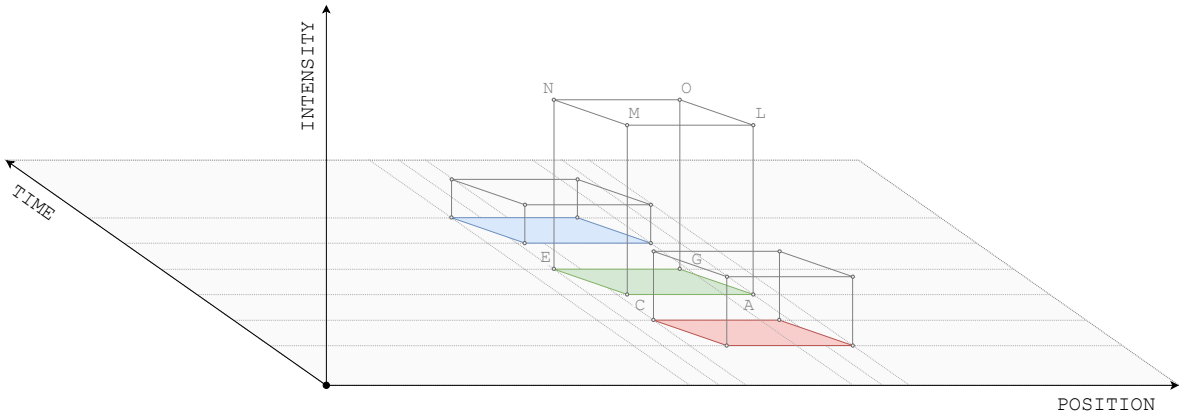

FIGURE 3.7: Space-time-intensity plot with three subframe bodies of one full frame cycle (illustration refers to EOC corresponding to CBU-characterizing Phase 1, see Section 3.5).

Color Coordinates of Subframes

STICA is finally completed by assigning color characteristics to every subframe. The color of light emitted during a subframe period can be defined by measuring the chromaticity

[11] Switching the projector's LEDs on or off by regulating the applied current does not lead to an instant jump to target luminance or zero light emission. In fact, the luminance level is continuously increasing/decreasing over time until the required level is reached. To quantify the LEDs response time, some measurements were performed for various frame rates at a luminance level of 157.0 cd/m^2 (see Appendix B.2.3). The LEDs switch quickly (on average 0.55 ± 0.01 µs for intensity increase to the desired output and 1.82 ± 0.21 µs for intensity decline to zero output). Consequently, the model assumes that desired light intensity changes during a subframe period are reached without delay (simplified, valid for increase/decrease of light emission).

coordinates x and y. The chromaticity coordinates of the three EOC subframes have the following values: $x = 0.6912$ and $y = 0.3078$ for the first subframe (red), $x = 0.3018$ and $y = 0.6276$ for the second subframe (green), and $x = 0.1527$ and $y = 0.0240$ for the third subframe (blue). The subframes are arranged in a typical RGB color pattern. The light colors of the red and the blue subframe are highly saturated, while the green subframe shows a reduced saturation. The resulting color gamut, however, is large enough to display a wide range of mixed colors with variable saturation (see right-side graphic in Figure 3.11).

3.5 Color Break-Up Characteristic

Regarding the current status of the model: physical stimulation is specified by quantifying light intensity and color for all included subframes. The physical stimulation of every subframe is spatially assigned to its retinal position. Furthermore, the presentation time for every subframe is defined. Defining the intensity/color of stimulation and the position/time of occurrence by applying STICA eventually leads to the determination of the complete physical stimulation at the retinal level under the given frame conditions. However, the single subframes have been characterized separately until now. The interaction between the individual subframes must now be dealt with. Color patterns as a result of temporal summation of all subframes within one frame cycle are analyzed. This step is essential for CBU prediction. A classification of CBU phases with different color patterns is established and the conditions for phase transitions are defined (see Section 3.5.1). Subsequently, the color structure of the CBU phases is qualitatively determined by calculating the boundaries of the homogeneous color sectors (see Section 3.5.2).

3.5.1 Phases and Transitions

Depending on the prevailing conditions (e.g., eye movement velocity or frame rate), CBU is either absent or appears in various color designs. These two options can be further classified into four phases, where Phase 0 (PH0) represents the phase with no objectively existent CBU and PH1 to PH3 include CBU appearance with different color patterns. All phases and their transition thresholds are described in the following subsections. Phase determinations and calculations of eye movement velocity thresholds required to switch from phase to phase are based on the spatio-temporal geometry of a subframe (see Section 3.4.1). The explanations below refer to the classic RGB pattern of three subframes within one frame cycle. Hence, the basic points A and E of all three subframes are of particular importance. The phases and transitions are determined considering the positioning of the subframes, not the timing.[12]

Definition of Phase 0

Formula 3.24 describes the spatial requirement for the basic point positioning that must be met to classify the situation into PH0:

$$A_{SF1} = A_{SF2} = A_{SF3} \;\cap\; E_{SF1} = E_{SF2} = E_{SF3} \tag{3.24}$$

The formula refers to the ideal overlapping of the retinal stimulation by the three subframes without any spatial deviation. The existence of PH0 is only given as long as eye movement

[12] In the MATLAB code, phases and transition thresholds are defined and calculated independently of the subframe count (within the applicable subframe range). The present CBU phase is determined in Segment VI, whereas transition thresholds of eye movement velocity are calculated in Segment VII. Phase determination and transition threshold calculation are executed for the frame cycle (out of all presented frame cycles) that features the highest angular eye movement velocity (frame cycle corresponds to the most central content position at display level, display position-dependent angular velocity due to the plane characteristic of the display unit).

is absent (CAT0 or CAT1). Color distortion in terms of CBU does not occur on either an objective or a subjective basis.

Transition from Phase 0 to Phase 1

In Formula 3.25, the basic requirement to trigger the appearance of CBU by switching from PH0 to PH1 is specified:

$$A_{SF1} \neq A_{SF2} \neq A_{SF3} \quad \cap \quad E_{SF1} \neq E_{SF2} \neq E_{SF3} \tag{3.25}$$

The moment eye movement is executed during the frame cycle presentation, PH0 immediately changes to PH1 (see Equation 3.26):

$$EMV_{PH0/1} \neq 0 \tag{3.26}$$

Regarding the general appearance of CBU, it is irrelevant which type of eye movement is executed — both saccades (CAT2) and pursuits (CAT3) trigger CBU.

Definition of Phase 1

Formula 3.27 clarifies the spatial requirement that must be fulfilled to classify the CBU effect into PH1:

$$E_{SF3} < E_{SF1} < A_{SF3} \tag{3.27}$$

In PH1, a stimulus intended to be white shows a colored distortion at the leading and trailing vertical edges, while the center of the stimulus is not affected (still white). The leading edge is colored blue and cyan, and on the trailing edge, red and yellow segments are visible (see Figure 3.8 illustrating rhomboids that provide a clearer arrangement than full subframe bodies). The dimension of retinal stimulation is larger than the CBU-provoking content's actual dimension at display level. The defined EOC conditions lead to a PH1 stimulation.

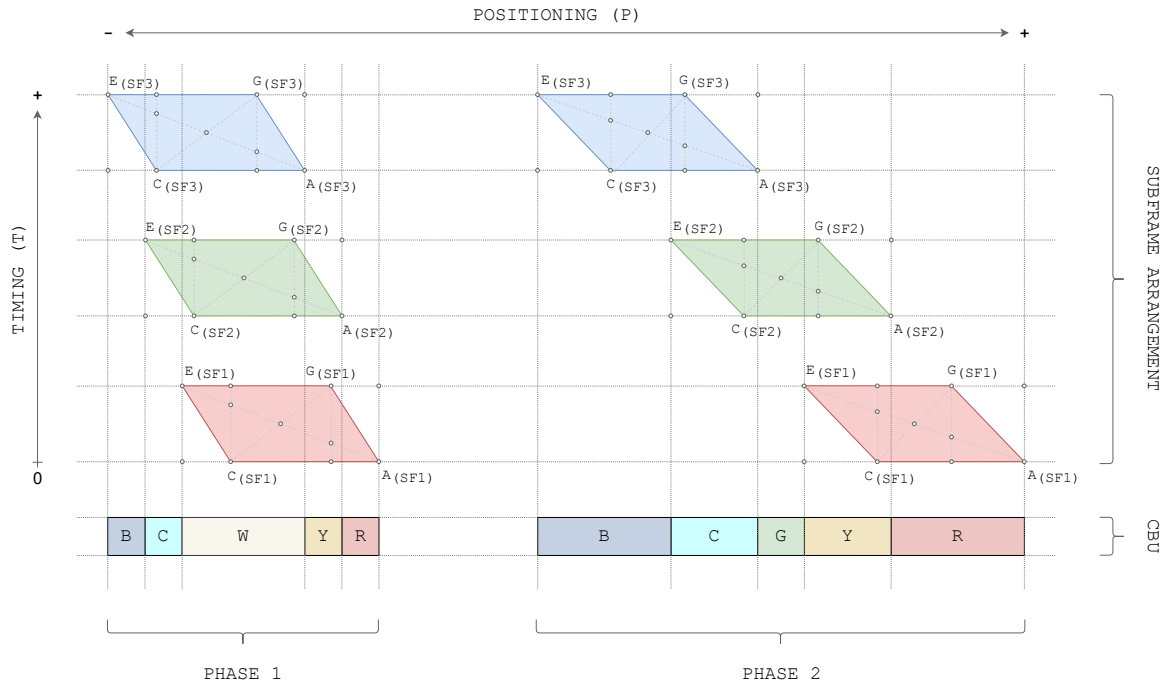

FIGURE 3.8: Subframe positioning/timing (three subframes, full frame cycle) and resulting CBU color patterns for PH1 (refers to EOC) and PH2.

Transition from Phase 1 to Phase 2

A transition from PH1 to PH2 is given as soon as the basic requirement in Formula 3.28 is fulfilled:

$$E_{SF1} = A_{SF3} \tag{3.28}$$

From the basic Formula 3.28, the more specific Formula 3.29 can be constructed, which calculates the threshold value of the eye movement velocity for a switch from PH1 to PH2 and vice versa:

$$EMV_{PH1/2} = (CW_{REG} \times SF_{CT} \times FR) / (2 - DC) \tag{3.29}$$

In Formula 3.29, regular content width CW_{REG} in [deg], subframe count SF_{CT}, frame rate FR in [Hz], and duty cycle DC are the parameters that define the eye movement velocity $EMV_{PH1/2}$ in [deg/s] that has to be overshot to switch from PH1 to PH2. Wider content, higher frame rate, and larger duty cycle increase the eye movement velocity for a phase transition. For the EOC conditions (see Table 3.2), the transition threshold of the eye movement velocity $EMV_{PH1/2}$ would be 317.6 deg/s at a frame rate of 90.0 Hz. Reducing the frame rate to 30.0 Hz while keeping all other EOC parameters stable would result in a decreased transition threshold of 105.9 deg/s as described by Formula 3.29.

Definition of Phase 2

The spatial requirement that has to be fulfilled to reach PH2 is described by the following Equation 3.30:

$$A_{SF3} < E_{SF1} < A_{SF2} \tag{3.30}$$

There are no more white shares of the stimulus in PH2 since there is no overlapping zone for all three subframes. Similar to PH1, the rainbow pattern (red, yellow, cyan, blue) is present at the leading and trailing edges. Furthermore, a green share occurs in the middle of the stimulus area (see Figure 3.8). The dimension of retinal stimulation during PH2 is larger when compared to PH1.

Transition from Phase 2 to Phase 3

The next transit between PH2 and PH3 is reached for the basic requirement specified by Formula 3.31:

$$E_{SF1} = A_{SF2} \tag{3.31}$$

The eye movement velocity for the transition from PH2 to PH3 can be calculated with the help of Formula 3.32:

$$EMV_{PH2/3} = (CW_{REG} \times SF_{CT} \times FR) / (1 - DC) \tag{3.32}$$

The threshold formula for the transition from PH2 to PH3 is almost identical to the formula for the transition from PH1 to PH2. The relevant parameters and their impact on the threshold eye movement velocity $EMV_{PH2/3}$ in [deg/s] are the same. Only the denominator in the formula is slightly different, leading to higher eye movement velocities. For the determined EOC conditions, $EMV_{PH2/3}$ would be 771.4 deg/s at a frame rate of 90.0 Hz.[13] Such an eye movement velocity corresponds to a saccade at the upper limit of the human visual system's capability (see Section 2.3.1).

[13] The derivations of Formula 3.29 on basis of Formula 3.28 (PH1/PH2) and Formula 3.32 on basis of Formula 3.31 (PH2/PH3) are provided in Appendix E. The Formulas 3.29 and 3.32 can be transposed to calculate the phase transition threshold of other parameters (e.g., frame rate threshold to avoid CBU effects of PH2/PH3).

Definition of Phase 3

The spatial requirement that has to be fulfilled to create CBU effects of PH3 is described by Formula 3.33:

$$E_{SF1} > A_{SF2} \tag{3.33}$$

In PH3, the primary RGB colors of the three subframes are fully separated at retinal level (see Figure 3.9). The dimensions of the unstimulated gaps between the blocks of red, green, and blue stimulation and the colored blocks itself depend on eye movement velocity, content width, subframe count, frame rate, and duty cycle (see previous formulas). No white shares and no other mixed colors are present (e.g., cyan or yellow). PH3 shows CBU effects with the most extensive color distortion.[14]

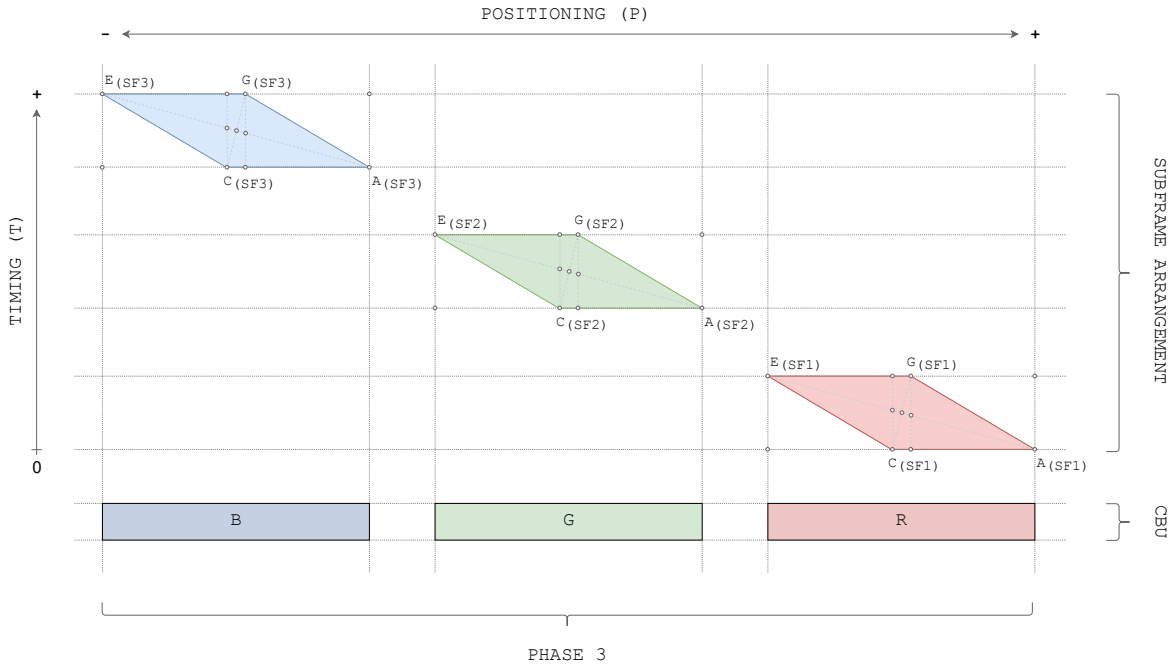

FIGURE 3.9: Subframe positioning/timing (three subframes, full frame cycle) and resulting CBU color pattern for PH3.

3.5.2 Color Sectors

Having described the key principles of CBU phases and their transitions, it is now time to quantify the color patterns of the established CBU phases in terms of their retinal positions. This requires to identify the borders of color sectors — the zone edges that separate zones of identical color characteristics. Assuming the color sector borders of a white CBU-provoking content during PH1 shall be determined (classic RGB subframe order, see left side of Figure 3.8). In this case, the borders between the white unbiased color sector in the middle and the colored sectors at the leading (blue and cyan) and trailing edges (yellow and red) must be distinguished. Hence, five different color sectors and their borders must be considered for the PH1 condition. The vertical dotted lines in Figure 3.8 represent the borders between the different color sectors. The borders of the color sectors are defined by the outer edges (*A*s and *E*s) of the rhomboid as the foundation of the three-dimensional subframe geometry (see Section 3.4.1). These outer edges have already been calculated during the determination

[14] Theoretical calculations on the transition between absence (PH0) and presence of CBU (PH1 to PH3) do not necessarily correspond to the subjective CBU detection threshold. Assuming objective CBU presence, an observer might still not notice an existent CBU effect as its magnitude might lie below his threshold of perceptibility (*TOP*). It is likely that the *TOP* arises in PH1 since PH0 is CBU-free and PH2/PH3 show distinct CBU.

of the retinal positions of the relevant basic points *A*, *C*, *E*, and *G* for all subframes implemented within all frame cycles of the full sequence.[15] The basic point positions can now be used for further calculations. The quantitative calculation of the borders of color sectors is always done by investigating the spatial overlapping of the time-integrated subframes of a closed frame cycle. For this purpose, a two-stage calculation process is executed by applying operations of the *set theory* in the following subsections.

Intersections and Unions

In a first step, the retinal positions of the intersections and unions for all possible subframe combinations within a closed frame cycle are determined under consideration of the single subframes' *A*s and *E*s as the spatial edges of the rhomboid subframe geometry. Therefore, operations of the set theory are applied to calculate intersections of sets and unions of sets.[16]

TABLE 3.3: Intersection and union sets for all possible combinations of subframe interactions under consideration of three/four subframes included within one frame cycle.

Division No. (= SF_{CT})	Subdivision No. (= SF_{IA})	Combination of Subframe Interactions		Substitution No. (SN)
		Intersection (I)	Union (U)	
3	1	(SF1)	(SF1)	[1]
		(SF2)	(SF2)	[2]
		(SF3)	(SF3)	[3]
	2	(SF1 ∩ SF2)	(SF1 ∪ SF2)	[4]
		(SF2 ∩ SF3)	(SF2 ∪ SF3)	[5]
	3	(SF1 ∩ SF2 ∩ SF3)	(SF1 ∪ SF2 ∪ SF3)	[6]
4	1	(SF1)	(SF1)	[1]
		(SF2)	(SF2)	[2]
		(SF3)	(SF3)	[3]
		(SF4)	(SF4)	[4]
	2	(SF1 ∩ SF2)	(SF1 ∪ SF2)	[5]
		(SF2 ∩ SF3)	(SF2 ∪ SF3)	[6]
		(SF3 ∩ SF4)	(SF3 ∪ SF4)	[7]
	3	(SF1 ∩ SF2 ∩ SF3)	(SF1 ∪ SF2 ∪ SF3)	[8]
		(SF2 ∩ SF3 ∩ SF4)	(SF2 ∪ SF3 ∪ SF4)	[9]
	4	(SF1 ∩ SF2 ∩ SF3 ∩ SF4)	(SF1 ∪ SF2 ∪ SF3 ∪ SF4)	[10]

Note. SF_{CT} = subframe count; SF_{IA} = interacting subframes; ∩ = intersection of sets (set theory); ∪ = union of sets (set theory).

Table 3.3 shows the intersection and union sets for all possible subframe combinations of a frame cycle with three or four subframes (see division number in table) to point out the subframe-dependent patterns during the following calculation steps. The total count of combinations in one division (e.g., three subframes) results from the cumulation of the combination counts in its subdivisions (limitation of interacting subframes to one, two, and three subframes, see table). In a division, a consecutive substitution number (SN) is assigned to every combination of subframe interaction. The general count of substitution numbers in

[15] Choosing the *A*s and *E*s for the determination of the color sector borders leads to inhomogeneous color characteristics within the color sectors. The color inhomogeneity originates from instable subframe presentation times at the sector borders (see rhomboid geometry) which is due to eye movement. To guarantee uniform color characteristics within the sectors, the *C*s and *G*s of the rhomboid would have to be additionally applied for border determination, leading to uniform color sectors (between the *C*s and *G*s) and heterogeneous color sectors for color transition (between *A*s and *G*s and between *C*s and *E*s). However, this approach is not implemented as it would increase the model's complexity significantly (could be worthwhile for future model revisions).

[16] Subframe intersections/unions are calculated in Segment VIII of the model. External code calculates areal intersections (Beudaert, 2012) and unions of ranges (Goodmanson, 2017) for all frame cycles of the sequence.

one division $SN_{CT\,(DIV)}$ solely depends on the subframe count SF_{CT} included within one frame cycle, and can be calculated with Formula 3.34. An assumption of four subframes per frame cycle leads to 10 possible combinations of different subframe interactions in the division. The count of possible combinations for a specific subdivision $SN_{CT\,(SDIV)}$ can be calculated with Formula 3.35. Assuming the interaction of only three of the four included subframes per frame cycle leads to a count of two possible combinations (see Table 3.3):

$$SN_{CT\,(DIV)} = ({SF_{CT}}^2 + SF_{CT}) / 2 \tag{3.34}$$

$$SN_{CT\,(SDIV)} = SF_{CT} - SF_{IA} + 1 \tag{3.35}$$

For the previous intersection and union sets, the existence of other subframes within the calculated range is not excluded. This requires the definition of exclusive subframe combinations excluding the appearance of all other subframes within a frame cycle.

Differences

In a second step, the retinal color sectors of exclusive subframe combinations are calculated. No other subframe than the defined subframes lies within the determined sector. Relevant data of the already calculated intersection and union sets of various subframe combinations are selected (see previous subsection), and combined by calculating their difference of sets. A specific arrangement of subframe interaction is created, representing the exclusive combination of selected subframes. The general set theory operation for the determination of the differences of sets is always identical, independently of CBU phase and subframe count (see Formula 3.36):

$$SEC = I \setminus (U_1 \cup U_2) \tag{3.36}$$

The color sector (SEC) that originates from the exclusive summation of selected subframes is determined by calculating the difference of sets between the intersection set (I) of the selected subframes and the union of the two union sets (U_1 and U_2) which include all other subframes within one frame cycle. To insert the correct subframe combinations of intersections and unions in Formula 3.36, the corresponding substitution numbers need to be read out (see Table 3.3). The choice of the correct substitution numbers always follows a general periodic pattern. However, this pattern is different for every CBU phase. It can even vary within a CBU phase, for example, if the subframe count of a frame cycle is changed.[17] The following tables present the patterns of substitution numbers for all CBU phases including three/four subframes, starting with PH1 (see Tables 3.4 and 3.5).

TABLE 3.4: Color sectors based on the interaction of three subframes within one frame cycle during PH1.

Color Sectors	Subframe Interaction (3SF)					
	Union (U_1)	SN	Intersection (I)	SN	Union (U_2)	SN
1	(—)	[—]	(SF1)	[1]	(SF2 ∪ SF3)	[5]
2	(—)	[—]	(SF1 ∩ SF2)	[4]	(SF3)	[3]
3	**(—)**	[—]	(SF1 ∩ SF2 ∩ SF3)	[6]	(—)	[—]
4	(SF1)	[1]	(SF2 ∩ SF3)	[5]	(—)	[—]
5	(SF1 ∪ SF2)	[4]	(SF3)	[3]	(—)	[—]

Note. U_1 = first union of sets; U_2 = second union of sets; I = intersection of sets; SN = substitution number; ∩ = intersection of sets; ∪ = union of sets.

Table 3.4 lists the resulting color sectors of the initially mentioned PH1 example (classic RGB sequence referring to the EOC) with five color sectors — red, yellow, white, cyan, and blue.

[17] The model's choice of substitution numbers is made by transferring the periodic pattern for their determination to MATLAB code (Segment IX calculates the color sectors for all frame cycles of the modeled sequence).

For example, the yellow color sector originates from the exclusive interaction between the first (red) and the second subframe (green) under exclusion of the existence of the third subframe (blue) within the determined retinal area. This genesis of the yellow color sector can be described by the corresponding set theory operation: $(SF1 \cap SF2) \setminus SF3$. The quantity of five color sectors for this condition depends on the subframe count within one frame cycle and can generally be calculated with Formula 3.37 (also valid for all other CBU phases):

$$SEC_{CT} = 2 \times SF_{CT} - 1 \tag{3.37}$$

By integrating a fourth subframe within a frame cycle, the color pattern during PH1 changes (see Table 3.5). Seven color sectors are formed in total. For example, the sixth color sector includes a mixed color by explicitly summing *SF3* and *SF4*. For this purpose, the difference of sets has to be calculated from the intersection of *SF3* and *SF4* and the union of *SF1* and *SF2* by operating $(SF3 \cap SF4) \setminus (SF1 \cup SF2)$ or calculating $[7] \setminus [5]$ under consideration of the substitution numbers.

TABLE 3.5: Color sectors based on the interaction of four subframes within one frame cycle during PH1.

Color Sector	Subframe Interaction (4SF)					
	Union (U_1)	SN	Intersection (I)	SN	Union (U_2)	SN
1	(—)	[—]	(SF1)	[1]	(SF2 ∪ SF3 ∪ SF4)	[9]
2	(—)	[—]	(SF1 ∩ SF2)	[5]	(SF3 ∪ SF4)	[7]
3	**(—)**	[—]	(SF1 ∩ SF2 ∩ SF3)	[8]	(SF4)	[4]
4	(—)	[—]	(SF1 ∩ SF2 ∩ SF3 ∩ SF4)	[10]	(—)	[—]
5	(SF1)	[1]	(SF2 ∩ SF3 ∩ SF4)	[9]	(—)	[—]
6	(SF1 ∪ SF2)	[5]	(SF3 ∩ SF4)	[7]	(—)	[—]
7	(SF1 ∪ SF2 ∪ SF3)	[8]	(SF4)	[4]	(—)	[—]

Note. U_1 = first union of sets; U_2 = second union of sets; I = intersection of sets; SN = substitution number; ∩ = intersection of sets; ∪ = union of sets.

Having described the color sectors for PH1, the following tables list the intersection and union sets and the corresponding substitution numbers to be combined for PH2. Table 3.6 refers to a frame cycle presentation including three subframes. A classic RGB succession results in the following sequence of five color sectors: red – yellow – green – cyan – blue (see right-side graphic in Figure 3.8). For example, the fourth color sector (cyan) is defined by the following operation: $(SF2 \cap SF3) \setminus SF1$.

TABLE 3.6: Color sectors based on the interaction of three subframes within one frame cycle during PH2.

Color Sector	Subframe Interaction (3SF)					
	Union (U_1)	SN	Intersection (I)	SN	Union (U_2)	SN
1	(—)	[—]	(SF1)	[1]	(SF2 ∪ SF3)	[5]
2	(—)	[—]	(SF1 ∩ SF2)	[4]	(SF3)	[3]
3	(SF1)	[1]	(SF2)	[2]	(SF3)	[3]
4	(SF1)	[1]	(SF2 ∩ SF3)	[5]	(—)	[—]
5	(SF1 ∪ SF2)	[4]	(SF3)	[3]	(—)	[—]

Note. U_1 = first union of sets; U_2 = second union of sets; I = intersection of sets; SN = substitution number; ∩ = intersection of sets; ∪ = union of sets.

For subframe counts of $SF_{CT} \geq 4$, the pattern of the substitution numbers determining the chronology of subframe combinations during PH2 does not only depend on the subframe count as in the previous examples. In this case, additional subcategories must be established. These subcategories are defined by the positions of the basic point E of the first subframe and all As of the second up to the last subframe within a frame cycle. For this reason, the number of subcategories depends on the subframe count. Four subframes within a frame cycle lead

to two subcategories. The requirement for the first subcategory for the condition of four subframes in PH2 is $A_{SF3} > E_{SF1} > A_{SF4}$. The resulting color sectors are listed in Table 3.7. For example, the fourth color sector would be created by applying the set theory operation $(SF2 \cap SF3) \setminus (SF1 \cup SF4)$ derived from the general difference set in Formula 3.36.

TABLE 3.7: Color sectors resulting from the interaction of four subframes within one frame cycle during PH2 under the requirement of $A_{SF3} > E_{SF1} > A_{SF4}$.

Color Sector	Subframe Interaction (4SF)					
	Union (U_1)	SN	Intersection (I)	SN	Union (U_2)	SN
1	(—)	[—]	(SF1)	[1]	(SF2 ∪ SF3 ∪ SF4)	[9]
2	(—)	[—]	(SF1 ∩ SF2)	[5]	(SF3 ∪ SF4)	[7]
3	**(—)**	[—]	(SF1 ∩ SF2 ∩ SF3)	[8]	(SF4)	[4]
4	(SF1)	[1]	(SF2 ∩ SF3)	[6]	(SF4)	[4]
5	(SF1)	[1]	(SF2 ∩ SF3 ∩ SF4)	[9]	(—)	[—]
6	(SF1 ∪ SF2)	[5]	(SF3 ∩ SF4)	[7]	(—)	[—]
7	(SF1 ∪ SF2 ∪ SF3)	[8]	(SF4)	[4]	(—)	[—]

Note. U_1 = first union of sets; U_2 = second union of sets; I = intersection of sets; SN = substitution number; ∩ = intersection of sets; ∪ = union of sets.

The requirement for the second and last subcategory is $A_{SF2} > E_{SF1} > A_{SF3}$ which results in a color sector chronology as described in Table 3.8.

TABLE 3.8: Color sectors resulting from the interaction of four subframes within one frame cycle during PH2 under the requirement of $A_{SF2} > E_{SF1} > A_{SF3}$.

Color Sector	Subframe Interaction (4SF)					
	Union (U_1)	SN	Intersection (I)	SN	Union (U_2)	SN
1	(—)	[—]	(SF1)	[1]	(SF2 ∪ SF3 ∪ SF4)	[9]
2	(—)	[—]	(SF1 ∩ SF2)	[5]	(SF3 ∪ SF4)	[7]
3	(SF1)	[1]	(SF2)	[2]	(SF3 ∪ SF4)	[7]
4	(SF1)	[1]	(SF2 ∩ SF3)	[6]	(SF4)	[4]
5	(SF1 ∪ SF2)	[5]	(SF3)	[3]	(SF4)	[4]
6	(SF1 ∪ SF2)	[5]	(SF3 ∩ SF4)	[7]	(—)	[—]
7	(SF1 ∪ SF2 ∪ SF3)	[8]	(SF4)	[4]	(—)	[—]

Note. U_1 = first union of sets; U_2 = second union of sets; I = intersection of sets; SN = substitution number; ∩ = intersection of sets; ∪ = union of sets.

For the inclusion of five subframes during PH2, three subcategories need to be distinguished under consideration of the first assumption of $A_{SF4} > E_{SF1} > A_{SF5}$, the second assumption of $A_{SF3} > E_{SF1} > A_{SF4}$, and the third assumption of $A_{SF2} > E_{SF1} > A_{SF3}$. The subcategory requirements for even higher subframe counts can be determined applying the same pattern.

The general calculations of the color sectors for PH3 — as illustrated in Figure 3.9 — are trivial since there are no overlapping subframes within one frame cycle (see Section 3.5.1 for phase definition). A retinal zone stimulated by a single subframe (first subframe = first color sector) is always followed by a gap with no light stimulation (second color sector) which is followed by a subframe stimulated zone (second subframe = third color sector). This process goes on until the last subframe is reached, i.e., the number of color sectors depends on the subframe count (see Formula 3.37). Three or four subframes within a frame cycle would result in five or seven color sectors, respectively. Moreover, the determination of explicit subframe combinations for PH3 by applying the set theory (intersections, unions, and differences) is obsolete because there are no overlapping single subframes. Consequently, there are no subframe combinations to be calculated. The retinal areas of the color sectors and their borders are defined by the edges of the included subframes' rhomboid structure (retinal positions of the As and Es), which are already available without further calculation.

3.6 Subframe Body Integration

The single subframes characterized in Section 3.4 are now temporally summated to determine the position-dependent profile of retinal stimulation with regard to the perceived light intensity and mixed color characteristics (see Section 3.6.3). However, before such a stimulation profile can be established, some fundamental features for the process of subframe fusion must first be defined in Sections 3.6.1 and 3.6.2.[18]

3.6.1 Temporal Summation

Figure 3.10 is a schematic reference to the EOC, and illustrates three subframe bodies as the representations of three subframes of one frame cycle in a space-time-intensity plot during PH1 (building on Figure 3.7).

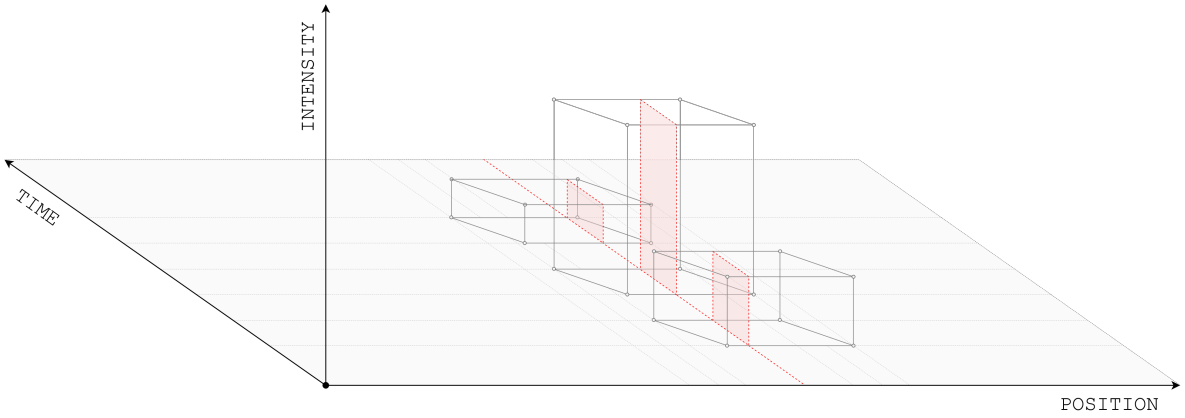

FIGURE 3.10: Space-time-intensity plot with positional slice (red dashed line) cutting through the subframe bodies (three SFs, full FC, EOC, PH1), revealing their slice planes (pale red surfaces).

A positional slice (red dashed line) cuts through the illustrated subframes. The resulting slice planes of the single subframes (pale red areas) represent their retinal stimulation with a defined light intensity over a certain period of time at the exact retinal position of the slice. In other words: The integral of a subframe's luminance level (see Section 3.4.2) over the subframe's on-time ($TP_{SF\,ON}$) represents the perceived light intensity at the determined position. Consequently, the light intensities of all three subframes have to be added up to determine the magnitude of light perception within a full frame cycle (TP_{FC}). Theoretically, the integration process can be extended even across multiple frame cycles. However, human visual perception limits the maximum time period for temporal summation. Thresholds of temporal summation for model specification are discussed in the following subsection.

Limits of Temporal Summation

The process of temporal summation of human vision is described by Bloch's law (1885) and is generally defined as follows:

$$Response = Intensity \times Time \tag{3.38}$$

The law is valid only for a "critical duration" (Hartline, 1934, p. 242) for which a complete integration of light energy over time can be assumed. In this thesis, the time period is called Bloch time (BT). Visual stimuli that fall within BT are summed up whereas stimuli that exceed those limits are not or at least not fully considered for temporal summation. On basis

[18] The MATLAB code on the model's process of temporal summation can be found in Segment X.

of a simplified assumption, the BT for temporal summation shows a fixed threshold of 0.05 s for cones and 0.10 s for rods (Hood and Finkelstein, 1986, as cited in Blake & Sekuler, 2006, p. 99).[19] Since the color characteristics of the CBU effect are the central attribute of interest, the threshold value of the color-sensitive cones is of paramount importance. Therefore, the cone threshold value of 0.05 s is used for comparisons with frame/subframe timings in digital imaging.

Summation of single Subframes

First, the limits of temporal summation are discussed for a single subframe as the smallest stimulation unit. The procedure of temporal summation is legitimate as long as the presentation time of one subframe does not fall below BT. Hence, Formula 3.39 must hold true:

$$TP_{SFON} \leq BT \tag{3.39}$$

By substituting the time period TP_{SFON} ($= DC/SFR$), the corresponding threshold subframe rate for temporal summation SFR_{TS} can be determined. The threshold subframe rate SFR_{TS} is not allowed to fall below 6.0 Hz under assumption of a DC of 0.3 and a BT of 0.05 s (see Formula 3.40).

$$SFR_{TS} \geq (DC \,/\, BT) \tag{3.40}$$

On the one hand, such low rates below SFR_{TS} are irrelevant in practical display unit application and, on the other hand, such values are blocked by the model anyway (see following subsection). In summary, the complete temporal summation within subframe presentation time is given in every model case.

Summation within Frame Cycles

Formula 3.41 states that the presentation time of all subframes within one frame cycle must not overshoot the BT to ensure the complete temporal summation of the emitted light intensity of all subframes. This is necessary to maintain the fundamental principle of color image creation on an FSC display system, which is based on the temporal summation of all subframes within a full frame cycle:

$$(TP_{FC} - TP_{SFOFF}) \leq BT \tag{3.41}$$

For this purpose, the following Equation 3.42 for the determination of the corresponding frame rate threshold of temporal summation FR_{TS} has to hold true:

$$FR_{TS} \geq [1 - (1 - DC) \,/\, SF_{CT}] \times BT^{-1} \tag{3.42}$$

[19] The BT for temporal summation of rods and cones is not stable but rather variable with changing conditions. The BT alters when changing the size of the stimulated area or the background luminance (Barlow, 1958), the retinal position or the state of light adaptation (Stewart, 1972; Ueno, 1978; Zuidema et al., 1981). Even changing the movement velocity of a stimulus (Burr, 1981) or switching between monocular and binocular viewing conditions reveals BT differences (Ueno, 1977). Therefore, a stable BT for rods or cones is a simplified assumption that does not hold for all conditions. Nevertheless, a fixed and balanced BT is chosen to reduce the complexity of subsequent calculations based on the BT (see following subsections). Furthermore, the origin of Bloch's law refers to visual stimulations with light intensities at detection threshold level, i.e., psychophysical research on the characteristics of temporal summation is mostly based on detection tasks. However, applying discrimination tasks or visual masking techniques confirms that the human visual system can execute comparable temporal integration processes for light stimuli at extremely low light levels (Holmes et al., 2017) and suprathreshold levels (Takayuki, 1994; Ueno, 1976). The confirmation of temporal summation at suprathreshold level validates the CBU model's approach of light intensity integration within and across subframe borders since light stimulation of display unit applications lies above the detection threshold. A full translation of the original paper of Bloch (1885) including a contemporary research review is provided by Gorea (2015).

Formula 3.42 can be derived from Formula 3.41 by substituting the time periods $TP_{FC} = 1/FR$ and $TP_{SF\,OFF} = (1 - DC)/SFR$. Under the previous assumptions of a stable DC of 0.3 and a fixed BT of 0.05 s, the imaginary increase of the subframe count within one frame cycle towards infinity leads to an asymptotic approximation towards the threshold frame rate for temporal summation FR_{TS} of 20.0 Hz. By avoiding frame rates below 20.0 Hz, it is impossible to violate the requirement that all subframes within one frame cycle are presented within BT. Accordingly, model calculations will be limited to $FR \geq 20.0$ Hz. This lower frame rate limit still makes it possible to analyze the effects of frame rates on CBU perception in the lower frame rate sector, which can be highly relevant for certain applications and is therefore of particular interest. Moreover, the lower frame rate limit does not require to consider negative side effects such as flickering.[20]

Summation across Frame Cycles

In addition to defining the principal conditions for temporal summation within one frame cycle, it is very important that the model defines the maximum time period for temporal summation. This has a fundamental impact on the color and intensity characteristics of the calculated CBU perception. The most obvious solution for the determination of the limits of temporal summation would be to take the determined BT of 0.05 s as threshold. The included amount of full frame cycles $FC_{CT\,(TS)}$ within the limits of temporal summation defined by BT can generally be calculated with Formula 3.43:

$$FC_{CT\,(TS)} = \lceil\, BT \times FR + (1 - DC) \,/\, SF_{CT} \,\rceil \tag{3.43}$$

However, the calculated integer frame cycle count $FC_{CT\,(TS)}$ is only valid as long as the following Equation 3.44 holds true. The equation tests the requirement that the threshold of temporal summation defined by BT lies within the time period in which the last subframe of the relevant frame cycle is switched off (lower/upper temporal limit is represented by the equation's left/right term in square brackets, respectively). If the equation does not hold true, the threshold time of temporal summation would separate subframe structures within the frame cycle number equal to the frame cycle count $FC_{CT\,(TS)}$:

$$[\, FC_{CT\,(TS)} \,/\, FR - (1 - DC) \,/\, FR \times SF_{CT} \,] \leq BT \leq [\, FC_{CT\,(TS)} \,/\, FR \,] \tag{3.44}$$

The pitfall of a fixed threshold for temporal summation is that Equation 3.44 does not hold true in most cases. A radical application of a fixed BT likely interrupts a frame cycle in progress. For the EOC conditions (see Table 3.2), a fixed BT of 0.05 s would interrupt the off-time of Subframe 14 within the fifth frame cycle (frame rate of 90.0 Hz, three subframes within one frame cycle). This is problematic because the main aim of temporal summation is not to split frame cycles (see previous subsection). Splitting frame cycles would have negative effects on the calculations of color specifications (see Section 3.6.3). Furthermore, a fixed threshold is not supported by the fact that the BT varies as soon as the surrounding conditions change (see Footnote 19). How to deal with this issue? On the one hand, shifting the threshold of temporal summation up or down the time axis towards the nearest frame cycle transition would solve the problem of dividing single frame cycles. On the other hand, it would suspend the comparability of the model output for different conditions. Comparability, however, is critical since the model is designed to compare CBU effects under different conditions. For example, model input parameters such as the frame rate could be changed to compare the resulting CBU effects (see Chapter 5).

[20] Empirical findings on flickering during a pre-testing phase of COBUS1 are provided in Appendix B.2.1.

A fixed threshold at 0.05 s has another disadvantage. For a lot of conditions, a multitude of frame cycles would have to be temporally summed up. The higher the frame rate, the larger the amount of frame cycles. However, the calculated color characteristics based on temporal summation of more than one frame cycle can deviate strongly from the color structure actually perceived by the viewer. For a PH1 example, the classic color structure reported by a viewer includes CBU effects at the leading and trailing edges and white unbiased content in the middle of the stimulus (see Figure 3.8). By implementing the discussed approach, the color structure determined by the model will deviate from a viewer's average subjective perception, particularly if the stimulated retinal areas of the included frame cycles partially overlap. This problem occurs when saccades are executed while the content is stable (slow saccade to stay in PH1) or when the viewer's pursuit eye movements do not follow the moving content precisely. The distorted model output might be a colored stimulus that could have no white shares at all. For precise pursuits, as assumed in the EOC, the inclusion of multiple frame cycles would not lead to such a discrepancy between model output and subjective perception. The stimulated areas — corresponding to the EOC's five frame cycles within the *BT* limits (rounded up) — are fully congruent on the retina. However, the model should work for all conditions for which it is developed.

An alternative would be to execute temporal summation for a single frame cycle only. This approach would result in a more robust color representation for the conditions mentioned above, because there are no partially overlapping frame cycles that can be summated to a color-distorted CBU reproduction. However, this will affect comparability, especially when the frame rate as model input parameter is varied and the outcomes have to be compared. Lowering the frame rate increases the cumulated subframe-on-time within one frame cycle. This does not mean that the content of a video sequence (succession of multiple frame cycles) which is presented at lower frame rates is perceived as brighter — this is not the case at all. In fact, brightness does not change when the frame rate is changed because the perception of brightness is triggered by a sequence of more than one frame cycles which lie within the limits of temporal summation. A cumulation of the subframes' on-times within the limits of temporal summation for lower and higher frame rates leads to the same result. The only difference is that for lower frame rates, the on-times of the included subframes are longer while less subframes lie within the limits of temporal summation. These two aspects cancel each other out. It follows that a model-based CBU calculation of light intensity considering only one frame cycle is not representative for a viewer's actual CBU perception provoked by a sequence of more than one frame cycle.

One solution could be a two-step process. First, the color structure and light intensity of the predicted stimulation are calculated based on a closed frame cycle's temporal summation. Second, the predicted intensity for one frame cycle is scaled up to the final CBU score (see Section 3.7.3). The scaling factor refers to the total amount of relevant frame cycles that actually contribute to the predicted perception. The count of contributing frame cycles $FC_{CT\,(CTB)}$ depends either on the eye or the content movement behavior defined by its movement velocity (*EMV* or *CMV*) and the distance of the movement path (*EMD* or *CMD*), see Formulas 3.45 and 3.46:

$$FC_{CT\,(CTB)} = (EMD_{EYE} \,/\, EMV_{EYE}) + 1 \tag{3.45}$$

$$FC_{CT\,(CTB)} = (CMD_{EYE} \,/\, CMV_{EYE}) + 1 \tag{3.46}$$

The correct choice between both Formulas 3.45 and 3.46 depends on the eye and content movement patterns (CAT2 or CAT3) and aspects of timing. However, the finally calculated frame cycle count $FC_{CT\,(CTB)}$ is always an integer no matter which of the two formulas is

applied.[21] For the determined EOC input parameters, a total of 55 frame cycles are contributing to the model prediction. By applying a scaling factor, the total occurrence time of the model-predicted stimulus is also taken into account. This is another positive aspect since it can be assumed that the extension of a stimulus' occurrence time — potentially including CBU shares — will lead to a higher CBU rating by the observer, even if the characteristic of the CBU effect itself remains unchanged. Weighing the pros and cons, implementing this approach into the model code can be considered a promising solution.

3.6.2 Retinal Scanning

The next intermediate step is to determine an accurate description of the perceived light intensity and color characteristics of every retinal spot within the zone of light exposure. To provide such a description, the whole zone of light exposure (or area of retinal stimulation) is scanned by a multitude of positional slices as described in Section 3.6.1. The result of every single scanning procedure is the perceived intensity and color specification for all relevant subframes within the frame cycle of choice (FCC).[22] It must be emphasized that the intensity levels and color characteristics of the single subframes are not yet summated. To get the perceived intensity values of the single subframes, it is necessary to determine the integral of light intensity (luminance) over the subframe's on-time referring to the retinal spot defined by the positional slice. Since the maximum on-time of one subframe does not exceed the threshold of temporal summation, this procedure is always valid (see Section 3.6.1). The color characteristics of the single subframes do not change over time. Therefore, the already established color specifications for the single subframes still apply (see Table 3.2). In general, the amount of relevant subframes to be considered varies for different retinal spots. For some spots, the characteristics of all subframes must be determined (see red positional slice in Figure 3.10). Other spots only require the calculation of one or two subframes.

$$SCN_{RES} = 0.0005^{\circ} \tag{3.47}$$

The stimulated retinal area is scanned with an accuracy specified by the scan resolution SCN_{RES} (see Formula 3.47), defined by the angle between two adjacent scanning lines at retinal level. The finer the resolution, the higher the degree of precision for the calculations across the stimulated area. However, the default value for the scan resolution is chosen to achieve sufficient accuracy without causing excessive computing time.

[21] All calculations on the frame cycle count assume that eye/content start their movement at the same time and that the content disappears directly after the stop point is reached (see Section 3.3.2). The frame cycle count $FC_{CT\,(CTB)}$ for CAT2 is calculated on basis of the eye movement duration (EMD_{EYE}/EMV_{EYE}) as no content movement is executed (see Formula 3.45). Regarding CAT3, two different scenarios have to be distinguished. First scenario: content movement duration is equal or longer than eye movement duration. The frame cycle count is calculated on basis of the eye movement duration (EMD_{EYE}/EMV_{EYE}) since CBU only occurs as long as eye movement is in progress (see Formula 3.45). Otherwise, the conditions would be categorized as non-CBU provoking CAT1. Second scenario: content movement duration is shorter than eye movement duration. The frame cycle count is calculated on basis of the content movement duration (CMD_{EYE}/CMV_{EYE}) as the content disappears after reaching the stop point of its movement path (there is no CBU without content presentation, see Formula 3.46). The calculated frame count considering eye/content movement distance and velocity is increased by 1 to include the first frame in start position. The calculations of the frame cycle count as a scaling factor for representative model indices are provided in MATLAB Segment III. The model calculated frame cycle count is always an integer as the model input parameters of eye/content movement distance in [px] and eye/content movement velocity in [px/fr] are always positive integers (see Segment IV).

[22] Out of all frame cycles of the modeled sequence, one frame cycle is chosen for the process of temporal summation. The FCC corresponds to the most central content position at display level and therefore features the highest angular eye movement velocity during presentation (display position-dependent angular velocity due to the plane display unit). Consequently, the FCC shows the highest CBU effect compared to other frame cycles (largest angular color distortion in eye movement direction). Regarding the EOC, the 27th out of 55 contributing frame cycles is chosen for temporal summation.

The number of executed scans SCN_{CT} is calculated with Formula 3.48 under consideration of the scan resolution and the area of retinal stimulation, reaching from the positions P of the first subframe's basic point A (scan start) to the last subframe's basic point E (scan stop) within the FCC:

$$SCN_{CT} = | P_{A\,(FC1/SF1)} - P_{E\,(FC1/SF3)} | \,/\, SCN_{RES} + RBP \tag{3.48}$$

Regarding the scan count, the positions of all rhomboid basic points (RBP) of the integrated subframes within the FCC are also included as important scan positions with changing intensity levels. Again, three included subframes within one frame cycle are assumed. For the determined EOC conditions, 4,625 scans are performed.

3.6.3 Subframe Fusion

The following subsection describes the determination of the ultimately perceived light intensity and the mixed color characteristics based on the additive color mixing of light. The calculations on subframe interactions are performed for the FCC. Analogous to the determination of the perceived light intensity and color characteristics for all single subframes (see previous subsection), the intensity and color characteristics after subframe fusion are calculated for every scanning line position within the stimulated retinal area. The calculation procedure for color mixture described by the Equations 3.49 to 3.57 is taken from Hunt and Pointer (2011, pp. 46–48) as well as Berns (2019, pp. 63–67). The first step of the procedure is to calculate the tristimulus values X, Y, and Z of the single subframes from their x/y chromaticity coordinates and their light intensity levels Y.[23] The calculations with the Equations 3.49 to 3.51 have to be executed separately for the first subframe (X_{SF1}, Y_{SF1}, Z_{SF1}), the second subframe (X_{SF2}, Y_{SF2}, Z_{SF2}), and the third subframe (X_{SF3}, Y_{SF3}, Z_{SF3}) for all scan positions:

$$X_{SF} = x_{SF} \times (Y_{SF} \,/\, y_{SF}) \tag{3.49}$$

$$Y_{SF} = Y_{SF} \tag{3.50}$$

$$Z_{SF} = (1 - x_{SF} - y_{SF}) \times (Y_{SF} \,/\, y_{SF}) \tag{3.51}$$

In a second step, the calculated tristimulus values X, Y, and Z of the single subframes can be added with respect to the additive color mixing of light. This results in the tristimulus values X_{MIX}, Y_{MIX}, and Z_{MIX} of the originating mixed color. Temporal summation of all subframes within one frame cycle is guaranteed under all circumstances that are covered by the model (see Section 3.6.1). Hence, temporally summing the subframes of the FCC is always permitted. Again, the calculations have to be executed for all scan positions. The stated Formulas 3.52 to 3.54 refer to the summation of all three subframes within the chosen frame cycle. However, depending on the position of the scanning line, different subframe combinations have to be summated. To calculate the tristimulus values of the mixed color for different subframe combinations (e.g., summation of only two subframes), the equations

[23] The x/y chromaticity coordinates for the three RGB subframes of the EOC are provided in Table 3.2. The light intensity Y has to be a photometric measure. The general choice of the luminance level L_v in [cd/m^2] is application-oriented (projector/screen). In this context, the integral of luminance level over time must be considered as the single subframes' light intensity Y (see previous subsection). This is essential for an accurate calculation of the subframe fusion as the duration of light emission during single subframe presentation is not the same for different positional slices. Position-dependent duration of light emission is existent between a subframe's basic points A and G and the basic points C and E (see rhomboid structure). To calculate the eventually perceived light intensity and the mixed color characteristics, luminance values must be weighted with a factor of time.

can be modified by removing the corresponding terms from the equations:

$$X_{MIX} = X_{SF1} + X_{SF2} + X_{SF3} \tag{3.52}$$

$$Y_{MIX} = Y_{SF1} + Y_{SF2} + Y_{SF3} \tag{3.53}$$

$$Z_{MIX} = Z_{SF1} + Z_{SF2} + Z_{SF3} \tag{3.54}$$

The last step is to convert the mixed color's chromaticity coordinates x_{MIX}/y_{MIX} and the finally perceived light intensity Y_{MIX} after subframe fusion from the mixed color's tristimulus values X_{MIX}, Y_{MIX}, and Z_{MIX} by applying Formulas 3.55 to 3.57 for all scan positions:

$$x_{MIX} = X_{MIX} \,/\, (X_{MIX} + Y_{MIX} + Z_{MIX}) \tag{3.55}$$

$$y_{MIX} = Y_{MIX} \,/\, (X_{MIX} + Y_{MIX} + Z_{MIX}) \tag{3.56}$$

$$Y_{MIX} = Y_{SF1} + Y_{SF2} + Y_{SF3} \tag{3.57}$$

Based on the determined EOC conditions (see Table 3.2), the left-side graphic in Figure 3.11 schematically illustrates the perceived light intensities of each scan position (gray lines as scanning lines), allowing an *intensity profile* to be determined along the stimulated retinal area (red line).

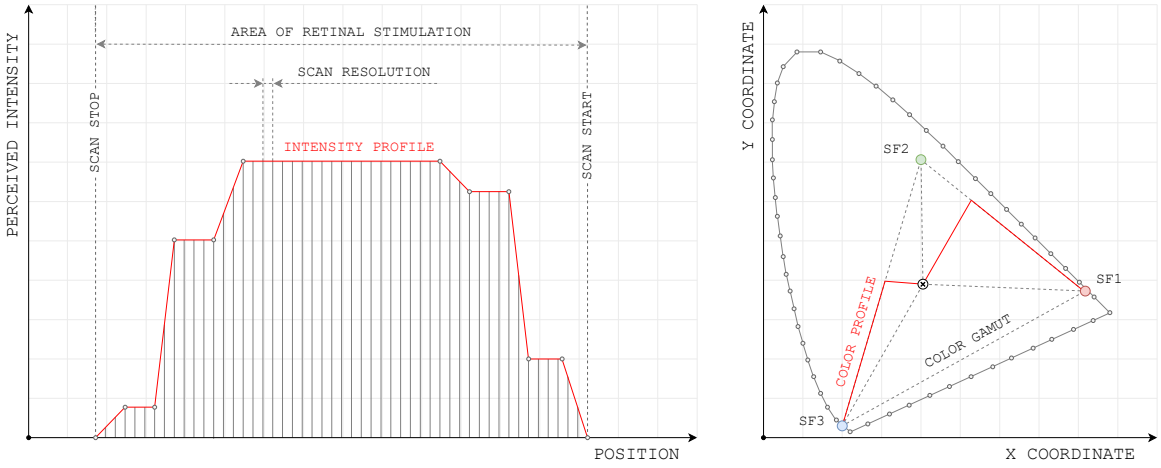

FIGURE 3.11: Intensity profile across area of retinal stimulation (left graphic, red line = intensity profile, vertical gray lines = scanning lines for retinal scanning) and color profile in CIE chromaticity diagram (right graphic, red line = color profile, red dot = first subframe, green dot = second subframe, blue dot = third subframe, white dot = harmonized mixed white color from all subframes, black cross = modified D65 as reference white point, dashed lines = color gamut of applied projector, see Appendix A.3.1, gray outline = spectral locus of 2.0° CIE 1931 color space) referring to the EOC.

Additionally, the full *color profile* over the stimulated retinal area for the EOC can be illustrated by applying the CIE chromaticity diagram (see Figure 3.11, right side). The color profile is visualized by a red line which in this case refers to a PH1 color profile derived from its course in the chromaticity diagram. The color profile starts at the right corner of the subframe color gamut representing a red color hue (only red subframe stimulates retina, coordinates are $x = 0.6912$ and $y = 0.3078$) and then goes over to a yellowish mixed color (mixture of red and green subframe), subsequently bending towards the unbiased white color characteristic (harmonized mixture of all subframes within the frame cycle, coordinates are $x = 0.3072$ and $y = 0.3147$ in close proximity to the modified D65 white point as reference). From that point, it changes into a cyan color characteristic as a mixture of green (second

subframe) and blue shares (third subframe). Finally, the color profile takes course towards its endpoint in the left corner of the gamut, which represents a blue color hue (only last blue subframe stimulates retina, coordinates are $x = 0.1527$, $y = 0.0240$). This is the classical sequence of color sectors in PH1: red – yellow – white – cyan – blue (see Section 3.5.2).[24]

3.6.4 Spatial Extension

Up to this point, the model simulation is determined only for the horizontal dimension of retinal stimulation. This has two reasons. First, the horizontal direction matters the most in terms of CBU genesis as the model only allows eye/content movement in horizontal direction (see Section 3.3.2). Second, the space-time-intensity plot that has been used to demonstrate aspects of retinal stimulation is limited to three dimensions (see Figure 3.10). Therefore, only one spatial dimension — the horizontal dimension — has been included. The vertical dimension would have found no place in a 3D coordinate system. However, the vertical dimension has to be added to allow the determination of retinal stimulation in all directions. Implementing this model add-on, the already determined intensity profile of retinal stimulation in horizontal direction (see left-side graphic in Figure 3.11) must be extended. The horizontal intensity profile is stretched vertically under consideration of the height of the displayed content at the retinal level (see Figure 3.12). The result is a schematic three-dimensional intensity body based on the temporal summation of all subframes within the FCC. The intensity body represents the perceived intensity in the horizontal and vertical directions at retinal level for the conditions determined by the EOC (see Table 3.2).

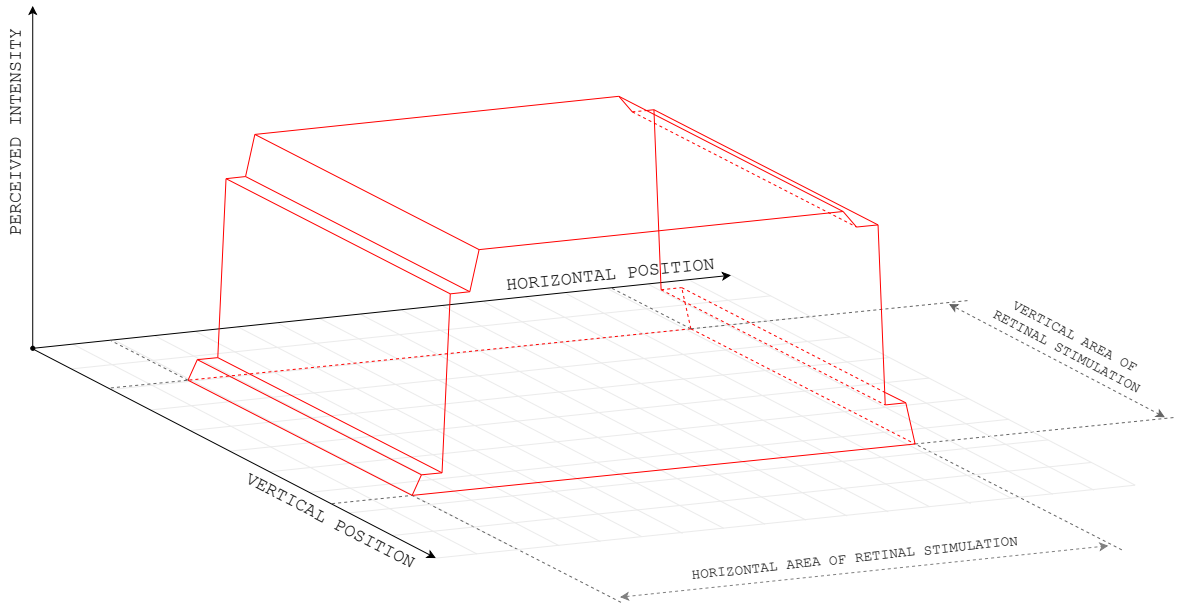

FIGURE 3.12: Schematic illustration of the intensity body's (red) retinal position-dependent (xy-plane) perceived intensity levels (z-axis) referring to the EOC.

Analogous to the temporal summation of visual stimuli (see Section 3.6.1), there is a spatial counterpart. The so-called spatial summation and its operating mode are described by

[24]The results of the model's subframe body integration are listed in matrix-structured tables in MATLAB Segment X (see XYL Table for chromaticity coordinates and XYZ Table for tristimulus values). The tables characterize all separately integrated subframes within the FCC as well as the resulting stimulation after temporal summation of all integrated subframes within the FCC (considering all retinal scanning positions within the stimulated retinal area). The x/y chromaticity coordinates and luminance levels L_v of the single subframes were harmonized to generate a mixed color that comes as close as possible to the modified D65 white point ($x = 0.3067$ and $y = 0.3180$, see Appendix B.1, reference to the EOC).

Ricco's law (1877), which essentially states that all stimuli that have the same product of stimulation intensity and stimulated area are equally detectable (see Equation 3.58):

$$Response = Intensity \times Area \tag{3.58}$$

Spatial summation has its anatomical genesis in the circuitry between retinal photoreceptors (rods and cones) and ganglion cells (and connecting intermediate cells such as horizontal cells, bipolar cells, and amacrine cells). Neural convergence in the connection between roughly 100 million photoreceptors and 1.25 million ganglion cells leads to the creation of receptive fields, which are of great importance for visual processing. These receptive fields are the reason for the ability of spatial summation. The process of spatial summation makes it possible to sum up all light stimulation within a receptive field to increase the eye's sensitivity and make very dim stimuli visible. The corresponding Ricco area (*RA*) defines the areal limits of full spatial summation (analogous to the Bloch time for temporal summation).[25]

The applicability of Ricco's law has strong limitations. First, it applies only to very small stimuli (referring to the *RA* size) within a limited areal around the fovea centralis (Blake & Sekuler, 2006). For a stimulus with a much larger retinal image than the region of spatial summation, "detection thresholds depend upon the stimulus luminance (or retinal luminance) and not on stimulus size" (Atchison & Smith, 2000, p. 103). A second limiting aspect must be considered: As previous explanations suggest, the origin of Ricco's law initially relates to visual stimulations at detection threshold level. There is no consensus in scientific research as to whether Ricco's law is also valid for suprathreshold light stimuli, which is the range of light emission during the use of display systems as the scope of the theoretical CBU model. Most of the previous research takes the position that spatial summation holds at detection threshold level but is reduced or even abolished for suprathreshold stimuli (Chirimuuta & Tolhurst, 2005; Legge & Foley, 1980; McIlhagga & Pääkkönen, 1999; Meese, 2004; Meese et al., 2005; Näsänen et al., 1998). More recent research attributes greater relevance to spatial summation at suprathreshold levels (Meese & Summers, 2007). However, even if spatial summation would occur to a relevant extent in suprathreshold stimuli, it can still be concluded that spatial summation — unlike temporal summation — is of no relevance to the theoretical CBU model, since it can be assumed that the areas of retinal stimulation during display application generally exceed the *RA* limits for which Ricco's law can be applied. As a consequence, spatial summation will not be considered in the model. However, irrespective of whether or not the size of a stimulated area contributes to the perceptual characteristics of a visual stimulation (e.g., regarding brightness or contrast), the areal size of CBU color distortion is used for model calculations on CBU perception (see Section 3.7).

3.7 Model Output

Having carried out all required calculations, the model output is now introduced based on model plots and indices referring to the EOC (see Sections 3.7.1 and 3.7.2).

3.7.1 Model Plots

Two standard model plots summarizing the previous model calculations are used for graphical illustration. Figure 3.13 illustrates an *intensity map* representing the levels of perceived intensity (z-axis) in horizontal and vertical direction at retinal level (xy-plane), based on the final result of temporal summation of all subframes within the FCC (compare with schematic illustration in Figure 3.12).

[25] Detailed information on spatial summation are provided by Blake and Sekuler (2006, pp. 71–110).

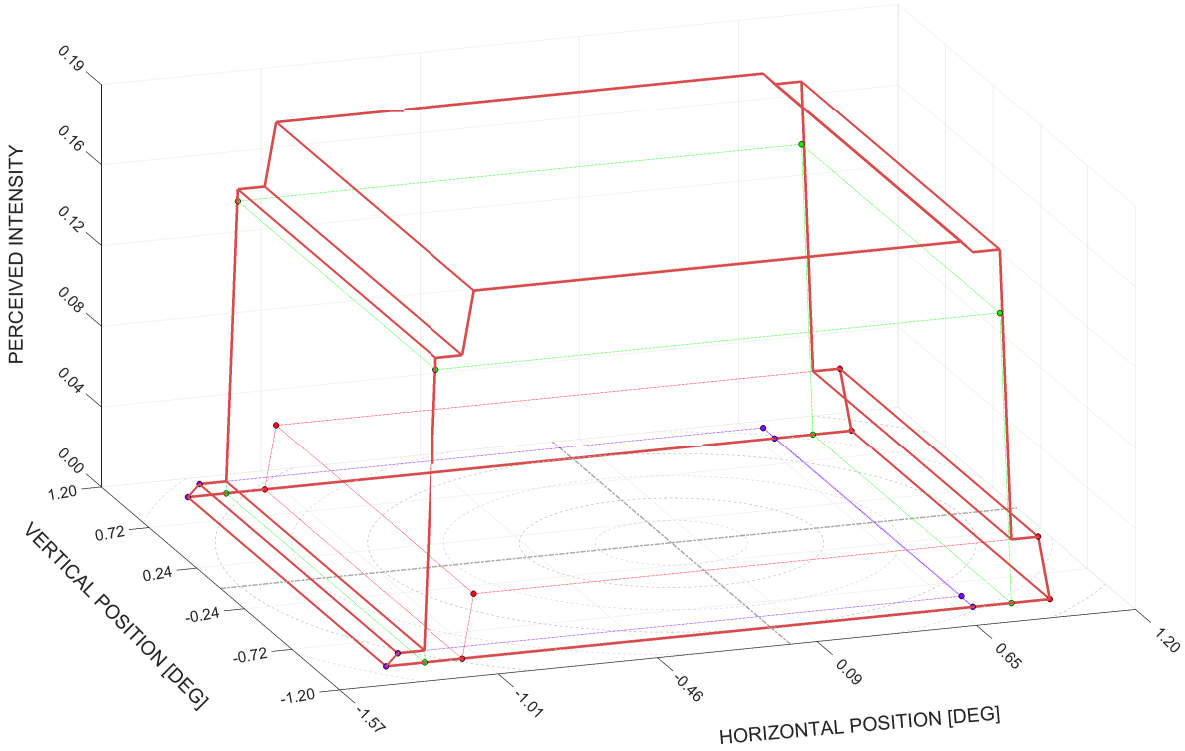

FIGURE 3.13: Intensity map plotted by the CBU model (based on EOC, see Table 3.2). Illustration of the retinal position-dependent (*xy*-plane) perceived intensity levels (*z*-axis) represented by the intensity body (red solid lines, temporal summation of all subframes within FCC) and the single subframe's intensity bodies (colored dotted lines, temporal summation of single subframe cycles within FCC); gray dash-dotted lines on *xy*-plane represent retinal center with fovea centralis as point of intersection, gray dashed circles illustrate retinal eccentricity steps of 0.25°.

Additionally, Figure 3.14 shows the *color map* at retinal level (*xy*-plane) which illustrates the resulting color characteristics of the CBU-provoking stimulus the viewer is confronted with. For the EOC, the CBU effect is classified into PH1. Colored artifacts at the leading and trailing stimulus edges frame the white unbiased content in the center of the stimulus.

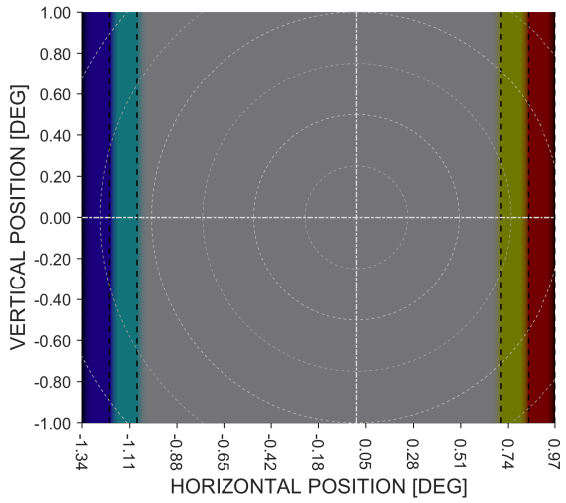

FIGURE 3.14: Color map plotted by the CBU model (based on EOC, see Table 3.2). Illustration of the mixed colors at retinal level in horizontal (*x*-axis) and vertical direction (*y*-axis) after temporal summation of all subframes within the FCC; gray dash-dotted lines represent retinal center with fovea centralis as point of intersection, gray dashed circles illustrate retinal eccentricity steps of 0.25°, black dashed lines represent borders between color zones.

Similar to the intensity map, the color map relates to the temporal summation within the single FCC at a relatively low frame rate of 90.0 Hz. As a result, the map's color representation is dimmed (e.g., unbiased white color zone is represented by a grayish area).[26]

3.7.2 Model Indices

Intensity and color map combined give a comprehensive graphical overview on the model findings (see Figures 3.13 and 3.14). However, some robust indices must be established as additional model output. These indices compress the complexity of the previous model calculations to single numbers.[27] Before the indices are introduced, two different kinds of zones of the intensity body in Figure 3.13 must be distinguished — the color-distorted zone representing the presence of CBU and the color-unbiased zone representing the absence of CBU. The intensity body's volume shares which are assigned to the CBU and the antagonistic non-CBU zones are calculated and used as representative indices. The volume shares of the intensity body are generally calculated by integrating the corresponding segments of the intensity profile function (see Figure 3.11) for each of the two zones. The intensity profile function represents the front surface of the intensity body (see Figure 3.13). By multiplying the result of the integration with the vertical dimension of the intensity body, the volume share for the CBU zones and the non-CBU zones can be determined separately. The borders that separate the zones have already been defined in Section 3.5.2.[28] Furthermore, a reference volume is calculated to classify the CBU and non-CBU index.

Color-Distorted Zones

The CBU index as a compressed model output allows a comparison with empirical study data (see Chapter 5). To calculate the corresponding CBU volume of the color-distorted zones, different mathematical approaches have to be applied for the relevant CBU phases (see Section 3.5.1). During PH1, the CBU effect occurs at the leading and trailing edges of the stimulus since not all subframes within the FCC are spatially congruent, leading to an incomplete summation. The volumes at both edges of the intensity body have to be added up to the final CBU-representing index $CBU_{IDX\,(PH1)}$ as described in Formula 3.59. To determine the volume at the leading edge VOL_{LE} and the volume at the trailing edge VOL_{TE}, the horizontal limits of the CBU effect at both edges must be determined. Therefore, the basic points of the subframes' rhomboid structure can be used. The zones of color distortion reach from the basic points A_{SF1} to A_{SF3} at the trailing edges and from E_{SF1} to E_{SF3} at the leading edges (three subframes within a frame cycle assumed):

$$CBU_{IDX\,(PH1)} = VOL_{LE} + VOL_{TE} \tag{3.59}$$

During PH2, the whole intensity body volume refers to CBU provocation because there is no color-unbiased zone, i.e., the calculation of $CBU_{IDX\,(PH2)}$ is straightforward as described

[26] The model's plots (intensity/color map) are defined in MATLAB Segment XIII. The mixed color effects illustrated in the color map refer to RGB triplet values (transferred from the existing XYZ tristimulus values).

[27] Model index calculations are performed in MATLAB Segment XI. Two different approaches are applied. The first approach considers the area of retinal stimulation while ignoring the intensity of retinal stimulation (Option 1). The second approach takes area and intensity of retinal stimulation into account (Option 2, as described by the intensity body in Figure 3.13). Both options are calculated by describing the stimulated retinal area in [mm] and [deg]. The finally applied model indices refer to Option 2 (angular values).

[28] The color sector borders are the foundation for model index calculations. The color sectors are determined considering the basic points A and E of the rhomboid subframe geometry. This leads to color deviations at the edges of the sectors due to the time variation of subframe light emission. As a consequence, the defined CBU zone and the corresponding index are underestimated, whereas the non-CBU zone/index is overestimated to the same extent (only in PH1, no error in PH2/PH3). For future model revisions, this can be avoided by defining color uniform sectors and color transition sectors that consider additional basic points (see Footnote 15).

in Formula 3.60. The total volume of the intensity body VOL_{TTL} lies within the horizontal borders of the complete area of retinal stimulation between A_{SF1} and E_{SF3}:

$$CBU_{IDX\,(PH2)} = VOL_{TTL} \tag{3.60}$$

The calculation of $CBU_{IDX\,(PH3)}$ is more complex, as it entails a decision on how to deal with the unstimulated gaps between the subframe-stimulated retinal zones. Put differently, the question is which approach best represents CBU perception in PH3? Even if the gap zones do not stimulate the retina, it seems unlikely that the gap size does not affect an observer's evaluation of perceived CBU intensity. Consequently, the total volume of the split intensity body VOL_{TTL} as the sum of the subframes' separated intensity bodies (see Formula 3.61) must be further processed:

$$VOL_{TTL} = VOL_{SF1} + VOL_{SF2} + VOL_{SF3} \tag{3.61}$$

Therefore, the ratio $R_{GP/SF}$ representing the relation between the horizontal dimensions of the unstimulated gap areas and the stimulated subframe areas is calculated with Formula 3.62. A gap width W_{GP} is always defined by the distance between the basic point E of a subframe and the basic point A of the subsequent subframe. The total width of subframe stimulation W_{SF} is defined by the dimension between its basic edge points A and E. The gap count depends on the amount of subframes included within one frame cycle. Assuming three subframes, two gaps need to be considered:

$$R_{GP/SF} = (\, W_{GP1} + W_{GP2} \,) \,/\, (\, W_{SF1} + W_{SF2} + W_{SF3} \,) \tag{3.62}$$

Besides the ratio $R_{GP/SF}$, an additional gap weighting factor WF_{GP} is included in the final formula for the calculation of the CBU index for PH3 (see Formula 3.63):

$$CBU_{IDX\,(PH3)} = VOL_{TTL} \times (\, 1 + R_{GP/SF} \times WF_{GP} \,) \tag{3.63}$$

WF_{GP} can be used to vary the weight with which the gaps contribute to the final CBU index. The default weighting factor WF_{GP} is 1.0, which means that both subframe-stimulated zones and unstimulated gap zones contribute to the final CBU index with equal weighting (changing the WF_{GP} to 0.5 would assign only half the weight of the subframe zones to the gap zones).

Color-Unbiased Zones

The antagonistic volume of the unbiased non-CBU zone must be calculated only for PH1 because there is no unbiased share in either PH2 or in PH3. The zone excluding the presence of CBU is always located in the horizontal center of the stimulus, framed by the CBU zones at the leading and trailing edges in horizontal direction:

$$NON\text{-}CBU_{IDX\,(PH1)} = VOL_{CTR} \tag{3.64}$$

The non-CBU index as described by Formula 3.64 is determined by the volume VOL_{CTR} of the central non-CBU zone which lies within the borders that go through the basic points A_{SF3} and E_{SF1}.

Reference Value

To put the established indices for the distorted CBU zones and the unbiased non-CBU zones in relation, a reference index REF_{IDX} is calculated. The reference index refers to the volume

of the intensity body for CAT0 conditions, i.e., a fixed content position and absence of eye movement (see Section 3.3.1).[29] For this condition, the complete intensity body is CBU-free. The total volume of the intensity body is identical to the intensity body's total volume in any other phase (PH1 to PH3). However, the total amount of perceived intensity (z-axis) is compressed onto a smaller retinal area (xy-plane) since the stimulation in horizontal direction is limited to the regular content width (no extended content width caused by eye movement during time-shifted subframe presentation, see Figure 3.4). This leads to the regular volume of the intensity body VOL_{REG} being equal to the reference index (see Formula 3.65). The reference index $REF_{IDX\,(PH0)}$ can be considered as the desired value and consequently is used to classify the calculated CBU and non-CBU indices:

$$REF_{IDX\,(PH0)} = VOL_{REG} \tag{3.65}$$

For the EOC with the defined frame rate of 90.0 Hz and the eye/content movement velocity of 36.0 deg/s (see Table 3.2 for further specifications), the indices $CBU_{IDX\,(PH1)}$ and $NON\text{-}CBU_{IDX\,(PH1)}$ are 0.0814 and 0.6232, respectively. Since the chosen example reflects the condition of PH1, the reference $REF_{IDX\,(PH0)}$ with a value of 0.7046 is the exact sum of both first mentioned indices.

3.7.3 Upscaling

It should be noted that all established indices generally refer to intensity bodies, as illustrated in Figure 3.13. The bodies are always based on the temporal summation of the subframes within one single frame cycle. As already described in Section 3.6.1, the inclusion of only one frame cycle has advantages, but also some important drawbacks, such as a lack of index comparability for changing model conditions (e.g., variable frame rates). The solution is to use the multiplier $FC_{CT\,(CTB)}$ to scale up the calculated indices for one frame cycle, as the multiplier considers the full amount of frame cycles contributing to CBU perception (see Formulas 3.45 and 3.46).[30] For the EOC, the contributing frame cycle count is $FC_{CT\,(CTB)} = 55$.

$$CBU_{IDX^*} = CBU_{IDX} \times FC_{CT\,(CTB)} \tag{3.66}$$

In Formula 3.66, the process of upscaling is described for CBU_{IDX^*} as an example (upscaled indices are marked with an asterisk). However, the remaining indices $NON\text{-}CBU_{IDX^*}$ and REF_{IDX^*} must also be scaled up as described in Formula 3.66. The upscaled EOC indices

[29] To allow a comparison between reference index and CBU/non-CBU index, the retinal position for which the reference is calculated is identical to the position of the FCC on which the CBU/non-CBU index is based.

[30] Calculating model indices for one FCC and multiplying them with the number of contributing frame cycles to establish comparable indices disregards the fact that the angular horizontal dimensions of CBU zones and non-CBU zones are different for every frame cycle of the modeled sequence (variable angular dimensions caused by different horizontal display positions of the frame cycles' corresponding content in combination with plane display unit). The FCC leads to the highest model indices due to the most central display position (per definition). Hence, the determined model indices (after scaling them up) overestimate the stimulation with color-distorted and unbiased content during the model sequence. However, the overestimation remains in acceptable limits with identical magnitudes for both stimulation types (color-distorted vs. unbiased). To compensate for variable angular zone dimensions across the display unit, an additional correction factor could be introduced. Alternatively, the temporal summation process could be separately applied for all frame cycles of the modeled sequence (considering different angular dimensions across the display unit). The calculated model indices for the CBU/non-CBU zones of all contributing frame cycles could be subsequently added up to the final model output. The approach is transferable to the CBU model as introduced in Chapter 3 since a model sequence always consists of an integer number of frame cycles. However, the loop function which uses the basic code of the model (see Chapter 5) cancels the requirement of integer frame cycles to determine model indices for a close meshed range of input parameters (leading to non-integer frame cycle counts in some cases). For non-integer frame cycle counts, the suggested approach is inapplicable and therefore discarded.

are 4.4760 for CBU_{IDX^*}, 34.2787 for $NON\text{-}CBU_{IDX^*}$, and 38.7548 for REF_{IDX^*}. These indices represent the essence of the model output for the defined conditions.[31]

3.8 Discussion

The model presented in Chapter 3 aims at predicting CBU effects for representative and well-defined conditions (see Section 3.3.2). The basis of the model is the Spatio-Temporal Intensity & Color Analysis — short STICA — which calculates position and timing as well as light intensity and color characteristics of all relevant single subframes as the smallest units involved in the genesis of CBU (see Section 3.4). The consideration of the interaction of relevant single subframes results in the position-dependent 3D profile of retinal stimulation (see Sections 3.5 and 3.6). The graphical illustration of the model results and further condensation of the model calculations into robust indices allow an adequate description and a clear distinction of the retinal areas with and without CBU (see Section 3.7). The original modeling goals, namely to provide graphical CBU reconstructions for visualization purposes and representative model indices for quantification purposes, were thus achieved (see Section 3.1). Thus, the model allows to gain insights at different levels, ranging from the genesis of CBU, to the impact of certain CBU determinants, to the classification of different CBU variants.

In summary, the current status of the introduced CBU model provides a solid basis for CBU prediction. However, the model could benefit from the implementation of some additional aspects. A critical review of other approaches for CBU evaluation and prediction may shed light on potential improvements to the presented model. The model's accuracy can be increased and the scope of application can be extended.

Other CBU evaluation and prediction methods are based on visualization or quantification processes (see Section 2.2.4). Objective CBU visualization is done either by applying a movable high-speed camera that simulates eye movement across a potentially CBU-provoking scenario (C.-H. Chen et al., 2008; C.-H. Chen et al., 2009; Y.-F. Chen et al., 2007b; Y.-K. Cheng et al., 2009; Hsu et al., 2007; Y.-P. Huang et al., 2009; Järvenpää, 2005; Koma & Uchida, 2003; F.-C. Lin et al., 2015; F.-C. Lin et al., 2012; F.-C. Lin, Huang, Wei, & Shieh, 2010; F.-C. Lin et al., 2019; F.-C. Lin, Teng, Chang, et al., 2016; F.-C. Lin et al., 2011a; Y.-J. Lin et al., 2018; Qin et al., 2018) or through computational CBU simulations by shifting and overlapping the field images to integrate them and simulate the final CBU image (H.-C. Cheng et al., 2010; Langendijk, 2007; Langendijk et al., 2009; Yoshida et al., 2011; Y. Zhang, Langendijk, Hammer, & Lin, 2011). For spatial shift calculations of the field images, frame rate and eye movement velocity are important factors, and additionally, color and brightness of the fields must be considered when overlapping and integrating them.

To quantify CBU effects rather than just visualize them, different theoretical formulas of variable complexity are applied — from simple formulas that only include the most relevant spatio-temporal factors such as frame rate, duty cycle, eye/content movement velocity, and stimulus width (S.-C. Chen et al., 2007; Y.-P. Huang et al., 2007; Koma & Uchida, 2003; Yan et al., 2007) to more comprehensive approaches that additionally consider the luminance characteristics of the content at a basic level (Sekiya et al., 2006) to even more elaborate approaches based on pixel level calculations (limited to ideal PEM) leading to a precise color and luminance description of the CBU stimulus (Wang, Zhang, Weng, et al., 2017). Another formula based on empirical investigations determines the field rate corresponding to the CBU detection threshold (Post et al., 1998; Post et al., 1997). However, most of the mentioned

[31] After executing the MATLAB function, the model indices are exported to an overview table. Relevant input parameters that define the model sequence are also listed. The table code is provided in MATLAB Segment XII.

formula approaches are tied to a specific technical setup, which limits their generality and utility. Device-independent methods avoid this problem by providing an objective content-based index. In most cases, such indices calculate the color differences between the ideal (original) image and the distorted CBU image on basis of the CIELAB (F.-C. Lin, Huang, Wei, & Shieh, 2010; Yang et al., 2016), CIELUV (Y.-P. Huang, Chen, et al., 2008; Kim et al., 2014; Yang et al., 2016), or CIEDE2000 color difference equation (Chang et al., 2012; Y.-P. Huang et al., 2009; F.-C. Lin et al., 2015; F.-C. Lin, Huang, & Shieh, 2010; F.-C. Lin et al., 2012; F.-C. Lin, Teng, Chang, et al., 2016; F.-C. Lin et al., 2011a; Teng et al., 2016). However, some of these color difference indices do not adequately represent subjective CBU perception. Therefore, Y. Zhang et al. (2012) proposed a new CBU index based mainly on the chromaticity difference between the single fields and the stimulus-to-background contrast. Another enhanced method related to the color difference indices determines a CBU metric at picture level by weighting certain high-potential CBU regions with a higher factor (F.-C. Lin et al., 2019; Y.-J. Lin et al., 2018; Qin et al., 2018). At last, vision-based methods go even one step further by considering the subjective response of the human visual system. With the goal of creating a robust single-valued index that is closer to the observer's actual CBU perception, spatio-temporal filtering of luminance and color-opponent channels of human visual perception are implemented (Y.-K. Cheng & Shieh, 2009; P. V. Johnson et al., 2014; Langendijk et al., 2006; Yi, 2008).

In comparison to the CBU model presented in this work, most of the other models use much simpler approaches with fewer variables (see simple CBU formula approaches) or apply a completely different calculation approach (see methods based on color difference equations) or pursue a different goal (see approaches for CBU visualization only). In addition, access to more complex and comparable models is limited in most cases, since their basic functionality is described by the available sources, but not the entire underlying CBU calculation procedure. This makes unrestricted traceability and direct comparability with the own model difficult, and does not even allow the transfer of useful model components. However, some external model descriptions — by P. V. Johnson et al. (2014) for instance — provide deeper insight, and therefore can be used to derive further model add-ons to improve the introduced model. In the following paragraphs, these adopted model add-ons and new proposals are discussed.

For example, viewer-related considerations could be integrated into the model to improve its output towards the actual subjective perception of a viewer. For this purpose, the current status of the model should first be classified. As the first stage of processing, the model determines the basal quantity of physical light stimulation that hits the retinal surface (see Section 3.4). Of course, the stimulation at retinal surface level is not equal to the final subjective perception by an observer. Additional steps of processing within the retinal layers as a second stage and further cognitive processing as a third stage have to be considered. For those deeper stages of processing, the wavelength-dependent sensitivity of the human eye (see Section 3.4.2) and the temporal summation of light stimuli (see Section 3.6) are implemented in the model. Furthermore, the process of spatial summation of light stimuli was discussed (see Section 3.6.4) but a model implementation proved irrelevant for the defined model conditions. However, some steps of retinal and cognitive processing are still missing. Implementation of the retinal and cognitive processing steps listed below would alter the general structure of the model and increase its depth. As a result, the model output would approximate the actual visual perception:

— eccentricity-dependent retinal sensitivity to light intensity and color (see Section 2.3.2) and its effect on the process of CBU perception (see empirical COBUS2 findings in Chapter 4 which could be used as foundation for a model add-on that implements position-dependent weighting factors)

— changes in visual perception during the execution of eye movements with a distinction between saccades and pursuits (see Section 2.3.2)

— state of light adaptation of the viewer's visual system based on the surrounding light conditions and its impact on the visual perception of color and intensity of light related to CBU perception (impact could be small, there is little research on this topic, see surrounding-based factors in Section 2.2.2)

— non-linear relation between objective visual stimulation and resulting subjective perception; filtering out separately the actually perceived light intensity and the visual area under consideration of the Weber-Fechner law (Fechner, 1860) or the Power law (S. S. Stevens, 1957) seems to be of particular importance, otherwise the impact of retinal light intensity exposure and stimulated retinal area on the model output does not appear balanced

— estimation of CBU perception and visibility based on spatio-temporal filtering in luminance channel and color-opponent channels (Y.-K. Cheng & Shieh, 2009; P. V. Johnson et al., 2014; Langendijk et al., 2006; Yi, 2008)

In addition, the implementation of other presentation-based factors such as specifications of the presented content and the applied hardware as additional model input parameters seems promising:

— contrast ratio between stimulus and background, which has a greater impact on CBU perception than the luminance level of the CBU stimulus itself; see Section 2.2.2 for overview and Y. Zhang et al. (2012) for implementation of contrast ratio during CBU index calculation

— variable switching behavior of the light sources during the transition time between on/off-status to extend the applicability of the model beyond the hardware components previously used (currently the model assumes an instant increase/decrease of the emitted light, which refers to the fast-switching LEDs applied, see Section 3.4.2)

Finally, some model-based aspects are listed, potentially leading to improvements of the model:

— differentiation between color sectors with uniform color characteristics and heterogeneous color sectors for color transitions (see Footnote 28 in Section 3.7.2)

— more flexible solution for the determination of the temporal summation limits, which gives greater consideration to the surrounding conditions (see Section 3.6.1)[32]

[32]The model-based calculations of a potentially CBU-provoking stimulus' color characteristics by temporally integrating a single frame cycle are suitable for most model conditions. However, the model does not represent a viewer's actual perception for all conditions. For example, the calculated color pattern of a fixed CBU-provoking stimulus during fast saccades (CAT2) under high frame rate conditions might not represent a viewer's actual perception. When viewing such a sequence, the CBU effect's color structure on the edges of the presented stimulus becomes complex (variety of spatially delimited mixed colors that deviate from the subframes' primary colors). It is assumed that such a color pattern does not result from the temporal summation of one single frame cycle's subframes but might rather originate from the overlapping of more than one frame cycle. Considering the spatio-temporal consequences of retinal stimulation for such conditions, a high frame rate leads to a fast repetition of sequential frame cycles with a small spatial offset between the frame cycles' content (even during fast saccades). A color-biased CBU effect with a complex color structure at the edges of the stimulus is the result. Such a color pattern that presumably originates from the overlapping of more than one frame cycle cannot be reproduced by the model's previous static concept of temporally summing up a closed frame cycle for all conditions. To meet all model conditions, more flexible temporal summation processes based on the present surrounding conditions have to be established.

— additional model index calculation process that considers specific color characteristics of the stimulated retinal areas (see Section 3.7.2)

— implementation of model structures that allow testing the effectiveness of various CBU compensation techniques such as Motion Interpolation (see Section 2.2.3)

— extension of the precise model indices to include a variability range (inter- and intraobserver variation) based on the data sets of the empirical COBUS series (see Chapter 4)

An alternative model index (see third bullet point) could calculate the volume shares of the intensity body as done previously (see Section 3.7.2), and additionally implement the color specification of retinal stimulation. This would be the most extensive approach, for which an additional color factor CF would have to be defined by the length of the vector between the position of the reference point and the position of the actual color point in the CIE xy chromaticity diagram (see Formula 3.67). The reference point refers to the unbiased color originating from the harmonized summation of all subframes within one frame cycle (e.g., white). The actual color point describes the CBU-biased color within the color-distorted zone (e.g., cyan):

$$CF = \sqrt{(x - x_{REF})^2 + (y - y_{REF})^2} \tag{3.67}$$

The color factor as defined in Formula 3.67 would have to be implemented after calculating the intensity profile across the area of retinal stimulation (see Section 3.6.3). By multiplying the perceived intensity with the color factor for every scan, the intensity profile would be modified under consideration of the color factor. The degree of color deviation would be incorporated. The subsequent procedure of spatial extension (see Section 3.6.4) and model index determination (see Section 3.7.2) would be maintained as described.

Finally, it is important that the newly introduced model keeps the balance between structural simplicity and predictive accuracy (see Section 3.3.3). In line with this principle, careful consideration must be given to which add-ons should ultimately be implemented. A suitable trade-off between over- and underfitting can be made using the established criteria of model selection.

Chapter 4

Color Break-Up Studies

4.1 Aim & Scope

After establishing a CBU model that predicts potential CBU perception on basis of theoretical calculations (see Chapter 3), the following chapter describes two empirical studies that investigated CBU perception using participant-based evaluations. Both Color Break-Up studies — COBUS1 and COBUS2 — analyzed the impact of hardware-based, content-based, or viewer-based factors on human CBU perception. Hence, young and healthy study participants (see Section 4.2.3) were invited to evaluate CBU effects provoked by different video sequence scenarios. The scenarios were presented with a DLP projector on a projection screen and controlled via CBU Scenario Player (see Section 4.2.4).[1]

The primary aim of COBUS1 was to investigate the impact of the display unit's frame rate and the luminance level of the CBU-provoking stimulus on CBU perception. In this context, the experimental arms of saccadic (CAT2) and pursuit eye movement (CAT3) were considered for CBU provocation. The results of COBUS1 provide the possibility to determine necessary hardware/content requirements for various settings that guarantee an acceptable CBU level (see Section 4.3.1). The secondary aim of COBUS1 was to investigate the influence of specific participant characteristics (visual performance, short-term state, and long-term personality traits) on CBU perception, and thus to explore the cause of interindividual differences in CBU perception.

The complementary goal of COBUS2 was to investigate subjective CBU perception in dependency of the size and position of the CBU-provoking stimulus. These stimulus-specific variables were tested during saccades and pursuits as in COBUS1. To the author's best knowledge, there is no robust quantitative research on the occurrence of CBU during stimulation of different retinal areas with different light sensitivities. New findings are of great interest for a more functional application of CBU compensation methods (see Section 4.4.2 and Chapter 6).[2]

In addition, the empirical data set of the COBUS series was used to evaluate the accuracy of the theoretical model-based approach for CBU prediction (see Chapter 5).

[1] The COBUS series was planned and executed in accordance with the ethical principles of the Declaration of Helsinki. COBUS1 and COBUS2 were approved in advance by the ethics committee (EC) of the FSU Jena. Both studies were reviewed separately by the EC. All required documents of COBUS1 (application form, study protocol, study information sheet, consent form, etc.) were submitted to the EC on 12th February 2019. After approaching the EC to personally present the project (5th March 2019), the proposal for study execution was accepted on 7th March 2019 without requiring any further amendments. Due to modifications of the study process, an amended proposal was submitted on 19th March 2019. The amendment was reviewed and finally permitted on 27th May 2019 without requiring any further rectification. The EC's approvals are documented and archived. COBUS1 was carried out between the 1st of April and the 9th of May 2019. The study documentation of COBUS2 was submitted to the EC on 16th January 2020. After personal presentation to the EC on 11th February 2020, the proposal for study execution was accepted on the same day. The EC's approval is documented and archived. COBUS2 took place from the 2nd to the 20th of March 2020.

[2] All investigated factors, target variables, and constants of the COBUS series are listed in the appendix in Tables H.1 (COBUS1) and H.2 (COBUS2).

4.2 Materials & Methods

4.2.1 Study Design

COBUS1 was designed as a prospective, monocentric, and multivariate cross-sectional study for hypothesis testing. Hypotheses H.1 to H.4 relate to the primary objective of COBUS1 to investigate the influence of the independent variables on the target variable of the study (subjective CBU perception):

H.1: Negative correlation between a display unit's frame rate and subjective CBU perception expressed by an exponential function.

H.2: Positive correlation between the luminance level of a CBU-provoking stimulus and subjective CBU perception expressed by a linear function.

Hypotheses H.1 and H.2 deal with assumptions *within* the subcategories of CAT2 and CAT3. In contrast, Hypotheses H.3 and H.4 refer to assumptions *across* the subcategories of CAT2 and CAT3:

H.3: Positive correlation between the length of a saccadic eye movement path (CAT2) and subjective CBU perception expressed by a power function.

H.4: Positive correlation between the velocity of pursuit eye movement (CAT3) and subjective CBU perception expressed by a linear function.

Hypotheses H.5 and H.6 correspond to the secondary objective of COBUS1 to investigate the influence of a viewer's visual performance (visual acuity, contrast sensitivity, and color vision) and personal characteristics (personality traits and current state) on his/her CBU perception:

H.5: Positive linear correlation between a viewer's visual performance and subjective CBU perception.

H.6: Positive linear correlation between a viewer's personal characteristics and subjective CBU perception.

COBUS2 was also designed as a prospective, monocentric, and multivariate cross-sectional study. However, both data collection and analysis were based on an exploratory approach (see results in Section 4.3.2).

4.2.2 Data Management

The study data were recorded in pseudonymized form. For this purpose, each participant was assigned a non-speaking pseudonym from which the identity of the participant cannot be deduced. To obtain unique participant identification numbers, a consecutive participant number was chosen. The assignment of a participant number to a participant's identity (full name and date of birth) is only possible via the pseudonymization list.

Data were collected via both a digital case report form (e-CRF, see Appendix A.2) and a direct software-based output of data in electronic form (CBU Scenario Player, see Appendix A.3.2). In accordance with the General Data Protection Regulation (GDPR), pseudonymized data collected through both the e-CRF and CBU Scenario Player were merged into a digital database through double data entry and protected from tampering by storage on an access-protected medium.

If the participant withdrew his/her consent to participate in the study (see Section 4.2.8), no further data were collected from the time of withdrawal. Data collected up to the point of withdrawal were not included in the final data analysis (only complete data sets were considered).

The originals of all essential study documents (e.g., consent form) will be kept for at least 10 years after completion of the study. All study documents are stored in a safe location and are kept confidential. The pseudonymization list is kept separately from the other study documents.

4.2.3 Inclusion and Exclusion

COBUS1 and COBUS2 aimed to include young volunteers between the ages of 18 and 35 years. The sample thus represented potential users of innovative technologies related to the described research. In addition, the sample should consist of equal numbers of male and female participants. All participants had to be healthy, i.e., they should not show any gerontological or pathological alteration of the visual system that would have impermissibly impaired their visual performance. Accordingly, the following exclusion criteria for COBUS1 and COBUS2 were set up.[3] All exclusion criteria related to the participant's visual system refer to monocular and binocular performance for COBUS1, but only to the dominant eye for COBUS2:

— maximum accommodative response < 4.0/5.50 D (COBUS1/COBUS2)

— visual acuity > 0.30 logMAR (test distance analogous to main examination)

— contrast sensitivity < 1.20 logCS (test distance analogous to main examination)

— prot-, deuter-, or tritanomaly (only COBUS2)

— prot-, deuter-, or tritanopia (COBUS1 and COBUS2)

— visual field defects of any kind (test area analogous to FOV of main examination)

— oculomotor dysfunction of any kind

— epilepsy

In COBUS2, the use of optical corrections of any kind (e.g., spectacles or contact lenses) directly led to the exclusion from study participation. To still ensure high visual performance, the spherical and cylindrical components of ametropia were limited to values below 0.75 D (myopia and hyperopia, dominant eye). In contrast, the use of a habitual optical correction

[3]Maximum accommodative response: The main study examination of COBUS1/COBUS2 was executed in a viewing distance of 0.58/0.29 m (participant to screen). The corresponding accommodative demand was 1.72/3.45 D. However, only two thirds of the maximum accommodative amplitude can be executed without stress for a longer period of time. Therefore, the maximum accommodative amplitude's threshold was 2.58/5.17 D. The exclusion criterion for the maximum accommodative response considers the calculated threshold. The maximum accommodative response during COBUS1 referred to the status with optical correction. During COBUS2, the maximum accommodative response was determined without optical correction. Visual acuity: The exclusion criterion is based on Hertenstein et al. (2016) that investigated 47 healthy participants (20–61 years) with FrACT (distance 2.5 m, photopic conditions) regarding normative values for visual acuity (MN = -0.12 logMAR, SD = 0.09). To exclude participants with a visual acuity that differs strongly from the standard values of a healthy sample, the exclusion criterion considers the fourfold SD: $-0.12 + 4 \times 0.09 = 0.24$ logMAR ≈ 0.30 logMAR (rounded up). Contrast sensitivity: The exclusion criterion is also based on Hertenstein et al. (2016), defining normative values of MN = 1.75 logCS, SD = 0.12 (N = 47, 20–61 years, FrACT in 0.5 m, photopic conditions). The exclusion criterion for contrast sensitivity considers the fourfold SD: $1.75 - 4 \times 0.12 = 1.27$ logCS ≈ 1.20 logCS (rounded down).

(e.g., spectacles or contact lenses) was generally allowed during COBUS1 as long as bifocals, trifocals, multifocals, or glasses with color filters were not used.[4] Furthermore, heterophoria greater than 10.0/5.0 prism diopters (horizontal/vertical) or heterotropia of any kind led to the exclusion from COBUS1 participation.

COBUS1 included a representative sample size of $N = 30$ (descriptive and confirmative stats possible, high effort to conduct study) as opposed to COBUS2 which was designed as a single case study ($N = 6$) for exploratory data collection and analysis (only descriptive statistics possible, no confirmative stats, reduced effort to conduct study).[5] A detailed characterization of the COBUS1/COBUS2 sample can be found in Sections 4.3.1 and 4.3.2.

4.2.4 Equipment and Devices

The following section lists all equipment and devices used during the planning and execution phase for the studies of the COBUS series.

Hardware Testing

The listed devices were used for initial testing of hardware components and surrounding conditions:

— projector lighting with spectroradiometer (Specbos 1211, JETI Technische Instrumente GmbH)

— projector timing with oscilloscope (TPS2024, Tektronix) including switchable gain detector (PDA36A2, Thorlabs)

— room illumination with luxmeter (Mini-Lux, MX-Electronic)

More detailed information on the listed devices and their application can be found in Appendix A.1.

Pre-Examination

The equipment used to test for suitability of potential participants and individual characteristics in different disciplines during pre-examination is listed below.[6] The applied tests

[4] Two options were evaluated for the determination of the participant's existing ametropia and its optical correction during COBUS1. The first option includes a subjective refraction and a subsequent correction of a potential ametropia with trial frame/lenses during examination (exclusion of refractive errors). The participant is optimally supplied during the inclusion/exclusion testing and the main examination phase. Furthermore, the size of the trial lenses and therefore the field of view through the trial lenses is the same for all participants (same corneal vertex distance assumed). The second option includes an objective refraction with autorefractor (preliminary investigation) and the use of the habitual correction during the study procedure. Option 2 allows a faster preliminary investigation (objective vs. subjective refraction) and leads to a sample's potentially wider visual acuity/contrast sensitivity range within defined exclusion criteria limits since small refractive errors are accepted (beneficial for investigation of the effect of visual performance variation on CBU perception). While both options offer specific benefits, the second option was chosen as it promised a higher level of the participant's attention/concentration during the time-consuming main examination phase (higher comfort due to habitual correction, faster pre-testing) which is of great importance for the quality of the test results. In addition, unacceptable limitations of visual performance caused by an inappropriate habitual correction were avoided with the defined exclusion criteria.

[5] The financial compensation for the participants was €15 per visit for COBUS1 and €30 per visit for COBUS2. The compensation was provided in full by the SeeReal Technologies GmbH.

[6] The dominant eye was only tested during COBUS2. Tests of phoria/tropia were only done during COBUS1. Color vision was tested with an anomaloscope and with color plates during COBUS1, whereas only color plates were applied during COBUS2.

and devices were selected with the primary consideration of a quick and reliable testing procedure during the COBUS series.

— habitual correction with lensmeter (VL3000, Visionix)

— objective refraction with autorefractor (i.Profiler, Carl Zeiss Vision GmbH)

— dominant eye with Hole-in-Card Test (Dominant Eye Test Card, USAEyes)

— accommodative amplitude with Push-Up and Push-Down Method via Smart Optometry (Version 3.4) presented on Galaxy S7 (Samsung)

— visual field with Amsler Grid via own illustration on T100T (ASUSTeK Computer Inc.)

— ocular motility with saccade/pursuit patterns via own illustration on T100T (ASUSTeK Computer Inc.)

— heterophoria/heterotropia with Cover-Uncover-Test (using occluder) and/or Maddox Rod Test (both VISUS GmbH)

— visual acuity via FrACT presented on Galaxy S7 (Samsung)

— contrast sensitivity via FrACT presented on ColorEdge CG246 (EIZO Corporation)

— color vision with anomaloscope (HMC Anomaloscope, OCULUS Optikgeräte GmbH) and/or color plates (Velhagen-Stilling Color Plates, Georg Thieme Verlag KG)

— questionnaire (self-developed)

A more detailed specification of the listed tests/devices and additional information on their application can be found in Appendix A.2.

Main Examination

The following hardware and software setup for the main study examination was selected to allow variation of technical and content-based factors (see Section 4.1) across a spectrum as wide as possible while eliminating or minimizing disruptive factors (e.g., inhomogeneity of luminance levels across the projection area):

— DLP projector (LightCrafter 4500, Texas Instruments) controlled via CBU Scenario Player (internal development of SeeReal Technologies GmbH)

— projection screen (Home Cinema Frame, Celexon Europe GmbH)

— eye-tracking system (Eyegaze Edge 600 Series, LC Technologies)

The technical specification of the listed equipment is provided in Appendix A.3.

4.2.5 Parameter Adjustment

Before launching the COBUS series, hardware limitations were investigated in a pre-testing phase. For example, not every luminance level and contrast ratio can be generated with the chosen DLP projector (see Appendix B.1). In this context, technical limitations of the projector (and the projection screen) as well as positioning of the hardware components have to be considered. The maximum luminance level that can be generated depends mainly on the projector's performance, the reflective characteristics of the projection screen and, of

course, the projection distance between projector and screen (reduction of luminance level regulated via LED current). The variability of the contrast ratio depends mainly on the applied color depth, for example, 1-bit color depth results in a fixed contrast ratio around 1.0 (only on- or off-mode for LED's possible, no intermediate luminance level steps realizable). A higher color depth allows to increase the variability of the contrast ratio to levels below 1.0. In turn, the choice of color depth has a direct impact on the maximum frame rate that can be displayed by the projector. The higher the color depth, the lower the maximum displayable frame rate (see Appendix B.2). Moreover, the duty cycle (fixed value of 0.3 during COBUS series) has an impact on the presentable frame rate range.

Characteristics of content creation such as movement patterns and velocities require consideration of additional limiting aspects (see Appendix C). When considering which patterns and velocities of content movement can be generated, projection and viewing distance are the main factors to keep in mind, as they determine the viewing angle for one pixel and the whole dimension of the projection area. These parameters determine the finite steps of feasible movement paths and limit the position and spatial dimension of the content presentation.

Moreover, content movement velocity and frame rate depend on each other, which means that not every combination is realizable. Limitations result from unfeasible combinations of content movement velocities and frame rates. Concluding, the considered parameters defining the study structure of the COBUS series are directly or at least indirectly connected, i.e., they are interdependent. Therefore, the study parameters have to be harmonized to generate balanced testing ranges representing practical applications for relevant display types. However, not every possible combination of study parameters is feasible. Expanding the range of one parameter may result in the need to reduce the range of another parameter. The determination of study content parameters described in the following Section 4.2.6 is based on this knowledge.

4.2.6 Content Creation

The following subsections describe the displayed content during the main examination phase of the COBUS series. Since CAT1 (eye static, content mobile) was not considered for the investigation, only the content applied for CAT2 and CAT3 is described. Figures 4.1 to 4.4 illustrate specific sequences related to defined study variables, e.g., a specific saccadic path length for COBUS1/CAT2 or a specific stimulus position for COBUS2/CAT3. Other sequences based on other study variables differ from the sequences illustrated below. A complete description of all object positions of all applied sequences during the COBUS series can be found in Appendix G.

Color Break-Up Study 1

The displayed content during CAT2 includes an adjustment point (AP, small red square, side length of 0.2°), a directional arrow (DA, red arrow, length of 1.0°, height of 0.5°), a fixation target (FT, green cross, side length of 1.0°), and the CBU-provoking stimulus (ST, upper and lower white square, side length of 2.0°) as illustrated in Figure 4.1. The objects are visualized in a defined chronological order to elicit the participant's desired behavior (visually-guided voluntary pro-saccade, see Section 2.3.1).[7] The chronological order of the

[7] The fixation target is visible during the presentation of the CBU-provoking stimulus. Therefore, the fixation target is defined as a small, green-colored cross (primary color), making it impossible to provoke CBU on its own. Furthermore, the fixation target's green coloring is not part of the CBU color pattern in PH1, avoiding disturbances during CBU perception. The adjustment point and the directional arrow disappear before starting the CBU-provoking process. Both objects are red-colored (primary color) to provoke initial attention and distinguish them from the fixation target.

objects' appearance and disappearance and their specific movement patterns are described in detail in Section 4.2.8.

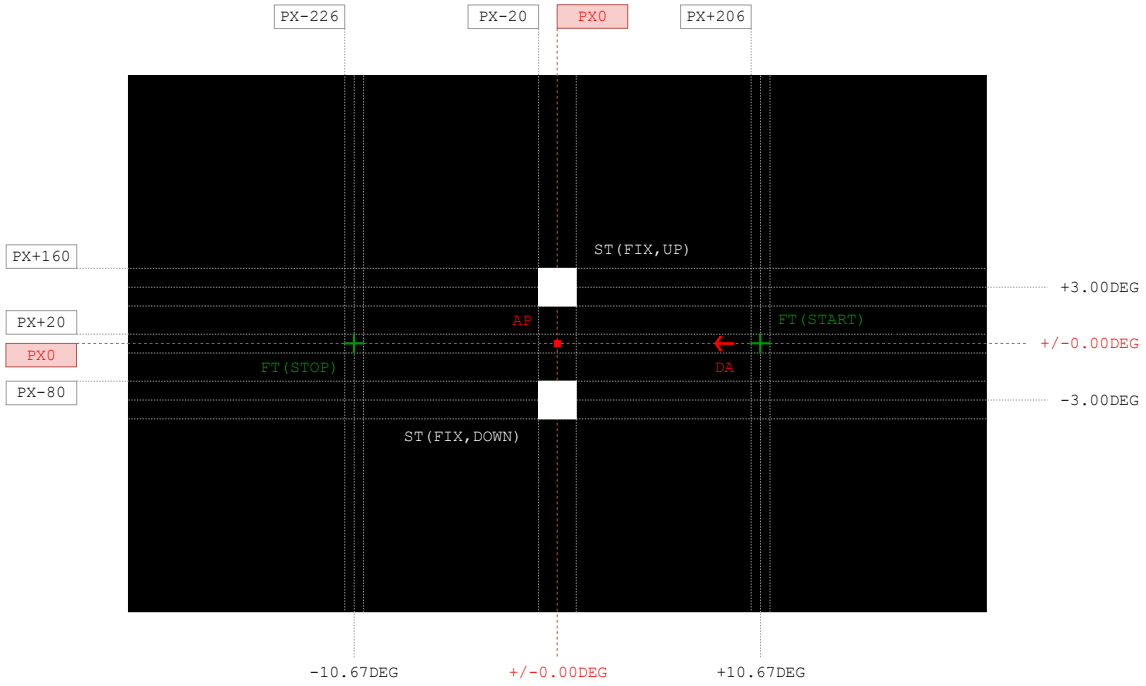

FIGURE 4.1: Content of main sequence for saccadic stimulation with path length of 21.3° during main examination phase of COBUS1/CAT2 (ST = 2.0×2.0° = 40×80 px, FT = 1.0×1.0° = 20×40 px, DA = 1.0×0.5° = 20×20 px, AP = 0.2×0.2° = 4×8 px, horizontal/vertical pixel pitch of 0.05°/0.025°).

Figure 4.1 shows a sequence that provokes saccadic eye movement from right-to-left (R2L) with an exemplary path length of 21.3°. Given variable display sizes and content characteristics that result in different eye movement behavior (e.g., gaming on television vs. office application on desktop display), a practicable and reasonable subcategory for CAT2 would be saccadic length. A variation of saccadic length from small (3.6°) to medium (9.0° and 14.3°) and large saccades (21.3° and 28.2°) covers a wide range of possible saccadic steps during display usage. In addition, the relation between saccadic length and eye movement velocity during saccades is adequately accounted for (see Figure 2.6). At least three values of saccadic length (3.6°, 9.0°, and 14.3°) lie within the zone of positive correlation to saccadic movement velocity. The largest values of saccadic length (21.3° and 28.2°) cover the plateau zone, i.e., saccadic movement velocity will not increase with larger saccadic length.

The content characteristics (size and shape) during CAT3 for CBU stimulus, fixation target, adjustment point, and directional arrow is similar to that of CAT2.[8] However, the locations and times of appearance are different when it comes to provoking PEM. Triggering PEM can be done in two ways — with or without saccadic shares. The use of a so-called step-ramp motion (Rashbass, 1961) would exclude saccadic shares from smooth PEM. The characteristic target movement path and the resulting eye movement response with and without the use of step-ramp stimulation is illustrated and described in Section 2.3.1 (see Figures 2.4 and 2.5). The exclusion of saccadic shares through the use of a step-ramp stimulation allows the

[8]The CBU stimulus size of 2.0° theoretically assures CBU perception in PH1 for eye movement velocities up to 105 deg/s (referring to Equation E.16, assuming the minimum frame rate of 30.0 Hz and a duty cycle of 0.3). Phase transitions from PH1 to PH2/PH3 (see Section 3.5.1) are avoided during CAT3 as the triggered pursuits do not overshoot the calculated transition velocity (not valid for CAT2 as faster saccades are triggered).

investigation of pure PEM without any other movement characteristics. This has the positive effect that CAT2 and CAT3 can be clearly differentiated by their different movement behavior. The necessary content to provoke step-ramp motion is illustrated in Figure 4.2.

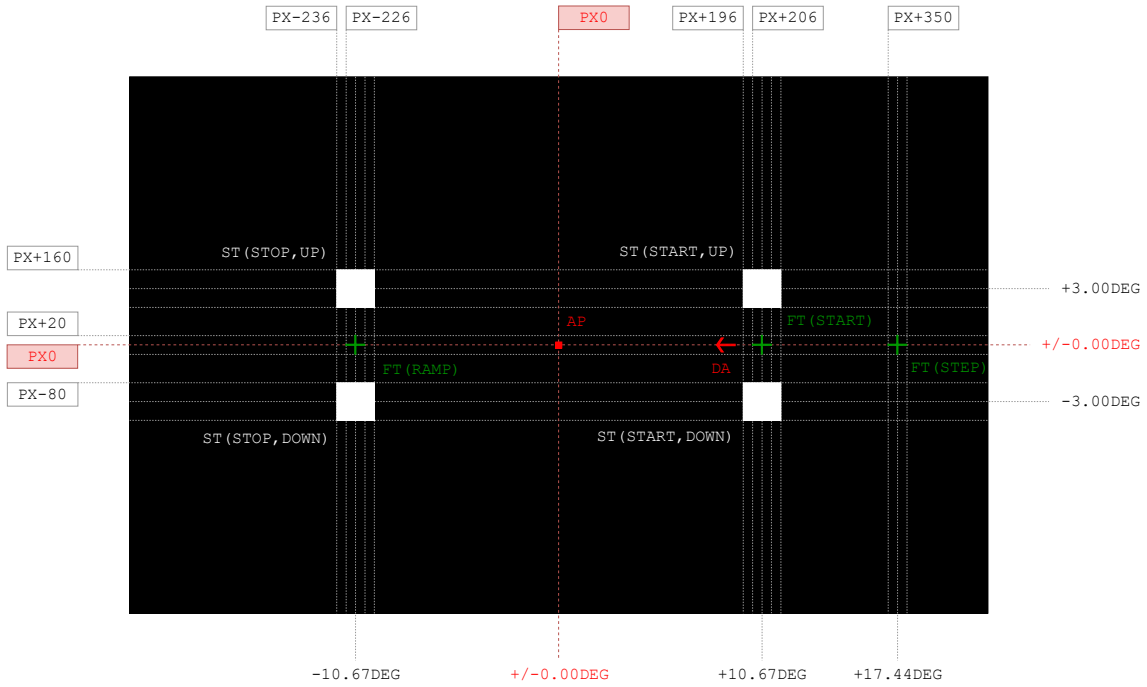

FIGURE 4.2: Content of main sequence for PEM stimulation with velocity of 36.0 deg/s during main examination phase of COBUS1/CAT3 (ST = 2.0×2.0° = 40×80 px, FT = 1.0×1.0° = 20×40 px, DA = 1.0×0.5° = 20×20 px, AP = 0.2×0.2° = 4×8 px, horizontal/vertical pixel pitch of 0.05°/0.025°).

To establish comparability between CAT2 and CAT3, identical eye movement path lengths of 21.3° are determined (compare Figures 4.1 and 4.2). Along this path, three PEM velocities (18.0, 36.0, and 54.0 deg/s) are included in the testing procedure as CAT3 subcategories. The determined velocities are below 70.0 deg/s as the upper limit for smooth PEM execution (Enderle, 2010).

Color Break-Up Study 2

First, the content for saccadic eye movement (CAT2) is illustrated. Compared to COBUS1, the basic objects illustrated during the main examination phase of COBUS2 (adjustment point, directional arrow, and fixation target) are similar in angular size and shape.[9] Figure 4.3 shows exemplary content presented to provoke a horizontal right-to-left pro-saccade (see fixation targets and directional arrow) which is executed voluntarily and visually-guided. In general, saccades are executed in right-to-left (R2L) and left-to-right (L2R) direction as well as in up-to-down (U2D) and down-to-up (D2U) direction. Saccades are executed from the start position of the fixation target to its stop position (assignment of start and stop position by presenting the fixation target time-shifted, see Section 4.2.8). The CBU-stimulating content (one white rectangle, see difference to COBUS1) is positioned upright during the horizontal saccades. The stimulus width is 3.0° (variable between 1.0 and 6.0° during COBUS2) and the stimulus length is 9.6° (kept stable during COBUS2). The position of the CBU stimulus during COBUS2 is changed over a horizontal range of ±50.0° in steps of 10.0°. Figure 4.3

[9] The absolute size of the basic objects of COBUS2 (adjustment point, directional arrow, and fixation target) is reduced when compared to COBUS1. However, the objects' angular size is identical in both studies as the viewing distance of COBUS2 is reduced.

shows the CBU stimulus exemplarily for an eccentricity of 50.0°. In case of vertical saccadic eye movement (up-to-down or down-to-up), the positions of the fixation targets have to be changed. Furthermore, the CBU stimulus is rotated by 90°.

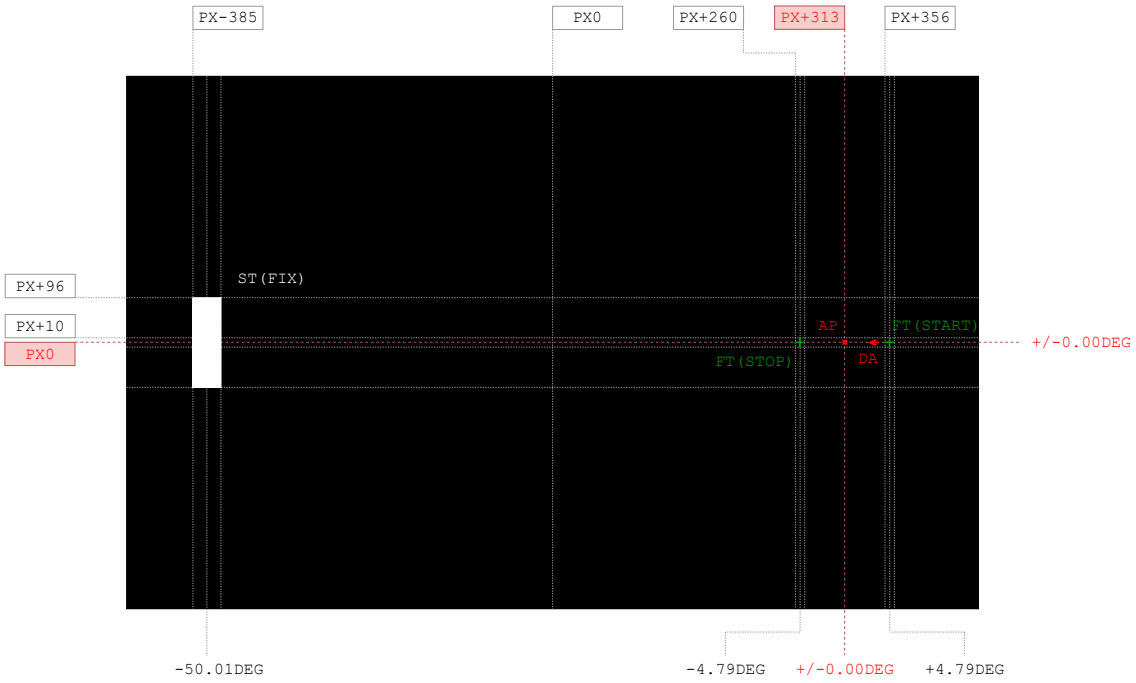

FIGURE 4.3: Content of main sequence for saccadic stimulation with path length of 9.6° during main examination phase of COBUS2/CAT2 (ST = 3.0×9.6° = 30×192 px, FT = 1.0×1.0° = 10×20 px, DA = 1.0×0.5° = 10×10 px, AP = 0.2×0.2° = 2×4 px, horizontal/vertical pixel pitch of 0.10°/0.05°).

As a consequence of the CBU stimulus size and the saccadic eye movement path, well-defined retinal areas are stimulated. For both movement directions (horizontal and vertical), the saccade's movement length of 9.6° as well as the CBU stimulus' dimension of 9.6° (perpendicular to the movement direction) are chosen to fit within a 10.0° quadratic sector of retinal stimulation. During CAT2, the quadratic sector is fully stimulated due to the relative retinal velocity of stimulation, leading to a movement of the CBU stimulus on the retina during its presentation. Stimulation within these quadratic sectors for different retinal eccentricities leads to a total CBU stimulation range from 50.0° in the nasal to 50.0° in the temporal direction.

Figure 4.4 shows all CAT3 objects presented to provoke a vertical PEM. Again, the content is created to provoke a step-ramp stimulation (see previous section). The figure depicts an example sequence, since the size and position of the CBU stimulus as well as the eye movement direction are variable during CAT3 as in CAT2.[10] The displayed CBU stimulus size and the PEM characteristics result in retinal stimulation within a quadratic sector of 10.0° side length. Due to the synchronous eye and content movement during CAT3 (see Section 4.2.8), the area provoked on the retina is defined by the dimensions of the CBU-stimulating content (white rectangle). Unlike CAT2, the CBU stimulus does not move across the retina with relative retinal velocity. During CAT3, the CBU stimulus is in a stable retinal position.

[10]For a CBU stimulus position in 0.0° during CAT3, the CBU stimulus (white rectangle) overlaps with the fixation target while they move synchronously. The moment both objects overlap, the fixation target (green cross, 10/20 px) is changed into a black square (minimum luminance, 2/4 px) to avoid biasing effects on CBU perception.

As a result, the horizontal and vertical movement directions lead to cross pattern stimulation within the quadratic sector of 10.0°, which does not completely cover the quadratic sector (different from CAT2 stimulation).

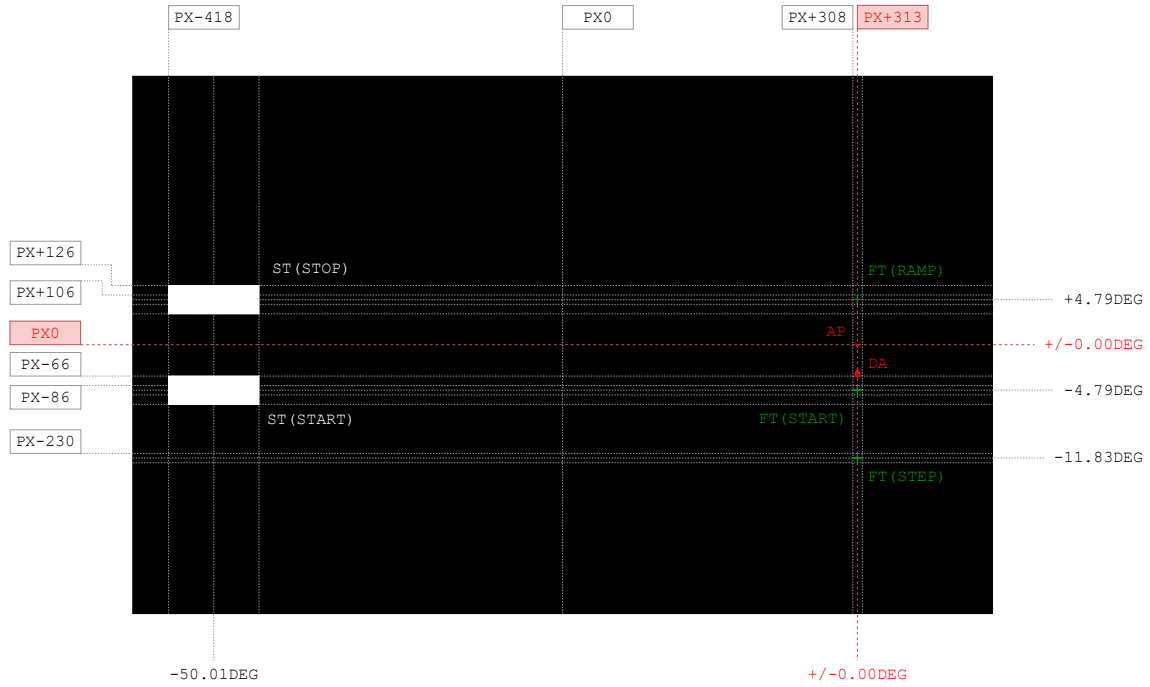

FIGURE 4.4: Content of main sequence for PEM stimulation with velocity of 36.0 deg/s during main examination phase of COBUS2/CAT3 (ST = 9.6×3.0° = 96×60 px, FT = 1.0×1.0° = 10×20 px, DA = 0.5×1.0° = 5×20 px, AP = 0.2×0.2° = 2×4 px, horizontal/vertical pixel pitch of 0.10°/0.05°).

4.2.7 Study Setup

The COBUS series was conducted at the EAH Jena (Faculty of SciTec, Room 05.-01.204). For a better idea of the study setup, some pictures illustrating important stations of COBUS1 and COBUS2 can be found in Appendix D.

Room Illumination

The main experiments of the COBUS series (see Section 4.2.8) were performed in a darkened room to exclude the impact of external light sources on the lighting conditions of the projection screen.[11] Scotopic lighting conditions were necessary to effectively utilize the limited maximum brightness of the DLP projector (see Appendix B.1). Furthermore, external light sources would have reduced the displayable contrast ratio on the projection screen. The pre-examination testing was conducted partially under photopic conditions of 775.1 ± 265.2 lx (ceiling lights on) and scotopic conditions (ceiling lights off).[12] Which lighting condition (scotopic or photopic) was chosen for each test is described in Appendix A.2.

[11] The ceiling lights of the room were switched off, and windows and other light sources of active devices were masked. The examiner's control displays were set to a minimum brightness as they could not be switched off or masked.

[12] The horizontal illuminance level for photopic conditions was determined with luxmeter (see Appendix A.1.3). The measurements were executed in 10 different measurement positions that were evenly distributed throughout the room at a height of 1.0 m above floor (active display systems were not considered during measurements). A high illuminance variation results from the ceiling lights' inhomogeneous arrangement (fluorescent tubes). However, for all participants, preliminary examinations were carried out in the same places, guaranteeing a stable illuminance level during specific tests.

Hardware Component Position

The determination of the depth positions of the central setup components, i.e., the projection distance between projector and screen, required to consider the following aspects:

— available focus range of projector

— achievable maximum luminance levels

Furthermore, the viewing distance from the first nodal point of the participant's eye(s) to the projection screen had to be defined under consideration of the following issues:

— desired horizontal field of view

— specific pixel size

A projection distance of 0.65 m and a viewing distance of 0.58/0.29 m (COBUS1/COBUS2) incorporated all mentioned aspects to achieve a balanced depth positioning between projector, screen, and participant during the main examination phase (see Appendix G). The resulting pixel size of 0.05°/0.10° (COBUS1/COBUS2) was of particular importance as it allowed to display the required content movement paths and velocities.

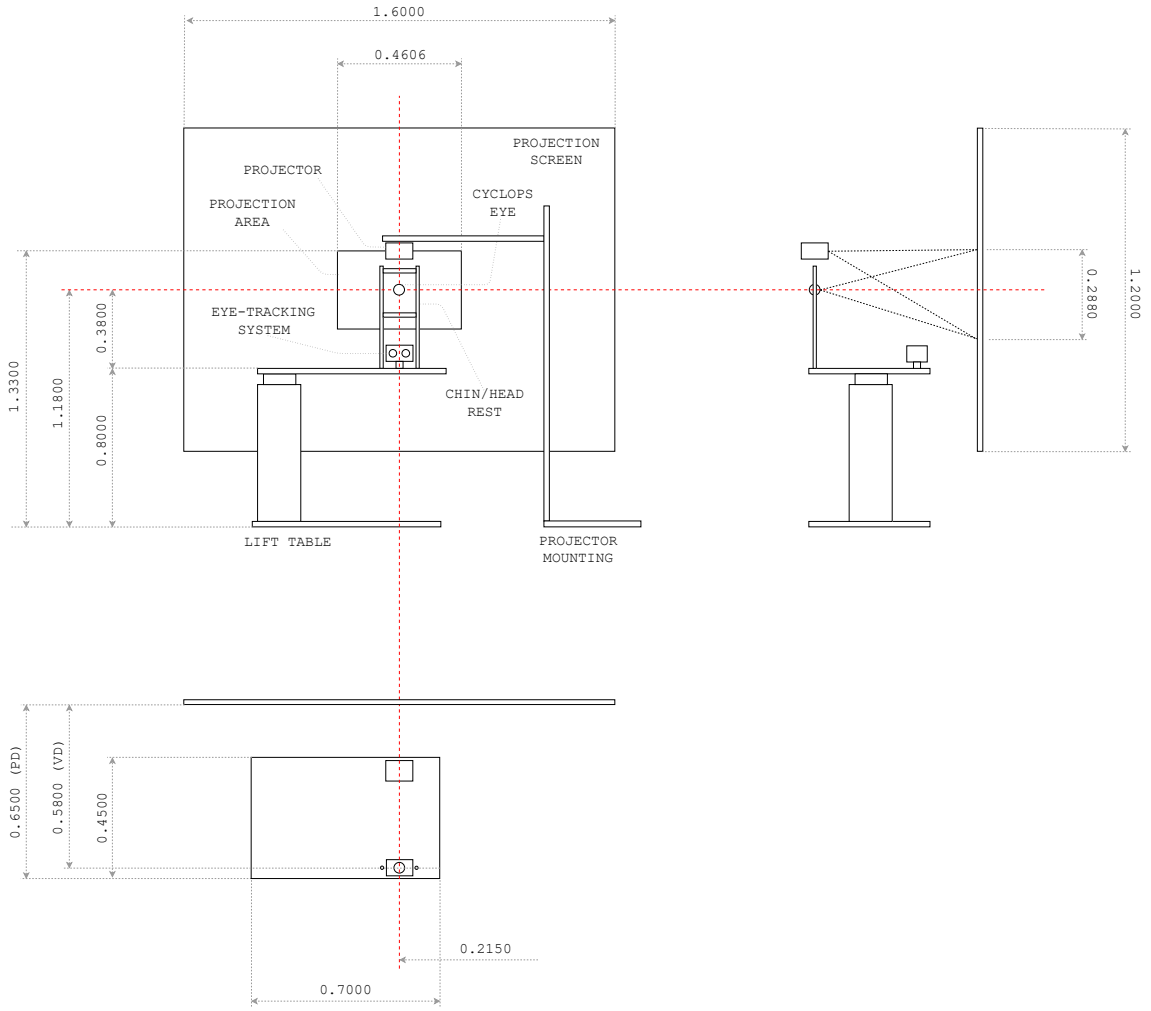

FIGURE 4.5: Hardware components and participant position during COBUS1 (top-left graphic: front view, top-right: side view, bottom-left: top view; projector mounting is left out in side/top view).

Figure 4.5 illustrates the final build-up for the main study examination of COBUS1 including the projector and its mounting, the projection screen, the eye-tracking system, and the lift table with head and chin rest.[13] In addition, the graphic shows the position of the participant. A projection distance greater than the viewing distance (projector positioned behind the observer's eye) made it necessary to place the projector above the observer's head and turn it upside-down. Fortunately, the projector is a 100% off-axis projector (see Appendix A.3.1) which allowed the positions of the projector and the participant's visual system to be displaced vertically.

The setup for the main study examination of COBUS2 included the same components as COBUS1 and only differed with regards to a few aspects. The viewing distance was reduced (0.29 m) to extend the field of view and allow investigation of central and peripheral CBU perception. Additionally, the participant's primary gaze position was no longer located in the projection area's horizontal/vertical center as in COBUS1 (see adjustment point in Figure 4.1). The gaze position was now shifted out of center, allowing even more peripheral areas to be stimulated (see adjustment point in Figure 4.3). In this setup, the projector was positioned horizontally to the right (Setup 1) or to the left (Setup 2) of the participant's position (vertical depth position of the projector was kept stable). Furthermore, the projector had to be rotated 180° when changing from Setup 1 to Setup 2 and vice versa. Both COBUS2 setups allowed the examination of a wide peripheral area in nasal and temporal retinal direction, covering up to $\pm 50.0°$.

4.2.8 Examination Process

All participants of COBUS1 and COBUS2 were invited to two visits (V1/V2), since time and effort required for study participation was extensive. Conducting each study on two different days allowed for a reduction in the participant's workload. A reduced workload had a positive effect on the concentration and compliance of the participant.[14] The examination process of the first visit (V1) during COBUS1 is shown in Figure 4.6, including the estimated durations for the different phases of the examination.

The second visit (V2) of COBUS1 required less time because only the main examination phase was executed. Visual acuity, contrast sensitivity, and color vision were tested and the questionnaire (pre/post) was applied. The COBUS2 examination process for V1/V2 was identical, except that the questionnaire was generally not applied and visual acuity, contrast sensitivity, and color vision were only tested once (V1). Study participation in COBUS1/COBUS2 was terminated upon completion of the second visit (no follow-up examinations or control visits).

[13] In Figure 4.5, the projection distance (PD) is defined as the distance from projection screen to a backward-shifted reference point behind the projector's back side since the optical path within the projector is unfolded. As the exact position of the projector's reference point is unknown, the horizontal adjustment of the projector position in reference to the screen requires to factor in the calculated dimensions of the projection area. An accurate size of the projection area implicates that the projection distance is also accurately adjusted. After adjusting the projection area, the projector's front/back side position lies approximately 540/640 mm away from the projection screen. The horizontal positioning of the projector is completed. An ideal projector position in vertical direction guarantees the participant's primary gaze position in the vertical center of the projection area. The available space between the participant's pupil center and the upper edge of the projector is 14.4 mm (projector is turned upside-down). Considering human anatomy, the distance between the participant's pupil center and the upper apex of his head is approximately 11.0 mm on average. The distance between the optical center and the upper edge of the projector (incl. cover) is approximately 3.0 mm. Consequently, there is less free space between the apex of the participant's head and the projector's upper edge. To avoid contact between participant and projector, the participant's final vertical position is adjusted via lift table while positioned on the head/chin rest (lift table's height is adjustable from 0.70 to 0.90 m).

[14] Visits were scheduled before 5 p.m. Later visits might have resulted in reduced concentration due to previous activities. In addition, V1 and V2 were aimed at being scheduled within a time span of 48 hr.

FIGURE 4.6: Study examination process during COBUS1/V1.

Pre-Examination

The first mandatory step was to do the necessary paperwork including the study information sheet, consent form, and account information.[15] After the participant gave his/her informed consent to participate in the study, the type and prescription of the habitual correction and the participant's refractive status were determined and documented. Before the participant was included into the study sample, the defined exclusion criteria were tested (see Section 4.2.3 for exclusion criteria and Appendix A.2.2 for test specifications). The participant was included if s/he did not meet one or more exclusion criteria. The test results regarding inclusion/exclusion were documented using a digital case report form (e-CRF, see Appendix A.2).

In a first training phase, the CBU effect and its various forms were explained to the participant. The aim was to illustrate the range of possible CBU characteristics and the different levels of CBU severity (from low to high).[16] In a second step, the participant's task during the main examination phase was described theoretically. The explanations of CBU

[15]The study information sheet informed the participant about the most important aspects such as the aim of the study, the process of study execution, and potential risks for the participant. The sheet was handed out prior to participation. By signing the consent form, the participant agreed to voluntarily participate. The appended data privacy statement informed the participant about the usage of the collected data and his/her rights. The participant's account information was documented for the transfer of the financial compensation after participation.

[16]Participants show a central tendency bias by avoiding extreme scale values during evaluation tasks (Guilford, 1954). Explaining CBU in advance led to a better comparability of the evaluated CBU scores of CAT2 and CAT3 (executed consecutively) as the participants were made aware of the full CBU range from the beginning. The training was executed before every main examination phase (V1 and V2).

and the task descriptions were clarified using animated illustrations (presented with tablet T100T, ASUSTeK Computer Inc.).

An additional questionnaire (integrated in the e-CRF, see Appendix A.2.4) was carried out before and after the main examination phase during V1/V2 (COBUS1), inquiring the participant's demographic data (gender, age), display usage behavior (profession, display types, average display time per day), general personality traits (e.g., affinity to technology), and current state (e.g., attention level).

Main Examination

Generally, the main examination phase included the presentation of CBU-provoking content and its assessment by the participant.[17] Recommendations of the International Telecommunication Union (ITU, 2012) give an overview of different methods to test video image quality/impairment and describe important aspects that need to be considered. At first, it had to be decided which general method of stimulus presentation was appropriate for the task of the COBUS series. "In SS [single-stimulus] methods, a single image ... is presented and the assessor provides an index of the entire presentation" (ITU, 2012, p. 16). Streijl et al. (2016) conclude that "methods such as single-stimulus can be used when subjects are presented with a wide impairment range" (p. 215). The main examination phase included two different experimental arms (CAT2/CAT3). Each experimental arm investigated different movement patterns. Within the experimental arms, several study parameters were changed so that a fixed number of CBU-provoking scenarios had to be presented for each arm. The provoked CBU intensity of the presented COBUS scenarios was expected to vary greatly. Hence, the application of a single-stimulus method was appropriate. However, further aspects had to be considered when applying the single-stimulus method:

> When two or more factors are examined, the images can be prepared in two ways. In the first, each image represents one level of one factor only. In the other, each image represents one level of every factor examined but, across images, each level of every factor occurs with every level of all other factors. Both methods permit results to be attributed clearly to specific factors. The latter method also permits the detection of interactions among factors (i.e., non-additive effects). (ITU, 2012, p. 17)

For the COBUS series, the latter method of multiple factors was applied. Another recommendation relates to the trial structure of the main examination phase:

> A typical assessment trial consists of two displays: a stimulus and a mid-grey post-exposure field. The duration of these displays may vary with viewer task, materials and the opinions or factors considered, but 10 and 5 s respectively are suggested. The viewer index, or indices, have to be collected during display of the post-exposure field only. (ITU, 2012, p. 17)

In this context, a single trial was defined by a loop consisting of pre-sequence (rest phase), main sequence (CBU provocation), and post-sequence (CBU evaluation). These central parts of the main examination phase as well as an additional training phase and general aspects such as breaks and the randomization process are described in the following (see Figure 4.7).

[17] During COBUS1, the habitual correction (spectacles or contact lenses) was worn during all study phases to compensate for a potential ametropia and assure adequate visual performance (visual acuity, contrast sensitivity, color vision). The main examination phase of COBUS1 was executed under binocular conditions. The participants of COBUS2 were not allowed to wear spectacles or contact lenses. To still guarantee an adequate visual performance, exclusion criteria for the refractive status were established (see Section 4.2.3). The main examination phase of COBUS2 was executed under monocular conditions to differentiate between nasal and temporal retinal stimulation.

FIGURE 4.7: Main examination phase of COBUS series.

After a general training phase (during pre-examination), an additional training phase on the DLP projector is recommended:

> At the beginning of the first session, about five 'dummy presentations' should be introduced to stabilize the observers' opinion. The data issued from these presentations must not be taken into account in the results of the test. If several sessions are necessary, about three dummy presentations are only necessary at the beginning of the following session. (ITU, 2012, p. 8)

In such a training phase, some selected total loops (consisting of pre-sequence, main sequence, and post-sequence) were displayed to clarify the participant's task (e.g., eye movement behavior) and visualize the full CBU range during the main examination phase. Data from the training sessions were not included in the statistical analysis. This training phase was conducted before each experiment (CAT2/CAT3) at each visit (V1/V2). The training loops were executed in the following order of CBU perception levels: high – medium – low – medium – high. However, the training loops for CAT2 and CAT3 differed from each other.[18] After the participant had completed the training, s/he was prepared to execute the entire set of loops during the main examination phase.

The pre-sequence of the main examination phase included a screen presentation that allowed the participant to prepare for the subsequent CBU-provoking main sequence. The pre-sequence displayed the text "Press Enter to start!" in blue color on black background to avoid disturbance of the participant's light adaptation and afterimages during the main sequence. The main sequence was initiated by pressing the enter key on the keypad as soon as the participant was ready.

[18] Training loops of CAT2/COBUS1 specified by frame rate, luminance, and saccadic length: low CBU level = 420.0 Hz, 10.0 cd/m^2, 9.0°; medium = 150.0 Hz, 80.0 cd/m^2, 14.3°; high = 30.0 Hz, 157.0 cd/m^2, 28.2°. Training loops of CAT3 specified by frame rate, luminance, and content movement velocity: low = 420.0 Hz, 10.0 cd/m^2, 18.0 deg/s; medium = 90.0 Hz, 80.0 cd/m^2, 36.0 deg/s; high = 30.0 Hz, 157.0 cd/m^2, 54.0 deg/s.

The main sequence aimed to provoke CBU by presenting different objects: adjustment point, directional arrow, fixation target, and CBU stimulus (see Section 4.2.6). The participants had different tasks during CAT2 (visually-guided voluntary pro-saccades, see Section 2.3.1) and CAT3 (pursuits provoked by step-ramp stimulation, see Section 2.3.1). As a consequence, the main sequence for CAT2 and CAT3 must be described separately.

The displayed content of the main sequence of CAT2 is illustrated in Figures 4.1 and 4.3 (COBUS1/COBUS2). At the start of the sequence, the participant saw the fixation target in its starting position. The adjustment point and a directional arrow were also visible from the start. The directional arrow gave the information in which direction the saccade had to be performed because the direction of the triggered saccade was randomized during the trial. Information about the saccade's direction helped the participant to execute the saccade in a more targeted way.[19] As there was a risk that the participant may unconsciously execute a compensatory rotation of the head toward the fixation target as the stop point of the desired eye movement, the adjustment point and notes from study staff helped the participant to adjust his/her head position. All three objects — fixation target, adjustment point, and directional arrow — were not allowed to provoke CBU. Therefore, these objects consisted of only one primary color. After the head position had been adjusted with the adjustment point, the participant fixated the fixation target without any head movement. At this point, it was important to instruct the participant to blink three times to reduce the likelihood of blinking during the following period of CBU provocation. With the correct head and eye position and no need to blink, the participant pressed the enter key to initiate the main sequence. The adjustment point and the directional arrow disappeared without delay. Only the fixation target in its start position was still visible. A randomized time between 750 and 1,500 ms after the button was pressed, the fixation target appeared in its stop position (to avoid learning effects that affect the participant's reaction time). This triggered the saccadic eye movement from the start to the stop position of the fixation target. The participant was instructed to perform a saccade from the start to the stop position as quickly and as precisely as possible as soon as s/he noticed the fixation target in the stop position. The fixation target in the start position disappeared 100 ms after the fixation target in the stop position had appeared, which means that there was an overlap between the presentation of the start and stop positions of the fixation target.[20] In the main sequence, the white CBU-provoking stimulus was not displayed until the start of the movement sequence. The CBU stimulus appeared exactly synchronized with the fixation target in stop position, i.e., the CBU stimulus was not visible until the saccadic eye movement was triggered. The perception of CBU prior to the relevant eye movement was avoided (e.g., looking around before the sequence was started by pressing the button). This was important because the influence of unwanted premature CBU perception on the final CBU evaluation could not be excluded. 1,000 ms after the fixation target had occurred in stop position, the main sequence was closed, and the post-sequence screen was displayed.[21]

[19] Erroneous eye movements were monitored with eye-tracking system to allow sequence repetitions.

[20] Regarding the fixation targets' appearance/disappearance, saccadic latency must be discussed. The Latency is highly individual; however, a typical saccade has a latency of about 200 ms (Carpenter, 1988). The latency depends on the sequential time arrangement of the two fixation targets that define the saccade. Latency is higher when the fixation targets overlap on the time line. The so-called gap effect (Saslow, 1967) reduces the latency by making the fixation target disappear shortly before the saccade-stimulating peripheral target occurs. However, latency reduction has no benefit for the purpose of the study. To the contrary: Placing a time gap between disappearing and reappearing fixation targets means that, for a short period of time, there is no target to fixate, potentially triggering uncontrolled eye movements. Therefore, the gap effect was not applied in CAT2.

[21] A time period of 1,000 ms allowed to complete the largest saccades of CAT2 before the CBU stimulus disappeared (even if the participant's reaction time was slower than average). However, the shorter the saccade, the larger the time gap between the completion of the saccade and the disappearance of the CBU stimulus. Therefore, participants were instructed to keep the gaze at the fixation target's stop position after the target was reached. Additional eye movements would have led to additional CBU perception falsifying the study results.

The presented content of the main sequence of CAT3 is illustrated in Figures 4.2 and 4.4 (COBUS1/COBUS2). The initial content presentation and procedure for the main sequence of CAT3 was identical to the procedure described for CAT2 until the participant pressed the enter key to start the main sequence. After pressing the button, a randomized time span between 750 and 1,500 ms elapsed until the fixation target disappeared in its start position and appeared horizontally to the right without any time delay (exemplary for a fixation target and CBU stimulus movement to the left). The fixation target made a step from the start position to its step position.[22] After execution of the step motion, the fixation target then immediately moved in opposite direction (to the left) to its stop position at a constant movement velocity — the so-called ramp movement. The whole movement behavior is called step-ramp stimulation (see Section 2.3.1). The initial step width of the fixation target (to the right) was calculated to guarantee that the fixation target moved in opposite direction (to the left) at a defined speed, so that it passed through the start position of the fixation target again after a period of 200 ms. This is the average reaction time of the participant, which means that the participant did not react until the fixation target passed through the start position. The moment when the fixation target passed through the start position, the participant followed the target's continuous movement with a smooth PEM without saccadic shares until the target reached its stop position. Ideally, the step-ramp stimulation provokes PEM without saccadic shares. The moment when the fixation target passed through its start position again was the moment when the CBU-provoking stimulus was made visible. The CBU stimulus was synchronized with the horizontal movement of the fixation target, and moved parallel to the fixation target from right to left once the fixation target had passed the start position until it reached its stop position.[23] After the stop position was reached, the fixation target and the CBU stimulus were present for another 500 ms. The participant was instructed to keep looking at the fixation target. Further eye movements had to be avoided to prevent provoking additional CBU. If this happens, the perceived CBU effect should not be considered when evaluating CBU via the continuous CBU scale. Regarding CBU perception during CAT3, theoretically, the participant should perceive constant CBU during the PEM since the velocity of both the fixation target and the CBU stimulus was constant. The participant was instructed to report inconsistent CBU perception during CAT3 (especially in the initial PEM phase). This could have been interpreted as initial shares of saccadic eye movement, for example, provoked by a deviation from the standard reaction time of the step-ramp stimulation. Documentation of inconsistent CBU perception during CAT3 was necessary so that the data set could be checked for exclusion.

The post-sequence allowed the participant to evaluate the perceived CBU effect. Since the single-stimulus method for CBU stimulation was applied, the evaluation process referred to Absolute Category Rating (ACR). An absolute CBU score was determined (no comparison between testing sequences). In ACR, categorical (adjectival or numerical) and non-categorical judgment scale approaches can be distinguished. An adjectival categorical judgment scale that is well established in CBU research is the ITU-R impairment scale (Y.-K. Cheng & Shieh, 2009; Y. Zhang et al., 2012). The scientific classification of this scale (advantages, disadvantages, areas of application) was critically reviewed by Streijl et al. (2016)

[22] The step motion of the fixation target can lead to unwanted eye movement in step direction. Goettker et al. (2018) investigated the effect of an additional time gap (50 ms) between the fixation target's disappearance and reappearance on unwanted eye movements during step motion — the so-called gap paradigm. Results show that eye movements caused by the step motion do not differ in the modified step-ramp sequences with time gap and the classic sequences without gap. Therefore, no time gap was integrated in the chronological procedure of the step-ramp stimulation. However, participants were instructed to avoid eye movements in step direction.

[23] All participants were instructed to precisely follow the fixation target and not gaze at the CBU stimulus. Slow pursuits might provoke such a behavior as there is enough time to fixate the CBU stimulus. Faster pursuits are executed more intuitively, making deviations from the fixation path unlikely.

who state that "the most common standard rating scale used to derive MOS [Mean Opinion Score] values is a category rating scale with five discrete levels. Due to the attachment of labels ... to these levels, it is non-linear, i.e. the levels are not equidistant across the scale" (p. 216). The scale's non-linearity results in an ordinal scale level. In other words, a metric scale level is not achieved.[24] Another aspect to bear in mind:

> The impairment scale ... is usually found that the stability of the results is greater for small impairments than for large impairments. Although the method sometimes has been used with limited ranges of impairments, it is more properly used with a full range of impairments. (ITU, 2012, p. 10)

In general, it has to be pointed out that the participant's ability to distinguish between steady variation of stimulation over a defined range is limited. The number of levels that a participant can distinguish are finite. Higher granularity is often not necessary since "potential higher resolution is lost in the noise due to the limits of human information processing capability" (Streijl et al., 2016, p. 217). In this context, Miller (1956) found that the number of stimulation levels that human perception can distinguish is 7 ± 2 (valid for different stimulation types). The granularity of a scale has to be adapted to these limits of human perception. First trials in a self-experimental setup confirmed Miller's conclusion, and indicated that a 5-point scale would be appropriate in terms of granularity for CAT2 and partially for CAT3. However, CAT3 granularity could be more precise than the 5-point score, especially in the area of low CBU provocation. In this area, slight CBU differences are easily distinguished since stimulus movement velocity in CAT3 is lower than for saccades in CAT2. For this CAT3 area, a higher granularity is appropriate.

Another categorical scale with a higher number of grades or continuous scaling as a non-categorical judgment method would deal with this problem.[25] In comparison to categorical judgment methods, the big advantage of continuous scaling is the scale level that can be achieved. Continuous scaling would result in metric scale level if only the poles are specified in semantic form (e.g., *imperceptible – very annoying*, based on the poles of the ITU-R impairment scale). A metric scale level for CBU evaluation is highly beneficial for inductive statistical analysis. However, with this design of continuous scaling, only the threshold of perceptibility *TOP* can be determined (Score 1 = *imperceptible*). In comparison, when applying the classic 5-point ITU-R impairment scale (adjectival categorical judgment methods), it is possible to determine the threshold of perceptibility (Score 1) and, beyond that, the threshold of annoyance *TOA* (Score 2 = *perceptible, but not annoying*). As pointed out above, the classic 5-point ITU-R impairment scale has only ordinal scale level, which makes it unsuitable for this task.

A solution is to use the continuous CBU scale and then ask the participant directly whether the CBU perception is annoying or not. This allows to evaluate the CBU level on a metric scale, and to determine the threshold of perceptibility and the threshold of annoyance (detailed description in Section 4.2.9). To implement this approach, the participant was invited to "Please evaluate CBU perception!" on the first CBU evaluation screen of the post-sequence (see Figure 4.8, left graphic). The participant selected the score that corresponded

[24] "In adjectival categorical judgements, observers assign an image or image sequence to one of a set of categories that, typically, are defined in semantic terms. The categories may reflect judgements of whether or not an attribute is detected (e.g., to establish the impairment threshold)" (ITU, 2012, p. 18). The verbal attributions to the numerical scale points of the ITU-R impairment scale from 1 to 5 are defined as follows: 1 = *very annoying*, 2 = *annoying*, 3 = *slightly annoying*, 4 = *perceptible, but not annoying*, 5 = *imperceptible*.

[25] "In non-categorical judgements, observers assign a value to each image or image sequence shown. There are two forms of the method. In continuous scaling, a variant of the categorical method, the assessor assigns each image or image sequence to a point on a line drawn between two semantic labels e.g. the ends of a categorical scale ... . The distance from an end of the scale is taken as the index for each condition. In numerical scaling, the assessor assigns each image or image sequence a number that reflects its judged level on a specified dimension (e.g. image sharpness). The range of the numbers used may be restricted (e.g. 0–100) or not" (ITU, 2012, p. 18).

to his/her CBU perception (CBU_{SCR}) on a continuous CBU scale. For this purpose, the participant moved the red grading line from the middle position as start point to the right or the left (via arrow keys of the keypad), and logged in his/her choice (via the enter key). As described earlier, the continuous CBU scale was adapted from the ITU-R impairment scale with its semantic specification of the poles of the scale (only) and its five tick marks for orientation (analogous to the five grading levels of the 5-point scale but without numerical or semantic specification of the inner tick marks). The lower pole of the scale represented a CBU score of 1.0, the upper pole represented a CBU score of 5.0 (also analogous to the ITU-R impairment scale). The smallest digital movement step on the scale referred to the size of a pixel, which resulted in 400 steps between the lower and upper pole and a granularity of 0.01 for the output of the CBU score (e.g., 3.21). On the second CBU evaluation screen (right graphic), the participant answered the question "Did you perceive CBU as annoying?" with "Yes" or "No" (choice with arrow and enter keys). The participant's decision closed the post-sequence, and started the loop from the beginning with the next selection of presentation parameter.[26]

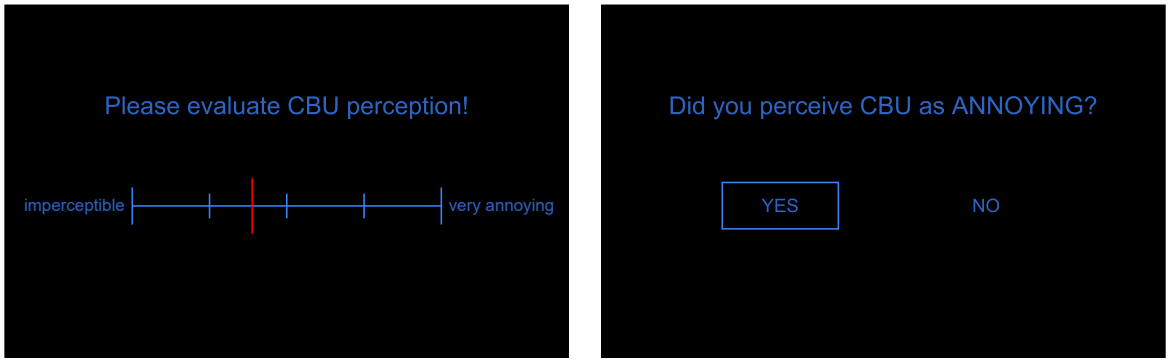

FIGURE 4.8: Evaluation screens during post-sequence of COBUS series. Left graphic: evaluation of CBU perception via continuous CBU scale. Right graphic: inquiry on the state of CBU annoyance.

It is important that test loops are "presented in random order and, preferably, in a different random sequence for each observer" (ITU, 2012, p. 17). Following this recommendation, the chronology of all sequence loops during the main examination phase had to be randomized individually for each participant. This avoided negative effects during the data collection resulting from fatigue or lack of concentration. The total number of sequence loops was calculated by multiplying the numbers of applied values for all variable parameters of the study (see Appendix G for a detailed description). This resulted in a total amount of 528 sequence loops for each participant during COBUS1 — 165 loops for CAT2 and 99 loops for CAT3, which made 264 loops during V1 and V2. During COBUS2, 1,152 sequence loops were presented in total. The total amount of loops was split to 576 loops per visit (288 CAT2 and CAT3 loops each for the two visits). At first, the chronology of exclusive nasal and temporal retinal CBU stimulation was randomized (www.random.org) and assigned to V1/V2 (only relevant for COBUS2). This exclusive assignment was necessary to change the study setup for nasal and temporal stimulation, which took some time and could not be done during the visit (see Section 4.2.7). The order of nasal and temporal stimulation for both visits was distributed as equal as possible over the sample. Second, during the visits, sequence loops referring to CAT2 and CAT3 were presented. All loops of CAT2 and CAT3 were presented in series, which means that either all CAT2 or all CAT3 loops were presented first. A mixed presentation of CAT2/CAT3 loops would have hampered the accomplishment of

[26] All items on the evaluation screens were blue-colored (except the emphasized red grading line) to prevent disturbance of the participants' light adaptation and avoid afterimages.

the task. The order of execution of the experimental categories (CAT2, CAT3) during a visit was randomized (relevant for COBUS1 and COBUS2). The order of the category execution during each visit was distributed as equally as possible. Third, all loops of one experimental category (CAT2 or CAT3) were randomized across the variable presentation parameters (also relevant for COBUS1 and COBUS2).[27] This avoided bias due to fatigue or inattention with increasing study duration.

Regarding test duration, the following recommendation applies: "A session should last up to half an hour" (ITU, 2012, p. 8). The conducted sessions (V1/V2) exceeded this recommended time span. However, breaks were taken to keep the participant's attention as high as possible. Short breaks with a defined duration followed a defined number of repetitions of sequence loops. The break was communicated by displaying "Break." on the projection screen. The remaining time for the break was displayed as well (break time of 30 s, clock ran backwards). The text was displayed in blue color on black background to minimize the effect on the main sequence (e.g., afterimages). During the break, the participant was allowed to rest in a comfortable position on his/her seat (during study examination, the participant was positioned on a head/chin rest). Pre-testing showed the best response to breaks after periods of 30 to 40 total loops. To guarantee a homogeneous integration into the chronology of the sequence loops, short breaks after 33/36 loops during COBUS1/COBUS2 were useful. Additionally, longer breaks of 900 s were included after all loops of an experimental category (CAT2/CAT3) were completed. During the longer breaks, the participant was allowed to stand up and walk around.

4.2.9 Statistical Analysis

Descriptive statistical data analysis including graphical editing of COBUS data was done using MATLAB (Version R2018b, The MathWorks, Inc.). Inductive statistical analysis was done by applying IBM SPSS Statistics (Version 25, IMB Corporation). Links to relevant MATLAB and SPSS files are integrated in the following sections.

Sample Size Estimation

To the best of the author's knowledge, there was no external research that could have been used to estimate the sample size of COBUS1. The determined sample size of $N = 30$ considered the recommendations ($N \geq 15$) of the methodical procedure guidelines for assessment of quality features in image reproduction of the ITU (2012). The COBUS2 data collection was based on the investigation of a limited number of individual cases ($N = 6$) for exploratory data analysis (no sample size estimation intended).

Statistical Analysis Plan

With regard to the primary objective of COBUS1 (see Hypotheses H.1 to H.4), the effect of the two independent technical variables (frame rate, luminance level) on the dependent variable (subjective CBU perception) was statistically analyzed for all subcategories of the experimental categories CAT2 and CAT3. The subcategories of CAT2 provoked CBU perception by triggering observer-dependent saccadic eye movements of variable distances. CAT3 and their subcategories related to CBU provocation by triggering observer-dependent PEM of variable velocity. 3D coordinate systems (x-axis: frame rate, y-axis: luminance level, z-axis: CBU score) were used to show the relationship between the metric variables frame

[27] The variables of COBUS1 were frame rate (11 values), saccadic length (CAT2 = 5) or pursuit velocity (CAT3 = 3), luminance level (3), and eye movement direction (2). The variables of COBUS2 were frame rate (2), eye movement direction (4), stimulus position (12) and size (6). All values are specified in Appendix H.

rate/luminance level and CBU score (CBU_{SCR}) as the metric target variable. The determination of CBU scores for the combinations of frame rate and luminance level allowed the creation of a 3D surface representing CBU perception for the test ranges applied (linear interpolation between the measurement points). The 3D models were created separately for every single subcategory of the included experimental categories (CAT2/CAT3). The graphical illustrations were complemented by tabular listings containing the mean values and standard deviations of the sample's CBU scores for all experimental conditions studied.

Statistical testing of Hypotheses H.1 to H.4 was based on curve fitting approaches for which the assumed relations between the independent variables within (frame rate, luminance level) and across the subcategories (saccadic path length, PEM velocity) and the CBU score were tested. Relations were classified in terms of their statistical goodness of fit, using the coefficient characteristics (B values) of the fitted function and the coefficients of determination r^2.[28] Additionally, within the subcategories (Hypotheses H.1 and H.2), a two-way repeated measures ANOVA with two within-subjects factors (luminance level, frame rate) was the method of choice for further inductive statistical testing. As foundation for the execution of a two-way repeated measures ANOVA, all participants evaluated all sequences that consisted of all possible combinations of the independent variables (independent variable consisted of related groups and dependent variable was measured at a continuous level). Furthermore, the surrounding conditions were kept stable during COBUS1. Generally, the statistical analysis was divided into pre-testing of an interaction between the independent variables (luminance level, frame rate) and main-testing for differences between groups of luminance levels, which included several statistical tests (significance level was set to $\alpha = .05$ by default, alpha error adjustment was applied when necessary).[29] After comparing the luminance level groups separately for each single experimental condition, it was additionally

[28]The assumed relation between an independent and a dependent variable of a specific experimental subcategory was confirmed for a curve fit with $r^2 \geq .90$. The corresponding hypothesis was confirmed as long as all hypothesis-related experimental subcategories were confirmed. For example, Hypothesis 1 was confirmed when the negative correlation between frame rate and subjective CBU perception (exponential regression) was verified for all investigated saccadic amplitudes (CAT2) and pursuit eye movement velocities (CAT3).

[29]The pre-testing of an interaction between the independent variables (luminance level, frame rate) was done within the two-way repeated measures ANOVA. A confirmation of a statistically significant interaction led to a breakup of the classic procedure of the Main Effects interpretation of the two-way repeated measures ANOVA, running statistical tests for the interpretation of Simple Main Effects instead. In a first step, Mauchly's Test of Sphericity was applied (luminance level, frame rate). The test decided if sphericity was confirmed ($p > .05$) or rejected ($p < .05$). A confirmation of sphericity led to a test of Within-Subjects Effects for the interaction between the independent variables under assumed sphericity (no correction necessary). In case of a rejection of sphericity, a corrected value was applied. Greenhouse-Geisser values lower than .750 made a Greenhouse-Geisser correction for the test of Within-Subjects Effects necessary, whereas Greenhouse-Geisser values higher than .750 resulted in an application of the Huynh-Feldt correction. The second step of pre-testing included the test of Within-Subjects Effects for potential interactions between the independent variables. Depending on the results of the sphericity test (confirmation or rejection), the relevant values (sphericity assumed, Greenhouse-Geisser, Huynh-Feldt) were chosen and interpreted. For a p value $< .05$, an interaction between the two independent variables had to be assumed. Consequently, the two-way repeated measures ANOVA could not be applied by considering the Main Effects interpretation, instead a Simple Main Effects interpretation had to be applied. The subsequent main-testing for differences between groups of luminance levels depended on the pre-testing results (see previous explanations). If no interactions between the independent variables were found, the classic procedure of the Main Effects interpretation of the two-way repeated measures ANOVA with two within-subjects factors (luminance level, frame rate) was method of choice. Otherwise, a Simple Main Effect interpretation was applied. At first, a global test was applied (valid for both approaches). If the test showed a p value $< .05$, different values in the tested sets/groups were existent and subsequent pairwise comparisons via Post Hoc Tests (adjusted Bonferroni, no alpha error adjustment) were executed to determine the exact differing sets/groups. If the p value of the global test was larger than .05 (significance level), no statistically significant differences between the compared sets/groups existed. The statistically significant pairwise comparisons were characterized by degrees of freedom (*df*), degrees of freedom for error (*error df*), F-ratio (F), significance level (p), and the Partial Eta Squared (ηp^2), following a defined notation: [$F(df, error\ df)$ = F-ratio (F), significance level (p), partial eta squared (ηp^2)].

tested whether there was a statistically significant difference of the CBU scores between the three luminance levels, averaged over a wider range of frame rates and movement patterns. This allowed the investigation of the general behavior within different ranges of experimental conditions. Two different ranges of frame rates and movement patterns were tested: the complete study range and a limited range (based on statistically significant CBU score differences between specific experimental conditions). Since the sample size was large enough ($N = 30$), parametric tests were assumed to hold the determined level of significance even if there was no normal distribution (Bortz & Schuster, 2010, p. 126). Consequently, parametric tests were applied, which means that the statistical comparison of the CBU scores (CBU_{SCR}) for the three luminance levels was done with a one-way repeated measures ANOVA followed by Post Hoc Tests (Bonferroni) for the two ranges of frame rates and movement patterns (for the same reason, a test for normal distribution did not play a role in the decision to use the two-way repeated measures ANOVA).

Based on the collected data of COBUS1, minimum technical requirements for the frame rate were determined to keep CBU perception within certain limits under defined framework conditions (luminance level, movement pattern). For this purpose, the threshold of annoyance *TOA* was established (threshold of perceptibility *TOP* corresponding to the lower pole of the continuous CBU scale was not considered for further analysis). The experimental paradigm that investigated the *TOA* was classified as a forced choice task, which means that the participant answered the closed question "Did you perceive CBU as annoying?" with "Yes" or "No" after rating the CBU effect (see Section 4.2.8). The next step was to establish a link between the portion of "Yes" answers — referred to as the success rate — and the CBU score. The success rate was calculated for fragments of 0.1 scale points along the continuous CBU scale (upper pole = 1, lower pole = 5). The relation between the success rate and the sample's CBU score was best represented by a nonlinear regression model, a so-called psychometric function defined separately for CAT2 and CAT3 without further classification into subcategories (x-axis: CBU score, y-axis: success rate). For psychometric curve fitting, a cumulative Gaussian function recommended by Wichmann and Hill (2001) was applied (see Formula 4.1).[30]

$$SUC = G + (1 - G - L) \times 0.5 \times \left\{ 1 + \mathrm{erf}\left[(CBU_{SCR} - U) \,/\, \sqrt{2 \times V^2} \right] \right\} \tag{4.1}$$

The success rate represents the accepted share of viewers that perceive CBU as annoying, for example, a success rate of 0.20 means that only 20% of the viewers perceive CBU as annoying. By defining the desired success rate for a specific situation, the selected psychometric function could be used to determine a CBU score that corresponded to the defined success rate. The determined CBU scores are the *TOA*s for the defined success rate under the chosen conditions. In a second step, the CBU scores representing the *TOA* were used to determine the required frame rates that had to be performed to avoid exceeding the initially defined success rate. For this purpose, the findings on the relation between perceived CBU score and frame rate were applied (averaged CBU scores for all three luminance levels were used in this case).

The secondary objective of COBUS1 referred to the effects of the sample's visual performance (e.g., visual acuity) and personal characteristics (short-term state and long-term personality traits) on CBU perception. The recorded characteristics of the sample (visualized via spider plots) were tested for their influence on a global CBU score (volume-based

[30] Two different psychometric functions — a cumulative Gaussian function (Fit 1) and a glmfit with binomial distribution (Fit 2) — were fitted to the empirical data. The MATLAB files »FitPsycheCurveWH« (Fit 1) and »FitPsycheCurveLogit« (Fit 2) used for psychometric curve fitting were created by Jones (2017). Fit 1 was finally chosen for psychometric curve fitting as it showed a superior goodness of fit (SUC = success rate, G = guess rate, L = lapse rate, U = mean value of the distribution, V = standard deviation of the distribution).

approach, see Hypotheses H.5 and H.6).[31] Parameters with metric scale level (i.e., visual performance parameters such as contrast sensitivity) were tested for linear correlation with the global CBU score by using appropriate statistical methods (paired samples, Pearson's correlation, graphical output via scatter plot). With regard to the inquired short- and long-term participant characteristics, five different items were evaluated via bipolar Likert scales (see Appendix A.2.4). The poles of the applied scales were semantically described by bipolar antagonistic word pairs. The single items had ordinal scale level with metric latent variable which means that the evaluated score had ordinal scale level. However, the scores could also be handled like metric data in statistical data analysis.[32] In case of reasonably high linear correlations between the sample's single features (visual performance and personal characteristics) and subjective CBU perception, subgroups of the sample could be formed and statistically compared with each other. Groups that presumably represent a high CBU potential (high visual performance, current state/personality traits favoring CBU perception) and a lower CBU potential (lower visual performance, state/traits making CBU perception less likely) could be defined by a Median Split to generate identical group sizes.

COBUS2 focused on the descriptive analysis of the effect of independent stimulus-based variables (size and position of the CBU stimulus) on subjective CBU perception as the dependent target variable. The experimental categories CAT2 (saccades) and CAT3 (pursuits) were included with further variation of the frame rate (30.0 and 60.0 Hz).[33] Due to the limited sample size ($N = 6$) inductive statistics were not applied. Again, 3D coordinate systems were used to illustrate the relationship between the metric influencing variables (x-axis: stimulus position, y-axis: stimulus size) and the metric target variable (y-axis: CBU_{SCR}). The 3D models were created separately for the experimental categories (CAT2 and CAT3) and the investigated frame rates (30.0 and 60.0 Hz). The CBU score referring to the *TOA* (same procedure as in COBUS1, psychometric function refers to Fit 1) was visualized as an xy-plane in the 3D coordinate systems. The intersection line between xy-plane and the 3D surface that represents CBU perception for various conditions (stimulus' size and position) allowed the assignment of stimulus-based threshold values for the size and position of the CBU-provoking stimulus that must be met to avoid exceeding the specified *TOA*.

4.3 Results

The empirical COBUS studies led to a considerable amount of data to be processed. A basic descriptive analysis was carried out for the complete data set of COBUS1 and COBUS2. Further statistical analysis was performed on selected data, since an all-encompassing analysis would have gone beyond the scope of the doctoral thesis. The selective access to the data was possible using self-developed MATLAB functions (see Sections 4.3.1 and 4.3.2).[34]

[31] Every participant stated a multitude of CBU scores for several COBUS1 conditions. To simplify correlation tests between CBU scoring and participant-dependent parameters, a global CBU score had to be defined. The score represents the general level of a participant's CBU perception and can be determined by either averaging all collected CBU scores or by referring to the volume under the CBU-characterizing surface in the 3D model (x-axis: frame rate, y-axis: luminance level, z-axis: mean CBU score, linear interpolation between data points, numerical integration along x-axis and y-axis). The final choice was made for the volume-based approach.

[32] The assumed linear relations between characteristics of the sample (visual performance, personal characteristics) and its CBU scoring were confirmed for linear regressions with $r^2 \geq .90$. The corresponding hypothesis could be confirmed for single sample characteristics. For example, Hypothesis 5 would be partially confirmed when the linear correlation was verified for visual acuity but not for contrast sensitivity and color vision.

[33] The impact of eye movement directions (nominal scale level) on CBU perception was not analyzed as CBU scores were averaged over all four movement directions to achieve a lower susceptibility against outliers.

[34] All MATLAB functions that relate to the empirical investigations during COBUS1 and COBUS2 were archived but not published to protect the raw data of the studies from unauthorized access. The raw data pertaining to the studies are available from the author upon reasonable request.

4.3.1 Color Break-Up Study 1

For COBUS1, three main MATLAB functions with different tasks were written. The first function »data select cobus1« helps to choose the correct data from the complete data set of the entire sample ($N = 30$) and outputs the corresponding data analysis. The second function »threshold« allows to determine thresholds for CBU scores and frame rates that correspond to a specific assumption that just a share of the viewers evaluates a scene with specific conditions as annoying. The third function »global cbu« visualizes the personal characteristics of the participants within the sample and tests these parameters for correlation with a global CBU score.[35]

Sample Characterization

A total of 33 participants were invited, two participants were excluded from participation (red-green color blindness, inadequate ocular motility), and one participant dropped out during participation (technical problems). This resulted in a data set of $N = 30$ to be analyzed. The sample of COBUS1 consisted of healthy students with an age distribution of 23.3 ± 2.7 years. Gender distribution was balanced, with a tendency towards female participation (57 to 43%).

TABLE 4.1: Power vector components and blurring strength for refractive error, habitual correction, and remaining ametropia of the sample (COBUS1).

Classification	Eye	M in [D]	J_0 in [D]	J_{45} in [D]	BS in [D]
PV_{RE}	OD	-1.67 ± 2.06	+0.13 ± 0.32	-0.07 ± 0.19	+1.81 ± 1.98
	OS	-1.50 ± 1.98	+0.16 ± 0.36	+0.02 ± 0.22	+1.66 ± 1.90
PV_{HC}	OD	-1.10 ± 1.79	+0.04 ± 0.16	-0.03 ± 0.13	+1.11 ± 1.80
	OS	-1.06 ± 1.73	+0.08 ± 0.24	0.00 ± 0.15	+1.09 ± 1.73
PV_{AM}	OD	-0.57 ± 0.53	+0.09 ± 0.25	-0.03 ± 0.13	+0.71 ± 0.43
	OS	-0.43 ± 0.52	+0.08 ± 0.25	+0.02 ± 0.14	+0.61 ± 0.42

Note. $N = 30$. Listed values refer to $MN \pm SD$. M = spherical equivalent; J_0 / J_{45} = Jackson vectors; BS = blurring strength; PV_{RE} = power vector of refractive error; PV_{HC} = power vector of habitual correction; PV_{AM} = power vector of remaining ametropia; OD = oculus dexter; OS = oculus sinister.

Regarding optical correction, more than half of the sample did not wear a habitual correction (63%), whereas the rest of the sample used spectacles (17%) or contact lenses (20%) in comparable shares. The refractive error without correction was investigated with autorefractor. For ametropia analysis, the spherocylindrical values for habitual correction and refractive error had to be transferred into power vectors.[36] From the collected data of habitual correction

[35] For the graphical output of the main MATLAB functions, the external functions »spider« (Arant, 2015), »intersections« (Schwarz, 2017), and »boundedline« (Kearney, 2014) were added to MATLAB's search path or placed in the same folder as the main functions.

[36] Following Thibos and Horner, "power vectors are a geometrical representation of spherocylindrical refractive errors in 3 fundamental dioptric components. The first component is a spherical lens with power M equal to the spherical equivalent of the given refractive error. If this spherical power is removed from the prescription, the result is a Jackson crossed cylinder (JCC) equivalent to a conventional cylinder of positive power J at axis $\alpha + 90°$ crossed with a cylinder of negative power -J at axis α. By convention, we describe this astigmatic component as a JCC of power J at axis α (the meridian of maximum positive power). This JCC can be further resolved into the sum of 2 other JCC lenses, one with power J_0 at axis $\alpha = 0° = 180°$ and the other with power J_{45} at axis $\alpha = 45°$. With this decomposition method, we are able to express any spherocylindrical refractive error by the 3 dioptric powers (M, J_0, J_{45})" (2001, p. 81). Transferring classic spherocylindrical to power vector description leads to a mathematical independence of the three power vector components which is necessary to combine, compare, and statistical analyze lens power or refractive error. Thibos and Horner state that the three components of the power vector (M, J_0, J_{45}) can be interpreted "geometrically as the (x, y, z) coordinates of a point in a 3-dimensional dioptric space. Thus, a power vector is that vector drawn from the coordinate origin of this space to the point (M, J_0, J_{45}). The length of this vector is a measure of the overall blurring strength B [changed to BS to avoid ambiguity within thesis] of a spherocylindrical lens or refractive error" (p. 81).

and refractive error values, the remaining ametropia (while wearing the habitual correction) was calculated. The power vector components (M, J_0, J_{45}) and the blurring strength BS for refractive error, habitual correction, and the remaining ametropia of the sample for right and left eye are summarized in Table 4.1. On average, the sample had a myopic refractive error (spherical equivalent). The habitual correction largely compensated for the refractive error, resulting in a slightly myopic ametropia (while wearing habitual correction). However, as the refractive error, habitual correction, and remaining ametropia refer to an infinite distance and the main study examination was performed at near distance (0.58 m), this slight myopic ametropia should not have affected the visual acuity during main study testing. With regards to the astigmatic component, Jackson cylinders J_0 and J_{45} have to be considered. The remaining astigmatic ametropia that resulted when refractive error was reduced by habitual correction was, on average, small. It was assumed that the remaining astigmatic ametropia did not affect the visual acuity during main study testing. However, the remaining astigmatic ametropia was calculated for infinite distance, which means that additional astigmatic components resulting from near astigmatism were not considered. Nevertheless, the influence of the sample's near astigmatism was likely to be marginal, even if it may have had a noticeable effect for the individual.[37]

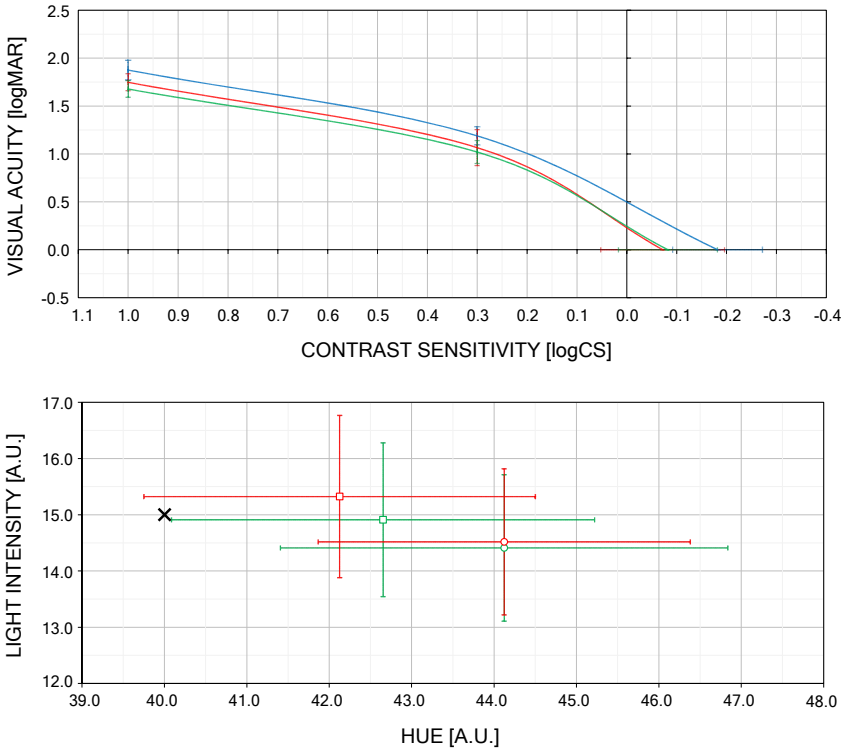

FIGURE 4.9: Sample's visual performance during COBUS1/V2 ($MN \pm SD$). Upper graphic: visual acuity and contrast sensitivity tested with FrACT (blue graph: binocular testing, red graph: right eye, green graph: left eye). Lower graphic: Pitt Diagram based on measurements with HMC Anomaloscope, illustrating sample's adjusted points for the right (green) and left eye (red) regarding first (square) and second measurement (circle), black cross represents ideal point of adjustment.

After compensation of the refractive error with the habitual correction, the small amount of remaining ametropia resulted in a high visual performance of the sample during COBUS1.

[37] The sample's habitual correction, refractive error, and remaining ametropia ($N = 30$, $MN \pm SD$, see Table 4.1) refer to emmetropic (no habitual correction) and ametropic participants (using habitual correction). The sample-averaged effect of the habitual correction on the refractive error (leading to the remaining ametropia) was weakened due to the consideration of emmetropic participants without habitual correction.

As visual acuity and contrast sensitivity during both visits differed only slightly, the visual performance parameter are illustrated only for V2 (see Figure 4.9, upper graphic). The sample's visual acuity under monocular conditions was -0.07 $\pm$ 0.12 logMAR ($MN \pm SD$) for the right eye and -0.08 $\pm$ 0.10 logMAR for the left eye. Under binocular conditions the visual acuity was slightly higher with -0.18 $\pm$ 0.09 logMAR. The contrast sensitivity of the sample's right and left eye was 1.75 $\pm$ 0.09 logCS and 1.68 $\pm$ 0.09 logCS, respectively. Under binocular conditions, the sample showed average values of 1.88 $\pm$ 0.10 logCS. These contrast sensitivity values refer to the optotype size of 50.0′ (corresponding to a visual acuity of 1.0 logMAR). For a smaller optotype size (10.0′ corresponding to 0.30 logMAR), the contrast sensitivity was lower with 1.07 $\pm$ 0.19 logCS, 1.02 $\pm$ 0.12 logCS, and 1.19 $\pm$ 0.09 logCS for monocular (right and left eye) and binocular conditions, respectively. The sample's values for visual acuity and contrast sensitivity were classified as age-appropriate.

Color vision is described via the Pitt Diagram in the lower graphic of Figure 4.9. In the graphic, the ideal point of adjustment (40.0/15.0) is marked with a black cross. With the ideal point of adjustment as center, an elliptic area from 34.0 to 46.0 for hue values (x-axis) and an area of 14.0 to 17.0 for light intensity (y-axis) is considered the normal range. All mean values of the sample lie within this range. However, some single values exceed this range on the right and lower borders of the normal range (see *SD* bars), i.e., some individuals adjusted hue and light conditions during the anomaloscope test outside the normal range. In this case, the Velhagen-Stilling Color Plates were tested to exclude color vision deficiencies (see exclusion criteria).

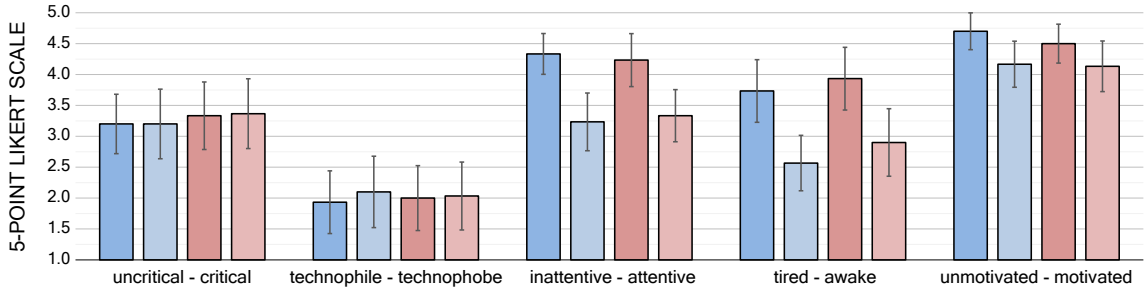

FIGURE 4.10: Sample's short-term state and long-term traits during COBUS1 ($MN \pm 0.5SD$); dark blue bars = pre-questionnaire before main examination phase during V1, pale blue bars = post-questionnaire after main examination phase during V1, dark red bars = pre-questionnaire during V2, pale red bars = post-questionnaire during V2 (Score 1 = *uncritical*, Score 5 = *critical*, etc.).

Figure 4.10 illustrates the sample's personal characteristics inquired through the applied questionnaire (see Appendix A.2.4). Predictably, the sample's long-term personality traits (*uncritical – critical*, *technophile – technophobe*) were quite stable over time (pre-evaluation vs. post-evaluation, first visit vs. second visit). The sample tended to be technophile and showed a moderate critical attitude. As expected, the items for the short-term state (*inattentive – attentive*, *tired – awake*, *unmotivated – motivated*) varied over time — particularly the scores determined before and after the main examination phase. The sample's attention decreased and its tiredness increased during the examination. However, the self-rated motivation remained at a consistently high level.

Effect of Technical Parameters

The following 3D graphics in the Figures 4.11 to 4.13 illustrate the effect of the main independent variables — frame rate (x-axis) and luminance level (y-axis) — on subjective CBU perception as target variable (z-axis). Every graphic represents the findings for one subcategory of CAT2 (variable saccadic length) or CAT3 (variable PEM velocity).

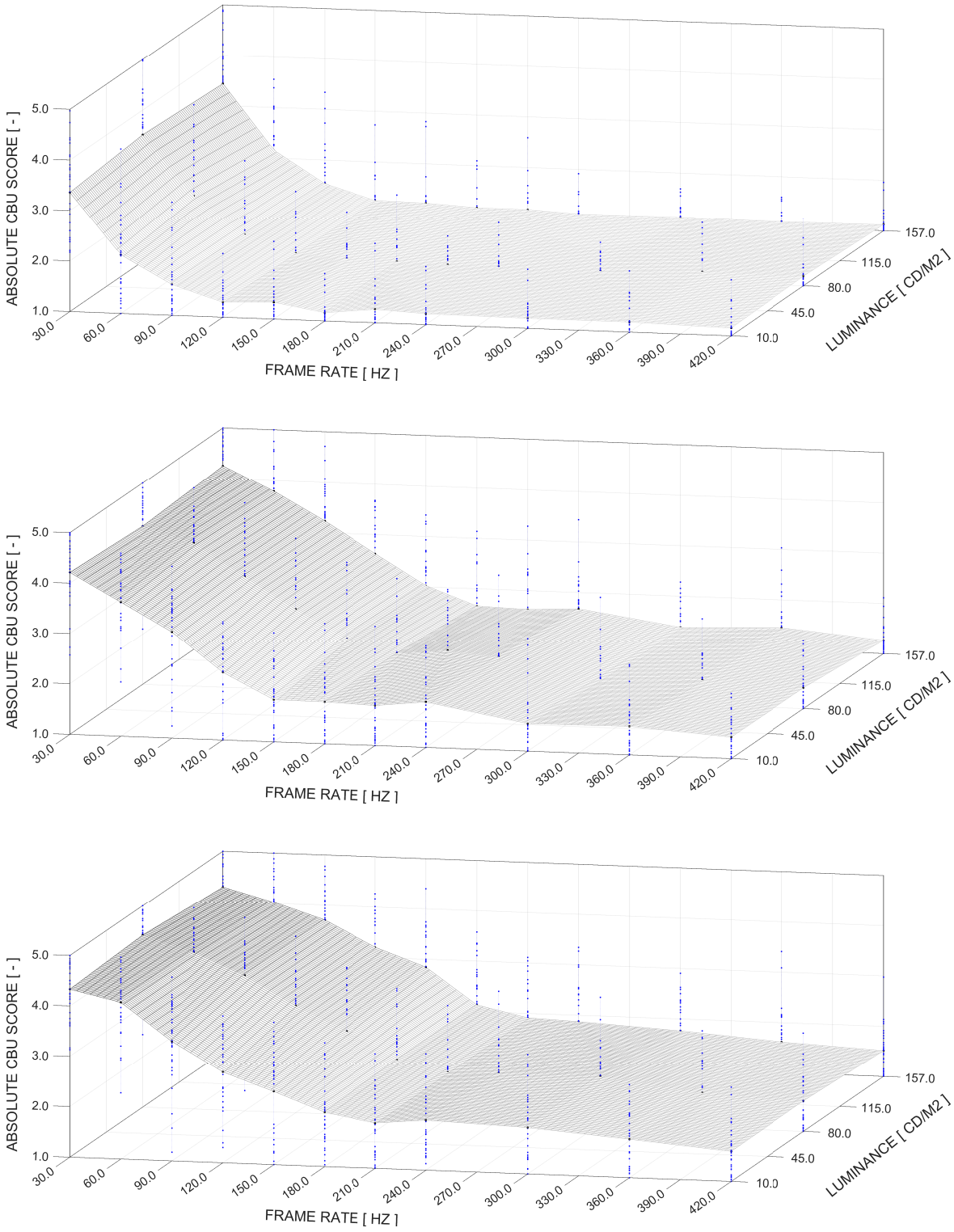

FIGURE 4.11: Sample's absolute CBU score in dependency of frame rate (30.0 to 420.0 Hz) and luminance level (10.0 to 157.0 cd/m^2) during saccadic eye movements (CAT2) with path lengths of 3.6° (upper graphic), 9.0° (middle graphic), and 14.3° (lower graphic); blue dots represent participants' CBU scores, black dots represent sample-averaged CBU scores, gray surfaces represent linear interpolations between averaged CBU scores (see Table F.1 for corresponding data of COBUS1/CAT2).

The graphics in Figure 4.11 and 4.12 refer to saccades with amplitudes of 3.6 to 28.2°, whereas the graphics in Figure 4.13 refer to pursuits with velocities of 18.0, 36.0, and 54.0 deg/s.

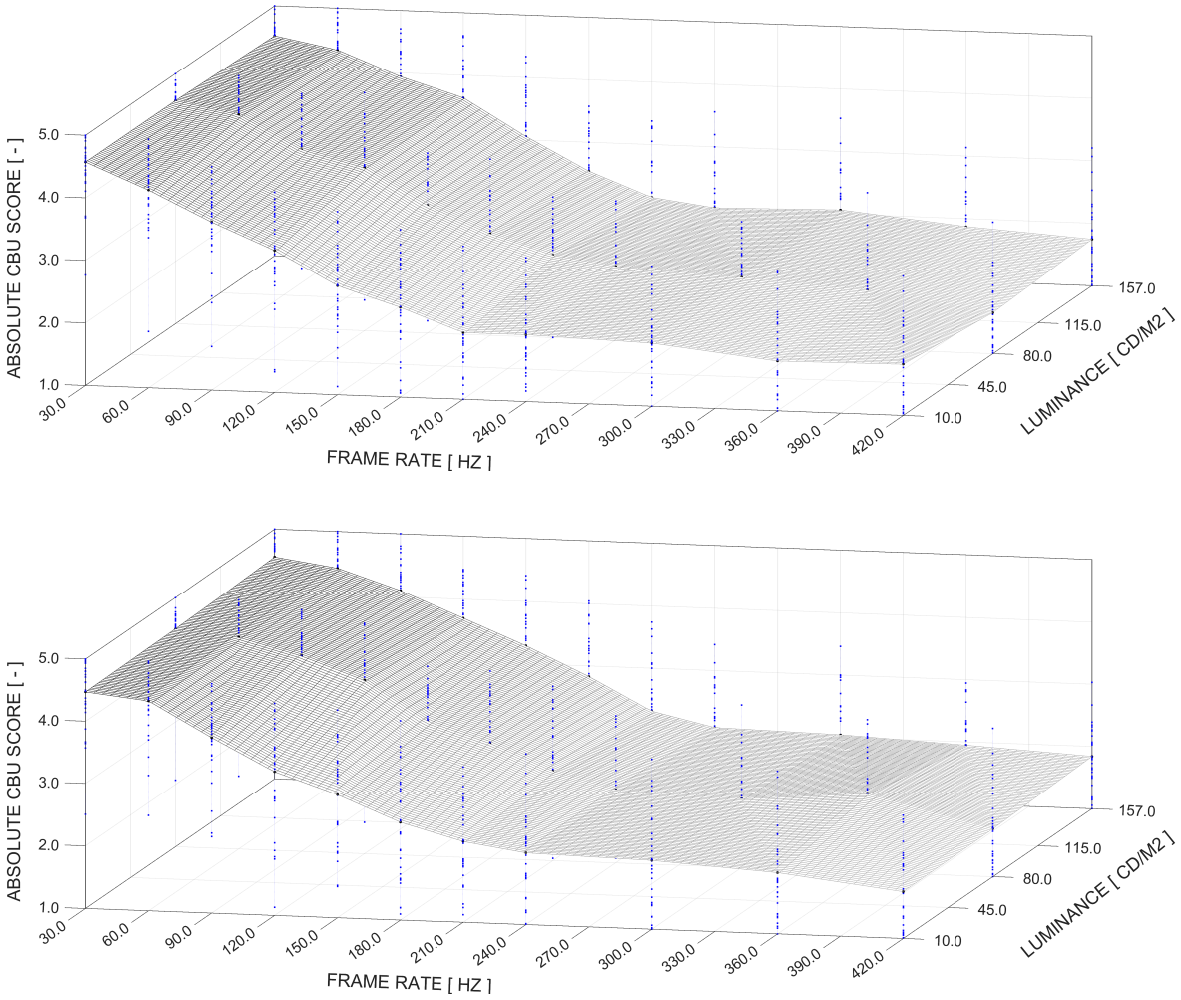

FIGURE 4.12: Sample's absolute CBU score in dependency of frame rate (30.0 to 420.0 Hz) and luminance level (10.0 to 157.0 cd/m^2) during saccadic eye movements (CAT2) with path lengths of 21.3° (upper graphic) and 28.2° (lower graphic); blue dots represent participants' CBU scores, black dots represent sample-averaged CBU scores, gray surfaces represent linear interpolations between averaged CBU scores (see Table F.1 for corresponding data of COBUS1/CAT2).

The graphics in Figures 4.11 to 4.13 provide a general overview of the collected data during COBUS1. What can be observed at first view? The graphics clearly show that the frame rate has a stronger impact on subjective CBU perception than the luminance level no matter which kind of eye movement is executed to provoke CBU (saccade or pursuit). This statement is particularly true for the range of low to medium frame rates (black dots are sample-averaged CBU scores). Likewise, the interindividual variability of CBU perception within the sample is clearly visible (blue dots are individual CBU scores).

The illustrated data sets are the foundation for the following statistical testing of Hypotheses H.1 to H.4 (see Section 4.2.1) which refer to the primary aim of COBUS1 to investigate the influence of frame rate and luminance level on subjective CBU perception.

$$CBU\ Score = B1 \times \exp\left(B2 \times Frame\ Rate \right) + B3 \tag{4.2}$$

Statistical testing starts with Hypothesis H.1 that assumes a negative correlation between frame rate and subjective CBU perception. It is assumed that the relationship between frame rate and CBU perception can be expressed by an exponential function. Therefore, a uniform exponential curve fitting function was applied for all tested conditions (see Formula 4.2).

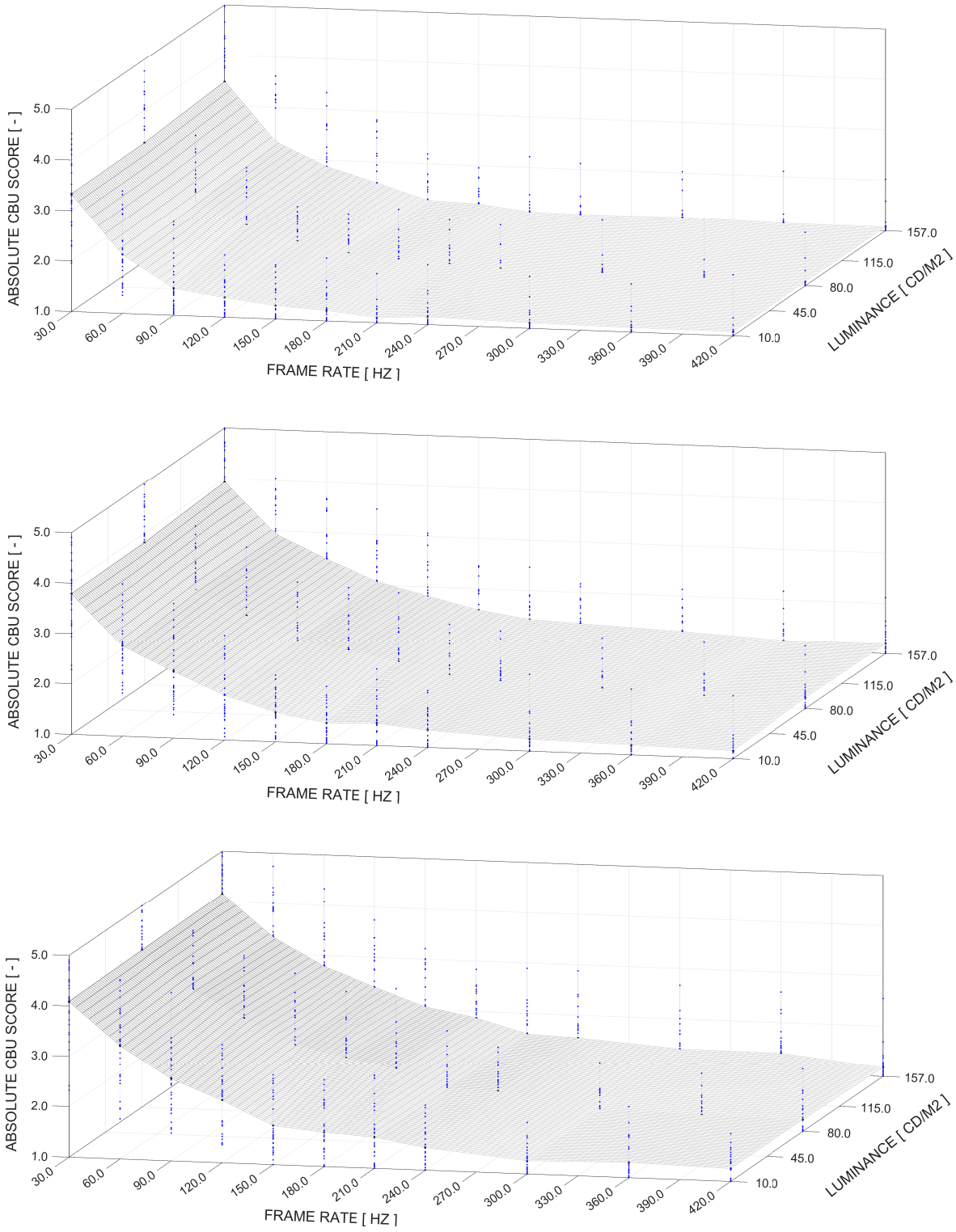

FIGURE 4.13: Sample's absolute CBU score in dependency of frame rate (30.0 to 420.0 Hz) and luminance level (10.0 to 157.0 cd/m^2) during pursuits (CAT3) with velocities of 18.0 deg/s (upper graphic), 36.0 deg/s (middle graphic), and 54.0 deg/s (lower graphic); blue dots represent participants' CBU scores, black dots represent sample-averaged CBU scores, gray surfaces represent linear interpolations between averaged CBU scores (see Table F.2 for relating data of COBUS1/CAT3).

Table 4.2 lists the coefficient characteristics (B values) for the fitted exponential functions for all tested conditions (variation of luminance levels and movement patterns). Furthermore,

the adjusted coefficient of determination r^2 was calculated to quantify the goodness of fit. The exponential function appropriately describes the relation between CBU perception and frame rate for all conditions ($r^2 > .93$). The nonlinear two-dimensional regression model expressed by Hypothesis H.1 is confirmed.

TABLE 4.2: Characteristics of the curve-fitted exponential functions representing the relation between frame rate and CBU score for all investigated luminance levels and subcategories of COBUS1.

LL in [cd/m²]		Saccadic Length in [deg]					PEM Velocity [deg/s]		
		3.6	**9.0**	**14.3**	**21.3**	**28.2**	**18.0**	**36.0**	**54.0**
10.0	**B1**	4.9924	4.1501	3.9924	4.0186	3.9100	4.7162	4.0184	4.1600
	B2	-0.0277	-0.0118	-0.0095	-0.0080	-0.0066	-0.0252	-0.0147	-0.0121
	B3	1.1918	1.4383	1.5425	1.5615	1.4954	1.1156	1.1831	1.2165
	adj. r^2	.995	.961	.964	.976	.970	.996	.996	.996
80.0	**B1**	5.2796	4.0652	4.1170	4.1589	4.0670	4.0630	3.8078	3.9731
	B2	-0.0263	-0.0093	-0.0078	-0.0057	-0.0051	-0.0202	-0.0124	-0.0094
	B3	1.1448	1.2699	1.3838	1.2692	1.2947	1.1022	1.1623	1.1172
	adj. r^2	.993	.964	.958	.971	.934	.996	.996	.996
157.0	**B1**	5.4125	4.3771	4.1095	4.1676	4.2474	4.2092	3.9698	3.9865
	B2	-0.0282	-0.0097	-0.0065	-0.0060	-0.0052	-0.0192	-0.0127	-0.0102
	B3	1.1207	1.1674	1.1359	1.3008	1.2063	1.0840	1.1811	1.2008
	adj. r^2	.998	.969	.954	.947	.947	.995	.997	.996

Note. $N = 30$. Curve fitting coefficients *B1*, *B2*, and *B3* refer to the exponential function in Formula 4.2. *B* values and the coefficients of determination (adjusted r^2) were determined under consideration of the sample's mean CBU score, not the single CBU scores of all participants. Variation of saccadic length during CAT2 and alteration of PEM velocity during CAT3. LL = luminance level.

Due to the great number of investigated conditions during COBUS1, the dependency between CBU score and frame rate is illustrated only for one subcategory of CAT2 and CAT3 (see Figure 4.14, *xz*-plane cuts of the CBU surfaces are illustrated in Figures 4.11 and 4.13).[38] The left-side graphics refer to saccades with a path length of 14.3°, whereas the right-side graphics refer to pursuits with an eye movement velocity of 18.0 deg/s. The illustrations include all tested luminance levels of 10.0, 80.0, and 157.0 cd/m². The fitted exponential functions in the graphics refer to the listed values in Table 4.2. It is of interest at which point the exponential flattening reaches a plateau of low CBU scores that are not significantly different. Therefore, inductive statistical analysis was used to test for statistically significant differences between CBU scores provoked by different frame rates (and different luminance levels). Inductive statistic was done by applying a two-way repeated measures ANOVA, since the effect of two independent variables (frame rate and luminance level) was investigated on the dependent variable CBU score.[39] The results for the impact of frame rate as one independent variable are described here, whereas the impact of the second independent variable (luminance level) is described in the result section referring to Hypothesis H.2. The number of discrete frame rate values (11) tested during COBUS1 yields a large number of potential combinations of frame rate-provoked CBU scores that could be statistically tested for significant differences.

[38] The complete data set of COBUS1 is accessible with the MATLAB function »data select cobus1«. With the help of the function, it is possible to obtain more detailed statistical information on other areas of interest covered by the complete data set (incl. graphical output). How to operate the function is described in detail in the m-file (definition of input/output arguments, etc.).

[39] Presenting all results of the two-way repeated measures ANOVA would go beyond the scope of this thesis. The statistical SPSS output of the full ANOVA procedure is documented in the spv-file »two way anova output« (generated via sps-file »two way anova syntax«) on basis of the raw data-containing sav-file »anova data set«. The SPSS documents were archived but not published to protect the raw data of the empirical study from unauthorized access.

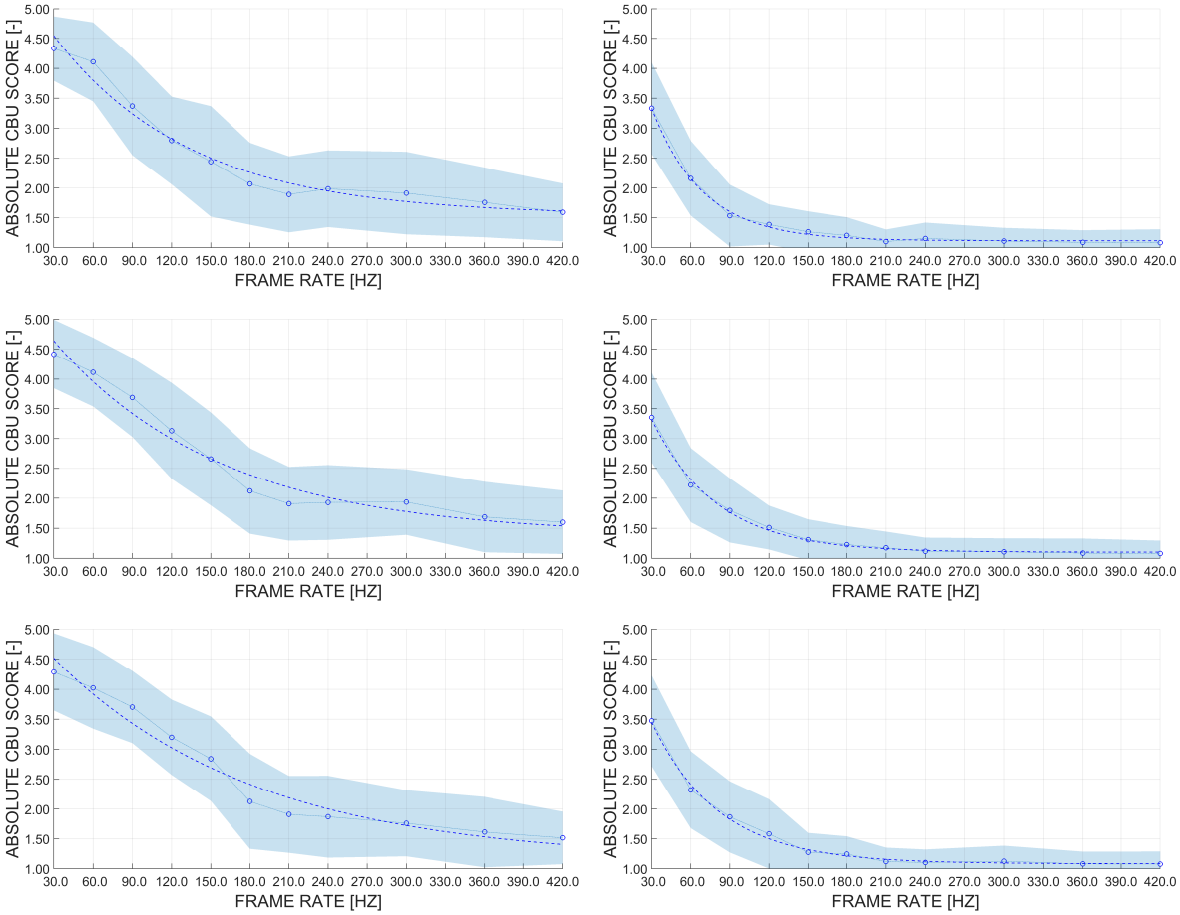

FIGURE 4.14: Absolute CBU score in dependency of frame rate during saccade with path length of 14.3° (CAT2, three left graphics) and pursuit with velocity of 18.0 deg/s (CAT3, three right graphics) for luminance levels of 10.0 cd/m^2 (two upper graphics), 80.0 cd/m^2 (two middle graphics), and 157.0 cd/m^2 (two lower graphics); blue circles are sample's mean CBU scores, blue dotted lines are linear CBU interpolations between mean values, pale blue areas are sample's CBU standard deviations (linear interpolation between data points), blue dashed lines are fitted exponential regressions.

Table 4.3 shows the probability values p as the statistical result of the hypothesis testing for CBU score differences for all possible frame rate combinations explicitly for the condition of a saccadic length of 14.3° (CAT2) and a luminance level of 80.0 cd/m^2 (see also Figure 4.14, left side). For example, there is a statistically significant difference between the CBU scores for the frame rates of 60.0 and 90.0 Hz [$F(10, 20) = 65.445$, $p < .001$, $\eta p^2 = .970$] or 90.0 and 120.0 Hz [$F(10, 20) = 65.445$, $p = .006$, $\eta p^2 = .970$] in the subcategory of a saccadic length of 14.3° (CAT2) and a luminance level of 80.0 cd/m^2. No statistically significant difference was found for the CBU scores referring to frame rates of 180.0 and 210.0 Hz ($p = 1.000$) or 240.0 and 300.0 Hz ($p = 1.000$). Looking at the entire table, it is clear that the plateau of statistically stable CBU scores with low values is reached at CBU scores referring to a frame rate of 180.0 Hz.[40]

[40]The frame rate threshold that separates areas of decreasing/stable CBU scores (see Figure 4.14, left side) is defined by a minimum of two subsequent CBU scores without statistically significant difference to the potential threshold value (arbitrary assumption). However, the absence of CBU score differences for frame rates above the defined threshold of 180.0 Hz cannot be confirmed for every case (e.g., 180.0/360.0 Hz) as the data set of COBUS1 is best but not perfectly represented by an exponential function (leading to erratic frame rate thresholds for different luminance levels and subcategories as well, see Table 4.5). Alternatively, the frame rate threshold could be determined by defining a specific gradient of the fitted exponential function, which would increase consistency.

TABLE 4.3: Analysis of CBU score differences of saccadic eye movement over 14.3° (CAT2) at a luminance level of 80.0 cd/m^2 for all tested frame rate combinations during COBUS1 (p values listed).

		Frame Rate in [Hz]										
		30.0	**60.0**	**90.0**	**120.0**	**150.0**	**180.0**	**210.0**	**240.0**	**300.0**	**360.0**	**420.0**
Frame Rate in [Hz]	**30.0**	—	.063	<.001	<.001	<.001	<.001	<.001	<.001	<.001	<.001	<.001
	60.0	.063	—	<.001	<.001	<.001	<.001	<.001	<.001	<.001	<.001	<.001
	90.0	<.001	<.001	—	.006	<.001	<.001	<.001	<.001	<.001	<.001	<.001
	120.0	<.001	<.001	.006	—	<.001	<.001	<.001	<.001	<.001	<.001	<.001
	150.0	<.001	<.001	<.001	<.001	—	.008	<.001	<.001	<.001	<.001	<.001
	180.0	<.001	<.001	<.001	<.001	.008	—	1.000	1.000	1.000	.001	<.001
	210.0	<.001	<.001	<.001	<.001	<.001	1.000	—	1.000	1.000	1.000	.726
	240.0	<.001	<.001	<.001	<.001	<.001	1.000	1.000	—	1.000	1.000	.251
	300.0	<.001	<.001	<.001	<.001	<.001	1.000	1.000	1.000	—	1.000	.158
	360.0	<.001	<.001	<.001	<.001	<.001	.001	1.000	1.000	1.000	—	1.000
	420.0	<.001	<.001	<.001	<.001	<.001	<.001	.726	.251	.158	1.000	—

Note. $N = 30$. Statistically significant difference between CBU scores under different conditions confirmed when corresponding p value smaller than the significance level of $\alpha = .05$, leading to the rejection of the null hypothesis of no difference between the CBU scores.

Another example referring to CAT3 (pursuit eye movement of 18.0 deg/s, luminance level of 80.0 cd/m^2) is illustrated in the second Table 4.4. Again, the p values were determined for the comparison of CBU scores of different frame rate combinations. For example, there is a statistically significant difference between the CBU scores for the frame rates of 30.0 and 60.0 Hz [$F(10, 20) = 24.659$, $p < .001$, $\eta p^2 = .925$] or 90.0 and 120.0 Hz [$F(10, 20) = 24.659$, $p = .003$, $\eta p^2 = .925$] in this CAT3 subcategory. No statistically significant difference was determined for the CBU scores referring to frame rates of 150.0 and 180.0 Hz ($p = 1.000$) or 180.0 and 210.0 Hz ($p = 1.000$). Looking at the entire table, statistically stable CBU scores are reached at the frame rate threshold of 150.0 Hz.

TABLE 4.4: Analysis of CBU score differences of PEM of 18.0 deg/s (CAT3) at a luminance level of 80.0 cd/m^2 for all tested frame rate combinations during COBUS1 (p values listed).

		Frame Rate in [Hz]										
		30.0	**60.0**	**90.0**	**120.0**	**150.0**	**180.0**	**210.0**	**240.0**	**300.0**	**360.0**	**420.0**
Frame Rate in [Hz]	**30.0**	—	<.001	<.001	<.001	<.001	<.001	<.001	<.001	<.001	<.001	<.001
	60.0	<.001	—	<.001	<.001	<.001	<.001	<.001	<.001	<.001	<.001	<.001
	90.0	<.001	<.001	—	.003	<.001	<.001	<.001	<.001	<.001	<.001	<.001
	120.0	<.001	<.001	.003	—	.215	<.001	<.001	<.001	<.001	<.001	<.001
	150.0	<.001	<.001	<.001	.215	—	1.000	.986	.042	.040	.010	.002
	180.0	<.001	<.001	<.001	<.001	1.000	—	1.000	.236	.345	.253	.136
	210.0	<.001	<.001	<.001	<.001	.986	1.000	—	1.000	1.000	1.000	1.000
	240.0	<.001	<.001	<.001	<.001	.042	.236	1.000	—	1.000	1.000	1.000
	300.0	<.001	<.001	<.001	<.001	.040	.345	1.000	1.000	—	1.000	1.000
	360.0	<.001	<.001	<.001	<.001	.010	.253	1.000	1.000	1.000	—	1.000
	420.0	<.001	<.001	<.001	<.001	.002	.136	1.000	1.000	1.000	1.000	—

Note. $N = 30$. Statistically significant difference between CBU scores under different conditions confirmed when corresponding p value smaller than the significance level of $\alpha = .05$, leading to the rejection of the null hypothesis of no difference between the CBU scores.

The following Table 4.5 shows the frame rate thresholds for a stable CBU score after overshooting. The thresholds are based on statistical tests without consideration of the human perception. The table includes the frame rate thresholds for the two mentioned examples and all other frame rate thresholds for the subcategories of CAT2/CAT3 (including all applied luminance levels).

TABLE 4.5: Frame rate thresholds for all tested luminance levels and subcategories of COBUS1.

LL in [cd/m²]	Saccadic Length in [deg]					PEM Velocity in [deg/s]		
	3.6	9.0	14.3	21.3	28.2	18.0	36.0	54.0
10.0	120.0	150.0	180.0	180.0	180.0	150.0	210.0	150.0
80.0	120.0	150.0	180.0	180.0	210.0	150.0	210.0	300.0
157.0	120.0	150.0	180.0	210.0	210.0	180.0	210.0	210.0

Note. Frame rate thresholds in [Hz] were determined under consideration of statistical testing of CBU score differences (see Tables 4.3 and 4.4) to separate frame rate ranges of variable and stable CBU scores. Variation of saccadic length during CAT2 and alteration of PEM velocity during CAT3. LL = luminance level.

The next Hypothesis H.2 states that there is a positive linear correlation between luminance level of the CBU-provoking stimulus and subjective CBU perception. A uniform linear function was applied to all experimental conditions (see Formula 4.3).

$$CBU\ Score = B1 \times Luminance\ Level + B2 \tag{4.3}$$

Table 4.6 shows the coefficient characteristics (B values) for the fitted linear functions of all tested conditions (variation of frame rates and movement patterns). Furthermore, the adjusted coefficients of determination r^2 are listed to quantify the goodness of fit.

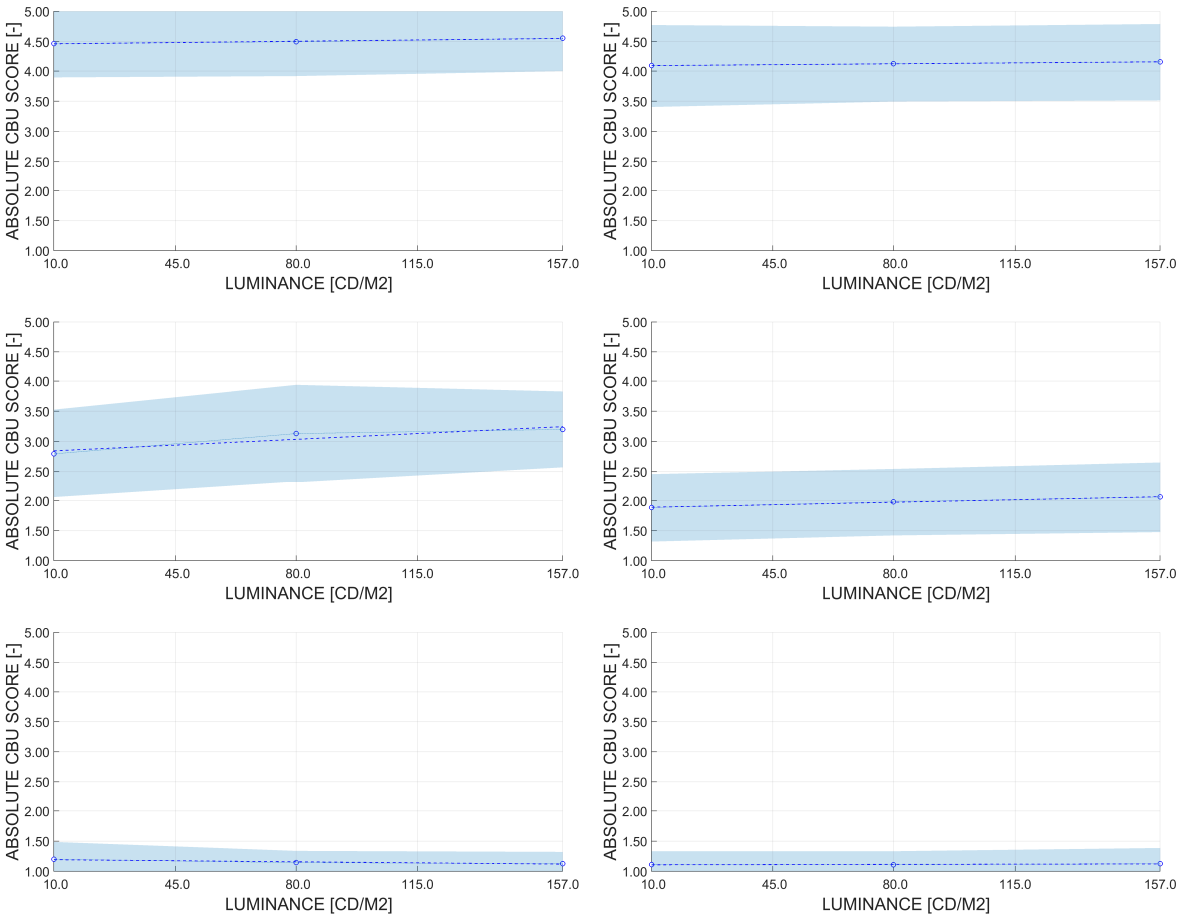

FIGURE 4.15: Absolute CBU score in dependency of luminance level under variation of frame rate and movement pattern during CAT2 (top-left graphic: large saccade of 28.2° at low frame rate of 30.0 Hz, middle-left: medium 14.3° saccade at medium 120.0 Hz, bottom-left: small 3.6° saccade at high 300.0 Hz) and CAT3 (top-right: fast pursuit of 54.0 deg/s at low frame rate of 30.0 Hz, middle-right: medium 36.0 deg/s pursuit at medium 120.0 Hz, bottom-right: slow 18.0 deg/s pursuit at high 300.0 Hz); blue circles are sample's mean CBU scores, blue dotted lines are linear CBU interpolations between mean values, pale blue areas are sample's CBU standard deviations (linear interpolation between data points), blue dashed lines are fitted linear regressions.

Looking at the slopes of the fitted linear functions (*B1*) across the complete test range, no uniform behavior can be observed (see Table 4.6). While no globally uniform behavior can be identified, some local patterns are observable. The assumed positive correlation between luminance level and CBU score with a marginal but relevant slope exists for a frame rate range between 90.0 and 150.0 Hz.[41] Within this area, the determined *B1* threshold is fully reached for larger saccadic lengths (14.3 to 28.2°) and on rare occasions for some PEM velocities. In all other cases, only weak positive correlations (with *B1* values less than 0.0017) or even negative correlations (expressed by negative *B1* values) were determined.

TABLE 4.6: Characteristics of the curve-fitted linear functions representing the relation between luminance level and CBU score for all investigated frame rates and subcategories of COBUS1.

Frame Rate in [Hz]		**Saccadic Length in [deg]**					**PEM Velocity in [deg/s]**		
		3.6	**9.0**	**14.3**	**21.3**	**28.2**	**18.0**	**36.0**	**54.0**
30.0	**B1**	0.0005	0.0003	-0.0003	-0.0004	0.0006	0.0010	0.0010	0.0004
	B2	3.3952	4.1780	4.3720	4.5826	4.4598	3.3068	3.7675	4.0857
	adj. r^2	-.569	-.685	-.755	.597	.951	.743	.791	.999
60.0	**B1**	-0.0001	0.0008	-0.0006	0.0011	0.0004	0.0011	0.0010	0.0005
	B2	2.2241	3.6985	4.1311	4.1982	4.3629	2.1466	2.7974	3.2784
	adj. r^2	-.996	-.213	.415	-.008	.794	.965	.646	-.428
90.0	**B1**	-0.0005	0.0009	0.0022	0.0017	0.0019	0.0022	0.0011	0.0010
	B2	1.6259	3.1150	3.4037	3.6856	3.8566	1.5508	2.3243	2.6647
	adj. r^2	.700	.613	.513	.894	.251	.770	.755	-.079
120.0	**B1**	-0.0004	0.0019	0.0027	0.0025	0.0026	0.0013	0.0012	0.0012
	B2	1.3023	2.3656	2.8170	3.3000	3.3740	1.3864	1.8808	2.2345
	adj. r^2	.950	.513	.710	.586	.123	.937	.990	.929
150.0	**B1**	-0.0007	0.0013	0.0027	0.0021	0.0022	0.0001	0.0015	0.0019
	B2	1.3142	1.8659	2.4268	2.7746	2.9587	1.2794	1.6196	1.8325
	adj. r^2	.247	.172	.989	.520	.955	-.944	.368	.048
180.0	**B1**	0.0000	-0.0012	0.0004	0.0007	0.0018	0.0003	0.0011	0.0013
	B2	1.1689	1.8551	2.0762	2.4758	2.5987	1.2054	1.4497	1.7251
	adj. r^2	-.898	.792	.600	-.477	.358	.967	-.019	-.075
210.0	**B1**	-0.0007	-0.0012	0.0001	0.0005	0.0001	0.0001	-0.0001	-0.0002
	B2	1.2522	1.8644	1.8963	2.1339	2.3381	1.1247	1.4328	1.6139
	adj. r^2	.305	-.197	.558	-.802	-.990	-.930	-.598	.492
240.0	**B1**	-0.0007	-0.0015	-0.0008	-0.0004	-0.0005	-0.0003	0.0003	0.0007
	B2	1.2193	1.9171	1.9955	2.1179	2.1700	1.1531	1.3235	1.4672
	adj. r^2	.969	.991	.999	-.772	.093	.800	-.005	.074
300.0	**B1**	-0.0005	-0.0011	-0.0011	0.0004	-0.0004	0.0001	0.0004	0.0010
	B2	1.1975	1.5415	1.9598	2.0196	2.1140	1.1072	1.2298	1.2384
	adj. r^2	.802	.848	.344	.148	.585	.278	.902	.808
360.0	**B1**	-0.0006	-0.0008	-0.0010	0.0005	-0.0003	-0.0001	0.0000	0.0006
	B2	1.2232	1.5665	1.7692	1.8301	2.0840	1.0909	1.1926	1.2625
	adj. r^2	.444	.953	.999	-.524	-.970	.861	-.713	-.133
420.0	**B1**	-0.0002	-0.0011	-0.0005	-0.0005	0.0006	0.0000	0.0003	-0.0005
	B2	1.1737	1.4558	1.6139	1.7777	1.7313	1.0834	1.1658	1.2650
	adj. r^2	-.497	.703	.393	-.633	.801	.946	-.104	.905

Note. $N = 30$. Curve fitting coefficients *B1* and *B2* refer to the linear function in Formula 4.3. *B* values and the coefficients of determination (adjusted r^2) were determined under consideration of the sample's mean CBU score, not the single CBU scores of all participants. Variation of saccadic length during CAT2 and alteration of PEM velocity during CAT3.

[41] A relevant slope was determined for *B1* values equal to or greater than 0.0017 which guaranteed a CBU score variation of at least 0.25 scale points along the tested range of luminance levels (10.0 to 157.0 cd/m^2).

The adjusted coefficients of determination r^2 are not constantly high in Table 4.6. The requirement of $r^2 \geq .90$ is only achieved for 9 out of 55 experimental CAT2 conditions and for 9 out of 33 conditions of CAT3. The linear function does not adequately represent most of the data. Hence, the use of a linear function is not appropriate for all study conditions (frame rate, experimental subcategories). Overall, a general linear relation between luminance level and subjective CBU perception cannot be confirmed. This leads to the rejection of Hypothesis H.2.

The exemplary illustrations in Figure 4.15 (representing yz-plane cuts of 3D graphics in the Figures 4.11 to 4.13) clarify these findings. The experimental conditions with lower (< 90.0 Hz) and higher frame rates (> 150.0 Hz) do not yield a relevant positive correlation between luminance level and CBU score (see upper/lower graphics). A positive and at least marginal effect of luminance level is only identifiable for a medium frame rate range (90.0 to 150.0 Hz) during larger saccades and partially during pursuits (see middle graphic).

Following the previous findings, it was additionally investigated if an inductive statistical group comparison of CBU scores referring to the luminance levels of 10.0, 80.0, and 157.0 cd/m^2 showed significant differences. The group comparison was performed for every single experimental condition of COBUS1 (variable frame rates and movement patterns). Therefore, a two-way repeated measures ANOVA with two within-subjects factors (luminance level, frame rate) was chosen. Generally, the statistical analysis was divided into pretesting of an interaction between the independent variables (luminance level, frame rate) and main-testing for differences between groups of luminance levels which included several statistical tests.[42] Summarizing, statistically significant CBU score differences are only confirmed within a frame rate range between 60.0 to 150.0 Hz in CAT2 and 60.0 to 180.0 Hz in CAT3 (with only one exception). However, within these ranges, the frame rate conditions that lead to statistical significance vary with different movement velocity patterns. For a saccadic length of 14.3° (CAT2), statistical significance is only shown for frame rates of 90.0 and 120.0 Hz, whereas a saccadic length of 21.3° shows statistical significance for frame rates of 60.0, 90.0, 120.0, and 150.0 Hz. The same variance can be identified for the movement velocity patterns of CAT3. For all frame rate conditions that lead to statistically significant CBU score differences, the majority (11) of the pairwise comparison by Post Hoc Testing shows statistically significant differences for the highest luminance levels (80.0 and 157.0 cd/m^2) compared to the lowest luminance level (10.0 cd/m^2). In the rest of the cases (6), at least one of the two highest luminance levels (80.0 or 157.0 cd/m^2) shows a statistically different CBU score compared to the lowest luminance level (10.0 cd/m^2). There is almost no experimental condition for which a statistically significant difference of CBU scores can be detected by comparing the two highest luminance levels (only one case). Finally, it can be concluded that the inductive statistical analysis confirms and specifies the initial findings on basis of the non-ideal linear model parameters (see earlier statements in this section). The statistically significant but marginal effects (maximum CBU score difference approximately 0.5 score points) only appear in a frame rate range between 60.0 and 180.0 Hz (CAT2 and CAT3 combined) This is roughly the lower half of the tested frame rate range. Comparing the different CAT2/CAT3 movement velocity patterns, the significant frame rates do not appear with a constant but rather an erratic pattern (within the mentioned range of frame rates). It is the pairwise comparison between the highest luminance levels (80.0 and 157.0 cd/m^2)

[42] Presenting all results of the two-way repeated measures ANOVA would exceed the limits of the result section (the Main Effects interpretation for pursuits of 36.0 deg/s was omitted due to the analysis without frame rate-dependent classification). All statistically significant ANOVA results are provided in Tables F.5 to F.12. The statistical SPSS output of the full ANOVA procedure is documented in the spv-file »two way anova output« (generated via sps-file »two way anova syntax«) on basis of the raw data-containing sav-file »anova data set«. The SPSS documents were archived but not published to protect the raw data of the empirical study from unauthorized access.

and the lowest luminance level (10.0 cd/m^2) that leads to a statistical significance — almost without exception.

After comparing the luminance level groups separately for each experimental condition, it was additionally tested whether there is a statistically significant difference in CBU scores between the three luminance levels averaged over a wider range of frame rates and movement patterns. This gives an overview of the general behavior under different experimental conditions. Two different ranges of frame rates and movement patterns were tested: a full range and a limited range. Regarding the limited test range, frame rates between 60.0 and 150.0 Hz and movement patterns between 9.0 and 28.2° were included for CAT2. For CAT3, frame rates between 60.0 and 180.0 Hz and all movement patterns (18.0 to 54.0 deg/s) were included. This selection contained the experimental conditions (frame rates and movement patterns) with the highest statistical significance in terms of the effect of luminance level on CBU perception. The excluded upper half of the frame rate range included the tail of the exponential regression lines with lower CBU values. It was expected that the plateau characteristic of the CBU scores for the upper half of the frame rate range weakens the impact of the luminance level on CBU scores. This is because all CBU scores are at a low level during high frame rate presentation, irrespective of the applied luminance level. Generally, the statistical comparison of the CBU scores for the three luminance levels was done with a one-way repeated measures ANOVA and Post Hoc Tests (Bonferroni).[43] In a first step, the CBU scores for all frame rates (30.0 to 420.0 Hz) and all movement patterns (3.6 to 28.2° for CAT2, 18.0 to 54.0 deg/s for CAT3) were averaged. As a result, every participant has one averaged CBU score for every luminance level ($MN \pm SD$). For CAT2, the CBU scores for the luminance levels of 10.0, 80.0, and 157.0 cd/m^2 are at 2.414 ± 0.385, 2.503 ± 0.363, and 2.458 ± 0.345. A statistically significant difference between the groups is confirmed for the luminance levels of 10.0 and 80.0 cd/m^2 [$F(1.289, 37.369) = 7.667$, $p = .002$, $\eta p^2 = .209$] as well as 80.0 and 157.0 cd/m^2 [$F(1.289, 37.369) = 7.667$, $p = .005$, $\eta p^2 = .209$]. Referring to CAT3, the CBU scores for the luminance of 10.0, 80.0, and 157.0 cd/m^2 are at 1.792 ± 0.323, 1.869 ± 0.327, and 1.887 ± 0.331. A statistically significant group difference is confirmed between the luminance of 10.0 and 80.0 cd/m^2 [$F(2, 58) = 25.824$, $p < .001$, $\eta p^2 = .471$] as well as 10.0 and 157.0 cd/m^2 [$F(2, 58) = 25.824$, $p < .001$, $\eta p^2 = .471$]. In a second step, the limited ranges of frame rates and movement patterns were tested. For CAT2, the CBU scores for the luminance levels of 10.0, 80.0, and 157.0 cd/m^2 are at 3.246 ± 0.551, 3.482 ± 0.533, and 3.493 ± 0.519 (averaged over frame rates and movement patterns). A statistically significant difference between the groups is confirmed for the luminance levels of 10.0 and 80.0 cd/m^2 [$F(1.289, 37.369) = 35.232$, $p < .001$, $\eta p^2 = .549$] as well as 10.0 and 157.0 cd/m^2 [$F(1.289, 37.369) = 35.232$, $p < .001$, $\eta p^2 = .549$]. With regard to CAT3, the CBU scores for the luminance levels of 10.0, 80.0, and 157.0 cd/m^2 are at 1.941 ± 0.411, 2.101 ± 0.442, and 2.106 ± 0.462. A statistically significant group difference is confirmed between the luminance levels of 10.0 and 80.0 cd/m^2 [$F(1.707, 49.495) = 37.568$, $p < .001$, $\eta p^2 = .564$] as well as 10.0 and 157.0 cd/m^2 [$F(1.707, 49.495) = 37.568$, $p < .001$, $\eta p^2 = .564$]. The statistical analysis reveals that the difference between the lowest luminance level (10.0 cd/m^2) and the two highest luminance levels (80.0 and 157.0 cd/m^2) increases as the frame rate and movement pattern ranges narrow. However, the differences in CBU scores between the low luminance and the two higher luminance levels are still marginal (while statistically significant). The CBU scores of the two highest luminance levels are comparable (no statistically significant difference found).

[43] Normal distribution is only confirmed for 10 out of 12 variables (Shapiro-Wilk); however, parametric tests could still be applied (see Section 4.2.9). The SPSS output of the one-way repeated measures ANOVA is documented in the spv-files »one way anova output 1« and »one way anova output 2« referring to the raw data-containing sav-file »anova data set«. The SPSS documents were archived but not published to protect the raw data of the empirical study from unauthorized access.

Hypotheses H.1 and H.2 concern assumptions within the subcategories of CAT2/CAT3 (impact of frame rate/luminance level on CBU), whereas Hypotheses H.3 and H.4 deal with assumptions across the subcategories (impact of movement behavior on CBU). Hypothesis H.3 states a positive correlation between saccadic amplitude (CAT2) and subjective CBU perception. It was assumed that a power function adequately represents this relationship. A uniform curve fitting function was used for all conditions (see Formula 4.4).

$$CBU\ Score = B1 \times Saccadic\ Length^{B2} + B3 \tag{4.4}$$

In contrast, Hypothesis H.4 states a positive linear correlation between the velocity of pursuit eye movement (CAT3) and subjective CBU perception (see Formula 4.5).

$$CBU\ Score = B1 \times Pursuit\ Eye\ Movement\ Velocity + B2 \tag{4.5}$$

Tables 4.7 and 4.8 list the coefficients (B values) for the fitted power (H.3) and linear functions (H.4) for all test conditions (variable frame rates and luminance levels). The adjusted coefficient of determination r^2 was calculated to quantify the goodness of fit.

TABLE 4.7: Characteristics of the curve-fitted power functions representing the relation between saccadic length and CBU score for all investigated frame rates and luminance levels during COBUS1.

LL in [cd/m²]		Frame Rate in [Hz]										
		30.0	**60.0**	**90.0**	**120.0**	**150.0**	**180.0**	**210.0**	**240.0**	**300.0**	**360.0**	**420.0**
10.0	**B1**	-5.826	-9.613	-8.079	-6.731	-243.299	-26.886	-8.291	-4.581	-8.662	-4.032	-5.193
	B2	-1.188	-1.070	-0.888	-0.288	-0.003	-0.027	-0.066	-1.198	-0.061	-0.118	-0.073
	B3	4.631	4.600	4.207	5.941	243.496	27.131	8.903	2.205	9.201	4.673	5.877
	adj. r^2	.970	.993	.995	.985	.969	.992	.960	.992	.950	.965	.906
80.0	**B1**	-3.668	-9.967	-8.687	-7.927	-13.379	-258.196	-5.125	-3.194	-132.621	-307.110	-109.937
	B2	-0.804	-1.146	-0.817	-0.320	-0.091	-0.003	-0.176	-0.637	-0.004	-0.002	-0.003
	B3	4.814	4.636	4.655	6.535	13.096	258.267	5.264	2.571	133.068	307.613	110.758
	adj. r^2	.967	.997	.995	.998	.984	.977	.929	.980	.915	.911	.982
157.0	**B1**	-4.603	-10.037	-9.602	-7.472	-20.145	-281.786	-139.594	-2.886	-174.540	-185.437	-257.736
	B2	-1.012	-1.082	-0.897	-0.477	-0.059	-0.003	-0.004	-0.518	-0.003	-0.002	-0.001
	B3	4.698	4.672	4.573	5.284	19.869	281.804	140.022	2.602	174.972	185.987	258.320
	adj. r^2	.967	.994	1.000	.992	.957	.965	.997	.999	.923	.985	.913

Note. $N = 30$. Curve fitting coefficients *B1*, *B2*, and *B3* refer to the power function in Formula 4.4. B values and the coefficients of determination (adjusted r^2) were determined under consideration of the sample's mean CBU score, not the single CBU scores of all participants. LL = luminance level.

TABLE 4.8: Characteristics of the curve-fitted linear functions representing the relation between PEM velocity and CBU score for all investigated frame rates and luminance levels during COBUS1.

LL in [cd/m²]		Frame Rate in [Hz]										
		30.0	**60.0**	**90.0**	**120.0**	**150.0**	**180.0**	**210.0**	**240.0**	**300.0**	**360.0**	**420.0**
10.0	**B1**	0.021	0.030	0.030	0.024	0.014	0.013	0.014	0.008	0.004	0.006	0.005
	B2	2.982	1.647	1.072	0.991	1.037	0.962	0.874	1.022	1.053	0.984	0.993
	adj. r^2	.970	.986	.882	.979	.950	.989	.935	.954	.735	1.000	.982
80.0	**B1**	0.021	0.032	0.029	0.023	0.023	0.020	0.012	0.013	0.005	0.005	0.004
	B2	2.996	1.681	1.317	1.113	0.933	0.885	0.973	0.881	1.037	1.010	1.024
	adj. r^2	.971	.974	.963	.989	.957	.990	.992	.993	.779	.988	.672
157.0	**B1**	0.019	0.028	0.025	0.023	0.022	0.017	0.013	0.012	0.008	0.009	0.003
	B2	3.176	1.860	1.462	1.195	0.936	0.937	0.907	0.902	0.998	0.911	1.053
	adj. r^2	.920	.968	.930	.982	.905	.998	.944	.961	.966	.942	.178

Note. $N = 30$. Curve fitting coefficients *B1* and *B2* refer to the linear function in Formula 4.5. B values and the coefficients of determination (adjusted r^2) were determined under consideration of the sample's mean CBU score, not the single CBU scores of all participants. LL = luminance level.

The power function accurately fits the data points of CAT2 for all tested conditions (see Table 4.7, $r^2 \geq .90$ for 33 out of 33 cases). This confirms Hypothesis H.3. The coefficient of determination r^2 for the linear functions generally shows values above .90 with some exceptions (see Table 4.8, 28 out of 33 cases), largely confirming Hypothesis H.4.

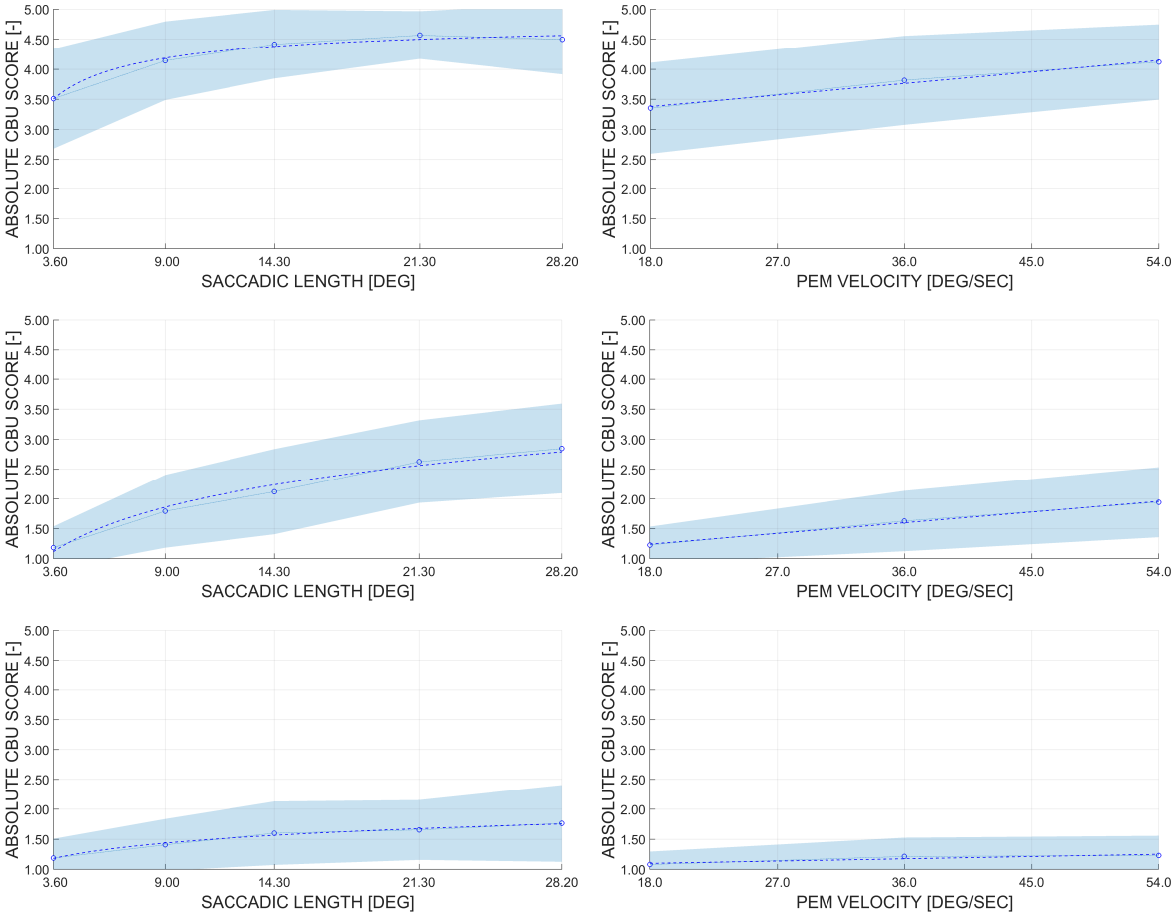

FIGURE 4.16: Absolute CBU score in dependency of saccadic path length (CAT2, three left graphics) and PEM velocity (CAT3, three right graphics) under variation of frame rate (two upper graphics: low frame rate of 30.0 Hz, two middle graphics: medium frame rate of 180.0 Hz, two lower graphics: high frame rate of 420.0 Hz) while luminance level was kept stable at 80.0 cd/m^2; blue circles are sample's mean CBU scores, blue dotted lines are linear CBU interpolations between mean values, pale blue areas are sample's CBU standard deviations (linear interpolation between data points), blue dashed lines are fitted regressions (power function for CAT2, linear function for CAT3).

The relationship between saccadic length and CBU score (H.3) is exemplarily illustrated for a low, a medium, and a high frame rate at a constant luminance level of 80.0 cd/m^2 (see Figure 4.16, three graphics on the left side). A positive correlation between dependent and independent variable is always given. However, the effect of increasing saccadic length on the CBU score decreases with higher frame rates. The relationship between PEM velocity and CBU score (H.4) is illustrated for the same conditions (see Figure 4.16, three graphics on the right side). Dependent and independent variable show a positive correlation for the three conditions. However, the effect of increasing PEM velocity on the CBU score decreases with higher frame rates (see also *B1* values in Table 4.8 representing the slope of the linear function).[44]

[44]Inductive statistics were not applied to test for statistically significant differences between CBU scores provoked by different saccadic lengths (H.3) or pursuit eye movement velocities (H.4).

Annoyance Threshold Determination

Having investigated the impact of frame rate and luminance level on the CBU score (see Hypotheses H.1 and H.2), threshold values for frame rates that guarantee a certain percentage of viewers without annoying CBU perception were determined for the experimental categories of CAT2/CAT3.

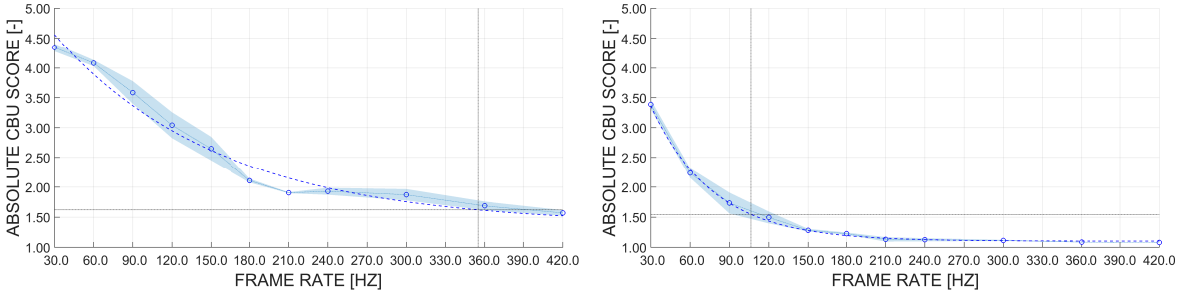

FIGURE 4.17: Averaged absolute CBU score over all tested luminance levels (10.0, 80.0, and 157.0 cd/m^2) in dependency of frame rate during saccade with path length of 14.3° (CAT2, left graphic) and pursuit with velocity of 18.0 deg/s (CAT3, right graphic); blue circles are sample's mean CBU scores, blue dotted lines are linear CBU interpolations between mean values, pale blue areas are sample's CBU standard deviations (linear interpolation between data points), black dash-dotted lines are threshold lines, blue dashed lines are fitted exponential regressions (CAT2: $B1 = 4.0368$, $B2 = -0.0078$, $B3 = 1.3701$, $r^2 = .964$; CAT3: $B1 = 4.2867$, $B2 = -0.0213$, $B3 = 1.1028$, $r^2 = .998$).

The luminance level has only a marginal impact on CBU perception, especially when compared to the impact of frame rate variation (see previous findings). This marginal effect was only found within a limited range of frame rates and movement patterns. Consequently, the annoyance thresholds were determined assuming that the luminance level has no significant impact on CBU score (at least within the tested range of luminance levels). Therefore, the CBU scores of the three tested luminance levels were averaged out within the CAT2/CAT3 subcategories. This procedure is exemplarily illustrated for a saccadic length of 14.3° in CAT2 and a PEM velocity of 18.0 deg/s in CAT3 (see graphics in Figure 4.14 for illustration of single luminance levels). The separate data sets for the three luminance levels were combined to determine the averaged CBU scores ($MN \pm SD$) as well as the fitted exponential function of the mixed data set of all tested luminance levels (see Figure 4.17). Subsequently, the frame rate threshold values for CBU annoyance control were determined on the basis of the mixed data set and its curve fitting.[45]

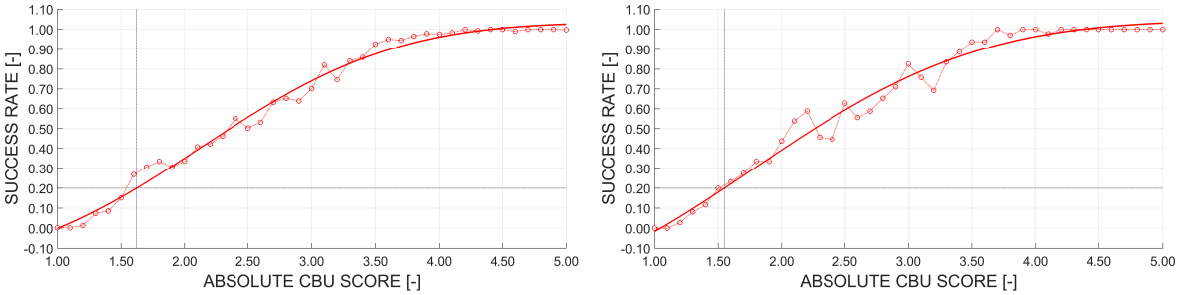

FIGURE 4.18: Fitted psychometric functions for saccades (CAT2, left graphic) and pursuits (CAT3, right graphic); red circles are sample's data points, red dotted lines are linear interpolations between data points, red lines are psychometric functions (Fit 1), black dash-dotted lines are threshold lines.

[45] Averaged CBU scores over three luminance levels simplified the threshold determination. For every subcategory of CAT2/CAT3, one instead of three frame rate thresholds was determined (fixed success rate assumed).

The experimental paradigm investigating the required thresholds for a limited CBU perception results in a psychometric function that describes the relation between the so-called success rate and CBU score (see Section 4.2.9 for information on the applied curve fitting approach). The psychometric function was separately defined for CAT2 and CAT3 without further classification into subcategories (see Figure 4.18). The success rate indicates the accepted share of viewers who perceive CBU as annoying, for example, a success rate of 0.20 means that only 20% of the viewers find CBU annoying. The psychometric function was used to determine a CBU score that corresponds to the defined success rate. For example, in CAT2 (saccade with path length of 14.3°) or CAT3 (pursuits of 18.0 deg/s), the CBU score corresponding to a success rate of 0.20 is 1.62 or 1.55, respectively (as illustrated in Figure 4.18 with the black dash-dotted threshold lines). The determined CBU scores are the so-called thresholds of annoyance (*TOA*). In a second step, the *TOA* was used to determine the required frame rates which have to be performed to avoid exceeding the initially defined success rate. To do that, the findings on the relation between perceived CBU score and frame rate were used (see black dash-dotted threshold lines in Figure 4.17). For the exemplary success rate of 0.20, the *TOA*s of 1.62 (CAT2) and 1.55 (CAT3) correspond to a frame rate of 354.9 Hz for saccades with a path length of 14.3° (CAT2) and 106.3 Hz for pursuits with a velocity of 18.0 deg/s (CAT3).

TABLE 4.9: Frame rate thresholds for selected success rates referring to all subcategories during COBUS1.

SUC	Experimental Category 2						Experimental Category 3			
	CBU_{SCR}	Saccadic Length in [deg]					CBU_{SCR}	PEM Velocity in [deg/s]		
		3.6	9.0	14.3	21.3	28.2		18.0	36.0	54.0
0.025	1.09	—	—	—	—	—	1.11	288.89	—	—
0.050	1.18	188.10	—	—	—	—	1.18	190.14	773.57	—
0.075	1.26	140.64	—	—	—	—	1.24	161.02	311.48	404.69
0.100	1.34	121.41	444.36	—	—	—	1.30	143.46	259.74	333.76
0.125	1.41	109.33	349.20	575.85	848.78	718.05	1.37	130.89	229.69	294.15
0.150	1.49	100.56	303.21	454.09	590.37	595.42	1.43	121.10	208.49	266.62
0.175	1.55	93.70	272.89	394.45	501.16	525.44	1.49	113.10	192.12	245.52
0.200	1.62	88.08	250.34	354.92	446.42	476.57	1.55	106.33	178.78	228.43
0.250	1.75	79.19	217.58	301.93	376.29	408.79	1.67	95.26	157.79	201.64
0.300	1.88	72.27	193.82	265.73	329.78	361.34	1.78	86.38	141.49	180.93
0.350	2.00	66.59	175.13	238.14	294.88	324.71	1.90	78.93	128.10	163.95
0.400	2.12	61.73	159.62	215.73	266.80	294.72	2.02	72.46	116.65	149.46
0.450	2.24	57.45	146.26	196.72	243.13	269.12	2.14	66.70	106.58	136.74
0.500	2.36	53.59	134.42	180.05	222.49	246.59	2.26	61.46	97.52	125.29
0.600	2.61	46.71	113.72	151.26	186.99	207.48	2.52	52.05	81.39	104.96
0.700	2.88	40.45	95.24	125.87	155.86	172.84	2.80	43.45	66.80	86.57
0.800	3.20	34.29	77.34	101.49	126.06	139.45	3.14	34.99	52.57	68.67
0.900	3.61	27.48	57.82	75.13	93.95	103.25	3.58	25.76	37.16	49.28
1.000	4.41	17.23	28.83	36.27	46.77	49.73	4.37	12.68	15.48	22.05

Note. Success rates (*SUC*) and their corresponding CBU scores (CBU_{SCR}) refer to the threshold of annoyance (*TOA*). Hence, the resulting frame rate thresholds in [Hz] represent annoyance thresholds. Crossed out table cells indicate that the frame rate threshold does not lie within the tested range.

For a general overview, Table 4.9 provides a summary of selected success rates, their corresponding CBU scores (*TOA*s), and required frame rates for all CAT2/CAT3 subcategories. The table does not give a complete picture of all possible success rates. More detailed insights are provided by the MATLAB function »threshold« (explanation of the function is embedded in the code).

Effect of Participant Characteristics

Hypotheses H.5 and H.6 relate to the secondary aim of COBUS1 to examine the influence of the participant's visual performance, short-term state, and long-term personality traits on CBU perception. Both hypotheses were tested by the MATLAB function »global cbu«.

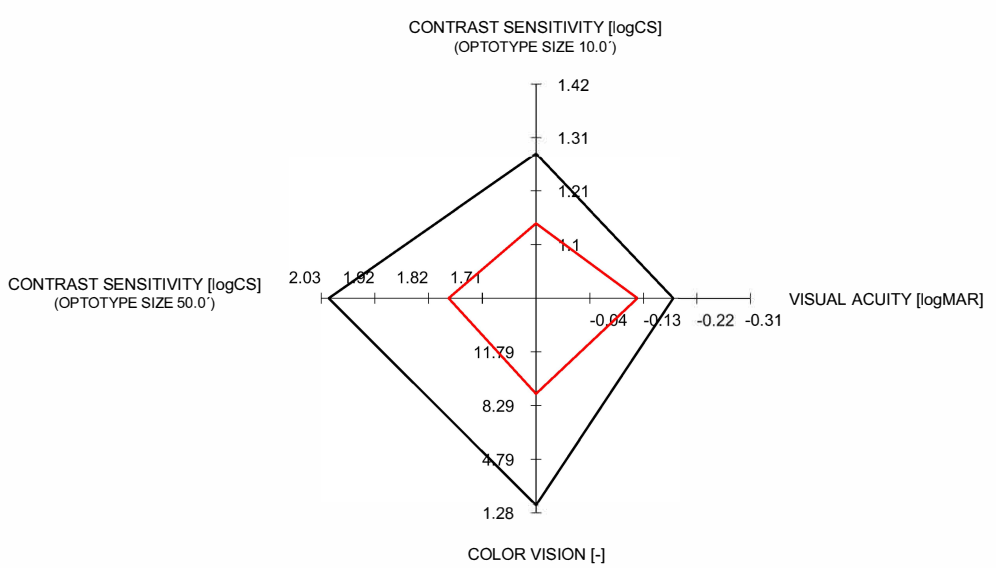

FIGURE 4.19: Visual acuity, contrast sensitivity (both binocular), and color vision (monocular) of Participant 1/4 (black/red) averaged over both COBUS1 visits; see Appendix A.2.3 for tests/procedures.

The visual performance of Participant 1 and 4 is exemplarily illustrated in a spider plot including visual acuity, contrast sensitivity, and color vision (see Figure 4.19).

TABLE 4.10: Curve-fitted linear regressions describing the relation between the sample's visual performance/personal characteristics and the global CBU score (COBUS1).

Variable	Condition	Experimental Category 2			Experimental Category 3		
		B1	B2	r^2	B1	B2	r^2
visual acuity	bino, V1/V2	-5.2340E+04	+1.2061E+05	.040	+7.5306E+02	+9.5436E+04	.000
contrast sensitivity	bino, V1/V2, 10.0′	+5.5305E+03	+1.2291E+05	.000	-1.4945E+03	+9.7100E+04	.000
	bino, V1/V2, 50.0′	-2.8879E+04	+1.8374E+05	.015	+3.1196E+04	+3.6767E+04	.024
color vision	mono, V1/V2	-5.6399E+02	+1.3348E+05	.010	+1.2323E+03	+8.6717E+04	.071
uncritical – critical	pre/post, V1/V2	-1.3501E+03	+1.3397E+05	.005	+2.0759E+03	+8.8508E+04	.016
	pre/post, V1	-3.9767E+02	+1.3453E+05	.000	+3.0993E+03	+8.7296E+04	.020
	pre/post, V2	-2.8635E+03	+1.3544E+05	.020	+3.2401E+02	+9.2314E+04	.000
technophile – technophobe	pre/post, V1/V2	-6.4824E+03	+1.4262E+05	.114	-2.0992E+03	+9.9541E+04	.017
	pre/post, V1	-9.5166E+03	+1.5245E+05	.198	-2.0269E+03	+1.0130E+05	.010
	pre/post, V2	-2.9485E+03	+1.3179E+05	.020	-2.1295E+03	+9.7694E+04	.018
inattentive – attentive	pre/post, V1	+6.0056E+03	+1.1053E+05	.030	-2.4064E+03	+1.0632E+05	.005
	pre/post, V2	-2.8633E+03	+1.3668E+05	.008	-6.4770E+03	+1.1790E+05	.066
tired – awake	pre/post, V1	+4.9495E+02	+1.3169E+05	.000	-7.9890E+03	+1.2238E+05	.090
	pre/post, V2	-3.9253E+03	+1.3926E+05	.026	-6.1605E+03	+1.1445E+05	.107
unmotivated – motivated	pre/post, V1	-1.2266E+04	+1.8763E+05	.096	-5.6367E+03	+1.2220E+05	.023
	pre/post, V2	-4.0677E+03	+1.4341E+05	.015	-4.4045E+03	+1.1241E+05	.030

Note. $N = 30$. Visual performance testing included the determination of the sample's visual acuity, contrast sensitivity, and color vision. Personal characteristics testing included the evaluation of short-term items (e.g., attention level) and long-term items (e.g., affinity to technology). V1/V2 = test results refer to Visit 1/2 of COBUS1; mono/bino = test results were collected under monocular/binocular viewing conditions of the participant (monocular testing with superior eye); pre/post = test results were collected before/after the main examination phase of COBUS1; 10.0′/50.0′ = test results refer to an optotype size of 10.0′/50.0′ (see Section 4.2.8 for further explanations of the examination process and Appendix A.2 for additional information of the applied tests/devices). *B1* = slope of linear regression; *B2* = *y*-intercept of linear regression; r^2 = coefficient of determination.

The spider plot in Figure 4.19 visualizes the averaged visual performance for both visits (V1/V2). The visual performance of Participant 1 is better than Participant 4's in all disciplines. The disciplines shown relate to Hypothesis H.5, which assumes a positive linear correlation between the participant's visual performance and his/her CBU perception.

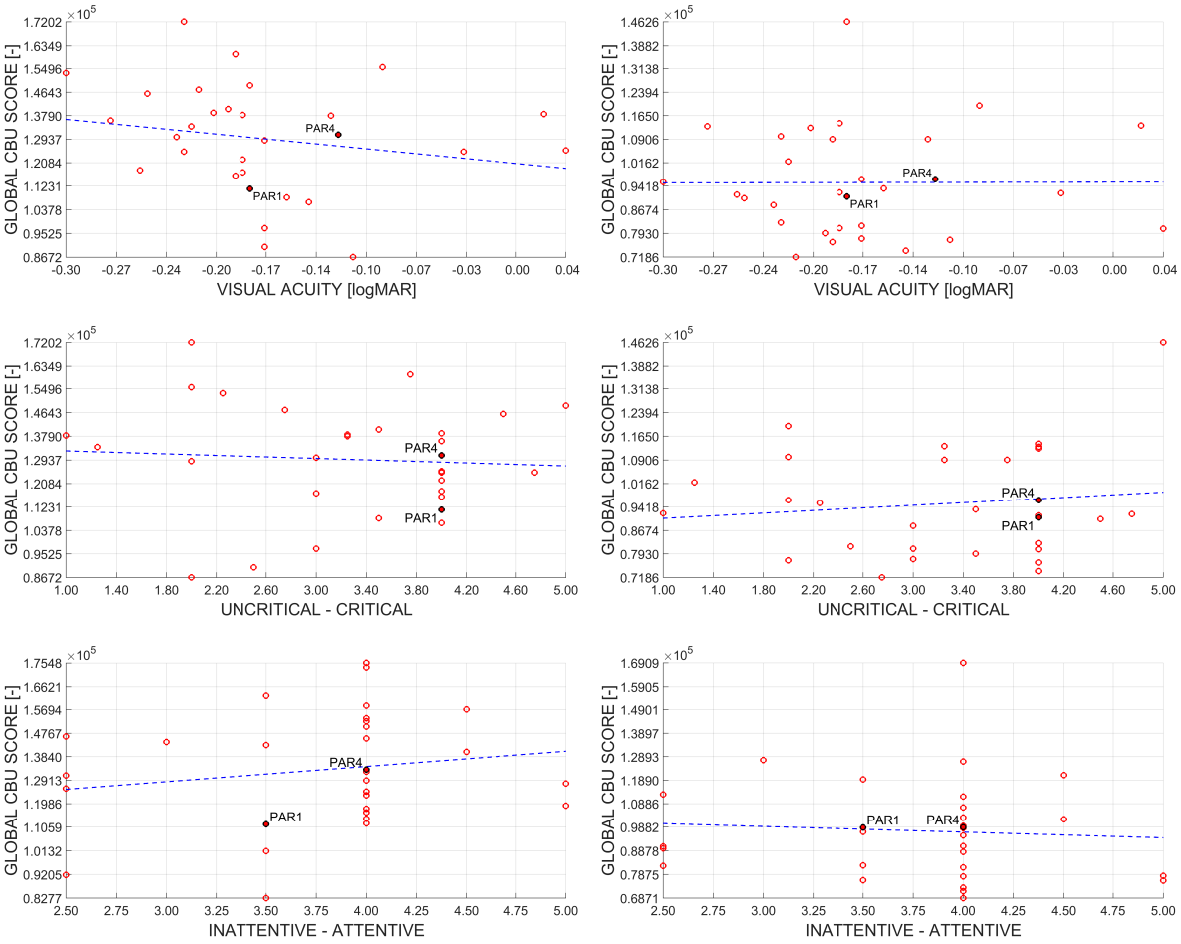

FIGURE 4.20: Global CBU score in dependency of visual acuity (binocular, visit-averaged, upper graphics), long-term (Score 1 = *uncritical*, Score 5 = *critical*, visit-averaged, middle graphics) and short-term item (Score 1 = *inattentive*, Score 5 = *attentive*, V1, lower graphics) for CAT2/CAT3 (left/right graphics); red circles are participants' data points, blue dashed lines are fitted linear regressions.

Figure 4.20 (two upper scatter plots) illustrates the relation between visual acuity and the global CBU score (averaged values of both visits).[46] Participant 1 and 4 are highlighted in the graphics representing CAT2 (left graphic) and CAT3 (right graphic). It is noticeable that Participant 1 shows lower CBU scores than Participant 4 even though s/he has a higher visual acuity (CAT2 and CAT3). To clarify the behavior of the entire sample, the regression line is illustrated as a dashed blue line. The CAT2 regression line symbolizes a positive correlation, meaning that the global CBU score increases with increasing visual acuity (mathematical smaller [logMAR] values indicate a higher visual acuity). In contrast, the regression line for CAT3 has a slope of almost zero, indicating that visual acuity does not have an impact on the global CBU score. However, the regression lines of both experimental categories

[46] In the course of hypothesis testing, CBU scores of different experimental conditions were compressed to a global CBU score. The global CBU score could be calculated with a volume-based or an average-based approach (the former was applied, see Section 4.2.9). However, it was irrelevant which approach was used as the comparison of both scores shows high coefficients of determination when fitting a linear regression (adjusted r^2 = .981 for CAT2 and .983 for CAT3, analyzed with supplementary MATLAB function »global cbu comparison«).

do not represent the data points well, i.e., the correlation between dependent and independent variable is generally weak (see Table 4.10). In conclusion, visual acuity alone is not an appropriate indicator for the prediction of the magnitude of CBU perception. The two other visual performance parameters — contrast sensitivity and color vision — do not show a strong positive correlation with the global CBU score either (see Table 4.10). Summing up, none of the three visual performance indicators tested (visual acuity, contrast sensitivity, color vision) can be used to reliably predict CBU perception provoked by saccades ($r^2 < .05$) or pursuits ($r^2 < .10$). As a result, Hypothesis H.5 must be rejected completely.

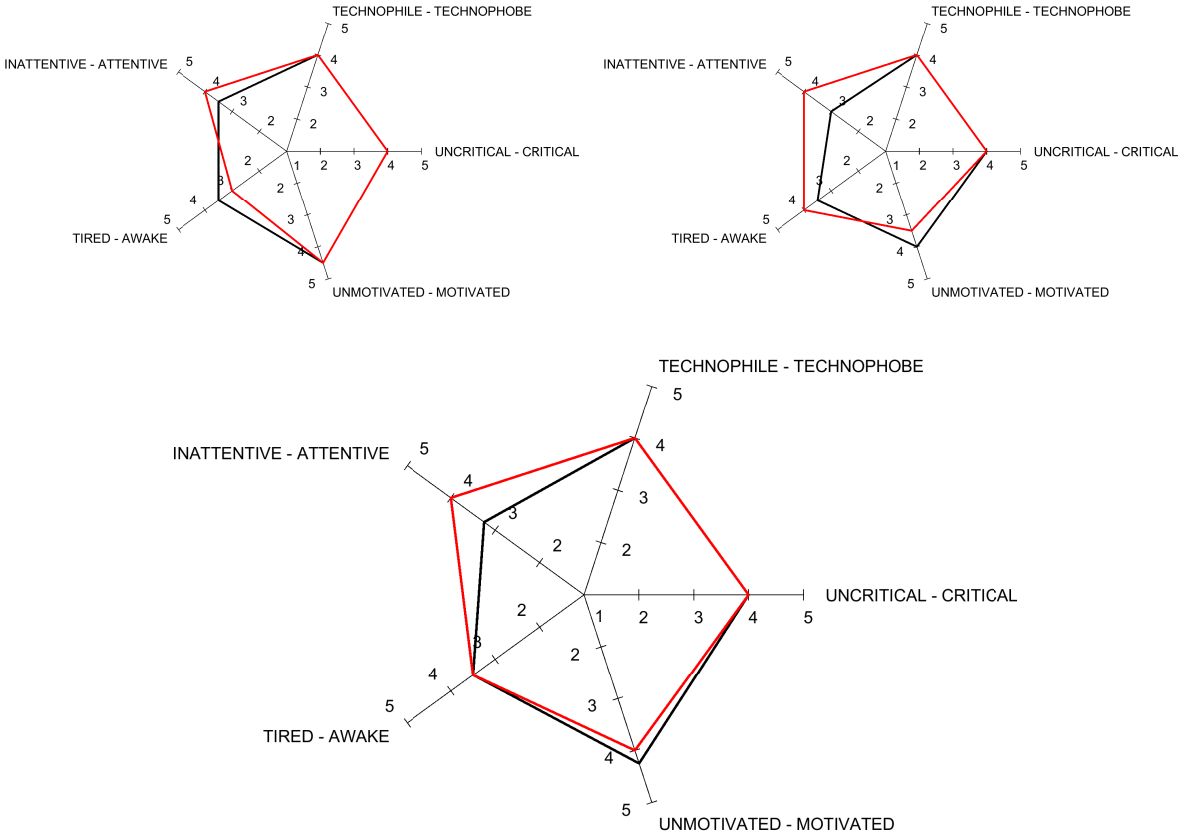

FIGURE 4.21: Short- and long-term characteristic items of Participant 1/4 (black/red) for first (top-left graphic) and second visit (top-right), and averaged over both visits (bottom) during COBUS1 (Score 1 = *uncritical/tired*, Score 5 = *critical/awake*, etc., averaged scores over evaluations before/after main examination phase, see Appendix A.2.4 for applied questionnaire).

The short-term state (*inattentive – attentive*, *tired – awake*, *unmotivated – motivated*) as well as the long-term traits (*uncritical – critical*, *technophile – technophobe*) of Participant 1 and 4 are illustrated in Figure 4.21. The spider plots refer to the data collection during V1 and V2 (two upper graphics) and the data average for both visits (lower graphic). Every spider plot visualizes the five short/long-term items. Every item was averaged over two evaluations during a visit (directly before and after the main study phase). For this reason, the averaged values of the single items can be interpreted as average characteristics during the main study phase. The tested long-term items of Participant 1 and 4 do not change from V1 to V2 (upper graphics) as personality traits are generally stable over time. The average value from both visits was additionally calculated (lower graphic) to increase data reliability. The three short-term items referring to the participants' current state change from V1 to V2 (upper graphics) as they are generally time-dependent variables. In this case, the informative value of a visit-averaged value (lower graphic) is rather low as the single values can strongly differ from each other. Hence, correlation testing for short-term items should only be done with the

visit-dependent data from V1 and V2, whereas correlation testing for the long-term items can also be done with visit-averaged data (see Table 4.10). It was generally expected that there is a positive linear correlation between the personal characteristic items (short- and long-term) and subjective CBU perception as expressed in Hypothesis H.6.

Figure 4.20 illustrates the effect of a long-term item (*uncritical – critical*) on the global CBU score (two middle graphics, left/right graphic refers to CAT2/CAT3). In CAT2, the sample shows no relevant positive correlation between the participant's personality trait and the global CBU score. It cannot be concluded that an increased critical attitude leads to higher global CBU scores. In CAT3, there is also no relevant positive correlation. As a second example, the impact of the short-term item of attention on the global CBU score is illustrated in the two lower graphics of Figure 4.20. In CAT2 (left graphic), the sample shows no relevant positive correlation between the participant's attention level and the global CBU score. Therefore, it cannot be concluded that an increased state of attention results in higher global CBU scores. The lack of a relevant positive correlation also applies to the CAT3 data set (right graphic). Both examples for a short-term and a long-term item are representative of all other personal characteristic items in terms of the absence of a relevant positive correlation (see Table 4.10, $r^2 < .20$ for CAT2, $r^2 < .15$ for CAT3). Consequently, Hypothesis H.6 has to be rejected as well.

4.3.2 Color Break-Up Study 2

Concerning COBUS2, the main MATLAB function »data select cobus2« helped to select data from the complete data set and output the corresponding data analysis for individual participants and the entire sample ($N = 6$).[47]

Sample Characterization

Seven participants were invited for study participation. While all seven participants passed the pre-examination inclusion tests, one participant discontinued the experiment after one quarter of the test sequences (PAR5). As the data set of this participant was incomplete, it had to be taken out. The data sets of six participants were included into the final analysis.

TABLE 4.11: Demographic data and visual performance parameters of COBUS2 participants.

Participant	Age in [years]	Gender	Dominant Eye	VA in [logMAR]	CS in [logCS]
PAR0	35	male	OS	-0.05	1.59
PAR1	23	male	OD	+0.03	1.35
PAR2	23	female	OS	-0.01	1.44
PAR3	22	female	OS	-0.10	1.44
PAR4	25	female	OS	+0.01	1.42
PAR6	26	male	OD	-0.11	1.34

Note. $N = 6$. VA = visual acuity; CS = contrast sensitivity; PAR = participant; OD = oculus dexter; OS = oculus sinister.

The participants' age and sex as well as the visual performance of their dominant eye are listed in Table 4.11 (only the dominant eye was used during the main examination phase).

Saccadic Eye Movement

All results illustrated in this subsection refer to CBU provocation during saccadic eye movement over a length of 9.6° (CAT2). The first part of this subsection presents the results that

[47] For the graphical output of the main MATLAB function, the external functions »intersections« (Schwarz, 2017) and »boundedline« (Kearney, 2014) were added to the MATLAB search path or placed in the same folder as the main function.

clarify correlations between the independent variables — stimulus position and size — and the score for CBU perception (CBU_{SCR}) as target variable.

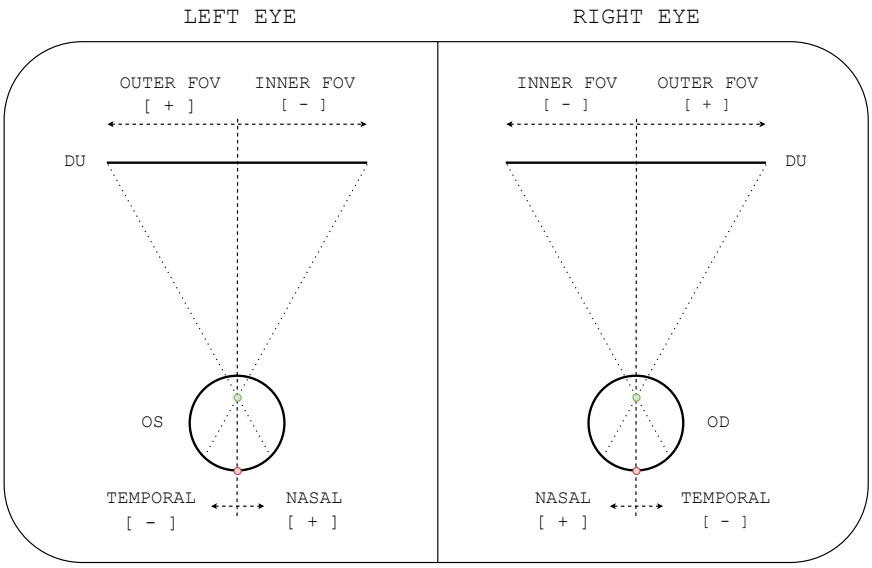

FIGURE 4.22: Sign conventions for retinal positions of a viewer's left (OS) or right eye (OD), and field of view (FOV) positions on the display unit (DU) during COBUS2.

The retinal stimulus position and the corresponding stimulus position within the field of view were specified with an identical mathematical leading sign (see Figure 4.22). Presentations of stimuli in the inner field of view — which correspond to a temporal retinal stimulation — were specified with a negative mathematical value, whereas presentations of stimuli in the outer field of view — which correspond to a nasal retinal stimulation — were specified with a positive mathematical value. This definition applies to both the right and the left eye. The validity of this definition for both eyes is important since tests during COBUS2 were conducted with the participants' dominant eye, which could be either the right or the left eye. Having assured a uniform definition for both eyes, the following figures illustrating CBU perception in dependency of stimulus position were designed without a reference to the examined participant eye.

Figure 4.23 (upper graphic) shows the effect of the independent variables of stimulus position (x-axis) and stimulus size (y-axis) on the sample's CBU score (z-axis) for a frame rate of 30.0 Hz. The black dots show the sample's mean CBU score for every combination of the tested study parameters (stimulus position, stimulus size). In between these data points, the CBU scores are linearly interpolated, resulting in the gray surface that represents CBU perception over the tested range. The gray CBU surface is cut by a xz-plane and yz-plane (red) which show the stimulus position and size that are explored in more detail. In this case, the chosen conditions are the stimulus position of 0.0° (fovea centralis) and the stimulus size of 3.0°.[48] The intersection (red dashed line) between the gray CBU surface and the red planes shows the effect of stimulus position and size on the CBU score. Likewise, the lower graphic in Figure 4.23 illustrates the effect of stimulus position (x-axis) and stimulus size (y-axis) on the sample's CBU score (z-axis) but relates to a frame rate of 60.0 Hz.

[48]The chosen xz/yz-planes exemplify the general procedure of data analysis (kept stable in the result section). The plane parameters can be changed via MATLAB function »data select cobus2« to determine new xz/yz-plane cuts through the CBU surface investigating the effect of other stimulus positions/sizes on CBU perception. How to operate the function is described in detail in the m-file (definition of input/output arguments, etc.).

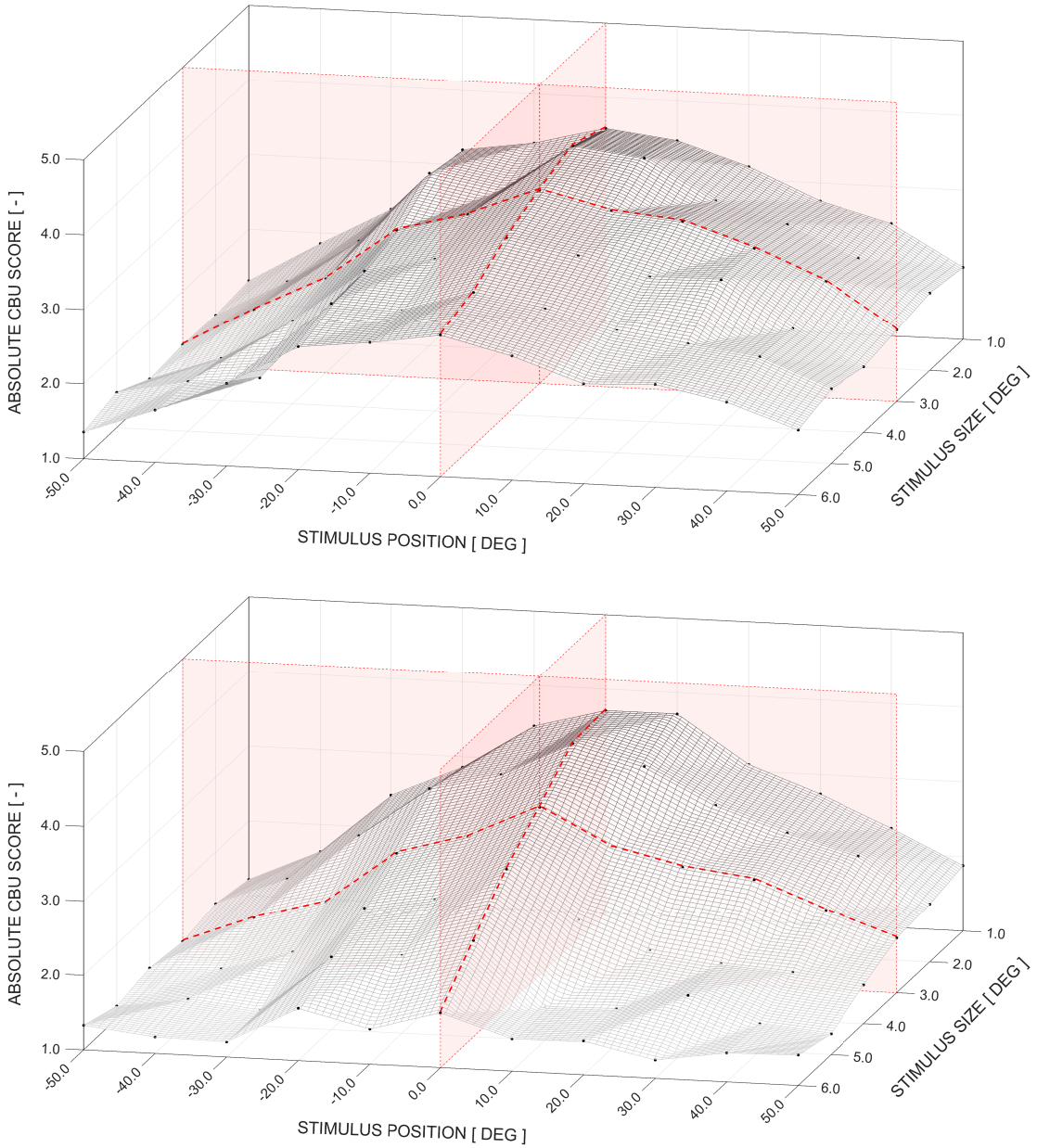

FIGURE 4.23: Sample's absolute CBU score in dependency of stimulus position/size during saccades (CAT2) at frame rates of 30.0/60.0 Hz (upper/lower graphic); black dots are sample-averaged CBU scores, gray surfaces are linear interpolations between averaged scores, reddish *xz*- and *yz*-planes determine stimulus size/position for further investigation (see Table F.3 for relating data).

A more detailed view on the intersection between CBU surface and *xz*-plane in Figure 4.23 allows to gain more information about the relationship between stimulus position and CBU score. Therefore, the upper two graphics of Figure 4.24 show the sample's mean CBU scores (red circles) for the applied frame rates of 30.0 and 60.0 Hz as visualized in Figure 4.23. Both graphics include the standard deviation of the sample's CBU scores (reddish zone). The participant-related CBU scores are also visualized by gray graphs. The participants' values refer to the mean value of all four movement directions tested for every position/size condition. The lower two graphics of Figure 4.24 refer to the intersection between CBU surface and *yz*-plane, which allows to analyze the relationship between stimulus size and CBU score in detail.

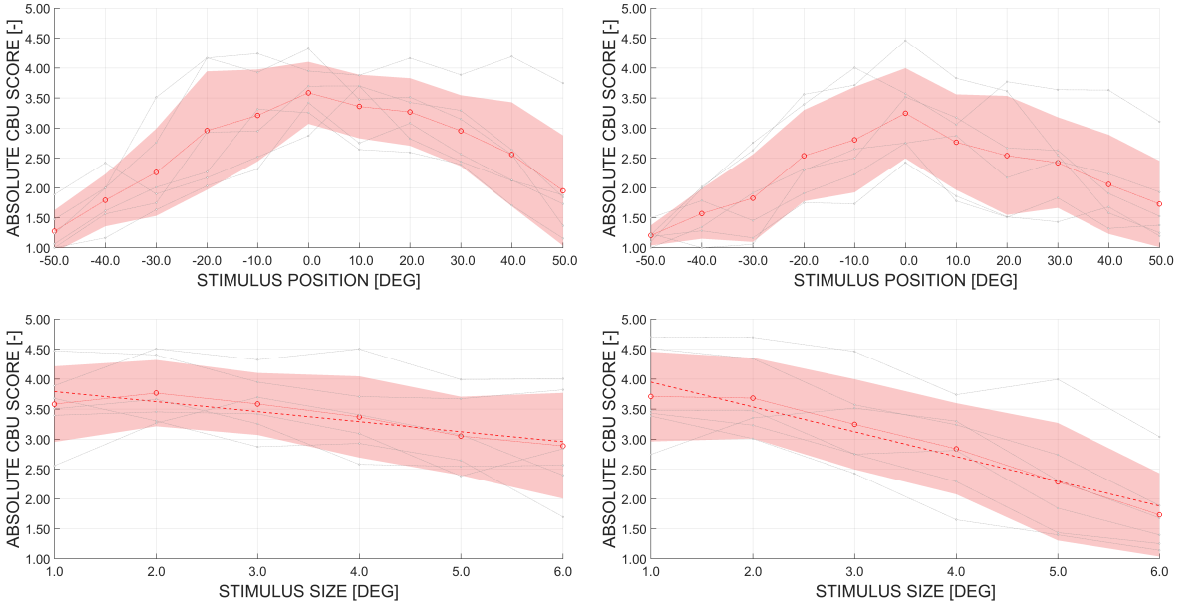

FIGURE 4.24: Sample's absolute CBU score for specific stimulus conditions during saccades (CAT2). Upper left/right graphic: stimulus position-dependent CBU score for a stimulus size of 3.0° at 30.0/60.0 Hz. Lower left/right graphic: stimulus size-dependent CBU score for a stimulus position of 0.0° at 30.0/60.0 Hz; red circles are sample's mean CBU scores, red dotted lines are linear CBU interpolations between mean values, pale red areas are sample's CBU standard deviations (linear interpolation between data points), red dashed lines are fitted linear regressions (lower graphics), grayed out data points (incl. linear interpolation lines) are participants' mean CBU scores.

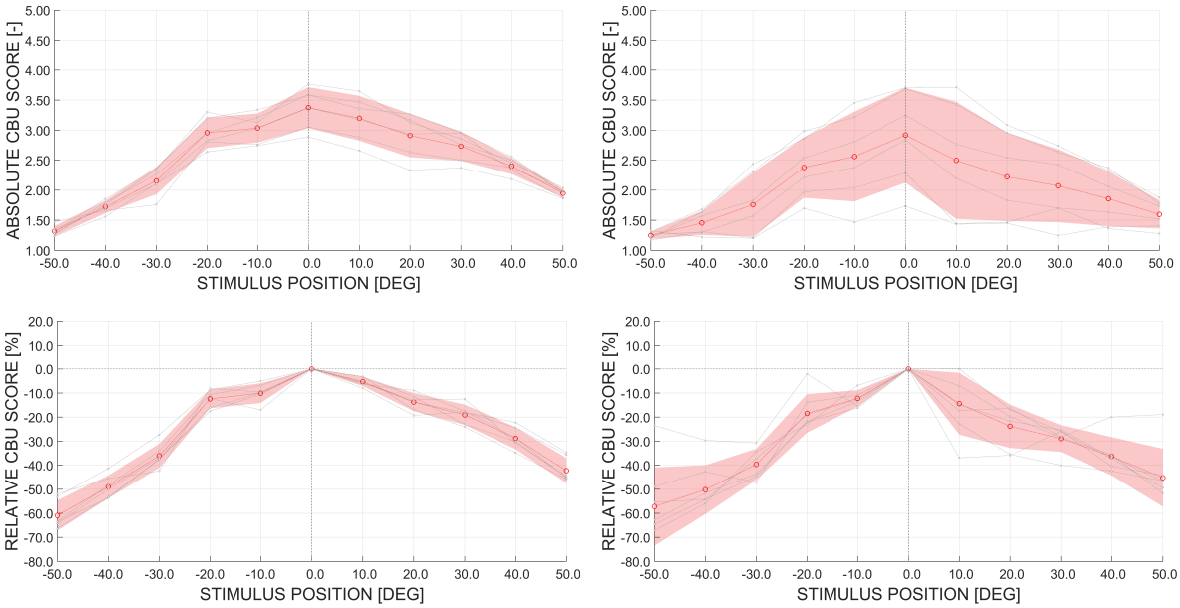

FIGURE 4.25: Sample's CBU score averaged over all stimulus sizes in dependency of stimulus position during saccades (CAT2). Upper left/right graphic: absolute CBU score at 30.0/60.0 Hz. Lower left/right graphic: relative CBU score compared to 0.0° reference position at 30.0/60.0 Hz; red circles are sample's mean CBU scores, red dotted lines are linear CBU interpolations between mean values, pale red areas are sample's CBU standard deviations (linear interpolation between data points), grayed out data points (incl. linear interpolation lines) are participants' mean CBU scores.

All four graphics in Figure 4.25 refer to the mean CBU scores (red circles with linearly interpolated red lines) that were calculated by averaging the scores of all stimulus sizes. Therefore, the graphics facilitate a comprehensive view on the relation between stimulus position

and CBU score. The 3D plots in Figure 4.23 were converted into 2D plots in Figure 4.25 by compressing the graphs of the 3D plot along the y-axis. The gray graphs represent the specific stimulus sizes from 1.0 to 6.0°. Again, the standard deviation is illustrated by the red zone. The upper two graphics refer to the absolute CBU scores evaluated with the continuous 5-point CBU scale. In contrast, the lower two graphics illustrate the relative CBU scores for the tested stimulus positions in relation to the score for the retinal center (0.0°).

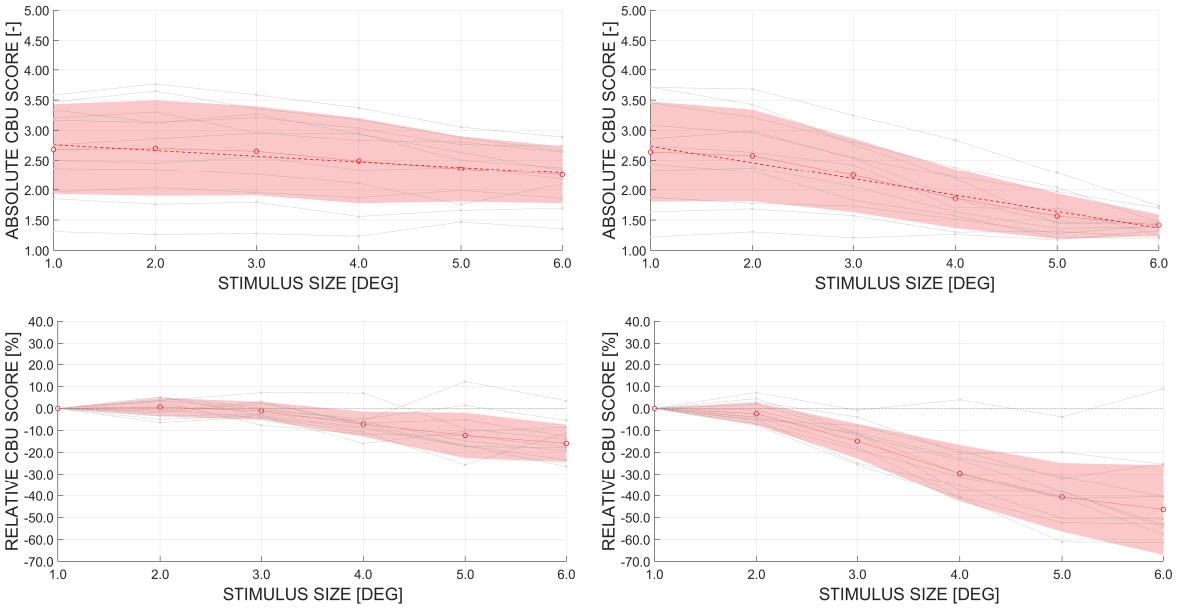

FIGURE 4.26: Sample's CBU score averaged over all stimulus positions in dependency of stimulus size during saccades (CAT2). Upper left/right graphic: absolute CBU score at 30.0/60.0 Hz. Lower left/right graphic: relative CBU score compared to 1.0° reference size at 30.0/60.0 Hz; red circles are sample's mean CBU scores, red dotted lines are linear CBU interpolations between mean values, pale red areas are sample's CBU standard deviations (linear interpolation between data points), red dashed lines are fitted linear regressions (upper graphics), grayed out data points (incl. linear interpolation lines) are participants' mean CBU scores.

The four graphics in Figure 4.26 illustrate the mean CBU scores calculated by averaging the scores of all investigated stimulus positions (as described for Figure 4.25). The graphics allow a global view on the relationship between stimulus size and CBU score.

Summarizing, the main findings on the effect of stimulus position on CBU perception (averaged CBU scores over all stimulus sizes) during saccadic eye movement are:

— approx. linear decrease of absolute CBU score from central (0.0°) to temporal/nasal retina (±50.0°), valid for 30.0 and 60.0 Hz (two upper graphics, Figure 4.25)

— maximum relative decrease of CBU score higher for inner (max. 57–61%) than for outer field of view (max. 42–45%), comparable behavior for both tested frame rates (two lower graphics, Figure 4.25)

Furthermore, the main effects of stimulus size on CBU perception (averaged CBU scores over all stimulus positions) during saccadic eye movement are:

— approx. linear decrease of absolute CBU score for stimulus sizes from 1.0 to 6.0°, valid for 30.0 and 60.0 Hz (two upper graphics, Figure 4.26)

— maximum relative decrease of CBU score clearly higher for 60.0 Hz (max. 46%) than for 30.0 Hz (max. 16%, two lower graphics in Figure 4.26)

Comparing the CBU scores for the presentation of frame rates of 30.0 and 60.0 Hz, it can be observed that the absolute CBU scores for the lower frame rate tend to be higher. Larger scores for lower frame rates are especially the case for larger stimulus sizes as visualized in Figure 4.23 (compare upper and lower graphic referring to frame rates of 30.0 and 60.0 Hz). This effect was expected due to the nature of CBU genesis. Regardless of the displayed frame rate, the interindividual variability of CBU perception within the sample is consistently high during the investigations of CAT2/COBUS2 (see Figure 4.24 for an exemplary illustration of the participant-dependent CBU variations).

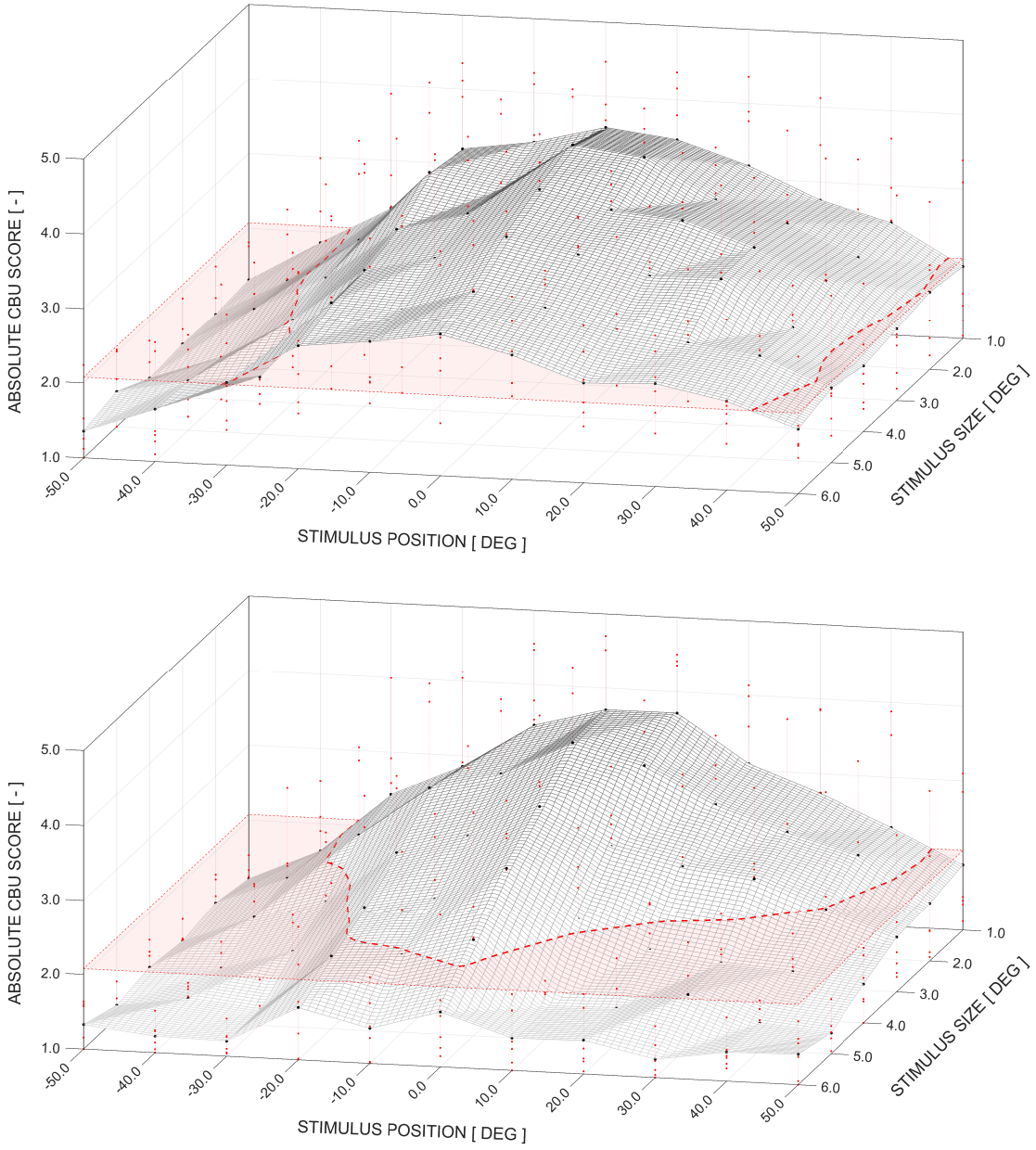

FIGURE 4.27: Sample's absolute CBU score in dependency of stimulus position/size during saccades (CAT2) at frame rates of 30.0/60.0 Hz (upper/lower graphic); black dots are sample-averaged CBU scores, red dots are participants' CBU scores, gray surfaces are linear interpolations between averaged scores, reddish *xy*-planes determine *TOA* borderlines for defined success rate.

The CBU scores that determine the thresholds of annoyance (*TOA*) during saccadic eye movement are presented in the second part of this subsection. Generally, the foundation

for the determination of the *TOA* is a psychometric function that describes the relation between CBU score and annoyance behavior (same procedure as in COBUS1).[49] With the help of the psychometric function for CAT2/COBUS2, the corresponding *TOA* for a defined success rate ("Yes" portion answered to the question "Did you perceive CBU as annoying?") can be determined. For example, a success rate of 0.30 (a share of 30% of the viewers perceive CBU as annoying) leads to a *TOA* of 2.08. The *TOA* is illustrated in the upper 3D graphic in Figure 4.27, which is based on the same data points as the upper graphic in Figure 4.23 since the experimental category (CAT2) and the frame rate of 30.0 Hz is identical for both plots. By implementing a *xy*-plane at the *z*-level of the *TOA* (2.08) for a success rate of 0.30, the intersection between the CBU surface (gray) and the *xy*-plane (reddish) can be determined (red dashed line, called *TOA* borderline from now on).[50] Furthermore, the *TOA* was analyzed for a frame rate of 60.0 Hz. The structure of analytical preparation was identical to the procedure for a frame rate of 30.0 Hz. The CBU surface in Figure 4.27 (lower graphic) is based on the same data points as Figure 4.23 (lower graphic), because the experimental category (CAT2) and the frame rate (60.0 Hz) are identical. The *xy*-plane is still positioned at the same *z*-level (2.08), as the psychometric function for CAT2 and the determined success rate of 0.30 are unchanged.

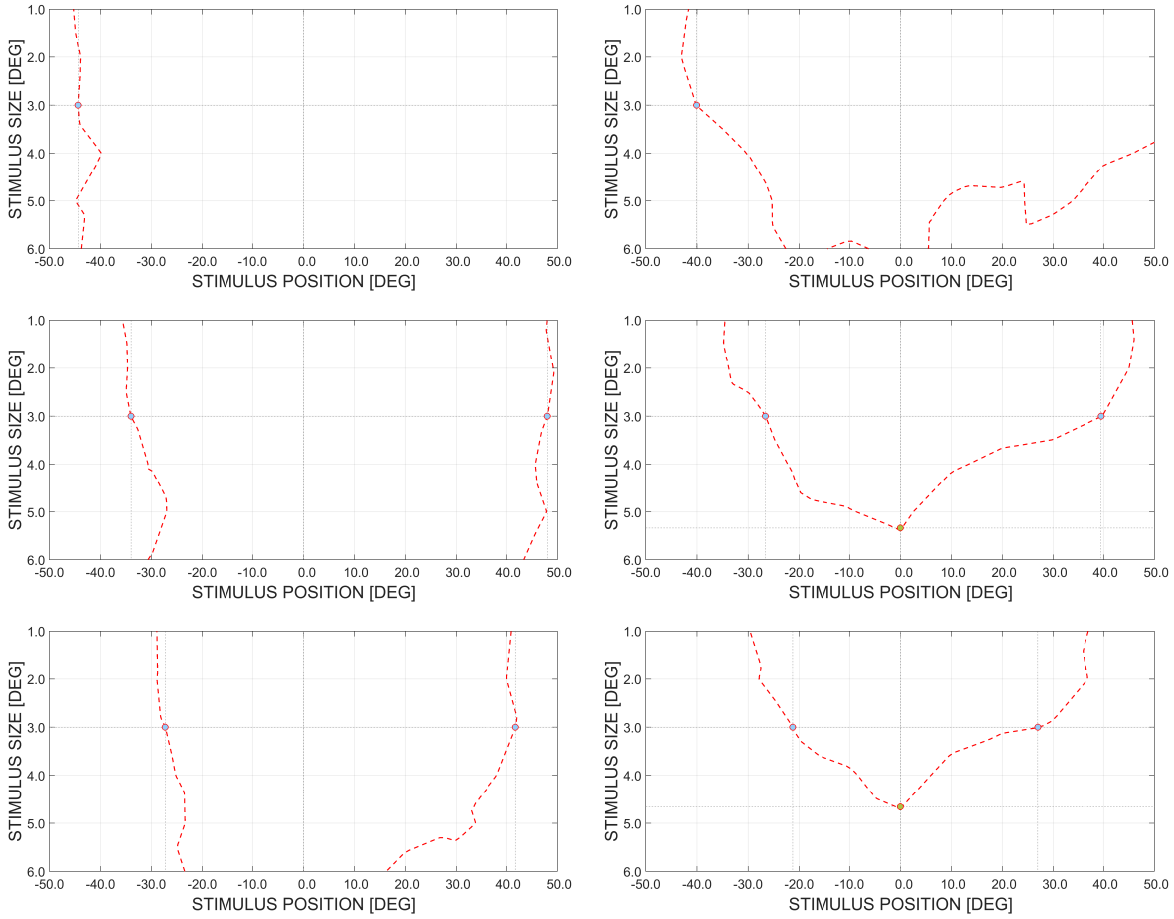

FIGURE 4.28: Sample's *TOA* borderlines during saccades (CAT2) for variable success rates (upper graphics: 0.10, middle: 0.30, lower: 0.50) at frame rates of 30.0/60.0 Hz (left/right graphics).

[49] The psychometric functions (Fit 1) for saccades and pursuits during COBUS2 can be viewed by running the MATLAB function »data select cobus2« (code deactivated by default).

[50] The chosen success rate and the corresponding *TOA* borderline exemplify the data analysis procedure. The success rate can be changed via MATLAB function »data select cobus2« to provide a new *TOA* borderline.

The top view onto such 3D plots in Figure 4.27 makes it possible to clearly identify the *TOA* borderline and the representing specific stimulus positions and sizes for which the defined success rate is exactly achieved (see Figure 4.28). The inner and outer areas that are separated by this *TOA* borderline (red dashed line) represent areas that fall below or exceed the success rate. The outer areas fall below the defined success rate. The stimulus position/size combinations that lie within the outer area can be used without exceeding the viewer share that is allowed to perceive CBU as annoying. The inner areas overshoot the success rate and therefore violate the determined requirement. The combinations of stimulus position and size that lie within the inner areas should be avoided, since too many viewers would be annoyed by CBU. In Figure 4.28, the *TOA* borderlines for success rates of 0.10, 0.30, and 0.50 are illustrated in the graphics top-down (graphics in the middle correspond to the 3D plots in Figure 4.27 with a success rate of 0.30). The graphics on the left and right refer to a frame rate of 30.0 and 60.0 Hz, respectively. The main findings on the effect of variable success rates on the *TOA* borderlines during saccadic eye movement are:

— stepwise lowering of the success rate from 0.50 to 0.10 (steps of 0.20) as illustrated in Figure 4.28

— lowering the success rate means that smaller viewer shares from 50% (lower graphics) to 30% (middle graphics) and 10% (upper graphics) are allowed to perceive CBU as annoying

— stricter requirements result in a stepwise decrease of the CBU score that corresponds to the defined success rate

— determined CBU score is equivalent to the *TOA* that is acceptable to fulfill the defined requirements

— smaller *TOA* leads to more combinations of stimulus position and size that result in CBU scores exceeding the *TOA* (see *TOA* borderlines, inner areas)

— *TOA* borderlines are shifted outwards which means that less combinations of stimulus position and size can be used without violating the applicable requirements (share of viewers that is allowed to find CBU annoying)

— potentially CBU-provoking content must be presented with larger size and higher eccentricity to avoid exceeding the applicable requirements

For both frame rate presentations (30.0 and 60.0 Hz), the general *TOA* borderline pattern is fairly similar. However, during lower frame rates, the *TOA* borderlines are stretched even further due to higher CBU scores.

Pursuit Eye Movement

All results illustrated in the following subsection refer to CBU perception during pursuit eye movement provoked by a content movement velocity of 36.0 deg/s (CAT3). The first segment clarifies the effect of stimulus position (x-axis) and stimulus size (y-axis) on the sample's CBU_{SCR} (z-axis). The results are illustrated in two 3D plots for the frame rates of 30.0 and 60.0 Hz (see Figure 4.29). In the graphics, the black dots represent the sample's mean CBU score for every combination of the tested study parameters (stimulus position, stimulus size). In between these data points, the CBU scores are linearly interpolated, resulting in the gray surface that represents CBU perception over the tested range. The gray CBU surface is cut by a xz-plane and yz-plane (red) which represent the stimulus position and stimulus size that are explored in more detail. As in the previous subsection on saccades,

the chosen conditions are the stimulus position of 0.0° (fovea centralis) and the stimulus size of 3.0°. The intersection (red dashed line) between the gray CBU surface and the red planes shows the effect of stimulus position and stimulus size on the CBU score (following graphical output has identical structure as previous subsection).

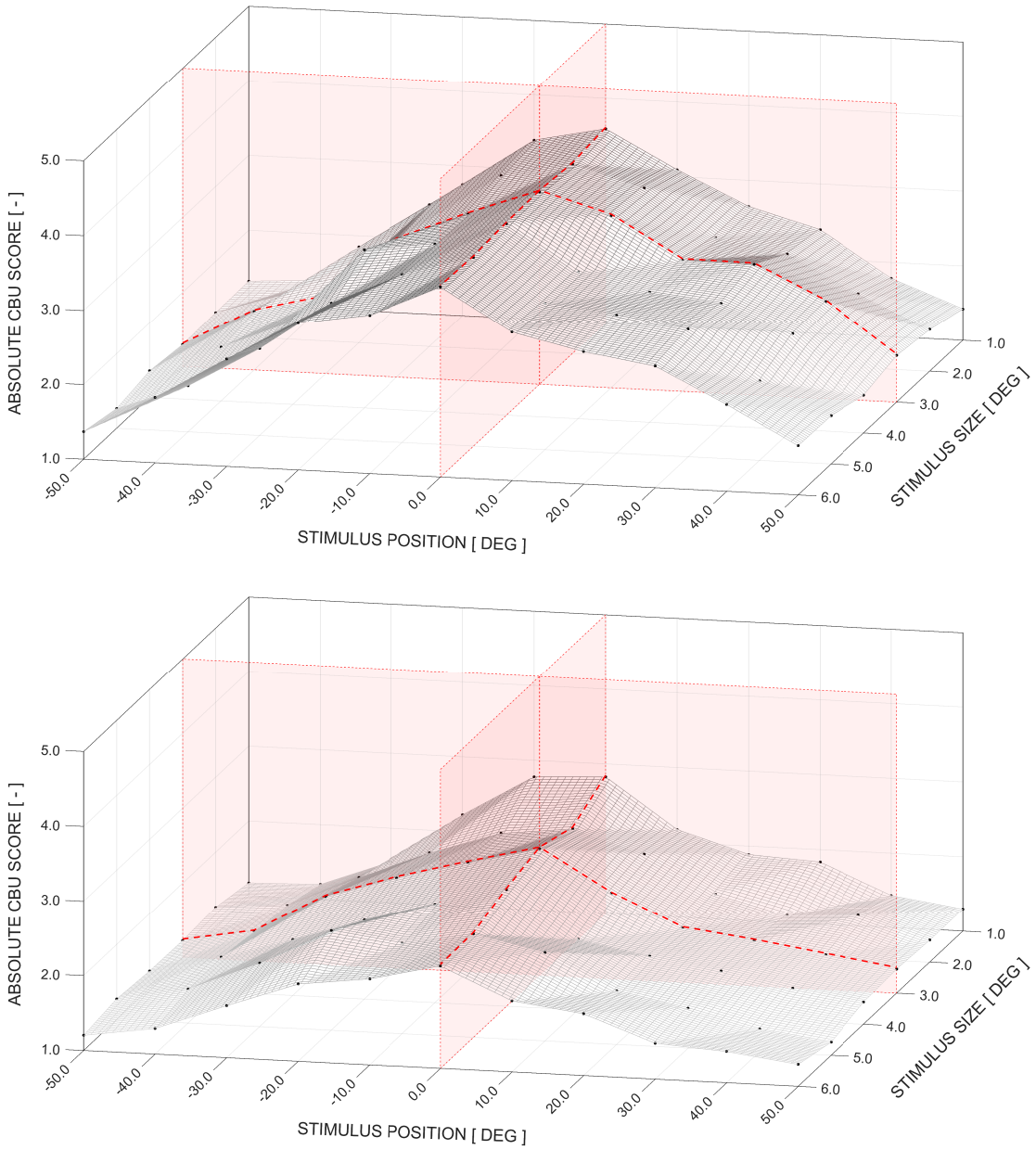

FIGURE 4.29: Sample's absolute CBU score in dependency of stimulus position/size during pursuits (CAT3) at frame rates of 30.0/60.0 Hz (upper/lower graphic); black dots are sample-averaged CBU scores, gray surfaces are linear interpolations between averaged scores, reddish xz- and yz-planes determine stimulus size/position for further investigation (see Table F.4 for relating data).

Figure 4.30 gives a more detailed view on the specific intersections between the CBU surface (gray) and the xz/yz-plane (reddish) in Figure 4.29. This allows to gain more information on the relationship between stimulus position and CBU score (upper two graphics, stimulus size of 3.0°). The relation between stimulus size and CBU score is illustrated in the lower two graphics (stimulus position of 0.0°). Both frame rates of 30.0 and 60.0 Hz are considered in Figure 4.30 (see graphics on the left and right).

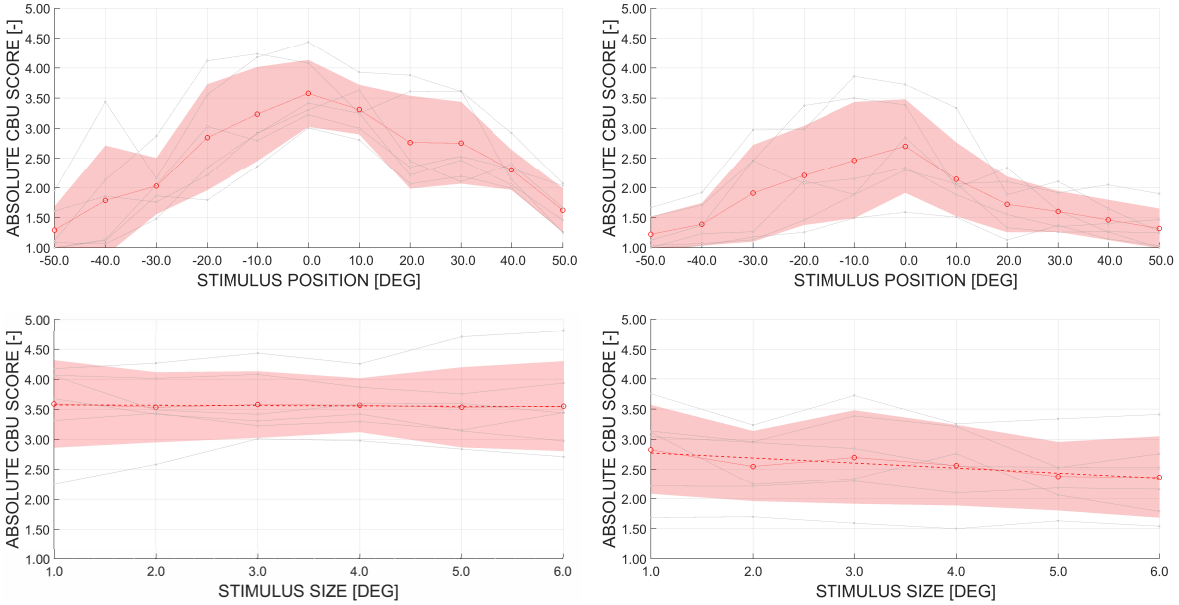

FIGURE 4.30: Sample's absolute CBU score for specific stimulus conditions during pursuits (CAT3). Upper left/right graphic: stimulus position-dependent CBU score for a stimulus size of 3.0° at 30.0/60.0 Hz. Lower left/right graphic: stimulus size-dependent CBU score for a stimulus position of 0.0° at 30.0/60.0 Hz; red circles are sample's mean CBU scores, red dotted lines are linear CBU interpolations between mean values, pale red areas are sample's CBU standard deviations (linear interpolation between data points), red dashed lines are fitted linear regressions (lower graphics), grayed out data points (incl. linear interpolation lines) are participants' mean CBU scores.

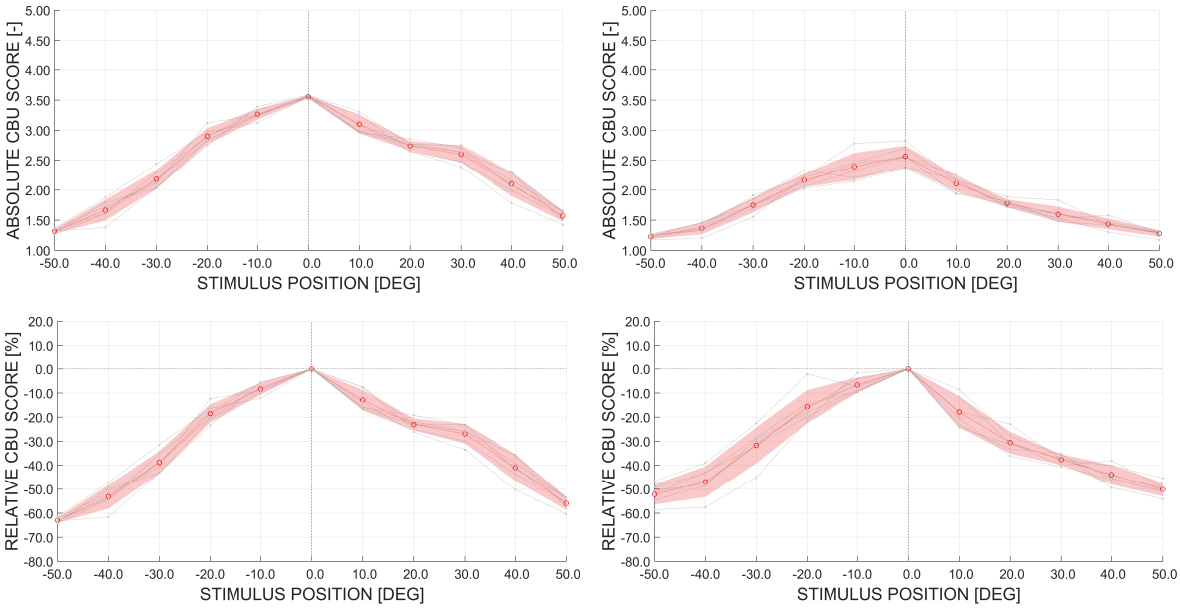

FIGURE 4.31: Sample's CBU score averaged over all stimulus sizes in dependency of stimulus position during pursuits (CAT3). Upper left/right graphic: absolute CBU score at 30.0/60.0 Hz. Lower left/right graphic: relative CBU score compared to 0.0° reference position at 30.0/60.0 Hz; red circles are sample's mean CBU scores, red dotted lines are linear CBU interpolations between mean values, pale red areas are sample's CBU standard deviations (linear interpolation between data points), grayed out data points (incl. linear interpolation lines) are participants' mean CBU scores.

The graphics in Figure 4.31 provide a global view on the relationship between stimulus position and CBU score by presenting the mean CBU scores averaged over all tested stimulus sizes (red circles with linearly interpolated red lines). The upper two graphics refer to the

absolute CBU scores, the lower two graphics illustrate the relative CBU scores (reference are CBU scores determined in the center of the retina at 0.0°). In addition, Figure 4.32 illustrates the mean CBU scores averaged over all investigated stimulus positions. Therefore, the graphics allow a global view on the relationship between stimulus size and CBU score.

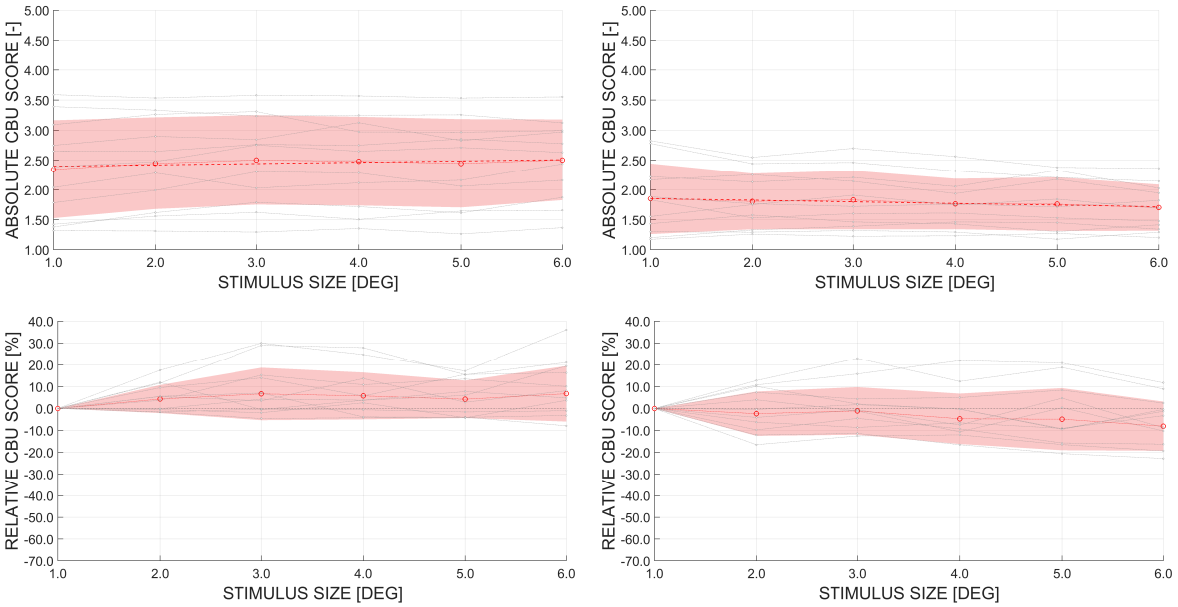

FIGURE 4.32: Sample's CBU score averaged over all stimulus positions in dependency of stimulus size during pursuits (CAT3). Upper left/right graphic: absolute CBU score at 30.0/60.0 Hz. Lower left/right graphic: relative CBU score compared to 1.0° reference size at 30.0/60.0 Hz; red circles are sample's mean CBU scores, red dotted lines are linear CBU interpolations between mean values, pale red areas are sample's CBU standard deviations (linear interpolation between data points), red dashed lines are fitted linear regressions (upper graphics), grayed out data points (incl. linear interpolation lines) are participants' mean CBU scores.

During PEM, the main findings on the effect of stimulus position on CBU perception (averaged CBU scores over all stimulus sizes) are:

— approx. linear decrease of absolute CBU score from retinal center (0.0°) to temporal and nasal periphery (±50.0°), valid for 30.0 and 60.0 Hz (see two upper graphics in Figure 4.31)

— maximum relative decrease of CBU score higher for inner (max. 52–63%) than for outer field of view (max. 50–56%), higher decrease values for 30.0 Hz than for 60.0 Hz (see two lower graphics in Figure 4.31)

Furthermore, the main effects of stimulus size on CBU perception (position-averaged CBU scores) during PEM are:

— approx. linear behavior of absolute CBU score for stimulus sizes from 1.0 to 6.0°, valid for 30.0 and 60.0 Hz (see two upper graphics in Figure 4.32)

— relative CBU scores are stable for variable stimulus sizes up to 6.0° (compared to stimulus size of 1.0°) within a range of +7 to -8%, valid for 30.0 and 60.0 Hz (see two lower graphics in Figure 4.32)

Comparing the CBU scores for frame rate presentations of 30.0 and 60.0 Hz, it can be observed that the absolute scores are generally higher for the lower frame rate (see Figure 4.29). This effect was expected due to the nature of CBU genesis.

The second segment of this subsection presents the results for the CBU scores that determine the *TOA*s for pursuit eye movement. In this context, a psychometric function for CAT3 as basis for *TOA* determination was applied (as done in the previous subsection). A success rate of 0.30 leads to a *TOA* of 2.20. The *TOA* is illustrated in the 3D plots in Figure 4.33. By implementing a *xy*-plane at the *z*-level of the *TOA* (2.20) for a success rate of 0.30, the intersection between the gray CBU surface and the reddish *xy*-plane can be determined (red dashed line which is called *TOA* borderline).

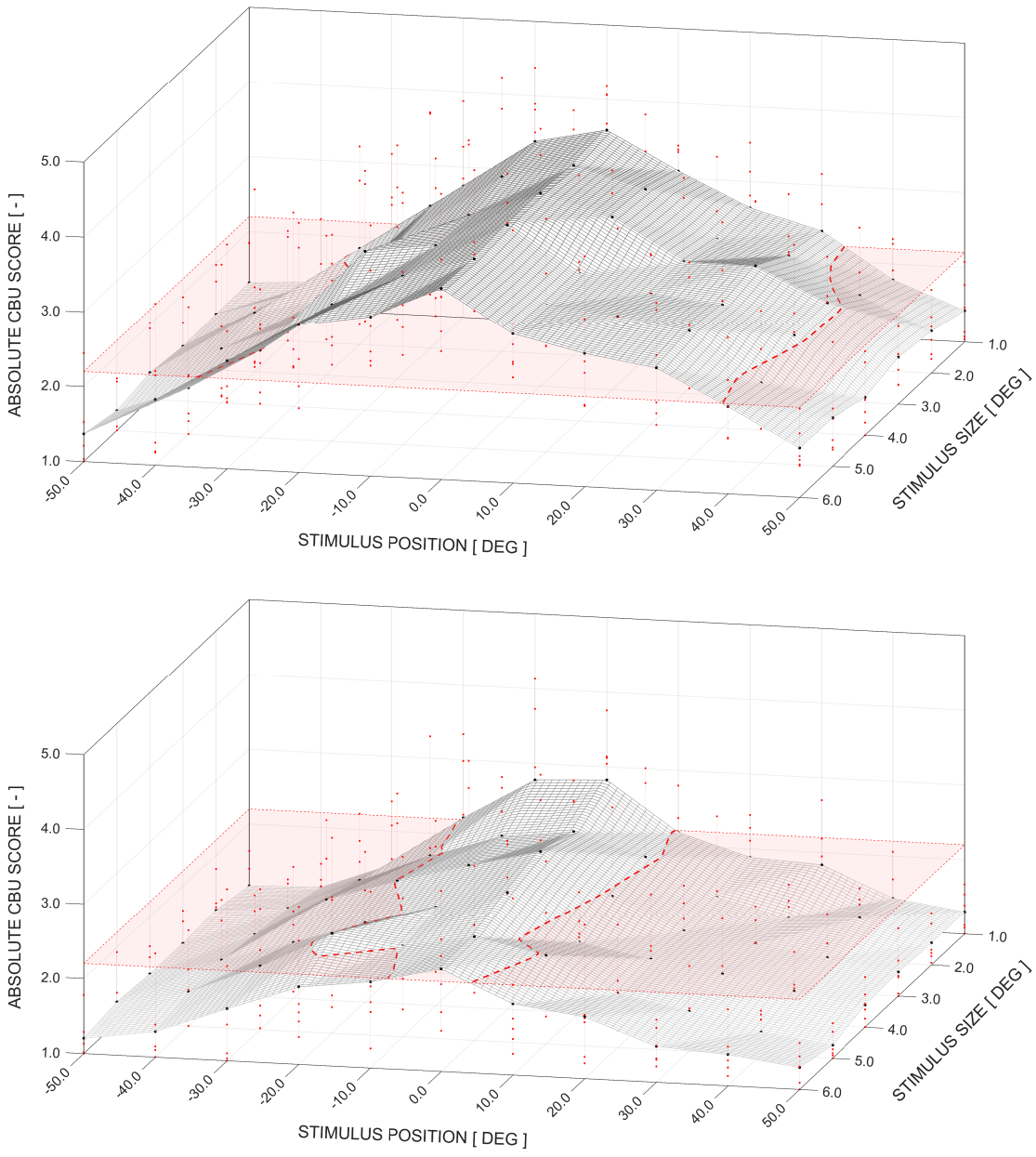

FIGURE 4.33: Sample's absolute CBU score in dependency of stimulus position/size during pursuits (CAT3) at frame rates of 30.0/60.0 Hz (upper/lower graphic); black dots are sample-averaged CBU scores, red dots are participants' CBU scores, gray surfaces are linear interpolations between averaged scores, reddish *xy*-planes determine *TOA* borderlines for defined success rate.

In a next step, the top view onto the 3D plots in Figure 4.33 allows the clear visualization of the *TOA* borderline (representing specific stimulus positions and sizes) for which the defined success rate is exactly achieved (see Figure 4.34). The outer and inner areas separated

by the *TOA* borderline (red dashed line) represent areas that fall below or overshoot the defined success rate and therefore fulfill or violate the determined requirements.

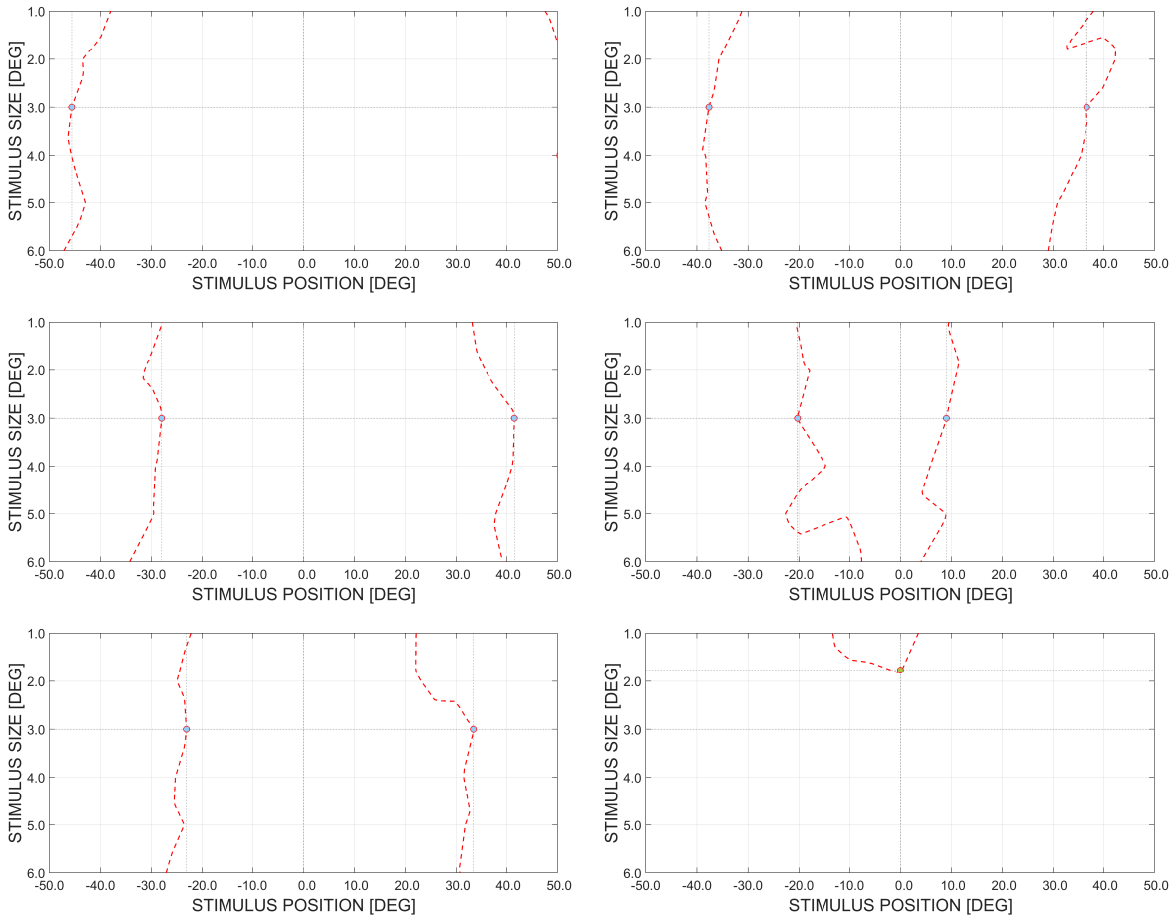

FIGURE 4.34: Sample's *TOA* borderlines during pursuits (CAT3) for variable success rates (upper graphics: 0.10, middle: 0.30, lower: 0.50) at frame rates of 30.0/60.0 Hz (left/right graphics).

Figure 4.34 illustrates the *TOA* borderlines for success rates of 0.10, 0.30, and 0.50 (graphics in the middle correspond to the 3D plots in Figure 4.33 with a success rate of 0.30). The graphics on the left/right refer to a frame rate of 30.0/60.0 Hz. The main findings on the effect of variable success rates on the *TOA* borderlines during PEM do not differ from the summary for saccadic eye movement. All statements can be transferred without exception (see explanations in previous subsection).

4.4 Discussion

4.4.1 Color Break-Up Study 1

In summary, it is undisputed that increasing the retinal velocity of a potential CBU stimulus elevates the magnitude of CBU perception, regardless of whether the stimulus movement on the retina is caused by actual eye movements such as pursuits (P. V. Johnson et al., 2014; Koma & Uchida, 2003) and saccades (Miettinen et al., 2008; X. Zhang & Farrell, 2003) or by experimental setups themselves (Mori et al., 1999; Post et al., 1998; Post et al., 1997). This fundamental finding is also reflected in the COBUS1 results. The higher the movement velocity of pursuits and saccades (provoked by larger saccadic amplitudes), the more pronounced the perceived CBU effect (see Figures 4.11 to 4.13). When analyzing the general

differences of CBU perception between saccades and pursuits, it can be seen that CBU score differences are not as large as expected. For example, the sample's general CBU level during saccades with a path length of 21.3° (see Figure 4.12, upper graphic) is higher than during provoked pursuits with a velocity of 36.0 deg/s (see Figure 4.13, middle graphic). However, such large saccades are normally performed with peak velocities around 500 deg/s (see Figure 2.6). With such differences between saccadic and pursuit eye movement velocity, larger CBU differences would have been expected. Why do the CBU levels not differ more clearly during saccades and pursuits? One reason could be that human visual perception changes during the execution of saccadic eye movements. Perceptual processes during saccades include saccadic suppression, mislocalization, and compression (Ross et al., 2001), all of which can affect participant's CBU perception. The perceived localization of brief stimuli before, during, and after saccades is not stable (Bischof & Kramer, 1968; Honda, 1989, 1991; Matin & Pearce, 1965). Saccadic mislocalization is thought to be part of the retinal stabilization process. The effect of reverse mislocalization for different retinal areas leads to saccadic compression — the compression of visual space and all perceived objects within it (Ross et al., 1997). In this context, Yohso and Ukai (2006) found that participants perceived CBU effects during saccades narrower than theoretically calculated (width of colored area in eye movement direction) — a result which the researchers link to the effect of saccadic compression. However, the effect of the aforementioned perceptual changes as an explanation for the limited CBU differences between saccades and pursuits in COBUS1 is hard to quantify, especially since misjudgments of stimulus localization also occur during PEM (Brenner et al., 2001; Kerzel et al., 2006; Rotman et al., 2002). Furthermore, the research on effects of saccadic mislocalization and compression refer to stimulus characteristics such as size and duration of presentation, which differ from the applied visual CBU stimuli of the COBUS series. The third perceptual process initially mentioned — saccadic suppression — leads to a reduction of retinal contrast sensitivity. The impact of saccadic suppression is higher on the magnocellular than on the parvocellular pathway, which means that the retina's sensitivity to luminance (exclusively for low spatial frequencies) is drastically reduced, while the retina's sensitivity to equiluminant color perception is not affected (Burr et al., 1994). In general, the magnitude of saccadic suppression increases with saccadic amplitude (Mitrani et al., 1970; Ridder & Tomlinson, 1997; Stevenson et al., 1986). This selective suppression of retinal sensitivity during saccades can be considered a plausible reason for the smaller differences in CBU perception during saccades and pursuits, as the suppression of contrast sensitivity during precise pursuits is insignificant compared to the strong effects of saccadic suppression (Schütz, Braun, & Gegenfurtner, 2007). Moreover, an improvement in sensitivity to colored stimuli, including red-green and blue-yellow stimuli, was found during pursuit tasks compared to fixation tasks (Braun et al., 2017; Schütz et al., 2008). It follows that perceptual processes during the execution of different forms of eye movements (saccades vs. pursuits) must be distinguished from one another and could be a possible reason for lower deviations in CBU perception (see also Section 2.3.2).

Effect of Technical Parameters

The structure of the COBUS1 discussion is based on the general structure of the testing of Hypotheses H.1 to H.6 (see Section 4.3.1) to allow easy transition between these sections. The first Hypothesis H.1 refers to alterations of CBU perception for frame rate variations of the applied presentation unit (30.0 to 420.0 Hz). Hypothesis H.1. states that there is a negative correlation between frame rate and CBU perception which can be adequately expressed by an exponential function. The formulation of Hypothesis H.1 is based on the genesis of CBU under consideration of temporal and spatial aspects of optical imaging (as described in Chapter 3) and subsequent stages of visual processing.

Generally, two conditions have to be fulfilled to provoke CBU perception. First, a display unit needs to present the subframes within one frame cycle sequentially. This is usually a succession of red, green, and blue subframes. Secondly, eye and optionally content movement must be performed during the frame presentation. Such a scenario leads to subframes that are spatially pulled apart and unfortunately do not fall on the same retinal area. Therefore, they are not fully summated to the desired mixed color. The retinal areas that are not illuminated by all subframes are the areas that provoke a deviant color perception — also known as CBU. The magnitude of CBU depends mainly on two factors: the eye movement velocity and the duration of frame and subframe presentation. This fact results from the basic physical equation of a linear motion with uniform acceleration, where the distance covered depends on the velocity of the motion and the time available for the motion ($s = v \times t$). The time available for the eye movement that leads to the spatial division of the subframes on the retina (which is the covered distance in movement direction in this case) depends on the frame rate of the display system. The lower the frame rate, the more time is available for eye movement within one single frame cycle, which results in a larger separation of the single subframes and accordingly leads to higher CBU effects. By varying the frame rate, the presentation time of one single frame cycle is changed in a reciprocal manner. For a frame rate of 60.0 Hz, the time span for one frame cycle is around 16.6 ms (1/60 s). When doubling the frame rate to 120.0 Hz, one single frame cycle will only need half the time of approx. 8.3 ms to run through. The relation between the applied frame rate and the resulting duration for one frame cycle can be expressed by a hyperbolic function. From this, one could conclude that the relationship between frame rate and CBU perception is also best explained by a hyperbolic function, as it perfectly explains the interaction between frame rate and frame duration (main factor for CBU genesis).

However, the magnitude of CBU does not only depend on aspects of optical imaging on the retinal surface. As the relationship between visual perception and physical stimulation is not linear, human image processing must also be considered. A steady increase of physical stimulation will always result in a saturation of visual perception. Referring to the Weber-Fechner law, the relationship between the intensity of a physical stimulus and the magnitude of subjective perception provoked by the stimulus can be described by a logarithmic function (Fechner, 1860). However, about 100 years after Fechner published his famous psychophysical law, S. S. Stevens (1957) postulated the Power law which "seems to govern nearly every sensory continuum for which the stimulus magnitude can be varied by known amounts. The universality formerly claimed for Fechner's logarithmic law seems to have fallen to the psychophysical power law" (S. S. Stevens, 2017, p. 14). Furthermore, the previously described perceptual alterations during the execution of saccades and pursuits also affect human image processing (see earlier remarks). Another psychophysical effect to consider: Higher CBU scores do not simply result from larger CBU areas. Another strengthening perceptual effect that is triggered by the enlarged colored CBU area itself influences human perception. Target size — in this case the size of the CBU area — is a critical parameter influencing color perception across the retina. Every measure of color perception from the center into the periphery of the human retina can be improved by applying a larger stimulus (Abramov et al., 1991; M. A. Johnson, 1986; Kuyk, 1982). For example, increasing the size of a colored area on the retina will improve the perceived saturation of this colored area. As a consequence, the perception of CBU effects cannot be derived from the size of the CBU-provoked retinal area alone.

Taking into account these various psychophysical aspects and the spatial and temporal assumptions on optical imaging, it seems reasonable to assume a correlation between frame rate and CBU perception that is best described by an exponential function (see Hypothesis H.1). Applying an exponential function shows a precise fit for the PEM data (see Table 4.2). Moreover, frame rate-dependent CBU perception during saccades can be accurately

described by exponential functions. While the adjusted coefficients of determination drop down slightly with increasing path length of saccadic eye movement, they do not fall below values of $r^2 = .93$. Finally, Hypothesis H.1 is confirmed.

The exponential relationship between frame rate and CBU perception makes it possible to effectively reduce CBU effects by increasing the applied frame rate. The statement is valid for increasing frame rates at a low level (e.g., 30.0 to 60.0 Hz). For higher levels, however, the same frame rate jump (e.g., 210.0 to 240.0 Hz) shows a significantly weakened effect on CBU perception — based on the inherent behavior of every exponential function. The location of the transition zone demarcating frame rate levels that allow an effective CBU reduction by increasing the applied frame rate from higher and therefore less effective frame rate levels depends on the kind of eye movement (saccade or pursuit) and its specific characteristics (saccadic length or pursuit velocity). The slower the eye movements, the earlier the frame rate level of reduced effectiveness is reached (see Figures 4.11 to 4.13). For further analysis, the position of the exponential function's horizontal asymptote allows important conclusions since it determines the absolute limit for CBU reduction under the theoretical assumption of no upper frame rate limit. Especially for eye movements with high movement velocities — such as saccades with large amplitudes — the horizontal asymptote shifts upwards to higher CBU scores (see *B3* values in Table 4.2), which means that raising the frame rate as a method of CBU compensation will never lead to a total elimination of CBU effects under worst-case conditions. This statement is further corroborated by the assessment of future technological developments with reference to FSC-LCD technology: "In spite of the emergence of new fast panel technologies, it is unlikely that affordable panels with frame rates higher than 240 Hz will be widely available in the foreseeable future" (F.-C. Lin, 2018, p. 22). Ideally, different CBU compensation techniques (including frame rate enhancement) are applied simultaneously to completely cancel the subjective perception of CBU effects during FSC presentation (see Section 2.2.3 for a listing of compensation techniques). However, as long as there is no prospect to set CBU effects to zero under all possible conditions, an approach to reduce CBU effects to the point that they are not perceived as annoying by a large share of viewers seems to be a suitable intermediate step (see following subsection that deals with the determination of the *TOA*).

With regard to Hypothesis H.2, it should be pointed out that while decreasing luminance of a CBU-provoking stimulus (157.0 to 10.0 cd/m^2) does have effects on CBU perception under specific experimental COBUS1 conditions, those effects are marginal in comparison to the effects of frame rate alteration. There is a relatively sharp distinction (at least for saccadic eye movement) between tested conditions (frame rate, movement pattern) that result in a confirmation or a rejection of a relevant positive correlation between luminance level and CBU score. A positive and at least marginal effect of luminance level only occurs for a medium frame rate range (90.0 to 150.0 Hz) mainly in CAT2 (higher saccadic length) and partially in CAT3 (pursuits). An effect of luminance level on CBU scores might be suppressed in the area of higher frame rates (> 150.0 Hz) as the left tail of the exponential function has a low plateau characteristic at this point, resulting in a compression of CBU scores no matter which luminance level is displayed (see Figure 4.13, upper graphic). The absence of a noticeable effect of luminance level on CBU scores for the lowest frame rates (< 90.0 Hz) might be explained by the fact that frame rates of 30.0 and 60.0 Hz lead to intensive CBU perception. Consequently, marginal effects of luminance variation might be overshadowed (see Figure 4.11, lower graphic). Beyond that, the non-linear relation between physical stimulus intensity and its subjective perception as well as saccadic suppression with its drastic effect on luminance perception can be further reasons for the absence of a relevant effect of luminance level on CBU perception (at least during saccades).

Consequently, the investigated interaction between luminance level and CBU perception cannot be properly described by a linear function for most of the tested experimental conditions (rejection of Hypothesis H.2). This becomes evident when studying the adjusted coefficients of determination r^2 for the regression lines fitted to the data set (see Table 4.6). However, it is difficult to derive a more complex function from only three luminance levels. Generally speaking, it seems that the luminance level only shows its marginal effect when falling below a certain threshold level. Above this threshold level, different luminance values do not have a significant effect on CBU perception (plateau). Unfortunately, this specific threshold level cannot be exactly determined from the available COBUS1 data. Presumably, the threshold level lies between 10.0 and 80.0 cd/m^2. This assumption is supported by other research findings (S.-C. Chen et al., 2007; Y.-P. Huang et al., 2007; Kobayashi et al., 2010; Miettinen et al., 2008; Yan et al., 2007; Y. Zhang et al., 2012) which point out that the effect of stimulus luminance level alone seems to be marginal up to the point of undershooting a certain luminance level threshold (stable background luminance assumed). Such a luminance level threshold might be determined at a level around 15 cd/m^2. Concluding, the relation between stimulus luminance and CBU perception investigated during COBUS1 cannot be satisfactorily described by a linear function, but rather by a power function as suggested by Post et al. Their study-based formula for CBU detection thresholds includes one power function term using stimulus luminance as the variable base with exponent values of 0.10 (1997) or 0.08 (1998).[51] Such a non-linear behavior can generally be derived from the non-linear relation between objective stimulation and subjective perception on basis of the psychophysical Power law (see discussion of Hypothesis H.1) which allows the description of marginal CBU score variations above and a rapid decrease of CBU scores below a certain luminance level threshold of approximately 15 cd/m^2. For further investigations, a test range above and below this threshold with a larger number of luminance levels is necessary since the complexity of a power function has to reproduced.

Hypotheses H.3 and H.4 both investigate the variation of a certain movement pattern on CBU perception. Hypothesis H.3 refers to saccades with various saccadic lengths (3.6 to 28.2°) whereas Hypothesis H.4 covers pursuits with different movement velocities (18.0 to 54.0 deg/s). Both hypotheses follow different approaches. A linear function (as proposed for Hypothesis H.4) does not seem appropriate for the definition of Hypothesis H.3 due to the indirect relation between saccadic length and a CBU effect's retinal extent. The two variables saccadic length and CBU score are linked by the velocity of saccadic eye movements, which depends on saccadic length. The relationship between saccadic eye movement velocity and the magnitude of the saccadic length is described in Section 2.3.1. In a nutshell, saccades have a typical spatial and temporal behavior of increasing eye movement velocity with increasing length of the saccadic path, which changes into a velocity plateau at a certain saccadic amplitude. The so-called main sequence describes this close and stereotypical relationship between the amplitude of saccadic eye movement and its peak velocity (Bahill, Clark, et al., 1975), which potentially provokes the most distinct CBU perception and therefore is the most relevant parameter for CBU evaluation during the execution of the saccade. To mathematically describe a saccade's peak velocity in dependency of its amplitude, some researchers propose a model based on an exponential function (Baloh et al., 1975; Smit et al.,

[51] The proposed formula by Post et al. also includes the contrast ratio between CBU-provoking stimulus and its background as a highly relevant factor for the determination of CBU detection thresholds. Miettinen et al. (2008) and Y. Zhang et al. (2012) corroborate Post et al. by concluding that the contrast ratio has a much stronger effect on CBU perception than the sole stimulus luminance. For example, increasing the background luminance while the stimulus luminance is kept stable (decline of contrast ratio) leads to a considerable reduction of CBU perception (X. Zhang & Farrell, 2003). During COBUS1, the contrast ratio's impact on CBU perception was not investigated as the Michelson contrast between stimulus and background was kept stable at approx. 0.99 for all investigated luminance levels *LL1* to *LL3* (see Appendix B.1.4).

1987) while others recommend a power function (Lebedev et al., 1996). There is no agreement in the scientific community as to which function best describes the relationship (see also Figure 2.6). For the execution of the visually-guided voluntary pro-saccades during COBUS1, a power function was chosen for uniform curve fitting under all conditions of frame rates and luminance levels. Statistical analysis of COBUS1 data supports this power function approach (see Table 4.7). Hypothesis H.3 is confirmed.

From a theoretical standpoint, a linear function adequately describes the relationship between pursuit eye movement and CBU perception as proposed in Hypothesis H.4 because there is a direct and constant relationship between PEM velocity and the retinal extent of CBU effects (constancy at least valid within but not across CBU phases, see Section 3.5). Hypothesis H.4 was formulated under the assumption that exclusive PEM without saccadic shares is provoked during CAT3 sequences. This assumption is based on two findings. First, applying a step-ramp stimulation (Rashbass, 1961) potentially avoids an initial retinal slip and the resulting catch-up saccade (see Figure 2.5). Second, realizing a subsequent steady movement of the fixation target with limited target movement velocities clearly below 90 deg/s (max. PEM velocity of 54.0 deg/s during COBUS1) potentially allows a smooth and precise pursuit of the target with a high gain and without the appearance of compensatory saccades (Meyer et al., 1985). Finally, the data set of COBUS1 and its statistical analysis largely confirm the theoretical foundation of a linear relation as proposed in Hypothesis H.4 (see Table 4.8).

Annoyance Threshold Determination

The frame rates required to avoid violating various success rates for all subcategories of CAT2 and CAT3 are listed in Table 4.9. The defined success rates determine the accepted share of viewers that perceive CBU as annoying. The CBU scores corresponding to the defined success rates are the *TOA*s. Based on this *TOA* determination, some practical examples point out the hardware requirements (frame rates) for relevant display types in different fields of application (see Table 4.12). The first display/application classification (Example 1) refers to the use of a classic television for film presentation (entertainment). It is expected that the viewer performs a short saccade of 3.6° between two points of interest in a film scene with shares of white content. The limited path length of the saccade within the dimensions of the TV is derived from the display size and the viewing distance. In this specific situation, a frame rate of 88.1 Hz is necessary to not violate the defined success rate of 0.20 (only 20% of the viewers should perceive CBU as annoying). The next display/application classification refers to a gaming scenario on a desktop display (Example 2). For instance, during a classic racing game, a gamer might make a saccadic jump from the driver's car in the center of the screen to the time/round note in the upper screen corner. In comparison to Example 1, the viewing distance is shorter, which results in a larger saccadic length (14.3°) even though the display diagonal is smaller. A larger saccadic length results in a higher eye movement velocity which finally leads to a drastically higher frame rate (265.7 Hz) that would assure a success rate of at least 0.30. Example 3 refers to navigation in road traffic realized with a Head-Up Display (HUD). Every now and then, large saccades — exceeding the dimensions of the HUD's field of view — have to be executed during road traffic. These saccades (28.2°) are provoked by real objects such as road signs or other cars. In the worst case, such large saccadic path lengths lead to ballistic eye movement velocities which make it necessary to operate very high frame rates (361.3 Hz) to control CBU effects (even if the success rate of 0.30 rate is moderate). A typical application for mobile use would be an office application via a tablet (Example 4), checking emails via Microsoft Outlook for instance. Scrolling down and following the content with PEM (18.0 deg/s) also provokes CBU predominantly on sharp light/dark boundaries. Due to the reduced eye movement velocity during PEM,

the necessary frame rate (121.1 Hz) is lower in comparison to the previous saccadic examples even if the success rate is tighter (0.15).

TABLE 4.12: Hardware requirements for CBU reduction regarding selected display types and applications.

	Example 1	Example 2	Example 3	Example 4
Display Type	TV	desktop	HUD	mobile / tablet
Display Diagonal in [in]	50.0	27.0	5.0	10.1
Display Format	16:9	16:9	16:9	4:3
Viewing Distance in [cm]	400	70	1,100	40
Application Area	motion picture	gaming	traffic navigation	office
Eye Movement in [deg]/[deg/s]	3.6 (SAC)	14.3 (SAC)	28.2 (SAC)	18.0 (PEM)
Success Rate	0.20	0.30	0.30	0.15
Frame Rate in [Hz]	88.1	265.7	361.3	121.1

Note. Eye movement characteristic was defined under consideration of the selected display type and the area of application (e.g., TV with large viewing distance leads to a small viewing angle, hence, shorter saccades are likely). Under further consideration of a defined success rate, the frame rate requirements to reduce CBU as demanded were calculated on basis of the COBUS1 findings (see Section 4.3.1). TV = television; HUD = Head-Up Display; SAC = saccadic eye movement; PEM = pursuit eye movement.

When interpreting the determined frame rates, it is important to consider some restricting aspects. The required frame rates are based on the average CBU perception of the COBUS1 sample since the involved curve fitting procedure (see Section 4.2.6) refers to the sample's mean CBU scores. This has the effect that significant inter- and intraindividual variations in CBU perception are not covered, i.e., the calculated frame rates are likely to over- or underestimate the actually required frame rates for an individual. However, a clearly arranged guideline cannot be achieved without simplification. Furthermore, the required frame rates are only valid for the defined experimental conditions of COBUS1, i.e., the calculated frame rate values refer to a constant CBU-provoking stimulus size (2.0°) and a constant contrast ratio (0.99). From the COBUS1 findings alone, the effect of a contrast ratio reduction or a stimulus size variation on CBU perception cannot be deduced (see Section 4.4.2). Nevertheless, the COBUS1 findings can be an intermediate step towards development guidelines for future display technology. As a concrete project, an extended display/application classification (exceeding the mentioned examples) could be developed, classifying the frame conditions for display usage and deriving the hardware requirements for these conditions to reduce CBU to an acceptable level.

The results of COBUS1 on required frame rates for reduced CBU perception can hardly be compared with empirical results of other researchers. Most external studies did not investigate the threshold of annoyance (*TOA*) but the threshold of perceptibility (*TOP*) by identifying the necessary frame rate at which CBU can no longer be detected. Under assumption of worst-case conditions — fast retinal stimulus velocities and high luminance levels of the CBU-provoking stimulus in combination with high stimulus-to-background contrast — the technical requirements to eliminate CBU effects are high. Post et al. (1998) and Post et al. (1997) determined frame rates of 1000 Hz and higher to completely eliminate CBU effects under unfavorable conditions (luminance level of stimulus up to 2,216 cd/m^2, stimulus-to-background contrast ratio of 1.0, retinal stimulus velocity of 200 deg/s). Confirming those high technical barriers, Miettinen et al. (2008) determined frame rates of a similar magnitude as high as 1200 Hz (stimulus luminance level at 500 cd/m^2, high Michelson contrast of approx. 1.0, saccadic length of 14°) lowering to a detection threshold slightly above 200 Hz for a low stimulus luminance level of 2 cd/m^2 and short saccadic length of 2°. Mori et al. (1999) reported a significantly lower frame rate threshold around 450 Hz for the most CBU-provoking conditions (stimulus luminance level of 250 cd/m^2 and retinal stimulus velocity of 400 deg/s), leading to an inconsistent picture of frame rate requirements for the *TOP*. The wide range of frame rate requirements highlights the fact that study results are only

valid for the applied study concept. Hence, a comparison between study results is difficult.[52] However, two conclusions can be drawn. First, regardless of the lack of precision when specifying the frame rate requirements for the *TOP*, it is certain that the current technological status quo cannot fully meet the requirements for CBU elimination solely on basis of higher frame rates. The less strict frame rate requirements for the *TOA* as proposed by COBUS1 are more achievable. This leads to the second conclusion. Even if the *TOP* values of other research experiments cannot be directly compared to the *TOA* values of COBUS1, the frame rate thresholds corresponding to CBU annoyance and CBU perceptibility are consistent. The majority of external frame rate values based on the *TOP* are significantly higher than values based on the *TOA* (see examples above). This makes sense, as the requirement that the CBU effect must not be perceived at all is much stricter than the requirement that it is not perceived as annoying by a certain share of the viewers.

Another empirical study based on a larger sample size by Seelmacher (2017, $N = 49$) investigated the general effect of frame rate variation (40 to 580 Hz) on the perceived CBU intensity (no detection thresholds determined). Seelmacher's findings show that the relationship between CBU perception and frame rate can be best described by applying a quadratic function with an initially steep drop of CBU intensities at a low frame rate range to a flatter decline in the middle and high ranges. The description of frame rate-dependent CBU perception by Seelmacher is related but not identical to the COBUS1 findings, which lead to an exponential function (see discussion on Hypothesis H.1). Seelmacher determined a transition from strong to medium CBU at 122 Hz, and from medium to mild CBU at 331 Hz. Again, different study setups must be taken into account (no active eye movement, stimulus luminance level of 457 $\mathrm{cd/m^2}$, background luminance level of 0.17 $\mathrm{cd/m^2}$, retinal stimulus velocity of 55 deg/s).

Effect of Participant Characteristics

High *interindividual* variability of CBU perception has been observed by various researchers such as Miettinen et al. (2008) and Yoshida et al. (2011) when investigating CBU detection thresholds or by Seelmacher (2017) when evaluating CBU under different testing conditions. Similarly, the results of COBUS1 show a high variation in CBU sensitivity from participant to participant (see Tables F.1 to F.2). Obviously, sensitivity in the perception of CBU depends strongly on individual human factors. On the one hand, factors potentially affecting CBU perception relate to the observer's visual system. Color perception has to be mentioned in the first place, although visual acuity and contrast sensitivity are also assumed to influence the perception of CBU. On the other hand, the viewer's general (long-term) personality traits such as his/her affinity to technology or critical attitude might affect CBU perception. However, to the author's best knowledge, research on the impact of visual performance parameters or specific personality traits on CBU perception is not existent. As assumed, distinct *intraindividual* variations can also be observed in the data set of COBUS1. To some extent, the same participant evaluated the same CBU-provoking scenario differently when repeated. Here, the short-term state such as the viewer's attention, concentration, and motivation might play a central role. Unfortunately, there is a research gap on this topic, too.

In this context, Hypothesis H.5 assumes a positive linear correlation between a viewer's visual performance and his/her subjective CBU perception, whereas Hypothesis H.6 refers to a positive linear relation between a viewer's short- and long-term characteristics and

[52] A high variance of the *TOP* might be explained by small samples combined with high interobserver variation of CBU perception. Furthermore, all studies used FSC-based apparatuses with different features (e.g., duty cycle) and setups (LED board vs. rotating filter wheel or chopper blade apparatus) leading to different CBU-provoking tasks (eye movement vs. fixation, perceptual changes as described in Section 2.3.2). Moreover, the presented content (stimulus/background) in the different studies was not similar and therefore not comparable.

his/her CBU perception. The obvious goal of the hypothesis testing was to gain information on the influence of individual viewer-based factors on CBU perception. The underlying idea was to find fast, reliable, and display-transferable tests that investigate specific aspects of visual performance (see Appendix A.2.3 for a description of the performance tests on visual acuity, contrast sensitivity, and color vision) and personal characteristics (see Appendix A.2.4 for the applied questionnaire) to predict the viewer's CBU sensitivity a priori.[53] For a practical implementation of such a procedure, the first step would be to record various viewer-based parameters (e.g., color vision and state of attention) and subsequently characterize the viewer with one global characterizing index that allows to estimate his/her current CBU sensitivity before s/he is confronted with potentially CBU-provoking content. In a second step, an individual adjustment of hardware and/or content parameters under consideration of the viewer's needs and limits could be made to reduce CBU perception during the usage of a potentially CBU-provoking display system.

A global index that describes the type of viewer by merging data of visual performance and personal characteristics to only one number holds a lot of appeal. Variables with the most promising correlations could be chosen and merged. While appealing, the empirical data show that this is not reasonable since the correlations between the global CBU score and the variables tested in COBUS1 are not strong enough or even non-existent (see Table 4.10). Summing up, the discipline of visual performance shows more variables with a positive correlation than the questionnaire-based items on personal characteristics. In CAT2, visual acuity shows the highest correlations of all visual performance parameters. In CAT3, it is contrast sensitivity. However, it has to be pointed out that the existing positive correlations are weak. Consequently, Hypotheses H.5 and H.6 are rejected. There is no high ranked variable that can effectively predict CBU sensitivity. Therefore, the creation of a global characterizing index on basis of the tests applied in COBUS1 is not promising at all. The correlation between a global viewer-characterizing index and the global CBU score would also be weak or even weaker than the correlations of the single variables.

A reason for the missing correlations between the global CBU score and the tested variables in COBUS1 (visual performance and short/long-term personal characteristics) might be the small variance of some of the characterizing variables within the sample. For example, visual performance parameters such as visual acuity, contrast sensitivity, and color vision are generally high within the sample of young and healthy participants, with only a few exceptions (see Section 4.2.6). Another reason for the missing correlation between variables of visual performance and CBU perception might be the fact that the variables of visual performance were determined under conditions that do not have that much in common with the requirements during the CBU testing for CAT2 and CAT3. For example, CBU perception was tested during eye movement. This is not the case during the standard optometric testing of visual acuity, contrast sensitivity, or color vision. It has to be pointed out that these measurements of visual performance investigate aspects of human vision that do play a role during CBU perception but are not specific enough to fit the requirements of the very specific task of CBU perception during saccades or pursuits. No previously existing optometric test applied in daily practice meets the requirements that would be necessary to make an adequate prediction on CBU sensitivity a priori. Regarding the short- and long-term personal characteristics, it must be noted that these parameters are highly subjective since they were self-evaluated by the participant and therefore subject to participant bias. In conclusion, it seems more promising to use an FSC setup and show a few representative CBU scenarios to the viewer which s/he then evaluates. This would make it possible to determine the current CBU sensitivity without detours.

[53] Previous findings do not support an effect of demographics such as age (Baron & Chase, 2004) or gender (Seelmacher, 2017) on CBU perception. Hence, demographics were not used to characterize participants.

4.4.2 Color Break-Up Study 2

The discussion of COBUS2 is structured analogous to the result presentation in Section 4.3.2 allowing a smooth transition between the sections.

Effect of Stimulus Size

The effect of increasing stimulus size on CBU perception can be quantified in a variance spectrum from a relative CBU increase of 7% to a decrease of 46% (stimulus size of 6.0° in reference to 1.0°, mean values averaged over all stimulus positions) over all tested frame rates (30.0 and 60.0 Hz) and experimental categories (CAT2 and CAT3) during COBUS2. The choice of frame rate and experimental category significantly affects the direction and strength of the effect of stimulus size (see Section 4.3.2). For example, the relative CBU decrease with increasing stimulus size during a CAT2 saccade at 60.0 Hz (-46%) in comparison to 30.0 Hz (-16%) is significantly higher (see Figure 4.26). One explanation could be a bias resulting from the perception of flickering at 30.0 Hz. It is possible that participants were affected by flickering during the presentation of CBU effects, and might have considered flickering as a negative effect when evaluating CBU. This could result in an upward shift of CBU scores under certain conditions. The flicker effect becomes more pronounced with larger stimulus sizes (larger flickering surface, see Appendix B.2.1), which could explain the lower relative decrease rates with larger stimulus sizes (up to 6.0°). The same general pattern can also be observed during pursuits (CAT3). Comparing the relative behavior while the stimulus size is changed from 1.0 to 6.0°, the relative CBU values increase by +7% for 30.0 Hz and decrease by -8% for 60.0 Hz (see Figure 4.32). Again, there is a discrepancy between the relative values for both frame rates with a higher relative CBU decrease for 60.0 Hz. As during saccades, this might be explained by flickering effects, even if the frame rate's effect during pursuits is less pronounced, possibly due to a lower sensitivity to flickering effects during pursuits.

In sum, it seems reasonable to focus mainly on results that are based on the 60.0 Hz presentation, since the results based on the 30.0 Hz presentation might be biased due to flickering effects. Therefore, the effect of increasing stimulus size on CBU perception is finally quantified with a relative CBU decrease of 46% for saccades and 8% for pursuits during a 60.0 Hz presentation. Based on these results, it must be concluded that an increase in stimulus size leads to a reduction of CBU perception for both saccades and pursuits, while the effect on CBU perception is larger for saccades than for pursuits. This finding is supported by the fact that the possibility of a transition from CBU-characterizing Phase 1 to a higher Phase 2 or even Phase 3 — which are normally rated with significantly higher CBU scores — is more likely provoked by a decreasing stimulus size during saccades than during pursuits due to potentially higher saccadic eye movement velocities (see Section 3.5.1). This discrepancy for the stimulus size's effect on CBU perception for saccades and pursuits can be confirmed by other research. Empirical studies showed that a larger stimulus size (width in eye movement direction) leads to a distinct reduction of perceived CBU effects during saccades (Kobayashi et al., 2011; Yoshida et al., 2011; X. Zhang & Farrell, 2003) whereas theoretical model simulations by P. V. Johnson et al. (2014) predicted only a small effect of stimulus width on CBU visibility during pursuits (no empirical data available for pursuits).

Effect of Stimulus Position

The effect of retinal stimulus position on CBU perception (averaged over all stimulus sizes) can be quantified for the maximum peripheral (50.0°) in reference to the central stimulus position (0.0°) with a relative CBU decrease of 52 to 63% (inner field of view) and 42 to 56%

(outer field of view) over all tested frame rates (30.0 and 60.0 Hz) and experimental categories (CAT2 and CAT3). Frame rate and experimental category slightly affect the strength of the positional effect as described in detail in Section 4.3.2 (see Figures 4.25 and 4.31). However, the values of relative CBU decrease are comparable to a certain degree as indicated by their small ranges.[54]

It is obvious that the reduced CBU perceptibility for higher retinal eccentricities as observed in COBUS2 is directly related to the well-known decline of retinal sensitivity from the fovea centralis to its periphery (see Section 2.3.2). Summing up other research findings, the human visual system's chromatic red-green and blue-yellow channels as well as the achromatic channel for light intensity response all show a decrease of sensitivity with rising eccentricity. In comparison, the red-green channel shows a more accentuated sensitivity reduction than the two other perceptual channels (Hansen et al., 2009; Martin et al., 2001; Mullen & Kingdom, 2002; Mullen et al., 2005), with a peripheral sensitivity for green stimuli even lower than for red stimuli (Newton & Eskew, 2003; Stromeyer et al., 1992). However, these research findings refer to detection/identification tasks which do not have informative value on quantitative aspects of color perception. In which way do color characteristics such as hue and saturation perceptually alter across the retina? From the fovea to the retinal periphery, a stimulus is more and more desaturated, and the perceived hue of the stimulus changes with increasing eccentricity (Boynton et al., 1964; Gordon & Abramov, 1977; Ikeda et al., 1985; McKeefry et al., 2007; B. Stabell & Stabell, 1979). Furthermore, there is a naso-temporal asymmetry which results in a faster reduction of saturation on the temporal side of the retina than on the corresponding nasal locus (Abramov et al., 1992; Ayama & Sakurai, 2003; Sakurai et al., 2003; U. Stabell & Stabell, 1982). Regarding hue perception in peripheral vision, the response of the blue-yellow channel is stronger than the response of the red-green channel. As an effect, the blue-yellow channel is largely unaffected with increasing eccentricity in all retinal directions (only the saturation decreases). Furthermore, mixed colors with a blue or yellow component such as blue-green and red-blue or green-yellow shift towards blue or yellow color perception. In contrast, color perception regarding the red-green channel deteriorates with increasing eccentricity in all retinal directions. Red and green colored stimuli or at least mixed color stimuli with an additional yellow component (yellow-red and green-yellow) shift towards a yellowish perception with increasing eccentricity. These color shifts tend to be more pronounced in temporal than in nasal direction. (Ayama & Sakurai, 2003; Hamada & Yujiri, 2004; Sakurai et al., 2003; Yujiri & Hamada, 2003).

Finally, the COBUS2 findings are clarified by the stated research findings. The general decline of CBU perceptibility with higher retinal eccentricities can be explained by the reduced retinal sensitivity to brightness and color. P. V. Johnson et al. (2014) affirm:

> We wondered whether breakup was more visible in the peripheral or central visual field. One might argue that it would be most noticeable in the peripheral field where high temporal frequencies are more visible. But one might also argue that breakup would be most noticeable near the fovea where spatial resolution and sensitivity to hue variation are greatest. All subjects reported that breakup was most visible when the rectangles [used CBU stimuli] passed nearest the fovea suggesting that the poor resolution and reduced sensitivity of the retinal periphery make color breakup less noticeable in that part of the visual field. (p. 9)

In addition, a higher relative CBU decrease from retinal center to periphery for the inner field of view (52 to 63%) in comparison to the outer field of view (42 to 56%) during COBUS2 can also be explained. The reason for this perceptual behavior mainly lies in the faster

[54] The small variances of relative CBU decrease for both frame rates indicate a limited impact of flickering on the study results. This is unexpected as the flickering effect depends on the stimulated retinal position (see Appendix B.2.1).

reduction of color saturation on the temporal retina (inner field of view) than on the nasal retina (outer field of view), whereas the tendency of stronger color shifts towards a dominant blue-yellow channel response in temporal rather than in nasal retinal direction is harder to estimate in terms of their effect on CBU perception (see statements above).

Effect of Movement Direction

During COBUS2, each test sequence defined by the independent variable range of CBU stimulus position and size included in every experimental category (CAT2 and CAT3) for all applied frame rates (30.0 and 60.0 Hz) was presented four times to the participant by executing two horizontal (L2R and R2L) and two vertical movement directions (U2D and D2U). It would be possible to investigate the effect of movement direction on CBU perception to obtain even more information. However, this has not been investigated since the CBU scores for all four movement directions have been averaged for all tested sequence conditions to assure a higher robustness against outliers. The robustness of the data set is more important than additional information on a secondary research question.

Other research results show that saccades with the same amplitude but different directions (horizontal, vertical, or diagonal) cause different intensities of the CBU effect — vertical and diagonal saccades provoke less CBU than horizontal saccades (Kobayashi et al., 2010). This deviation can be explained by the fact that a saccade's velocity for a defined amplitude depends on the direction in which it is executed. A horizontal saccade can be performed with a higher peak velocity than a vertical saccade (Garbutt et al., 2003). As a consequence, the averaged CBU scores over four different movement directions during COBUS2 have to be distinguished from CBU effects for a specific eye movement direction.

Under the theoretical assumption of perfectly precise PEM with a gain of 1.0, it would be expected that there is no difference in CBU perception for pursuits in horizontal and vertical direction. However, it has been shown that the actual gain of horizontal pursuits is greater than that of vertical pursuits in the phase of pursuit maintenance (Rottach et al., 1996). This means that horizontal pursuits are executed more precisely whereas vertical pursuits tend to fall behind the fixation target. The resulting effect on the viewer's CBU evaluation during vertical pursuits is difficult to predict, as this behavior may lead to potentially higher CBU perception due to the need to execute catch-up saccades or to lower CBU perception caused by slower PEM and/or reduced visual performance outside the fovea. Again, it cannot be ruled out that the CBU scores averaged over four different PEM directions (COBUS2) deviate from CBU scores assigned to a specific movement direction.

Threshold of Annoyance

Since flickering at 30.0 Hz might have a biasing effect when varying the CBU stimulus size, more emphasis should be put on the *TOA* results based on the frame rate of 60.0 Hz as illustrated in the right-side graphics in Figure 4.28 (saccades) and Figure 4.34 (pursuits). In the graphics, the *TOA* borderlines provide a quick overview of all combinations of CBU stimulus sizes and positions that do or do not violate the determined *TOA* (based on the defined success rate). The outer area stands for all size-to-position combinations that do not violate the determined CBU annoyance requirements whereas the inner area delimited by the *TOA* borderline defines all combinations that violate the requirements (more viewers than desired perceive CBU as annoying). This graphical output and the underlying data set can be a useful tool for an application-dependent specification of content creation guidelines.

When analyzing the single graphics in Figures 4.28 and 4.34 in more detail, it becomes clear that the variation of the success rates leads to consistent *TOA* borderlines due to a steady decrease of CBU scores with more peripheral stimulus positions and larger stimulus

sizes. Furthermore, it can be concluded that the variation of the success rate has a direct effect on the range of stimulus positions that can be considered for content presentation without a violation of the determined requirements (success rate, *TOA*). The higher the success rate (larger viewer share that is allowed to be annoyed by CBU), the more the *TOA* borderlines reach towards the viewer's central field of view. Potentially CBU-provoking stimuli can be presented more centrally without annoying more viewers with CBU than specified. This statement applies to both experimental categories (CAT2/CAT3). In terms of applicable stimulus sizes, it can be concluded that the variation of the success rate also has an effect on the course of the *TOA* borderline. However, increasing success rates only leads to wider ranges of applicable stimulus sizes above a certain level of the success rate. Below this level, the effect of success rate variation is marginal to non-existent. This is true for both CAT2 and CAT3.

In conclusion, higher success rates — which represent a less strict requirement by accepting a larger share of viewers who are allowed to be annoyed by CBU — lead to a greater flexibility in choosing stimulus position and size combinations that meet the specified CBU annoyance requirements. Ultimately, this is a trade-off between the CBU effect's acceptable impact on the viewer and the degrees of freedom in content creation.

4.4.3 Shortcomings

The COBUS series sheds light on the impact of hardware-based, content-based, and viewer-based factors on human CBU perception, allowing the definition of important requirements to reduce CBU. However, the processes of study preparation, execution, and post-processing have a few shortcomings that require attention.

The pixel structure presented on the projection screen differs from the common horizontal/vertical alignment structure due to the micromirror diamond array of the applied DLP projector (see Figure A.2). As a consequence, the edges of the presented objects during the main sequence of the main examination phase (e.g., CBU-provoking stimulus) were partially saw-toothed (no straight edges, pixel-sized structure). However, due to the small pixel sizes applied during the COBUS series, this is unlikely to have had a relevant effect on the participant's CBU perception and evaluation.

Some participants reported slight color effects at the upper and lower edges of the CBU-provoking stimulus (eye movement in horizontal direction assumed, greenish/reddish coloring at the upper/lower edge of the CBU-provoking white square, see Section 4.2.6). These color effects are thought to be elicited by the participants through unwanted executions of vertical eye movements during the presentation of the CBU-provoking stimulus. It is unlikely that these color effects affected the CBU evaluations during the COBUS series, as all participants were requested to consider only CBU effects that occur in eye movement direction and report irregularities as soon as they occurred (irregular test sequences were repeated).

It can be assumed that all participants perceived flickering effects during a frame rate presentation of 30.0 Hz (see pre-testing in Appendix B.2.1). A participant might erroneously consider the negative effect of flickering while evaluating CBU perception and therefore overestimate the CBU effect. Furthermore, after presenting a specific number of 30.0 Hz sequences, a participant might be conditioned to expect high CBU perception each time flickering occurs since the previous flickering sequences are likely to provoke high CBU effects. Therefore, the participant might select higher CBU scores than warranted (e.g., for small saccadic jumps of 3.6°). As a result, a bias during the CBU evaluation of 30.0 Hz sequences cannot be ruled out even if all participants are told not to consider flickering effects during CBU evaluation.

While a controlled laboratory testing is necessary to collect data in a similarly controlled manner, a lab setting "may be considered 'unnatural' when compared to the way a user would typically experience the content" (Streijl et al., 2016, p. 215). Hence, the CBU perception and evaluation during COBUS might deviate from the way a viewer would perceive CBU at home in front of his/her TV. As a consequence, COBUS results are not representative for all everyday uses of all available display systems. In this context, it should be emphasized that the main study examinations of the COBUS series took place in a darkened room (see Section 4.2.7). This lighting condition does not cover the full range of possible lighting conditions during everyday display use. Surrounding lighting conditions have a strong impact on perception across a viewer's field of view: Surrounding illuminance triggers retinal adaptation processes and influences the degree of rod/cone activity, chromatic sensitivity deteriorates and hue perception alters with decreasing illuminance levels over the whole retinal area (Hamada & Yujiri, 2004; Yujiri & Hamada, 2003). In a dark-adapted state, rod intrusion strongly influences peripheral color vision (B. Stabell & Stabell, 1980; U. Stabell & Stabell, 1981). Therefore, CBU effects during display usage in broad daylight are likely to differ from the COBUS results.

Describing content movement velocities in [deg/s] results in a center-to-periphery bias when the content is displayed on a presentation unit with a flat screen characteristic as during the COBUS series. The disadvantage is that a movement with constant velocity on such a plane surface cannot be expressed by a constant movement velocity value in [deg/s], since angles in [deg] spanned by identical absolute distances in [px] and covered in the same time span are smaller in the periphery than in the center of the screen. Consequently, the movement velocity in [deg/s] for a constant movement is smaller in the periphery than in the center, i.e., the velocity value in [deg/s] for a constant movement is not stable for all possible positions on the screen. The center-to-periphery-bias is described in detail in Appendix C.3.

Due to the close positioning of the upper apex of the participant's head and the projector (see Section 4.2.7), a precise alignment of the displayed content with a straight forward eye gaze on the fixation target (see 4.2.6) could not be realized. In fact, a slight upward eye position (approx. 5°) was adjusted for all participants to offer some free space between head and projector so that the participant did not bump against the projector (for example, when leaning back from the head/chin rest position during breaks). The upward deviation of eye gaze within the sample was slightly variable (approx. $\pm$2.5°) as every participant has an individual anatomical head structure. It is not expected that these variations affected the study results since the retinal position of the study content was not affected by the described deviations. However, it cannot be completely ruled out that the vertical gaze position has an impact on the quality of pursuits and saccades.

These shortcomings were known and analyzed prior to starting the COBUS series. However, the shortcomings could not be addressed due to lack of alternative approaches and/or were deemed negligible in terms of their impact on the study results.

Chapter 5

Model Output vs. Study Data

5.1 Data Selection

CBU perception has been investigated using two different approaches — a theoretical model-based approach as described in Chapter 3 and an empirical study-based approach as presented in Chapter 4. In the following, both approaches are compared in terms of outcomes. Adopting the conditions of the empirical study as the model's input parameters, the modeled output CBU_{IDX^*} and the participants' subjective CBU perception represented by the CBU_{SCR} can be compared. Comparing CBU_{IDX^*} and CBU_{SCR} allows the evaluation of the accuracy of the theoretical model. The comparison is based on a selected share of the complete data set of COBUS1 (with its two experimental arms of CAT2 and CAT3 that include further experimental subgroups). The chosen data set refers to the study condition of precise PEM provoked by a content movement velocity of 36.0 deg/s over a path length of 21.3° (CAT3) under consideration of frame rate variations from 30.0 to 420.0 Hz.[1]

5.2 Model Loop

To calculate the model output for various frame rates, the loop function »cbu loop« was written in MATLAB (Version R2018b, The MathWorks, Inc.). The code has been made available as open source, accessible on GitHub (https://github.com/markusleicht/ColorBreakUp) and archived via Zenodo (https://doi.org/10.5281/zenodo.6749170).

The aim of the loop function is to repeatedly run the fundamental CBU model function »cbu model« for model index calculation (see Chapter 3) while varying the frame rate for each new run, covering the defined frame rate range of 30.0 to 420.0 Hz in 5.0 Hz steps by default.[2] A basic code description for the loop function is embedded in the MATLAB code itself. Before running the loop for various frame rates, the input parameters of eye and content movement velocity in [px/fr] have to be adapted to guarantee the same angular movement velocity in [deg/s] for different frame rates (see Table 5.1). This adaption process in the loop function is necessary to mirror the PEM condition of COBUS1 with equal eye/content movement velocity of 36.0 deg/s for all applied frame rates. For example, a content movement velocity of 36.0 deg/s at a frame rate of 90.0 Hz is achieved by applying frame-to-frame shifts of 8 px/fr (EOC condition for general model description in Chapter 3). To guarantee the same angular movement velocity of 36.0 deg/s for a frame rate of only 30.0 Hz, the frame-to-frame shifts of the moving content have to be adjusted to 24 px/fr.

[1] In Chapter 3, the input parameters of the same COBUS1 setting are used to explain the structure of the new CBU model. However, the model description refers to one discrete frame rate of 90.0 Hz (see Table 3.2).

[2] The variation of the determined frame rates is executed in Segment A of MATLAB's main loop function. For the graphical output of Segment A, the external functions »cprintf« (Altman, 2020), »blandaltmanplot« (Wisselink, 2019), and »boundedline« (Kearney, 2014) must be available by adding the folders to the MATLAB search path or placing them in the same folder as the main function.

TABLE 5.1: Possible ranges and determined values of CBU loop calculation for various input parameters concerning display system, viewer characteristics, and surrounding condition.

Classification		Input Parameter	Abbrev.	Range	Value	Unit
display	hardware	frame rate	FR	20.0 – unlimited	30.0 – 420 (5.0 steps)	Hz
		subframe number	SF_{CT}	2 – 6	3	—
		duty cycle	DC	0.0 – 1.0	0.3	—
		native resolution (hor.×vert.)	RES	positive integers ≠ 0	912×1140	px
		aspect ratio	AR	positive values ≠ 0	1.60	—
		display diagonal	DD	positive values ≠ 0	0.54322	m
	lighting [a]	radiance level	RL	0.0 – unlimited	0.1224 / 0.2456 / 0.1576	$W/(sr \times m^2)$
		luminance level	LL	0.0 – unlimited	27.39 / 126.03 / 5.14	cd/m^2
		chromaticity coordinate (x value)	x	ltd. by color space	0.6912 / 0.3018 / 0.1527	—
		chromaticity coordinate (y value)	y	ltd. by color space	0.3078 / 0.6276 / 0.0240	—
	content	width (regular)/height [b]	CW_{REG} / CH	integer w/i display lmt.	40 / 80	px
		vertical position [c]	CP_{VER}	integer w/i display lmt.	+40	px
		mov. positions (hor. start/stop) [d]	CP_{T0} / CP_{T1}	integer w/i display lmt.	-236 / +196	px
		movement velocity (hor.) [e]	CMV	0 – unlimited	+1.7 to +24.0	px/fr
viewer	anatomy [f]	$\overline{CV\text{-}N}$ (relaxed)	—	—	0.00706	m
		$\overline{CV\text{-}N'}$ (relaxed)	—	—	0.00736	m
		$\overline{CV\text{-}F'}$ (relaxed)	—	—	0.02389	m
		$\overline{CV\text{-}N}$ (accommodated)	—	—	0.00656	m
		$\overline{CV\text{-}N'}$ (accommodated)	—	—	0.00691	m
		$\overline{CV\text{-}F'}$ (accommodated)	—	—	0.02125	m
		$\overline{CV\text{-}Z'}$	—	—	0.01350	m
		radius of retina	RR	—	0.01200	m
	cognition	Bloch time (cones) [g]	BT_{CO}	0.0 – unlimited	0.0 (inactive)	s
		Bloch time (rods)	BT_{RO}	0.0 – unlimited	0.0 (inactive)	s
		Ricco area (rods/cones) [h]	$RA_{RO/CO}$	0.0 – unlimited	0.0 (inactive)	m
	eye	vertical position [i]	EP_{VER}	integer w/i display lmt.	0	px
		mov. positions (hor. start/stop) [j]	EP_{T0} / EP_{T1}	integer w/i display lmt.	-216 / +216 (PEM)	px
		movement velocity (hor.) [k]	EMV	0 – unlimited	+1.7 to +24.0 (PEM)	px/fr
surrounding		viewing distance [l]	VD	positive values ≠ 0	0.57169	m

Note. *CV* = corneal vertex; *N* = first nodal point; *N′* = second nodal point; *F′* = second principal focus; *Z′* = eye's center of rotation.

[a] For every single subframe, all lighting parameters are specified separately under consideration of the determined number of three subframes within one frame cycle (*SF1* = red / *SF2* = green / *SF3* = blue).

[b] Content is assumed to have a simple geometrical shape. In this case, it is a quadratic stimulus with a width of 40 px and a height of 80 px corresponding to an angular side length of 2.0° in horizontal and vertical direction (angular side length in [deg] is valid for content in a central display position in horizontal/vertical direction, undistorted content at display level).

[c] Vertical content position is defined by the upper content edge at display level (constant), point of origin is vertical center of the display unit (down = negative, up = positive), determined vertical content position for model calculation (+40) leads to a vertically centered display position which deviates from COBUS1 presentation setting with one upper (+160) and one lower stimulus (-80) since model only allows the determination of one stimulus in a defined position.

[d] Horizontal movement path is defined by position of left content edge (display level) at the time movement starts (*T0*) and after movement is finished (*T1*), point of origin is the horizontal center of the display unit (left = negative, right = positive).

[e] Horizontal content movement velocity in [px/fr] has to be adapted regarding the application of different frame rates to guarantee a constant corresponding angular content movement velocity of +36.0 deg/s for the defined conditions (angular movement velocity in [deg/s] refers to a rotation around the eye's center of rotation *Z′*, angular movement velocity is only valid for a central display position, positive values = left to right movement, negative values = right to left movement).

[f] Anatomical parameters of standard observer eye refer to Gullstrand-Emsley's schematic human eye model (except retinal radius), *relaxed* values refer to anatomical status of no accommodative effort, *accommodated* values refer to status of an accommodative effort of 10.9 D (Emsley, 1936); simplistically, it is assumed that the schematic retina has a spherical shape with a radius of 12.0 mm (Smith & Atchison, 1997).

[g] Bloch time is defined as time period for which temporal summation of light stimulation is assumed.

[h] Ricco area is defined as area for which spatial summation of light stimulation is assumed (no differentiation for rods and cones).

[i] Constant vertical eye gaze position (cyclops eye's fixation line at display level), point of origin is vertical center of the display unit (down = negative, up = positive).

[j] Movement path is defined by eye gaze position (cyclops eye's fixation line at display level) at the time movement starts (*T0*) and after movement is finished (*T1*), point of origin is the horizontal center of the display unit (left = negative, right = positive), eye movement path for model calculation is determined to follow CBU-provoking content with idealized PEM, eye gaze position during PEM determined to be in the horizontal/vertical center of the CBU-provoking content at the start of every frame cycle.

[k] Horizontal eye movement velocity in [px/fr] has to be adapted regarding the application of different frame rates to guarantee a constant corresponding angular eye movement velocity of +36.0 deg/s for the defined conditions (angular movement velocity in [deg/s] refers to a rotation around the eye's center of rotation *Z′*, angular movement velocity is only valid for a central display position, positive values = left to right movement, negative values = right to left movement).

[l] Distance from display level to corneal vertex of cyclops eye.

Figure 5.1 illustrates the frame rate-dependent output of the loop function for the model indices CBU_{IDX^*} (red graph) and $NON\text{-}CBU_{IDX^*}$ (green graph), representing the model-based calculations for the perception of color-distorted and color-unbiased shares of the presented CBU-provoking stimulus, respectively. Furthermore, the reference index REF_{IDX^*} (black graph) is plotted to allow a classification of the indices (see Section 3.7 for a detailed explanation of model indices). Both indices CBU_{IDX^*} and $NON\text{-}CBU_{IDX^*}$ show an opposing behavior with changing frame rate. CBU_{IDX^*} decreases with increasing frame rate whereas $NON\text{-}CBU_{IDX^*}$ approximates the ideal upper limit of CBU-free stimulation represented by REF_{IDX^*}. Within the determined frame rate range, CBU_{IDX^*} and $NON\text{-}CBU_{IDX^*}$ never reach the zero level, i.e., the color characteristics of the investigated CBU-provoking stimulus are constantly classified into PH1 with color-unbiased shares in the central area of the stimulus and color-distorted leading and trailing stimulus edges (see Section 3.5 for an explanation of CBU phases).[3]

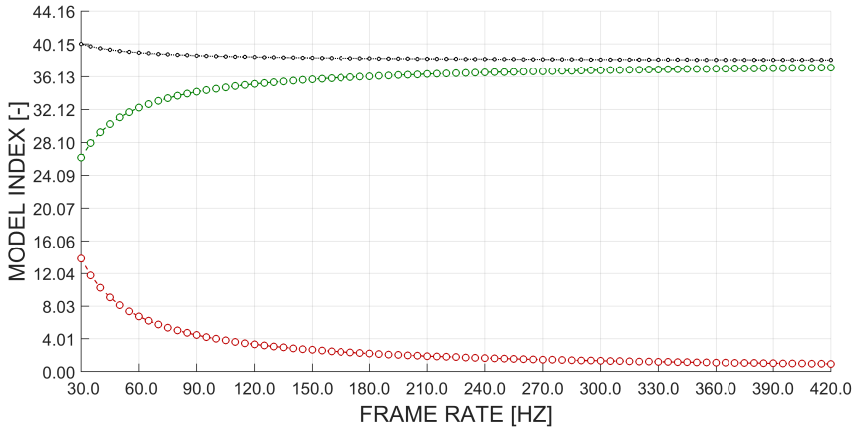

FIGURE 5.1: Model indices CBU_{IDX^*} (red graph), $NON\text{-}CBU_{IDX^*}$ (green), and REF_{IDX^*} (black) in dependency of frame rate (30.0 to 420.0 Hz, 5.0 Hz steps) for PEM sequence with eye/content movement velocity of 36.0 deg/s (see Table 5.1), calculated/plotted with MATLAB loop function.

Additionally, Figure 5.2 shows the color maps for three selected frame rates of 30.0, 90.0, and 180.0 Hz to visualize the actual color characteristics of the investigated CBU-provoking stimulus at retinal level.[4] The illustrated CBU effects are all classified into PH1. However, the three color maps show CBU effects of varying degrees. The apparently strongest CBU effect occurs at the lowest frame rate of 30.0 Hz. The extent of the CBU effect decreases at the leading and trailing stimulus edges as the frame rate increases. The final model indices corresponding to the visualized color maps at 30.0, 90.0, and 180.0 Hz in Figure 5.2 are 13.8960, 4.4760, and 2.2177 for CBU_{IDX^*} and 26.2540, 34.2787, and 36.1861 for $NON\text{-}CBU_{IDX^*}$, respectively. REF_{IDX^*} for the frame rates of 30.0, 90.0, and 180.0 Hz is 40.1484, 38.7548, and 38.4039, respectively (see Figure 5.1).

[3] Besides Segment A for frame rate variation, the main loop function contains further code segments. Segments B to E theoretically allow a variation of other factors of CBU perception (Segment B: eye movement velocity, Segment C: duty cycle, Segment D: content width, Segment E: subframe number/count). However, the functionality of these code segments is not yet established (segments are deactivated). Before the Segments B to E can be used, the code structure from Segment A must be transferred to the other segments.

[4] Color maps are calculated on basis of temporal summation of the subframes' light emission within a single frame cycle of choice (FCC). Different frame rates lead to different on-times of light emission within the FCC. As a result, dimmed color representations can occur in the color maps, especially for scenarios with high frame rates (see right-side graphic in Figure 5.2, unbiased white color zone is represented by a grayish area). However, the final model indices CBU_{IDX^*}, $NON\text{-}CBU_{IDX^*}$, and REF_{IDX^*} are scaled up to compensate for the frame rate-dependent duration of light emission within the FCC (see Section 3.7).

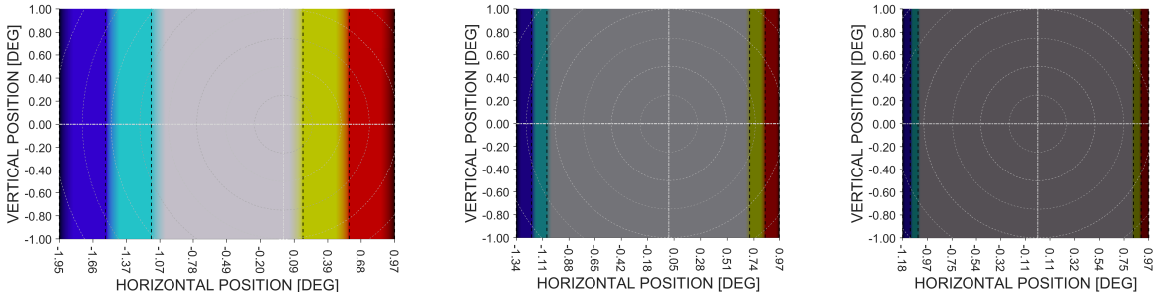

FIGURE 5.2: Color maps for PEM sequence with eye/content movement velocity of 36.0 deg/s (see Table 5.1), considering frame rates of 30.0 (left graphic), 90.0 (middle), and 180.0 Hz (right). Illustration of mixed colors at retinal level after temporal summation of all subframes within the FCC, calculated/plotted with MATLAB model function (dash-dotted gray lines represent horizontal/vertical retinal center with fovea centralis as point of intersection, dashed gray circles illustrate retinal eccentricity steps of 0.25°, dashed black lines represent borders between color zones).

5.3 Data Scaling

The range of values for the calculated model index CBU_{IDX^*} starts at zero, indicating the absence of CBU (lower limit). In upwards direction, there is no limit for the CBU_{IDX^*}, which means that index values can theoretically range from zero to infinity. In COBUS1, by contrast, the sample's CBU perception was evaluated on a continuous CBU scale with a range from 1.0 to 5.0, and a granularity of 0.01 for the finally determined score CBU_{SCR} (see Section 4.2.8). Since the scale limits of CBU_{IDX^*} and CBU_{SCR} differ, both data sets have to be adjusted for comparison. There are different scaling methods that can be applied. By applying a min-max-normalization, the model index CBU_{IDX^*} is adapted by compressing/stretching the index values to match the minimum and maximum values of the empirical CBU score data set. Alternatively, a standardization process can be used to rescale both data sets so that the condition of $MN = 0$ and $SD = 1$ is satisfied. For the purpose of this study, a standardization process is used.[5]

$$CBU_{S\text{-}MN\,(SPL,FR)} = \left(CBU_{MN\,(SPL,FR)} - CBU_{MN\,(SPL,FRR)} \right) / CBU_{SD\,(SPL,FRR)} \tag{5.1}$$

The standardization process has to be applied to both the empirical study-based and the theoretical model-based data set. For the empirical data set, the standardized mean sample values of the CBU scores for all frame rates are calculated with Formula 5.1 where $CBU_{MN\,(SPL,FR)}$ is the mean score of all participants ($N = 30$) for one discrete frame rate within the tested frame rate range and $CBU_{MN\,(SPL,FRR)}$ is the mean score for all tested frame rates within the range of 30.0 and 420.0 Hz (referring to all 30 participants). $CBU_{SD\,(SPL,FRR)}$ is the standard deviation of the mean sample scores of the full frame rate range (30.0 to 420.0 Hz). The result of the calculation is $CBU_{S\text{-}MN\,(SPL,FR)}$ as the standardized mean sample score for one discrete frame rate. By executing this calculation for all discrete frame rate values from 30.0 to 420.0 Hz, the standardized mean sample CBU scores for all discrete frame rate values within the test range can be calculated.

$$CBU_{S\text{-}SGL\,(PAR,FR)} = \left(CBU_{SGL\,(PAR,FR)} - CBU_{MN\,(SPL,FRR)} \right) / CBU_{SD\,(SPL,FRR)} \tag{5.2}$$

After standardizing the mean sample value of the CBU scores for all single frame rates, the standardized standard deviation must also be calculated. Therefore, the single CBU scores for each participant have to be standardized using Formula 5.2 where $CBU_{SGL\,(PAR,FR)}$ is the

[5] In the MATLAB loop function, the code for the standardization and normalization processes is provided in Segment A under »Standardization of Data« (activated) and »Min-Max-Normalization of Data« (deactivated).

score of one single participant and one discrete frame rate within the tested range of 30.0 to 420.0 Hz. It is important to notice that $CBU_{MN\,(SPL,FRR)}$ and $CBU_{SD\,(SPL,FRR)}$ are identical to the terms used in Formula 5.1 which refer to the mean values of the entire sample (all participants, full frame rate range). The result of the calculation is the standardized score $CBU_{S\text{-}SGL\,(PAR,FR)}$ of one single participant and one discrete frame rate. This calculation has to be executed for all participants and all discrete frame rate values. After standardizing the whole data set as explained, the standard deviation of the standardized single CBU scores of all 30 participants can be calculated for all tested frame rates from 30.0 to 420.0 Hz. Now the standardized mean sample values and standard deviations of the CBU scores are available for the empirical data set. The data set of the theoretical model has to be standardized as well. However, only the explicitly calculated model indices CBU_{IDX^*} for the applied range of frame rates have to be standardized since there is no established spread for the theoretical model. The standardization of the explicit model indices of the theoretical model is done like the standardization of the mean sample values of the empirical CBU scores (see Formula 5.1). Aiming to provide stability during standardization, the values for the terms $CBU_{MN\,(SPL,FRR}$ and $CBU_{SD\,(SPL,FRR)}$ refer to the full frame rate range between 30.0 and 420.0 Hz by default. Furthermore, the frame rate steps are kept stable at 5.0 Hz during the standardization process.

5.4 Data Comparison

After model output and empirical data set are standardized, it is finally possible to combine and compare the outcomes of empirical research and applied model in Figure 5.3. The model's CBU index (CBU_{IDX^*}) is illustrated by a red dashed graph (based on the calculations for frame rates from 30.0 to 420.0 Hz in 5.0 Hz steps). The sample's average CBU scores (CBU_{SCR}) are represented by blue dots covering the applied frame rates during COBUS1. A fitted exponential function on basis of the sample's average CBU scores is also plotted as a blue dashed graph.

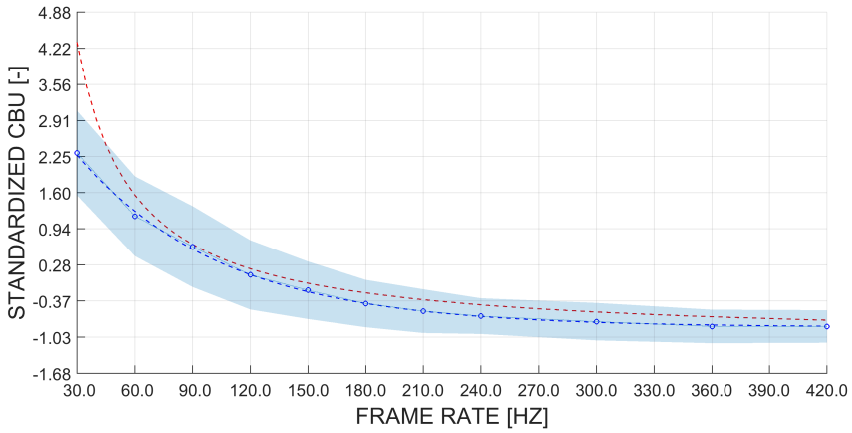

FIGURE 5.3: Model index CBU_{IDX^*} and empirical study score CBU_{SCR} of COBUS1 (both standardized) in dependency of frame rate (30.0 to 420.0 Hz) for PEM sequence with eye/content movement velocity of 36.0 deg/s; red dashed graph represents CBU_{IDX^*}, blue circles represent CBU_{SCR} (sample-averaged), blue dashed graph represents exponential function fitted to empirical data, pale blue area represents standard deviation of empirical data (linear interpolation between data points).

When comparing the model-predicted CBU effect (red dashed graph) with the subjective CBU perception during COBUS1 (blue dashed graph), it can be concluded that both graphs run in close proximity for a large share of the investigated frame rate range — approximately from 60.0 to 420.0 Hz. Within this range, the model predicts subjective CBU perception

with sufficient accuracy. With decreasing frame rates, however, both graphs diverge. As a result, the model-based CBU_{IDX^*} clearly exceeds the empirical CBU_{SCR} between 30.0 and approximately 60.0 Hz. The model graph runs out of the sample's spread (pale blue zone) because of its steep rise within the low frame rate range.

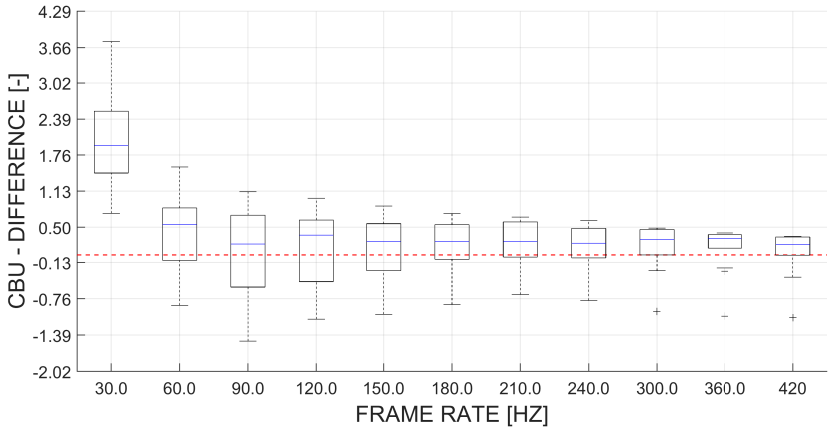

FIGURE 5.4: Differences between model index CBU_{IDX^*} and study score CBU_{SCR} (both standardized, difference = index - score) for PEM sequence with eye/content movement velocity of 36.0 deg/s, consideration of all frame rates investigated during the execution of COBUS1 (elements of the box-and-whisker plot: lower/upper whisker represents minimum/maximum value of the data set with outliers excluded, box represents interquartile range, blue solid line represents median, black cross represents outliers; red dashed line represents zero CBU difference).

Furthermore, discrepancies between the sample's CBU_{SCR} and the model's CBU_{IDX^*} (both standardized) are illustrated by a box-and-whisker plot in Figure 5.4. The sample score and the model index are compared for all frame rates investigated during COBUS1. The plotted zero line (red dashed line) represents the ideal case of no difference between CBU_{SCR} and CBU_{IDX^*}. The zero line lies within the interquartile range for all tested frame rates from 60.0 to 420.0 Hz (with the notable exception of 360.0 Hz where at least the minimum-maximum limits enclose the zero line). However, the increased CBU deviation between the theoretical model and the empirical study for the lowest frame rate of 30.0 Hz stands out in comparison to all other investigated frame rates.

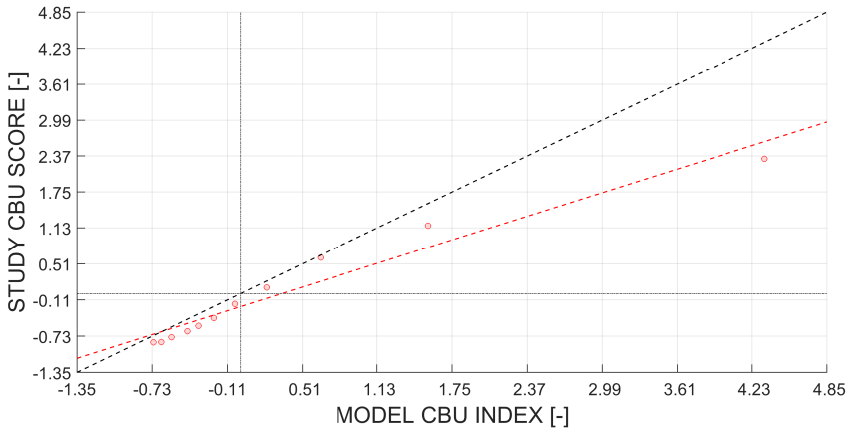

FIGURE 5.5: Model index CBU_{IDX^*} and study score CBU_{SCR} (both standardized) for PEM sequence with eye/content movement velocity of 36.0 deg/s, considering all frame rates investigated during COBUS1 (red circles represent CBU_{IDX^*}/CBU_{SCR} data points, red dashed line represents linear regression fitted to CBU data points, black dashed line represents angle bisector of xy-coordinate system, dash-dotted lines represent horizontal/vertical zero lines).

Finally, a scatter plot shows the relation between the model's CBU_{IDX^*} (x-axis) and the sample's average CBU_{SCR} (y-axis) for the investigated frame rates during COBUS1 without assigning the applied frame rates (see Figure 5.5). A linear regression (red dashed line) is fitted to the resulting CBU data points (red circles) with adequate fitting accuracy of $r^2 = .946$. The fitted regression shows a flatter slope ($B1 = 0.6559$) and a slight downward shift ($B2 = -0.2235$) in comparison to the bisecting line (black dashed line) that represents the ideal state of identical values for CBU_{IDX^*} and CBU_{SCR}. The flatter slope of the linear regression is caused by an increasing discrepancy between CBU_{SCR} and CBU_{IDX^*} for higher CBU effects.

5.5 Model Improvements

The theoretical model provides a solid foundation for predicting CBU perception. Its basic framework is the determination of the basal quantity of physical light stimulation hitting the retinal surface. Further steps of processing within the retinal layers up to the brain are also implemented (wavelength-dependent sensitivity of the human eye and temporal summation of light stimuli). However, the inclusion of supplementary steps of retinal and cognitive processing could improve the accuracy of the final output, approximating the actual CBU perception (see Section 3.8 for the complete list of proposed model add-ons). For example, it is widely known that the relationship between the intensity of a physical stimulus and its corresponding subjective perception is clearly non-linear (not integrated into the model so far). The Power law by S. S. Stevens (1957) addresses this circumstance (see Formula 5.3):

$$\psi = k \times \phi^{\beta^*} \tag{5.3}$$

Where ψ is the subjective magnitude of perception and ϕ is the physical magnitude of stimulation. The constant k is used as a scaling factor and depends on the unit of measurement. The exponent β^* of the power function describing the relation between stimulation and perception "serves as a kind of signature that may differ from one sensory continuum to another" (S. S. Stevens, 2017, p. 13).[6] In other words, for every sensory category, there is a specific β^* for the given surrounding conditions. Concerning the CBU model, there are two sensory categories that are of particular importance — the processing of brightness and visual area (see Section 3.7.2, model calculations are based on area and light intensity of stimulation). With regards to the perception of brightness, a dark-adapted eye has a corresponding β^* of 0.33 (S. S. Stevens, 1961), whereas a light-adapted eye shows a higher value of 0.44 (J. C. Stevens & Stevens, 1963). Lowering the duration of stimulus presentation also increases β^* close to 0.5 (J. C. Stevens & Hall, 1966). The exponent β^* for the perception of visual areas is determined around 0.7 (Kerst & Howard, 1978, averaged value for immediate and memory-based response).

Applying a psychophysical filter on basis of the acquired knowledge could attenuate the model's CBU_{IDX^*} for conditions that currently provoke overvalued CBU indices, exceeding actual subjective CBU perception (see Figure 5.3). For the moment, the filter will not be embedded in the model code; after running the code, only the model output is filtered. To modify the previous model output, a power function with β^* values ranging from 0.3 to 0.7 and a constant of $k = 1.0$ is applied (see Figure 5.6).[7] This has the effect of reducing, in particular, the highest model indices provoked by the lowest frame rates. The model output (pale red area) approximates the empirical output (pale blue area).

[6] S. S. Stevens originally used the symbol β as exponent of the power function. The symbol has been changed to β^* to avoid ambiguity within the thesis.

[7] The applied range for the exponent β^* is based on the mentioned research on the determination of representative power functions for the sensory categories of brightness and visual area. The constant k of the power function is set to 1.0 by default as the subsequent standardization process offsets its effect anyway.

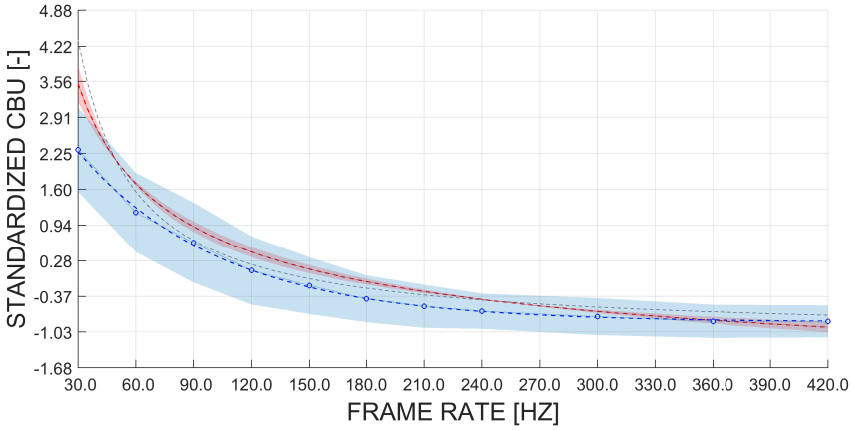

FIGURE 5.6: Model index CBU_{IDX^*} after applying a psychophysical filter and empirical study score CBU_{SCR} of COBUS1 (both standardized) in dependency of frame rate (30.0 to 420.0 Hz) for PEM sequence with eye/content movement velocity of 36.0 deg/s; red dashed graph represents CBU_{IDX^*} filtered with power function (see Formula 5.3, $k = 1.0$, $\beta^* = 0.5$), pale red area represents CBU_{IDX^*} filtered with power functions ($k = 1.0$, $\beta^* = 0.3$–0.7), gray dashed graph represents CBU_{IDX^*} without filtering, blue circles represent CBU_{SCR} (sample-averaged), blue dashed graph represents exponential function fitted to empirical data, pale blue area represents standard deviation of empirical data (linear interpolation between data points).

In addition, the approximation of the model calculations to the empirical data is visualized with a new box-and-whisker plot. The increased deviation between the sample's CBU_{SCR} and the model's CBU_{IDX^*} for the lowest frame rates (see Figure 5.4) is reduced after applying the psychophysical filter (see Figure 5.7). Implementing the psychophysical model upgrade also leads to a rotational shift of the previous linear regression within the scatter plot in Figure 5.5. The new regression line in Figure 5.8 shows a slightly higher fitting accuracy of $r^2 = .987$, a steeper slope ($B1 = 0.7852$), and a comparable y-intercept ($B2 = -0.2413$). This indicates that the filtered model results are approximating the empirical data, hence, approaching the target of a perfectly representative model output (represented by the plotted bisecting line).

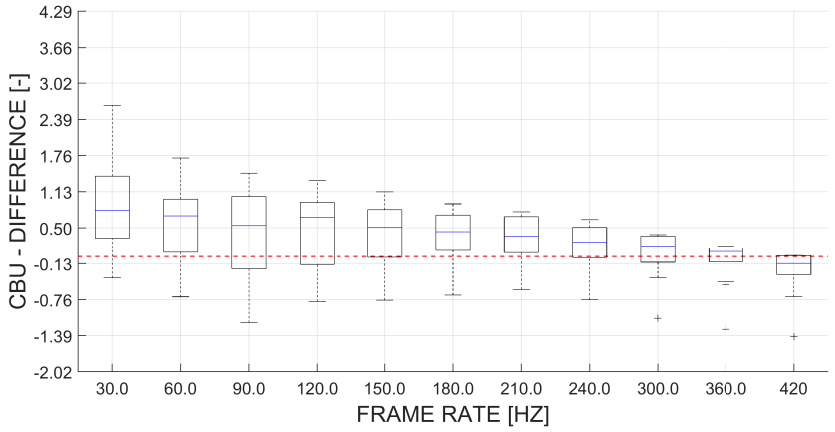

FIGURE 5.7: Differences between filtered model index CBU_{IDX^*} (see Formula 5.3, $k = 1.0$, $\beta^* = 0.3$) and study score CBU_{SCR} (both standardized, difference = index - score) for PEM sequence with eye/content movement velocity of 36.0 deg/s, consideration of all frame rates investigated during the execution of COBUS1 (elements of the box-and-whisker plot: lower/upper whisker represents minimum/maximum value of the data set with outliers excluded, box represents interquartile range, blue solid line represents median, black cross represents outliers; red dashed line represents zero CBU difference).

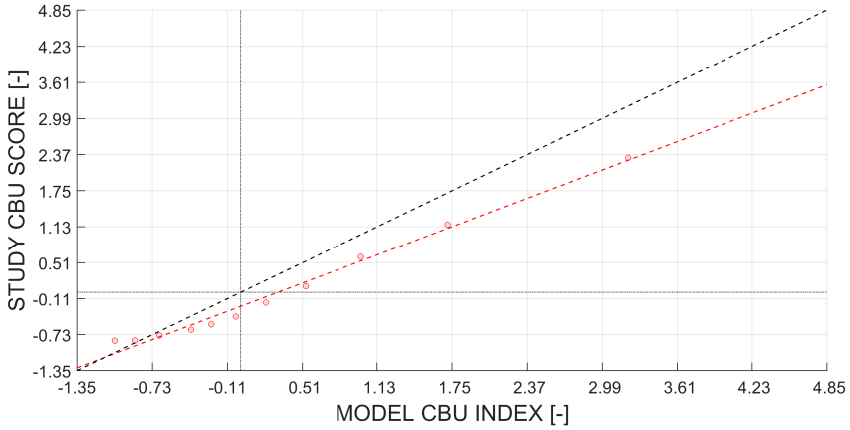

FIGURE 5.8: Filtered model index CBU_{IDX^*} (see Formula 5.3, $k = 1.0$, $\beta^* = 0.3$) and study score CBU_{SCR} (both standardized) for PEM sequence with eye/content movement velocity of 36.0 deg/s, considering all frame rates investigated during COBUS1 (red circles represent CBU_{IDX^*}/CBU_{SCR} data points, red dashed line represents linear regression fitted to CBU data points, black dashed line represents angle bisector of xy-coordinate system, dash-dotted lines represent horizontal/vertical zero lines).

As the positive effect of the comprehensive filtering of the model output could be confirmed, an individual filtering of brightness and visual area within the model code promises to bring further benefits. This adjustment would take into account that the previous model index calculation overestimates the weight of light intensity stimulation in comparison to the weight of the stimulated retinal area. By embedding two separate power functions as specific filters for the simulation of intensity and area within the model, this imbalance can be counteracted (lower β^* values for intensity filter than for area filter). The proposed modification would enhance CBU_{IDX^*} calculations, especially in PH2.

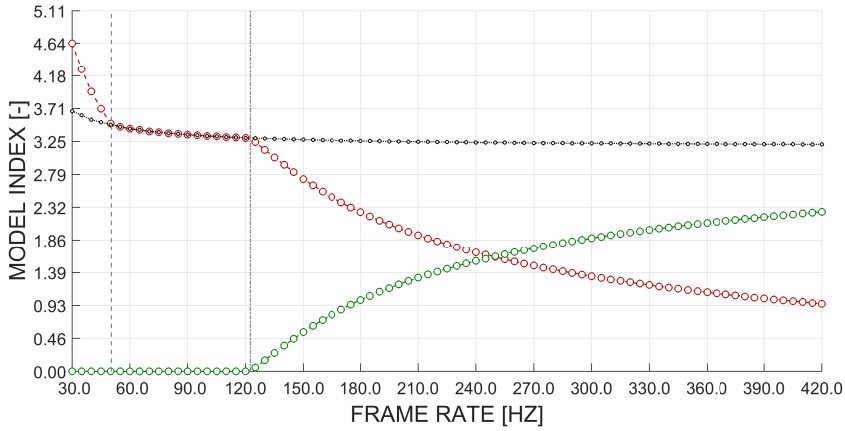

FIGURE 5.9: Model indices CBU_{IDX^*} (red graph), $NON\text{-}CBU_{IDX^*}$ (green), and REF_{IDX^*} (black) in dependency of frame rate (30.0 to 420.0 Hz, 5.0 Hz steps) for PEM sequence with increased eye/content movement velocity of 108.0 deg/s and reduced CBU-provoking stimulus width of 0.5° (other input parameters unchanged, see Table 5.1), calculated/plotted with MATLAB loop function (gray dash-dotted vertical line is PH1/PH2 transition, gray dashed vertical line is PH2/PH3 transition).

Unfortunately, the previously applied loop conditions in Chapter 5 lead to model indices that only refer to CBU effects of PH1, as illustrated in Figure 5.1. Therefore, loop conditions are changed to include CBU effects of PH2. The new conditions represent a PEM sequence with an increased eye/content movement velocity of 108.0 deg/s and a reduced CBU-provoking stimulus width of 0.5° (equals 10 px, all other input parameters remain unchanged, see Table 5.1). The altered model input parameters lead to a provocation of CBU

effects from PH1 to PH3 along the tested frame rate range as illustrated in Figure 5.9. The phase transition thresholds are illustrated by gray vertical lines. The CBU phases are arranged from left to right as follows: PH3 – PH2 – PH1. Apparently, the model's CBU_{IDX^*} increases only slightly while running through PH2 (by decreasing the frame rates). The attenuated index gain in PH2 results from a significant expansion of the color-distorted retinal area (underestimated by the model) but a stable level of CBU-related light intensity stimulation (overestimated by the model). It can be assumed that the flat PH2 course of the CBU_{IDX^*} graph in Figure 5.9 does not represent the perceived CBU increase by a viewer. The model's corresponding color maps (PH2) for the frame rates of 60.0, 90.0, and 120.0 Hz in Figure 5.10 support this assumption, as the three color maps are clearly distinguishable. By adjusting the weighting of light intensity and area of retinal stimulation, the problem of non-representative CBU indices in PH2 can be resolved.

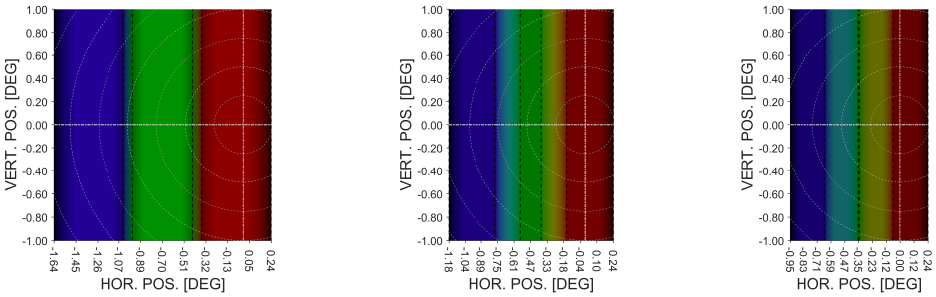

FIGURE 5.10: Color maps for PEM sequence with increased eye/content movement velocity of 108.0 deg/s and reduced CBU-provoking stimulus width of 0.5° (other input parameters unchanged, see Table 5.1), considering frame rates of 60.0 (left graphic), 90.0 (middle), and 120.0 Hz (right). Illustration of mixed colors at retinal level after temporal summation of all subframes within the FCC, calculated/plotted with MATLAB model function (dash-dotted gray lines represent horizontal/vertical retinal center with fovea centralis as point of intersection, dashed gray circles illustrate retinal eccentricity steps of 0.25°, dashed black lines represent color zone borders).

Other add-ons (see Section 3.8) could also enhance the model's accuracy. Three aspects in particular could have a strong impact. First, include detailed information on the color characteristics of the CBU-provoking stimulus in the process of model index calculation. This would go beyond simply distinguishing color-unbiased and color-distorted zones. Second, consider the contrast ratio between CBU-provoking stimulus and its background as a major factor during the genesis of CBU. Third, implement code that covers the variability of visual perception by considering eccentricity-dependent retinal sensitivity as well as perceptual differences during saccades and pursuits. These recommended model upgrades are likely to improve the model output substantially.

Chapter 6

Conclusion

Using a mixed design with empirical experiments and theoretical model development, this thesis has shed light on previously unconsidered but essential research questions about CBU perception during FSC presentation, expanding the current field of research. These research findings are not only an academic exercise but provide crucial information for practical application. In combination with other research, the research findings of this work can help provide a condensed but substantive guideline for future FSC-based display technology. The guideline should address minimum hardware requirements (e.g., setup-dependent frame rate standards for CBU reduction), content creation recommendations (e.g., content characteristic-dependent use of specific display areas), and proposals for the implementation of CBU compensation techniques (e.g., transferability and effectiveness in dependency of display type and field of application). Such a guideline would make previous knowledge about CBU widely available and provide the tools to reduce CBU effects to the greatest possible extent or even eliminate them.

While this thesis provides essential information for a comprehensive guideline, more CBU research is required to fill the existing knowledge gaps. For instance, a follow-up project should investigate the effect of stimulus and background luminance. To this end, it would be useful to separately vary (1) the luminance level of the potentially CBU-provoking stimulus, (2) the background luminance level, and (3) the contrast ratio between stimulus and background to examine their exclusive impact on CBU perception. With respect to the CBU stimulus, an integration of luminance levels below $15\,cd/m^2$ (while background luminance is stable) seems to be reasonable, since a faster decline of CBU perception is expected in this low-level area than for luminance levels above this threshold (see COBUS1 findings). Furthermore, a stable stimulus luminance during background luminance increase promises a faster CBU reduction compared to stimulus luminance reduction with stable background luminance because the contrast ratio drops faster. Finally, by smartly selecting the ranges of stimulus and background luminance, the influence of variable combinations of balanced stimulus and background luminance on the perceived CBU effect can be investigated while keeping the contrast ratio stable. The collected study data on the effect of stimulus and background luminance on CBU perception can be used to feed the theoretical CBU model and thus expand it with new important features (see corresponding proposal in Section 5.5).

Research consolidation, i.e., comparing and combining research results from multiple scientific sources, is tremendously important, particularly for the field of CBU perception. In the following, a cursory glance at the literature is provided, identifying how the findings of this research could complement, add-on, or advance other research on methods for CBU compensation.

So far, the most promising CBU compensation techniques such as Local Primary Desaturation (LPD) can only be applied to digital display systems that allow a desaturation of the emitted light within a subframe cycle. Such a desaturation can only be achieved by mixing the primary colors of the display system's light sources within the subframe cycle. The

application of LPD is possible for specific FSC-LCDs, but unfortunately not for all display systems that are based on the FSC principle. For example, the technical design of the H3D display system of SeeReal Technologies (mentioned in Chapter 1) prevents the implementation of such compensation techniques. Therefore, methods for CBU compensation that can be used for such display systems are limited to a few options, such as increasing the frame rate or applying Motion Interpolation (MI). However, even the available methods are only effective to a limited extent due to technical or methodological restrictions. Therefore, it is necessary to improve previous approaches or develop other methods to provide effective tools for CBU reduction for all FSC-based technologies.

COBUS2 findings could be used in two ways to compensate CBU. First, specific content creation guidelines under consideration of stimulus position and size can be defined. Such guidelines could be used to avoid the creation of content with a high CBU potential. However, such restrictions at this early stage of content creation are not applicable if there is no tolerance to modify the content without compromising the central purpose behind the content presented. Therefore, while this approach — which is based solely on own research — can be helpful, it is limited in scope. Second, a more selective application of externally developed CBU compensation techniques such as the previously mentioned MI can be applied by considering only objects that have a high potential to annoy a defined share of viewers. Relevant objects can be predicted on basis of the object's size and position within the user's field of view based on the data set of COBUS2. Different MI zones that are limited to a certain central part of the full presentation area could be determined for specific object sizes. This would allow the application of MI for a limited number of potentially CBU-provoking objects within the MI zones. All other objects outside the MI zone would not be considered because they do not provoke annoying CBU effects. Hence, the computational effort for MI implementation would be decreased, consequently reducing the time required for MI calculation processes. The feasibility of a compensation technique such as MI would be increased. This approach — exemplary for a fruitful combination of own and external research results — derives its value from potentially wide-ranging practical applicability across different display types.

Another possible approach is based on the so-called Foveated Rendering Technique (FRT), which is actually used for HMD applications. FRT reduces computational effort by decreasing the displayed image quality within the viewer's peripheral field of view, which corresponds to the retinal areas that are not able to process higher display resolutions anyway (Kaplanyan et al., 2019). Based on the dependence of CBU sensitivity on retinal eccentricity, this general FRT concept can be transferred to a CBU compensation method. The fovea centralis and its adjacent structures are extremely sensitive to the perception of light intensity and color, and consequently also to CBU perception (see COBUS2 results). By changing the characteristics of light stimulation within the foveal area, CBU effects can be reduced significantly. For the most effective application, it is advised to focus on reducing the contrast between high-potential CBU objects and their background by setting a gradual luminance transition rather than just considering alterations of the CBU object's characteristics alone (in this context, the earlier proposed follow-up project on luminance effects promises to deliver directly transferable results). This approach is based on the idea on which the FRT is built. However, the FRT principle would be implemented with reverse logic, as image quality is reduced by blurred edges in the retinal area with the highest resolution and the most sensitive light and color perception. Under most conditions, such a qualitative degradation of a scene would be classified as insufficient by the viewer. However, the conditions under which the viewer would perceive this blurring most strongly are static conditions such as the fixation of a static object in a scene. The beauty of this solution is that no compensation is needed for such conditions, as no CBU effect is caused (CAT0/CAT1).

A compensation is only required the moment the viewer executes saccades (CAT2) or pursuits (CAT3). Fortunately, the human eye's sensitivity to detect blurred edges is significantly reduced during eye movements — not least due to perceptual changes, particularly during saccades (see explanations on saccadic suppression in Section 2.3.2). This circumstance is advantageous because intensified edge blurring must be performed, especially for saccades, since strong CBU effects are expected without compensation. These combined perceptual effects could enable the desired CBU reduction based on an objective image quality reduction which might not be perceived by the viewer at all. Existing knowledge in the field of FRT can be adapted to speed-up the development of this derived method of Foveated Blurring. However, high technical requirements such as a real-time content adaptation based on gaze-tracking data have to be met. Such processes lead to high computational effort which has to be carried out in a very short period of time. Therefore, further technological leaps are essential.

In the context of FRT implementation, Lu et al. (2020) proposed another ambitious approach of blending different display regions with different frame rates in the same frame to improve the perceptual experience in the focused region. Again, this general concept of displaying only regions of interest with higher frame rates can be adapted and used in the course of CBU compensation. Findings on frame rate-dependent CBU reduction (COBUS1) and retinal position-dependent CBU sensitivity (COBUS2) form the basis for the concept transfer, varying applied frame rates in dependency of variable CBU sensitivity for different retinal eccentricities. For instance, for a display region containing an object with high CBU potential that passes through the viewer's fovea during eye movement, the applied frame rate would need to be increased to provide targeted protection from CBU perception. At the same time, lower frame rates would be acceptable for the surrounding display areas, as the CBU potential is lower in these areas. Of course, this approach does not exempt from the need to generally increase achievable frame rates, which are currently subject to hardware-related limitations. However, as soon as suitably high frame rates are available for various display types, this approach can help reduce the computational effort to accelerate real-time processes that must be integrated for the application of CBU compensation techniques (see previous proposals).

A new approach for CBU compensation that has not yet been considered is based on a targeted variation of every subframe's light emission behavior over time. The basic idea for this approach is derived from the Overdrive Technology used to reduce annoying motion artifacts on conventional LCDs (no FSC presentation).[1] Although the CBU compensation method to be introduced makes use of the same technical approach, it clearly differs from the Overdrive Technology in terms of its specific application and the resulting effect. The underlying idea is to change the light emission profile over time for all individual subframes implemented within one frame cycle, especially during the time periods that include the initial increase of the luminance level towards maximum output and the subsequent decrease of the luminance level towards zero output. More specifically, the starting points of luminance level increase/decrease, the slops of luminance incline/decline as well as the

[1]Motion artifacts on conventional LCDs are characterized by blurred edges of moving objects which occur while the viewer's eyes trace these objects. Such artifacts are caused by (1) a pixel cell's slow response time for the transition from off- to on-state and vice versa and (2) the general hold-type character of an LCD, leading to continuous light emission during a frame cycle. The motion blurring at the object's edges results from different outcomes of the integration processes (emitted light over time) across the stimulated retinal area due to eye movements in combination with the LCD's light emission behavior over time. Motion artifacts that are caused by (1) the slow response times of the LC panel can be avoided/reduced by overdriving the initial pixel voltage which raises the gain of the light intensity function towards the desired luminance level. With higher initial pixel driving voltage, the target value is reached faster and the off/on-transition of a pixel cell has a sharper temporal edge. Motion artifacts that are caused by (2) the LCD's continuous light emission behavior can be reduced by applying a scanning backlight that emulates an impulse-type display (den Boer, 2005).

maximum luminance level would be customized under consideration of the present conditions (e.g., viewer's eye movement velocity or frame rate of the display unit). Assuming an implementation of three subframes within one frame cycle, the following procedure would be applied: The temporal starting point of the first subframe's light emission increase zone is shifted backwards. An accelerated increase towards a higher maximum luminance level compensates for the reduced time of light emission. In other words: The first subframe's light emission phase is shifted to the second half of its previous on-time. For the second subframe, the increase zone is also shifted backwards. Additionally, the decrease zone is shifted forward leading to a temporal compression of the second subframe's light emission phase into the middle of the previous on-time. For the third subframe, the phase of light emission is shifted into the first half of its previous on-time by initially overdriving towards a higher light output. Consequently, the third subframe's decrease of light emission starts earlier. By temporally shifting and compressing the light emission phases of the three subframes, their zones of highest light emission move closer together. This has no negative effect on the conditions in which no eye movements and consequently no CBU occur (CAT0/CAT1), since the result of the temporal summation of light intensity by the eye is not changed, i.e., the viewer's perception of the displayed content is not changed. Under conditions requiring CBU compensation, the altered light emission behavior of the implemented subframe set hypothetically results in reduced CBU zones at the leading and trailing edges of the retinal stimulation, as the light emission for these zones is temporally shifted towards the middle of the frame cycle. Although the effectiveness of this approach diminishes under worst-case conditions (e.g., triggering fast saccades), this proposal could be an element of situation-related CBU reduction that is particularly useful during pursuits that provoke reduced CBU effects.

Evidently, further research is required to pursue the proposed follow-up projects. It is worthwhile to push ahead with research in this area, because the FSC principle has advantages that will become increasingly important in the future. For instance, the potentially ultra-low power consumption of FSC-LCDs (Y.-P. Huang et al., 2011) is a major advantage that not only saves costs but also helps to reduce energy consumption — an essential feature given the current climate crisis. Until now, CBU is the main pitfall of the FSC technology. High market shares of different FSC-based display types such as trendsetting low-power HMD/HUD applications (Abeeluck et al., 2018) for private or professional use are only feasible if CBU can be eliminated to ensure high consumer acceptance.

Appendix A

Device Specification

A.1 Testing of Hardware

A.1.1 Spectroradiometer

The light measurements on the DLP projector were executed with a spectroradiometer (Specbos 1211). The usage of the measurement device and its technical features are described in the operating instructions and the data sheet provided by the manufacturer (JETI Technische Instrumente GmbH, 2021a, 2021b).

A.1.2 Oscilloscope

The DLP projector's timing measurements were executed with a four-channel digital storage oscilloscope (TPS2024) and a switchable gain detector (PDA36A2). Operating information and technical specifications of the oscilloscope are described in the user's manual (Tektronix, 2004). The detector is specified in the corresponding user's guide (Thorlabs, 2020).

A.1.3 Luxmeter

The illumination in the examination room of the COBUS series was measured with a luxmeter (Mini-Lux). Device information can be found in the user's guide (MX-Electronic, n.d.).

A.2 Pre-Examination

The application of a digital case report form (e-CRF, self-developed) allowed digital data collection during the COBUS series. The e-CRF is based on a xlsm-file and contains the pre-examination data (date/time of examination, Participant ID, demographics and optical correction of the participant, results of inclusion/exclusion and visual performance testing, etc.) and the questionnaire for participant characterization.

A.2.1 Optical Correction

The dioptric power of a participant's spectacles (habitual correction) was either requested or determined with lensmeter (VL3000, Visionix). In case of using contact lenses, the refractive power was inquired (and validated via blister/packing in the best case). Additionally, the type of habitual correction was noted (spectacles or contact lenses).

The objective refraction (distance) was executed with autorefractor (i.Profiler, Carl Zeiss Vision GmbH) under photopic room illumination (ceiling lights on, illuminance level described in Section 4.2.7). The refraction was determined with a device-internal adjustment of an analyze aperture of 3.0 mm and a corneal vertex distance of 12.0 mm. The measurement was done while the participant did not use any optical correction.

The participant's visual system was tested for sighting dominance (Coren & Kaplan, 1973). Testing sighting dominance is recommended for fixation tasks and/or monocular tasks. Both was the case during COBUS2 (no execution during COBUS1). Therefore, a Hole-in-Card Test was used to determine the participant's sighting dominant eye. The test was executed while the participant looked at a target in a near viewing distance of 0.29 m (similar to the viewing distance during the main examination of COBUS2).

A.2.2 Inclusion/Exclusion

The maximum amplitude of accommodation was tested with the Push-Up/Push-Down Method to exclude participants with a reduced amplitude (see Section 4.2.3). Every method was executed once — first Push-Up, then Push-Down. The measurement was done using a digital application (Smart Optometry, Version 3.4.full) on a mobile phone with adequate technical features (Samsung Galaxy S7, 5.1 in., 1440x2560 px, 577 ppi). The Landolt C was used for testing (row of five optotypes; optotype size corresponded to a visual acuity that was two logarithmic steps below the maximum visual acuity in near distance). The participant passed the test when the defined threshold for the accommodative amplitude was not undershot (both measurements were averaged). The measurements of the accommodative amplitude were executed under photopic room illumination (ceiling lights on).

The screening of visual field losses was done with the Amsler Grid. The test was presented as a self-made digital version via tablet (T100T, ASUSTeK Computer Inc.). The classic black grid on white background was created via PPT file, guaranteeing a test area similar to the field of view that was stimulated during the main study examination of the COBUS series (COBUS1: $\pm 25.0°$, COBUS2: $\pm 50.0°$). The line distance of approx. 1.0° was adapted from the classic Amsler Grid. The testing of the visual field was done under photopic room illumination (ceiling lights on).

The participant's ocular motility was tested to rule out dysfunctions that could affect the execution of saccades and pursuits (required during main study examination). The motility tests were embedded within PPT files (self-developed) and presented with a tablet (T100T, ASUSTeK Computer Inc.). The test procedure included movement patterns that were similar to the movement paths during the main study examination of the COBUS series.[1] The participant's ocular motility was assessed under binocular conditions during COBUS1 and COBUS2 (critical for the testing procedure). The tests were executed under photopic room illumination (ceiling lights on).

The existence of a heterophoria/tropia was tested with the Cover-Uncover-Test using a hand-held eye occluder. In case of a confirmed heterophoria/tropia, the magnitude of the misalignment was subsequently determined with the Maddox Rod Test (maddox rod, compensation prism, point light source). The test distance was derived from the applied viewing distance (participant to screen) during the main experimental setup. The Cover-Uncover-Test was executed under photopic room illumination (ceiling lights on). The room light was dimmed during Maddox Rod Test in case of a reduced visibility of the light line. Heterophoria/tropia testing was only executed during COBUS1 (no execution during COBUS2).

A.2.3 Visual Performance

Visual acuity in [logMAR] was determined with the Freiburger Visual Acuity and Contrast Test (Version 3.9.9a), abbreviated FrACT (Bach, 1996). FrACT was presented on a smartphone with a high resolution (Samsung Galaxy S7, 5.1 in., 1440x2560 px, 577 ppi) to meet

[1] For example, the ocular motility testing during COBUS1 included saccades with amplitudes of 3.6, 9.0, 14.3, 21.3, and 28.2° and pursuits with velocities of 18.0, 36.0, and 54.0 deg/s (step-ramp stimulation). All movements were tested in left-to-right direction and vice versa.

the standards for visual acuity testing in a shortened test distance. The test distance was similar to the viewing distance (participant to screen) during the main experimental setup of COBUS1 (0.58 m) and COBUS2 (0.29 m). The distance was kept stable via head/chin rest (see Figure D.1). The display's native resolution allowed to investigate a sufficient visual acuity range with an upper limit of 2.57 (decimal visual acuity) for the applied test distance during COBUS1. The test results were used for exclusion and correlation testing. The upper visual acuity limit of 1.28 (decimal) for COBUS2 was sufficient as only the exclusion criterion for visual acuity of the participants was checked (visual acuity of 0.30 logMAR equals decimal visual acuity of 0.50). No further statistical testing was performed.

During visual acuity testing, the Landolt C was used in eight different positions (up, down, left, right, top-right, bottom-right, top-left, bottom-left). For every trial, a single Landolt C was presented on the smartphone. The participant responded via numeric keypad. Correct and false answers were accompanied with an acoustic signal (no visual feedback), as these signals can stimulate participants' motivation and compliance. Before starting the visual acuity test, the test procedure was explained to the participant and a test trial was carried out to familiarize the participant with the task.

The visual acuity threshold was finally determined by presenting 24 successive trials (every 6th trial was a trial above threshold to increase motivation). An ascending threshold strategy was applied as recommended (Bach, 2018, typical for chart testing, DIN/ISO corrected threshold definition). The black Landolt C was presented on white background. The luminance of the background was set to $200.51 \pm 0.86\,\mathrm{cd/m^2}$ ($MN \pm SD$, measured with Specbos 1211, JETI Technische Instrumente GmbH) as a level of $200\,\mathrm{cd/m^2}$ is recommended for visual acuity testing on electronic devices (International Organization for Standardization [ISO], 2020). Chromaticity coordinates of the background were $x = 0.3067 \pm 0.0006$ and $y = 0.3276 \pm 0.0004$ (CIE 1931, 2.0°, measured with Specbos 1211). The contrast ratio was set to 1.0 as the standard for visual acuity testing. The visual acuity testing was done under scotopic lighting conditions (room light was deactivated).

Contrast sensitivity in [logCS] was also tested with FrACT.[2] The tests were presented on the ColorEdge CG246, a professional monitor from the EIZO Corporation (2013, user's manual). The monitor met the standards for contrast sensitivity testing in a shortened test distance (resolution, contrast ratio, luminance levels). The test distance was adapted to the viewing distance (participant to screen) during the main experimental setup of COBUS1 (0.58 m) and COBUS2 (0.29 m). The distance was kept stable via head/chin rest (see Figure D.1).

During contrast sensitivity testing, the Landolt C was presented in eight different positions (up, down, left, right, top-right, bottom-right, top-left, bottom-left).[3] For every trial, a single Landolt C was presented on the monitor. The participant responded via numeric keypad. Just as during visual acuity testing, correct and false answers were accompanied with an acoustic signal (no visual feedback). Before starting the contrast sensitivity testing, the test procedure was explained to the participant and a test trial was carried out to familiarize the participant with the task.

The contrast sensitivity threshold was finally determined by presenting 24 successive trials (every 6th trial was a trial above threshold to increase motivation). The Landolt C and its background were presented with variable contrast ratios. An ascending threshold strategy

[2]The definition of visual acuity in [logMAR] as well as contrast sensitivity in [logCS] assured an interval level of the measured values which allowed an extended use of statistical methods such as parametric testing (Bach et al., 2017, pp. 345–346).

[3]Sinus gratings with their bandpass characteristics have some advantages. However, the applied monitor could not display the pattern in an appropriate manner. Hence, the Landolt C with its lowpass characteristics was applied (connecting the contrast sensitivity and visual acuity testings as the same optotype was used). Information on the application of optotypes (lowpass) and sinus gratings (bandpass) during contrast sensitivity testing are provided by Bach et al. (2008).

was applied as recommended (typical for chart testing, DIN/ISO corrected threshold definition). During COBUS1, the contrast sensitivity threshold was determined for two different sizes of the Landolt C. One version of the Landolt C had a diameter of 10.0′, corresponding to a visual acuity level of 0.30 logMAR which equals a decimal visual acuity of 0.50 (upper test limit at 0.56). The second size was 50.0′, analog to a visual acuity of 1.0 logMAR which equals a decimal visual acuity of 0.10. Both optotype sizes were included to consider the influence of optotype size on contrast sensitivity as described by the contrast sensitivity curve (Bach et al., 2008). With an optotype size of 50.0′, the plateau of the contrast sensitivity curve was represented. The optotype size of 10.0′ incorporated the curve's area of decline towards the maximum visual acuity (highest contrast, lowest optotype size). The test results during COBUS1 were used for exclusion and correlation testing. During the pre-testing of COBUS2, only one size was applied for the Landolt C. The diameter of the Landolt C was set to 50.0′, analogous to a visual acuity of 1.0 logMAR which equals a decimal visual acuity of 0.10 (upper test limit at 0.28). The optotype size was determined for an appropriate exclusion criterion testing (no further statistical testing).

For the monitor calibration of the contrast sensitivity testing, the background luminance was set to a value of $200.07 \pm 0.49\,\mathrm{cd/m^2}$ ($MN \pm SD$) while a Landolt C for visual acuity testing was displayed to establish comparability (measured with Specbos 1211). The chromaticity coordinates of the background were $x = 0.3143 \pm 0.0001$ and $y = 0.3240 \pm 0.0003$ (CIE 1931, 2.0°, measured with Specbos 1211). The luminance linearization for the applied monitor was done using the FrACT-integrated tool (gamma value determination). The contrast sensitivity testing was executed under scotopic lighting conditions (room light was deactivated).

Color vision was quantitatively tested with HMC Anomaloscope (OCULUS Optikgeräte GmbH) under the standards of use as defined in the user guidelines (Krastel, 2006). The anomaloscope was applied during COBUS1 (no execution during COBUS2). During the testing, the participant looked through the anomaloscope's ocular using the investigated eye. The other eye was covered with an eye patch (photopic room illumination). Testing was done for the Rayleigh equation (red/green anomaly), whereas the Moreland equation was not applied (blue-yellow anomaly). The test procedure was executed in manual mode under determination of the absolute adjustment width (neutral stimulation by showing a white adaptation field every 3.0 s). The participant adjusted hue value (x-axis in Pitt Diagram) and light intensity (y-axis) by him-/herself to generate identical semi-circles. After the participant finished two trials with different starting points, the whole procedure was repeated once more (four repetitions in total).[4] For every repetition, hue value and light intensity as well as the anomaly quotient were determined and documented. However, the anomaly quotient as the classic color vision measure was not used in further statistical analysis as it only considers hue values but not light intensity values. Addressing this shortcoming, the Euclidean distance between the ideal point of adjustment (40.0/15.0) and the actually adjusted point by the participant was calculated as an alternative color vision measure (applied during correlation testing between color vision and CBU perception).

Completing the anomaloscope test outside the normal range (colored area in Pitt Diagram), a commonly used method to screen color vision deficiencies — the Velhagen-Stilling Color Plates — was additionally executed to exclude red-green and blue-yellow color vision deficiencies (see exclusion criteria). The color plates were used to screen the sample under monocular conditions referring to the standards of use (e.g., viewing distance, order of

[4] The starting point of the first trial was set to 0.0/19.1 (hue/light), whereas the second trial started at 73.0/1.8 (no standard defined to the author's best knowledge). The starting points assured the crossing of areas that cannot be distinguished with color vision deficiency to reach the ideal point of adjustment (40.0/15.0) in the Pitt Diagram.

plate presentation). The Velhagen-Stilling Color Plates were used under exclusion of natural lighting conditions (photopic room illumination via ceiling lights).

A.2.4 Questionnaire

A self-developed questionnaire was applied to characterize the participant during COBUS1 (see Figure A.1). Five different items were requested via a bipolar 5-point Likert scale. The items refer to general long-term personality traits (Item 1 to 2) and the current short-term state of the participant (Item 3 to 5). The poles of the applied item scales are semantically described by bipolar antagonistic word pairs (e.g., *uncritical – critical*).

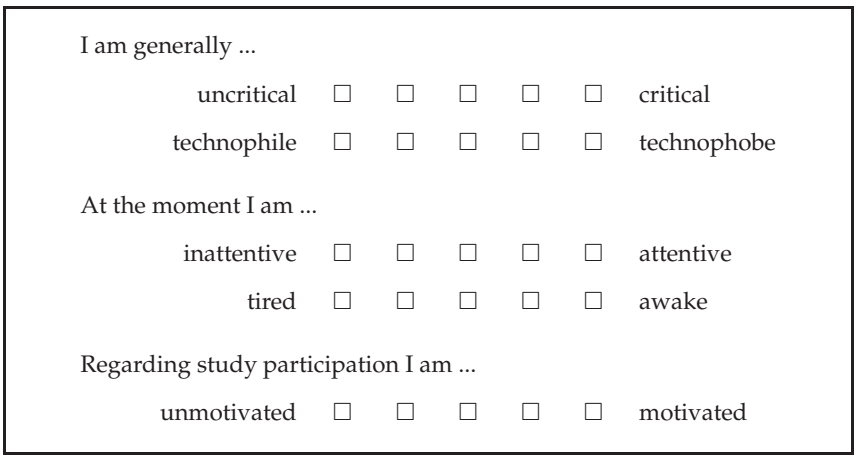

FIGURE A.1: Questionnaire with five different items requesting general long-term personality traits (Item 1 to 2) and the current short-term state of the participant (Item 3 to 5) during COBUS1.

After a brief introduction, the participant chose a box for every item. For data analysis, the ticked box was assigned an integer value between 1 (e.g., *uncritical*) and 5 (e.g., *critical*).

A.3 Main Examination

A.3.1 DLP Projector

The LightCrafter 4500 (Texas Instruments) was applied to display the content during the main examination phase of the COBUS series. The DLP projector is a 100% off-axis system.[5] Its internal structure is illustrated in Figure D.4. The key technical specifications of the projector are listed below:

— 0.45 in. diagonal micromirror array

— native resolution of 912×1140 px

— 7.6 µm micromirror pitch

— maximum bandwidth of 5.8 Gbps

— binary pattern rates up to 4 kHz

The micromirrors of the projector's DMD are arranged as a diagonal array, i.e., the projected pixel structure is saw-toothed (see Figure A.2). The diamond pixel geometry is rotated by 45° in comparison to a conventional pixel arrangement with horizontal and vertical edges.

[5]The optical axis of the projector is (roughly) aligned with the lower edge of the projection area. The projection is directed upwards when the projector is positioned with its metal base on the ground.

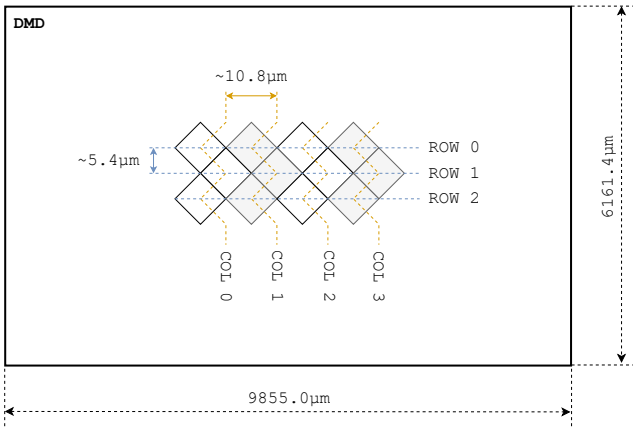

FIGURE A.2: Diamond array structure of DLP projector's digital micromirror device (DMD).

Table A.1 specifies the projection parameters for four projection distances. The listed distance of 650 mm refers to the COBUS series.

TABLE A.1: Projection parameters in dependency of different projection distances.

	Projection Distance in [mm]			
	500	**650**	**1000**	**2000**
Diagonal Size in [in]	16.70	21.39	32.80	65.00
Diagonal Size in [mm]	424.18	543.22	833.12	1651.00
Horizontal Size in [mm]	359.70	460.61	706.48	1400.05
Vertical Size in [mm]	224.81	287.97	441.55	875.03
Horizontal Half Angle in [deg]	19.78	19.51	19.46	19.29
Vertical Half Angle in [deg]	12.67	12.49	12.45	12.34
Aspect Ratio	1.60			
Magnification [a]	36.50	46.74	71.69	142.06
Pixel Size in [mm] [b]	0.3944	0.5051	0.7747	1.5351
Pixel Size in [deg] [c]	0.0390	0.0500	0.0767	0.1520

[a] Calculated by dividing horizontal width of projection area by horizontal width of DMD.
[b] Calculated by multiplying DMD pixel size with magnification.
[c] Calculated for distance of 578.7495 mm between first nodal point of viewer's eyes and projection screen level.

The stated technical specifications of the DLP projector were either taken from the user's guide of Texas Instruments (TI, 2017) or calculated using the given technical data. Further information on the projector and its periphery is provided in the DLP data sheet (TI, 2021) and the controller data sheet (TI, 2019).

A.3.2 CBU Scenario Player

The CBU Scenario Player is the software that triggers the DLP projector's output. The software was developed with the programming language C++, using Direct3D (Version 11, Microsoft Corp.) for graphics generation and output. The projector is basically controlled by a customized version of the official software for the LightCrafter 4500 (Texas Instruments). This software was modified to receive commands from the CBU Scenario Player to check/update projector settings. At first, several projector and display output settings (e.g., frame rate) need to be set by the software. In a second step, the software accesses prepared scenarios with defined content (e.g., white CBU-provoking stimulus on dark background) to be presented via projector for the defined settings. The defined scenarios are finally viewed by the participant who then evaluates his/her CBU perception for every scenario with a

CBU score and an annoyance estimation. For every participant, the evaluated data set from a multitude of scenarios is written into an evaluation protocol for documentation. The protocol can be exported for further processing.

A.3.3 Projection Screen

During the COBUS series, the front projection screen Home Cinema Frame (Celexon Europe GmbH) was used in combination with the mentioned projector. The screen has a gain of 1.2 and is classified as Type D. The selection of screen and projector enabled a high reflective homogeneity over the entire projection area (see preliminary test results in Appendix B.1).

A.3.4 Eye-Tracking System

The Eyegaze Edge 600 Series (LC Technologies) allowed the examiner to visually monitor the participant's eye movements during the main study execution of the COBUS series. Sequences with apparently erroneous eye movements were identified and repeated. The manual of the Eyegaze (n.d.) provides all relevant information. The eye-tracking system is controlled with the analysis software Nyan 2.0 (Interactive Minds).

Appendix B

Hardware Testing

B.1 Light Measurement

In preparation for the COBUS series, various light measurements were carried out. The light measurements refer to the COBUS setup with the DLP projector and the projection screen specified in Appendix A.3. The measurements were executed with a spectroradiometer (see Appendix A.1.1) under scotopic lighting conditions (darkened room).

B.1.1 Input and Output

The input current applied to the projector's LEDs can be adjusted to alter their light output. The LED current is regulated with the current number (CN) via graphical user interface of the projector's control software. Generally, the current number can be set within a range from 0 to 255. For a zeroed current number, no current is applied and no light is emitted. A maximum LED current ($CN = 255$) results in a high light output. The linear relation between the determined current number and the applied LED current I in [A] is described by the Equations B.1 to B.3 from TI (2017, p. 25).

$$I_R = 0.0175 \times CN_R + 0.4495 \tag{B.1}$$

$$I_G = 0.0181 \times CN_G + 0.3587 \tag{B.2}$$

$$I_B = 0.0160 \times CN_B + 0.1529 \tag{B.3}$$

To prevent damage to the projector, some technical limitations must be respected. The projector has a "thermal limit resulting in total simultaneous red, green, and blue LED currents less than 4.3 A for continuous LED operation" (TI, 2017, p. 25). During the COBUS series, the projector's LEDs were activated time-sequentially, i.e., only one LED was switched on at any time. Hence, the threshold value of 4.3 A is valid for every single LED. Using the Equations B.1 to B.3, the maximum current number corresponding to the current threshold of 4.3 A can be calculated. For the red and the green LED, the current numbers of $CN_R = 220.02 \approx 220$ and $CN_G = 217.75 \approx 217$ should never be overshot to avoid damage to the projector. The threshold value of the blue LED is $CN_B = 259.19 \approx 259$. The calculated value is above the maximum adjustable current number. Therefore, the full current number range can be applied.

In a preliminary test sequence, the separate light output of the red, green, and blue LED was investigated over the full current number range. Luminance levels were measured with the spectroradiometer's measurement spot in the horizontal/vertical center of the projection area. The optical axis of the measurement device was adjusted perpendicular to the screen while a homogeneously illuminated screen was presented (red, green, or blue). The projection distance was set to 0.65 m (adapted from the COBUS setup) while the distance between measurement device and screen was set to 1.0 m. Tests were executed at a frame rate of

400.0 Hz (base frame rate = 100.0 Hz, equivalent to the HDMI refresh rate) with a duty cycle of 0.3. Current numbers were altered from 0 to 250 in steps of 10 (see Table B.1).[1]

TABLE B.1: Measurement conditions during the investigation of the relation between current number and luminance level of the applied projector's LEDs.

Hardware / Content	Parameter	Specification	Value	Unit
projector	base frame rate / frame rate	—	100.0 / 400.0	Hz
	duty cycle	—	0.3	—
	subframe order	—	R–D–D / D–G–D / D–D–B [a]	—
	current number	R / G / B	0–250, steps of 10	—
	projection distance	—	0.65	m
test object	displayed content	—	full red / green / blue [b]	—
	white point adjustment	x/y coordinate	—	—
spectroradiometer	synch. frequency	white	1200	Hz
	max. integration time	white	60.0	s
	observer	—	CIE1931 (2.0°)	—
	measurement distance	—	1.0	m

Note. R = red; G = green; B = blue; D = dark.
[a] Separate testing of single LEDs (red, green, blue); tested LED was only switched on within its corresponding time slot (classic RGB order), all other LEDs were switched off within their slots.
[b] Complete projection area was displayed in red or green or blue color with variable luminance level depending on the current number of the chosen LED.

Figure B.1 shows the approximately linear increase of the luminance levels with rising current numbers. The green LED has the highest output compared to the red and blue LED. Furthermore, the linear relation between current numbers and LED currents is illustrated.

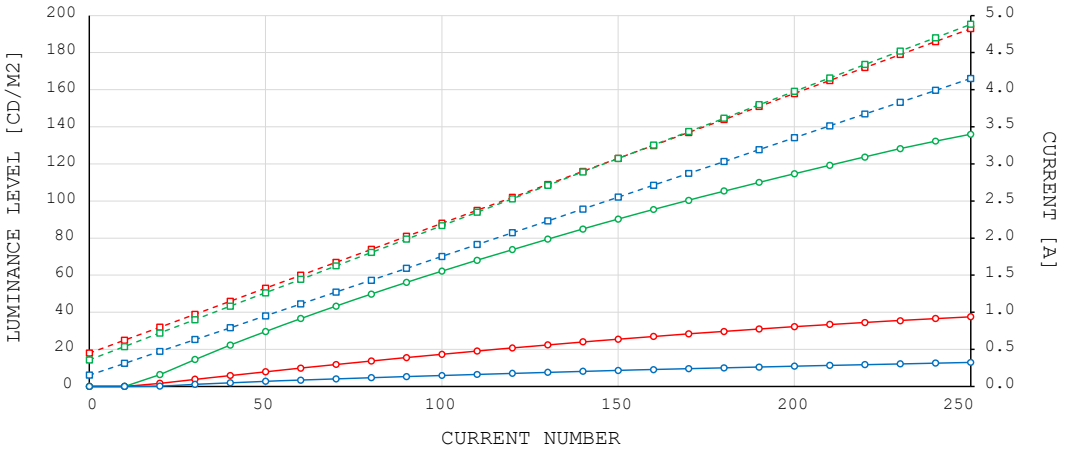

FIGURE B.1: Applied current and measured luminance level of DLP projector's red, green, and blue LEDs in dependency of current number; solid lines represent luminance level on primary y-axis, dashed lines represent current on secondary y-axis (calculated with Equations B.1 to B.3).

B.1.2 Position Dependency

In a next step, the maximum luminance level for white content was investigated. The achievable luminance with the applied projector/screen combination was measured for a projection distance of 0.65 m. The corresponding current numbers were determined under fulfillment of two requirements. First, the white point adjustment was executed to approximate the chromaticity coordinates of the white content to a reference white point.[2] Second, the

[1] The measurement distance between device/screen did not affect the measured luminance levels. Hence, a variation from the viewing distances during the COBUS series was irrelevant for the validity of the results.

[2] The white point adjustment referred to a temporary reference white point at $x = 0.3333$ and $y = 0.3333$ in the CIE xy chromaticity diagram (different from the final reference white point in Section B.1.3).

maximum luminance was adjusted in compliance with the current number thresholds (see Section B.1.1). The adjusted current numbers that met both requirements are $CN_R = 220$, $CN_G = 217$, and $CN_B = 75$ for red, green, and blue LED. After adjusting the current numbers, the luminance level over the complete projection area was measured, investigating the variability from center to periphery. The measurement spots were arranged as a two-dimensional grid pattern (209 spots with 1.25° horizontal/vertical distance, see Table B.2).

TABLE B.2: Measurement conditions for the investigation of luminance level and chromaticity coordinate variation over the full projection area in horizontal and vertical direction.

Hardware / Content	Parameter	Specification	Value	Unit
projector	base frame rate / frame rate	—	100.0 / 400.0	Hz
	duty cycle	—	0.3	—
	subframe order	—	R–G–B	—
	current number	R / G / B	220 / 217 / 75	—
	projection distance	—	0.65 [a]	m
test object	displayed content	—	full black / white [b]	—
	white point adjustment	x/y coordinate	0.3333 / 0.3333	—
spectroradiometer	synch. frequency	min. / max. LL	1200 / 1200	Hz
	max. integration time	min. / max. LL	2.0 / 60.0	s
	observer	—	CIE1931 (2.0°)	—
	measurement distance	—	1.0	m

Note. R = red; G = green; B = blue; LL = luminance level.
[a] Measured luminance values are representative for COBUS series as projection distance during light measurement and COBUS series was identical.
[b] Complete projection area was displayed in black/white (1-bit color depth off/on-mode) for the investigation of the minimum/maximum luminance level.

Figure B.2 shows the maximum luminance level (brightest white for 1-bit color depth on-mode) over the whole projection area for the defined current numbers.

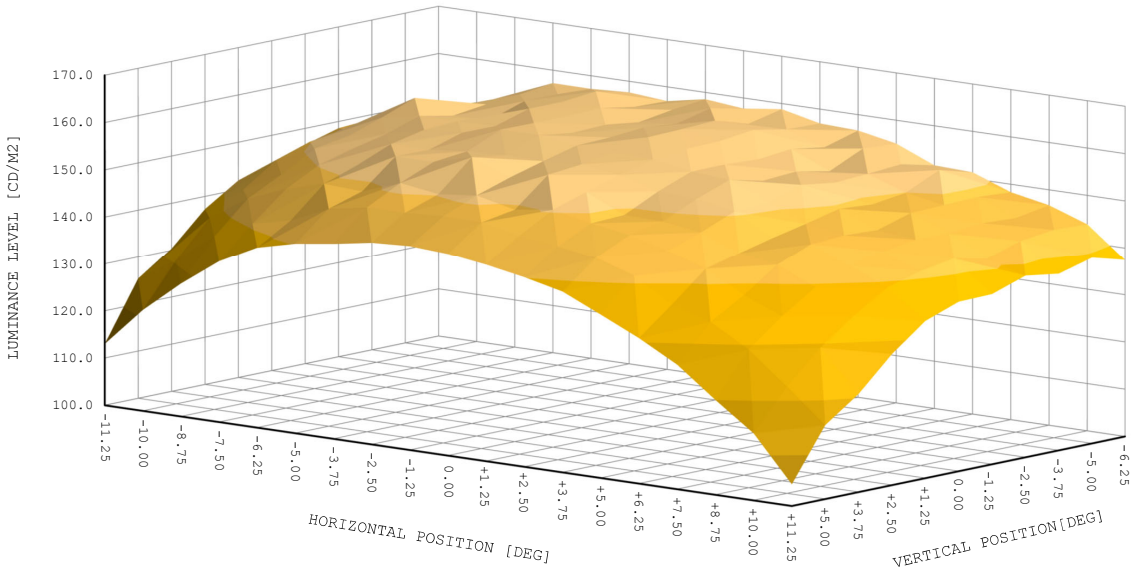

FIGURE B.2: Maximum luminance level across projection area incl. 209 measurement spots with linear interpolation between spots (1-bit color depth on-mode, DLP projector in upright position, positive/negative angular values refer to rightward/leftward and upward/downward screen positions, angular values for horizontal/vertical screen positions deviate from viewing angles during COBUS series as light measurement distance was different to viewing distance during COBUS series).

The achievable luminance level ($MN \pm SD = 147.58 \pm 10.11\,\mathrm{cd/m^2}$) depends on the screen position. The variability of luminance levels can be observed in horizontal and vertical direction. However, there is a greater decline on the vertical screen axis. The decline runs from

bottom to top as the projector is a 100% off-axis system (projector in upright position). The lowest luminance levels are located at the upper edges of the screen (approx. 30% decline).[3]

More than 98% of the measured color coordinates for the white content presentation over the projection area (209 spots, maximum luminance level, on-mode) are enclosed by a circle with a radius of 0.008 around the applied reference white point at $x = 0.3333$ and $y = 0.3333$ in the CIE chromaticity diagram. The variability of the color characteristics from screen center to periphery is negligible. However, the applied RGB mixture (based on the determined current numbers to reach the reference white point coordinates) leads to the subjective perception of slightly yellowish content. Therefore, the reference white point had to be redefined and the final LED currents for the COBUS series had to be readjusted.

B.1.3 Frame Rate Dependency

The reference for the white point adjustment was redefined from the idealized coordinates ($x = 0.3333/y = 0.3333$) to the coordinates that correspond to D65 (0.3127/0.3290). Subsequently, the current numbers for the red (157), green (217), and blue LED (76) were adapted to shift the resulting color coordinates of the displayed content towards the new reference point. As a result, the yellowish coloring of the content was reduced but still visible. This is a common problem. Subjective color perception provoked by new displays or projectors (based on LEDs, OLEDs, etc.) cannot always be precisely described by applying the CIE xy chromaticity diagram which is based on the CIE 1931 Color Matching Functions (CMF). Therefore, other CMFs or offsets for the x/y chromaticity coordinates have been proposed to bypass the mismatch (Bakhrakh & Görlich, 2017). To further reduce the yellowish coloring, an offset of Δx = -0.006 and Δy = -0.011 was applied as suggested by the Society of Motion Picture and Television Engineers (SMPTE, 2014).[4] The new x/y coordinates for the corrected D65 white point were $x = 0.3067$ and $y = 0.3180$. The modified current numbers $CN_R = 153$, $CN_G = 217$, and $CN_B = 82$ were tested for compliance with the new reference point.

TABLE B.3: Measurement conditions for the investigation of luminance level and color coordinate reproduction under BFR/FR variation after fine adjustment on basis of corrected D65 white point.

Hardware / Content	Parameter	Specification	Value	Unit
projector	base frame rate / frame rate	—	30.0 and 60.0 / 30.0 – 420.0 [a]	Hz
	duty cycle	—	0.3	—
	subframe order	—	R – G – B	—
	current number	R / G / B	153 / 217 / 82	—
	projection distance	—	0.65	m
test object	displayed content	—	quadratic shape [b]	—
	white point adjustment	x/y coordinate	0.3067 / 0.3180	—
spectroradiometer	synch. frequency	stimulus/background	variable, depending on frame rate	Hz
	max. integration time	stimulus/background	60.0 / 2.0	s
	observer	—	CIE1931 (2°)	—
	measurement distance	—	0.58	m

Note. R = red; G = green; B = blue.
[a] All possible BFR/FR combinations were tested, BFR of 30.0 Hz made FR testing of 30.0, 60.0, 90.0, 120.0, 150.0, 180.0, and 210.0 Hz possible, BFR of 60.0 Hz led to FR testing of 60.0, 120.0, 180.0, 240.0, 300.0, 360.0, and 420.0 Hz (see Appendix B.2).
[b] Two squares with side length of 3.0° were displayed in two measurement positions (horizontally centered on screen, vertically above/below screen center), squares included either CBU stimulus-representing white content (1-bit color depth on-mode) or background-representing black content (1-bit color depth off-mode).

[3] The minimum luminance level over the projection area was additionally measured (black screen, 1-bit color depth off-mode, same current numbers, same measurement spots). The achieved luminance level is $0.386 \pm 0.052\,\mathrm{cd/m^2}$ ($MN \pm SD$) with the same tendency of reduced luminance levels from bottom to top in vertical direction and from center to periphery in horizontal direction.

[4] The recommended offset by the SMPTE refers to LCDs with LED backlight. Since the applied projector uses the same light source (LED) with a comparable emission spectrum, it was reasonable to use the same offset.

Luminance levels and color characteristics for the new current numbers were tested at two different spots. The spots corresponded to the upper/lower position of the CBU-provoking stimulus during COBUS1/CAT2 (see Figure 4.1). Measurements were executed for white content, representing the CBU-provoking stimulus (maximum luminance level, 1-bit color depth on-mode). Black content was also investigated, representing the background setting (minimum luminance level, 1-bit color depth off-mode). Based on these measurements, the achievable contrast ratio was calculated. All technically available frame rates and base frame rates were applied to assess their effect on luminance levels and color characteristics (see Table B.3).

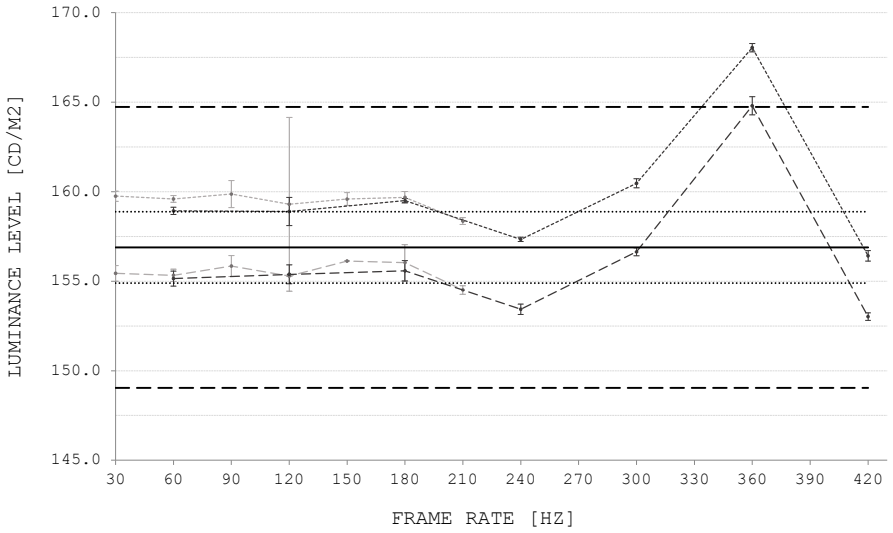

FIGURE B.3: Maximum luminance level for different BFR/FR combinations (all LEDs activated, time-sequential white content, 1-bit color depth on-mode); gray dotted/dashed graph = luminance levels for all frame rates at base frame rate of 30.0 Hz in lower/upper measurement position ($MN \pm 1.96SD$, 10 measurements for every BFR/FR combination and measurement position), black dotted/dashed graph = luminance levels for all frame rates at base frame rate of 60.0 Hz in lower/upper measurement position, solid horizontal line = averaged luminance level over all measurements, upper/lower dashed horizontal lines = upper/lower 5% tolerance limit of averaged luminance level (all measurements), upper/lower dotted horizontal line = averaged luminance level over all measurements in lower/upper position.

The averaged luminance level of all measurements for white content with maximum luminance is $157.39 \pm 2.59\,\mathrm{cd/m^2}$ (10 repeated measures for every BFR/FR combination in every measurement position). All measured luminance levels are located within the acceptable $\pm 5\%$ tolerance range (see Figure B.3). However, an exception occurs during the BFR/FR combination of 60.0/360.0 Hz (corrections are carried out in Section B.1.4).[5] The discrepancies for the upper and lower measurement positions (dotted vs. dashed graphs) are caused by the projector's position-dependent output (especially in vertical direction, see Section B.1.2). To investigate the base frame rate's impact on the achieved luminance levels, the overlapping frame rates feasible with both base frame rates of 30.0/60.0 Hz are compared (gray vs. black graphs). The differences for the relevant frame rates of 60.0, 120.0, and 180.0 Hz are below $1.0\,\mathrm{cd/m^2}$. Therefore, the applied base frame rate does not significantly affect the projector's output.

The averaged luminance level of all measurements for black content with minimum luminance is $0.453 \pm 0.004\,\mathrm{cd/m^2}$ (five repeated measures for every BFR/FR combination in

[5]The variability of 10 repeated measures for 30.0/120.0 Hz (BFR/FR) in the lower position is elevated. This might be due to measurement device-dependent outliers or an instability of the projector's output.

every measurement position). Combining the results for the minimum and maximum luminance levels, a high Michelson contrast of $C_M = 0.994$ on average can be achieved. The contrast ratio shows negligible changes for different BFR/FR combinations.

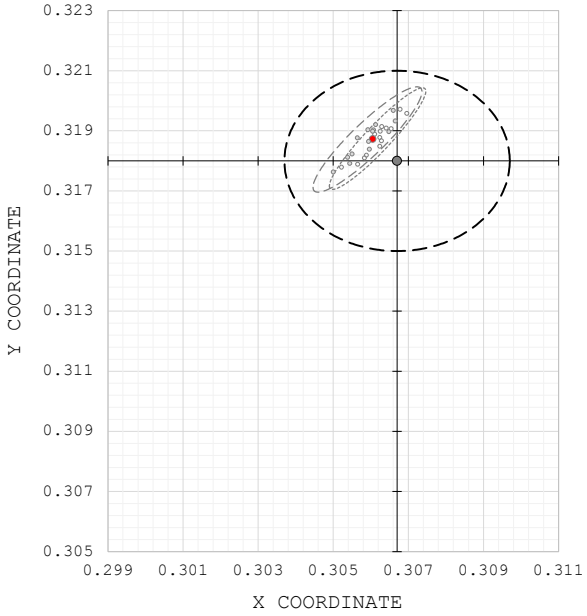

FIGURE B.4: CIE xy chromaticity diagram illustrating chromaticity coordinate distributions of white content with maximum luminance level for different frame rates (30.0 to 420.0 Hz) at base frame rates of 30.0/60.0 Hz (all LEDs activated, time-sequential color mixture, 1-bit color depth on-mode); central gray dot = corrected D65 white point ($x = 0.3067/y = 0.3180$), pale gray dots = averaged x/y chromaticity coordinates of all BFR/FR combinations in upper measurement position (10 measurements for every BFR/FR combination), white dots = averaged x/y chromaticity coordinates of all BFR/FR combinations in lower measurement position, red dot = averaged x/y chromaticity coordinate over all measurement conditions, gray dashed ellipse = Fisher's 95% confidence ellipse referring to averaged x/y chromaticity coordinates in upper measurement position (pale gray dots), gray dotted ellipse = Fisher's 95% confidence ellipse referring to averaged x/y chromaticity coordinates in lower measurement position (white dots), black dashed circle = tolerance circle with radius of 0.003 around the corrected D65 white point (central gray dot) defining tolerable color deviations.

The x/y color coordinates of white content (maximum luminance) were determined for the applied BFR/FR combinations in both measurement positions (see Figure B.4). The coordinate distribution for the measurement session was compared to the corrected D65 white point (0.3067/0.3180) as target value. The measured coordinate distribution scatters within a tolerable range around the target value. Hence, the presentation of white-colored content can be classified as stable when altering the applied BFR/FR combination (with a slight tendency of increasing x/y values for higher frame rates).

B.1.4 Test Range Determination

Determining the luminance levels for the white-colored CBU-provoking stimulus of the COBUS series, the projector's upper output limit of approximately 158 cd/m^2 must be respected. Furthermore, the x/y coordinates for white content at low luminance levels are harder to adjust as the corresponding current numbers are getting smaller. This restricts the current number range for a balanced adjustment of the red, green, and blue LED's output.[6]

[6]Color adjustments at low luminance levels are difficult as stepwise current number changes are limited to integer values. Changing current numbers by the smallest possible steps has a higher relative effect on the x/y chromaticity coordinates when the adjustable values are small. Hence, inaccuracies are inevitable during color coordinate adjustment at low luminance levels.

A precise white point adjustment can only be assured for luminance levels around 10 cd/m^2 (lower limit). Within the defined limits of available luminance levels, the non-linear relation between objective light intensity and subjective perceived brightness must be kept in mind when projecting the COBUS series.[7] Aiming to guarantee a wide range of subjective CBU perception, stimuli have to be displayed at the lowest and the highest luminance level of the available range. A third luminance level can be added approximately equidistant to the upper and lower limit. The corresponding LED currents were adjusted via current numbers. During this process, a white point calibration was incorporated. The displayed content and the applied BFR/FR combinations remained unchanged (compare Tables B.3 and B.4). The final current numbers for the lowest luminance level (*LL1* approx. 10 cd/m^2) are $CN_R = 18$, $CN_G = 21$, and $CN_B = 20$. The values for the intermediate luminance level (*LL2* approx. 80 cd/m^2) are $CN_R = 76$, $CN_G = 98$, and $CN_B = 47$. The maximum luminance level (*LL3* approx. 158 cd/m^2) is achieved by setting $CN_R = 153$, $CN_G = 217$, and $CN_B = 82$.[8]

TABLE B.4: Measurement conditions for the investigation of included luminance levels during the COBUS series under BFR/FR variation (further inclusion of measurements on chromaticity coordinate distribution).

Hardware / Content	Parameter	Specification	Value	Unit
projector	base frame rate / frame rate	—	30.0 and 60.0 / 30.0 – 420.0 [a]	Hz
	duty cycle	—	0.3	—
	subframe order	—	Scenario 1 / Scenario 2 [b]	—
	current number	R / G / B	variable [c]	—
	projection distance	—	0.65	m
test object	displayed content	—	quadratic shape [d]	—
	white point adjustment	x/y coordinate	0.3067 / 0.3180	—
spectroradiometer	synch. frequency	stimulus / background	variable, depending on frame rate	Hz
	max. integration time	stimulus / background	60.0 / 2.0	s
	observer	—	CIE1931 (2°)	—
	measurement distance	—	0.58	m

Note. R = red; G = green; B = blue.
[a] All possible BFR/FR combinations were tested, BFR of 30.0 Hz made FR testing of 30.0, 60.0, 90.0, 120.0, 150.0, 180.0, and 210.0 Hz possible, BFR of 60.0 Hz led to FR testing of 60.0, 120.0, 180.0, 240.0, 300.0, 360.0, and 420.0 Hz (see Appendix B.2).
[b] To investigate the LL for the red, green, and blue LED separately with altering LED current during Scenario 1, only one LED (red or green or blue) was switched on (e.g., R – D – D = red – dark – dark). For the investigation of the resulting LL of color mixed white content during Scenario 2, all LEDs (red and green and blue) were switched on time-sequentially (R – G – B = red – green – blue).
[c] Current numbers for red, green, and blue LED for minimum luminance level *LL1* (approx. 10 cd/m^2) are $CN_R = 18$, $CN_G = 21$, and $CN_B = 20$; current numbers for intermediate luminance level *LL2* (approx. 80 cd/m^2) are $CN_R = 76$, $CN_G = 98$, and $CN_B = 47$; current numbers for maximum luminance level *LL3* (approx. 158 cd/m^2) are $CN_R = 153$, $CN_G = 217$, and $CN_B = 82$.
[d] Two squares with side length of 3.0° were displayed in two measurement positions (horizontally centered on screen, vertically above/below screen center), squares included either CBU stimulus-representing white content (1-bit color depth on-mode) or background-representing black content (1-bit color depth off-mode).

Corresponding to the determined current numbers, the measured luminance levels *LL1* to *LL3* for white content (1-bit color depth on-mode) are illustrated in Figure B.5. In all three graphics, the ±5% tolerance range for an acceptable luminance variation (dashed horizontal lines) is not exceeded for any BFR/FR combination in any measurement position.[9] Finally, the averaged luminance levels for white content are $LL1 = 10.23 \pm 0.18$ cd/m^2 ≈ 10 cd/m^2,

[7] The Weber-Fechner law describes the relation between a physical stimulus intensity and its corresponding subjective perception by a logarithmic function (Fechner, 1860). In contrast, S. S. Stevens (1957) postulated the Power law that applies a power function to describe the relation between stimulus and stimulation.

[8] At first, the final current numbers were adjusted for one BFR/FR combination (base frame rate = 30.0 Hz, frame rate = 180.0 Hz) to approach the defined white point coordinates and luminance levels as precise as possible. The best fitting current numbers for the chosen BFR/FR combination were then adopted to all BFR/FR combinations, assuming that the color coordinates and luminance levels of all BFR/FR combinations show a uniformly distributed scattering around the target values within a limited range.

[9] The maximum luminance level (*LL3*) for 60.0/360.0 Hz (BFR/FR) initially exceeded the upper 5% tolerance limit (see Figure B.3). This violation of limits was due to a deviation between the initially adjusted on/off-times and the actually measured on/off-times within a subframe cycle (see Table B.5). By adapting the subframe timings of the projector's LEDs, the luminance level was shifted into the tolerance zone (see Figure B.5).

$LL2 = 80.38 \pm 1.49\,\mathrm{cd/m^2} \approx 80\,\mathrm{cd/m^2}$, and $LL3 = 156.79 \pm 2.59\,\mathrm{cd/m^2} \approx 157\,\mathrm{cd/m^2}$ ($MN \pm SD$). The averaged luminance levels for the corresponding black content (1-bit color depth off-mode, identical current numbers and BFR/FR combinations) are $LL1 = 0.027 \pm 0.003\,\mathrm{cd/m^2}$, $LL2 = 0.230 \pm 0.013\,\mathrm{cd/m^2}$, and $LL3 = 0.451 \pm 0.019\,\mathrm{cd/m^2}$.[10] The achieved values guarantee a high Michelson contrast of $C_M > 0.99$ between the white CBU stimulus and its dark background for the luminance levels *LL1* to *LL3* during the COBUS series (see Section 4.2.6).

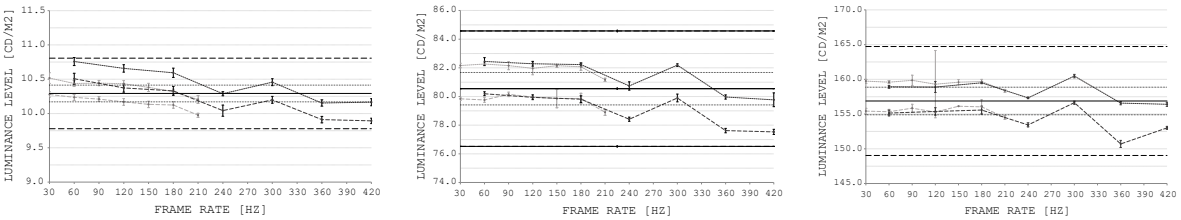

FIGURE B.5: Luminance levels *LL1* (left graphic), *LL2* (middle), and *LL3* (right) for different BFR/FR combinations (all LEDs activated, time-sequential white content, 1-bit color depth on-mode); gray dotted/dashed graph = luminance levels for all frame rates at base frame rate of 30.0 Hz in lower/upper measurement position ($MN \pm 1.96SD$, 10 measurements for every BFR/FR combination and measurement position), black dotted/dashed graph = luminance levels for all frame rates at base frame rate of 60.0 Hz in lower/upper measurement position, solid horizontal line = averaged luminance level over all measurements, upper/lower dashed horizontal lines = upper/lower 5% tolerance limit of averaged luminance level (all measurements), upper/lower dotted horizontal line = averaged luminance level over all measurements in lower/upper position.

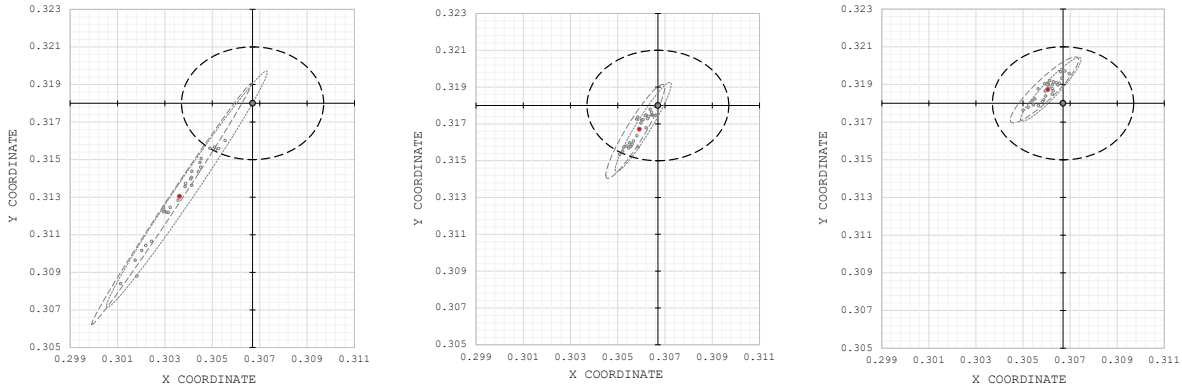

FIGURE B.6: CIE *xy* chromaticity diagram illustrating chromaticity coordinate distributions of white content with luminance levels *LL1* (left graphic), *LL2* (middle), and *LL3* (right) for different frame rates (30.0 to 420.0 Hz) at base frame rates of 30.0/60.0 Hz (all LEDs activated, time-sequential color mixture, 1-bit color depth on-mode); central gray dot = corrected D65 white point ($x = 0.3067/y = 0.3180$), pale gray dots = averaged x/y chromaticity coordinates of all BFR/FR combinations in upper measurement position (10 measurements for every BFR/FR combination), white dots = averaged x/y chromaticity coordinates of all BFR/FR combinations in lower measurement position, red dot = averaged x/y chromaticity coordinate over all measurement conditions, gray dashed ellipse = Fisher's 95% confidence ellipse referring to averaged x/y chromaticity coordinates in upper measurement position (pale gray dots), gray dotted ellipse = Fisher's 95% confidence ellipse referring to averaged x/y chromaticity coordinates in lower measurement position (white dots), black dashed circle = tolerance circle with radius of 0.003 around the corrected D65 white point (central gray dot) defining tolerable color deviations.

[10] Some frame rates can be created with both base frame rates of 30.0 and 60.0 Hz (see overlapping graphs in Figure B.5). The first option would be to take all available frame rates on basis of the base frame rate of 30.0 Hz and the remaining frame rates on basis of the base frame rate of 60.0 Hz, leading to a lower variance of the luminance levels *LL1* and *LL2* over the full frame rate range from 30.0 to 420.0 Hz. A second option would be to apply all available frame rates on basis of the base frame rate of 60.0 Hz and the remaining frame rates on basis of the base frame rate of 30.0 Hz, leading to a slightly lower variance of the highest luminance level *LL3*. Taking the whole picture into account, the BFR/FR combinations of the first option were applied in the COBUS series.

The chromaticity coordinate distributions for the three defined luminance levels *LL1* to *LL3* are illustrated in Figure B.6 (white content in 1-bit color depth on-mode, time-sequential RGB pattern, all BFR/FR combinations for lower/upper measurement positions). An acceptable color coordinate variation is defined by a tolerance circle around the corrected D65 white point. The tolerances are not exceeded for the luminance levels *LL2* and *LL3* (only single outliers). However, the lowest luminance level *LL1* shows a clear violation of limits as the scatter plot is widely stretched into the third quadrant. A more centered scattering around the corrected D65 white point fails due to the reduced ability of fine adjustment during the calibration of low luminance (see Footnote 6) and the applied adjustment procedure (see Footnote 8, no uniformly distributed scattering). The deviations are classified as acceptable as the color distortions are not subjectively perceived ($N = 1$, Participant ML).

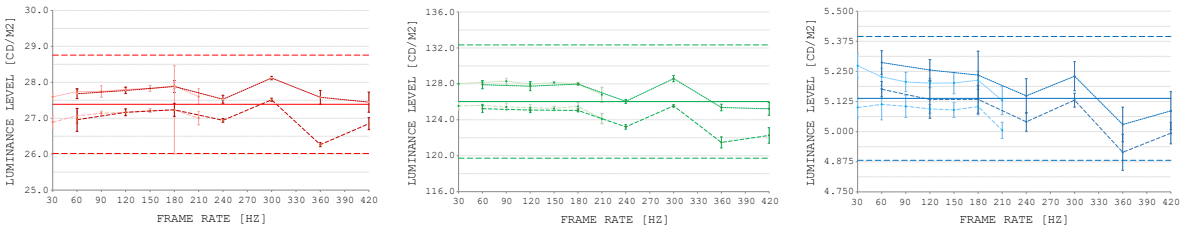

FIGURE B.7: Separate luminance levels for red (left graphic), green (middle), and blue LED (right) corresponding to *LL3* for different frame rate/base frame rate combinations (single LEDs activated, colored content); pale red/green/blue dotted graph = luminance levels for all frame rates at base frame rate of 30.0 Hz in lower measurement position ($MN \pm 1.96SD$, 10 measurements for every BFR/FR combination and measurement position), red/green/blue dotted graph = luminance levels for all frame rates at base frame rate of 60.0 Hz in lower measurement position, pale red/green/blue dashed graph = luminance levels for all frame rates at base frame rate of 30.0 Hz in upper measurement position, red/green/blue dashed graph = luminance levels for all frame rates at base frame rate of 60.0 Hz in upper measurement position, solid horizontal line = averaged luminance level over all measurements, upper/lower dashed horizontal line = upper/lower 5% tolerance limit of averaged luminance level (all measurements), upper/lower dotted horizontal line = averaged luminance level over all measurements in lower/upper position.

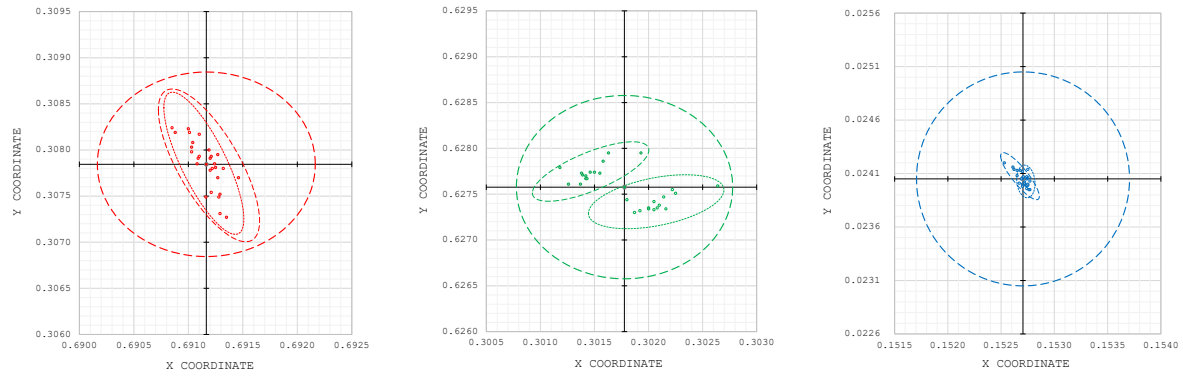

FIGURE B.8: CIE xy chromaticity diagram illustrating chromaticity coordinate distributions of red (left graphic), green (middle), and blue content (right) corresponding to *LL3* for different frame rates (30.0 to 420.0 Hz) at base frame rates of 30.0/60.0 Hz (single LEDs activated, colored content); pale gray dots = averaged x/y chromaticity coordinates of all BFR/FR combinations in upper measurement position (10 measurements for every BFR/FR combination), white dots = averaged x/y chromaticity coordinates of all BFR/FR combinations in lower measurement position, central red/green/blue dot = averaged x/y chromaticity coordinate over all measurement conditions, red/green/blue dashed ellipse = Fisher's 95% confidence ellipse referring to averaged x/y chromaticity coordinates in upper measurement position (pale gray dots), red/green/blue dotted ellipse = Fisher's 95% confidence ellipse referring to averaged x/y chromaticity coordinates in lower measurement position (white dots), red/green/blue dashed circle = tolerance circle with radius of 0.001 around the averaged x/y chromaticity coordinate for all measurement conditions (red/green/blue dot) defining tolerable color deviations.

For the highest luminance level (*LL3*), the light measurements were additionally executed while only one LED was active (other LEDs were switched off). This scenario allowed to collect further information on the individual light emission behavior of the single LEDs during BFR/FR variation (see Scenario 1 in Table B.4). The results for the separate red, green, and blue channel are illustrated in Figure B.7. The lower/upper 5% tolerance limits for acceptable luminance level variations are not violated.

The color-dependent scatter plots in Figure B.8 (only one LED active, all other LEDs were switched off) illustrate the chromaticity coordinate distributions for the maximum luminance level (*LL3*) under BFR/FR variation. An acceptable color coordinate variation is marked with the tolerance circle (radius of 0.001) around the averaged x/y chromaticity coordinate for all measurements. There is no violation of the defined tolerances for the coordinate distribution of the red, green, and blue LED.

B.2 Frame Rate Testing

The limits of applicable frame rates for the COBUS series have to be discussed. The lower limit depends on the participant's perception of flickering effects (see Section B.2.1). The upper limit is determined by technical features of the applied projector (see Section B.2.2). After setting the frame rate limits, experimental results of corresponding on/off-times of the projector's LEDs are presented in Section B.2.3.

B.2.1 Flicker Effect

Flickering arises when the off-times that separate the on-times of a pulsed light source exceed a certain period of time. At some point, the human eye is able to resolve the successive light stimuli over time. The emitted light flickers and is not perceived as a continuous stimulation. The flicker fusion frequency (FFF) of the human eye determines the threshold of perceivable flickering. The FFF depends on factors such as the strength and color of stimulation, the illuminated area's size and its retinal position as well as the human eye's state of adaptation. Generally, the FFF ranges from approximately 22 Hz for low-level scotopic stimulations up to about 90 Hz for high-level photopic stimulations (Eysel, 2017). The FFF's dependency on the stimulus color is of particular importance during the investigation of CBU effects that are based on the time-sequential emission of RGB patterns. Yamada and Sakaguchi (2006) state that red, green, and blue stimuli have different FFFs of 30, 50, and 35 Hz, respectively. Therefore, the highest color-dependent FFF of 50 Hz would be necessary to rule out the possibility of flickering on FSC-based display units.

During preliminary tests, flicker effects were investigated for frame rates from 30.0 to 420.0 Hz as the potential range of the COBUS series ($N = 1$, Participant ML). Perceptual thresholds of flickering were determined during the execution of pursuits and saccades provoked by sequences identical to those of COBUS1 (see Section 4.2.6). All sequences were presented for the lowest (approx. 10 cd/m^2) and the highest possible luminance of the white CBU stimulus (> 150 cd/m^2). The threshold determination was designed as upward stimulation, starting with the lowest frame rate of 30.0 Hz. The frame rate was increased (steps of 30.0 Hz) until the complete absence of flickering was achieved for all tested sequences. The frame rate that led to flicker-free conditions was clearly detectable by the participant. At a frame rate of 30.0 Hz, flickering was existent for all tested sequences of CAT2/CAT3. Flicker-free conditions were reached at 60.0 Hz and higher (valid for all luminance levels). However, the exact FFF threshold could not be determined because of the applied frame rate graduation. The participant's threshold lies somewhere between 30.0 and 60.0 Hz.

The test results confirm the previous knowledge on the FFF. Flickering at a frame rate of 30.0 Hz could be assumed during the COBUS series. For particularly sensitive participants,

even frame rates of 60.0 Hz might provoke flickering. Nevertheless, the lower limit for applicable frame rates in the COBUS series was set at 30.0 Hz as the lower sector of frame rates was of particular interest. The lower the frame rate, the potentially higher the CBU level. Covering low frame rates is highly relevant, especially for display technologies that currently operate at low rates (e.g., displays or projectors at a development stage). Including a wide range of frame rates in the COBUS series allowed to collect findings that are transferable to various technological approaches. As a consequence, all participants of the COBUS series had to be aware that flickering could occur during the study. Participants were briefed to disregard flickering during the evaluation of CBU effects. The appearance of flickering during the COBUS series was documented and discussed.

B.2.2 Projector Limitations

During the COBUS series, large saccadic path lengths were investigated. Such path lengths provoke ballistic saccades (CAT2). The higher the executed eye movement velocity, the greater the potential for strong CBU effects. Generally, the upper limit of the applied range of frame rates should provoke the absence of CBU effects or at least a sharp CBU reduction. Therefore, frame rates as high as possible had to be implemented in the COBUS series. The upper limit of realizable frame rates was determined by the technical features of the applied DLP projector and its periphery (see Appendix A.3.1). There are two limiting factors. First, the HDMI refresh rate (or, synonymously, base frame rate) can either be set to 30.0 Hz or 60.0 Hz by adjusting the output settings of the graphics adapter. The displayable frame rates are always multiples of the HDMI refresh rate since one refresh cycle contains a sequence of up to seven sequential full RGB images (set via control software of the projector).[11] The finally executed frame rate is calculated by multiplying the HDMI refresh rate with the number of included RGB images within one refresh cycle. For example, assuming a HDMI refresh rate of 30.0 Hz with four included RGB images leads to an FSC presentation at a frame rate of 120.0 Hz. By applying the maximum HDMI refresh rate (60.0 Hz) while including the maximum of seven RGB images, the highest displayable frame rate of 420.0 Hz is operated. The second limitation is the projector's minimum exposure time of 235 µs for the defined 1-bit color depth. The LED's on/off-times within a subframe cycle are both not allowed to fall below this time limit. Assuming a duty cycle of 0.3, the on-time is 238 µs and the off-time is 555 µs for the maximum frame rate of 420.0 Hz. The minimum exposure time is not violated when operating the maximum frame rate. Consequently, the exposure time requirement is also met for all lower frame rates. For the defined conditions, the projector's feasible frame rates are 30.0, 60.0, 90.0, 120.0, 150.0, 180.0, and 210.0 Hz as multiples of the HDMI refresh rate of 30.0 Hz as well as 60.0, 120.0, 180.0, 240.0, 300.0, 360.0, and 420.0 Hz for a HDMI refresh rate of 60.0 Hz.

B.2.3 Subframe Timing

The theoretically calculated and adjusted on/off-times of the projector's LEDs for all possible BFR/FR combinations (see Section B.2.2) were now compared with the actually measured on/off-times within a subframe cycle. The aim was to ensure error-free projector output before the start of the COBUS series. The on/off-times were measured with an oscilloscope/detector device (see Appendix A.1.2) by directly illuminating the detector with the projector's beam path without involving the projection screen. All luminance levels of the

[11] A refresh cycle includes a maximum of 24 color channels. One channel must be entirely black, used for the off-times of a subframe cycle as the duty cycle is 0.3. The remaining 23 channels can be used to integrate seven full RGB channels — one channel for every color, which adds up to 21 channels for digital color reproduction. The two leftover channels are not used as they do not allow to include another complete RGB color triplet.

COBUS series were investigated (*LL1* to *LL3*, see Section B.1.4). However, the listed on/off-timings in Table B.5 are limited to the maximum luminance of 157.0 cd/m^2 as the results of the other luminance levels are similar. The measured subframe timings differ only slightly from the adjusted timings via control software of the projector. The differences between the measured and adjusted timings are below the 5% tolerance. There is only one exception. The measured timings for the BFR/FR combination of 60.0/360.0 Hz (on-time = 292 µs, off-time = 636 µs) differ from the adjusted timings (on = 277 µs, off = 648 µs) by +5.42% for the on-time and -1.85% for the off-time. The LEDs are in on-mode for too long, whereas the time period in off-mode is too short. The result is an increased luminance level for 60.0/360.0 Hz (BFR/FR) compared to all other BFR/FR combinations (see Figure B.3). As a consequence, the initially adjusted timing values (on = 277 µs, off = 648 µs) were changed by ±3.0 µs to the new timing values (on = 274 µs, off = 651 µs). The new timing values show a positive effect on the measured subframe timings (on = 267 µs, off = 659 µs). The timings are now within the 5% tolerance zone (see Table B.5). Furthermore, the corresponding luminance is within the tolerable limits (see right graphic in Figure B.5).

TABLE B.5: Subframe cycle's calculated, adjusted, and measured on/off-times for BFR/FR combinations.

BFR in [Hz]	FR in [Hz]	Calculated Time in [µs]		Adjusted Time in [µs]		Measured Time in [µs]		Time Difference in [µs]		Time Difference in [%]	
		On	Off	On	Off	On	Off	On	Off	On	Off
30.0	**30.0**	3333.3	7777.8	3333.0	7777.0	3320.0	7760.0	-13.0	-17.0	-0.39	-0.22
	60.0	1666.7	3888.9	1666.0	3888.0	1660.0	3892.0	-6.0	4.0	-0.36	0.10
	90.0	1111.1	2592.6	1111.0	2592.0	1110.0	2586.0	-1.0	-6.0	-0.09	-0.23
	120.0	833.3	1944.4	833.0	1944.0	835.0	1934.0	2.0	-10.0	0.24	-0.51
	150.0	666.7	1555.6	666.0	1555.0	670.0	1544.0	4.0	-11.0	0.60	-0.71
	180.0	555.6	1296.3	555.0	1296.0	565.0	1296.0	10.0	0.0	1.80	0.00
	210.0	476.2	1111.1	476.0	1111.0	485.0	1116.0	9.0	5.0	1.89	0.45
60.0	**60.0**	1666.7	3888.9	1666.0	3888.0	1670.0	3780.0	4.0	-108.0	0.24	-2.78
	120.0	833.3	1944.4	833.0	1944.0	810.0	1970.0	-23.0	26.0	-2.76	1.34
	180.0	555.6	1296.3	555.0	1296.0	550.0	1296.0	-5.0	0.0	-0.90	0.00
	240.0	416.7	972.2	416.0	972.0	415.0	980.0	-1.0	8.0	-0.24	0.82
	300.0	333.3	777.8	333.0	777.0	330.0	780.0	-3.0	3.0	-0.90	0.39
	360.0	277.8	648.1	277.0	648.0	292.0	636.0	15.0	-12.0	5.42	-1.85
	C 360.0	277.8	648.1	274.0	651.0	267.0	659.0	-7.0	8.0	-2.55	1.23
	420.0	238.1	555.6	238.0	555.0	232.0	561.0	-6.0	6.0	-2.52	1.08

Note. BFR = base frame rate; FR = frame rate. Calculated timing values were derived from the BFR/FR combination. Adjusted timing values were regulated via graphical user interface of the projector's control software. Measured timings values were quantified via oscilloscope/detector setup. Time difference values were calculated by subtracting a subframe cycle's adjusted and measured on/off-timing values. Two different timing adjustments for BFR/FR combination of 60.0/360.0 Hz since light measurement with initial on/off-timings (60.0/360.0 Hz) results in luminance level that exceeds the threshold for acceptable variation, adapted timing values (60.0/C 360.0 Hz) lead to luminance level that does not violate the determined thresholds (see also Appendices B.1.3 and B.1.4).

Additionally, the duration of a LED's increase/decrease zone within a subframe cycle was investigated. The increase zone includes the initial boost from zero to maximum light emission, whereas the decrease zone covers the subsequent decline towards zero output.[12] The measurements were executed for all possible BFR/FR combinations (identical to the on/off-time measurements) while the projector was set to maximum light emission. On average, the duration from zero to maximum emission is fast with only 0.55 ± 0.01 µs (increase zone). The time span for the output reduction towards zero is longer with 1.82 ± 0.21 µs (decrease zone). However, it can be concluded that the projector's LEDs show a rapid switching behavior between on- and off-mode.

[12]Within the decrease zone, the LED's output slowly runs out towards the zero level (after a fast decline). Therefore, the decrease zone's stop point is defined by a decline of 90% of the maximum output value. All other reference points of time measurement are defined by zero/maximum light emission.

Appendix C

Content Creation

The content files that define the displayed content in the main sequences of the COBUS series were written with Notepad++. The files were read out by the CBU Scenario Player (see Appendix A.3.2) and finally presented with the applied DLP projector (see Appendix A.3.1). The pixel numbering within the content files is based on the 912×1140 diamond pixel array of the projector and is described in Figure C.1 (left graphic). The zero-pixel is positioned in the upper left corner of the projection area. The pixels are consecutively numbered to the right from PX 0 to PX +911 and downwards from PX 0 to PX +1139.

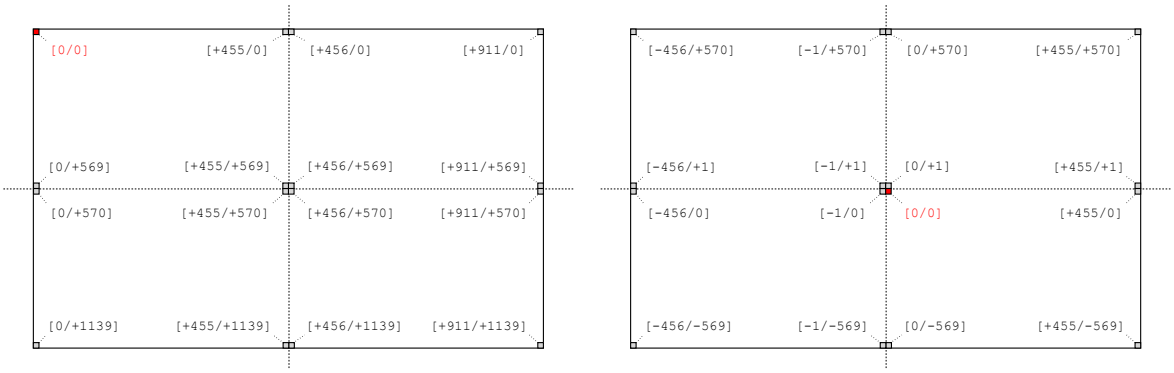

FIGURE C.1: Pixel numbering during content creation for the main sequences of the COBUS series (left graphic, applied in content files) and altered pixel numbering to match the zero-pixel [0/0] with the point of origin of the applied display unit's coordinate system (right graphic, applied in thesis).

The pixel numbering in the doctoral thesis differs from the numbering in the content files. For descriptions of the theoretical CBU model (see Figure 3.2) and the empirical studies (see Figure 4.1), the coordinate system of the projection area has its point of origin in the horizontal/vertical center. The position of the zero-pixel coincides with the coordinate system's point of origin (see Figure C.1, right graphic).[1]

C.1 Judder Effect

During the creation of content for the COBUS series, disturbing effects such as juddering had to be avoided. The judder effect is defined as a stuttering movement of displayed content. The content movement is not perceived as continuous movement with a stable velocity but as a skipping movement from one position to the next. A judder effect potentially occurs when the content's movement velocity in [px/fr] and the display unit's frame rate in [Hz] are not balanced. The content movement velocity is too high for the applied frame rate. In such a case, large frame-to-frame jumps of the displayed content are executed within an extended time period (provoked by a low frame rate). Such a disadvantageous combination

[1] The point of origin and the zero-pixel match as the reference point of every pixel is its upper left corner.

potentially results in judder perception. To the author's best knowledge, there are no formulas or calculation tables that could be used to theoretically determine judder-free conditions on FSC-based display units. Therefore, judder perception was empirically investigated in a pre-testing phase ($N = 1$, Participant ML). The aim was to avoid unsteady content movement during the COBUS series as it might affect the participant's eye movement behavior and, subsequently, the intensity of CBU perception.

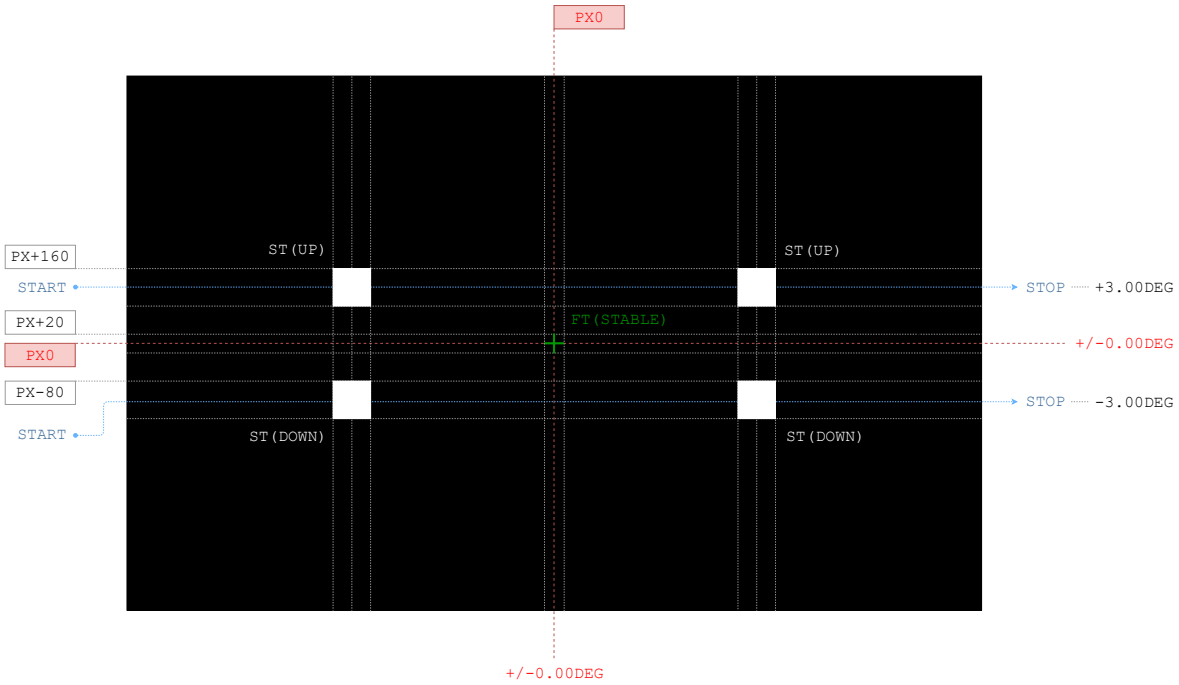

FIGURE C.2: Content for judder testing (CAT1) during pre-testing phase (ST = 2.0×2.0° = 40×80 px, FT = 1.0×1.0° = 20×40 px, referring to horizontal/vertical pixel pitch of 0.05°/0.025°).

Judder detection thresholds were determined for content movement velocities from 1.0 to 100.0 px/fr at frame rates of 30.0, 60.0, 90.0, 120.0, 180.0, 240.0, and 360.0 Hz.[2] The projector's configuration and the distances between participant, projector, and screen were adapted from the setup of COBUS1 to reach comparability (see Table H.1). The displayed content is illustrated in Figure C.2. The upper and lower stimulus for judder evaluation (white square) was moving synchronically from left to right. The start and stop positions of the stimulus were virtually outside the screen limits. The participant was instructed to fixate the stable fixation target (green cross) and evaluate possible judder effects of the moving white squares (without pursuing the stimulus). The applied eye/content movement pattern is categorized as CAT1 (eye static, content mobile).[3]

[2]Not all frame rates of the COBUS series were considered for judder testing. However, the lowest frame rates with the highest potential for juddering were included (e.g., 30.0 or 60.0 Hz). The content's movement velocity was changed in 0.5 px/fr steps from 1.0 to 10.0 px/fr and in 1.0 px/fr steps from 10.0 to 100.0 px/fr. An ascending and a descending test strategy was executed (two repetitions each). The test range of content movement velocities in [px/fr] covered the movement velocities of 18.0, 36.0, and 54.0 deg/s that were tested in CAT3 during the COBUS series (valid for all tested frame rates from 30.0 to 360.0 Hz, see Tables G.8 to G.11 for conversion).

[3]The least common multiple of the pixel count that represented a constant content movement distance for all content movement velocities exceeded the screen dimensions. Therefore, the stimulus moved into the screen from the left and moved out to the right. Pursuing the moving stimulus would have provoked CBU effects (CAT3) which could have affected the judder evaluation. Moreover, at a certain point, the tested content movement velocities became too fast to be tracked. Therefore, the participant was instructed to fixate the central fixation target.

Figure C.3 illustrates the results of the judder testing. The blue graphs refer to content movement velocities in [px/fr] and the red graphs cover content movement velocities in [deg/s]. The graphs with a solid line represent the maximum content movement velocities applied during CAT3/COBUS1. The values in [deg/s] are stable over the tested frame rate range (54.0 deg/s), whereas the values in [px/fr] change with changing frame rates (3.0 to 36.0 px/fr, calculated on basis of a variable frame duration). The graphs with the dotted lines illustrate the empirically determined content movement velocities as the detection thresholds for juddering. The graphs with the dashed lines represent theoretical calculations of the detection threshold. The calculated thresholds in [px/fr] are based on the assumption that a ratio between content movement velocity in [px/fr] and frame rate in [Hz] greater than 0.5 provokes perceivable juddering.[4] With increasing frame rate, the empirically determined content movement velocities in [px/fr] do not show a linear increase as theoretically assumed (dotted vs. dashed blue graph). The empirical threshold initially rises and then slowly falls with increasing frame rate (no constant gain). Converting the empirical velocity values from [px/fr] to [deg/s], an approximately linear relationship between content movement velocity and frame rate can be observed (dotted red line, primary *y*-axis is logarithmized).

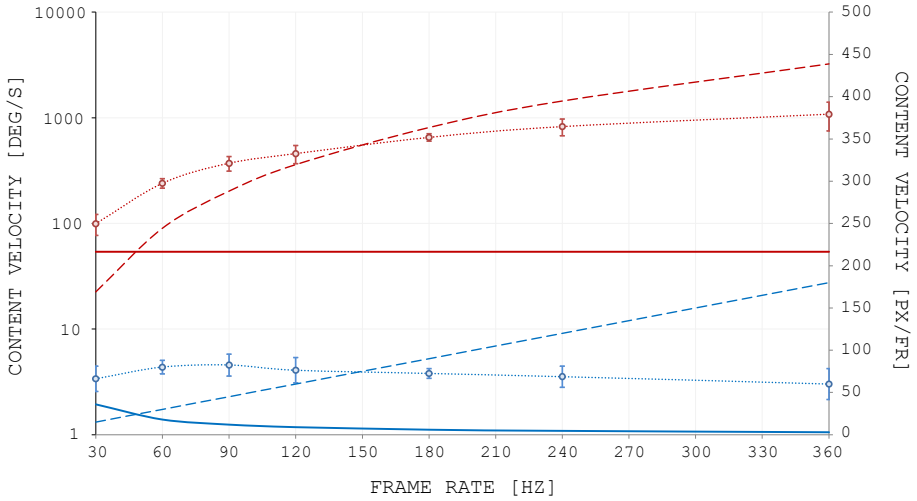

FIGURE C.3: Content movement velocities corresponding to judder detection threshold for different frame rates; red graphs refer to content movement velocity in [deg/s] on primary *y*-axis (logarithmized), blue graphs refer to content movement velocity in [px/fr] on secondary *y*-axis, dotted graphs represent empirically detected thresholds ($MN \pm 2SD$), dashed graphs represent theoretically detected thresholds, solid graphs represent maximum content movement velocity during COBUS1.

It is of utmost importance that the content's maximum velocity during CAT3/COBUS1 (solid graphs) does not exceed the empirically determined judder detection thresholds (dotted graphs). This requirement is achieved for all tested frame rates from 30.0 to 360.0 Hz (valid for values in [px/fr] and [deg/s] likewise). Even for the lowest frame rate of 30.0 Hz, the difference between the applied velocity (36.0 px/fr or 54.0 deg/s) and the corresponding threshold (66.3 px/fr or 99.4 deg/s) is high enough to tolerate inter- and intraindividual variability (of high importance since pre-testing referred to a single participant). Hence, the absence of judder effects during the worst-case conditions of the COBUS series was likely. In case of judder perception, the occurrence was documented and the corresponding data set was excluded.

[4]The theoretical detection thresholds for judder-free conditions assume that the absolute distance of pixel jumps per frame in [px/fr] can be increased when higher frame rates are applied. A conversion of the theoretical detection threshold in [px/fr] to the thresholds in [deg/s] is described in the notes of Table G.8.

C.2 Half-Pixel Jump

When creating moving content on a digital display unit, the content's movement path is defined by its start and stop position. Both positions define the distance of content movement. The number of frames that are necessary to display the movement define the duration of content movement. By dividing the movement distance in [px] by the duration of the movement in [fr], the content movement velocity in [px/fr] is calculated. The graduation for content shifts from frame to frame is generally limited to pixel jumps. Fortunately, the DMD array of the applied DLP projector has a diamond pixel array (see Appendix A.3.1). Therefore, the smallest graduation for horizontal content shifts is half the pixel size. Such content shifts are called half-pixel jumps. If the desired content movement velocity in [px/fr] is a multiple of a half-pixel jump, the movement is feasible without further effort. For COBUS1, the distances between projector, screen, and participant guaranteed a horizontal pixel size of 0.05°. The pixel size of one twentieth of a degree allows that multiples of half-pixel jumps via frame-to-frame displacement in [px/fr] can be transferred to integer values of content movement velocity in [deg/s]. For an exemplary frame-to-frame shift of 6.5 px while applying a frame rate of 120.0 Hz, the content movement velocity would be 39.0 deg/s (see Table G.8). Content movement based on half-pixel jumps results in a limited number of displayable movement velocities in [deg/s] for a single frame rate. Moreover, the discrete movement velocities in [deg/s] have to be compared for all frame rates within the desired range. There is an even stronger limitation for content movement velocities in [deg/s] that are achievable at all frame rates of the applied range. Concluding, the number of displayable content movement velocities in [deg/s] that are based on half-pixel jumps and are realizable at all frame rates is inadequate (see half-pixel jump violations in Table G.9).

There are possibilities to extend the range of applicable content movement velocities in [deg/s]. For velocities that violate the rule of half-pixel jumps, the closest possible velocity that is achievable with a multiple of half-pixel jumps could be chosen. For example, the content movement velocity of 36.0 deg/s at a frame rate of 210.0 Hz is not realizable with half-pixel jumps. The calculated shift for the defined conditions is 3.43 px (see Table G.9). The closest valid velocity would be 36.8 deg/s, deviating by +2.1% from the desired velocity (see Table G.8). Movement velocities would be displayed with a deviation from the desired value but the movement would be steady. However, the gap between displayed and desired velocity is not always tolerable as the percentage difference can be in the high double-digit range for some conditions. An alternative approach could be applied. Even if the content movement velocity in [px/fr] is not a multiple of a half-pixel jump, the content movement is still presentable via display unit (without rounding up/down as initially suggested). For an exemplary velocity of 2.67 px/fr (12.0 deg/s at 90.0 Hz), the movement is defined by a 2.5 px jump for the first and second frame-to-frame transition and a 3.0 px jump for the third transition.[5] The code that defines this movement behavior initially calculates the exact pixel position under consideration of a linear interpolation between the previous and the following key frame that define the start and stop position of the defined movement path. This procedure is done for all frame-to-frame transitions within the defined movement

[5]The horizontal content movement of a single pixel from pixel position PX +200 to PX +800 (see Figure C.1, left-side graphic) between Frame 1 and Frame 225 would lead to a linear content movement velocity of [(PX +800) - (PX +200)] / 225 fr = 2.67 px/fr. The first pixel shift of 2.67 px/fr for the first transition from Frame 1 to Frame 2 defines the new pixel position at (PX +200 + 2.67 px) = PX +202.67. However, this fractional pixel position cannot be displayed since only integer half pixel positions are displayable. Therefore, the fractional pixel position of PX +202.67 is rounded off. The pixel is actually shifted to the pixel position of PX +202.5. Consequently, the content movement velocity for the first pixel jump is [(PX +202.5) - (PX +200)] / 1 fr = 2.5 px/fr (not 2.67 px/fr). The second pixel jump from Frame 2 to Frame 3 is (PX +202.67 + 2.67 px) = PX +205.34. This position is rounded off again, which leads to an integer pixel position of PX +205. The second pixel shift would result in a content movement velocity of [(PX +205) - (PX +202.5)] / 1 fr = 2.5 px/fr and so forth.

path. Then — not until the level of pixel presentation is reached — all content positions are rounded off to bypass the shortcoming that fractional pixel positions are not displayable. As a result, the content movement is unsteady but the averaged movement velocity from start to stop position corresponds to the desired movement velocity (2.67 px/fr).

Before implementing this approach for content presentation during the COBUS series, the perceptibility of unsteady content movement caused by a violation of the rule of half-pixel jumps was tested. As long as the unsteadiness of a content movement is below the detection threshold, content-triggered eye movements might be unaffected by the unsteady behavior of the content movement (CAT3). In this case, the characteristic of CBU perception should be unimpaired, too. The tests were executed by a single participant ($N = 1$, Participant ML). The applied hardware components during the pre-testing were identical to the COBUS series (projector, processor, screen). A stuttering content movement due to limited computing power was excluded by applying a suitable processor. The projector setup was also adapted from the adjustments during the COBUS series (e.g., duty cycle of 0.3). All tests were executed for the movement pattern of CAT1 (stable eye, moving content).[6] The positions of the presented objects such as the fixation target and the stimulus that potentially provoked unsteady content movement (white square) were identical to the judder testing (see Figure C.2). The luminance level of the stimulus was 157.0 cd/m^2 and the contrast ratio to the dark background was 1.0. All combinations within a defined range of frame rates (30.0 to 420.0 Hz) and content movement velocities (multiples of 9.0 deg/s up to 45.0 deg/s) that violate the half-pixel jump rule were tested (see Table C.1).

TABLE C.1: Perceptibility of unsteady content movement on a digital display unit concerning various frame rates and content movement velocities.

FR in [Hz]	Content Movement Velocity in [deg/s]				
	9.0	**18.0**	**27.0**	**36.0**	**45.0**
30.0	NV (6.00)	NV (12.00)	NV (18.00)	NV (24.00)	NV (30.00)
60.0	NV (3.00)	NV (6.00)	NV (9.00)	NV (12.00)	NV (15.00)
90.0	NV (2.00)	NV (4.00)	NV (6.00)	NV (8.00)	NV (10.00)
120.0	NV (1.50)	NV (3.00)	NV (4.50)	NV (6.00)	NV (7.50)
150.0	PI (1.20)	NI (2.40)	NI (3.60)	NI (4.80)	NV (6.00)
180.0	NV (1.00)	NV (2.00)	NV (3.00)	NV (4.00)	NV (5.00)
210.0	PI (0.86)	NI (1.71)	NI (2.57)	NI (3.43)	NI (4.29)
240.0	NI (0.75)	NV (1.50)	NI (2.25)	NV (3.00)	NI (3.75)
300.0	NI (0.60)	NI (1.20)	NI (1.80)	NI (2.40)	NV (3.00)
360.0	NV (0.50)	NV (1.00)	NV (1.50)	NV (2.00)	NV (2.50)
420.0	NI (0.43)	NI (0.86)	NI (1.29)	NI (1.71)	NI (2.14)

Note. Pre-testing of a single participant for subjective perceptibility of unsteady content movements ($N = 1$, Participant ML). FR = frame rate; NV = no violation of half-pixel jump rule; PI = violation of half-pixel jump rule with perceivable irregularity in content movement velocity; NI = violation of half-pixel jump rule with no perceivable irregularity in content movement velocity. Corresponding content movement velocity in [px/fr] in brackets.

The preliminary tests show that stuttering content movement is perceptible for the combinations with the lowest frame rates (150.0 and 210.0 Hz) and the lowest movement velocity (9.0 deg/s) that violate the half-pixel jump rule. All other rule-breaking combinations do not lead to the perception of unsteady content movement. Concluding, the applied content movement velocity affects the ability to detect unsteady movements. An unsteady movement is easier to perceive while the content moves slowly (stable frame rate assumed). For clarification, the content movement velocities of 9.0 deg/s and 36.0 deg/s at a stable frame rate of 150.0 Hz are compared. The lower velocity of 9.0 deg/s equates to 1.2 px/fr, whereas

[6] It was assumed that the sensitivity to perceive unsteady content movements is higher when the human eye is in a stable position (CAT1) rather than pursuing the moving content (CAT3). Moreover, there was no necessity to integrate CAT2 as no content movement is executed in this category.

the higher velocity of 36.0 deg/s corresponds to 4.8 px/fr (see Table C.1). The initial steps of the frame-to-frame movement for the slower content movement of 1.2 px/fr are 1.0 – 1.0 – 1.5 – 1.0 – 1.5 px/fr. The steps for the faster movement of 4.8 px/fr are 4.5 – 5.0 – 4.5 – 5.0 – 5.0 px/fr. The maximum discrepancy of the consecutive pixel jumps is 0.5 px/fr for the slower movement. This makes a relative discrepancy of 41.7% in relation to the targeted velocity of 1.2 px/fr. For the higher content movement velocity of 4.8 px/fr, the relative discrepancy has a maximum of only 10.4%. The higher relative discrepancy for the slower content movement indicates a higher potential to perceive stuttering movement (as the pre-testings revealed).[7]

The applied frame rate also affects the perceptibility of unsteady movement patterns. The impact of an increased frame rate during stable content movement velocity will be analyzed. Therefore, the scenario with a content movement velocity of 9.0 deg/s is compared for two different frame rates of 150.0 and 300.0 Hz. For the lower frame rate, the content's velocity of 9.0 deg/s (equals 1.2 px/fr) is realized with frame-to-frame shifts of 1.0 – 1.0 – 1.5 – 1.0 – 1.5 px/fr. Applying a higher frame rate leads to smaller content shifts of 0.5 – 0.5 – 0.5 – 0.5 – 1.0 px/fr to create the same velocity of 9.0 deg/s (equals 0.6 px/fr). The maximum relative discrepancy within the sequence of content shifts is larger for the higher frame rate (83.3%) in comparison to the lower frame rate (41.7%). At first sight, the results imply that higher frame rates allow an easier detection of unsteady content movement. However, distance and duration of the content movement must be altered simultaneously to increase the frame rate during a stable content movement velocity.[8] The impact of a reduced content movement duration at higher frame rates seems to be larger than the simultaneous presence of the counteracting force of larger relative discrepancies between the content shifts. Ultimately, the pre-testing shows that unsteady content movement is perceived more easily at lower frame rates.

Summing up, unsteady content movements caused by a violation of the rule of half-pixel jumps are visible during slow content movements at medium frame rates (9.0 deg/s at 150.0 or 210.0 Hz). To avoid the perception of unsteady content movement, it was sufficient to exclude the velocity of 9.0 deg/s from the COBUS series. As long as unsteady content movements are below the threshold of perception, it can be assumed that there is no negative effect on the provoked eye movement behavior and the triggered CBU perception. Therefore, the applicable range of the COBUS series was extended by combinations of content movement velocities and frame rates that, while violating the rule of half-pixel jumps, do not provoke perceivable unsteadiness of the content movement.

C.3 Center-to-Periphery Bias

The velocity of a movement can be specified in different units. Commonly, content movement velocities on a flat screen of a digital display unit are described in [px/fr]. The unit relates to distance fragments in [px] that are covered within a fragmental time period in [fr] as the way of digitally creating content movements. On the display unit's pixel array, the content position is gradually shifted from frame to frame. Specifying content movements in [px/fr] has the advantage that stable velocities can be described adequately with constant

[7] Changes of the content movement velocity at a stable frame rate are realized by modifying the magnitude of the content shifts from frame to frame. The duration of a frame cycle is kept stable. Therefore, the stated relative discrepancies refer to the content shifts from frame to frame. The larger the relative discrepancies of the content shifts along the movement path, the clearer the perceptibility of unsteady content movement.

[8] Higher frame rates reduce the content movement duration (described more accurately, it is the time period between the content shifts). To keep the content movement velocity stable, the content movement distance must be reduced. For higher frame rates, a stable velocity is achieved with smaller content shifts over a shorter period of time.

values in [px/fr] as they are stable for all position changes across the flat screen. Alternatively, movement velocities can be expressed in [deg/s]. The unit refers to angle values in [deg] that are covered within a certain time period in [s]. It is commonly used to describe eye movement velocities.

The present work dealt with both — content movement velocities on a flat projection screen and eye movement velocities triggered by the presented content. It was essential that both movement velocities were specified using the same unit. When describing eye/content movement velocities on a plane surface in [deg/s], a movement with a constant velocity cannot be expressed by a constant value in [deg/s]. Movement angles in [deg] that are spanned by the same absolute distances in [px] are smaller in the periphery than in the center of the screen (see Figure C.4). Consequently, the velocity value in [deg/s] for a movement with a constant velocity is smaller in the screen's periphery than in the center. The so-called center-to-periphery bias (CPB) is due to the screen's flat surface. Hence, it could have appeared best to use velocity values in [px/fr] for the description of all movement velocities on a plane surface. However, eye movement velocities played a key role in this thesis and are generally expressed in [deg/s]. Consequently, all eye/content movement velocities were specified in [deg/s], allowing comparisons with other research findings. Stated movement velocities in [deg/s] always refer to a central screen position (see Tables G.8 to G.11). For peripheral screen positions, the stated values are invalid. During COBUS1, the actual velocity values in [deg/s] declined by less than 4% from the screen center to the periphery. The CPB's scale was tolerable as it loses relevance with higher viewing distances (VD = 0.58 m, PD = 0.65 m). The CPB was also present during COBUS2 since the same projector and projection screen were used. While the viewing distance was shorter (VD = 0.29 m, PD = 0.65 m), the CPB was limited to approximately 1% as the applied movement paths were shorter in comparison to COBUS1. The CPBs provoked by the setups of the COBUS series were classified as tolerable.

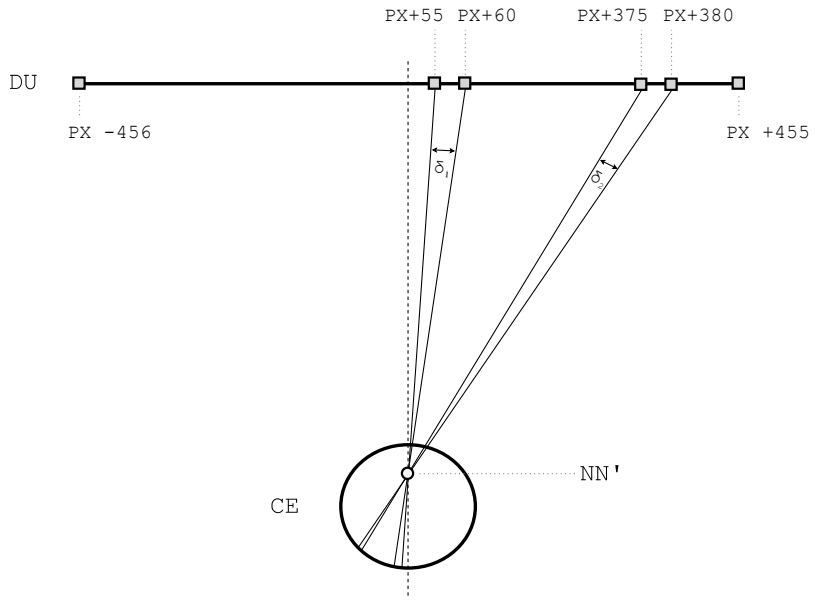

FIGURE C.4: Clarification of the center-to-periphery bias: The comparison of a central and a peripheral pixel position transition with the same absolute pixel distance on the display unit (DU) leads to different angular distances ($\delta_1 > \delta_2$) from the perspective of a cyclops eye (CE).

With respect to the CPB, potential deviations of the positions and sizes of the applied content have to be discussed. The content positions were correctly calculated by compensating for the CPB. For example, the included saccadic amplitudes from 3.6° to 28.2° during COBUS1 were calculated as stated (see Table G.1). The eccentricities from 0.0° to 50.0° for

the CBU-provoking stimulus during COBUS2 were precisely complied with as well (see Table G.2, negligible deviations caused by the stepwise positioning via pixel array). For the content size, there were two possible approaches. A position-adapted content size in [px] would have guaranteed identical retinal angles in [deg] for all content positions. The CBU perception during COBUS2 would have been tested for various eccentricities while keeping the stimulus-covered retinal area in [deg] stable. This approach would have provided controlled study conditions by excluding additional factors that potentially affect CBU perception. The alternative was a stable content size in [px] regardless of the screen position. The covered retinal area in [deg] would have been reduced with increasing eccentricity. The CBU investigations for various eccentricities (COBUS2) would have been affected by the variable retinal area in [deg] that would have been covered by the CBU-provoking stimulus. For example, the CBU-provoking stimulus' longer side covered 96 px perpendicular to the vertical movement path. The idealized angle of retinal stimulation for a central stimulus position is 9.6° (idealized pixel size of 0.10° in horizontal direction). For peripheral content positions of 10.0° and 50.0°, the covered horizontal retinal area is reduced to 9.29° and 3.97°, respectively (see Figure 4.4). The higher the eccentricity of the content position, the smaller the covered retinal area. The second approach has a higher practical relevance as an object's absolute size typically does not change when shifting its scene position (no depth variation assumed). Therefore, the final choice was made for the second approach. Consequently, all stated content sizes in [deg] are only valid for a central position of the content (see Tables G.1 to G.7).

Appendix D

Study Setup Illustration

To illustrate the experimental setup of the COBUS series, some pictures of important test stations are appended. With regard to COBUS1, pictures of the participant's visual acuity and contrast sensitivity testing during the pre-examination as well as the main examination setup including DLP projector, projection screen, and eye-tracking system are illustrated in Figures D.1 and D.2. Illustrations regarding the main examination phase of the COBUS2 setup are attached in Figure D.3. Additionally, the disassembled DLP projector is pictured in Figure D.4.

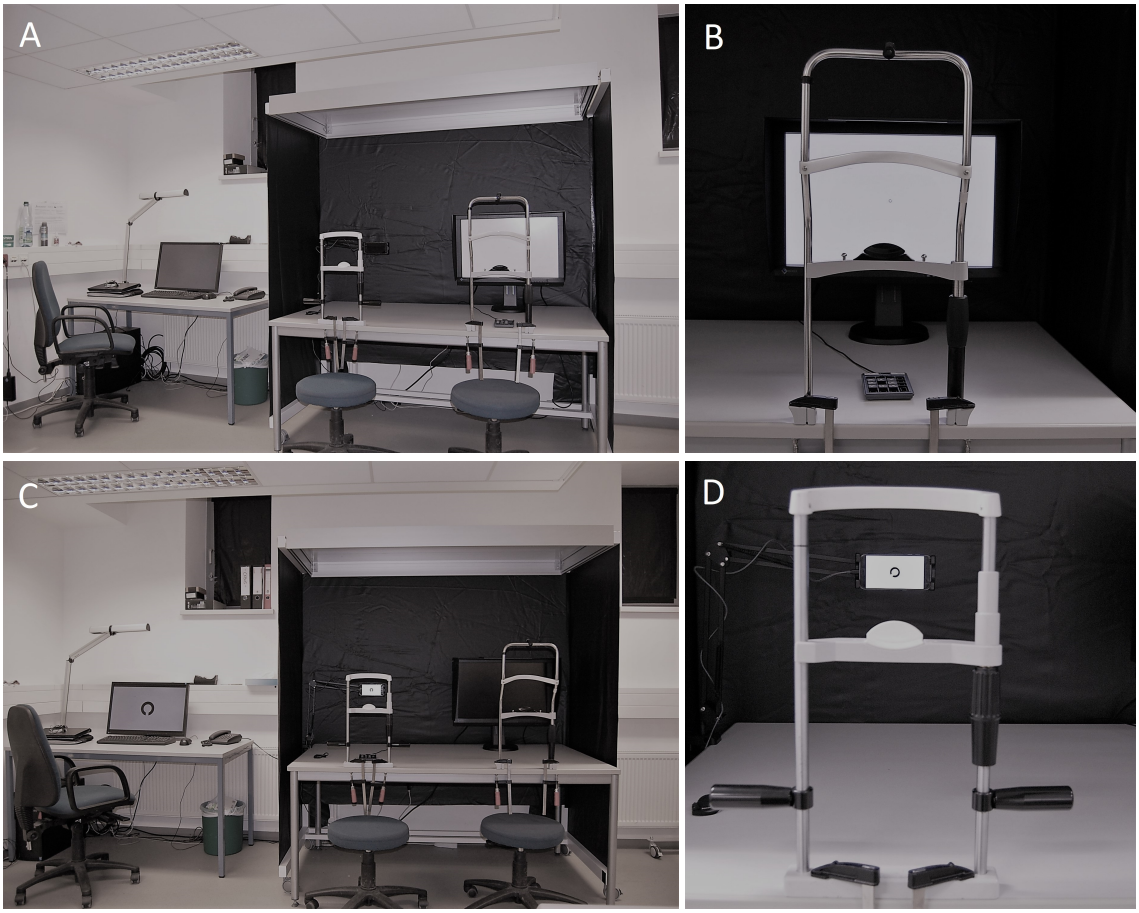

FIGURE D.1: Pre-examination setup of COBUS1. A: Overview of complete test station, testing of participant's visual acuity and contrast sensitivity (two monitors on right side) while examiner controls procedure (single monitor on left side). B: Testing of participant's contrast sensitivity on EIZO monitor (ColorEdge CG246) while participant is positioned on head and chin rest, keypad for participant response. C: Simultaneous presentation of the Landolt C on examiner's control monitor (left side) and participant's test monitor (right side). D: Testing of participant's visual acuity on Samsung Galaxy S7 while participant is positioned on head and chin rest.

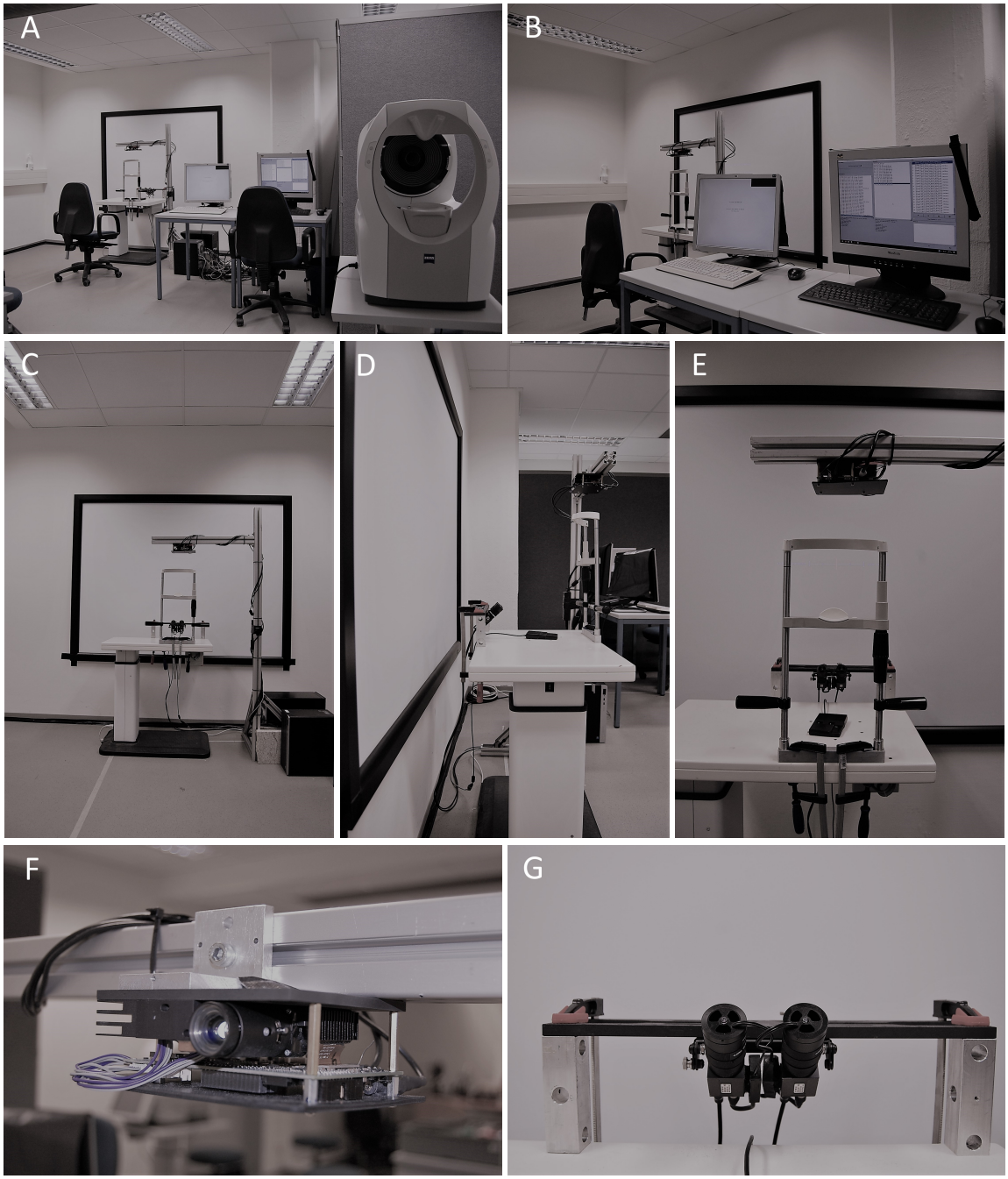

FIGURE D.2: Main study examination setup of COBUS1. A: Overview of complete main examination test station (left side) and i.Profiler (Carl Zeiss Vision GmbH) for inclusion/exclusion testing of objective refraction (right side). B: Examiner control station (eye-tracking controlled with left monitor, CBU Scenario Player displayed on right monitor). C: Front view of participant's test position (including projection screen, lift table with eye-tracking system and head/chin rest, DLP projector fixed on aluminum mounting, processors). D: Side view of participant's test position (including projection screen, lift table with eye-tracking system, keypad for participant response, head and chin rest, DLP projector fixed on aluminum mounting). E: Detailed front view from participant's test position (including projection screen, lift table with eye-tracking system, keypad for participant response, head and chin rest, DLP projector fixed on aluminum mounting). F: DLP projector (LightCrafter 4500, Texas Instruments) fixed on aluminum mounting. G: Eye-tracking system (Eyegaze Edge 600 Series, LC Technologies) mounted on lift table.

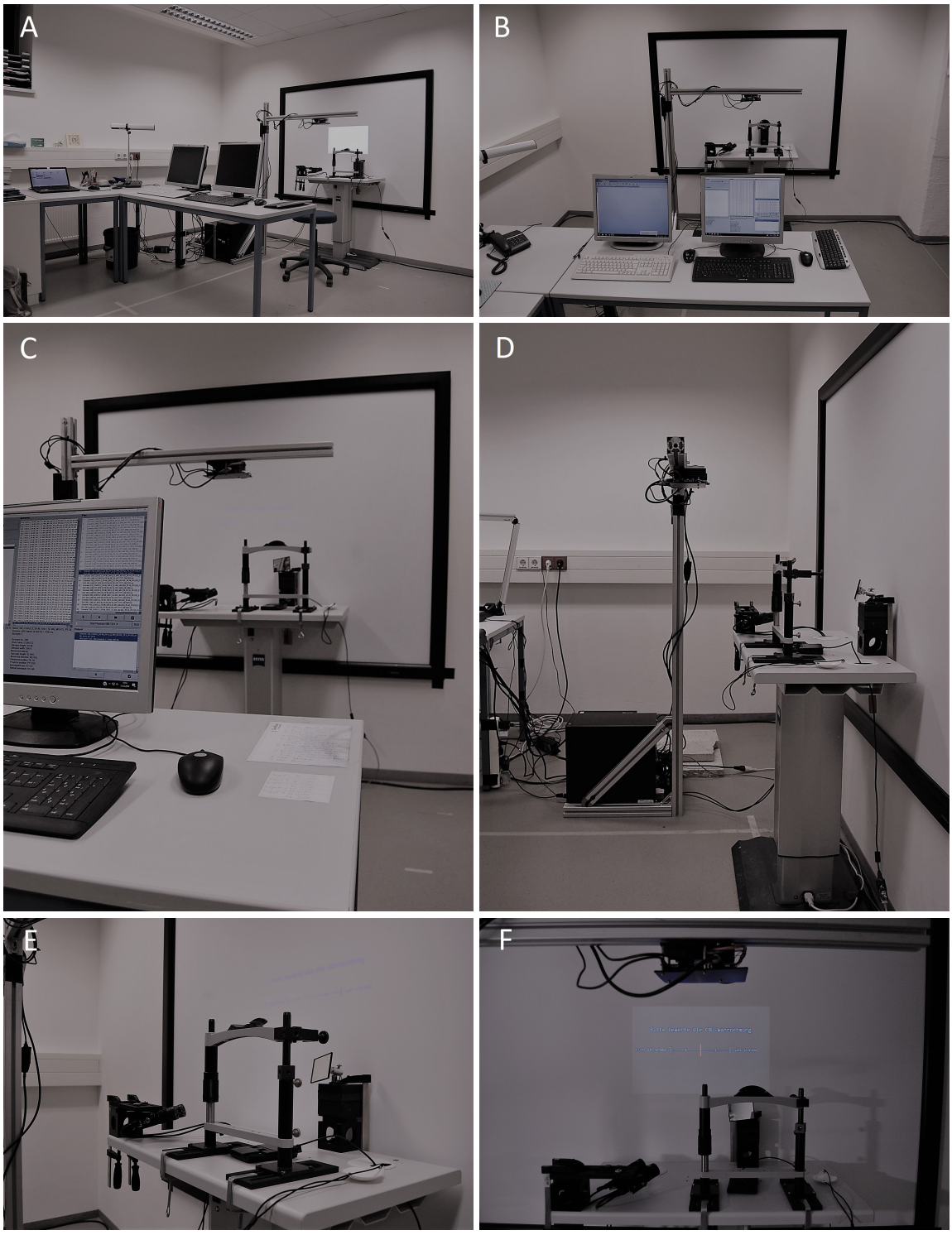

FIGURE D.3: Main study examination setup of COBUS2. A: Overview of complete test station, examiner's control station (front, two monitors) and participant's test position defined by the chin rest on the lift table in front of the projection screen (back). B: Examiner's control station in the front (eye-tracking monitor on the left, CBU Scenario Player on right monitor) and participant's test position in the back. C: Examiner's control monitor with CBU Scenario Player for test scenario selection (front) and participant's test position (back). D: Side view of participant's test position (including projection screen, lift table with eye-tracking and chin rest, DLP projector fixed on aluminum mounting, processors). E: Detailed view of participant's test position (lift table setup including chin rest, keypad for participant response, and eye-tracking system with mirror arrangement). F: Front view of projection screen presenting post-sequence for CBU evaluation from participant's test position.

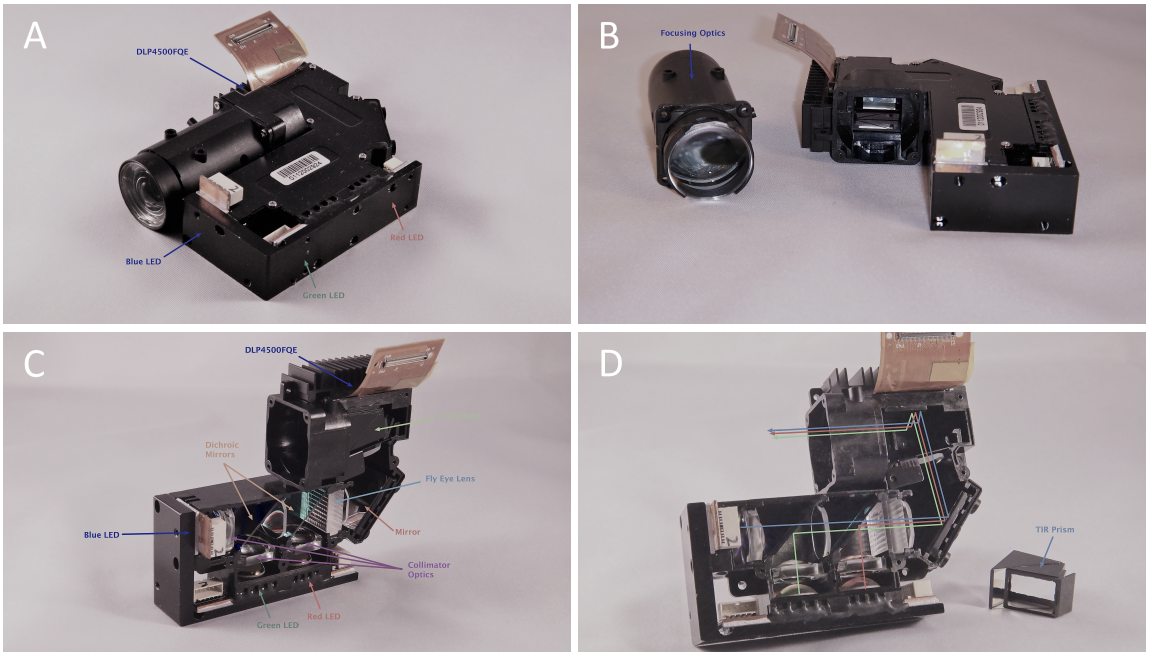

FIGURE D.4: Disassembled DLP projector (LightCrafter 4500, Texas Instruments). A: DLP projector with removed bottom thermal plate, heat sinks, and driver board. B: Disassembled light engine of DLP projector. C: Optical path of DLP projector. D: Optical path of red, green, and blue LED while TIR prism is removed (LEDs from OSRAM Licht AG, red LED: LE A Q9WP, green LED: LE CG Q9WP, blue LED: LE B Q9WP). Adapted from *A look inside the iView Engine in LightCrafter4500*, by P. Gelabert, 2013, Texas Instruments: DLP products forum (https://e2e.ti.com/support/dlp-products-group/dlp/f/dlp-products-forum/278008/a-look-inside-the-iview-engine-in-lightcrafter4500). Copyright 2013 by Pedro Gelabert. Adapted with permission.

Appendix E

Phase Transition Equations

The spatial requirement for a phase transition from PH1 to PH2 (see Formula E.1) is defined on basis of the relevant basic points (*A*, *C*, *D*, and *E*) under assumption of three subframes (*SF1*, *SF2*, and *SF3*) within one frame cycle (see Sections 3.4 and 3.5). A more specific Formula E.16 can be derived from the expressed requirement in Formula E.1 by substitution and transposition as described in Formulas E.2 to E.15.[1]

$$E_{SF1} = A_{SF3} \tag{E.1}$$

$$\mid\ E_{SF1} = A_{SF1} + \overline{A_{SF1}C_{SF1}} + \overline{C_{SF1}D_{SF1}} \tag{E.2}$$

$$\mid\ A_{SF3} = A_{SF1} + \overline{A_{SF1}A_{SF3}} \tag{E.3}$$

$$A_{SF1} + \overline{A_{SF1}C_{SF1}} + \overline{C_{SF1}D_{SF1}} = A_{SF1} + \overline{A_{SF1}A_{SF3}} \tag{E.4}$$

$$\mid\ \overline{A_{SF1}C_{SF1}} = CW_{REG} \tag{E.5}$$

$$\mid\ \overline{C_{SF1}D_{SF1}} = EMV_{PH1/2} \times TP_{SFON} \tag{E.6}$$

$$\mid\ \overline{A_{SF1}A_{SF3}} = 2 \times EMV_{PH1/2} \times TP_{SFC} \tag{E.7}$$

$$A_{SF1} + CW_{REG} + EMV_{PH1/2} \times TP_{SFON} = A_{SF1} + 2 \times EMV_{PH1/2} \times TP_{SFC} \tag{E.8}$$

$$CW_{REG} + EMV_{PH1/2} \times TP_{SFON} = 2 \times EMV_{PH1/2} \times TP_{SFC} \tag{E.9}$$

$$(\, CW_{REG} + EMV_{PH1/2} \times TP_{SFON} \,) \,/\, (\, 2 \times EMV_{PH1/2} \times TP_{SFC} \,) = 1 \tag{E.10}$$

$$\mid\ DC = TP_{SFON} \,/\, TP_{SFC} \tag{E.11}$$

$$CW_{REG} \,/\, (\, 2 \times EMV_{PH1/2} \times TP_{SFC} \,) + DC \,/\, 2 = 1 \tag{E.12}$$

$$CW_{REG} \,/\, (\, 2 \times EMV_{PH1/2} \times TP_{SFC} \,) = 1 - DC \,/\, 2 \tag{E.13}$$

$$(\, 2 \times EMV_{PH1/2} \times TP_{SFC} \,) \,/\, CW_{REG} = 1 \,/\, (\, 1 - DC \,/\, 2 \,) \tag{E.14}$$

$$\mid\ TP_{SFC} = 1 \,/\, (\, SF_{CT} \times FR \,) \tag{E.15}$$

$$EMV_{PH1/2} = (\, CW_{REG} \times SF_{CT} \times FR \,) \,/\, (\, 2 - DC \,) \tag{E.16}$$

Formula E.16 allows the calculation of an eye movement velocity threshold $EMV_{PH1/2}$ for the phase transition from PH1 to PH2 under defined conditions.

[1] Abbreviations in the transition formulas: CW_{REG} = regular content width in [deg], SF_{CT} = subframe count within frame cycle, FR = display unit's frame rate in [Hz], DC = display unit's duty cycle, TP_{SFON} = time period a single subframe is switched on in [s], TP_{SFC} = time period of full subframe cycle including subframe's on/off-time in [s], $EMV_{PH1/2}$ = eye movement velocity threshold for transition from Phase 1 to Phase 2 in [deg/s].

The derivation of Formula E.32 from Formula E.17 allows to calculate the threshold for the eye movement velocity $EMV_{PH2/3}$ that must be exceeded to switch from the CBU-characterizing PH2 to PH3 (analogous to the initial annotations for the phase transition from PH1 to PH2).[2]

$$E_{SF1} = A_{SF2} \tag{E.17}$$

$$\mid E_{SF1} = A_{SF1} + \overline{A_{SF1}C_{SF1}} + \overline{C_{SF1}D_{SF1}} \tag{E.18}$$

$$\mid A_{SF2} = A_{SF1} + \overline{A_{SF1}A_{SF2}} \tag{E.19}$$

$$A_{SF1} + \overline{A_{SF1}C_{SF1}} + \overline{C_{SF1}D_{SF1}} = A_{SF1} + \overline{A_{SF1}A_{SF2}} \tag{E.20}$$

$$\mid \overline{A_{SF1}C_{SF1}} = CW_{REG} \tag{E.21}$$

$$\mid \overline{C_{SF1}D_{SF1}} = EMV_{PH2/3} \times TP_{SFON} \tag{E.22}$$

$$\mid \overline{A_{SF1}A_{SF2}} = EMV_{PH2/3} \times TP_{SFC} \tag{E.23}$$

$$A_{SF1} + CW_{REG} + EMV_{PH2/3} \times TP_{SFON} = A_{SF1} + EMV_{PH2/3} \times TP_{SFC} \tag{E.24}$$

$$CW_{REG} + EMV_{PH2/3} \times TP_{SFON} = EMV_{PH2/3} \times TP_{SFC} \tag{E.25}$$

$$(\, CW_{REG} + EMV_{PH2/3} \times TP_{SFON} \,) \,/\, (\, EMV_{PH2/3} \times TP_{SFC} \,) = 1 \tag{E.26}$$

$$\mid DC = TP_{SFON} \,/\, TP_{SFC} \tag{E.27}$$

$$CW_{REG} \,/\, (\, EMV_{PH2/3} \times TP_{SFC} \,) + DC = 1 \tag{E.28}$$

$$CW_{REG} \,/\, (\, EMV_{PH2/3} \times TP_{SFC} \,) = 1 - DC \tag{E.29}$$

$$(\, EMV_{PH2/3} \times TP_{SFC} \,) \,/\, CW_{REG} = 1 \,/\, (\, 1 - DC \,) \tag{E.30}$$

$$\mid TP_{SFC} = 1 \,/\, (\, SF_{CT} \times FR \,) \tag{E.31}$$

$$EMV_{PH2/3} = (\, CW_{REG} \times SF_{CT} \times FR \,) \,/\, (\, 1 - DC \,) \tag{E.32}$$

Generally, Formula E.16 for the transition from PH1 to PH2 and Formula E.32 for the transition from PH2 and PH3 can both be transposed to calculate the phase transition thresholds of other parameters included in the formulas. For example, it might be of particular interest to determine hardware requirements such as the minimum frame rate that needs to be achieved to avoid CBU effects classified into PH2 or PH3. Furthermore, requirements for content creation (e.g., content width in eye movement direction) could be determined to reduce the intensity of CBU effects by preventing a transition into higher CBU phases.

[2] Abbreviations in the transition formulas: CW_{REG} = regular content width in [deg], SF_{CT} = subframe count within frame cycle, FR = display unit's frame rate in [Hz], DC = display unit's duty cycle, TP_{SFON} = time period a single subframe is switched on in [s], TP_{SFC} = time period of full subframe cycle including subframe's on/off-time in [s], $EMV_{PH2/3}$ = eye movement velocity threshold for transition from Phase 2 to Phase 3 in [deg/s].

Appendix F

Statistical Appendix

The statistical appendix includes the complete data set of COBUS1, considering all investigated experimental categories (CAT2/CAT3) and their subcategories (different eye movement pattern). Table F.1 lists the data set of CAT2 and Table F.2 refers to the data of CAT3. The mean values and standard deviations of the sample's CBU scores are listed, corresponding to the graphics in the Figures 4.11 to 4.13. Furthermore, the calculated success rates are specified separately for all study conditions.

The data sets for all experimental conditions of COBUS2 can be found in the Tables F.3 (CAT2) and F.4 (CAT3). The tables include the sample's CBU scores ($MN \pm SD$) and the success rates for all study conditions. The listed data sets are visualized in the corresponding Figures 4.23 (CAT2) and 4.29 (CAT3).

The subsequent Tables F.5 to F.12 contain the inductive statistical SPSS analysis of CBU score differences for the investigated luminance levels on basis of a two-way repeated measures ANOVA with two within-subjects factors (luminance level and frame rate) for all subcategories of saccadic (CAT2) and pursuit eye movement (CAT3) during COBUS1. Only statistically significant pairwise comparisons are listed. All other statistical SPSS values for pairwise comparisons without statistical significance are documented in the spv-file »two way anova output« (created via sps-file »two way anova syntax« on basis of the raw data-containing sav-file »anova data set«). The SPSS documents were archived but not published to protect the raw data of the empirical study from unauthorized access.

TABLE F.1: Sample's CBU scores ($MN \pm SD$) and success rates (SUC) for various path lengths of saccadic eye movement (CAT2) under variation of luminance level and frame rate during COBUS1.

LL in [cd/m^2]	FR in [Hz]	Saccadic Length in [deg]									
		3.6		9.0		14.3		21.3		28.2	
		CBU	SUC	CBU	SUC	CBU	SUC	CBU	SUC	CBU	SUC
10.0	30.0	3.36 ± 1.03	0.83	4.21 ± 0.70	0.93	4.33 ± 0.70	0.98	4.57 ± 0.55	0.98	4.47 ± 0.68	0.97
	60.0	2.16 ± 1.06	0.43	3.66 ± 0.81	0.88	4.11 ± 0.71	0.97	4.16 ± 0.66	0.97	4.36 ± 0.63	1.00
	90.0	1.61 ± 0.75	0.17	3.11 ± 0.95	0.72	3.37 ± 0.93	0.87	3.68 ± 0.75	0.93	3.81 ± 0.73	0.93
	120.0	1.30 ± 0.40	0.08	2.34 ± 0.85	0.48	2.79 ± 0.85	0.65	3.27 ± 0.87	0.85	3.30 ± 0.91	0.83
	150.0	1.33 ± 0.56	0.13	1.83 ± 0.73	0.32	2.44 ± 1.06	0.53	2.74 ± 0.83	0.72	2.97 ± 0.85	0.75
	180.0	1.16 ± 0.34	0.08	1.83 ± 0.80	0.28	2.07 ± 0.81	0.38	2.43 ± 0.88	0.52	2.56 ± 0.99	0.53
	210.0	1.27 ± 0.56	0.08	1.79 ± 0.79	0.25	1.89 ± 0.80	0.28	2.07 ± 0.77	0.35	2.29 ± 0.83	0.47
	240.0	1.22 ± 0.36	0.03	1.90 ± 0.80	0.27	1.99 ± 0.76	0.35	2.07 ± 0.75	0.33	2.15 ± 0.84	0.32
	300.0	1.20 ± 0.33	0.02	1.54 ± 0.67	0.18	1.92 ± 0.84	0.30	2.01 ± 0.71	0.35	2.10 ± 0.83	0.32
	360.0	1.20 ± 0.38	0.05	1.56 ± 0.67	0.17	1.76 ± 0.75	0.20	1.80 ± 0.81	0.27	1.98 ± 0.81	0.37
	420.0	1.15 ± 0.32	0.03	1.42 ± 0.58	0.08	1.59 ± 0.63	0.17	1.82 ± 0.78	0.25	1.75 ± 0.79	0.23
80.0	30.0	3.51 ± 0.90	0.85	4.14 ± 0.71	0.98	4.42 ± 0.61	0.98	4.57 ± 0.46	1.00	4.50 ± 0.66	0.98
	60.0	2.34 ± 1.03	0.55	3.85 ± 0.75	0.93	4.12 ± 0.67	0.98	4.38 ± 0.52	1.00	4.40 ± 0.73	0.98
	90.0	1.60 ± 0.78	0.17	3.22 ± 1.00	0.85	3.69 ± 0.77	0.88	3.86 ± 0.77	0.97	4.14 ± 0.64	1.00
	120.0	1.28 ± 0.56	0.10	2.61 ± 0.92	0.65	3.13 ± 0.92	0.83	3.61 ± 0.88	0.83	3.78 ± 0.78	0.93
	150.0	1.21 ± 0.35	0.05	2.06 ± 0.84	0.42	2.66 ± 0.87	0.63	3.04 ± 0.86	0.78	3.16 ± 0.85	0.78
	180.0	1.19 ± 0.50	0.07	1.80 ± 0.76	0.33	2.12 ± 0.82	0.38	2.63 ± 0.89	0.67	2.85 ± 0.92	0.72
	210.0	1.16 ± 0.28	0.08	1.89 ± 0.79	0.27	1.91 ± 0.79	0.33	2.32 ± 0.79	0.53	2.43 ± 0.94	0.52
	240.0	1.16 ± 0.30	0.05	1.80 ± 0.75	0.27	1.93 ± 0.72	0.35	2.17 ± 0.82	0.35	2.17 ± 0.87	0.42
	300.0	1.14 ± 0.27	0.03	1.43 ± 0.62	0.13	1.94 ± 0.78	0.32	2.08 ± 0.69	0.38	2.10 ± 0.80	0.35
	360.0	1.21 ± 0.48	0.10	1.49 ± 0.59	0.15	1.69 ± 0.71	0.20	1.94 ± 0.76	0.30	2.26 ± 0.83	0.42
	420.0	1.19 ± 0.44	0.07	1.41 ± 0.53	0.05	1.60 ± 0.64	0.17	1.66 ± 0.70	0.220	1.76 ± 0.72	0.27
157.0	30.0	3.43 ± 1.09	0.82	4.26 ± 0.67	0.98	4.29 ± 0.74	0.95	4.52 ± 0.65	0.98	4.56 ± 0.61	0.98
	60.0	2.16 ± 0.93	0.48	3.79 ± 0.86	0.93	4.02 ± 0.77	0.93	4.33 ± 0.59	1.00	4.42 ± 0.63	0.98
	90.0	1.53 ± 0.76	0.17	3.23 ± 0.91	0.78	3.70 ± 0.68	0.93	3.94 ± 0.65	0.98	4.10 ± 0.59	0.98
	120.0	1.24 ± 0.44	0.08	2.62 ± 0.84	0.70	3.20 ± 0.87	0.75	3.64 ± 0.79	0.92	3.70 ± 0.77	0.93
	150.0	1.22 ± 0.59	0.08	2.02 ± 0.83	0.42	2.84 ± 0.83	0.72	3.05 ± 0.91	0.75	3.29 ± 0.92	0.83
	180.0	1.17 ± 0.39	0.05	1.66 ± 0.72	0.23	2.13 ± 0.88	0.43	2.54 ± 0.85	0.62	2.83 ± 0.93	0.65
	210.0	1.17 ± 0.46	0.05	1.63 ± 0.72	0.23	1.91 ± 0.78	0.28	2.15 ± 0.80	0.42	2.31 ± 0.91	0.52
	240.0	1.12 ± 0.25	0.03	1.67 ± 0.64	0.18	1.87 ± 0.80	0.28	2.02 ± 0.73	0.37	2.08 ± 0.74	0.33
	300.0	1.13 ± 0.25	0.02	1.38 ± 0.52	0.07	1.76 ± 0.71	0.23	2.06 ± 0.71	0.30	2.04 ± 0.74	0.35
	360.0	1.11 ± 0.23	0.03	1.45 ± 0.62	0.10	1.61 ± 0.72	0.15	1.87 ± 0.74	0.30	1.95 ± 0.67	0.28
	420.0	1.12 ± 0.26	0.03	1.27 ± 0.39	0.05	1.52 ± 0.54	0.15	1.74 ± 0.72	0.27	1.84 ± 0.72	0.22

Note. $N = 30$. For reasons of completeness, the sample's success rate is listed separately for every single experimental condition of COBUS1 (saccadic path length, frame rate, and luminance level); however, the psychometric function in Section 4.3.1 was calculated by pooling the whole data set of CAT2. LL = luminance level; FR = frame rate.

TABLE F.2: Sample's CBU scores ($MN \pm SD$) and success rates (SUC) for various velocities of pursuit eye movement (CAT3) under variation of luminance level and frame rate during COBUS1.

LL in [cd/m^2]	FR in [Hz]	PEM Velocity in [deg/s]					
		18.0		36.0		54.0	
		CBU	SUC	CBU	SUC	CBU	SUC
10.0	30.0	3.33 ± 0.85	1.00	3.79 ± 0.81	0.98	4.09 ± 0.78	0.97
	60.0	2.16 ± 0.68	0.57	2.79 ± 0.75	0.78	3.25 ± 0.84	0.88
	90.0	1.54 ± 0.57	0.18	2.32 ± 0.72	0.60	2.63 ± 0.79	0.67
	120.0	1.39 ± 0.47	0.08	1.89 ± 0.68	0.35	2.24 ± 0.77	0.43
	150.0	1.27 ± 0.41	0.10	1.59 ± 0.50	0.22	1.77 ± 0.69	0.27
	180.0	1.21 ± 0.36	0.05	1.41 ± 0.47	0.08	1.68 ± 0.64	0.23
	210.0	1.10 ± 0.23	0.03	1.44 ± 0.60	0.08	1.62 ± 0.71	0.13
	240.0	1.15 ± 0.31	0.02	1.34 ± 0.42	0.08	1.45 ± 0.60	0.17
	300.0	1.11 ± 0.25	0.03	1.24 ± 0.42	0.02	1.26 ± 0.34	0.05
	360.0	1.09 ± 0.23	0.02	1.20 ± 0.34	0.05	1.30 ± 0.48	0.05
	420.0	1.08 ± 0.24	0.02	1.15 ± 0.30	0.02	1.25 ± 0.39	0.07
80.0	30.0	3.35 ± 0.86	0.98	3.82 ± 0.82	0.98	4.12 ± 0.78	0.98
	60.0	2.22 ± 0.73	0.60	2.91 ± 0.82	0.90	3.38 ± 0.81	0.92
	90.0	1.80 ± 0.63	0.38	2.44 ± 0.72	0.68	2.84 ± 0.81	0.77
	120.0	1.51 ± 0.51	0.18	1.98 ± 0.68	0.37	2.35 ± 0.80	0.55
	150.0	1.31 ± 0.42	0.03	1.83 ± 0.69	0.37	2.13 ± 0.63	0.42
	180.0	1.23 ± 0.38	0.03	1.63 ± 0.61	0.23	1.95 ± 0.71	0.32
	210.0	1.17 ± 0.35	0.02	1.40 ± 0.44	0.12	1.59 ± 0.56	0.20
	240.0	1.12 ± 0.25	0.02	1.32 ± 0.41	0.12	1.57 ± 0.61	0.12
	300.0	1.11 ± 0.25	0.03	1.25 ± 0.41	0.05	1.29 ± 0.36	0.02
	360.0	1.09 ± 0.26	0.02	1.18 ± 0.31	0.02	1.25 ± 0.33	0.03
	420.0	1.08 ± 0.22	0.02	1.21 ± 0.36	0.02	1.23 ± 0.38	0.05
157.0	30.0	3.48 ± 0.85	0.95	3.93 ± 0.80	0.98	4.15 ± 0.73	0.98
	60.0	2.32 ± 0.74	0.65	2.93 ± 0.79	0.92	3.32 ± 0.73	0.92
	90.0	1.87 ± 0.67	0.38	2.47 ± 0.79	0.72	2.78 ± 0.83	0.77
	120.0	1.58 ± 0.62	0.13	2.06 ± 0.68	0.48	2.41 ± 0.75	0.60
	150.0	1.28 ± 0.38	0.05	1.81 ± 0.63	0.30	2.05 ± 0.77	0.45
	180.0	1.24 ± 0.39	0.05	1.58 ± 0.54	0.15	1.87 ± 0.63	0.32
	210.0	1.12 ± 0.26	0.05	1.42 ± 0.46	0.13	1.59 ± 0.56	0.25
	240.0	1.11 ± 0.24	0.03	1.38 ± 0.43	0.08	1.55 ± 0.57	0.13
	300.0	1.13 ± 0.33	0.02	1.30 ± 0.49	0.08	1.40 ± 0.52	0.05
	360.0	1.08 ± 0.22	0.02	1.19 ± 0.34	0.02	1.39 ± 0.54	0.05
	420.0	1.08 ± 0.24	0.03	1.20 ± 0.34	0.02	1.18 ± 0.38	0.05

Note. $N = 30$. For reasons of completeness, the sample's success rate is listed separately for every single experimental condition of COBUS1 (pursuit eye movement velocity, frame rate, and luminance level); however, the psychometric function in Section 4.3.1 was calculated by pooling the whole data set of CAT3. LL = luminance level; FR = frame rate; PEM = pursuit eye movement.

TABLE F.3: Sample's CBU scores ($MN \pm SD$) and success rates (SUC) for saccadic eye movement with a path length of 9.6° (CAT2) under variation of stimulus size and stimulus position for a frame rate presentation of 30.0 and 60.0 Hz during COBUS2.

FR in [Hz]	SP in [deg]	Stimulus Size in [deg]											
		1.0		2.0		3.0		4.0		5.0		6.0	
		CBU	SUC	CBU	SUC	CBU	SUC	CBU	SUC	CBU	SUC	CBU	SUC
30.0	-50.0	1.31 ± 0.54	0.00	1.27 ± 0.50	0.00	1.28 ± 0.45	0.00	1.23 ± 0.45	0.00	1.47 ± 0.67	0.08	1.36 ± 0.57	0.00
	-40.0	1.86 ± 0.87	0.25	1.76 ± 0.78	0.13	1.80 ± 0.78	0.17	1.56 ± 0.74	0.13	1.66 ± 0.78	0.21	1.70 ± 0.78	0.17
	-30.0	2.36 ± 1.05	0.38	2.35 ± 1.01	0.46	2.26 ± 0.83	0.42	2.11 ± 0.88	0.25	1.76 ± 0.76	0.21	2.10 ± 0.94	0.29
	-20.0	3.20 ± 1.08	0.83	3.31 ± 1.00	0.83	2.96 ± 1.05	0.75	2.83 ± 1.11	0.67	2.81 ± 1.02	0.71	2.64 ± 0.96	0.67
	-10.0	3.34 ± 0.88	0.83	3.13 ± 0.94	0.75	3.21 ± 0.91	0.75	3.04 ± 1.10	0.75	2.76 ± 1.03	0.58	2.74 ± 1.09	0.71
	-0.0	3.35 ± 0.78	0.83	3.54 ± 1.00	0.88	3.42 ± 0.97	0.83	3.25 ± 1.03	0.83	2.94 ± 0.87	0.75	2.96 ± 1.18	0.71
	+0.0	3.82 ± 0.68	1.00	3.99 ± 0.60	1.00	3.76 ± 0.52	0.96	3.50 ± 0.78	0.92	3.17 ± 0.94	0.79	2.82 ± 0.90	0.63
	+10.0	3.47 ± 0.80	0.96	3.65 ± 0.54	1.00	3.36 ± 0.73	0.83	3.18 ± 0.71	0.83	2.88 ± 0.82	0.67	2.66 ± 0.90	0.63
	+20.0	3.17 ± 0.93	0.88	3.13 ± 0.64	0.79	3.27 ± 0.76	0.88	2.94 ± 0.85	0.67	2.63 ± 0.91	0.54	2.33 ± 0.70	0.46
	+30.0	2.76 ± 0.95	0.63	2.86 ± 0.89	0.75	2.96 ± 0.76	0.75	2.95 ± 0.93	0.79	2.50 ± 0.84	0.54	2.37 ± 0.69	0.42
	+40.0	2.51 ± 0.82	0.58	2.46 ± 0.86	0.46	2.56 ± 0.99	0.50	2.34 ± 0.70	0.38	2.38 ± 0.76	0.29	2.19 ± 0.84	0.38
	+50.0	1.97 ± 1.09	0.33	2.04 ± 0.88	0.25	1.96 ± 0.94	0.25	1.87 ± 0.73	0.25	2.00 ± 0.76	0.21	1.86 ± 0.76	0.25
60.0	-50.0	1.22 ± 0.27	0.00	1.31 ± 0.38	0.04	1.21 ± 0.31	0.00	1.27 ± 0.38	0.00	1.17 ± 0.25	0.00	1.33 ± 0.38	0.00
	-40.0	1.64 ± 0.90	0.13	1.69 ± 0.86	0.13	1.57 ± 0.62	0.08	1.30 ± 0.43	0.00	1.31 ± 0.40	0.04	1.22 ± 0.32	0.04
	-30.0	2.44 ± 1.00	0.38	2.31 ± 0.91	0.50	1.83 ± 0.82	0.25	1.57 ± 0.74	0.13	1.21 ± 0.34	0.00	1.20 ± 0.26	0.00
	-20.0	2.86 ± 1.05	0.63	2.99 ± 1.06	0.71	2.54 ± 1.08	0.50	2.22 ± 1.12	0.42	1.97 ± 1.02	0.29	1.70 ± 0.96	0.17
	-10.0	3.46 ± 1.07	0.88	3.22 ± 0.92	0.83	2.81 ± 0.92	0.71	2.38 ± 1.17	0.42	2.04 ± 0.95	0.33	1.47 ± 0.61	0.04
	-0.0	3.45 ± 1.01	0.88	3.55 ± 1.01	0.83	3.20 ± 1.06	0.71	2.85 ± 0.92	0.71	2.27 ± 1.11	0.46	1.57 ± 0.82	0.13
	+0.0	3.97 ± 0.68	1.00	3.82 ± 0.69	0.96	3.30 ± 0.97	0.71	2.83 ± 1.02	0.75	2.31 ± 1.22	0.42	1.90 ± 0.92	0.25
	+10.0	3.71 ± 0.81	1.00	3.43 ± 0.76	0.96	2.77 ± 0.95	0.63	2.20 ± 1.12	0.38	1.44 ± 0.41	0.17	1.43 ± 0.51	0.08
	+20.0	3.09 ± 0.93	0.88	2.96 ± 0.77	0.79	2.54 ± 1.02	0.58	1.83 ± 0.75	0.25	1.47 ± 0.61	0.08	1.45 ± 0.65	0.04
	+30.0	2.74 ± 1.05	0.71	2.64 ± 1.00	0.63	2.43 ± 0.96	0.42	1.70 ± 0.71	0.21	1.70 ± 0.78	0.17	1.25 ± 0.38	0.08
	+40.0	2.33 ± 1.10	0.42	2.37 ± 0.95	0.50	2.06 ± 0.95	0.29	1.64 ± 0.60	0.17	1.36 ± 0.40	0.04	1.39 ± 0.31	0.08
	+50.0	1.88 ± 0.93	0.17	1.78 ± 0.90	0.25	1.73 ± 0.84	0.21	1.52 ± 0.61	0.13	1.28 ± 0.38	0.04	1.41 ± 0.65	0.13

Note. $N = 6$. For reasons of completeness, the sample's success rate is listed separately for every single experimental condition of COBUS2 (stimulus size, stimulus position, and frame rate); however, the psychometric function in Section 4.3.2 was calculated by pooling the whole data set of CAT2. FR = frame rate; SP = stimulus position.

TABLE F.4: Sample's CBU scores ($MN \pm SD$) and success rates (SUC) for pursuit eye movement with a velocity of 36.0 deg/s (CAT3) under variation of stimulus size and stimulus position for a frame rate presentation of 30.0 and 60.0 Hz during COBUS2.

FR in [Hz]	SP in [deg]	Stimulus Size in [deg]											
		1.0		2.0		3.0		4.0		5.0		6.0	
		CBU	SUC	CBU	SUC	CBU	SUC	CBU	SUC	CBU	SUC	CBU	SUC
30.0	-50.0	1.32 ± 0.54	0.00	1.31 ± 0.50	0.00	1.29 ± 0.47	0.00	1.35 ± 0.69	0.08	1.26 ± 0.54	0.04	1.37 ± 0.65	0.04
	-40.0	1.38 ± 0.56	0.08	1.62 ± 0.84	0.08	1.79 ± 0.97	0.17	1.72 ± 0.86	0.17	1.62 ± 0.86	0.17	1.88 ± 0.94	0.21
	-30.0	2.04 ± 0.88	0.38	2.29 ± 1.09	0.42	2.03 ± 0.84	0.33	2.12 ± 0.96	0.50	2.17 ± 0.87	0.50	2.44 ± 1.12	0.58
	-20.0	2.75 ± 0.95	0.67	2.90 ± 1.04	0.79	2.85 ± 1.02	0.71	3.13 ± 0.85	0.83	2.83 ± 0.91	0.75	2.97 ± 1.16	0.83
	-10.0	3.39 ± 0.98	0.92	3.33 ± 1.06	0.92	3.24 ± 0.85	0.92	3.25 ± 0.88	0.92	3.26 ± 1.03	0.88	3.12 ± 0.85	0.88
	-0.0	3.45 ± 0.90	0.88	3.52 ± 0.90	0.96	3.63 ± 0.77	0.96	3.53 ± 0.67	0.92	3.51 ± 0.92	0.92	3.47 ± 0.99	0.96
	+0.0	3.73 ± 0.70	0.96	3.55 ± 0.57	0.92	3.53 ± 0.57	0.92	3.61 ± 0.61	0.96	3.55 ± 0.80	0.92	3.64 ± 0.78	0.96
	+10.0	3.09 ± 0.71	0.75	3.26 ± 0.67	0.83	3.31 ± 0.66	0.92	2.97 ± 0.91	0.79	2.97 ± 0.84	0.75	2.99 ± 1.00	0.79
	+20.0	2.65 ± 0.76	0.71	2.65 ± 0.76	0.63	2.76 ± 0.84	0.75	2.75 ± 0.62	0.67	2.86 ± 0.88	0.67	2.78 ± 1.01	0.71
	+30.0	2.39 ± 0.82	0.50	2.48 ± 0.76	0.63	2.76 ± 0.81	0.63	2.65 ± 0.84	0.63	2.71 ± 0.76	0.71	2.63 ± 0.78	0.63
	+40.0	1.79 ± 0.66	0.21	2.00 ± 0.68	0.21	2.31 ± 0.69	0.42	2.29 ± 0.79	0.42	2.06 ± 0.78	0.33	2.16 ± 0.71	0.38
	+50.0	1.43 ± 0.46	0.00	1.56 ± 0.57	0.08	1.63 ± 0.60	0.08	1.51 ± 0.48	0.00	1.65 ± 0.68	0.08	1.66 ± 0.53	0.17
60.0	-50.0	1.17 ± 0.34	0.04	1.26 ± 0.49	0.04	1.23 ± 0.41	0.00	1.23 ± 0.35	0.00	1.27 ± 0.48	0.04	1.20 ± 0.45	0.04
	-40.0	1.20 ± 0.26	0.00	1.33 ± 0.46	0.00	1.39 ± 0.53	0.04	1.46 ± 0.76	0.08	1.45 ± 0.64	0.13	1.34 ± 0.67	0.04
	-30.0	1.56 ± 0.73	0.04	1.75 ± 0.90	0.13	1.91 ± 0.89	0.21	1.75 ± 0.78	0.13	1.85 ± 0.94	0.21	1.69 ± 1.00	0.17
	-20.0	2.23 ± 1.10	0.42	2.13 ± 1.00	0.42	2.21 ± 1.00	0.33	2.06 ± 1.00	0.42	2.33 ± 1.10	0.50	2.03 ± 0.91	0.33
	-10.0	2.78 ± 1.03	0.54	2.44 ± 0.98	0.54	2.47 ± 1.04	0.63	2.32 ± 0.95	0.54	2.21 ± 0.96	0.38	2.15 ± 0.89	0.33
	-0.0	2.90 ± 1.12	0.63	2.45 ± 0.99	0.46	2.76 ± 1.09	0.67	2.68 ± 1.10	0.50	2.50 ± 0.98	0.50	2.33 ± 1.07	0.50
	+0.0	2.76 ± 0.90	0.63	2.65 ± 0.80	0.46	2.64 ± 0.88	0.58	2.45 ± 0.79	0.42	2.26 ± 0.76	0.46	2.41 ± 0.77	0.42
	+10.0	2.17 ± 0.70	0.42	2.26 ± 0.84	0.46	2.15 ± 0.90	0.29	1.94 ± 0.67	0.33	2.18 ± 0.89	0.38	1.95 ± 0.83	0.38
	+20.0	1.89 ± 0.76	0.21	1.77 ± 0.73	0.17	1.72 ± 0.51	0.04	1.76 ± 0.59	0.13	1.72 ± 0.66	0.13	1.83 ± 0.81	0.25
	+30.0	1.83 ± 0.76	0.21	1.53 ± 0.54	0.00	1.60 ± 0.60	0.13	1.61 ± 0.56	0.08	1.53 ± 0.39	0.08	1.48 ± 0.38	0.08
	+40.0	1.44 ± 0.47	0.00	1.58 ± 0.65	0.13	1.47 ± 0.37	0.00	1.43 ± 0.41	0.00	1.30 ± 0.36	0.00	1.42 ± 0.45	0.00
	+50.0	1.30 ± 0.41	0.00	1.29 ± 0.35	0.00	1.32 ± 0.36	0.00	1.30 ± 0.33	0.00	1.18 ± 0.26	0.00	1.29 ± 0.33	0.04

Note. $N = 6$. For reasons of completeness, the sample's success rate is listed separately for every single experimental condition of COBUS2 (stimulus size, stimulus position, and frame rate); however, the psychometric function in Section 4.3.2 was calculated by pooling the whole data set of CAT3. FR = frame rate; SP = stimulus position.

TABLE F.5: Statistical analysis of CBU score differences for investigated luminance levels on basis of a two-way repeated measures ANOVA with two within-subjects factors (luminance level and frame rate) referring to the execution of saccadic eye movement with a path length of 3.6° (CAT2) during COBUS1.

Pre-Testing [a]		**Main-Testing** [b]							
Mauchly's Test [c]	**Within-Sub Effects** [d]	**Global Test (ME)** [e]	**Post Hoc Test** [f]						
			FR in [Hz]	**LL in [cd/m²]**	**df**	**error df**	**F**	**p**	**ηp²**
.000 / .352	.609	.116	30.0	10.0 / 80.0	—	—	—	—	—
				10.0 / 157.0	—	—	—	—	—
				80.0 / 157.0	—	—	—	—	—
			60.0	10.0 / 80.0	—	—	—	—	—
				10.0 / 157.0	—	—	—	—	—
				80.0 / 157.0	—	—	—	—	—
			90.0	10.0 / 80.0	—	—	—	—	—
				10.0 / 157.0	—	—	—	—	—
				80.0 / 157.0	—	—	—	—	—
			120.0	10.0 / 80.0	—	—	—	—	—
				10.0 / 157.0	—	—	—	—	—
				80.0 / 157.0	—	—	—	—	—
			150.0	10.0 / 80.0	—	—	—	—	—
				10.0 / 157.0	—	—	—	—	—
				80.0 / 157.0	—	—	—	—	—
			180.0	10.0 / 80.0	—	—	—	—	—
				10.0 / 157.0	—	—	—	—	—
				80.0 / 157.0	—	—	—	—	—
			210.0	10.0 / 80.0	—	—	—	—	—
				10.0 / 157.0	—	—	—	—	—
				80.0 / 157.0	—	—	—	—	—
			240.0	10.0 / 80.0	—	—	—	—	—
				10.0 / 157.0	—	—	—	—	—
				80.0 / 157.0	—	—	—	—	—
			300.0	10.0 / 80.0	—	—	—	—	—
				10.0 / 157.0	—	—	—	—	—
				80.0 / 157.0	—	—	—	—	—
			360.0	10.0 / 80.0	—	—	—	—	—
				10.0 / 157.0	—	—	—	—	—
				80.0 / 157.0	—	—	—	—	—
			420.0	10.0 / 80.0	—	—	—	—	—
				10.0 / 157.0	—	—	—	—	—
				80.0 / 157.0	—	—	—	—	—

Note. $N = 30$. Section 4.2.9 offers a detailed description of the applied statistical test procedure. FR = frame rate; LL = luminance level.
[a] Pre-testing for interaction between independent variables (frame rate and luminance level).
[b] Main-testing for differences between groups of luminance levels.
[c] Mauchly's Test of Sphericity (Significance/Greenhouse-Geisser).
[d] Test of Within-Subjects Effects for independent variables (frame rate and luminance level).
[e] Application of Main Effects (ME) interpretation since no interaction between independent variables (frame rate and luminance level) identified.
[f] Adjusted Bonferroni executed as Post Hoc Test (no further adjustment of alpha error necessary), pairwise comparison characterized by degrees of freedom (*df*), degrees of freedom for error (*error df*), F-Ratio (*F*), significance level (*p*), and the Partial Eta Squared (ηp^2).

TABLE F.6: Statistical analysis of CBU score differences for investigated luminance levels on basis of a two-way repeated measures ANOVA with two within-subjects factors (luminance level and frame rate) referring to the execution of saccadic eye movement with a path length of 9.0° (CAT2) during COBUS1.

Pre-Testing [a]		**Main-Testing** [b]							
Mauchly's Test [c]	**Within-Sub Effects** [d]	**Global Test (SME)** [e]	**Post Hoc Test** [f]						
			FR in [Hz]	**LL in [cd/m²]**	**df**	**error df**	**F**	**p**	**ηp²**
.043 / .560	.005	.253	30.0	10.0 / 80.0	—	—	—	—	—
				10.0 / 157.0	—	—	—	—	—
				80.0 / 157.0	—	—	—	—	—
		.031	60.0	10.0 / 80.0	2.000	28.000	3.956	.024	.220
				10.0 / 157.0	—	—	—	—	—
				80.0 / 157.0	—	—	—	—	—
		.518	90.0	10.0 / 80.0	—	—	—	—	—
				10.0 / 157.0	—	—	—	—	—
				80.0 / 157.0	—	—	—	—	—
		.003	120.0	10.0 / 80.0	2.000	28.000	7.035	.006	.334
				10.0 / 157.0	2.000	28.000	7.035	.031	.334
				80.0 / 157.0	—	—	—	—	—
		.143	150.0	10.0 / 80.0	—	—	—	—	—
				10.0 / 157.0	—	—	—	—	—
				80.0 / 157.0	—	—	—	—	—
		.139	180.0	10.0 / 80.0	—	—	—	—	—
				10.0 / 157.0	—	—	—	—	—
				80.0 / 157.0	—	—	—	—	—
		.086	210.0	10.0 / 80.0	—	—	—	—	—
				10.0 / 157.0	—	—	—	—	—
				80.0 / 157.0	—	—	—	—	—
		.144	240.0	10.0 / 80.0	—	—	—	—	—
				10.0 / 157.0	—	—	—	—	—
				80.0 / 157.0	—	—	—	—	—
		.182	300.0	10.0 / 80.0	—	—	—	—	—
				10.0 / 157.0	—	—	—	—	—
				80.0 / 157.0	—	—	—	—	—
		.348	360.0	10.0 / 80.0	—	—	—	—	—
				10.0 / 157.0	—	—	—	—	—
				80.0 / 157.0	—	—	—	—	—
		.062	420.0	10.0 / 80.0	—	—	—	—	—
				10.0 / 157.0	—	—	—	—	—
				80.0 / 157.0	—	—	—	—	—

Note. $N = 30$. Section 4.2.9 offers a detailed description of the applied statistical test procedure. FR = frame rate; LL = luminance level.
[a] Pre-testing for interaction between independent variables (frame rate and luminance level).
[b] Main-testing for differences between groups of luminance levels.
[c] Mauchly's Test of Sphericity (Significance/Greenhouse-Geisser).
[d] Test of Within-Subjects Effects for independent variables (frame rate and luminance level).
[e] Application of Simple Main Effects (SME) interpretation since interaction between independent variables (frame rate and luminance level) was identified.
[f] Adjusted Bonferroni executed as Post Hoc Test (no further adjustment of alpha error necessary), pairwise comparison characterized by degrees of freedom (*df*), degrees of freedom for error (*error df*), F-Ratio (*F*), significance level (*p*), and the Partial Eta Squared (ηp^2).

TABLE F.7: Statistical analysis of CBU score differences for investigated luminance levels on basis of a two-way repeated measures ANOVA with two within-subjects factors (luminance level and frame rate) referring to the execution of saccadic eye movement with a path length of 14.3° (CAT2) during COBUS1.

Pre-Testing [a]		**Main-Testing** [b]							
Mauchly's Test [c]	**Within-Sub Effects** [d]	**Global Test (SME)** [e]	**Post Hoc Test** [f]						
			FR in [Hz]	**LL in [cd/m²]**	**df**	**error df**	**F**	**p**	**ηp²**
.000 / .492	.003	.234	30.0	10.0 / 80.0	—	—	—	—	—
				10.0 / 157.0	—	—	—	—	—
				80.0 / 157.0	—	—	—	—	—
		.350	60.0	10.0 / 80.0	—	—	—	—	—
				10.0 / 157.0	—	—	—	—	—
				80.0 / 157.0	—	—	—	—	—
		.012	90.0	10.0 / 80.0	2.000	28.000	5.201	.047	.271
				10.0 / 157.0	2.000	28.000	5.201	.010	.271
				80.0 / 157.0	—	—	—	—	—
		.001	120.0	10.0 / 80.0	2.000	28.000	8.963	.009	.390
				10.0 / 157.0	2.000	28.000	8.963	.001	.390
				80.0 / 157.0	—	—	—	—	—
		.098	150.0	10.0 / 80.0	—	—	—	—	—
				10.0 / 157.0	—	—	—	—	—
				80.0 / 157.0	—	—	—	—	—
		.873	180.0	10.0 / 80.0	—	—	—	—	—
				10.0 / 157.0	—	—	—	—	—
				80.0 / 157.0	—	—	—	—	—
		.981	210.0	10.0 / 80.0	—	—	—	—	—
				10.0 / 157.0	—	—	—	—	—
				80.0 / 157.0	—	—	—	—	—
		.586	240.0	10.0 / 80.0	—	—	—	—	—
				10.0 / 157.0	—	—	—	—	—
				80.0 / 157.0	—	—	—	—	—
		.126	300.0	10.0 / 80.0	—	—	—	—	—
				10.0 / 157.0	—	—	—	—	—
				80.0 / 157.0	—	—	—	—	—
		.241	360.0	10.0 / 80.0	—	—	—	—	—
				10.0 / 157.0	—	—	—	—	—
				80.0 / 157.0	—	—	—	—	—
		.552	420.0	10.0 / 80.0	—	—	—	—	—
				10.0 / 157.0	—	—	—	—	—
				80.0 / 157.0	—	—	—	—	—

Note. $N = 30$. Section 4.2.9 offers a detailed description of the applied statistical test procedure. FR = frame rate; LL = luminance level.
[a] Pre-testing for interaction between independent variables (frame rate and luminance level).
[b] Main-testing for differences between groups of luminance levels.
[c] Mauchly's Test of Sphericity (Significance/Greenhouse-Geisser).
[d] Test of Within-Subjects Effects for independent variables (frame rate and luminance level).
[e] Application of Simple Main Effects (SME) interpretation since interaction between independent variables (frame rate and luminance level) was identified.
[f] Adjusted Bonferroni executed as Post Hoc Test (no further adjustment of alpha error necessary), pairwise comparison characterized by degrees of freedom (*df*), degrees of freedom for error (*error df*), F-Ratio (*F*), significance level (*p*), and the Partial Eta Squared (ηp^2).

TABLE F.8: Statistical analysis of CBU score differences for investigated luminance levels on basis of a two-way repeated measures ANOVA with two within-subjects factors (luminance level and frame rate) referring to the execution of saccadic eye movement with a path length of 21.3° (CAT2) during COBUS1.

Pre-Testing [a]		**Main-Testing** [b]							
Mauchly's Test [c]	**Within-Sub Effects** [d]	**Global Test (SME)** [e]	**Post Hoc Test** [f]						
			FR in [Hz]	**LL in [cd/m²]**	**df**	**error df**	**F**	**p**	**ηp²**
.002 / .516	.048	.699	30.0	10.0 / 80.0	—	—	—	—	—
				10.0 / 157.0	—	—	—	—	—
				80.0 / 157.0	—	—	—	—	—
		.002	60.0	10.0 / 80.0	2.000	28.000	7.546	.001	.350
				10.0 / 157.0	2.000	28.000	7.546	.028	.350
				80.0 / 157.0	—	—	—	—	—
		.014	90.0	10.0 / 80.0	—	—	—	—	—
				10.0 / 157.0	2.000	28.000	4.947	.011	.261
				80.0 / 157.0	—	—	—	—	—
		.001	120.0	10.0 / 80.0	2.000	28.000	9.087	.002	.394
				10.0 / 157.0	2.000	28.000	9.087	.003	.394
				80.0 / 157.0	—	—	—	—	—
		.034	150.0	10.0 / 80.0	2.000	28.000	3.834	.044	.215
				10.0 / 157.0	—	—	—	—	—
				80.0 / 157.0	—	—	—	—	—
		.106	180.0	10.0 / 80.0	—	—	—	—	—
				10.0 / 157.0	—	—	—	—	—
				80.0 / 157.0	—	—	—	—	—
		.048	210.0	10.0 / 80.0	—	—	—	—	—
				10.0 / 157.0	—	—	—	—	—
				80.0 / 157.0	—	—	—	—	—
		.388	240.0	10.0 / 80.0	—	—	—	—	—
				10.0 / 157.0	—	—	—	—	—
				80.0 / 157.0	—	—	—	—	—
		.722	300.0	10.0 / 80.0	—	—	—	—	—
				10.0 / 157.0	—	—	—	—	—
				80.0 / 157.0	—	—	—	—	—
		.581	360.0	10.0 / 80.0	—	—	—	—	—
				10.0 / 157.0	—	—	—	—	—
				80.0 / 157.0	—	—	—	—	—
		.120	420.0	10.0 / 80.0	—	—	—	—	—
				10.0 / 157.0	—	—	—	—	—
				80.0 / 157.0	—	—	—	—	—

Note. $N = 30$. Section 4.2.9 offers a detailed description of the applied statistical test procedure. FR = frame rate; LL = luminance level.
[a] Pre-testing for interaction between independent variables (frame rate and luminance level).
[b] Main-testing for differences between groups of luminance levels.
[c] Mauchly's Test of Sphericity (Significance/Greenhouse-Geisser).
[d] Test of Within-Subjects Effects for independent variables (frame rate and luminance level).
[e] Application of Simple Main Effects (SME) interpretation since interaction between independent variables (frame rate and luminance level) was identified.
[f] Adjusted Bonferroni executed as Post Hoc Test (no further adjustment of alpha error necessary), pairwise comparison characterized by degrees of freedom (*df*), degrees of freedom for error (*error df*), F-Ratio (*F*), significance level (*p*), and the Partial Eta Squared (ηp^2).

TABLE F.9: Statistical analysis of CBU score differences for investigated luminance levels on basis of a two-way repeated measures ANOVA with two within-subjects factors (luminance level and frame rate) referring to the execution of saccadic eye movement with a path length of 28.2° (CAT2) during COBUS1.

Pre-Testing [a]		**Main-Testing** [b]							
Mauchly's Test [c]	**Within-Sub Effects** [d]	**Global Test (SME)** [e]	**Post Hoc Test** [f]						
			FR in [Hz]	**LL in [cd/m²]**	**df**	**error df**	**F**	**p**	**ηp²**
.000 / .466	.010	.287	30.0	10.0 / 80.0	—	—	—	—	—
				10.0 / 157.0	—	—	—	—	—
				80.0 / 157.0	—	—	—	—	—
		.586	60.0	10.0 / 80.0	—	—	—	—	—
				10.0 / 157.0	—	—	—	—	—
				80.0 / 157.0	—	—	—	—	—
		.002	90.0	10.0 / 80.0	2.000	28.000	7.703	.002	.355
				10.0 / 157.0	2.000	28.000	7.703	.002	.355
				80.0 / 157.0	—	—	—	—	—
		.000	120.0	10.0 / 80.0	2.000	28.000	10.116	.000	.419
				10.0 / 157.0	2.000	28.000	10.116	.010	.419
				80.0 / 157.0	—	—	—	—	—
		.040	150.0	10.0 / 80.0	—	—	—	—	—
				10.0 / 157.0	2.000	28.000	3.607	.038	.205
				80.0 / 157.0	—	—	—	—	—
		.079	180.0	10.0 / 80.0	—	—	—	—	—
				10.0 / 157.0	—	—	—	—	—
				80.0 / 157.0	—	—	—	—	—
		.385	210.0	10.0 / 80.0	—	—	—	—	—
				10.0 / 157.0	—	—	—	—	—
				80.0 / 157.0	—	—	—	—	—
		.572	240.0	10.0 / 80.0	—	—	—	—	—
				10.0 / 157.0	—	—	—	—	—
				80.0 / 157.0	—	—	—	—	—
		.077	300.0	10.0 / 80.0	—	—	—	—	—
				10.0 / 157.0	—	—	—	—	—
				80.0 / 157.0	—	—	—	—	—
		.022	360.0	10.0 / 80.0	—	—	—	—	—
				10.0 / 157.0	—	—	—	—	—
				80.0 / 157.0	2.000	28.000	4.412	.023	.240
		.586	420.0	10.0 / 80.0	—	—	—	—	—
				10.0 / 157.0	—	—	—	—	—
				80.0 / 157.0	—	—	—	—	—

Note. $N = 30$. Section 4.2.9 offers a detailed description of the applied statistical test procedure. FR = frame rate; LL = luminance level.
[a] Pre-testing for interaction between independent variables (frame rate and luminance level).
[b] Main-testing for differences between groups of luminance levels.
[c] Mauchly's Test of Sphericity (Significance/Greenhouse-Geisser).
[d] Test of Within-Subjects Effects for independent variables (frame rate and luminance level).
[e] Application of Simple Main Effects (SME) interpretation since interaction between independent variables (frame rate and luminance level) was identified.
[f] Adjusted Bonferroni executed as Post Hoc Test (no further adjustment of alpha error necessary), pairwise comparison characterized by degrees of freedom (*df*), degrees of freedom for error (*error df*), F-Ratio (*F*), significance level (*p*), and the Partial Eta Squared (ηp^2).

TABLE F.10: Statistical analysis of CBU score differences for investigated luminance levels on basis of a two-way repeated measures ANOVA with two within-subjects factors (luminance level and frame rate) referring to the execution of pursuit eye movement with a movement velocity of 18.0 deg/s (CAT3) during COBUS1.

Pre-Testing [a]		**Main-Testing** [b]							
Mauchly's Test [c]	**Within-Sub Effects** [d]	**Global Test (SME)** [e]	**Post Hoc Test** [f]						
			FR in [Hz]	**LL in [cd/m²]**	**df**	**error df**	**F**	**p**	**ηp²**
.000 / .471	.000	.045	30.0	10.0 / 80.0	—	—	—	—	—
				10.0 / 157.0	—	—	—	—	—
				80.0 / 157.0	—	—	—	—	—
		.031	60.0	10.0 / 80.0	—	—	—	—	—
				10.0 / 157.0	2.000	28.000	3.943	.023	.220
				80.0 / 157.0	—	—	—	—	—
		.000	90.0	10.0 / 80.0	2.000	28.000	16.197	.000	.536
				10.0 / 157.0	2.000	28.000	16.197	.000	.536
				80.0 / 157.0	—	—	—	—	—
		.003	120.0	10.0 / 80.0	2.000	28.000	6.981	.016	.333
				10.0 / 157.0	2.000	28.000	6.981	.015	.333
				80.0 / 157.0	—	—	—	—	—
		.757	150.0	10.0 / 80.0	—	—	—	—	—
				10.0 / 157.0	—	—	—	—	—
				80.0 / 157.0	—	—	—	—	—
		.720	180.0	10.0 / 80.0	—	—	—	—	—
				10.0 / 157.0	—	—	—	—	—
				80.0 / 157.0	—	—	—	—	—
		.290	210.0	10.0 / 80.0	—	—	—	—	—
				10.0 / 157.0	—	—	—	—	—
				80.0 / 157.0	—	—	—	—	—
		.407	240.0	10.0 / 80.0	—	—	—	—	—
				10.0 / 157.0	—	—	—	—	—
				80.0 / 157.0	—	—	—	—	—
		.914	300.0	10.0 / 80.0	—	—	—	—	—
				10.0 / 157.0	—	—	—	—	—
				80.0 / 157.0	—	—	—	—	—
		.851	360.0	10.0 / 80.0	—	—	—	—	—
				10.0 / 157.0	—	—	—	—	—
				80.0 / 157.0	—	—	—	—	—
		.957	420.0	10.0 / 80.0	—	—	—	—	—
				10.0 / 157.0	—	—	—	—	—
				80.0 / 157.0	—	—	—	—	—

Note. $N = 30$. Section 4.2.9 offers a detailed description of the applied statistical test procedure. FR = frame rate; LL = luminance level.
[a] Pre-testing for interaction between independent variables (frame rate and luminance level).
[b] Main-testing for differences between groups of luminance levels.
[c] Mauchly's Test of Sphericity (Significance/Greenhouse-Geisser).
[d] Test of Within-Subjects Effects for independent variables (frame rate and luminance level).
[e] Application of Simple Main Effects (SME) interpretation since interaction between independent variables (frame rate and luminance level) was identified.
[f] Adjusted Bonferroni executed as Post Hoc Test (no further adjustment of alpha error necessary), pairwise comparison characterized by degrees of freedom (*df*), degrees of freedom for error (*error df*), F-Ratio (*F*), significance level (*p*), and the Partial Eta Squared (ηp^2).

TABLE F.11: Statistical analysis of CBU score differences for investigated luminance levels on basis of a two-way repeated measures ANOVA with two within-subjects factors (luminance level and frame rate) referring to the execution of pursuit eye movement with a movement velocity of 36.0 deg/s (CAT3) during COBUS1.

Pre-Testing [a]		**Main-Testing** [b]						
Mauchly's Test [c]	**Within-Sub Effects** [d]	**Global Test (ME)** [e]	**Post Hoc Test** [f]					
			FR in [Hz]	**LL in [cd/m^2]**	**df**	**error df**	**F**	**p**	**ηp^2**
.004 / .523	.097	.000	30.0	10.0 / 80.0	2.000	58.000	11.697	.010	.287
				10.0 / 157.0	2.000	58.000	11.697	.000	.287
				80.0 / 157.0	—	—	—	—	—
			60.0	10.0 / 80.0	2.000	58.000	11.697	.010	.287
				10.0 / 157.0	2.000	58.000	11.697	.000	.287
				80.0 / 157.0	—	—	—	—	—
			90.0	10.0 / 80.0	2.000	58.000	11.697	.010	.287
				10.0 / 157.0	2.000	58.000	11.697	.000	.287
				80.0 / 157.0	—	—	—	—	—
			120.0	10.0 / 80.0	2.000	58.000	11.697	.010	.287
				10.0 / 157.0	2.000	58.000	11.697	.000	.287
				80.0 / 157.0	—	—	—	—	—
			150.0	10.0 / 80.0	2.000	58.000	11.697	.010	.287
				10.0 / 157.0	2.000	58.000	11.697	.000	.287
				80.0 / 157.0	—	—	—	—	—
			180.0	10.0 / 80.0	2.000	58.000	11.697	.010	.287
				10.0 / 157.0	2.000	58.000	11.697	.000	.287
				80.0 / 157.0	—	—	—	—	—
			210.0	10.0 / 80.0	2.000	58.000	11.697	.010	.287
				10.0 / 157.0	2.000	58.000	11.697	.000	.287
				80.0 / 157.0	—	—	—	—	—
			240.0	10.0 / 80.0	2.000	58.000	11.697	.010	.287
				10.0 / 157.0	2.000	58.000	11.697	.000	.287
				80.0 / 157.0	—	—	—	—	—
			300.0	10.0 / 80.0	2.000	58.000	11.697	.010	.287
				10.0 / 157.0	2.000	58.000	11.697	.000	.287
				80.0 / 157.0	—	—	—	—	—
			360.0	10.0 / 80.0	2.000	58.000	11.697	.010	.287
				10.0 / 157.0	2.000	58.000	11.697	.000	.287
				80.0 / 157.0	—	—	—	—	—
			420.0	10.0 / 80.0	2.000	58.000	11.697	.010	.287
				10.0 / 157.0	2.000	58.000	11.697	.000	.287
				80.0 / 157.0	—	—	—	—	—

Note. $N = 30$. Section 4.2.9 offers a detailed description of the applied statistical test procedure. FR = frame rate; LL = luminance level.
[a] Pre-testing for interaction between independent variables (frame rate and luminance level).
[b] Main-testing for differences between groups of luminance levels.
[c] Mauchly's Test of Sphericity (Significance/Greenhouse-Geisser).
[d] Test of Within-Subjects Effects for independent variables (frame rate and luminance level).
[e] Application of Main Effects (ME) interpretation since no interaction between independent variables (frame rate and luminance level) identified.
[f] Adjusted Bonferroni executed as Post Hoc Test (no further adjustment of alpha error necessary), pairwise comparison characterized by degrees of freedom (*df*), degrees of freedom for error (*error df*), F-Ratio (*F*), significance level (*p*), and the Partial Eta Squared (ηp^2).

TABLE F.12: Statistical analysis of CBU score differences for investigated luminance levels on basis of a two-way repeated measures ANOVA with two within-subjects factors (luminance level and frame rate) referring to the execution of pursuit eye movement with a movement velocity of 54.0 deg/s (CAT3) during COBUS1.

Pre-Testing [a]		**Main-Testing** [b]							
Mauchly's Test [c]	**Within-Sub Effects** [d]	**Global Test (SME)** [e]	**Post Hoc Test** [f]						
			FR in [Hz]	**LL in [cd/m^2]**	**df**	**error df**	**F**	**p**	**ηp^2**
.047 / .552	.011	.654	30.0	10.0 / 80.0	—	—	—	—	—
				10.0 / 157.0	—	—	—	—	—
				80.0 / 157.0	—	—	—	—	—
		.085	60.0	10.0 / 80.0	—	—	—	—	—
				10.0 / 157.0	—	—	—	—	—
				80.0 / 157.0	—	—	—	—	—
		.093	90.0	10.0 / 80.0	—	—	—	—	—
				10.0 / 157.0	—	—	—	—	—
				80.0 / 157.0	—	—	—	—	—
		.133	120.0	10.0 / 80.0	—	—	—	—	—
				10.0 / 157.0	—	—	—	—	—
				80.0 / 157.0	—	—	—	—	—
		.000	150.0	10.0 / 80.0	2.000	28.000	12.364	.001	.469
				10.0 / 157.0	2.000	28.000	12.364	.000	.469
				80.0 / 157.0	—	—	—	—	—
		.037	180.0	10.0 / 80.0	2.000	28.000	3.730	.035	.210
				10.0 / 157.0	—	—	—	—	—
				80.0 / 157.0	—	—	—	—	—
		.954	210.0	10.0 / 80.0	—	—	—	—	—
				10.0 / 157.0	—	—	—	—	—
				80.0 / 157.0	—	—	—	—	—
		.114	240.0	10.0 / 80.0	—	—	—	—	—
				10.0 / 157.0	—	—	—	—	—
				80.0 / 157.0	—	—	—	—	—
		.073	300.0	10.0 / 80.0	—	—	—	—	—
				10.0 / 157.0	—	—	—	—	—
				80.0 / 157.0	—	—	—	—	—
		.125	360.0	10.0 / 80.0	—	—	—	—	—
				10.0 / 157.0	—	—	—	—	—
				80.0 / 157.0	—	—	—	—	—
		.273	420.0	10.0 / 80.0	—	—	—	—	—
				10.0 / 157.0	—	—	—	—	—
				80.0 / 157.0	—	—	—	—	—

Note. $N = 30$. Section 4.2.9 offers a detailed description of the applied statistical test procedure. FR = frame rate; LL = luminance level.
[a] Pre-testing for interaction between independent variables (frame rate and luminance level).
[b] Main-testing for differences between groups of luminance levels.
[c] Mauchly's Test of Sphericity (Significance/Greenhouse-Geisser).
[d] Test of Within-Subjects Effects for independent variables (frame rate and luminance level).
[e] Application of Simple Main Effects (SME) interpretation since interaction between independent variables (frame rate and luminance level) was identified.
[f] Adjusted Bonferroni executed as Post Hoc Test (no further adjustment of alpha error necessary), pairwise comparison characterized by degrees of freedom (*df*), degrees of freedom for error (*error df*), F-Ratio (*F*), significance level (*p*), and the Partial Eta Squared (ηp^2).

Appendix G

Conversion Tables

The positional arrangement of the main hardware components (projector and screen) and the participant during the COBUS series was determined under consideration of various aspects (e.g., focus range of the projector, required luminance level on the screen, field of view and pixel size for content creation):

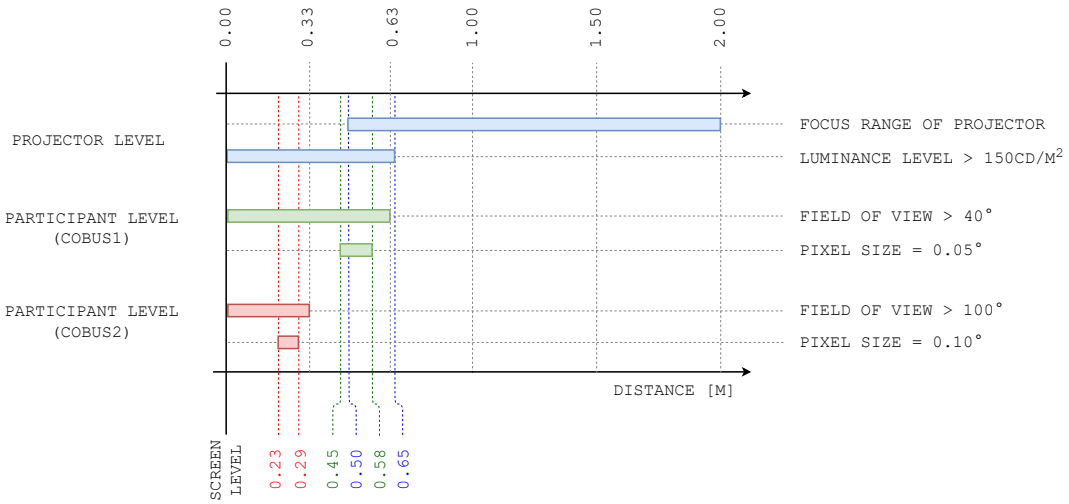

FIGURE G.1: Depth position of projector/participant with reference to screen position (COBUS).

[1] The projector's focus range is adjustable from 0.5 to 2.0 m (projector to screen, front projection) with a projection angle of about ±19.5° in horizontal direction and ±12.5° in vertical direction (see Table A.1).

[2] Doubling the projection distance between projector and screen leads to a reduction of light intensity to one fourth on the screen. The aim was to reach a maximum luminance level greater than 150 cd/m^2. A projection distance of 0.65 m results in a maximum luminance level that fulfills the required lighting conditions (approx. 157 cd/m^2, see Appendix B.1). Larger projection distances shift the luminance level below the determined threshold.

[3] With regard to [1] and [2], the projection distance must lie between 0.50 and 0.65 m to fulfill both requirements (see dashed blue lines in Figure G.1).

[4] The fixed range of applicable projection distances defines the corresponding range of participant levels that assure the desired horizontal field of view for content creation. During COBUS1, the field of view had to be greater than 40°, at least 100° were required for COBUS2. Hence, the viewing distance between participant and screen could not exceed 0.63 m and 0.33 m for COBUS1 and COBUS2, respectively.

[5] Projection distance and viewing distance had to be matched to guarantee a horizontal pixel size of 0.05°/0.10° from the viewer point (COBUS1/COBUS2). With these pixel sizes, the desired integer content movement velocities could be presented without discrepancy (at least for the better part of the applied frame rates, see Table G.8). The corresponding viewing distances were calculated to guarantee the defined pixel sizes for projection distances from 0.50 to 0.65 m. The viewing distances reached from 0.45 to 0.58 m for COBUS1 and from 0.23 to 0.29 m for COBUS2 (see dashed green/red lines in Figure G.1). Within the defined ranges, one specific participant level corresponded to one specific projector level.

[6] Smaller pixel sizes would also allow integer movement velocities (e.g., 0.025° during COBUS1). As a positive effect, the lower limit of adjustable movement velocities would be shifted downwards and the graduation of applicable movement velocities would be finer (valid for the highest frame rate of the test range, determining the intersection of realizable movement velocities over the complete frame rate range would impact the range of valid movement velocities). For a fixed projection distance between 0.50 and 0.65 m, the viewing distance would have to be increased to realize a pixel size of 0.025°. This would violate the field of view requirement. The defined content of CAT2/CAT3 could not be realized. Larger pixel sizes would also guarantee integer movement velocities (e.g., 0.10° for COBUS1). Considering a projection distance between 0.50 and 0.65 m, the viewing distance would have to be reduced to realize a pixel size of 0.10°. This would have a positive effect on the available field of view. Nevertheless, the slowest content movement velocity (for the highest frame rate) would be shifted upwards and the graduation of the movement velocity range would be stretched. Therefore, it was reasonable to keep the pixel sizes for the COBUS series as stated under [5].

[7] Summing up, the projection distance could be varied between 0.50 and 0.65 m. Simultaneously, the participant had to be positioned in a distance to the screen between 0.45 to 0.58 m for COBUS1 and 0.23 to 0.29 m for COBUS2. To guarantee an accommodative demand during the COBUS series that did not overshoot the participant's accommodative capacity, the largest possible distances between projector/participant and screen were chosen. This reduced the risk of a lowered retinal image quality as a disturbing factor during CBU perception. The projection distance was set to 0.65 m and the viewing distance was determined at 0.58 m for COBUS1 and 0.29 m for COBUS2.

Based on the determined projection and viewing distances for the COBUS series, the Tables G.1 to G.7 list the content sizes and positions in [px] and [deg] for all single objects applied during the main sequences of COBUS1 and COBUS2.[1] Furthermore, the Tables G.8 to G.11 convert content movement velocities from [px/fr] to [deg/s] and vice versa for the applied frame rates during the COBUS series.

[1]The object positions in Tables G.1 to G.7 are listed only for the L2R movement paths as long as the R2L path has identical, horizontally mirrored end points (see START and STOP positions in tables). For position changes between the L2R and R2L path, the end point positions are listed separately (see STEP positions in tables). Regarding the vertical movement paths, the end point descriptions of the U2D paths are only complemented by the D2U path descriptions if both paths are more different than merely horizontally mirrored. Abbreviations in the content size/position tables: AP = adjustment point, DA = directional arrow, FT = fixation target, ST (UP/DOWN) = upper/lower CBU-provoking stimulus, ST (HOR/VER) = CBU-provoking stimulus (horizontally/vertically aligned rectangle), FIX = fixed position during presentation, START/STOP = start/stop position of linear movement path, STEP/RAMP = step/ramp or stop position of step-ramp movement path, SAC3.6 = saccade with 3.6° path length (exemplary), PEM18 = pursuit with velocity of 18.0 deg/s (exemplary), L2R/R2L = left-to-right/right-to-left movement direction, U2D/D2U = up-to-down/down-to-up movement direction, CW1 = content width of 1.0° (exemplary), CH3 = content height of 3.0° (exemplary), ECC50 = eccentricity of 50.0° (exemplary).

TABLE G.1: Content size/position for objects presented in the main sequences of the experimental categories CAT2 and CAT3 during COBUS1.

CAT	Object Characteristic		Object Dimension [a]		Horizontal Location [b]		Vertical Location [b]	
	Type	Specification	Size [px]	Size [deg]	Pos. [px]	Pos. [deg]	Pos. [px]	Pos. [deg]
2	AP	FIX	4×8	0.2×0.2	-2	0.000	+4	0.000
	DA	FIX, SAC3.6, L2R	20×20	1.0×0.5	-24	-0.700	+10	0.000
		FIX, SAC9.0, L2R	20×20	1.0×0.5	-60	-2.498	+10	0.000
		FIX, SAC14.4, L2R	20×20	1.0×0.5	-114	-5.186	+10	0.000
		FIX, SAC21.6, L2R	20×20	1.0×0.5	-186	-8.732	+10	0.000
		FIX, SAC28.8, L2R	20×20	1.0×0.5	-258	-12.212	+10	0.000
	ST (UP)	FIX	40×80	2.0×2.0	-20	0.000	+160	+2.998
	ST (DOWN)	FIX	40×80	2.0×2.0	-20	0.000	-80	-2.998
	FT	START, SAC3.6, L2R	20×40	1.0×1.0	-46	-1.799	+20	0.000
		STOP, SAC3.6, L2R	20×40	1.0×1.0	+26	1.799	+20	0.000
		START, SAC9.0, L2R	20×40	1.0×1.0	-100	-4.491	+20	0.000
		STOP, SAC9.0, L2R	20×40	1.0×1.0	+80	+4.491	+20	0.000
		START, SAC14.4, L2R	20×40	1.0×1.0	-154	-7.163	+20	0.000
		STOP, SAC14.4, L2R	20×40	1.0×1.0	+134	+7.163	+20	0.000
		START, SAC21.6, L2R	20×40	1.0×1.0	-226	-10.675	+20	0.000
		STOP, SAC21.6, L2R	20×40	1.0×1.0	+206	+10.675	+20	0.000
		START, SAC28.8, L2R	20×40	1.0×1.0	-298	-14.108	+20	0.000
		STOP, SAC28.8, L2R	20×40	1.0×1.0	+278	+14.108	+20	0.000
3	AP	FIX	4×8	0.2×0.2	-2	0.000	+4	0.000
	DA	FIX, L2R	20×20	1.0×0.5	-186	-8.7318	+10	0.000
	ST (UP)	START, L2R	40×80	2.0×2.0	-236	-10.675	+160	+2.998
		STOP, L2R	40×80	2.0×2.0	+196	+10.675	+160	+2.998
	ST (DOWN)	START, L2R	40×80	2.0×2.0	-236	-10.675	-80	-2.998
		STOP, L2R	40×80	2.0×2.0	+196	+10.675	-80	-2.998
	FT	START, L2R	20×40	1.0×1.0	-226	-10.675	+20	0.000
		STEP, PEM18, L2R	20×40	1.0×1.0	-298	-14.108	+20	0.000
		STEP, PEM36, L2R	20×40	1.0×1.0	-370	-17.441	+20	0.000
		STEP, PEM54, L2R	20×40	1.0×1.0	-442	-20.656	+20	0.000
		RAMP, L2R	20×40	1.0×1.0	+206	+10.675	+20	0.000
		START, R2L	20×40	1.0×1.0	+206	+10.675	+20	0.000
		STEP, PEM18, R2L	20×40	1.0×1.0	+278	+14.108	+20	0.000
		STEP, PEM36, R2L	20×40	1.0×1.0	+350	+17.441	+20	0.000
		STEP, PEM54, R2L	20×40	1.0×1.0	+422	+20.656	+20	0.000
		RAMP, R2L	20×40	1.0×1.0	-226	-10.675	+20	0.000

Note. See Figures 4.1 and 4.2 for exemplary visualization of mentioned objects.

[a] Object size (CW×CH) in [px] in horizontal and vertical direction (HOR×VER) is defined by the object's maximum dimension in horizontal and vertical direction. Object size (CW×CH) in [deg] in horizontal and vertical direction (HOR×VER) is defined by the object's maximum dimension in horizontal and vertical direction, angular object size is valid for a central display position of the object in horizontal and vertical direction in reference to the position of the adjustment point AP (horizontal/vertical center) as the observer's primary gaze position, coinciding with the central point of origin of the display unit's coordinate system (see red dashed lines in Figures 4.1 and 4.2, see also Appendix C.3 for further information on the center-to-periphery bias).

[b] Horizontal/vertical object position in [px] refers to the position of the left/upper edge of the rectangular box that frames the object at its horizontal and vertical edges (no horizontal or vertical box rotation), object position in [px] refers to the defined pixel numbering as illustrated in Figure C.1 (right-side graphic). Horizontal/vertical object position in [deg] refers to the horizontal/vertical center of the object, reference point is defined by the position of the adjustment point AP (horizontal/vertical center) as the observer's primary gaze position, coinciding with the central point of origin of the display unit's coordinate system (see red dashed lines in Figures 4.1 and 4.2).

TABLE G.2: Content size/position for objects presented in the main sequence of CAT2H with horizontal eye movement during COBUS2.

CAT	Object Characteristic		Object Dimension [a]		Horizontal Location [b]		Vertical Location [b]	
	Type	Specification	Size [px]	Size [deg]	Pos. [px]	Pos. [deg]	Pos. [px]	Pos. [deg]
2H	AP	FIX	2×4	0.2×0.2	+312	0.000	+2	0.000
	DA	FIX, L2R	10×10	1.0×0.5	+280	-3.296	+5	0.000
	ST (VER)	FIX, CW1, ECC50	10×192	1.0×9.6	-375	-50.007	+96	0.000
		FIX, CW2, ECC50	20×192	2.0×9.6	-380	-50.007	+96	0.000
		FIX, CW3, ECC50	30×192	3.0×9.6	-385	-50.007	+96	0.000
		FIX, CW4, ECC50	40×192	4.0×9.6	-390	-50.007	+96	0.000
		FIX, CW5, ECC50	50×192	5.0×9.6	-395	-50.007	+96	0.000
		FIX, CW6, ECC50	60×192	6.0×9.6	-400	-50.007	+96	0.000
		FIX, CW1, ECC40	10×192	1.0×9.6	-173	-40.014	+96	0.000
		FIX, CW2, ECC40	20×192	2.0×9.6	-178	-40.014	+96	0.000
		FIX, CW3, ECC40	30×192	3.0×9.6	-183	-40.014	+96	0.000
		FIX, CW4, ECC40	40×192	4.0×9.6	-188	-40.014	+96	0.000
		FIX, CW5, ECC40	50×192	5.0×9.6	-193	-40.014	+96	0.000
		FIX, CW6, ECC40	60×192	6.0×9.6	-198	-40.014	+96	0.000
		FIX, CW1, ECC30	10×192	1.0×9.6	-23	-30.015	+96	0.000
		FIX, CW2, ECC30	20×192	2.0×9.6	-28	-30.015	+96	0.000
		FIX, CW3, ECC30	30×192	3.0×9.6	-33	-30.015	+96	0.000
		FIX, CW4, ECC30	40×192	4.0×9.6	-38	-30.015	+96	0.000
		FIX, CW5, ECC30	50×192	5.0×9.6	-43	-30.015	+96	0.000
		FIX, CW6, ECC30	60×192	6.0×9.6	-48	-30.015	+96	0.000
		FIX, CW1, ECC20	10×192	1.0×9.6	+99	-20.041	+96	0.000
		FIX, CW2, ECC20	20×192	2.0×9.6	+94	-20.041	+96	0.000
		FIX, CW3, ECC20	30×192	3.0×9.6	+89	-20.041	+96	0.000
		FIX, CW4, ECC20	40×192	4.0×9.6	+84	-20.041	+96	0.000
		FIX, CW5, ECC20	50×192	5.0×9.6	+79	-20.041	+96	0.000
		FIX, CW6, ECC20	60×192	6.0×9.6	+74	-20.041	+96	0.000
		FIX, CW1, ECC10	10×192	1.0×9.6	+207	-9.997	+96	0.000
		FIX, CW2, ECC10	20×192	2.0×9.6	+202	-9.997	+96	0.000
		FIX, CW3, ECC10	30×192	3.0×9.6	+197	-9.997	+96	0.000
		FIX, CW4, ECC10	40×192	4.0×9.6	+192	-9.997	+96	0.000
		FIX, CW5, ECC10	50×192	5.0×9.6	+187	-9.997	+96	0.000
		FIX, CW6, ECC10	60×192	6.0×9.6	+182	-9.997	+96	0.000
		FIX, CW1, ECC0	10×192	1.0×9.6	+308	0.000	+96	0.000
		FIX, CW2, ECC0	20×192	2.0×9.6	+303	0.000	+96	0.000
		FIX, CW3, ECC0	30×192	3.0×9.6	+298	0.000	+96	0.000
		FIX, CW4, ECC0	40×192	4.0×9.6	+293	0.000	+96	0.000
		FIX, CW5, ECC0	50×192	5.0×9.6	+288	0.000	+96	0.000
		FIX, CW6, ECC0	60×192	6.0×9.6	+283	0.000	+96	0.000
	FT	START, SAC9.6, L2R	10×20	1.0×1.0	+260	-4.789	+10	0.000
		STOP, SAC9.6, L2R	10×20	1.0×1.0	+356	+4.789	+10	0.000

Note. See Figure 4.3 for exemplary visualization of mentioned objects.

[a] Object size (CW×CH) in [px] in horizontal and vertical direction (HOR×VER) is defined by the object's maximum dimension in horizontal and vertical direction. Object size (CW×CH) in [deg] in horizontal and vertical direction (HOR×VER) is defined by the object's maximum dimension in horizontal and vertical direction, angular object size is valid for a symmetrically aligned display position of the object in horizontal and vertical direction in reference to the position of the adjustment point AP (horizontal/vertical center) as the observer's primary gaze position (see red dashed lines in Figure 4.3) which does not coincide with the central point of origin of the display unit's coordinate system (see Appendix C.3 for further information on the center-to-periphery bias).

[b] Horizontal/vertical object position in [px] refers to the position of the left/upper edge of the rectangular box that frames the object at its horizontal and vertical edges (no horizontal or vertical box rotation), object position in [px] refers to the defined pixel numbering as illustrated in Figure C.1 (right-side graphic). Horizontal/vertical object position in [deg] refers to the horizontal/vertical center of the object, reference point is defined by the position of the adjustment point AP (horizontal/vertical center) as the observer's primary gaze position (see red dashed lines in Figure 4.3) which does not coincide with the central point of origin of the display unit's coordinate system.

TABLE G.3: Content size/position for objects presented in the main sequence of CAT2V with vertical eye movement during COBUS2.

CAT	Object Characteristic		Object Dimension [a]		Horizontal Location [b]		Vertical Location [b]	
	Type	**Specification**	**Size [px]**	**Size [deg]**	**Pos. [px]**	**Pos. [deg]**	**Pos. [px]**	**Pos. [deg]**
2V	AP	FIX	2×4	0.2×0.2	+312	0.000	+2	0.000
	DA	FIX, U2D	5×20	0.5×1.0	+310	0.000	+66	+3.297
	ST (HOR)	FIX, CH1, ECC50	96×20	9.6×1.0	-418	-50.007	+10	0.000
		FIX, CH2, ECC50	96×40	9.6×2.0	-418	-50.007	+20	0.000
		FIX, CH3, ECC50	96×60	9.6×3.0	-418	-50.007	+30	0.000
		FIX, CH4, ECC50	96×80	9.6×4.0	-418	-50.007	+40	0.000
		FIX, CH5, ECC50	96×100	9.6×5.0	-418	-50.007	+50	0.000
		FIX, CH6, ECC50	96×120	9.6×6.0	-418	-50.007	+60	0.000
		FIX, CH1, ECC40	96×20	9.6×1.0	-216	-40.014	+10	0.000
		FIX, CH2, ECC40	96×40	9.6×2.0	-216	-40.014	+20	0.000
		FIX, CH3, ECC40	96×60	9.6×3.0	-216	-40.014	+30	0.000
		FIX, CH4, ECC40	96×80	9.6×4.0	-216	-40.014	+40	0.000
		FIX, CH5, ECC40	96×100	9.6×5.0	-216	-40.014	+50	0.000
		FIX, CH6, ECC40	96×120	9.6×6.0	-216	-40.014	+60	0.000
		FIX, CH1, ECC30	96×20	9.6×1.0	-66	-30.015	+10	0.000
		FIX, CH2, ECC30	96×40	9.6×2.0	-66	-30.015	+20	0.000
		FIX, CH3, ECC30	96×60	9.6×3.0	-66	-30.015	+30	0.000
		FIX, CH4, ECC30	96×80	9.6×4.0	-66	-30.015	+40	0.000
		FIX, CH5, ECC30	96×100	9.6×5.0	-66	-30.015	+50	0.000
		FIX, CH6, ECC30	96×120	9.6×6.0	-66	-30.015	+60	0.000
		FIX, CH1, ECC20	96×20	9.6×1.0	+56	-20.041	+10	0.000
		FIX, CH2, ECC20	96×40	9.6×2.0	+56	-20.041	+20	0.000
		FIX, CH3, ECC20	96×60	9.6×3.0	+56	-20.041	+30	0.000
		FIX, CH4, ECC20	96×80	9.6×4.0	+56	-20.041	+40	0.000
		FIX, CH5, ECC20	96×100	9.6×5.0	+56	-20.041	+50	0.000
		FIX, CH6, ECC20	96×120	9.6×6.0	+56	-20.041	+60	0.000
		FIX, CH1, ECC10	96×20	9.6×1.0	+164	-9.997	+10	0.000
		FIX, CH2, ECC10	96×40	9.6×2.0	+164	-9.997	+20	0.000
		FIX, CH3, ECC10	96×60	9.6×3.0	+164	-9.997	+30	0.000
		FIX, CH4, ECC10	96×80	9.6×4.0	+164	-9.997	+40	0.000
		FIX, CH5, ECC10	96×100	9.6×5.0	+164	-9.997	+50	0.000
		FIX, CH6, ECC10	96×120	9.6×6.0	+164	-9.997	+60	0.000
		FIX, CH1, ECC0	96×20	9.6×1.0	+265	0.000	+10	0.000
		FIX, CH2, ECC0	96×40	9.6×2.0	+265	0.000	+20	0.000
		FIX, CH3, ECC0	96×60	9.6×3.0	+265	0.000	+30	0.000
		FIX, CH4, ECC0	96×80	9.6×4.0	+265	0.000	+40	0.000
		FIX, CH5, ECC0	96×100	9.6×5.0	+265	0.000	+50	0.000
		FIX, CH6, ECC0	96×120	9.6×6.0	+265	0.000	+60	0.000
	FT	START, SAC9.6, U2D	10×20	1.0×1.0	+308	0.000	+106	+4.790
		STOP, SAC9.6, U2D	10×20	1.0×1.0	+308	0.000	-86	-4.790

Note. See Figure 4.3 for exemplary visualization of mentioned objects.

[a] Object size (CW×CH) in [px] in horizontal and vertical direction (HOR×VER) is defined by the object's maximum dimension in horizontal and vertical direction. Object size (CW×CH) in [deg] in horizontal and vertical direction (HOR×VER) is defined by the object's maximum dimension in horizontal and vertical direction, angular object size is valid for a symmetrically aligned display position of the object in horizontal and vertical direction in reference to the position of the adjustment point AP (horizontal/vertical center) as the observer's primary gaze position (see red dashed lines in Figure 4.3) which does not coincide with the central point of origin of the display unit's coordinate system (see Appendix C.3 for further information on the center-to-periphery bias).

[b] Horizontal/vertical object position in [px] refers to the position of the left/upper edge of the rectangular box that frames the object at its horizontal and vertical edges (no horizontal or vertical box rotation), object position in [px] refers to the defined pixel numbering as illustrated in Figure C.1 (right-side graphic). Horizontal/vertical object position in [deg] refers to the horizontal/vertical center of the object, reference point is defined by the position of the adjustment point AP (horizontal/vertical center) as the observer's primary gaze position (see red dashed lines in Figure 4.3) which does not coincide with the central point of origin of the display unit's coordinate system.

TABLE G.4: Content size/position for objects presented in the main sequence of CAT3H with horizontal eye/content movement during COBUS2 (Part 1).

CAT	Object Characteristic		Object Dimension [a]		Horizontal Location [b]		Vertical Location [b]	
	Type	**Specification**	**Size [px]**	**Size [deg]**	**Pos. [px]**	**Pos. [deg]**	**Pos. [px]**	**Pos. [deg]**
3H	AP	FIX	2×4	0.2×0.2	+312	0.000	+2	0.000
	DA	FIX, L2R	10×10	1.0×0.5	+280	-3.296	+5	0.000
	ST (VER)	START, L2R, CW1, ECC50	10×192	1.0×9.6	-423	-52.100	+96	0.000
		STOP, L2R, CW1, ECC50	10×192	1.0×9.6	-327	-48.164	+96	0.000
		START, L2R, CW2, ECC50	20×192	2.0×9.6	-428	-52.288	+96	0.000
		STOP, L2R, CW2, ECC50	20×192	2.0×9.6	-332	-48.385	+96	0.000
		START, L2R, CW3, ECC50	30×192	3.0×9.6	-433	-52.474	+96	0.000
		STOP, L2R, CW3, ECC50	30×192	3.0×9.6	-337	-48.605	+96	0.000
		START, L2R, CW4, ECC50	40×192	4.0×9.6	-438	-52.659	+96	0.000
		STOP, L2R, CW4, ECC50	40×192	4.0×9.6	-342	-48.822	+96	0.000
		START, L2R, CW5, ECC50	50×192	5.0×9.6	-443	-52.842	+96	0.000
		STOP, L2R, CW5, ECC50	50×192	5.0×9.6	-347	-49.038	+96	0.000
		START, L2R, CW6, ECC50	60×192	6.0×9.6	-448	-53.024	+96	0.000
		STOP, L2R, CW6, ECC50	60×192	6.0×9.6	-352	-49.252	+96	0.000
		START, L2R, CW1, ECC40	10×192	1.0×9.6	-221	-42.984	+96	0.000
		STOP, L2R, CW1, ECC40	10×192	1.0×9.6	-125	-37.396	+96	0.000
		START, L2R, CW2, ECC40	20×192	2.0×9.6	-226	-43.251	+96	0.000
		STOP, L2R, CW2, ECC40	20×192	2.0×9.6	-130	-37.711	+96	0.000
		START, L2R, CW3, ECC40	30×192	3.0×9.6	-231	-43.515	+96	0.000
		STOP, L2R, CW3, ECC40	30×192	3.0×9.6	-135	-38.022	+96	0.000
		START, L2R, CW4, ECC40	40×192	4.0×9.6	-236	-43.777	+96	0.000
		STOP, L2R, CW4, ECC40	40×192	4.0×9.6	-140	-38.331	+96	0.000
		START, L2R, CW5, ECC40	50×192	5.0×9.6	-241	-44.036	+96	0.000
		STOP, L2R, CW5, ECC40	50×192	5.0×9.6	-145	-38.637	+96	0.000
		START, L2R, CW6, ECC40	60×192	6.0×9.6	-246	-44.294	+96	0.000
		STOP, L2R, CW6, ECC40	60×192	6.0×9.6	-150	-38.941	+96	0.000
		START, L2R, CW1, ECC30	10×192	1.0×9.6	-71	-33.830	+96	0.000
		STOP, L2R, CW1, ECC30	10×192	1.0×9.6	+25	-26.687	+96	0.000
		START, L2R, CW2, ECC30	20×192	2.0×9.6	-76	-34.174	+96	0.000
		STOP, L2R, CW2, ECC30	20×192	2.0×9.6	+20	-27.084	+96	0.000
		START, L2R, CW3, ECC30	30×192	3.0×9.6	-81	-34.515	+96	0.000
		STOP, L2R, CW3, ECC30	30×192	3.0×9.6	+15	-27.479	+96	0.000
		START, L2R, CW4, ECC30	40×192	4.0×9.6	-86	-34.853	+96	0.000
		STOP, L2R, CW4, ECC30	40×192	4.0×9.6	+10	-27.871	+96	0.000
		START, L2R, CW5, ECC30	50×192	5.0×9.6	-91	-35.188	+96	0.000
		STOP, L2R, CW5, ECC30	50×192	5.0×9.6	+5	-28.261	+96	0.000
		START, L2R, CW6, ECC30	60×192	6.0×9.6	-96	-35.521	+96	0.000
		STOP, L2R, CW6, ECC30	60×192	6.0×9.6	0	-28.647	+96	0.000

Note. See Figure 4.4 for exemplary visualization of mentioned objects.
[a] Object size (CW×CH) in [px] in horizontal and vertical direction (HOR×VER) is defined by the object's maximum dimension in horizontal and vertical direction. Object size (CW×CH) in [deg] in horizontal and vertical direction (HOR×VER) is defined by the object's maximum dimension in horizontal and vertical direction, angular object size is valid for a symmetrically aligned display position of the object in horizontal and vertical direction in reference to the position of the adjustment point AP (horizontal/vertical center) as the observer's primary gaze position (see red dashed lines in Figure 4.4) which does not coincide with the central point of origin of the display unit's coordinate system (see Appendix C.3 for further information on the center-to-periphery bias).
[b] Horizontal/vertical object position in [px] refers to the position of the left/upper edge of the rectangular box that frames the object at its horizontal and vertical edges (no horizontal or vertical box rotation), object position in [px] refers to the defined pixel numbering as illustrated in Figure C.1 (right-side graphic). Horizontal/vertical object position in [deg] refers to the horizontal/vertical center of the object, reference point is defined by the position of the adjustment point AP (horizontal/vertical center) as the observer's primary gaze position (see red dashed lines in Figure 4.4) which does not coincide with the central point of origin of the display unit's coordinate system.

TABLE G.5: Content size/position for objects presented in the main sequence of CAT3H with horizontal eye/content movement during COBUS2 (Part 2).

CAT	Object Characteristic		Object Dimension [a]		Horizontal Location [b]		Vertical Location [b]	
	Type	Specification	Size [px]	Size [deg]	Pos. [px]	Pos. [deg]	Pos. [px]	Pos. [deg]
3H	ST (VER)	START, L2R, CW1, ECC20	10×192	1.0×9.6	+51	-24.573	+96	0.000
		STOP, L2R, CW1, ECC20	10×192	1.0×9.6	+147	-16.158	+96	0.000
		START, L2R, CW2, ECC20	20×192	2.0×9.6	+46	-24.986	+96	0.000
		STOP, L2R, CW2, ECC20	20×192	2.0×9.6	+142	-16.618	+96	0.000
		START, L2R, CW3, ECC20	30×192	3.0×9.6	+41	-25.395	+96	0.000
		STOP, L2R, CW3, ECC20	30×192	3.0×9.6	+137	-17.076	+96	0.000
		START, L2R, CW4, ECC20	40×192	4.0×9.6	+36	-25.802	+96	0.000
		STOP, L2R, CW4, ECC20	40×192	4.0×9.6	+132	-17.532	+96	0.000
		START, L2R, CW5, ECC20	50×192	5.0×9.6	+31	-26.206	+96	0.000
		STOP, L2R, CW5, ECC20	50×192	5.0×9.6	+127	-17.985	+96	0.000
		START, L2R, CW6, ECC20	60×192	6.0×9.6	+26	-26.607	+96	0.000
		STOP, L2R, CW6, ECC20	60×192	6.0×9.6	+122	-18.436	+96	0.000
		START, L2R, CW1, ECC10	10×192	1.0×9.6	+159	-15.044	+96	0.000
		STOP, L2R, CW1, ECC10	10×192	1.0×9.6	+255	-5.780	+96	0.000
		START, L2R, CW2, ECC10	20×192	2.0×9.6	+154	-15.510	+96	0.000
		STOP, L2R, CW2, ECC10	20×192	2.0×9.6	+250	-6.275	+96	0.000
		START, L2R, CW3, ECC10	30×192	3.0×9.6	+149	-15.973	+96	0.000
		STOP, L2R, CW3, ECC10	30×192	3.0×9.6	+245	-6.768	+96	0.000
		START, L2R, CW4, ECC10	40×192	4.0×9.6	+144	-16.434	+96	0.000
		STOP, L2R, CW4, ECC10	40×192	4.0×9.6	+240	-7.261	+96	0.000
		START, L2R, CW5, ECC10	50×192	5.0×9.6	+139	-16.893	+96	0.000
		STOP, L2R, CW5, ECC10	50×192	5.0×9.6	+235	-7.752	+96	0.000
		START, L2R, CW6, ECC10	60×192	6.0×9.6	+134	-17.350	+96	0.000
		STOP, L2R, CW6, ECC10	60×192	6.0×9.6	+230	-8.243	+96	0.000
		START, L2R, CW1, ECC0	10×192	1.0×9.6	+260	-5.285	+96	0.000
		STOP, L2R, CW1, ECC0	10×192	1.0×9.6	+356	4.292	+96	0.000
		START, L2R, CW2, ECC0	20×192	2.0×9.6	+255	-5.780	+96	0.000
		STOP, L2R, CW2, ECC0	20×192	2.0×9.6	+351	3.794	+96	0.000
		START, L2R, CW3, ECC0	30×192	3.0×9.6	+250	-6.275	+96	0.000
		STOP, L2R, CW3, ECC0	30×192	3.0×9.6	+346	3.296	+96	0.000
		START, L2R, CW4, ECC0	40×192	4.0×9.6	+245	-6.768	+96	0.000
		STOP, L2R, CW4, ECC0	40×192	4.0×9.6	+341	2.798	+96	0.000
		START, L2R, CW5, ECC0	50×192	5.0×9.6	+240	-7.261	+96	0.000
		STOP, L2R, CW5, ECC0	50×192	5.0×9.6	+336	2.299	+96	0.000
		START, L2R, CW6, ECC0	60×192	6.0×9.6	+235	-7.752	+96	0.000
		STOP, L2R,, CW6, ECC0	60×192	6.0×9.6	+331	1.799	+96	0.000
	FT	START, L2R	10×20	1.0×1.0	+260	-4.789	+10	0.000
		STEP, PEM36, L2R	10×20	1.0×1.0	+188	-11.829	+10	0.000
		RAMP, L2R	10×20	1.0×1.0	+356	+4.789	+10	0.000
		START, R2L	10×20	1.0×1.0	+356	+4.789	+10	0.000
		STEP, PEM36, R2L	10×20	1.0×1.0	+428	+11.829	+10	0.000
		RAMP, R2L	10×20	1.0×1.0	+260	-4.789	+10	0.000

Note. See Figure 4.4 for exemplary visualization of mentioned objects.
[a] See corresponding note in Table G.4 for additional information on the object dimension.
[b] See corresponding note in Table G.4 for additional information on the object location.

TABLE G.6: Content size/position for objects presented in the main sequence of CAT3V with vertical eye/content movement during COBUS2 (Part 1).

CAT	Object Characteristic		Object Dimension [a]		Horizontal Location [b]		Vertical Location [b]	
	Type	Specification	Size [px]	Size [deg]	Pos. [px]	Pos. [deg]	Pos. [px]	Pos. [deg]
3V	AP	FIX	2×4	0.2×0.2	+312	0.000	+2	0.000
	DA	FIX, U2D	5×20	0.5×1.0	+310	0.000	+66	+3.297
	ST (HOR)	START, U2D, CH1, ECC50	96×20	9.6×1.0	-418	-50.007	+106	+4.790
		STOP, U2D, CH1, ECC50	96×20	9.6×1.0	-418	-50.007	-86	-4.790
		START, U2D, CH2, ECC50	96×40	9.6×2.0	-418	-50.007	+116	+4.790
		STOP, U2D, CH2, ECC50	96×40	9.6×2.0	-418	-50.007	-76	-4.790
		START, U2D, CH3, ECC50	96×60	9.6×3.0	-418	-50.007	+126	+4.790
		STOP, U2D, CH3, ECC50	96×60	9.6×3.0	-418	-50.007	-66	-4.790
		START, U2D, CH4, ECC50	96×80	9.6×4.0	-418	-50.007	+136	+4.790
		STOP, U2D, CH4, ECC50	96×80	9.6×4.0	-418	-50.007	-56	-4.790
		START, U2D, CH5, ECC50	96×100	9.6×5.0	-418	-50.007	+146	+4.790
		STOP, U2D, CH5, ECC50	96×100	9.6×5.0	-418	-50.007	-46	-4.790
		START, U2D, CH6, ECC50	96×120	9.6×6.0	-418	-50.007	+156	+4.790
		STOP, U2D, CH6, ECC50	96×120	9.6×6.0	-418	-50.007	-36	-4.790
		START, U2D, CH1, ECC40	96×20	9.6×1.0	-216	-40.014	+106	+4.790
		STOP, U2D, CH1, ECC40	96×20	9.6×1.0	-216	-40.014	-86	-4.790
		START, U2D, CH2, ECC40	96×40	9.6×2.0	-216	-40.014	+116	+4.790
		STOP, U2D, CH2, ECC40	96×40	9.6×2.0	-216	-40.014	-76	-4.790
		START, U2D, CH3, ECC40	96×60	9.6×3.0	-216	-40.014	+126	+4.790
		STOP, U2D, CH3, ECC40	96×60	9.6×3.0	-216	-40.014	-66	-4.790
		START, U2D, CH4, ECC40	96×80	9.6×4.0	-216	-40.014	+136	+4.790
		STOP, U2D, CH4, ECC40	96×80	9.6×4.0	-216	-40.014	-56	-4.790
		START, U2D, CH5, ECC40	96×100	9.6×5.0	-216	-40.014	+146	+4.790
		STOP, U2D, CH5, ECC40	96×100	9.6×5.0	-216	-40.014	-46	-4.790
		START, U2D, CH6, ECC40	96×120	9.6×6.0	-216	-40.014	+156	+4.790
		STOP, U2D, CH6, ECC40	96×120	9.6×6.0	-216	-40.014	-36	-4.790
		START, U2D, CH1, ECC30	96×20	9.6×1.0	-66	-30.015	+106	+4.790
		STOP, U2D, CH1, ECC30	96×20	9.6×1.0	-66	-30.015	-86	-4.790
		START, U2D, CH2, ECC30	96×40	9.6×2.0	-66	-30.015	+116	+4.790
		STOP, U2D, CH2, ECC30	96×40	9.6×2.0	-66	-30.015	-76	-4.790
		START, U2D, CH3, ECC30	96×60	9.6×3.0	-66	-30.015	+126	+4.790
		STOP, U2D, CH3, ECC30	96×60	9.6×3.0	-66	-30.015	-66	-4.790
		START, U2D, CH4, ECC30	96×80	9.6×4.0	-66	-30.015	+136	+4.790
		STOP, U2D, CH4, ECC30	96×80	9.6×4.0	-66	-30.015	-56	-4.790
		START, U2D, CH5, ECC30	96×100	9.6×5.0	-66	-30.015	+146	+4.790
		STOP, U2D, CH5, ECC30	96×100	9.6×5.0	-66	-30.015	-46	-4.790
		START, U2D, CH6, ECC30	96×120	9.6×6.0	-66	-30.015	+156	+4.790
		STOP, U2D, CH6, ECC30	96×120	9.6×6.0	-66	-30.015	-36	-4.790

Note. See Figure 4.4 for exemplary visualization of mentioned objects.
[a] Object size (CW×CH) in [px] in horizontal and vertical direction (HOR×VER) is defined by the object's maximum dimension in horizontal and vertical direction. Object size (CW×CH) in [deg] in horizontal and vertical direction (HOR×VER) is defined by the object's maximum dimension in horizontal and vertical direction, angular object size is valid for a symmetrically aligned display position of the object in horizontal and vertical direction in reference to the position of the adjustment point AP (horizontal/vertical center) as the observer's primary gaze position (see red dashed lines in Figure 4.4) which does not coincide with the central point of origin of the display unit's coordinate system (see Appendix C.3 for further information on the center-to-periphery bias).
[b] Horizontal/vertical object position in [px] refers to the position of the left/upper edge of the rectangular box that frames the object at its horizontal and vertical edges (no horizontal or vertical box rotation), object position in [px] refers to the defined pixel numbering as illustrated in Figure C.1 (right-side graphic). Horizontal/vertical object position in [deg] refers to the horizontal/vertical center of the object, reference point is defined by the position of the adjustment point AP (horizontal/vertical center) as the observer's primary gaze position (see red dashed lines in Figure 4.4) which does not coincide with the central point of origin of the display unit's coordinate system.

TABLE G.7: Content size/position for objects presented in the main sequence of CAT3V with vertical eye/content movement during COBUS2 (Part 2).

CAT	Object Characteristic		Object Dimension [a]		Horizontal Location [b]		Vertical Location [b]	
	Type	Specification	Size [px]	Size [deg]	Pos. [px]	Pos. [deg]	Pos. [px]	Pos. [deg]
3V	ST (HOR)	START, U2D, CH1, ECC20	96×20	9.6×1.0	+56	-20.041	+106	+4.790
		STOP, U2D, CH1, ECC20	96×20	9.6×1.0	+56	-20.041	-86	-4.790
		START, U2D, CH2, ECC20	96×40	9.6×2.0	+56	-20.041	+116	+4.790
		STOP, U2D, CH2, ECC20	96×40	9.6×2.0	+56	-20.041	-76	-4.790
		START, U2D, CH3, ECC20	96×60	9.6×3.0	+56	-20.041	+126	+4.790
		STOP, U2D, CH3, ECC20	96×60	9.6×3.0	+56	-20.041	-66	-4.790
		START, U2D, CH4, ECC20	96×80	9.6×4.0	+56	-20.041	+136	+4.790
		STOP, U2D, CH4, ECC20	96×80	9.6×4.0	+56	-20.041	-56	-4.790
		START, U2D, CH5, ECC20	96×100	9.6×5.0	+56	-20.041	+146	+4.790
		STOP, U2D, CH5, ECC20	96×100	9.6×5.0	+56	-20.041	-46	-4.790
		START, U2D, CH6, ECC20	96×120	9.6×6.0	+56	-20.041	+156	+4.790
		STOP, U2D, CH6, ECC20	96×120	9.6×6.0	+56	-20.041	-36	-4.790
		START, U2D, CH1, ECC10	96×20	9.6×1.0	+164	-9.997	+106	+4.790
		STOP, U2D, CH1, ECC10	96×20	9.6×1.0	+164	-9.997	-86	-4.790
		START, U2D, CH2, ECC10	96×40	9.6×2.0	+164	-9.997	+116	+4.790
		STOP, U2D, CH2, ECC10	96×40	9.6×2.0	+164	-9.997	-76	-4.790
		START, U2D, CH3, ECC10	96×60	9.6×3.0	+164	-9.997	+126	+4.790
		STOP, U2D, CH3, ECC10	96×60	9.6×3.0	+164	-9.997	-66	-4.790
		START, U2D, CH4, ECC10	96×80	9.6×4.0	+164	-9.997	+136	+4.790
		STOP, U2D, CH4, ECC10	96×80	9.6×4.0	+164	-9.997	-56	-4.790
		START, U2D, CH5, ECC10	96×100	9.6×5.0	+164	-9.997	+146	+4.790
		STOP, U2D, CH5, ECC10	96×100	9.6×5.0	+164	-9.997	-46	-4.790
		START, U2D, CH6, ECC10	96×120	9.6×6.0	+164	-9.997	+156	+4.790
		STOP, U2D, CH6, ECC10	96×120	9.6×6.0	+164	-9.997	-36	-4.790
		START, U2D, CH1, ECC0	96×20	9.6×1.0	+265	0.000	+106	+4.790
		STOP, U2D, CH1, ECC0	96×20	9.6×1.0	+265	0.000	-86	-4.790
		START, U2D, CH2, ECC0	96×40	9.6×2.0	+265	0.000	+116	+4.790
		STOP, U2D, CH2, ECC0	96×40	9.6×2.0	+265	0.000	-76	-4.790
		START, U2D, CH3, ECC0	96×60	9.6×3.0	+265	0.000	+126	+4.790
		STOP, U2D, CH3, ECC0	96×60	9.6×3.0	+265	0.000	-66	-4.790
		START, U2D, CH4, ECC0	96×80	9.6×4.0	+265	0.000	+136	+4.790
		STOP, U2D, CH4, ECC0	96×80	9.6×4.0	+265	0.000	-56	-4.790
		START, U2D, CH5, ECC0	96×100	9.6×5.0	+265	0.000	+146	+4.790
		STOP, U2D, CH5, ECC0	96×100	9.6×5.0	+265	0.000	-46	-4.790
		START, U2D, CH6, ECC0	96×120	9.6×6.0	+265	0.000	+156	+4.790
		STOP, U2D, CH6, ECC0	96×120	9.6×6.0	+265	0.000	-36	-4.790
	FT	START, U2D	10×20	1.0×1.0	+308	0.000	+106	+4.790
		STEP, PEM36, U2D	10×20	1.0×1.0	+308	0.000	+250	+11.832
		RAMP, U2D	10×20	1.0×1.0	+308	0.000	-86	-4.790
		START, D2U	10×20	1.0×1.0	+308	0.000	-86	-4.790
		STEP, PEM36, D2U	10×20	1.0×1.0	+308	0.000	-230	-11.832
		RAMP, D2U	10×20	1.0×1.0	+308	0.000	+106	+4.790

Note. See Figure 4.4 for exemplary visualization of mentioned objects.
[a] See corresponding note in Table G.6 for additional information on the object dimension.
[b] See corresponding note in Table G.6 for additional information on the object location.

TABLE G.8: Content movement velocity in [deg/s] for various combinations of content movement velocity in [px/fr] and frame rate in [Hz] during COBUS1.

		Frame Rate in [Hz]										
		30.0	**60.0**	**90.0**	**120.0**	**150.0**	**180.0**	**210.0**	**240.0**	**300.0**	**360.0**	**420.0**
Content Movement Velocity in [px/fr]	**0.5**	0.75	1.50	2.25	3.00	3.75	4.50	5.25	6.00	7.50	9.00	10.50
	1.0	1.50	3.00	4.50	6.00	7.50	9.00	10.50	12.00	15.00	18.00	21.00
	1.5	2.25	4.50	6.75	9.00	11.25	13.50	15.75	18.00	22.50	27.00	31.50
	2.0	3.00	6.00	9.00	12.00	15.00	18.00	21.00	24.00	30.00	36.00	42.00
	2.5	3.75	7.50	11.25	15.00	18.75	22.50	26.25	30.00	37.50	45.00	52.50
	3.0	4.50	9.00	13.50	18.00	22.50	27.00	31.50	36.00	45.00	54.00	63.00
	3.5	5.25	10.50	15.75	21.00	26.25	31.50	36.75	42.00	52.50	63.00	73.50
	4.0	6.00	12.00	18.00	24.00	30.00	36.00	42.00	48.00	60.00	72.00	84.00
	4.5	6.75	13.50	20.25	27.00	33.75	40.50	47.25	54.00	67.50	81.00	94.50
	5.0	7.50	15.00	22.50	30.00	37.50	45.00	52.50	60.00	75.00	90.00	105.00
	5.5	8.25	16.50	24.75	33.00	41.25	49.50	57.75	66.00	82.50	99.00	115.50
	6.0	9.00	18.00	27.00	36.00	45.00	54.00	63.00	72.00	90.00	108.00	126.00
	6.5	9.75	19.50	29.25	39.00	48.75	58.50	68.25	78.00	97.50	117.00	136.50
	7.0	10.50	21.00	31.50	42.00	52.50	63.00	73.50	84.00	105.00	126.00	147.00
	7.5	11.25	22.50	33.75	45.00	56.25	67.50	78.75	90.00	112.50	135.00	157.50
	8.0	12.00	24.00	36.00	48.00	60.00	72.00	84.00	96.00	120.00	144.00	168.00
	8.5	12.75	25.50	38.25	51.00	63.75	76.50	89.25	102.00	127.50	153.00	178.50
	9.0	13.50	27.00	40.50	54.00	67.50	81.00	94.50	108.00	135.00	162.00	189.00
	9.5	14.25	28.50	42.75	57.00	71.25	85.50	99.75	114.00	142.50	171.00	199.50
	10.0	15.00	30.00	45.00	60.00	75.00	90.00	105.00	120.00	150.00	180.00	210.00
	11.0	16.50	33.00	49.50	66.00	82.50	99.00	115.50	132.00	165.00	198.00	231.00
	12.0	18.00	36.00	54.00	72.00	90.00	108.00	126.00	144.00	180.00	216.00	252.00
	13.0	19.50	39.00	58.50	78.00	97.50	117.00	136.50	156.00	195.00	234.00	273.00
	14.0	21.00	42.00	63.00	84.00	105.00	126.00	147.00	168.00	210.00	252.00	294.00
	15.0	22.50	45.00	67.50	90.00	112.50	135.00	157.50	180.00	225.00	270.00	315.00
	16.0	24.00	48.00	72.00	96.00	120.00	144.00	168.00	192.00	240.00	288.00	336.00
	17.0	25.50	51.00	76.50	102.00	127.50	153.00	178.50	204.00	255.00	306.00	357.00
	18.0	27.00	54.00	81.00	108.00	135.00	162.00	189.00	216.00	270.00	324.00	378.00
	19.0	28.50	57.00	85.50	114.00	142.50	171.00	199.50	228.00	285.00	342.00	399.00
	20.0	30.00	60.00	90.00	120.00	150.00	180.00	210.00	240.00	300.00	360.00	420.00
	22.0	33.00	66.00	99.00	132.00	165.00	198.00	231.00	264.00	330.00	396.00	462.00
	24.0	36.00	72.00	108.00	144.00	180.00	216.00	252.00	288.00	360.00	432.00	504.00
	26.0	39.00	78.00	117.00	156.00	195.00	234.00	273.00	312.00	390.00	468.00	546.00
	28.0	42.00	84.00	126.00	168.00	210.00	252.00	294.00	336.00	420.00	504.00	588.00
	30.0	45.00	90.00	135.00	180.00	225.00	270.00	315.00	360.00	450.00	540.00	630.00
	32.0	48.00	96.00	144.00	192.00	240.00	288.00	336.00	384.00	480.00	576.00	672.00
	34.0	51.00	102.00	153.00	204.00	255.00	306.00	357.00	408.00	510.00	612.00	714.00
	36.0	54.00	108.00	162.00	216.00	270.00	324.00	378.00	432.00	540.00	648.00	756.00
	38.0	57.00	114.00	171.00	228.00	285.00	342.00	399.00	456.00	570.00	684.00	798.00
	40.0	60.00	120.00	180.00	240.00	300.00	360.00	420.00	480.00	600.00	720.00	840.00

Note. Content movement velocity in [deg/s] = content movement velocity in [px/fr] × idealized pixel size in [deg] × frame rate in [Hz], content movement velocity in [deg/s] is determined for COBUS1 setup conditions (PD = 0.65 m, VD = 0.58 m, idealized pixel size of 0.05°/0.025° in horizontal/vertical direction), content movement velocity in [deg/s] is calculated without consideration of the center-to-periphery bias (CPB), i.e., the listed content movement velocities in [deg/s] correspond to the content's pixel jump (or content shift) between two frames for which it is simplistically assumed that (1) the content positions for both frames are symmetrically aligned in direct proximity around the horizontal center of the screen (equal to the adjustment point position) while (2) the participant's gaze position is also determined at the horizontal screen center. Deviations of these assumptions lead to a peripheral presentation of moving content in relation to the eye gaze position, resulting in reduced velocity values in [deg/s] (see Appendix C.3 for further information on the CPB). Regarding content movement velocity in [px/fr]: half-pixel jumps are possible in horizontal direction, therefore, half-pixel steps are included for content movement velocity in [px/fr] (see Appendix C.2 for further information on this topic).

TABLE G.9: Content movement velocity in [px/fr] for various combinations of content movement velocity in [deg/s] and frame rate in [Hz] during COBUS1.

		Frame Rate in [Hz]										
		30.0	**60.0**	**90.0**	**120.0**	**150.0**	**180.0**	**210.0**	**240.0**	**300.0**	**360.0**	**420.0**
Content Movement Velocity in [deg/s]	**1.0**	0.67	0.33	0.22	0.17	0.13	0.11	0.10	0.08	0.07	0.06	0.05
	2.0	1.33	0.67	0.44	0.33	0.27	0.22	0.19	0.17	0.13	0.11	0.10
	3.0	2.00	1.00	0.67	0.50	0.40	0.33	0.29	0.25	0.20	0.17	0.14
	4.0	2.67	1.33	0.89	0.67	0.53	0.44	0.38	0.33	0.27	0.22	0.19
	5.0	3.33	1.67	1.11	0.83	0.67	0.56	0.48	0.42	0.33	0.28	0.24
	6.0	4.00	2.00	1.33	1.00	0.80	0.67	0.57	0.50	0.40	0.33	0.29
	7.0	4.67	2.33	1.56	1.17	0.93	0.78	0.67	0.58	0.47	0.39	0.33
	8.0	5.33	2.67	1.78	1.33	1.07	0.89	0.76	0.67	0.53	0.44	0.38
	9.0	6.00	3.00	2.00	1.50	1.20	1.00	0.86	0.75	0.60	0.50	0.43
	10.0	6.67	3.33	2.22	1.67	1.33	1.11	0.95	0.83	0.67	0.56	0.48
	12.0	8.00	4.00	2.67	2.00	1.60	1.33	1.14	1.00	0.80	0.67	0.57
	14.0	9.33	4.67	3.11	2.33	1.87	1.56	1.33	1.17	0.93	0.78	0.67
	16.0	10.67	5.33	3.56	2.67	2.13	1.78	1.52	1.33	1.07	0.89	0.76
	18.0	12.00	6.00	4.00	3.00	2.40	2.00	1.71	1.50	1.20	1.00	0.86
	20.0	13.33	6.67	4.44	3.33	2.67	2.22	1.90	1.67	1.33	1.11	0.95
	22.0	14.67	7.33	4.89	3.67	2.93	2.44	2.10	1.83	1.47	1.22	1.05
	24.0	16.00	8.00	5.33	4.00	3.20	2.67	2.29	2.00	1.60	1.33	1.14
	26.0	17.33	8.67	5.78	4.33	3.47	2.89	2.48	2.17	1.73	1.44	1.24
	28.0	18.67	9.33	6.22	4.67	3.73	3.11	2.67	2.33	1.87	1.56	1.33
	30.0	20.00	10.00	6.67	5.00	4.00	3.33	2.86	2.50	2.00	1.67	1.43
	32.0	21.33	10.67	7.11	5.33	4.27	3.56	3.05	2.67	2.13	1.78	1.52
	34.0	22.67	11.33	7.56	5.67	4.53	3.78	3.24	2.83	2.27	1.89	1.62
	36.0	24.00	12.00	8.00	6.00	4.80	4.00	3.43	3.00	2.40	2.00	1.71
	38.0	25.33	12.67	8.44	6.33	5.07	4.22	3.62	3.17	2.53	2.11	1.81
	40.0	26.67	13.33	8.89	6.67	5.33	4.44	3.81	3.33	2.67	2.22	1.90
	42.0	28.00	14.00	9.33	7.00	5.60	4.67	4.00	3.50	2.80	2.33	2.00
	44.0	29.33	14.67	9.78	7.33	5.87	4.89	4.19	3.67	2.93	2.44	2.10
	46.0	30.67	15.33	10.22	7.67	6.13	5.11	4.38	3.83	3.07	2.56	2.19
	48.0	32.00	16.00	10.67	8.00	6.40	5.33	4.57	4.00	3.20	2.67	2.29
	50.0	33.33	16.67	11.11	8.33	6.67	5.56	4.76	4.17	3.33	2.78	2.38
	52.0	34.67	17.33	11.56	8.67	6.93	5.78	4.95	4.33	3.47	2.89	2.48
	54.0	36.00	18.00	12.00	9.00	7.20	6.00	5.14	4.50	3.60	3.00	2.57
	56.0	37.33	18.67	12.44	9.33	7.47	6.22	5.33	4.67	3.73	3.11	2.67
	58.0	38.67	19.33	12.89	9.67	7.73	6.44	5.52	4.83	3.87	3.22	2.76
	60.0	40.00	20.00	13.33	10.00	8.00	6.67	5.71	5.00	4.00	3.33	2.86
	64.0	42.67	21.33	14.22	10.67	8.53	7.11	6.10	5.33	4.27	3.56	3.05
	68.0	45.33	22.67	15.11	11.33	9.07	7.56	6.48	5.67	4.53	3.78	3.24
	72.0	48.00	24.00	16.00	12.00	9.60	8.00	6.86	6.00	4.80	4.00	3.43
	76.0	50.67	25.33	16.89	12.67	10.13	8.44	7.24	6.33	5.07	4.22	3.62
	80.0	53.33	26.67	17.78	13.33	10.67	8.89	7.62	6.67	5.33	4.44	3.81

Note. Content movement velocity in [px/fr] = content movement velocity in [deg/s] / (idealized pixel size in [deg] × frame rate in [Hz]), content movement velocity in [px/fr] is determined for COBUS1 setup conditions (PD = 0.65 m, VD = 0.58 m, idealized pixel size of 0.05°/0.025° in horizontal/vertical direction), calculated velocity values in [px/fr] can only be executed with a steady horizontal content movement (no vertical movement in COBUS1) as long as the calculated values in [px/fr] are multiples of 0.5 (half-pixel jumps possible in horizontal direction), velocity values in [px/fr] that do not meet the assumption to be a multiple of 0.5 and therefore violate the half-pixel jump condition can also be created but lead to unsteady content movement (see also Appendix C.2). Content movement velocity in [deg/s] is calculated without consideration of the center-to-periphery bias (CPB), i.e., the listed content movement velocities in [deg/s] correspond to the content's pixel jump (or content shift) between two frames for which it is simplistically assumed that (1) the content positions for both frames are symmetrically aligned in direct proximity around the horizontal center of the screen (equal to the adjustment point position) while (2) the participant's gaze position is also determined at the horizontal screen center. Deviations of these assumptions lead to a peripheral presentation of moving content in relation to the eye gaze position, resulting in reduced velocity values in [deg/s] (see Appendix C.3 for further information on the CPB).

TABLE G.10: Content movement velocity in [deg/s] for various combinations of content movement velocity in [px/fr] and frame rate in [Hz] during COBUS2.

		Frame Rate in [Hz]										
		30.0	**60.0**	**90.0**	**120.0**	**150.0**	**180.0**	**210.0**	**240.0**	**300.0**	**360.0**	**420.0**
Content Movement Velocity in [px/fr]	**0.5**	1.50	3.00	4.50	6.00	7.50	9.00	10.50	12.00	15.00	18.00	21.00
	1.0	3.00	6.00	9.00	12.00	15.00	18.00	21.00	24.00	30.00	36.00	42.00
	1.5	4.50	9.00	13.50	18.00	22.50	27.00	31.50	36.00	45.00	54.00	63.00
	2.0	6.00	12.00	18.00	24.00	30.00	36.00	42.00	48.00	60.00	72.00	84.00
	2.5	7.50	15.00	22.50	30.00	37.50	45.00	52.50	60.00	75.00	90.00	105.00
	3.0	9.00	18.00	27.00	36.00	45.00	54.00	63.00	72.00	90.00	108.00	126.00
	3.5	10.50	21.00	31.50	42.00	52.50	63.00	73.50	84.00	105.00	126.00	147.00
	4.0	12.00	24.00	36.00	48.00	60.00	72.00	84.00	96.00	120.00	144.00	168.00
	4.5	13.50	27.00	40.50	54.00	67.50	81.00	94.50	108.00	135.00	162.00	189.00
	5.0	15.00	30.00	45.00	60.00	75.00	90.00	105.00	120.00	150.00	180.00	210.00
	5.5	16.50	33.00	49.50	66.00	82.50	99.00	115.50	132.00	165.00	198.00	231.00
	6.0	18.00	36.00	54.00	72.00	90.00	108.00	126.00	144.00	180.00	216.00	252.00
	6.5	19.50	39.00	58.50	78.00	97.50	117.00	136.50	156.00	195.00	234.00	273.00
	7.0	21.00	42.00	63.00	84.00	105.00	126.00	147.00	168.00	210.00	252.00	294.00
	7.5	22.50	45.00	67.50	90.00	112.50	135.00	157.50	180.00	225.00	270.00	315.00
	8.0	24.00	48.00	72.00	96.00	120.00	144.00	168.00	192.00	240.00	288.00	336.00
	8.5	25.50	51.00	76.50	102.00	127.50	153.00	178.50	204.00	255.00	306.00	357.00
	9.0	27.00	54.00	81.00	108.00	135.00	162.00	189.00	216.00	270.00	324.00	378.00
	9.5	28.50	57.00	85.50	114.00	142.50	171.00	199.50	228.00	285.00	342.00	399.00
	10.0	30.00	60.00	90.00	120.00	150.00	180.00	210.00	240.00	300.00	360.00	420.00
	11.0	33.00	66.00	99.00	132.00	165.00	198.00	231.00	264.00	330.00	396.00	462.00
	12.0	36.00	72.00	108.00	144.00	180.00	216.00	252.00	288.00	360.00	432.00	504.00
	13.0	39.00	78.00	117.00	156.00	195.00	234.00	273.00	312.00	390.00	468.00	546.00
	14.0	42.00	84.00	126.00	168.00	210.00	252.00	294.00	336.00	420.00	504.00	588.00
	15.0	45.00	90.00	135.00	180.00	225.00	270.00	315.00	360.00	450.00	540.00	630.00
	16.0	48.00	96.00	144.00	192.00	240.00	288.00	336.00	384.00	480.00	576.00	672.00
	17.0	51.00	102.00	153.00	204.00	255.00	306.00	357.00	408.00	510.00	612.00	714.00
	18.0	54.00	108.00	162.00	216.00	270.00	324.00	378.00	432.00	540.00	648.00	756.00
	19.0	57.00	114.00	171.00	228.00	285.00	342.00	399.00	456.00	570.00	684.00	798.00
	20.0	60.00	120.00	180.00	240.00	300.00	360.00	420.00	480.00	600.00	720.00	840.00
	22.0	66.00	132.00	198.00	264.00	330.00	396.00	462.00	528.00	660.00	792.00	924.00
	24.0	72.00	144.00	216.00	288.00	360.00	432.00	504.00	576.00	720.00	864.00	1008.00
	26.0	78.00	156.00	234.00	312.00	390.00	468.00	546.00	624.00	780.00	936.00	1092.00
	28.0	84.00	168.00	252.00	336.00	420.00	504.00	588.00	672.00	840.00	1008.00	1176.00
	30.0	90.00	180.00	270.00	360.00	450.00	540.00	630.00	720.00	900.00	1080.00	1260.00
	32.0	96.00	192.00	288.00	384.00	480.00	576.00	672.00	768.00	960.00	1152.00	1344.00
	34.0	102.00	204.00	306.00	408.00	510.00	612.00	714.00	816.00	1020.00	1224.00	1428.00
	36.0	108.00	216.00	324.00	432.00	540.00	648.00	756.00	864.00	1080.00	1296.00	1512.00
	38.0	114.00	228.00	342.00	456.00	570.00	684.00	798.00	912.00	1140.00	1368.00	1596.00
	40.0	120.00	240.00	360.00	480.00	600.00	720.00	840.00	960.00	1200.00	1440.00	1680.00

Note. Content movement velocity in [deg/s] = content movement velocity in [px/fr] × idealized pixel size in [deg] × frame rate in [Hz], content movement velocity in [deg/s] is determined for COBUS2 setup conditions (PD = 0.65 m, VD = 0.29 m, idealized pixel size of 0.10°/0.05° in horizontal/vertical direction), content movement velocity in [deg/s] is calculated without consideration of the center-to-periphery bias (CPB), i.e., the listed content movement velocities in [deg/s] correspond to the content's pixel jump (or content shift) between two frames for which it is simplistically assumed that (1) the content positions for both frames are symmetrically aligned in direct proximity around the adjustment point (AP) on the screen while (2) the participant's gaze position is also determined by the AP position. Deviations of these assumptions lead to a peripheral presentation of moving content in relation to the eye gaze position, resulting in reduced velocity values in [deg/s] (see Appendix C.3 for further information on the CPB). Regarding content movement velocity in [px/fr]: half-pixel jumps are possible in horizontal direction, therefore, half-pixel steps are included for content movement velocity in [px/fr] (see Appendix C.2 for further information on this topic).

TABLE G.11: Content movement velocity in [px/fr] for various combinations of content movement velocity in [deg/s] and frame rate in [Hz] during COBUS2.

		Frame Rate in [Hz]										
		30.0	**60.0**	**90.0**	**120.0**	**150.0**	**180.0**	**210.0**	**240.0**	**300.0**	**360.0**	**420.0**
Content Movement Velocity in [deg/s]	**1.0**	0.33	0.17	0.11	0.08	0.07	0.06	0.05	0.04	0.03	0.03	0.02
	2.0	0.67	0.33	0.22	0.17	0.13	0.11	0.10	0.08	0.07	0.06	0.05
	3.0	1.00	0.50	0.33	0.25	0.20	0.17	0.14	0.13	0.10	0.08	0.07
	4.0	1.33	0.67	0.44	0.33	0.27	0.22	0.19	0.17	0.13	0.11	0.10
	5.0	1.67	0.83	0.56	0.42	0.33	0.28	0.24	0.21	0.17	0.14	0.12
	6.0	2.00	1.00	0.67	0.50	0.40	0.33	0.29	0.25	0.20	0.17	0.14
	7.0	2.33	1.17	0.78	0.58	0.47	0.39	0.33	0.29	0.23	0.19	0.17
	8.0	2.67	1.33	0.89	0.67	0.53	0.44	0.38	0.33	0.27	0.22	0.19
	9.0	3.00	1.50	1.00	0.75	0.60	0.50	0.43	0.38	0.30	0.25	0.21
	10.0	3.33	1.67	1.11	0.83	0.67	0.56	0.48	0.42	0.33	0.28	0.24
	12.0	4.00	2.00	1.33	1.00	0.80	0.67	0.57	0.50	0.40	0.33	0.29
	14.0	4.67	2.33	1.56	1.17	0.93	0.78	0.67	0.58	0.47	0.39	0.33
	16.0	5.33	2.67	1.78	1.33	1.07	0.89	0.76	0.67	0.53	0.44	0.38
	18.0	6.00	3.00	2.00	1.50	1.20	1.00	0.86	0.75	0.60	0.50	0.43
	20.0	6.67	3.33	2.22	1.67	1.33	1.11	0.95	0.83	0.67	0.56	0.48
	22.0	7.33	3.67	2.44	1.83	1.47	1.22	1.05	0.92	0.73	0.61	0.52
	24.0	8.00	4.00	2.67	2.00	1.60	1.33	1.14	1.00	0.80	0.67	0.57
	26.0	8.67	4.33	2.89	2.17	1.73	1.44	1.24	1.08	0.87	0.72	0.62
	28.0	9.33	4.67	3.11	2.33	1.87	1.56	1.33	1.17	0.93	0.78	0.67
	30.0	10.00	5.00	3.33	2.50	2.00	1.67	1.43	1.25	1.00	0.83	0.71
	32.0	10.67	5.33	3.56	2.67	2.13	1.78	1.52	1.33	1.07	0.89	0.76
	34.0	11.33	5.67	3.78	2.83	2.27	1.89	1.62	1.42	1.13	0.94	0.81
	36.0	12.00	6.00	4.00	3.00	2.40	2.00	1.71	1.50	1.20	1.00	0.86
	38.0	12.67	6.33	4.22	3.17	2.53	2.11	1.81	1.58	1.27	1.06	0.90
	40.0	13.33	6.67	4.44	3.33	2.67	2.22	1.90	1.67	1.33	1.11	0.95
	42.0	14.00	7.00	4.67	3.50	2.80	2.33	2.00	1.75	1.40	1.17	1.00
	44.0	14.67	7.33	4.89	3.67	2.93	2.44	2.10	1.83	1.47	1.22	1.05
	46.0	15.33	7.67	5.11	3.83	3.07	2.56	2.19	1.92	1.53	1.28	1.10
	48.0	16.00	8.00	5.33	4.00	3.20	2.67	2.29	2.00	1.60	1.33	1.14
	50.0	16.67	8.33	5.56	4.17	3.33	2.78	2.38	2.08	1.67	1.39	1.19
	52.0	17.33	8.67	5.78	4.33	3.47	2.89	2.48	2.17	1.73	1.44	1.24
	54.0	18.00	9.00	6.00	4.50	3.60	3.00	2.57	2.25	1.80	1.50	1.29
	56.0	18.67	9.33	6.22	4.67	3.73	3.11	2.67	2.33	1.87	1.56	1.33
	58.0	19.33	9.67	6.44	4.83	3.87	3.22	2.76	2.42	1.93	1.61	1.38
	60.0	20.00	10.00	6.67	5.00	4.00	3.33	2.86	2.50	2.00	1.67	1.43
	64.0	21.33	10.67	7.11	5.33	4.27	3.56	3.05	2.67	2.13	1.78	1.52
	68.0	22.67	11.33	7.56	5.67	4.53	3.78	3.24	2.83	2.27	1.89	1.62
	72.0	24.00	12.00	8.00	6.00	4.80	4.00	3.43	3.00	2.40	2.00	1.71
	76.0	25.33	12.67	8.44	6.33	5.07	4.22	3.62	3.17	2.53	2.11	1.81
	80.0	26.67	13.33	8.89	6.67	5.33	4.44	3.81	3.33	2.67	2.22	1.90

Note. Content movement velocity in [px/fr] = content movement velocity in [deg/s] / (idealized pixel size in [deg] × frame rate in [Hz]), content movement velocity in [px/fr] is determined for COBUS2 setup conditions (PD = 0.65 m, VD = 0.29 m, idealized pixel size of 0.10°/0.05° in horizontal/vertical direction), calculated velocity values in [px/fr] can only be executed with a steady horizontal content movement (no vertical movement in COBUS2) as long as the calculated values in [px/fr] are multiples of 0.5 (half-pixel jumps possible in horizontal direction), velocity values in [px/fr] that do not meet the assumption to be a multiple of 0.5 and therefore violate the half-pixel jump condition can also be created but lead to unsteady content movement (see Appendix C.2 for further information). Content movement velocity in [deg/s] is calculated without consideration of the center-to-periphery bias (CPB), i.e., the listed content movement velocities in [deg/s] correspond to the content's pixel jump (or content shift) between two frames for which it is simplistically assumed that (1) the content positions for both frames are symmetrically aligned in direct proximity around the adjustment point (AP) on the screen while (2) the participant's gaze position is also determined by the AP position. Deviations of these assumptions lead to a peripheral presentation of moving content in relation to the eye gaze position, resulting in reduced velocity values in [deg/s] (see Appendix C.3 for further information on the CPB).

Appendix H

Summary Tables

For both parts of the empirical study series — COBUS1 and COBUS2 — factors, targets, and constants were determined (see Tables H.1 and H.2), aiming to investigate the effect of the independent variables (factors) on the dependent variables (targets) while keeping certain study conditions stable.

A primary and a secondary target have to be distinguished. The primary target was the participant's CBU perception evaluated by a continuous CBU scale and the second target was the annoyance threshold determined by forced choice (see Section 4.2.8). Both targets were identical for COBUS1 and COBUS2.

The CBU-associated factors of COBUS1 and COBUS2 differed from each other as different research questions were addressed. During COBUS1, the factors were frame rate (FR = 11 specific values), saccadic length for CAT2 (SL = 5) or movement velocity for CAT3 (MV = 3), luminance level (LL = 3), and movement direction (MD = 2). For COBUS2, the factors were frame rate (FR = 2), stimulus position (SP = 12), stimulus size (SS = 6), and movement direction (MD = 4). The determined values of the investigated factors cover a specific range and can be looked up in Table H.1 for COBUS1 and Table H.2 for COBUS2. The total number of sequence loops that had to be presented to a participant during the main examination phase (see Section 4.2.8) can be calculated by multiplying the applied value count of all investigated factors during the study. This results in a total amount of 528 sequence loops for every participant during COBUS1, consisting of 330 loops for CAT2 (11 FR×3 LL×5 SL×2 MD) and 198 loops for CAT3 (11 FR×3 LL×3 MV×2 MD). Participants of COBUS2 were confronted with a total of 1,152 sequence loops, consisting of equal shares of 576 loops for CAT2 and CAT3 (2 FR×12 SP×6 SS×4 MD).

Specific hardware settings (e.g., subframe order within a frame period or duty cycle within a subframe period) and surrounding conditions (e.g., room illumination) were kept stable during the COBUS series to assure a controlled study execution and guarantee comparability of the results of COBUS1 and COBUS2. Other constants were kept stable only during COBUS1 or COBUS2 (e.g., viewing distance and angular pixel size), aiming to fulfill different requirements for content presentation.

TABLE H.1: Summary of independent variables (factors) and dependent variables (targets) as well as constants during COBUS1.

Classification	Factor / Target / Constant	Value [Unit]	Scale of Measurement
target (primary/secondary) [a]	subjective CBU perception (evaluated by continuous CBU scale)	lower scale pole = imperceptible (1.0), upper scale pole = very annoying (5.0)	metric
	annoyance threshold (evaluated by forced choice)	yes – no	nominal
projector setting	frame rate	30.0 – 60.0 – 90.0 – 120.0 – 150.0 – 180.0 – 210.0 – 240.0 – 300.0 – 360.0 – 420.0 [Hz]	metric
	duty cycle	0.3	metric
	subframe order	R – G – B	nominal
	native resolution	912×1140 [px]	metric
	(hor.) pixel size	0.05 [deg]	metric
stimulus setting	stimulus size [b]	quadratic shape, side length 2.0 [deg]	metric
	stimulus position [c]	0.0 [deg]	metric
	movement direction	L2R – R2L (randomized for Visit 1/2)	nominal
	saccadic length (only CAT2) [c]	3.6 – 9.0 – 14.3 – 21.3 – 28.2 [deg]	metric
	movement velocity (only CAT3) [d]	18.0 – 36.0 – 54.0 [deg/s]	metric
	stimulus luminance level	10.0 – 80.0 – 157.0 [cd/m^2]	metric
study setting	illuminance (room)	scotopic conditions during main examination (see appendix)	metric
	viewing / projection distance	0.58 / 0.65 [m]	metric
demographics	age of participant	18 – 35 [years] (see exlcusion criteria)	metric
	sex of participant	male – female	nominal
visual performance	visual acuity	$\leq$ 0.30 [logMAR] (see exclusion criteria)	metric
	contrast sensitivity	$\geq$ 1.20 [logCS] (see exlcusion criteria)	metric
	color perception	normal – anomaly, anopia excluded (see exclusion criteria)	metric
profession	job title	open question (group assignment afterwards)	nominal
	display type	tv – desktop – laptop – tablet – smartphone – others	nominal
	everyday usage duration	average time [hr]	metric
personality traits [e]	uncritical – critical	bipolar 5-point Likert scale	ordinal with metric latent variable
	technophile – technophobe	bipolar 5-point Likert scale	ordinal with metric latent variable
current state [e]	inattentive – attentive	bipolar 5-point Likert scale	ordinal with metric latent variable
	unmotivated – motivated	bipolar 5-point Likert scale	ordinal with metric latent variable
	tired – awake	bipolar 5-point Likert scale	ordinal with metric latent variable

[a] Participant's CBU perception was evaluated in two steps: first, assignment of score for perceived CBU effect on continuous CBU scale, second, answer to closed question if CBU is perceived as annoying, see post-sequence description in Section 4.2.8.
[b] Stimulus size in [deg] only valid for a central stimulus position regarding the participant's eye gaze position, deviations lead to reduced stimulus sizes in [deg] because of the center-to-periphery bias (CPB), see Appendix C.3 for more information.
[c] Stimulus position and saccadic movement paths in [deg] calculated correctly under consideration of the CPB.
[d] Content movement velocities in [deg/s] only valid for symmetrically aligned movements in direct proximity around the adjustment point (AP) on the screen, CPB induced deviations lead to reduced velocity values in [deg/s], see Appendix C.3.
[e] Evaluation of participant's personality traits (long-term items) and current state (short-term items) via bipolar 5-point Likert scales (poles of the applied scales are described semantically by bipolar antagonistic word pairs, see Appendix A.2.4).

TABLE H.2: Summary of independent variables (factors) and dependent variables (targets) as well as constants during COBUS2.

Classification	Factor / Target / Constant	Value [Unit]	Scale of Measurement
target (primary/secondary) [a]	subjective CBU perception (evaluated by continuous CBU scale)	lower scale pole = imperceptible (1.0), upper scale pole = very annoying (5.0)	metric
	annoyance threshold (evaluated by forced choice)	yes – no	nominal
projector setting	frame rate	30.0 – 60.0 [Hz]	metric
	duty cycle	0.3	metric
	subframe order	R – G – B	nominal
	native resolution	912×1140 [px]	metric
	(hor.) pixel size	0.10 [deg]	metric
stimulus setting	stimulus size (width/length) [b]	rectangular shape, 1.0 – 2.0 – 3.0 – 4.0 – 5.0 – 6.0 / 9.6 [deg]	metric
	stimulus position [c]	nasal and temporal retinal stimulation, 0.0 – 10.0 – 20.0 – 30.0 – 40.0 – 50.0 [deg]	metric
	movement direction	L2R – R2L – U2D – D2U	nominal
	saccadic length (only CAT2) [c]	9.6 [deg]	metric
	movement velocity (only CAT3) [d]	36.0 [deg/s]	metric
	stimulus luminance level	157.0 [cd/m^2]	metric
study settings	illuminance (room)	scotopic conditions during main examination (see appendix)	metric
	viewing / projection distance	0.29 / 0.65 [m]	metric
demographics	age of participant	18 – 35 [years] (see exlcusion criteria)	metric
	sex of participant	male – female	nominal
visual performance	visual acuity	$\leq$ 0.30 [logMAR] (see exclusion criteria)	metric
	contrast sensitivity	$\geq$ 1.20 [logCS] (see exlcusion criteria)	metric
	color perception	normal – anomaly, anopia excluded (see exclusion criteria)	metric
profession	job title	open question (group assignment afterwards)	nominal
	display type	—	—
	everyday usage duration	—	—
personality traits [e]	uncritical – critical	—	—
	technophile – technophobe	—	—
current state [e]	inattentive – attentive	—	—
	unmotivated – motivated	—	—
	tired – awake	—	—

[a] Participant's CBU perception was evaluated in two steps: first, assignment of score for perceived CBU effect on continuous CBU scale, second, answer to closed question if CBU is perceived as annoying, see post-sequence description in Section 4.2.8.
[b] Stimulus sizes in [deg] only valid for a central stimulus position regarding the participant's eye gaze position, deviations lead to reduced stimulus sizes in [deg] because of the center-to-periphery bias (CPB), see Appendix C.3 for more information.
[c] Stimulus positions and saccadic movement path in [deg] calculated correctly under consideration of the CPB, stimulus position of 0.0° investigated twice (nasal and temporal).
[d] Content movement velocity in [deg/s] only valid for symmetrically aligned movements in direct proximity around the adjustment point (AP) on the screen, CPB induced deviations lead to reduced velocity values in [deg/s], see Appendix C.3.
[e] No evaluation of participant's personality traits (long-term items) and current state (short-term items) via bipolar 5-point Likert scales during COBUS2.

References

Abeeluck, A. K., Iverson, A., Goetz, H., & Passon, E. (2018). 58-2: Invited paper: High-performance displays for wearable and HUD applications. *SID Symposium Digest of Technical Papers*, *49*(1), 768–771. https://doi.org/10.1002/sdtp.12358

Abramov, I., Gordon, J., & Chan, H. (1991). Color appearance in the peripheral retina: Effects of stimulus size. *Journal of the Optical Society of America A*, *8*(2), 404–414. https://doi.org/10.1364/josaa.8.000404

Abramov, I., Gordon, J., & Chan, H. (1992). Color appearance across the retina: Effects of a white surround. *Journal of the Optical Society of America A*, *9*(2), 195–202. https://doi.org/10.1364/JOSAA.9.000195

Altman, Y. (2020). *Cprintf - display formatted colored text in command window (Version 1.11.0.0)* [Code]. MATLAB File Exchange. https://de.mathworks.com/matlabcentral/fileexchange/24093-cprintf-display-formatted-colored-text-in-command-window

Arant, M. (2015). *Spider (data, tle, rng, lbl, leg, f) (Version 1.2.0.0)* [Code]. MATLAB File Exchange. https://de.mathworks.com/matlabcentral/fileexchange/22708-spider-data-tle-rng-lbl-leg-f?s_tid=prof_contriblnk

Atchison, D. A., & Smith, G. (2000). *Optics of the human eye*. Butterworth-Heinemann.

Awater, H., & Lappe, M. (2004). Perception of visual space at the time of pro- and anti-saccades. *Journal of Neurophysiology*, *91*(6), 2457–2464. https://doi.org/10.1152/jn.00821.2003

Ayama, M., & Sakurai, M. (2003). Changes in hue and saturation of chromatic lights presented in the peripheral visual field. *Color Research & Application*, *28*(6), 413–424. https://doi.org/10.1002/col.10194

Bach, M., Hoffmann, M. B., Jägle, H., Heinrich, S. P., Schiefer, U., & Wesemann, W. (2017). Kontrastsehen – Definitionen, Umrechnungen und Äquivalenztabelle [Contrast vision – definitions, conversions, and equivalence tables]. *Der Ophthalmologe*, *114*(4), 341–347. https://doi.org/10.1007/s00347-016-0379-5

Bach, M., Wesemann, W., Kolling, G., Bühren, J., Krastel, H., & Schiefer, U. (2008). Photopisches Kontrastsehen. Örtliche Kontrastempfindlichkeit [Photopic contrast sensitivity. Local contrast perception]. *Der Ophthalmologe*, *105*(1), 46–59. https://doi.org/10.1007/s00347-007-1605-y

Bach, M. (1996). The Freiburg Visual Acuity Test — Automatic measurement of visual acuity. *Optometry and Vision Science*, *73*(1), 49–53. https://doi.org/10.1097/00006324-199601000-00008

Bach, M. (2018). *Manual of the Freiburg Vision Test FrACT, Version 3.10.0*. https://michaelbach.de/fract/media/FrACT3_Manual.pdf

Bahill, A. T., Adler, D., & Stark, L. (1975). Most naturally occurring human saccades have magnitudes of 15 degrees or less. *Investigative Ophthalmology & Visual Science*, *14*(6), 468–469. https://iovs.arvojournals.org/arvo/content_public/journal/iovs/933061/468.pdf

Bahill, A. T., Clark, M. R., & Stark, L. (1975). The main sequence, a tool for studying human eye movements. *Mathematical Biosciences*, *24*, 191–204. https://doi.org/10.1016/0025-5564(75)90075-9

Bakhrakh, L., & Görlich, S. (2017). Improvement of monitor calibration using other than CIE 1931 color matching functions. *Proceedings of the Lux Europa Ljubljana*, 434–440. http://www.sdr.si/pdf/le2017_proceedings.pdf

Baloh, R. W., Sills, A. W., Kumley, W. E., & Honrubia, V. (1975). Quantitative measurement of saccade amplitude, duration, and velocity. *Neurology*, *25*(11), 1065. https://doi.org/10.1212/WNL.25.11.1065

Barlow, H. B. (1958). Temporal and spatial summation in human vision at different background intensities. *The Journal of Physiology*, *141*(2), 337–350. https://doi.org/10.1113/jphysiol.1958.sp005978

Barnes, G. R. (2008). Cognitive processes involved in smooth pursuit eye movements. *Brain and Cognition*, *68*(3), 309–326. https://doi.org/10.1016/j.bandc.2008.08.020

Baron, P. C., Monnier, P., Negy, A. L., Post, D. L., Christianson, L., Elcher, J., & Ewart, R. (1996). Can motion compensation eliminate color breakup of moving objects in field-sequential color displays? *SID International Symposium: Digest of Technical Papers*, *27*, 843–846.

Baron, P. C., & Chase, W. (2004). P-29: Variability in susceptibility to the color flash effect in field sequential color displays. *SID Symposium Digest of Technical Papers*, *35*(1), 338–341. https://doi.org/10.1889/1.1830983

Becker, W., & Jürgens, R. (1979). An analysis of the saccadic system by means of double step stimuli. *Vision Research*, *19*(9), 967–983. https://doi.org/10.1016/0042-6989(79)90222-0

Bedell, H. E., & Lott, L. A. (1996). Suppression of motion-produced smear during smooth pursuit eye movements. *Current Biology*, *6*(8), 1032–1034. https://doi.org/10.1016/S0960-9822(02)00650-4

Bergquist, J., & Wennstam, C. (2006). 49.2: Field-sequential-colour display with adaptive gamut. *SID Symposium Digest of Technical Papers*, *37*(1), 1594–1597. https://doi.org/10.1889/1.2433303

Berns, R. S. (2019). *Billmeyer and Saltzman's principles of color technology* (4th ed.). John Wiley & Sons. https://doi.org/10.1002/9781119367314

Beudaert, X. (2012). *Range intersection (Version 1.10.0.0)* [Code]. MATLAB File Exchange. https://de.mathworks.com/matlabcentral/fileexchange/31753-range-intersection

Bischof, N., & Kramer, E. (1968). Untersuchungen und Überlegungen zur Richtungswahrnehmung bei willkürlichen sakkadischen Augenbewegungen [Investigations and considerations of directional perception during voluntary saccadic eye movements]. *Psychologische Forschung*, *32*, 185–218. https://doi.org/10.1007/BF00418660

Blake, R., & Sekuler, R. (2006). *Perception* (5th ed.). McGraw-Hill.

Bloch, A.-M. (1885). Expériences sur la vision [Experiments on vision]. *Comptes Rendus des Séances de la Société de Biologie*, *37*, 493–495.

Bono, F., Oliveri, R. L., Zappia, M., Aguglia, U., Puccio, G., & Quattrone, A. (1996). Computerized analysis of eye movements as a function of age. *Archives of Gerontology and Geriatrics*, *22*(3), 261–269. https://doi.org/10.1016/0167-4943(96)00698-X

Bortz, J., & Schuster, C. (2010). *Statistik für Human-und Sozialwissenschaftler [Statistics for human and social scientists]* (7th ed.). Springer-Verlag. https://link.springer.com/book/10.1007/978-3-642-12770-0

Boynton, R. M., Schafer, W., & Neun, M. E. (1964). Hue-wavelength relation measured by color-naming method for three retinal locations. *Science*, *146*(3644), 666–668. https://doi.org/10.1126/science.146.3644.666

Braun, D. I., Schütz, A. C., & Gegenfurtner, K. R. (2017). Visual sensitivity for luminance and chromatic stimuli during the execution of smooth pursuit and saccadic eye movements. *Vision Research*, *136*, 57–69. https://doi.org/10.1016/j.visres.2017.05.008

Brenner, E., Smeets, J. B. J., & van den Berg, A. V. (2001). Smooth eye movements and spatial localisation. *Vision Research*, *41*(17), 2253–2259. https://doi.org/10.1016/S0042-6989(01)00018-9

Bridgeman, B., van der Heijden, A. H. C., & Velichkovsky, B. M. (1994). A theory of visual stability across saccadic eye movements. *Behavioral and Brain Sciences*, *17*(2), 247–258. https://doi.org/10.1017/S0140525X00034361

Brown, B. (1972). Dynamic visual acuity, eye movements and peripheral acuity for moving targets. *Vision Research*, *12*(2), 305–321. https://doi.org/10.1016/0042-6989(72)90120-4

Brown, M. R. G., DeSouza, J. F. X., Goltz, H. C., Ford, K., Menon, R. S., Goodale, M. A., & Everling, S. (2004). Comparison of memory- and visually guided saccades using event-related fMRI. *Journal of Neurophysiology*, *91*(2), 873–889. https://doi.org/10.1152/jn.00382.2003

Burr, D. C. (1981). Temporal summation of moving images by the human visual system. *Proceedings of the Royal Society B: Biological Sciences*, *211*(1184), 321–339. https://doi.org/10.1098/rspb.1981.0010

Burr, D. C., Holt, J., Johnstone, J. R., & Ross, J. (1982). Selective depression of motion sensitivity during saccades. *The Journal of Physiology*, *333*(1), 1–15. https://doi.org/10.1113/jphysiol.1982.sp014434

Burr, D. C., Morrone, M. C., & Ross, J. (1994). Selective suppression of the magnocellular visual pathway during saccadic eye movements. *Nature*, *371*(6497), 511–513. https://doi.org/10.1038/371511a0

Carpenter, R. H. S. (1988). *Movements of the eyes*. Pion Ltd.

Chang, C.-W., Lin, F.-C., Huang, Y.-P., Shieh, H.-P. D., Hsu, K.-Y., Langendijk, E. H. A., & Huang, Y.-S. (2012). 55.3: Development of a 65-inch color-filter-less LCD and Stencil-LPD method for high quality 120Hz 2-field displays. *SID Symposium Digest of Technical Papers*, *43*(1), 745–748. https://doi.org/10.1002/j.2168-0159.2012.tb05891.x

Chen, C.-H., Chen, K.-H., Huang, Y.-P., Shieh, H.-P. D., & Ho, M.-T. (2008). 71.2: Gray level redistribution in field sequential color LCD technique for color breakup reduction. *SID Symposium Digest of Technical Papers*, *39*(1), 1096–1099. https://doi.org/10.1889/1.3069326

Chen, C.-H., Lin, F.-C., Hsu, Y.-T., Huang, Y.-P., & Shieh, H.-P. D. (2009). A field sequential color LCD based on color fields arrangement for color breakup and flicker reduction. *Journal of Display Technology*, *5*(1), 34–39. https://doi.org/10.1109/jdt.2008.2001578

Chen, R. H. (2011). *Liquid crystal displays: Fundamental physics and technology*. John Wiley & Sons. https://doi.org/10.1002/9781118084359

Chen, S.-C., Yan, S.-P., Cheng, Y.-K., Lin, F.-C., Wei, C.-M., Huang, Y.-P., & Shieh, H.-P. D. (2007). A human visual model for color break-up artifact in design field-sequential color LCDs. *Proceedings of the International Display Manufacturing Conference and FPD Expo*, 872–875. https://scholar.nycu.edu.tw/en/publications/a-human-visual-model-for-color-break-up-artifact-in-design-field-

Chen, Y.-F., Chen, C.-C., & Chen, K.-H. (2007a). 11.3: Mixed color sequential technique for high contrast LCD with optimum power consumption. *SID Symposium Digest of Technical Papers*, *38*(1), 134–137. https://doi.org/10.1889/1.2785245

Chen, Y.-F., Chen, C.-C., & Chen, K.-H. (2007b). Mixed color sequential technique for reducing color breakup and motion blur effects. *Journal of Display Technology*, *3*(4), 377–385. https://doi.org/10.1109/JDT.2007.903160

Cheng, H.-C., Rao, L., & Wu, S.-T. (2010). Color breakup suppression in field-sequential five-primary-color LCDs. *Journal of Display Technology*, *6*(6), 229–234. https://doi.org/10.1109/JDT.2010.2042678

Cheng, Y.-K., Huang, Y.-P., Cheng, Y.-R., & Shieh, H.-P. D. (2009). Two-field scheme: Spatiotemporal modulation for field sequential color LCDs. *Journal of Display Technology*, *5*(10), 385–390. https://doi.org/10.1109/JDT.2009.2026186

Cheng, Y.-K., & Shieh, H.-P. D. (2009). Relative contrast sensitivity for color break-up evaluation in field-sequential-color LCDs. *Journal of Display Technology*, *5*(10), 379–384. https://doi.org/10.1109%2FJDT.2009.2025708

Chirimuuta, M., & Tolhurst, D. J. (2005). Does a Bayesian model of V1 contrast coding offer a neurophysiological account of human contrast discrimination? *Vision Research*, *45*(23), 2943–2959. https://doi.org/10.1016/j.visres.2005.06.022

Chu, C.-L., Chiu, T.-L., & Chen, K.-H. (2010). Pseudo zero-dimension dimming for power reduction in field sequential color liquid crystal display systems. *Journal of Display Technology*, *6*(8), 323–331. https://doi.org/10.1109/JDT.2010.2056353

Collewijn, H., & Tamminga, E. P. (1986). Human fixation and pursuit in normal and open-loop conditions: Effects of central and peripheral retinal targets. *The Journal of Physiology*, *379*(1), 109–129. https://doi.org/10.1113/jphysiol.1986.sp016243

Coren, S., & Kaplan, C. P. (1973). Patterns of ocular dominance. *Optometry and Vision Science*, *50*(4), 283–292. https://journals.lww.com/optvissci/abstract/1973/04000/patterns_of_ocular_dominance_.2.aspx

Crisler, M. C., Held, R. T., Latta, S., Michail, A. A., Shetter, M., & Tomlin, A. (2018). *Avoidance of color breakup in late-stage re-projection* (U.S. Patent No. 9,874,932). U.S. Patent and Trademark Office. https://patft.uspto.gov/netacgi/nph-Parser?patentnumber=9874932

Dalhaus, R. N., & Gunther, K. L. (2012). A tritan Waldo would be easier to detect in the periphery than a red/green one: Evidence from visual search. *Journal of the Optical Society of America A*, *29*(2), A298–A305. https://doi.org/10.1364/JOSAA.29.00A298

de Brouwer, S., Yuksel, D., Blohm, G., Missal, M., & Lefèvre, P. (2002). What triggers catch-up saccades during visual tracking? *Journal of Neurophysiology*, *87*(3), 1646–1650. https://doi.org/10.1152/jn.00432.2001

den Boer, W. (2005). *Active matrix liquid crystal displays: Fundamentals and applications*. Elsevier.

Diamond, M. R., Ross, J., & Morrone, M. C. (2000). Extraretinal control of saccadic suppression. *Journal of Neuroscience*, *20*(9), 3449–3455. https://doi.org/10.1523/JNEUROSCI.20-09-03449.2000

Dodge, R. (1903). Five types of eye movement in the horizontal meridian plane of the field of regard. *American Journal of Physiology-Legacy Content*, *8*(4), 307–329. https://doi.org/10.1152/ajplegacy.1903.8.4.307

EIZO Corporation. (2013). *ColorEdge CG246 calibration color LCD monitor: User's manual*. https://www.eizoglobal.com/support/db/files/manuals/03V24050F1/Manual-EN.pdf

Eliav, D., Langendijk, E. H. A., Swinkels, S., & Baruchi, I. (2005). 47.3: Suppression of color breakup in color-sequential multi-primary projection displays. *SID Symposium Digest of Technical Papers*, *36*(1), 1510–1513. https://doi.org/10.1889/1.2036297

Emsley, H. H. (1936). *Visual optics*. Hatton Press Ltd.

Enderle, J. D. (2010). *Models of horizontal eye movements, part I: Early models of saccades and smooth pursuit*. Morgan & Claypool Publishers. https://doi.org/dfbch4

Eyegaze. (n.d.). *Eyegaze Edge: User manual*. https://eyegaze.com/wp-content/uploads/Eyegaze-Edge-Manual.pdf

Eysel, U. (2017). Sehen und Augenbewegungen [Vision and eye movement]. In R. F. Schmidt, F. Lang, & M. Heckmann (Eds.), *Physiologie des Menschen* (pp. 345–385). Springer-Verlag. https://doi.org/10.1007/978-3-642-01651-6

Fechner, G. T. (1860). *Elemente der Psychophysik [Elements of psychophysics]* (Vol. 2). Breitkopf und Härtel.

Findlay, J. M., & Harris, L. R. (1984). Small saccades to double-stepped targets moving in two dimensions. In A. G. Gale & F. Johnson (Eds.), *Theoretical and applied aspects of eye movement research* (pp. 71–78). North-Holland Publishing. https://www.sciencedirect.com/bookseries/advances-in-psychology/vol/22/suppl/C

Fischer, B. (1999). *Blickpunkte: Neurobiologische Prinzipien des Sehens und der Blicksteuerung [Viewpoints: Neurobiological principles of vision and gaze control]*. Verlag Hans Huber.

Fischer, B., Biscaldi, M., & Gezeck, S. (1997). On the development of voluntary and reflexive components in human saccade generation. *Brain Research*, *754*(1-2), 285–297. https://doi.org/10.1016/S0006-8993(97)00094-2

Flipse, J. P., van der Wildt, G. J., Rodenburg, M., Keemink, C. J., & Knol, P. G. M. (1988). Contrast sensitivity for oscillating sine wave gratings during ocular fixation and pursuit. *Vision Research*, *28*(7), 819–826. https://doi.org/10.1016/0042-6989(88)90029-6

Garbutt, S., Han, Y., Kumar, A. N., Harwood, M., Harris, C. M., & Leigh, R. J. (2003). Vertical optokinetic nystagmus and saccades in normal human subjects. *Investigative Ophthalmology & Visual Science*, *44*(9), 3833–3841. https://doi.org/10.1167/iovs.03-0066

Gelabert, P. (2013, July 15). *A look inside the iView engine in LightCrafter4500* [Online forum post]. Texas Instruments. https://e2e.ti.com/support/dlp-products-group/dlp/f/dlp-products-forum/278008/a-look-inside-the-iview-engine-in-lightcrafter4500

Gibaldi, A., & Sabatini, S. P. (2021). The saccade main sequence revised: A fast and repeatable tool for oculomotor analysis. *Behavior Research Methods*, *53*(1), 167–187. https://doi.org/10.3758/s13428-020-01388-2

Gilchrist, I. D. (2011). Saccades. In S. P. Liversedge, I. D. Gilchrist, & S. Everling (Eds.), *The Oxford handbook of eye movements* (pp. 85–94). Oxford University Press. https://doi.org/10.1093/oxfordhb/9780199539789.001.0001

Goettker, A., Braun, D. I., Schütz, A. C., & Gegenfurtner, K. R. (2018). Execution of saccadic eye movements affects speed perception. *Proceedings of the National Academy of Sciences*, *115*(9), 2240–2245. https://doi.org/10.1073/pnas.1704799115

Goldmark, P. C. (1949). *Color television* (U.S. Patent No. 2,480,571). U.S. Patent and Trademark Office. https://patft.uspto.gov/netacgi/nph-Parser?patentnumber=2480571

Goodmanson, D. (2017, November 14). *Overlapping time-intervals* [Online forum post]. MATLAB Answers. https://de.mathworks.com/matlabcentral/answers/366626-overlapping-time-intervals

Gordon, J., & Abramov, I. (1977). Color vision in the peripheral retina. II. Hue and saturation. *Journal of the Optical Society of America*, *67*(2), 202–207. https://doi.org/10.1364/JOSA.67.000202

Gorea, A. (2015). A refresher of the original Bloch's law paper (Bloch, July 1885). *i-Perception*, *6*(4), 1–6. https://doi.org/10.1177/2041669515593043

Guenther, B. D., & Steel, D. G. (Eds.). (2018). *Encyclopedia of modern optics* (2nd ed.). Elsevier. https://www.elsevier.com/books/encyclopedia-of-modern-optics/guenther/978-0-12-809283-5

Guilford, J. P. (1954). *Psychometric methods*. McGraw-Hill.

Hamada, H., & Yujiri, A. (2004). Color zone map in peripheral vision at various illuminance levels. *Optical Review*, *11*(4), 240–248. https://doi.org/10.1007/s10043-004-0240-y

Hansen, T., Pracejus, L., & Gegenfurtner, K. R. (2009). Color perception in the intermediate periphery of the visual field. *Journal of Vision*, *9*(4), 1–12. https://doi.org/drq36h

Hartline, H. K. (1934). Intensity and duration in the excitation of single photoreceptor units. *Journal of Cellular & Comparative Physiology*, *5*(2), 229–247. https://doi.org/10.1002/jcp.1030050210

Hasebe, H., & Kobayashi, S. (1985). A full-color field sequential LCD using modulated backlight. *SID Symposium Digest of Technical Papers*, *16*, 81–83.

Häussler, R., Gritsai, Y., Zschau, E., Missbach, R., Sahm, H., Stock, M., & Stolle, H. (2017). Large real-time holographic 3D displays: Enabling components and results. *Applied Optics*, *56*(13), F45–F52. https://doi.org/10.1364/AO.56.000F45

Hertenstein, H., Bach, M., Gross, N. J., & Beisse, F. (2016). Marked dissociation of photopic and mesopic contrast sensitivity even in normal observers. *Graefe's Archive for Clinical and Experimental Ophthalmology*, *254*(2), 373–384. https://doi.org/10.1007/s00417-015-3020-4

Holmes, R., Victora, M., Wang, R. F., & Kwiat, P. G. (2017). Measuring temporal summation in visual detection with a single-photon source. *Vision Research*, *140*, 33–43. https://doi.org/10.1016/j.visres.2017.06.011

Honda, H. (1989). Perceptual localization of visual stimuli flashed during saccades. *Perception & Psychophysics*, *45*(2), 162–174. https://doi.org/10.3758/BF03208051

Honda, H. (1991). The time courses of visual mislocalization and of extraretinal eye position signals at the time of vertical saccades. *Vision Research*, *31*(11), 1915–1921. https://doi.org/10.1016/0042-6989(91)90186-9

Hsu, Y.-T., Lin, F.-C., Chen, C.-H., Huang, Y.-P., & Shieh, H.-P. D. (2007). A field sequential color LCD based on color field arrangement for color breakup and flicker reduction. *Proceedings of the 14th International Display Workshops*, 59–62.

Hu, K.-T., Lin, T.-P., Tsai, C.-C., Tai, W.-C., & Chien, K.-H. (2011). 20.1: A method for color breakup suppression in a color sequential display. *SID Symposium Digest of Technical Papers*, *42*(1), 251–254. https://doi.org/10.1889/1.3621286

Huang, F.-C., Pająk, D., Kim, J., Kautz, J., & Luebke, D. (2017). Mixed-primary factorization for dual-frame computational displays. *ACM Transactions on Graphics*, *36*(4), 1–13. https://doi.org/10.1145/3072959.3073654

Huang, Y.-P., Chen, K.-H., Chen, C.-H., Lin, F.-C., & Shieh, H.-P. D. (2008). Adaptive LC/BL feedback control in field sequential color LCD technique for color breakup minimization. *Journal of Display Technology*, *4*(3), 290–295. https://doi.org/10.1109/JDT.2008.926494

Huang, Y.-P., Lin, F.-C., & Shieh, H.-P. D. (2011). Eco-displays: The color LCD's without color filters and polarizers. *Journal of Display Technology*, *7*(12), 630–632. https://doi.org/10.1109/JDT.2011.2166056

Huang, Y.-P., Lin, F.-C., Tsai, C.-C., & Shieh, H.-P. D. (2009). Stencil field-sequential color method for color breakup suppression on 180Hz LCD-TV. *Proceedings of the Eurodisplay Conference*, 564–567. https://scholar.nycu.edu.tw/en/publications/invited-stencil-field-sequential-color-method-for-color-breakup-s

Huang, Y.-P., Lin, F.-C., Wei, C.-M., Shieh, H.-P. D., Tsai, C.-C., Tai, W.-C., & Mo, C.-N. (2008). A color break-up suppression method, Stencil-FSC method, for field-sequential-color (FSC) LCDs with low power consumption. *SID Conference Record of the International Display Research Conference*, 59–62. https://scholar.nycu.edu.tw/en/publications/a-color-break-up-suppression-method-stencil-fsc-method-for-field-

Huang, Y.-P., Yan, S.-P., Hsu, Y.-T., Cheng, Y.-K., Chen, C.-H., Lin, F.-C., & Shieh, H.-P. D. (2007). Human vision model for color break-up (CBU) and a CBU-less 5.6" field sequential color display. *10th Asian Symposium on Information Display*, 71–74. https://scholar.nycu.edu.tw/en/publications/human-vision-model-for-color-break-upcbu-and-a-cbu-less-56-field-

Hunt, R. W. G., & Pointer, M. R. (2011). *Measuring colour* (4th ed.). John Wiley & Sons. https://doi.org/10.1002/9781119975595

Ikeda, M., Sekiguchi, N., & Shioiri, S. (1985). Color perimetry with a color naming method. In A. Heijl & E. L. Greve (Eds.), *Sixth international visual field symposium* (pp. 273–277). Dr. W. Junk Publishers. https://doi.org/10.1007/978-94-009-5512-7

International Organization for Standardization. (2020). *Ophthalmic optics — Chart displays for visual acuity measurement — Printed, projected and electronic*. (ISO Standard No. 10938). https://www.iso.org/standard/63691.html.

International Telecommunication Union. (2012). *Methodology for the subjective assessment of the quality of television pictures*. (ITU-R BT.500-13). https://www.itu.int/rec/R-REC-BT.500.

Jak, M. J. J., Hekstra, G. J., Hoppenbrouwers, J. J. L., Vossen, F. J., Raman, N., & Belik, O. (2005). 25.3: Spectrum sequential liquid crystal display. *SID Symposium Digest of Technical Papers*, *36*(1), 1120–1123. https://doi.org/10.1889/1.2036197

Järvenpää, T. (2005). Measuring color breakup of stationary images in field-sequential-color displays. *Journal of the Society for Information Display*, *13*(2), 139–144. https://doi.org/10.1889/1.2012596

JETI Technische Instrumente GmbH. (2021a). *JETI Spectroradiometer Specbos 12x1 / Specbos 1211-2: Operating instructions*. https://www.jeti.com/files/content/products/spectroradiometer/JETI_specbos.pdf

JETI Technische Instrumente GmbH. (2021b). *Spectroradiometer Specbos 1211-2: Data sheet*. https://www.jeti.com/files/content/support/downloads/specbos%201211-2.pdf

Johnson, M. A. (1986). Color vision in the peripheral retina. *American Journal of Optometry and Physiological Optics*, *63*(2), 97–103. https://doi.org/10.1097/00006324-198602000-00003

Johnson, P. V., Kim, J., & Banks, M. S. (2014). The visibility of color breakup and a means to reduce it. *Journal of Vision*, *14*(14), 1–13. https://doi.org/10.1167/14.14.10

Jones, G. (2017). *PsychometricCurveFitting* [Code]. GitHub. https://github.com/garethjns/PsychometricCurveFitting

Kalesnykas, R. P., & Hallett, P. E. (1994). Retinal eccentricity and the latency of eye saccades. *Vision Research*, *34*(4), 517–531. https://doi.org/10.1016/0042-6989(94)90165-1

Kaplanyan, A. S., Sochenov, A., Leimkühler, T., Okunev, M., Goodall, T., & Rufo, G. (2019). DeepFovea: Neural reconstruction for foveated rendering and video compression using learned statistics of natural videos. *ACM Transactions on Graphics*, *38*(6), 1–13. https://doi.org/10.1145/3355089.3356557

Kearney, K. (2014). *Boundedline.m: Line with shaded error/confidence bounds (Version 1.3.0.0)* [Code]. MATLAB File Exchange. https://de.mathworks.com/matlabcentral/fileexchange/27485-boundedline-m

Kerst, S. M., & Howard, J. H., Jr. (1978). Memory psychophysics for visual area and length. *Memory & Cognition*, *6*(3), 327–335. https://doi.org/10.3758/BF03197463

Kerzel, D., Aivar, M. P., Ziegler, N. E., & Brenner, E. (2006). Mislocalization of flashes during smooth pursuit hardly depends on the lighting conditions. *Vision Research*, *46*(6-7), 1145–1154. https://doi.org/10.1016/j.visres.2005.06.032

Kim, J. U., Yang, C. M., Bae, J. H., Kim, C.-W., Lee, H.-S., & Kim, D. (2014). Evaluation of static color breakup for natual images on field sequential displays. *Color Imaging XIX: Displaying, Processing, Hardcopy, and Applications*, *9015*, 90150L. https://doi.org/10.1117/12.2041437

Klein, C., & Ettinger, U. (Eds.). (2019). *Eye movement research: An introduction to its scientific foundations and applications*. Springer-Verlag. https://doi.org/10.1007/978-3-030-20085-5

Klinke, R., & Silbernagl, S. (2005). *Lehrbuch der Physiologie [Textbook of physiology]* (4th ed.). Thieme.

Knox, P. C., Davidson, J. H., & Anderson, D. (2005). Age-related changes in smooth pursuit initiation. *Experimental Brain Research*, *165*(1), 1–7. https://doi.org/10.1007/s00221-005-2265-2

Kobayashi, M., Yoshida, A., & Yoshida, Y. (2010). P-51: A basic assessment for color break-up on a field-sequential color display. *SID Symposium Digest of Technical Papers*, *41*(1), 1434–1437. https://doi.org/10.1889/1.3499974

Kobayashi, M., Yoshida, A., & Yoshida, Y. (2011). An evaluation of perceived color break-up on field-sequential color displays. *Human Vision and Electronic Imaging XVI*, *7865*, 1–9. https://doi.org/10.1117/12.872325

Koma, N., & Uchida, T. (2003). A new field-sequential-color LCD without moving-object color break-up. *Journal of the Society for Information Display*, *11*(2), 413–417. https://doi.org/10.1889/1.1825656

Kowler, E. (2011). Eye movements: The past 25 years. *Vision Research*, *51*(13), 1457–1483. https://doi.org/10.1016/j.visres.2010.12.014

Kowler, E., van der Steen, J., Tamminga, E. P., & Collewun, H. (1984). Voluntary selection of the target for smooth eye movement in the presence of superimposed, full-field stationary and moving stimuli. *Vision Research*, *24*(12), 1789–1798. https://doi.org/10.1016/0042-6989(84)90010-5

Krastel, H. (2006). *Anomaloskop: Leitfaden für die Untersuchung in der Praxis [Anomaloscope: Guideline for the investigation in practice]*. https://www.oculus.de/uploads/media/oculus_hmc_anomaloskop_kurzanleitung.pdf

Krauzlis, R. J. (2004). Recasting the smooth pursuit eye movement system. *Journal of Neurophysiology*, *91*(2), 591–603. https://doi.org/10.1152/jn.00801.2003

Kuyk, T. K. (1982). Spectral sensitivity of the peripheral retina to large and small stimuli. *Vision Research*, *22*(10), 1293–1297. https://doi.org/10.1016/0042-6989(82)90142-0

Langendijk, E. H. A. (2007). A novel spectrum-sequential display design with a wide color gamut and reduced color breakup. *Journal of the Society for Information Display*, *15*(4), 261–266. https://doi.org/10.1889/1.2723883

Langendijk, E. H. A., Cennini, G., & Belik, O. (2009). Color-breakup evaluation of spatio-temporal color displays with two- and three-color fields. *Journal of the Society for Information Display*, *17*(11), 933–940. https://doi.org/10.1889/JSID17.11.933

Langendijk, E. H. A., Swinkels, S., Eliav, D., & Ben-Chorin, M. (2006). Suppression of color breakup in color-sequential multi-primary projection displays. *Journal of the Society for Information Display*, *14*(3), 325–329. https://doi.org/10.1889/1.2185281

Lappe, M., Awater, H., & Krekelberg, B. (2000). Postsaccadic visual references generate presaccadic compression of space. *Nature*, *403*(6772), 892–895. https://doi.org/10.1038/35002588

Lebedev, S., Van Gelder, P., & Tsui, W. H. (1996). Square-root relations between main saccadic parameters. *Investigative Ophthalmology & Visual Science*, *37*(13), 2750–2758. https://iovs.arvojournals.org/article.aspx?articleid=2161749

Legge, G. E., & Foley, J. M. (1980). Contrast masking in human vision. *Journal of the Optical Society of America*, *70*(12), 1458–1471. https://doi.org/10.1364/JOSA.70.001458

Leigh, R. J., & Zee, D. S. (2015). *The neurology of eye movements* (5th ed.). Oxford University Press. https://doi.org/10.1093/med/9780199969289.001.0001

Lin, F.-C. (2018). Color formation of LCD – spatial and temporal. In B. D. Guenther & D. G. Steel (Eds.), *Encyclopedia of modern optics* (2nd ed., pp. 17–24). Elsevier. https://www.elsevier.com/books/encyclopedia-of-modern-optics/guenther/978-0-12-809283-5

Lin, F.-C., Chang, C.-W., Huang, Y.-P., & Shieh, H.-P. D. (2015). High-image reproduction by the low-field-rate Stencil-LPD method for field-sequential-color LCDs. *Journal of Display Technology*, *11*(12), 1069–1075. https://doi.org/10.1109/JDT.2015.2448762

Lin, F.-C., Huang, Y.-P., & Shieh, H.-P. D. (2010). Color breakup reduction by 180 Hz Stencil-FSC method in large-sized color filter-less LCDs. *Journal of Display Technology*, *6*(3), 107–112. https://doi.org/10.1109/JDT.2009.2027034

Lin, F.-C., Huang, Y.-P., Teng, C.-Y., & Shieh, H.-P. D. (2012). Image saturation improvement for 180 Hz Stencil-FSC LCD with side-lit LED backlight. *Journal of Display Technology*, *8*(12), 699–706. https://doi.org/10.1109/JDT.2012.2215839

Lin, F.-C., Huang, Y.-P., Wei, C.-M., & Shieh, H.-P. D. (2009). Color-breakup suppression and low-power consumption by using the Stencil-FSC method in field-sequential LCDs. *Journal of the Society for Information Display*, *17*(3), 221–228. https://doi.org/10.1889/JSID17.3.221

Lin, F.-C., Huang, Y.-P., Wei, C.-M., & Shieh, H.-P. D. (2010). Color filter-less LCDs in achieving high contrast and low power consumption by Stencil field-sequential-color method. *Journal of Display Technology*, *6*(3), 98–106. https://doi.org/10.1109%2FJDT.2009.2025395

Lin, F.-C., Huang, Y.-P., Wei, C.-M., Shieh, H.-P. D., Tsai, C.-C., & Tai, W.-C. (2008). 71.5: Stencil-FSC method for color break-up suppression and low power consumption in field-sequential LCDs. *SID Symposium Digest of Technical Papers*, *39*(1), 1108–1111. https://doi.org/10.1889/1.3069330

Lin, F.-C., Qin, Z., Teng, K.-T., & Huang, Y.-P. (2019). Color breakup suppression based on global dimming for field sequential color displays using edge information in images. *Optics Express*, *27*(3), 2335–2343. https://doi.org/10.1364/OE.27.002335

Lin, F.-C., Teng, K.-T., Chang, C.-W., Lin, C.-H., Huang, Y.-P., & Shieh, H.-P. D. (2016). 15-2: Effective color breakup suppression by a low-cost global dimming backlight for field-sequential-color displays. *SID Symposium Digest of Technical Papers*, *47*(1), 171–174. https://doi.org/10.1002/sdtp.10628

Lin, F.-C., Teng, K.-T., Huang, Y.-P., & Shieh, H.-P. D. (2016). Color breakup reduction using global Edge-FSC method. *23rd International Display Workshops in conjunction with Asia Display*, 656–657. https://scholar.nycu.edu.tw/en/publications/color-breakup-reduction-using-global-edge-fsc-method

Lin, F.-C., Zhang, Y., & Langendijk, E. H. A. (2011a). 65.1: Color breakup reduction by local-primary-desaturation in color-filterless LCDs. *SID Symposium Digest of Technical Papers*, *42*(1), 960–963. https://doi.org/10.1889/1.3621500

Lin, F.-C., Zhang, Y., & Langendijk, E. H. A. (2011b). Color breakup suppression by local primary desaturation in field-sequential color LCDs. *Journal of Display Technology*, *7*(2), 55–61. https://doi.org/10.1109/JDT.2010.2090493

Lin, Y.-J., Qin, Z., Lin, F.-C., Shieh, H.-P. D., & Huang, Y.-P. (2018). 85-3: Distinguished student paper: Image-content-adaptive color breakup index for field-sequential-color displays using dominant visual saliency method. *SID Symposium Digest of Technical Papers*, *49*(1), 1159–1162. https://doi.org/10.1002/sdtp.12104

Lisberger, S. G., & Westbrook, L. E. (1985). Properties of visual inputs that initiate horizontal smooth pursuit eye movements in monkeys. *Journal of Neuroscience*, *5*(6), 1662–1673. https://doi.org/10.1523/JNEUROSCI.05-06-01662.1985

Lisberger, S. G., Morris, E. J., & Tychsen, L. (1987). Visual motion processing and sensory-motor integration for smooth pursuit eye movements. *Annual Review of Neuroscience*, *10*(1), 97–129. https://doi.org/10.1146/annurev.ne.10.030187.000525

Lu, H.-C., Hsieh, W.-T., & Chien, S.-Y. (2020). Boosting perceptual resolution of VR displays. *CVPR Workshop on Computer Vision for Augmented and Virtual Reality*, 1–4. https://xr.cornell.edu/workshop/2020/papers

Ludvigh, E., & Miller, J. W. (1958). Study of visual acuity during the ocular pursuit of moving test objects. I. Introduction. *Journal of the Optical Society of America*, *48*(11), 799–802. https://doi.org/10.1364/JOSA.48.000799

Ludwig, C. J. H., Gilchrist, I. D., & McSorley, E. (2004). The influence of spatial frequency and contrast on saccade latencies. *Vision Research*, *44*(22), 2597–2604. https://doi.org/10.1016/j.visres.2004.05.022

Ludwig, C. J. H., Mildinhall, J. W., & Gilchrist, I. D. (2007). A population coding account for systematic variation in saccadic dead time. *Journal of Neurophysiology*, *97*(1), 795–805. https://doi.org/10.1152/jn.00652.2006

Makino, T., Yoshihara, T., Shiroto, H., & Kiyota, Y. (2003). *Liquid crystal display* (U.S. Patent No. 6,570,554). U.S. Patent and Trademark Office. https://patft.uspto.gov/netacgi/nph-Parser?patentnumber=6570554

Mallot, H. A. (2000). *Sehen und die Verarbeitung visueller Information [Vision and the processing of visual information]* (2nd ed.). Vieweg+Teubner Verlag. https://doi.org/10.1007/978-3-663-11347-8

Martin, P. R., Lee, B. B., White, A. J. R., Solomon, S. G., & Rüttiger, L. (2001). Chromatic sensitivity of ganglion cells in the peripheral primate retina. *Nature*, *410*(6831), 933–936. https://doi.org/10.1038/35073587

Matin, L., & Pearce, D. G. (1965). Visual perception of direction for stimuli flashed during voluntary saccadic eye movements. *Science*, *148*(3676), 1485–1488. https://doi.org/10.1126/science.148.3676.1485

Maxwell, J. C. (1857). XVIII.—Experiments on colour, as perceived by the eye, with remarks on colour-blindness. *Transactions of the Royal Society of Edinburgh*, *21*(2), 275–298. https://doi.org/10.1017/S0080456800032117

Maxwell, J. C. (1860). On the theory of compound colours, and the relations of the colours of the spectrum. *Proceedings of the Royal Society of London*, *10*, 404–409. https://doi.org/10.1098/rspl.1859.0074

McIlhagga, W., & Pääkkönen, A. (1999). Noisy templates explain area summation. *Vision Research*, *39*(2), 367–372. https://doi.org/10.1016/S0042-6989(98)00141-2

McKeefry, D. J., Murray, I. J., & Parry, N. R. A. (2007). Perceived shifts in saturation and hue of chromatic stimuli in the near peripheral retina. *Journal of the Optical Society of America A*, *24*(10), 3168–3179. https://doi.org/10.1364/JOSAA.24.003168

Meese, T. S. (2004). Area summation and masking. *Journal of Vision*, *4*(10), 930–943. https://doi.org/10.1167/4.10.8

Meese, T. S., Hess, R. F., & Williams, C. B. (2005). Size matters, but not for everyone: Individual differences for contrast discrimination. *Journal of Vision*, *5*(11), 928–947. https://doi.org/10.1167/5.11.2

Meese, T. S., & Summers, R. J. (2007). Area summation in human vision at and above detection threshold. *Proceedings of the Royal Society B: Biological Sciences*, *274*(1627), 2891–2900. https://doi.org/10.1098/rspb.2007.0957

Meyer, C. H., Lasker, A. G., & Robinson, D. A. (1985). The upper limit of human smooth pursuit velocity. *Vision Research*, *25*(4), 561–563. https://doi.org/10.1016/0042-6989(85)90160-9

Miettinen, I., Näsänen, R., & Häkkinen, J. (2008). Effects of saccade length and target luminance on the refresh frequency threshold for the visibility of color break-up. *Journal of Display Technology*, *4*(1), 81–85. https://doi.org/10.1109/JDT.2007.901568

Miller, G. A. (1956). The magical number seven, plus or minus two: Some limits on our capacity for processing information. *Psychological Review*, *63*(2), 81–97. https://doi.org/10.1037/h0043158

Mitrani, L., Yakimoff, N., & Mateeff, S. (1970). Dependence of visual suppression on the angular size of voluntary saccadic eye movements. *Vision Research*, *10*(5), 411–415. https://doi.org/10.1016/0042-6989(70)90121-5

Mori, M., Hatada, T., Ishikawa, K., Saishouji, T., Wada, O., Nakamura, J., & Terashima, N. (1999). Mechanism of color breakup in field-sequential-color projectors. *Journal of the Society for Information Display*, *7*(4), 257–259. https://sid.onlinelibrary.wiley.com/doi/abs/10.1889/1.1985291

Morrone, M. C., Ross, J., & Burr, D. (2005). Saccadic eye movements cause compression of time as well as space. *Nature Neuroscience*, *8*(7), 950–954. https://doi.org/10.1038/nn1488

Moschner, C., & Baloh, R. W. (1994). Age-related changes in visual tracking. *Journal of Gerontology*, *49*(5), M235–M238. https://doi.org/10.1093/geronj/49.5.M235

Mullen, K. T., & Kingdom, F. A. A. (2002). Differential distributions of red–green and blue-yellow cone opponency across the visual field. *Visual Neuroscience*, *19*(1), 109–118. https://doi.org/10.1017/S0952523802191103

Mullen, K. T., Sakurai, M., & Chu, W. (2005). Does L/M cone opponency disappear in human periphery? *Perception*, *34*(8), 951–959. https://doi.org/10.1068%2Fp5374

Munoz, D. P., Broughton, J. R., Goldring, J. E., & Armstrong, I. T. (1998). Age-related performance of human subjects on saccadic eye movement tasks. *Experimental Brain Research*, *121*(4), 391–400. https://doi.org/10.1007/s002210050473

Murphy, B. J. (1978). Pattern thresholds for moving and stationary gratings during smooth eye movement. *Vision Research*, *18*(5), 521–530. https://doi.org/10.1016/0042-6989(78)90196-7

MX-Electronic. (n.d.). *Bedienungsanleitung zum Mini-Lux [Operating instructions for the Mini-Lux]*. http://www.mx-electronic.com/pdf-texte/link-lichtmess-systeme/bedienungsanleitungdeutsch.pdf

Näsänen, R., Tiippana, K., & Rovamo, J. (1998). Contrast restoration model for contrast matching of cosine gratings of various spatial frequencies and areas. *Ophthalmic and Physiological Optics*, *18*(3), 269–278. https://doi.org/fpnhxr

Newton, J. R., & Eskew, R. T., Jr. (2003). Chromatic detection and discrimination in the periphery: A postreceptoral loss of color sensitivity. *Visual Neuroscience*, *20*(5), 511–521. https://doi.org/10.1017/S0952523803205058

Post, D. L., Nagy, A. L., Monnier, P., & Calhoun, C. S. (1998). 38.3: Predicting color breakup on field-sequential displays: Part 2. *SID Symposium Digest of Technical Papers*, *29*(1), 1037–1040. https://doi.org/10.1889/1.1833662

Post, D. L., Monnier, P., & Calhoun, C. S. (1997). Predicting color breakup on field-sequential displays. *Head-Mounted Displays II*, *3058*, 57–65. https://doi.org/10.1117/12.276660

Poulos, A., Jentz, L. H., Brown, C., Ambrus, A., Tomlin, A., Dack, J., Kohler, J., Rehmeyer, E. S., Parker, E. D., Denhez, N., & Boesel, B. (2018). *Control device with holographic element* (U.S. Patent No. 10,126,553). U.S. Patent and Trademark Office. https://patft.uspto.gov/netacgi/nph-Parser?patentnumber=10126553

Qin, Z., Lin, F.-C., Huang, Y.-P., & Shieh, H.-P. D. (2019). 2.2: Invited paper: Towards picture-level color breakup assessment for sequential color displays. *SID Symposium Digest of Technical Papers*, *50*(S1), 18–21. https://doi.org/10.1002/sdtp.13369

Qin, Z., Lin, Y.-J., Lin, F.-C., Kuo, C.-W., Lin, C.-H., Sugiura, N., Shieh, H.-P. D., & Huang, Y.-P. (2018). Image content adaptive color breakup index for field sequential color displays using a dominant visual saliency method. *Journal of the Society for Information Display*, *26*(2), 85–97. https://doi.org/10.1002/jsid.644

Qin, Z., Zhang, Y., Lin, F.-C., Huang, Y.-P., & Shieh, H.-P. D. (2019). A review of color breakup assessment for field sequential color display. *Information Display*, *35*(2), 13–43. https://doi.org/10.1002/msid.1019

Rashbass, C. (1961). The relationship between saccadic and smooth tracking eye movements. *The Journal of Physiology*, *159*(2), 326–338. https://doi.org/10.1113/jphysiol.1961.sp006811

Riccò, A. (1877). Relazione fra il minimo angolo visuale e l'intensità luminosa [Relationship between the minimum visual angle and the luminous intensity]. *Memorie della Societa Degli Spettroscopisti Italiani*, *6*, B29–B58. https://adsabs.harvard.edu/pdf/1877MmSSI...6B..29R

Ridder, W. H., III, & Tomlinson, A. (1997). A comparison of saccadic and blink suppression in normal observers. *Vision Research*, *37*(22), 3171–3179. https://doi.org/10.1016/S0042-6989(97)00110-7

Robinson, D. A. (1965). The mechanics of human smooth pursuit eye movement. *The Journal of Physiology*, *180*(3), 569–591. https://doi.org/10.1113/jphysiol.1965.sp007718

Ross, J., Morrone, M. C., & Burr, D. C. (1997). Compression of visual space before saccades. *Nature*, *386*(6625), 598–601. https://doi.org/10.1038/386598a0

Ross, J., Morrone, M. C., Goldberg, M. E., & Burr, D. C. (2001). Changes in visual perception at the time of saccades. *Trends in Neurosciences*, *24*(2), 113–121. https://doi.org/10.1016/S0166-2236(00)01685-4

Rotman, G., Brenner, E., & Smeets, J. B. J. (2002). Spatial but not temporal cueing influences the mislocalisation of a target flashed during smooth pursuit. *Perception*, *31*(10), 1195–1203. https://doi.org/10.1068%2Fp3411

Rottach, K. G., Zivotofsky, A. Z., Das, V. E., Averbuch-Heller, L., Discenna, A. O., Poonyathalang, A., & Leigh, R. J. (1996). Comparison of horizontal, vertical and diagonal smooth pursuit eye movements in normal human subjects. *Vision Research*, *36*(14), 2189–2195. https://doi.org/10.1016/0042-6989(95)00302-9

Sakurai, M., Ayama, M., & Kumagai, T. (2003). Color appearance in the entire visual field: Color zone map based on the unique hue component. *Journal of the Optical Society of America A*, *20*(11), 1997–2009. https://doi.org/10.1364/JOSAA.20.001997

Saslow, M. G. (1967). Effects of components of displacement-step stimuli upon latency for saccadic eye movement. *Journal of the Optical Society of America*, *57*(8), 1024–1029. https://doi.org/10.1364/JOSA.57.001024

Schütz, A. C., Braun, D. I., & Gegenfurtner, K. R. (2007). Contrast sensitivity during the initiation of smooth pursuit eye movements. *Vision Research*, *47*(21), 2767–2777. https://doi.org/10.1016/j.visres.2007.07.006

Schütz, A. C., Braun, D. I., & Gegenfurtner, K. R. (2011). Eye movements and perception: A selective review. *Journal of Vision*, *11*(5), 1–30. https://doi.org/10.1167/11.5.9

Schütz, A. C., Braun, D. I., Kerzel, D., & Gegenfurtner, K. R. (2008). Improved visual sensitivity during smooth pursuit eye movements. *Nature Neuroscience*, *11*(10), 1211–1216. https://doi.org/10.1038/nn.2194

Schütz, A. C., Delipetkos, E., Braun, D. I., Kerzel, D., & Gegenfurtner, K. R. (2007). Temporal contrast sensitivity during smooth pursuit eye movements. *Journal of Vision*, *7*(13), 1–15. https://doi.org/10.1167/7.13.3

Schwarz, D. M. (2017). *Fast and robust curve intersections (Version 2.0.0.0)* [Code]. MATLAB File Exchange. https://de.mathworks.com/matlabcentral/fileexchange/11837-fast-and-robust-curve-intersections

Seelmacher, D. (2017). *Color Break-Up: Bestimmung des Akzeptanzlevels für praxisrelevante Darbietungsszenarien [Color break-up: Determination of the acceptance level for practice-relevant scenarios]* [Unpublished bachelor's thesis]. University of Applied Sciences, Jena, Germany.

Sekiya, K., Miyashita, T., & Uchida, T. (2006). L-4: Late-news paper: A simple and practical way to cope with color breakup on field sequential color LCDs. *SID Symposium Digest of Technical Papers*, *37*(1), 1661–1664. https://doi.org/10.1889/1.2433323

Sekiya, K., Wako, K., Ishinabe, T., Miyashita, T., & Uchida, T. (2003). On the effect of motion interpolation and blanking on color-field sequential LCDs. *Proceedings of the 10th International Display Workshops*, 1731–1734.

Sharpe, J. A., & Sylvester, T. O. (1978). Effect of aging on horizontal smooth pursuit. *Investigative Ophthalmology & Visual Science*, *17*(5), 465–468. https://iovs.arvojournals.org/article.aspx?articleid=2175671

Sharpe, J. A., & Zackon, D. H. (1987). Senescent saccades: Effects of aging on their accuracy, latency and velocity. *Acta Oto-Laryngologica*, *104*(5-6), 422–428. https://doi.org/10.3109/00016488709128270

Shieh, H.-P. D., Huang, Y.-P., Lin, F.-C., Chen, H.-M. P., & Cheng, Y.-K. (2009). 18.1: Invited paper: Eco-display - an LCD-TV powered by a battery? *SID Symposium Digest of Technical Papers*, *40*(1), 228–231. https://doi.org/10.1889/1.3256748

Siemianowski, S., Bremer, M., Plummer, E., Fiebranz, B., Klasen-Memmer, M., & Canisius, J. (2016). 15-3: Invited paper: Liquid crystal technologies towards realising a field sequential colour (FSC) display. *SID Symposium Digest of Technical Papers*, *47*(1), 175–178. https://doi.org/10.1002/sdtp.10629

Silverstein, L. D. (2005). 25.1: Distinguished contributed paper: STColor: Hybrid spatial-temporal color synthesis for enhanced display image quality. *SID Symposium Digest of Technical Papers*, *36*(1), 1112–1115. https://doi.org/10.1889/1.2036195

Sluka, T., Kvasov, A., Kubes, T., Masson, J., Fotinos, A., Smolik, G., Suruceanu, G., Ergunay, S., Michoud, A., Hirt, G., Kabengera, P., & Comminot, J. (2021). Light-field brings augmented reality to the personal space. *Optical Architectures for Displays and Sensing in Augmented, Virtual, and Mixed Reality (AR, VR, MR) II*, *11765*, 179–194. https://doi.org/10.1117/12.2584091

Smit, A. C., van Gisbergen, J. A. M., & Cools, A. R. (1987). A parametric analysis of human saccades in different experimental paradigms. *Vision Research*, *27*(10), 1745–1762. https://doi.org/10.1016/0042-6989(87)90104-0

Smith, G., & Atchison, D. A. (1997). *The eye and visual optical instruments*. Cambridge University Press. https://doi.org/10.1017/CBO9780511609541

Society of Motion Picture and Television Engineers. (2014). *SMPTE Standard - Measurement and Calibration Procedure for HDTV Display Luminance Levels and Chromaticity*. (RP 2080-2:2014). https://ieeexplore.ieee.org/document/7289952.

Souman, J. L., Hooge, I. T. C., & Wertheim, A. H. (2005). Perceived motion direction during smooth pursuit eye movements. *Experimental Brain Research*, *164*(3), 376–386. https://doi.org/10.1007/s00221-005-2261-6

Spering, M., & Montagnini, A. (2011). Do we track what we see? Common versus independent processing for motion perception and smooth pursuit eye movements: A review. *Vision Research*, *51*(8), 836–852. https://doi.org/10.1016/j.visres.2010.10.017

Spooner, J. W., Sakala, S. M., & Baloh, R. W. (1980). Effect of aging on eye tracking. *Archives of Neurology*, *37*(9), 575–576. https://doi.org/10.1001/archneur.1980.00500580071012

Srivastava, A. K., Shi, L., & Kwok, H. S. (2019). 40.1: Invited paper: Electrically suppressed helix ferroelectric liquid crystals (FLCD) for modern LCDs. *SID Symposium Digest of Technical Papers*, *50*(S1), 441–444. https://doi.org/10.1002/sdtp.13522

Stabell, B., & Stabell, U. (1979). Rod and cone contributions to change in hue with eccentricity. *Vision Research*, *19*(10), 1121–1125. https://doi.org/c9x68b

Stabell, B., & Stabell, U. (1980). Spectral sensitivity in the far peripheral retina. *Journal of the Optical Society of America*, *70*(8), 959–963. https://doi.org/10.1364/JOSA.70.000959

Stabell, U., & Stabell, B. (1981). Spectral sensitivity of the dark-adapted extrafoveal retina at photopic intensities. *Journal of the Optical Society of America*, *71*(7), 841–844. https://doi.org/10.1364/JOSA.71.000841

Stabell, U., & Stabell, B. (1982). Color vision in the peripheral retina under photopic conditions. *Vision Research*, *22*(7), 839–844. https://doi.org/10.1016/0042-6989(82)90017-7

Stevens, J. C., & Hall, J. W. (1966). Brightness and loudness as functions of stimulus duration. *Perception & Psychophysics*, *1*(9), 319–327. https://doi.org/10.3758/BF03215796

Stevens, J. C., & Stevens, S. S. (1963). Brightness function: Effects of adaptation. *Journal of the Optical Society of America*, *53*(3), 375–385. https://doi.org/10.1364/JOSA.53.000375

Stevens, S. S. (1957). On the psychophysical law. *Psychological Review*, *64*(3), 153–181. https://doi.org/10.1037/h0046162

Stevens, S. S. (1961). To honor Fechner and repeal his law: A power function, not a log function, describes the operating characteristic of a sensory system. *Science*, *133*(3446), 80–86. https://doi.org/10.1126/science.133.3446.80

Stevens, S. S. (2017). *Psychophysics: Introduction to its perceptual, neural and social prospects*. Routledge. https://doi.org/10.4324/9781315127675

Stevenson, S. B., Volkmann, F. C., Kelly, J. P., & Riggs, L. A. (1986). Dependence of visual suppression on the amplitudes of saccades and blinks. *Vision Research*, *26*(11), 1815–1824. https://doi.org/10.1016/0042-6989(86)90133-1

Stewart, B. R. (1972). Temporal summation during dark adaptation. *Journal of the Optical Society of America*, *62*(3), 449–457. https://doi.org/10.1364/JOSA.62.000449

Streijl, R. C., Winkler, S., & Hands, D. S. (2016). Mean opinion score (MOS) revisited: Methods and applications, limitations and alternatives. *Multimedia Systems*, *22*(2), 213–227. https://doi.org/10.1007/s00530-014-0446-1

Stromeyer, C. F., III, Lee, J., & Eskew, R. T., Jr. (1992). Peripheral chromatic sensitivity for flashes: A post-peceptoral red-green asymmetry. *Vision Research*, *32*(10), 1865–1873. https://doi.org/10.1016/0042-6989(92)90047-M

Takayuki, T. (1994). Temporal integration characteristics of the human visual system for the suprathreshold flashes: I. Suprathreshold analogue of Bloch's law. *Tohoku Psychologica Folia*, *53*, 27–39. http://hdl.handle.net/10097/56167

Teich, M., Schuster, T., Leister, N., Zozgornik, S., Fugal, J., Wagner, T., Zschau, E., Häussler, R., & Stolle, H. (2022). Real-time, large-depth holographic 3D head-up display: Selected aspects. *Applied Optics*, *61*(5), B156–B163. https://doi.org/10.1364/AO.442924

Tektronix. (2004). *TPS2000 series digital storage oscilloscope: User manual*. https://download.tek.com/manual/071144105web.pdf

Teng, K.-T., Lin, F.-C., Chang, C.-W., Lin, C.-H., Huang, Y.-P., & Shieh, H.-P. D. (2016). 59-4: Reduction of possible flicker and color breakup using Deflicker-FSC method for field-sequential-color displays. *SID Symposium Digest of Technical Papers*, *47*(1), 809–812. https://doi.org/10.1002/sdtp.10796

Terao, M., Watanabe, J., Yagi, A., & Nishida, S. (2010). Smooth pursuit eye movements improve temporal resolution for color perception. *PLOS ONE*, *5*(6), Article e11214. https://doi.org/10.1371/journal.pone.0011214

Texas Instruments. (2017). *TI DLP LightCrafter 4500 evaluation module: User's guide*. http://www.ti.com/lit/ug/dlpu011f/dlpu011f.pdf

Texas Instruments. (2019). *DLPC350 DLP Digital Controller for DLP4500 and DLP4500NIR DMDs* [Data sheet]. http://www.ti.com/lit/ds/symlink/dlpc350.pdf

Texas Instruments. (2021). *DLP4500 .45 WXGA DMD* [Data sheet]. http://www.ti.com/lit/ds/symlink/dlp4500.pdf

Thibos, L. N., & Horner, D. (2001). Power vector analysis of the optical outcome of refractive surgery. *Journal of Cataract & Refractive Surgery*, *27*(1), 80–85. https://doi.org/10.1016/S0886-3350(00)00797-5

Thorlabs. (2020). *PDA36A2 Si switchable gain detector: User guide*. https://www.thorlabs.com/drawings/7caa293c902496e3-277F0C17-CE31-BBC5-39565350367E5FA0/PDA36A2-Manual.pdf

Turano, K. A., & Heidenreich, S. M. (1999). Eye movements affect the perceived speed of visual motion. *Vision Research*, *39*(6), 1177–1187. https://doi.org/10.1016/S0042-6989(98)00174-6

Tychsen, L., & Lisberger, S. G. (1986). Visual motion processing for the initiation of smooth-pursuit eye movements in humans. *Journal of Neurophysiology*, *56*(4), 953–968. https://doi.org/10.1152/jn.1986.56.4.953

Ueno, T. (1976). Temporal summation and reaction time to double-light pulses at suprathreshold levels. *Perception & Psychophysics*, *19*(5), 399–404. https://doi.org/10.3758/BF03199399

Ueno, T. (1977). Reaction time as a measure of temporal summation at suprathreshold levels. *Vision Research*, *17*(2), 227–232. https://doi.org/10.1016/0042-6989(77)90086-4

Ueno, T. (1978). Temporal summation in human vision: Simple reaction time measurements. *Perception & Psychophysics*, *23*(1), 43–50. https://doi.org/10.3758/bf03214293

Van Dijk, R., & Shimizu, J. A. (2004). *System and method for motion compensation of image planes in color sequential displays* (U.S. Patent No. 6,831,948). U.S. Patent and Trademark Office. https://patft.uspto.gov/netacgi/nph-Parser?patentnumber=6831948

Van Dijk, R., & Shimizu, J. A. (2009). *System and method for motion compensation of image planes in color sequential displays* (U.S. Patent No. 7,486,730). U.S. Patent and Trademark Office. https://patft.uspto.gov/netacgi/nph-Parser?patentnumber=7486730

Vel. (2017). *Masters/doctoral thesis (Version 2.5)* [LaTeX Template]. Creodocs. https://www.latextemplates.com/template/masters-doctoral-thesis

Volkmann, F. C., Riggs, L. A., White, K. D., & Moore, R. K. (1978). Contrast sensitivity during saccadic eye movements. *Vision Research*, *18*(9), 1193–1199. https://doi.org/10.1016/0042-6989(78)90104-9

Walker, R., Deubel, H., Schneider, W. X., & Findlay, J. M. (1997). Effect of remote distractors on saccade programming: Evidence for an extended fixation zone. *Journal of Neurophysiology*, *78*(2), 1108–1119. https://doi.org/10.1152/jn.1997.78.2.1108

Wang, J., Zhang, Y., Li, X., & Weng, Y. (2017). Color breakup visibility thresholds for 2-field sequential colors. *Color Research & Application*, *42*(5), 580–590. https://doi.org/10.1002/col.22125

Wang, J., Zhang, Y., Weng, Y., & Li, X. (2017). Simulation of color breakup based on measured display temporal responses. *Journal of the Society for Information Display*, *25*(11), 653–662. https://doi.org/10.1002/jsid.614

Welch, B. L., & Fernie, A. (1997). *Field sequential color head mounted display with suppressed color break-up* (U.S. Patent No. 5,684,498). U.S. Patent and Trademark Office. https://patft.uspto.gov/netacgi/nph-Parser?patentnumber=5684498

Wichmann, F. A., & Hill, N. J. (2001). The psychometric function: I. Fitting, sampling, and goodness of fit. *Perception & Psychophysics*, *63*(8), 1293–1313. https://doi.org/10.3758/BF03194544

Wisselink, H. J. (2019). *BlandAltmanPlot (Version 1.0)* [Code]. MATLAB File Exchange. https://de.mathworks.com/matlabcentral/fileexchange/71052-blandaltmanplot

Wolf, W., Hauske, G., & Lupp, U. (1978). How presaccadic gratings modify postsaccadic modulation transfer function. *Vision Research*, *18*(9), 1173–1179. https://doi.org/10.1016/0042-6989(78)90101-3

Wurtz, R. H. (2008). Neuronal mechanisms of visual stability. *Vision Research*, *48*(20), 2070–2089. https://doi.org/10.1016/j.visres.2008.03.021

Yamada, F., & Sakaguchi, Y. (2006). *Matrix driven liquid crystal display module system, apparatus and method* (U.S. Patent No. 7,079,162). U.S. Patent and Trademark Office. https://patft.uspto.gov/netacgi/nph-Parser?patentnumber=7079162

Yan, S.-P., Cheng, Y.-K., Lin, F.-C., Wei, C.-M., Huang, Y.-P., & Shieh, H.-P. D. (2007). P-40: A visual model of color break-up for design field-sequential LCDs. *SID Symposium Digest of Technical Papers*, *38*(1), 338–341. https://doi.org/10.1889/1.2785300

Yang, C.-M., Bae, J.-H., Kim, J.-U., Kim, C.-W., Kim, D.-S., Cho, S.-P., & Lee, H.-S. (2016). Content-dependent reduction of static color breakup on field sequential color LCDs. *Journal of Display Technology*, *12*(7), 673–680. https://doi.org/10.1109/JDT.2016.2521820

Yi, W.-C. (2008). *Color break-up evaluation by relative contrast sensitivity index* [Master's thesis, National Chiao Tung University, Hsinchu, Taiwan]. Institutional Repository of NCTU. https://ir.nctu.edu.tw/bitstream/11536/38623/1/551301.pdf

Yohso, A., & Ukai, K. (2006). How color break-up occurs in the human-visual system: The mechanism of the color break-up phenomenon. *Journal of the Society for Information Display*, *14*(12), 1127–1133. https://doi.org/10.1889/1.2408396

Yoshida, A., Kobayashi, M., & Yoshida, Y. (2011). 24.4: Subjective and objective assessments of color break-up on field sequential color display devices. *SID Symposium Digest of Technical Papers*, *42*(1), 313–316. https://doi.org/10.1889/1.3621307

Yujiri, A., & Hamada, H. (2003). Color appearance of object colors in peripheral vision at various illuminance levels. *Journal of Light & Visual Environment*, *27*(2), 83–91. https://doi.org/10.2150/jlve.27.83

Zackon, D. H., & Sharpe, J. A. (1987). Smooth pursuit in senescence: Effects of target acceleration and velocity. *Acta Oto-Laryngologica*, *104*(3-4), 290–297. https://doi.org/10.3109/00016488709107331

Zhang, X., & Farrell, J. E. (2003). Sequential color breakup measured with induced saccades. *Human Vision and Electronic Imaging VIII*, *5007*, 210–217. https://doi.org/10.1117/12.497843

Zhang, Y., Langendijk, E. H. A., Hammer, M., & Hinnen, K. (2012). A new color breakup measure based on color difference between fields and contrast to the surrounding. *Journal of Display Technology*, *8*(3), 145–153. https://doi.org/10.1109%2FJDT.2011.2165936

Zhang, Y., Langendijk, E. H. A., Hammer, M., & Lin, F.-C. (2011). A hybrid spatial-temporal color display with local-primary-desaturation backlight scheme. *Journal of Display Technology*, *7*(12), 665–673. https://doi.org/10.1109/JDT.2011.2159774

Zhang, Y., Lin, F.-C., & Langendijk, E. H. A. (2011). A field-sequential-color display with a local-primary-desaturation backlight scheme. *Journal of the Society for Information Display*, *19*(3), 258–264. https://doi.org/10.1889/JSID19.3.258

Zhang, Y., Wang, J., Wang, L., Tu, Y., & Li, X. (2016). 59-1: Invited paper: Modeling and suppressing of color breakup. *SID Symposium Digest of Technical Papers*, *47*(1), 798–801. https://doi.org/10.1002/sdtp.10793

Zuidema, P., Verschuure, H., Bouman, M. A., & Koenderink, J. J. (1981). Spatial and temporal summation in the human dark-adapted retina. *Journal of the Optical Society of America*, *71*(12), 1472–1480. https://doi.org/10.1364/JOSA.71.001472